POLYMORPHISM AND CYCLODEXTRIN INCLUSION COMPLEXES OF ANTIHYPERTENSIVE AGENTS

By: Welcome Thabani Mhlongo

B.Sc. (Hons.)

Thesis Presented for the Degree of

DOCTOR OF PHILOSOPHY

in the Department of Chemistry

Faculty of Science

University of Cape Town

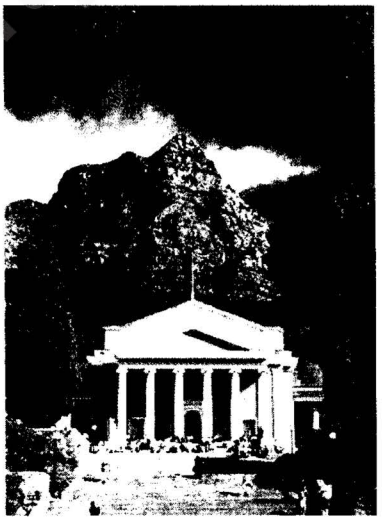

January 2006

Acknowledgements

I would like to thank:

Supervisors

Professor M. R. Caira, for his patience, kindness, understanding, excellent supervision and expertise that are second to none.

Professor L. R. Nassimbeni for his advice, help as well as knowing absolutely everything.

Thanks are due to Professor M. T. Bojita, Rector of the University of Medicine and Pharmacy, "Iuliu Hatieganu," Cluj-Napoca, Romania for hosting me as a visiting researcher in his laboratory and for guidance in the selection of drugs for this study.

Dr J. Bacsa and Dr H. Su for single crystal X-ray diffraction data collected on the Kappa CCD diffractometer.

The members of the University of Cape Town Supramolecular Chemistry Group for their assistance during the project, especially Dr C. Oliver and Mr V. Smith, and making my daily working environment pleasant.

My family, and friends for their support and encouragement.

The National Research Foundation, the Centre for Scientific and Industrial Research and the University of Cape Town for financial support.

Journal Articles Published and Conferences Attended

Journal articles published

1. M. R. Caira, S. A. Bourne, W. T. Mhlongo, P. M. Dean, New crystalline forms of permethylated beta-cyclodextrin, Chem. Commun., **19**, 2216-2217, **2004**.

Conferences attended

International Immunopharmacology Congress 2001, Sun City, Pilanesberg, South Africa, September 16-20, 2001.
Poster: Structure and thermal analysis of the antihypertensive Metoprolol.
M R Caira, L R Nassimbeni and W Mhlongo.

Annual Meeting of the South African Crystallographic Society, University of Stellenbosch, RSA, 4-5 April, 2002.
Structure and thermal analysis of the antihypertensive Metoprolol.
M R Caira, L R Nassimbeni and W Mhlongo.

21st European Crystallographic Meeting, ECM-21, Durban, South Africa, 24-29 August 2003.
Poster f4.m6.p3: Cyclodextrin inclusion complexes of antihypertensive agents: thermal and X-ray diffraction studies. W T Mhlongo, M R Caira and L R Nassimbeni.

Academy of Pharmaceutical Sciences 24th Annual Congress, Durban, South Africa, 7-10 September 2003.
Poster T15: Cyclodextrin inclusion of antihypertensive agents: thermal and X-ray diffraction studies. W T Mhlongo, M R Caira and L R Nassimbeni.

Abstract

Polymorphism and Cyclodextrin Inclusion Complexes of Antihypertensive Agents

The objective of the project described in this thesis was to isolate polymorphs, solvates and cyclodextrin inclusion complexes of antihypertensive agents. The physical properties of different polymorphs of a given drug are of significant interest to the pharmaceutical industry. The solubility enhancement of poorly soluble drugs by encapsulating them within cyclodextrins is also an important pharmaceutical consideration.

The drugs investigated were atenolol, metoprolol, oxprenolol free bases and two salts, namely oxprenolol hydrochloride and metoprolol tartrate. No polymorphs of these antihypertensive agents were isolated but metoprolol yielded a solvate with n-hexane. Single crystals of atenolol, metoprolol, metoprolol tartrate and oxprenolol were isolated and their X-ray structures are reported here for the first time.

Inclusion complexes of atenolol, metoprolol and oxprenolol free bases with cyclodextrins were successfully investigated in the solid state. The cyclodextrin hosts used for drug inclusion were β-cyclodextrin, γ-cyclodextrin, heptakis(2,6-di-O-methyl)-β-cyclodextrin, heptakis(2,3,6-tri-O-methyl)-β-cyclodextrin and hexakis(2,3,6-tri-O-methyl)-α-cyclodextrin. A new crystal form of heptakis(2,3,6-tri-O-methyl)-β-cyclodextrin as a trihydrate was isolated in an attempt to produce an inclusion complex between this host compound and the drug substance atenolol. The first crystal form of this host compound, a monohydrate, was previously discovered by the Supramolecular Chemistry Research Unit at the University of Cape Town.

The various analytical techniques utilised for the characterisation of the solid-state properties of the species were elemental analysis as well as thermal, X-ray diffraction and spectroscopic techniques. Single crystal X-ray diffraction was the principal technique used for investigation of structural features. The structure of metoprolol revealed one

molecule per asymmetric unit while the structure of the metoprolol solvate revealed eight molecules of metoprolol and one of n-hexane per asymmetric unit.

Structure solution was successful for six cyclodextrin inclusion complexes. The oxprenolol guest molecule was successfully modelled in β-cyclodextrin and heptakis(2,3,6-tri-O-methyl)-β-cyclodextrin. Metoprolol was successfully modelled in hexakis(2,3,6-tri-O-methyl)-α-cyclodextrin but could not be modelled in heptakis(2,3,6-tri-O-methyl)-β-cyclodextrin and β-cyclodextrin due to its severe disorder.

The computed powder X-ray diffraction (PXRD) patterns of the oxprenolol-β-cyclodextrin (OXPRBCD) and atenolol-β-cyclodextrin (ATBCD) inclusion complexes were different from their experimental PXRD patterns. This indicated that phase transformation had occurred upon grinding the single crystals for each of these complexes. These two complexes crystallise in space group P1 [with unit cell parameters a ~ 18, b ~15 and c ~ 15 Å]; thus, they are isostructural. However, their experimental PXRD patterns are different from each other. The comparison of these experimental PXRDs with published reference patterns for β-cyclodextrin complexes showed that grinding OXPRBCD transformed this material into a form crystallising in the space group $P2_1$ while grinding ATBCD resulted in its transformation to a phase belonging to the space group C2. Such transformations have not been reported previously.

Among the free bases studied, atenolol is the only one that is currently commercially available as a medicinal agent. Exploitation of metoprolol and oxprenolol free bases as guests for cyclodextrin inclusion has led to the isolation and full characterisation of new inclusion complexes that have potential for further pharmaceutical development.

Abbreviations and Symbols

Compounds

CD	cyclodextrin
β-CD	beta-cyclodextrin
γ-CD	gamma-cyclodextrin
DIMEB	heptakis(2,6-di-O-methyl)-beta-cyclodextrin
TRIMEA	hexakis(2,3,6-tri-O-methyl)-alpha-cyclodextrin
TRIMEB	heptakis(2,3,6-tri-O-methyl)-beta-cyclodextrin
ATBCD	atenolol-β-CD inclusion complex
SATBCD	(S-)-atenolol-β-CD inclusion complex
METBCD	metoprolol-β-CD inclusion complex
OXPRBCD	oxprenolol-β-CD inclusion complex
ATGCD	atenolol-γ-CD inclusion complex
METGCD	metoprolol-γ-CD inclusion complex
OXPRGCD	oxprenolol-γ-CD inclusion complex
DMBOXP	DIMEB•oxprenolol inclusion complex
METTMEA	metoprolol•TRIMEA inclusion complex
METTMB	metoprolol•TRIMEB inclusion complex
OXPTMB	oxprenolol•TRIMEB inclusion complex
NTMB	TRIMEB trihydrate
TRIB	NTMB after dehydration

Techniques

HSM	Hot Stage Microscopy
DSC	Differential Scanning Calorimetry
TGA	Thermogravimetric analysis
PXRD	Powder X-ray Diffraction
FTIR	Fourier Transform Infrared Spectroscopy
NMR	Nuclear Magnetic Resonance
UV	Ultraviolet Spectrophotometry

Symbols

CSD	Cambridge Structural Database
α	The angle between b and c unit cell axes
β	The angle between a and c unit cell axes
γ	The angle between a and b unit cell axes
E	Normalised structure factor
Endo	Endotherm
e.s.d	Estimated standard deviation
F	Structure factor
F(000)	Number of electrons in the unit cell
S	Goodness of fit (F^2)
s.o.f.	Site-occupancy factor
τ	Torsion angle
T_{on}	Onset temperature

Table of Contents

Chapter 3 – Antihypertensive Agents

Chapter 7 – TRIMEA and DIMEB Inclusion Complexes

Chapter 1 - Introduction

Supramolecular Chemistry

In 1988 Jean-Marie Lehn[1] defined supramolecular chemistry in his Nobel lecture as "chemistry beyond the molecule". Hence supramolecular chemistry can be described as a discipline of chemistry that involves all intermolecular interactions where covalent bonds are not established between the interacting species, namely molecules, ions or radicals. This discipline was triggered by the discovery of the chlorine clathrate hydrate [$Cl_2 \cdot 6H_2O$] by Davey[2] in 1811. The discovery of X-rays and their use in structure elucidation in 1895 and 1912 respectively enhanced the growth in this field. In this thesis the structure elucidation of the antihypertensive agents atenolol, metoprolol tartrate, oxprenolol hydrochloride and the free bases of the salts and the cyclodextrin inclusion of the free bases atenolol, metoprolol and oxprenolol will be treated.

Polymorphism

Polymorphism is a technical term used in crystallography to describe the ability of the same compound to crystallise in more than one distinct crystal form. This phenomenon is associated with different crystal packing arrangements and is very common in pharmaceuticals.[3,4] Since they have different crystal structures, polymorphs have different chemical and physical properties; they have different melting points, different chemical reactivity, different dissolution rates and different bioavailability. The existence of different conformers of the same molecule in different polymorphic modifications is referred to as conformational polymorphism.[5] Solvates are species with included solvent molecules.[6] When the entire material lacks long-range order it is referred to as amorphous.[7] Figure 1.1 illustrates the concept of polymorphs and solvates. A thorough examination of the polymorphic properties of a drug accompanied by its isolation and characterisation are necessary in the pharmaceutical industry for patents and characterisation regulations. This information may also be subsequently used to 'engineer' an optimum polymorphic type of the pharmaceutical under study.[8]

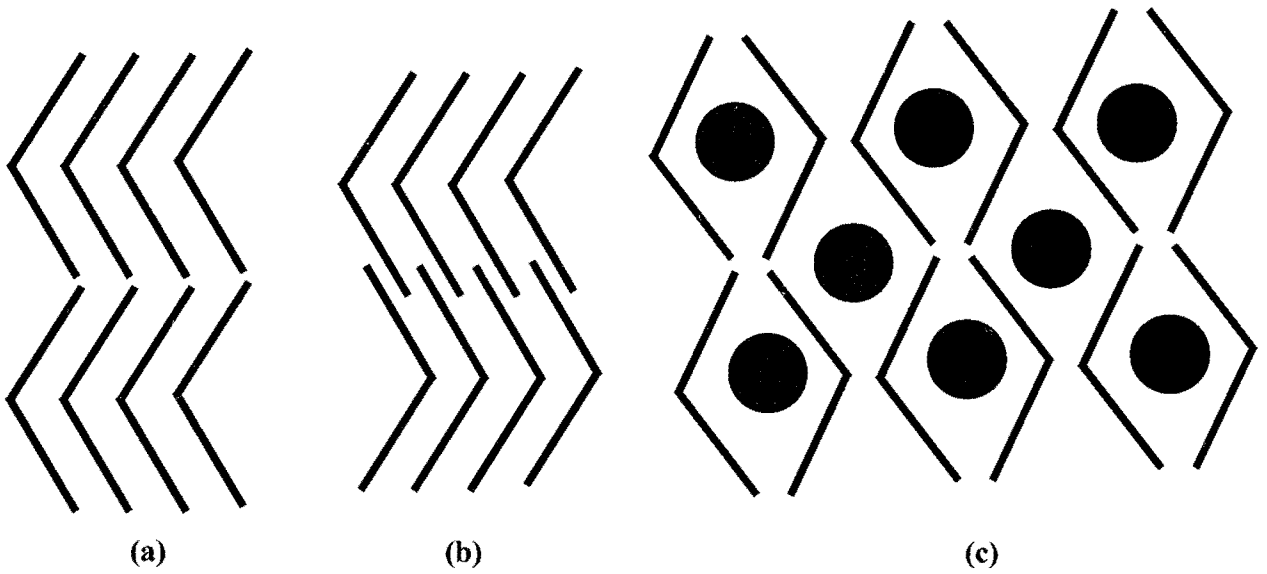

Figure 1.1 Schematic diagram illustrating polymorphs **(a)**, **(b)** and **(c)** solvate. ● represents a solvent molecule.

Brief Historical Perspective of Polymorphism

The first appearance of this term, according to the Oxford English Dictionary, was in 1656 referring to the diversity of fashion. The first recognition of the different crystal morphologies of the same compound $NaH_2PO_4 \cdot H_2O$ was by Mitscherlich[9] in 1822. In 1844, Amici[10] invented the first polarising microscope instrument that was destined to play a crucial role in the development of polymorphism. In 1870 Mallard[11] studied geometrical crystallography and considered the structural basis for polymorphism in a paper he published in 1876. In 1891 Lehman[12] discovered two different types of polymorphism, namely monotropic and enantiotropic. The former involves two forms in which one undergoes an irreversible phase change to the second form while the latter involves two phases that can undergo a reversible phase transition. Based on the

principles of thermodynamics a major development in polymorphism came with the work by Ostwald[13] in 1897 on the relative stability of different polymorphs. With the advent of X-ray crystallography, Tamman[14] considered two polymorphic molecular crystals as being identical molecular species being arranged in different structures. This is today used as the basic criterion for the identification of polymorphs.

The Significance of Polymorphism

Polymorphism plays a crucial role in a number of industrial and commercial applications. In the photographic industry, differences in solubility of polymorphs can pose problems during manufacture, and can lead to impaired performance of the film for negatives.[15] Polymorphism also plays an essential role in the fat-based industries where the melting point and melting behaviour are clearly important physical properties of materials such as ice cream, chocolate and margarine.[16] In the pharmaceutical industry polymorphism is very important from the viewpoints of bioavailability,[17,18,19] stability and handling,[20,21] because the difference in crystal form causes a change in physical properties. In 1998 Abbott halted the production of the HIV protease inhibitor, ritonavir, due to the appearance of an undesired form of the drug during its manufacturing process.[22] The thermodynamically stable, undesired form, had health consequences since it had lower solubility with greatly reduced bioavailability. The economic consequence was due to the removal of the drug from the market and the duration of time spent in rectifying the problem. In this study various solvents and crystallisation methods were employed to determine whether the antihypertensive agents atenolol, metoprolol and oxprenolol have the potential to crystallise in more than one crystal form. Metoprolol and oxprenolol free bases are novel substances and they were obtained by the author from metoprolol tartrate and oxprenolol hydrochloride respectively.

Antihypertensive Agents

Background

Antihypertensive agents used for this work are racemic β-blockers. β-blockers were introduced into clinical practice in the 1960s as racemic mixtures consisting of (R-)- and (S-)-enantiomers in a fixed 1:1 ratio.[23] Little has changed on this issue although it has been clearly shown in vitro as well as in human studies that only the (S-)-enantiomers are biologically active when clinical doses of the racemic drugs are used. Therefore the biologically inactive (R-)-form may cause serious side effects on its own; thus the (R-)- and (S-)-enantiomers should be recognised and used as individual drugs independently. The β-blockers that have been studied for this work are oxprenolol hydrochloride, atenolol and metoprolol tartrate and the free bases of the salts, i.e. oxprenolol and metoprolol.

Oxprenolol hydrochloride

Oxprenolol hydrochloride (1-[(methylethyl)amino]-3-[2-(2-propenyloxy)phenoxy]-2-propanol hydrochloride) is a non-selective β-blocker, recognised as being an important drug and usually prescribed for the treatment of hypertension, angina pectoris, migraine and dysfunctional labour.[24,25,26] The half-life of this compound ranges between 1.3-1.5 h for oral doses of 80 mg of the conventional tablet.[27] The crystal structure of this substance was first determined from X-ray diffraction data in 1977.[28] It crystallises in the monoclinic space group $P2_1/c$ with the unit cell parameters a = 10.477 b = 22.114, c = 7.433 Å and β = 103.86° with four molecules in the unit cell. The use of various solvents to generate polymorphs resulted in the known crystal forms of these substances.

The oxprenolol free base was isolated in this work for the first time and its crystal structure is reported. The molecular structures of the salt and the free base are illustrated in Figure 1.2.

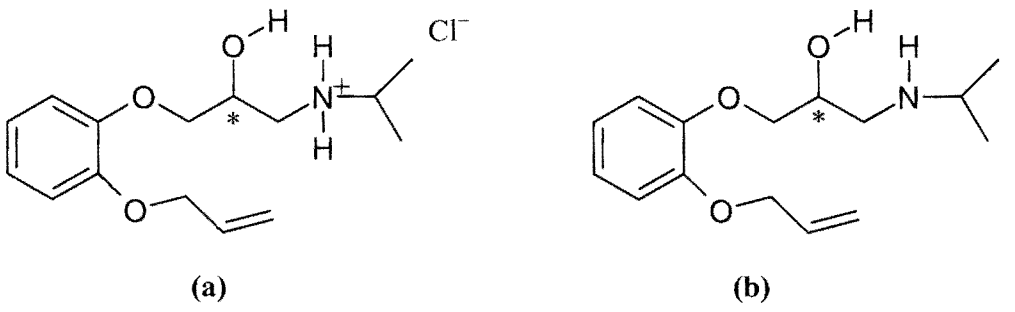

Figure 1.2 Schematic diagrams of the (a) hydrochloride salt and (b) free base of oxprenolol. '*' denotes the chiral centre.

Atenolol

The synthesis of atenolol ((RS)-4-[2-(hydroxy-3-isopropylaminopropoxy)phenyl]-acetamide) was first reported in 1970,[29] and the first pharmacological and clinical studies were made in 1973 and 1974.[30,31,32] Unlike oxprenolol [non-specific β-blocker, i.e. it has both β_1- and β_2-effects], atenolol is a β_1-blocker. β_1-blockers mainly affect the heart while β_2-blockers affect receptors in bronchial tissue. Atenolol is a white odourless powder and it has a slightly bitter taste. Atenolol has been resolved using capillary electrophoresis,[33] HPLC[34] and impregnated TLC.[35] This substance has also been prepared from p-hydroxyphenylacetamide and (R-)- or (S-)-epichlorohydrin followed by preferential crystallisation to yield the enantiopure form.[36] Atenolol hydrochloride is also commercially available in addition to the atenolol free base. This salt is highly soluble in water relative to its free base. The chemical structure of atenolol is shown in Figure 1.3. The crystal structure of atenolol is reported in this work.

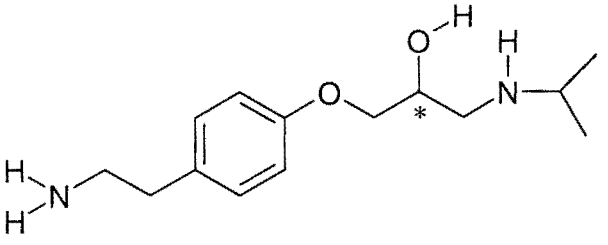

Figure 1.3 Schematic diagram of the atenolol molecule. '*' denotes the chiral centre.

Metoprolol tartrate

Metoprolol tartrate, ([(RS)-3-[4-(2-methoxyethyl)phenoxy]-1-(isopropylamino)propan-2-ol] tartrate) is a synthetic, selective β_1-adrenoreceptor blocking agent.[37,38,39] It is a 2:1 salt consisting of a racemic mixture of optical isomers of the metoprolol base and naturally occurring *dextro*-tartaric acid. It is a white, odourless crystalline powder. This compound is physically and chemically stable. Under high humidity metoprolol tartrate is hygroscopic and rapidly adsorbs water at relative humidities greater than 70%. However upon drying and re-analysis, the material is found to have retained its chemical and physical integrity.[40] It has been reported that after oral administration metoprolol tartrate is readily and rapidly absorbed and is rapidly distributed to body tissues.[41] The schematic diagrams of metoprolol tartrate and its free base are illustrated in Figure 1.4. The isolation of metoprolol free base is reported for the first time in this work. In addition to metoprolol tartrate there is also metoprolol succinate. These salts are both currently commercially available.

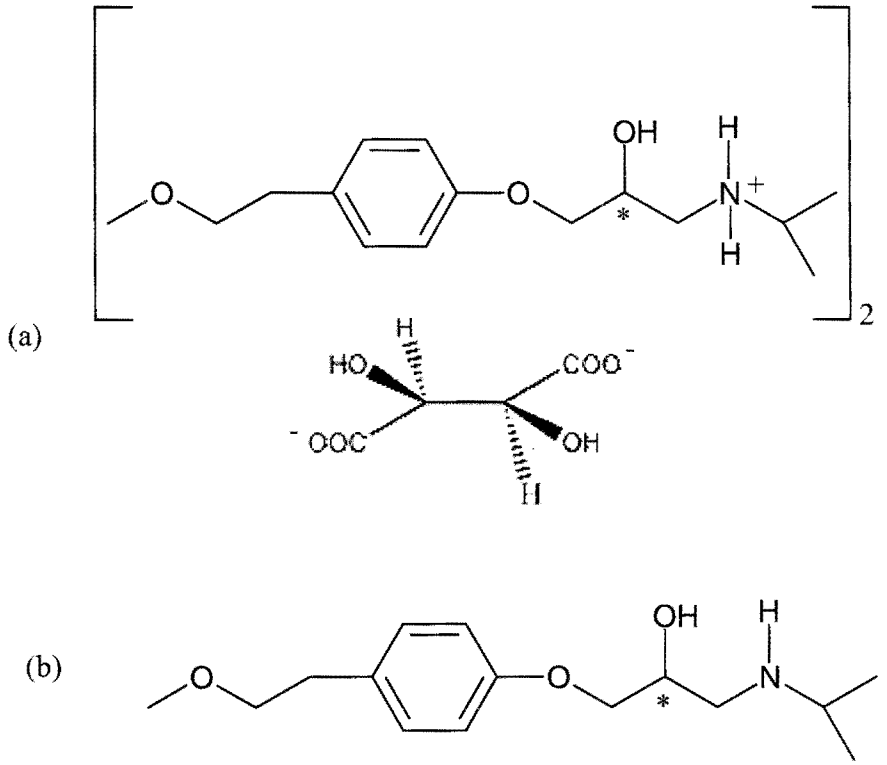

Figure 1.4 Schematic diagrams of the (a) tartrate salt and (b) free base of metoprolol. '*' denotes the chiral centre.

Cyclodextrins

Natural Origin of Cyclodextrins

Since part of this thesis deals with attempts to include the forementioned drugs in cyclodextrins, a description of these macrocyclic host compounds follows. The degradation of starch by the glucosyltransferase enzyme (CGT) results in the primary product of chain splitting undergoing an intramolecular reaction without the participation of water. This subsequently leads to the formation of α-1,4-linked cyclic products known as cyclodextrins [hereinafter CDs]. The enzyme CGT was first isolated from the microbe *Bacillus macerans*.[42] Cyclodextrins contain different numbers of glucopyranose units due to the lack of specificity of the enzyme action in producing these compounds. The most abundant of the CDs produced naturally are α-, β- and γ-CDs consisting of 6, 7 and 8 glucopyranose units respectively [Figure 1.5]. Cyclodextrins with fewer than six ring members cannot be formed for steric reasons. Theoretically, CDs with ten or even higher glucose units could be prepared; however, their high solubility in water and weak complex forming ability, make them of less significance.

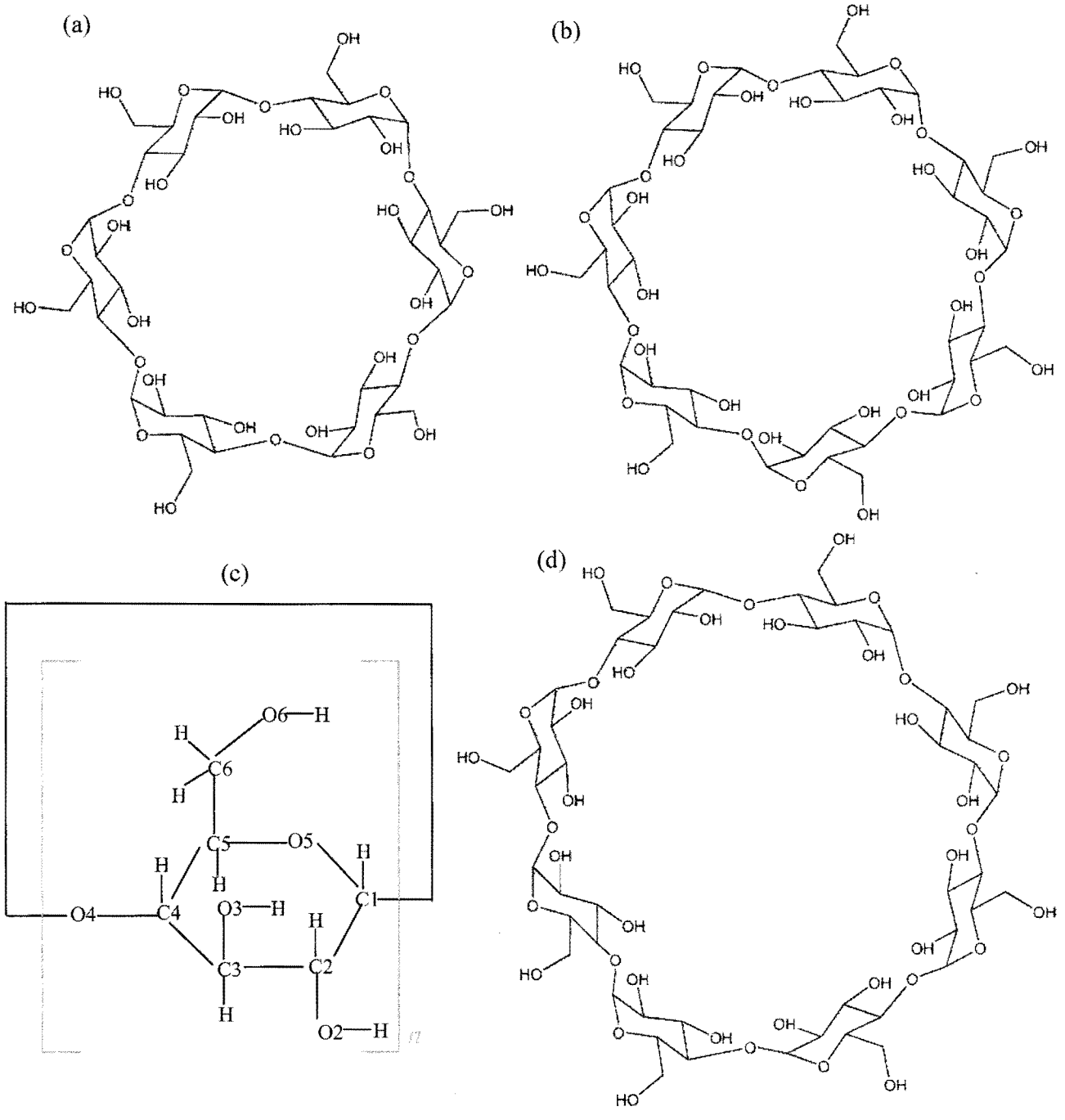

Figure 1.5 (a) α-CD, (b) β-CD, (c) the glucopyranose unit labelling and (d) γ-CD.

Historical Overview

In 1891 Villiers first published a paper that referred to a substance which later proved to be a cyclodextrin.[43] In 1903 Schardinger studied and characterised the degradation product of starch and referred to it as a cyclic oligosaccharide.[44] In the 1930s Pringsheim's phenomenal discovery was that CDs had a high tendency to form complexes with various organic compounds.[45,46] Between 1930 and 1970 Freudenberg and his co-workers, based on their own experiments and the work published by Karrer[47] and Miekeley,[48] concluded that CDs are built from maltose units and contain only α-1,4-glycosidic linkages and in 1936 postulated the structure of these crystalline dextrins.[49] In the 1950s French *et al*[50] and Cramer *et al*[51] produced CDs enzymatically, purified them and characterised their chemical and physical properties. French[50] discovered that there were even larger CDs than γ-CD while Cramer[51] and his co-workers focused on the inclusion complex forming properties of the CDs. In 1953 Freudenberg, Cramer and Plieninger obtained a patent that covered the application of CDs in drug formulations.[52] In 1957 French published the first fundamental review on CDs,[50] which was followed by a monograph by Thoma and Steward[53] in 1965, and in 1968 by Caeser.[54] Once adequate toxicological studies had been performed and the cost of purchase had become relatively cheap, the utilisation of CDs profoundly increased. Today cyclodextrins have a wide variety of applications. They are used in biomedical products, pharmaceutical industries, cosmetics and toiletries, foods and pesticides.

Structural Features

The glucose units almost invariably adopt the $^4C_1$-chair conformation and their conformations are fairly rigid.[55,56,57] However the O6 atom possesses rotational freedom around the C5-C6 bond. The limited conformational flexibility is the rotational freedom around the C1-O4'-C4' glycosidic link [' = refer to the next glucose unit].

Hydrogen bonding

The *cis*-orientation of glucose units relative to one another leads to intramolecular hydrogen bonds between the secondary hydroxyl groups [labelled O2-H and O3-H] of adjacent units. Saenger *et al*[58] discovered this hydrogen bonding to be of a 'flip-flop' nature by neutron diffraction studies. A complete secondary belt is formed by these hydrogen bonds in CDs thus stabilising the macrocyclic conformation except in α-CD. The hydrogen bond-belt is incomplete in this CD due to the irregular rotation of one of the glucose units relative to the remaining five glucose units. The O2•••O3' distance between adjacent glucose units becomes shorter in the order α-, β- and γ-CD [3.05, 2.92, 2.84 Å]; thus the intramolecular hydrogen bond becomes stronger with an increase in the number of units.[57]

Conformational Parameters of Cyclodextrins

There are three principal torsion angles that define the conformational flexibility of a cyclodextrin molecule. These are the primary hydroxyl, glycosidic and pyranoid torsion angles. The primary hydroxyl or O5-C5-C6-O6 torsion angle (ω) describes the rotation around the C5-C6 bond, indicating the direction of the C6-O6 bond. There are three possible conformations that can be adopted by this C6-O6 bond, namely the (+)-*gauche*, (-)-*gauche* or *trans* conformations. The (-)-*gauche* conformation [ω = -60°] with the C6-O6 bond pointing away from the centre of the CD cavity is the most preferred orientation. The presence of a hydrogen bond formed between the O6 hydroxyl group and an included guest leads to the C6-O6 bond pointing toward the centre of the CD cavity [(+)-*gauche*, ω = +60°]. The trans conformation [ω = 180°] has not been observed in CD structures for steric reasons. The rotation around the C1-O4'-C4' linkage is described by two glycosidic torsion angles, namely **Φ** [O5-C1- O4'-C4'] and **ψ** [C1- O4'-C4'-C3']. The two pyranoid torsion angles Θ_1 [C2-C3-C4-C5] and Θ_2 [C3-C4-C5-O5] describe the conformational relationship around the C4 atom of each glucose unit. The mean values of the principal torsion angles for α-, β- and γ-CDs are listed in Table 1.1.

Table 1.1 Mean values for principal torsion angles [°] of CDs

CD	$\|\omega\|$ [59]	Φ [60]	ψ [60]	Θ_1 [60]	Θ_2 [60]
α	68	108	130	+52	-53
β	64	112	128	+56	-56
γ	68	110	130	+62	-62

O4 Polygon

The macrocyclic structures of CDs are best described in terms of a polygon model composed of 6, 7 and 8 glycosidic O4 atoms for α-, β- and γ-CDs respectively. The various geometrical parameters of the O4 polygon defined by Saenger[56] and Harata[57] are illustrated in Figure 1.6. Those parameters are the O4 distance to the polygon centroid, **r** [the centroid is labelled **C** in Figure 1.6], the O4•••O4' distance, **l**, the O4•••O4'•••O4" angle, **a**, the O4•••O4'•••O4"•••O4"' torsion angle, **t**, and the deviation of each O4 atom from the mean O4 plane, **d**. For a planar macrocycle the deviation (**d**) of each O4 atom from the O4 mean plane would be zero and the O4•••O4'•••O4"•••O4"' torsion angles (**t**) would all be zero.

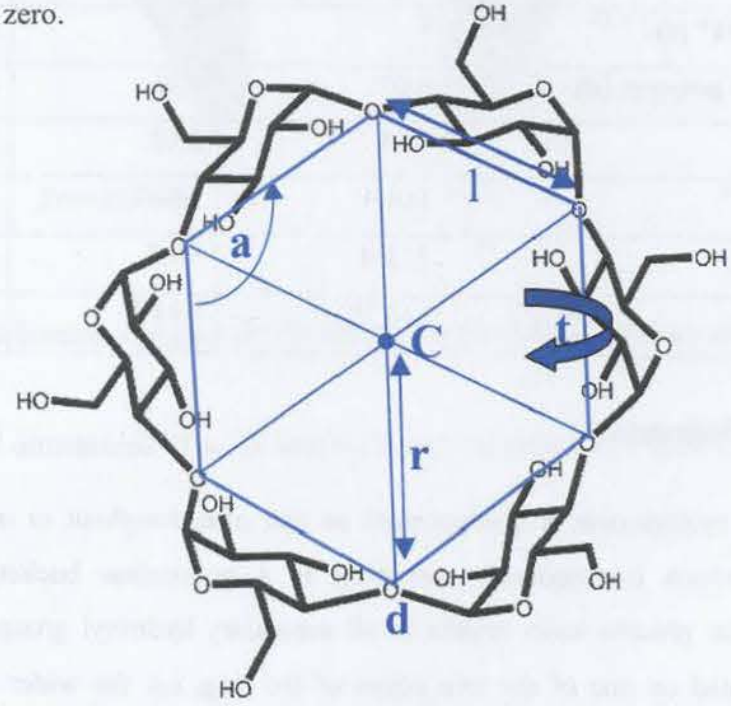

Figure 1.6 Principal geometrical parameters of the O4 polygon illustrated for α-CD.

Other useful parameters that are not directly defined by this polygon are the O2•••O3' distance, the intersaccharidic bond angle, φ [C1'-O4-C4], and the tilt angle, τ, which is defined in two ways. The first tilt angle τ_1[61] is defined as the angle made between the mean plane through the six atoms C1, C2, C3, C4, C5 and O5 of each glucose unit and the normal to the O4 mean plane, while the second tilt angle τ_2[62] is defined as the angle made between the mean plane through O4, C4, C1 and O4' atoms and the O4 mean plane. Ideally both definitions should yield the same value; however the distortion of the conformation around the glycosidic linkages due to the formation of the macrocycle results in these defined tilt angles having different values. Table 1.2 presents the mean values for these parameters obtained from average structure values in the literature.

Table 1.2 Mean values for the structural parameters describing the macrocyclic conformations of CD molecules

Parameter	**α-CD**	**β-CD**	**γ-CD**
O4•••O4' (**l**) / Å [57]	4.2	4.3	4.5
Radius (**r**) of the O4 polygon / Å [57]	4.2	5.0	5.9
O4•••O4'•••O4" (**a**) / ° [59]	120	128	132
O4•••O4'•••O4"•••O4"' (**t**) / ° [59]	5	5	2
Planarity of the O4 polygon (**d**) / Å [59]	0.07	0.08	0.02
O2•••O3' / Å [61]	3.05	2.92	2.84
C1'-O4-C4 (φ) / ° [61]	118.4	117.7	115.0
Tilt angle (τ_1) / °	+11.4	+9.5	+14.5
Tilt angle (τ_2) / °	+13 [63]	+14 [64]	+17 [65]

The Shape of Cyclodextrins

The shape of the cyclodextrin is characterised as that of a doughnut or wreath-shaped truncated cone [which is frequently compared to a bottomless bucket]. The $^4C_1$ conformation of the glucose units results in all secondary hydroxyl groups [O2-H and O3-H] being situated on one of the two edges of the ring, i.e. the wider edge. These hydroxyl groups are in equatorial positions, with the O2 groups pointing towards the

cavity and the O3 groups pointing away from the cavity. The primary hydroxyl groups [O6] are situated on the narrower edge of the ring and their free rotation reduces the effective diameter of the cavity [Figure 1.7]. The glycosidic oxygen bridges [O4] and hydrogen atoms from the methine [C3-H and C5-H] and methylene groups [C6-H_2] line the inner wall of the CD cavity. The electron lone pairs of the O4 bridges are directed towards the inside of the cavity resulting in a high electron density there. Consequently the CD cavity is relatively apolar and hydrophobic compared to water. The lining of the hydroxyl groups at both ends of the cavity renders the external faces polar and hydrophilic. This is due to a dipole moment parallel to the pseudo-symmetry axis as a result of twice the number of hydroxyl groups on the secondary side when compared to the primary side.

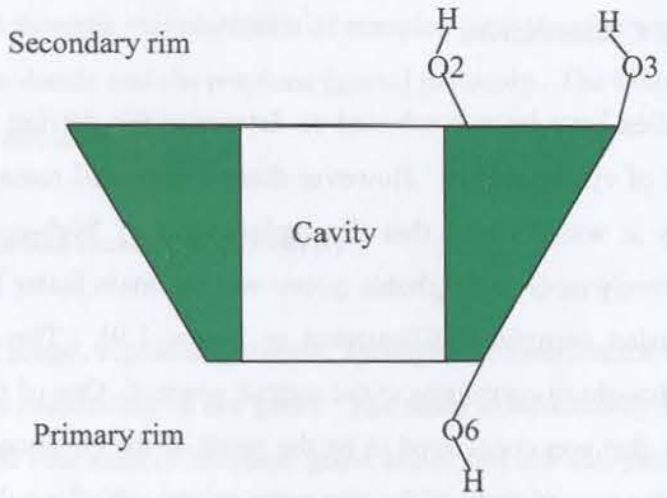

Figure 1.7 Schematic diagram of CD illustrating the cavity, primary and secondary faces.

The physical dimensions of α-, β- and γ-CD vary as shown in Figure 1.8.

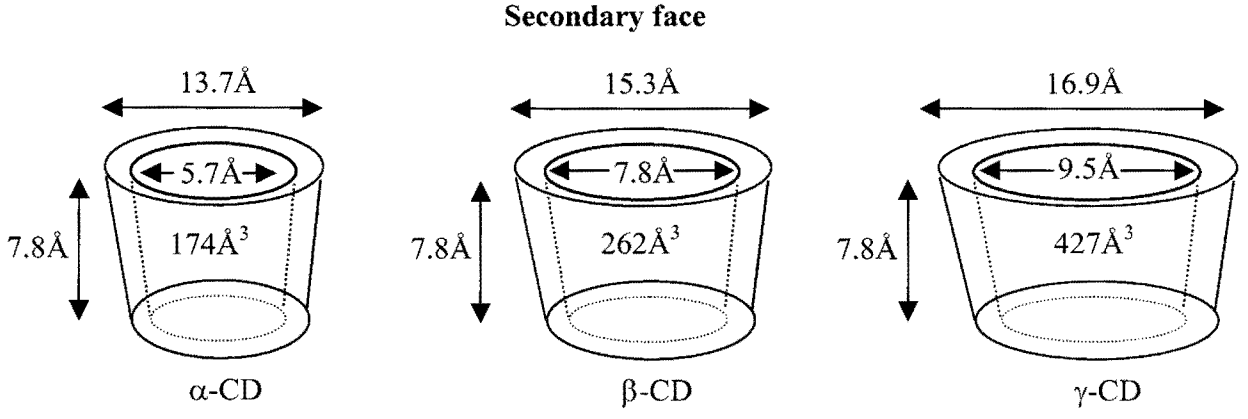

Figure 1.8 Schematic diagram showing physical dimensions of α-, β- and γ-CD. [66]

Inclusion Complexes of Cyclodextrins

A large number of studies have been conducted to determine the driving forces in the inclusion complexation of cyclodextrins. However these forces still remain unclear or controversial.[67] Initially it was thought that the replacement of 'high-enthalpy' water molecules with the relatively more hydrophobic guests was the main factor leading to the formation of CD inclusion complexes [illustrated in Figure 1.9]. There are several driving forces that are thought to contribute to the overall process. One of these forces is hydrophobic interaction that was considered to be the result of the enhanced structure of the water molecules in the near vicinity of the non-polar solute, which would bring about very large entropy loss during the hydration.[68] However, neither neutron scattering measurements nor computer simulations could elucidate the nature of the hydrophobic interaction.[69] The other driving forces such as electrostatic, van der Waals, hydrogen-bonding, charge-transfer interactions, and relief of conformational strain on complexation are thought to contribute to the formation of CD complexes. A recent review assigns more weight to these forces except for the relief of conformational strain.[67]

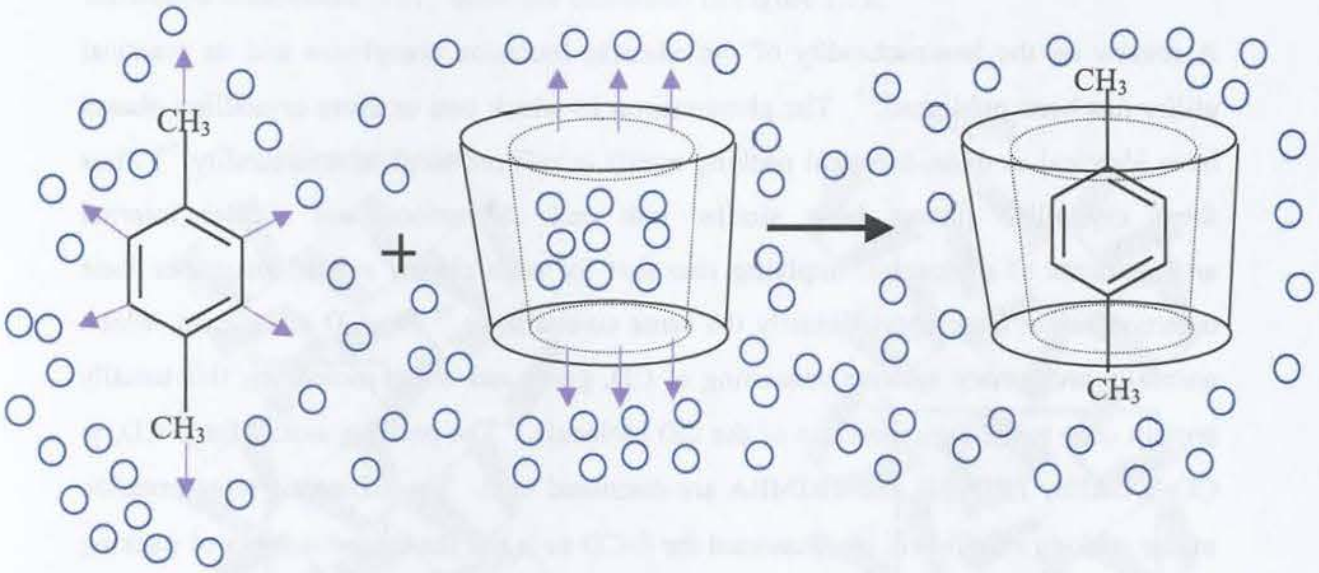

Figure 1.9 Schematic representation of complex formation between the CD [host] molecule and the p-xylene [guest] molecule. The blue circles show water molecules.[66]

Guest orientation inside the CD cavity

The size and shape, dipole alignments, hydrophobic interactions and other driving forces determine the orientation of the guest. The study conducted by Kitagawa et al indicated that the dipole moments of aromatic guest molecules are anti-parallel to that of their host CDs.[70,71] The analyses of computer-generated molecular lipophilicity patterns [MLPs] have shown a close relationship between the hydrophobic and hydrophilic regions of cyclodextrins and the included guests.[72] The alignment occurs between the hydrophobic portion of the guest and the hydrophobic cavity, while the polar group of the guest is situated close to the secondary hydroxyls or even on the outside of the cavity. The reverse of these patterns was observed with per-O-methylated CDs resulting in the reverse orientations of the guest molecules within the cavities of these hosts.

Crystal Packing

A review on the isostructurality of cyclodextrin inclusion complexes and its practical utility has been published.[73] The phenomenon in which two or more crystalline phases have identical or quasi-identical packing motifs is referred to as isostructurality. [74] Thus these crystalline phases have similar unit cell dimensions and similar internal arrangements of molecules, implying also that for such closely related structures their common atoms have approximately the same co-ordinates.[75] For CD complexes, which normally are ternary systems consisting of CD, guest and water molecules, this usually applies only to the rigid portions of the CD molecule.[73] The packing motifs for β-CD, γ-CD, DIMEB, TRIMEB and TRIMEA are discussed next. The schematic representation of the packing motifs will be illustrated for β-CD as it has the largest number of packing motifs.

Packing Arrangements of β-CD species

The packing arrangements of β-CD structures are categorised into monomeric, dimeric [two β-CD molecules that are connected at their secondary rim by multiple hydrogen bonds] and tetrameric structures [consisting of two dimers]. There are five different types of monomeric packing arrangements, namely: herringbone [$P2_1$], zigzag [$P2_12_12_1$], brickwork [$P2_1$], layer [$P2_1$] and helical channel [$P6_1$] and they are presented in Figure 1.10.[56, 76] The monomeric herringbone packing arrangement is preferred for small guest molecules that do not protrude from the cavity and it shows efficient packing of the β-CD molecules.

For the dimeric structures of β-CD there are four different types of packing arrangements, namely channel [P1 or C2], screw channel [$P2_1$], chessboard [$C222_1$] and intermediate [P1]. These packing arrangements are presented schematically in Figure 1.11. The majority of β-CD complexes consist of dimers that are arranged in a head-to-head fashion and they are stabilised by multiple hydrogen bonds across the secondary face. This results in a large cavity that is able to accommodate bulky guest molecules. There are

two types of tetrameric packing arrangements, namely tetrameric intermediate [P1] and tetrameric chessboard [$P2_1$]; these are illustrated in Figure 1.12.

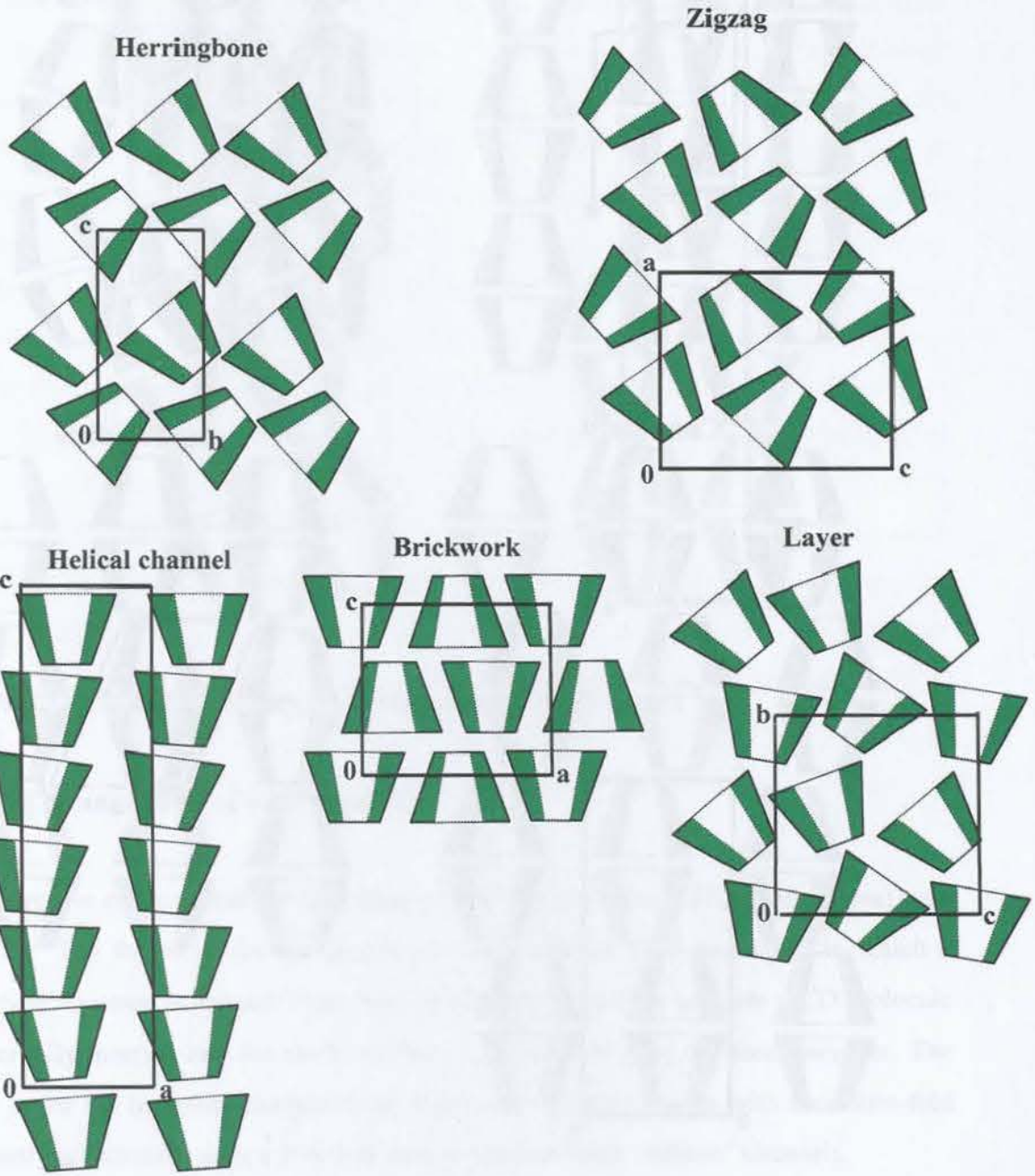

Figure 1.10 The packing arrangements of β-CD molecules in monomeric complexes.

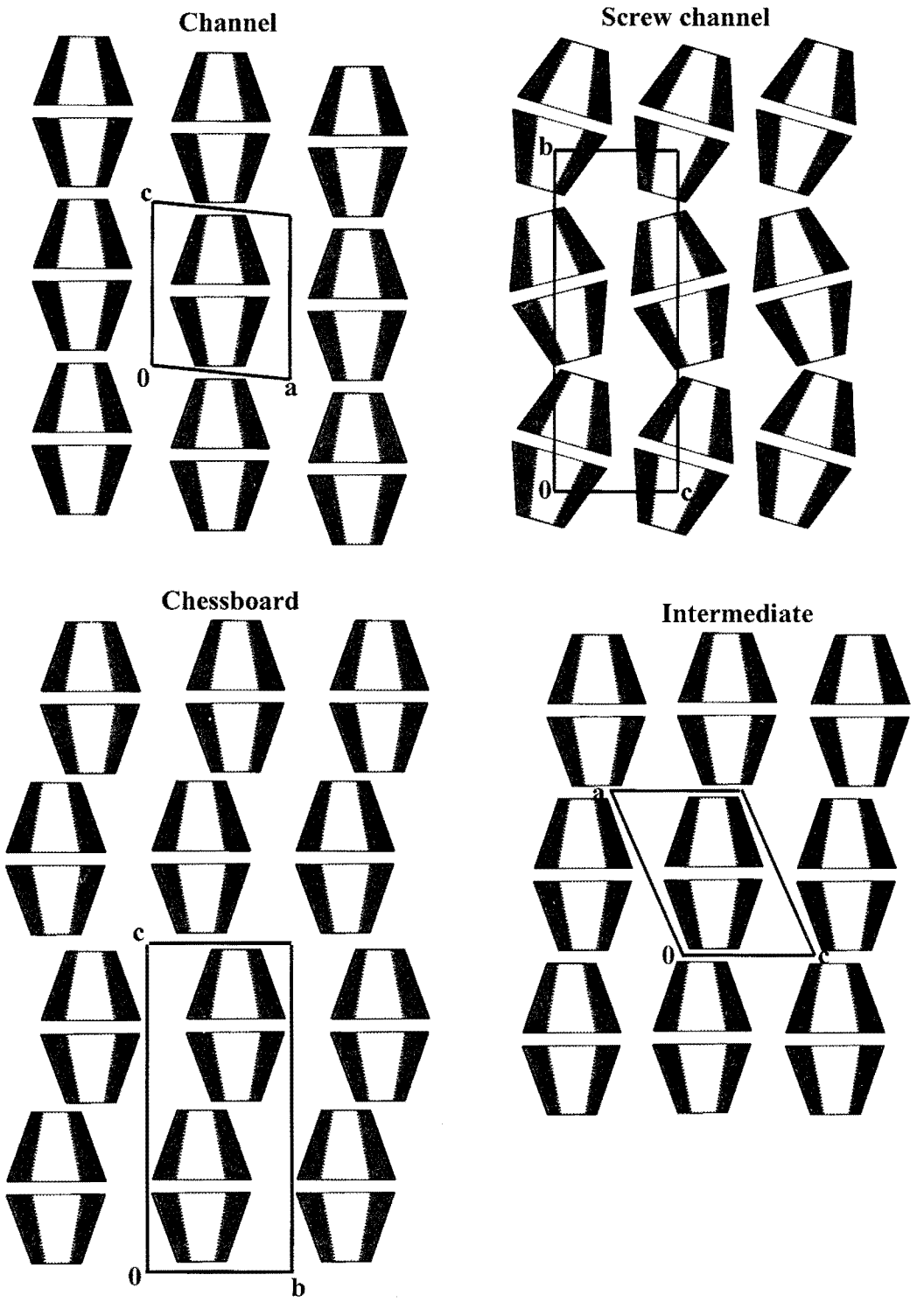

Figure 1.11 The packing arrangements of β-CD dimers in β-CD complexes.[56, 76]

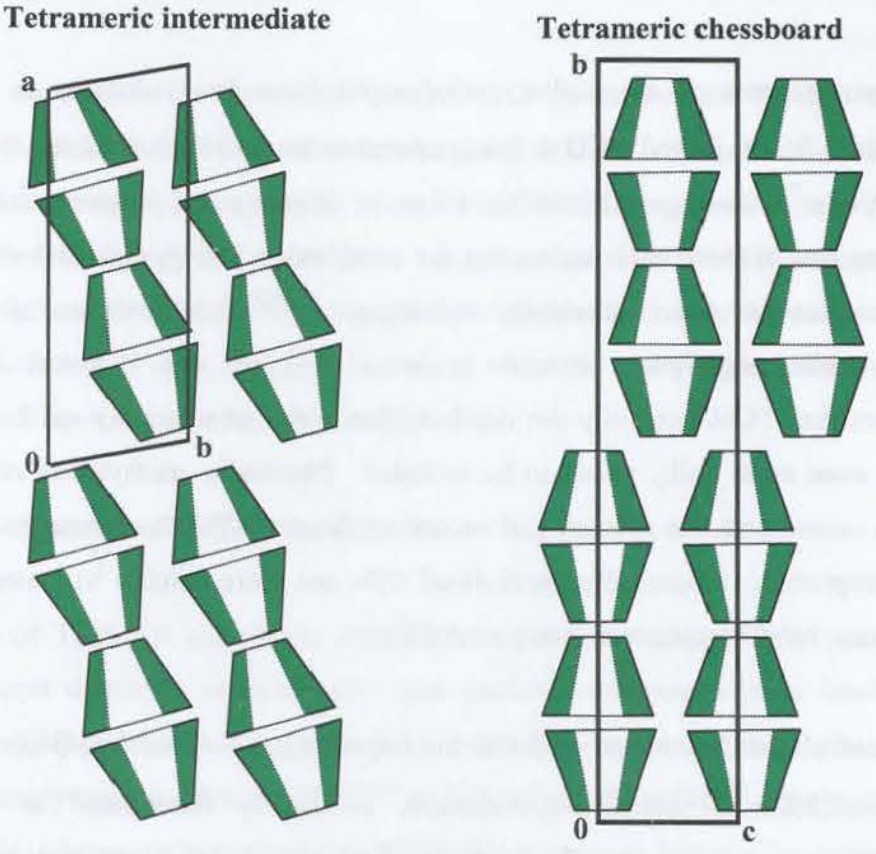

Figure 1.12 The tetrameric packing arrangements of β-CD dimers.[56]

Packing arrangements of γ-CD molecules

There are two types of packing arrangements, namely herringbone [$P2_1$] and channel type [$P42_12$]. The former is for the monomeric uncomplexed γ-CD molecules in which a cage-type structure is formed where two glucose units from an adjacent γ-CD molecule are partially inserted into the cavity of the γ-CD molecule from the secondary rim. The latter is for the inclusion complexes in which the γ-CD molecules with their four-fold symmetry are stacked along a four-fold axis to produce linear 'infinite' channels.

Methylated Cyclodextrins

At room temperature the native cyclodextrins have low solubility in water. The solubilities for α-, β- and γ-CD at this temperature are 0.1211, 0.0163 and 0.168 mol dm^{-3} respectively.[77] Consequently, in an effort to improve the aqueous solubility while retaining and in some cases enhancing the complexing ability, chemical modification of cyclodextrins has been extensively investigated.[78,79,80,81] Methylation of the hydroxyl group causes significant changes in some physical and chemical properties of cyclodextrins. Geometrically the depth of the cavity increases by ca. 2 Å which then allows even more bulky guests to be included. Physically, methylation of the hydroxyl groups causes both the primary and secondary faces of CDs to change from hydrophilic to hydrophobic. Chemically, methylated CDs are more soluble in water and organic solvents at room temperature than parent CDs.

Two methylated derivatives of β-CD are heptakis(2,6-di-O-methyl)-β-cyclodextrin and heptakis(2,3,6-tri-O-methyl)-β-cyclodextrin, commonly abbreviated as DIMEB and TRIMEB respectively. Another methylated CD which has been used in this study is hexakis(2,3,6-tri-O-methyl)-α-cyclodextrin abbreviated as TRIMEA. These have been proposed as drug carriers in the pharmaceutical industry; thus they have formed part of this study. The structures of these compounds are given in Figure 1.13.

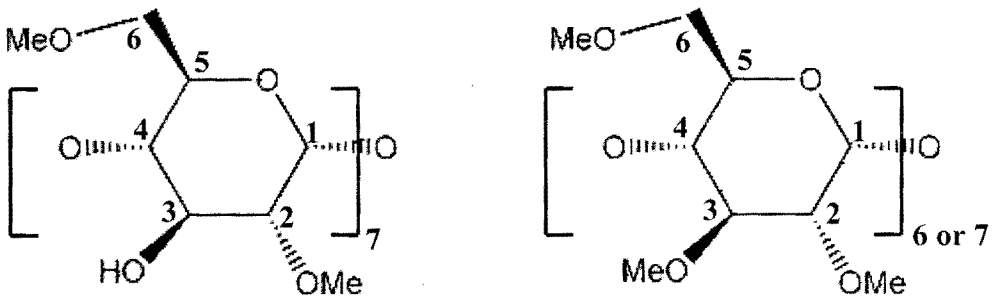

Figure 1.13 The methylated positions for the glucose units of (a) DIMEB and (b) TRIMEA [6 glucose units in a ring] or TRIMEB [7 glucose units in a ring].

Packing arrangements of DIMEB molecules

A search of the Cambridge Structural Database [CSD] shows that DIMEB and its complexes crystallise in the monoclinic space group $P2_1$ and the orthorhombic space group $P2_12_12_1$.[82] Various packing modes observed in DIMEB complexes include channel type to modified brickwork and herringbone type packing. The DIMEB molecules are stacked in a head-to-tail fashion with the guest located either in the cyclodextrin cavity as with 2-naphthoic acid,[83] or in the interstitial sites, while the cavity is occupied by water molecules as with *p*-iodophenol and *p*-nitrophenol.[84]

Packing arrangements of TRIMEB molecules

The majority of TRIMEB complexes crystallise in the space group $P2_12_12_1$ and their crystal structures display a screw-channel type packing arrangement in a head-to-tail mode.[82] Two TRIMEB crystal structures have been reported in the monoclinic space group $P2_1$, namely the butamben-TRIMEB[85] and (E)-ajoene-TRIMEB[86] complexes. The former complex shows a channel-type packing with successive layers of complex units having alternating polarities, while the latter forms channels as a result of translated units.

Packing arrangements of TRIMEA molecules

The packing arrangements of TRIMEA itself and its inclusion complexes are of a channel-type.[73] However, the nature of these crystal packing schemes is quite different since the host crystallises in the orthorhombic space group $P2_12_12_1$, whilst the TRIMEA complexes crystallise in the monoclinic space group $P2_1$.

Mechanism by which CDs modify drug release

There has been growing interest in developing rate-controlled oral preparations, since appropriate drug release from dosage forms is of critical importance in realising their therapeutic efficacy.[87,88] Among the various kinds of carrier materials that are being

developed, cyclodextrins are potential candidates to deliver the necessary amount of drug to the targeted site for a necessary period of time, both efficiently and precisely.[89,90,91] The unique characteristic of CDs is that they form inclusion complexes both in solution and in the solid state, in which each guest molecule is surrounded by the hydrophobic environment of the CD cavity. This can lead to alteration of physical, chemical and biological properties of guest molecules, and can finally have considerable pharmaceutical potential. The biodegradation of CDs is important for their function as colon-targeting carriers.

The rate and extent of oral bioavailability of a poorly water-soluble drug from its CD complex can be optimised by adjusting various factors that affect the dissociation equilibrium of the complex both in the formulation and in the biophase in which the complex is administered.[92,93] The displacement of the drug from the CD cavity by exogenous and endogenous substances that exist at the absorption site is responsible for acceleration of drug absorption.[94,95] Figure 1.14 illustrates the overall process of drug absorption from a solid complex in the presence of a competing agent. Various types of CDs are utilised for the controlled rate of drug release. The controlled rate is classified into three types, namely immediate release, prolonged release and modified release.

The hydrophilic CDs [e.g. DIMEB] are used for the immediate release formulations of drugs [e.g. analgesics, antipyretics, coronary vasodilators] in emergency situations.[96]

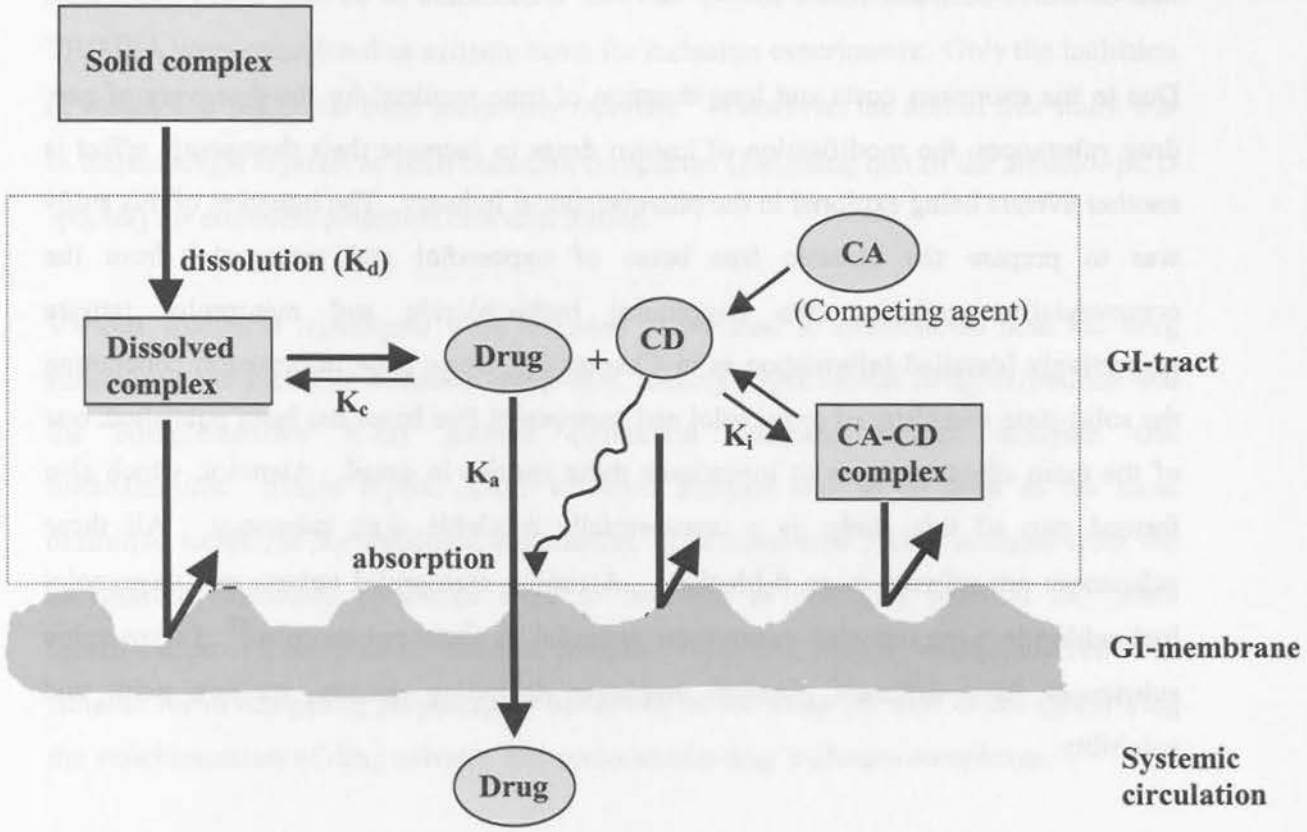

Figure 1.14 Overall process of drug absorption from an inclusion complex following dissolution and dissociation in the gastrointestinal tract.[96] K_d = dissolution rate constant of drug-CD complex; K_c = stability constant of drug-CD complex; K_i = stability constant of competing agent-CD complex; K_a = absorption rate constant of drug.

Motivation and Objectives of the Study

Due to the enormous costs and long duration of time required for the discovery of new drug substances, the modification of known drugs to increase their therapeutic effect is another avenue being explored in the pharmaceutical industry. The intention of this study was to prepare the racemic free bases of oxprenolol and metoprolol from the commercially available salts oxprenolol hydrochloride and metoprolol tartrate respectively [detailed information is in Chapter 3]. Since little information concerning the solid-state chemistry of oxprenolol and metoprolol free bases has been published, one of the main objectives was to investigate these species in detail. Atenolol, which also formed part of this study, is a commercially available drug substance. All these substances are referred to as β-blockers. Atenolol, metoprolol tartrate and oxprenolol hydrochloride were reported to have the potential to show polymorphs.[97] Polymorphic substances have different physical properties including density, melting point and solubility.

The first aim of this study was to investigate the potential for each of these compounds [oxprenolol, metoprolol and atenolol] to display polymorphism [as highlighted on page 1 of this Chapter], not only for academic interest, but also for the extension of their chemistry and pharmaceutical applications. Various solvents of different polarity, ranging from single solvent systems to binary solvent systems and various methods were to be employed to possibly isolate polymorphs or solvates of these drugs.

The second objective was to modify the chemical properties of these drug substances by encapsulating them in cyclodextrins. The low aqueous solubilities of oxprenolol, metoprolol and atenolol free bases render them highly suitable as guests for supramolecular modification by this route. The CD encapsulation of these substances would have advantages, namely (a) the provision of previously unexplored CD-oxprenolol, CD-metoprolol and CD-atenolol inclusion complexes [new chemical entities] and (b) possible improvement of the performances [enhanced dissolution rate, drug stability, bioavailability] of these drugs. The cyclodextrin inclusion of these drug

substances might also be of commercial interest. β-CD, γ-CD, DIMEB, TRIMEB and TRIMEA were considered as suitable hosts for inclusion experiments. Only the inclusion of atenolol in β-CD has been previously reported.[98] However, the aim of this study was to isolate single crystals of such inclusion complexes [including that of the atenolol-βCD species] for complete structural characterisation.

Various analytical techniques were intended to be used to characterise both the drug substances and their CD inclusion complexes, namely single crystal X-ray diffraction and the complementary X-ray powder diffraction analyses, thermal analyses and microanalysis. Single crystal X-ray structure analysis was to be used as the most definitive technique for structural elucidation. The computed PXRD patterns from the successfully modelled structures were to be used as reference patterns for future identification of these phases. Thermal analysis [TGA, DSC, HSM] was considered to be suitable for investigating polymorphic behaviour of the drugs as well as for quantifying the stoichiometries of drug solvates and cyclodextrin-drug inclusion complexes.

Chapter 2 – Experimental and Computational Methods

Materials

Atenolol, oxprenolol hydrochloride and metoprolol tartrate were purchased from Sigma Chemical Company [St. Louis, Missouri, USA] and used as received. Oxprenolol and metoprolol free bases were prepared by the addition of excess 1.0 **M** NaOH to aqueous solutions of oxprenolol hydrochloride and metoprolol tartrate respectively. These free bases were each extracted from the aqueous phase using dichloromethane after which the product was obtained by allowing the solvent to slowly evaporate at room temperature. The host compounds β-cyclodextrin, γ-cyclodextrin, heptakis(2,6-di-O-methyl)-β-cyclodextrin [DIMEB], heptakis(2,3,6-tri-O-methyl)-β-cyclodextrin [TRIMEB] and hexakis(2,3,6-tri-O-methyl)-α-cyclodextrin [TRIMEA] were purchased from Cyclolab [Budapest, Hungary] and used without further purification.

Preparation Methods

Slow cooling and slow evaporation were employed for the preparation of crystals of antiyhpertensive agents and cyclodextrin complexes. Cyclodextrin inclusion complexes were obtained by the methods of co-precipitation, kneading or co-solvent. Co-precipitation involved the addition of equimolar amounts of drug to a hot [for β- and γ-CDs] or cold [methylated CDs] saturated aqueous solution of the cyclodextrin. Kneading involved making a paste of the cyclodextrin with water using a mortar and pestle and adding equimolar amount of drug after which kneading continued for an hour. The consistency of the paste was maintained by the addition of an appropriate amount of water during this period. The co-solvent method involved dissolving a drug in a small volume of organic solvent [methanol or ethanol], and slowly adding that to a saturated aqueous cyclodextrin solution. The solutions were filtered with 0.45 μm microfilter to encourage the growth of larger crystals, and were subsequently allowed to cool and evaporate slowly.

Microanalysis

A Fisons EA1108 CHNS-O Elemental Analyser was used to determine the amount of carbon, hydrogen and nitrogen that was present in each prepared compound. The antihypertensive agents generally proved to be anhydrous from thermal analysis and their crystals were kept in open vials for an hour prior to microanalysis. Crystals of cyclodextrin inclusion complexes were dried on filter paper, and stored in an open vial for a week prior to microanalysis. This was performed to allow the crystals to reach equilibrium with the atmospheric water vapour. Microanalysis of these compounds was performed concurrently with the thermal gravimetric analysis to ascertain their water content at the time of their microanalysis. Microanalysis was used to validate the host:guest ratio found for each cyclodextrin inclusion compound. In addition to microanalysis confirming the purity of the prepared species, it also provided additional information, the nature of which depended on the species. In the case of drugs, microanalysis can be used to confirm whether the species are polymorphs or solvates.

Thermal Analyses

Thermal analysis is a technique which shows the behaviour of a compound when exposed to a controlled heating and cooling in a controlled atmosphere. It is used to measure the changes in the physical properties of a sample as a function of temperature. In this study there are three thermal analytical methods that were used to elucidate the physical changes that take place, namely Hot Stage Microscopy [HSM], Thermogravimetric Analysis [TGA] and Differential Scanning Calorimetry [DSC].

HSM is used for the qualitative analysis of any possible physical changes that occur in a sample as it is subjected to heating. Information may also be recorded visually and it is often related to thermal events measured quantitatively on the TGA and DSC apparatus. DSC is used to quantitatively determine onset temperatures [T_{on}] of fusion, dehydration, recrystallisation and transformation. DSC is also used to indicate complex formation, solvation and degradation.[99] It is also used to determine the enthalpy changes associated

with these events - this is important for the stability relationship study of solvates and the unsolvated forms of a sample. TGA is used to quantitatively determine mass loss of a sample on heating. This in turn allows for the determination of the mass percentage of included solvent.

DSC experiments were performed on a Perkin Elmer PC7-Series instrument, namely the PE DSC7 Differential Scanning Calorimeter. Some of the TGA experiments were performed on a Perkin Elmer PC7-Series instrument, namely PE TGA7 while others were carried out on a Mettler Toledo STAR^e thermal analysis system, namely TGA/SDTA 851^e, Version 6.10. All DSC and TGA runs were performed at 10 K/min under a nitrogen flow rate of 30 ml/min.

Hot Stage Microscopy [HSM]

A Linkam TP92 temperature control unit fitted with a Linkam TH MS600 was used to heat the crystals at a controlled rate. Images were captured using a real-time Sony Digital Hyper HAD colour video camera fitted to a Nikon SMZ-10 stereoscopic microscope. A heating rate of 10°C / min was used and the crystals, in most cases, were submerged in an inert medium of silicone oil to observe the evolution of gas bubbles upon dehydration. Images that were recorded were analysed by the Soft Imaging System, analySIS.[100]

Thermogravimetric Analysis [TGA]

TGA was used to measure mass loss of the sample upon heating it at a controlled rate. For the TGA experiments performed on a Perkin Elmer PC7-Series instrument, an open platinum pan was used, which was connected to the hanging wire of a thermobalance. Both crystalline and powder samples of weight 2-4 mg were analysed on the TGA. Calibration of the TGA instrument was performed against the Curie points of alumel [163°C] and nickel [354°C].

For the TGA experiments performed on a Mettler Toledo STAR^e, an open aluminium oxide crucible was used, which was placed horizontally onto the thermobalance crucible holder. In both cases the mass loss was used to determine qualitatively and quantitatively the presence of the included solvent. Samples masses of 0.5-6 mg were placed in a crucible and put in a furnace purged with N_2 [flow rate = 30 ml/min] and run at a heating rate of 10°C / min. The Mettler TGA instrument was calibrated using indium [melting point = 156.6°C] and aluminium [melting point = 660.3°C] in an automated process in which temperature calibration, tau lag calibration and sensor calibration are performed simultaneously.

Differential Scanning Calorimetry [DSC]

DSC experiments measure the difference in energy inputs [i.e. the enthalpy] between the sample and the reference, in a controlled atmosphere, as a function of temperature. A sample of weight 0.8-5.0 mg was placed in a crimped, vented aluminium sample pan, while the reference pan was left empty. Endothermic and exothermic peaks appearing in the DCS traces were analysed in terms of their onset temperatures, temperature ranges as well as their associated enthalpies [ΔH in J/g]. The DSC analyser was calibrated against the melting points of indium [156.6°C] and zinc [419.5°C] and the fusion enthalpy of indium [28.5 J/g].

Fourier Transform Infrared Spectroscopy [FTIR]

FTIR spectroscopy was utilised to investigate the effect of cyclodextrin complexation on the -C=O, -N-C=O and -NH_2 stretching frequencies of the guest molecule. FTIR spectra for a drug, complexed material and the CD host molecule were recorded on a Perkin Elmer 983 FTIR spectrophotometer over the range 4000-600 cm^{-1}. Samples were prepared by grinding the material in Nujol mull and the percentage transmittance was recorded against frequency.

Proton Nuclear Magnetic Resonance Spectroscopy [PNMR in solution]

PNMR was used as a diagnostic tool to ascertain that the two polymorphic forms of a host in solution were chemically identical. The reason for performing this analysis was to verify that one of the products of an unsuccessful attempt to form an inclusion complex was the host compound in a new polymorphic form [as indicated by preliminary X-ray analysis]. Thus necessary chemical analyses to ensure the absence of a guest were imperative. PNMR experiments were performed at 300 MHz with a Varian-Gemini 300 spectrometer. The 1H NMR spectra were recorded in D_2O solution at 298 ± 0.5 K.

X-ray Crystallographic Analysis

Single crystal X-ray Diffraction

The single crystal X-ray crystallographic technique was the main tool used to elucidate the crystal structures in this study. Single crystals for all new species reported in this study were obtained. In each case single crystals of desired quality with dimensions 0.1-0.5 mm were selected for X-ray analysis. Their selection was based on their ability to uniformly extinguish plane polarised light. Crystals were mounted on a glass fibre and coated with Paratone N oil, to prevent dehydration in the case of the solvated crystals and to 'glue' the crystal to the fibre when cooling the crystal for low-temperature data-collection. The glass fibre was then mounted on a goniometer head.

X-ray Photography

The preliminary unit cell dimensions and crystal systems for some of the crystals were obtained by X-ray photography. Oscillation and 0-level Weissenberg photographs were sufficient for this purpose. The generation of X-rays was on a Phillips PW1120/100 generator using Ni-filtered CuKα radiation [1.5418 Å] and they were produced at 20 mA and 40 kV. The photographs were recorded on a Stoë goniometer with a film radius of 28.65 mm.

Oscillation photography

One crystallographic unit cell axis length and any symmetry associated with it were determined from oscillation photography.[101] A crystal was mounted on the goniometer head with one of its crystallographic axes orientated parallel to the oscillation axis and orthogonal to the X-ray beam. The photographic alignment was done with a series of short oscillation photographs and that was a prerequisite for the accurate cell axis determination as well as for Weissenberg photography. A full oscillation photograph was used to determine the length of the unit cell axes and the associated symmetry.

Weissenberg photography

The determination of the remaining unit cell axes, angle between them and their associated symmetry was carried out using Weissenberg photography.[101] In most cases, the 0-level line on the oscillation photograph was chosen. A screen was used in order for the selected layer line to reach the film. The film was moved parallel to the oscillation axis so that the diffraction pattern from the chosen layer line was spread over the entire film. The resulting photograph was placed on a transparent Weissenberg co-ordinate chart, from which the co-ordinates of each point were located and plotted onto graph paper to portray a representation of the reciprocal lattice. The Laue symmetry could also be inspected leading to the establishment of the crystal system and space group.

Data-collection

Intensity data were collected on a Nonius Kappa CCD Single Crystal X-ray Diffractometer using graphite-monochromated MoKα radiation [0.71073 Å]. Radiation was generated by a Nonius FR590 generator, operated at 23 mA and 53 kV. Data-collections were performed at room [~ 298K] and low [113-193K] temperatures. The exact temperatures for each data-collection are given in appropriate chapters. A constant flow of the N_2 gas [flow rate = 20 mL/min] produced by a Cryostream cooler [Oxford Cryosystems] was responsible for the maintenance of low temperatures. DENZO and

SCALEPACK were used for cell refinement and data reduction and data were corrected for Lorentz-polarisation effects.[102] Assignment of the correct space group was confirmed using the XPREP program[103] by examining systematic absences. This program was also used for the preparation of the SHELXS-97[104] input files.

Crystal Structure Solution and Refinement

Different structure solution programs and different methods were used to solve the structures in this work. These depended on the size of the structure, quality of the data and nature of the problem. SHELXS-97[104] was used to solve structures of antihypertensive agents [small structures]. For the CD complexes however, this program was not adequate due to their larger structures and the poor diffraction of the crystals. CD structures were solved by isomorphous replacement in cases where isostructural complexes existed, using the coordinates of their cyclodextrin non-hydrogen atoms. An alternative to this method was to use SHELXD,[117] a program specifically designed for solving larger structures. All structures were refined on F^2 using full-matrix least-squares in the program SHELXL-97.[113] Both SHELXS-97[104] and SHELXL-97[113] were accessed via the X-SEED[105] interface.

SHELXD

SHELXD[117] is a program used to solve larger *ab initio* problems than those amenable to solution with SHELXS-97.[104] The structure solution strategy of this program is based on the dual-space iteration strategy, called 'Shake-and Bake',[106] and has been coined the 'half-baked' method.[107] Conventional 'direct methods' successfully solve few structures that have more than 200 independent atoms,[107] whereas the dual-space iteration strategies solve structures of up to 1000 independent atoms with native data to at least 1.2 Å resolution.

SHELXL-97

Model refinement was performed in SHELXL-97[113] employing full-matrix least-squares minimisation of the function $\Sigma\ w(F_o^2 - F_c^2)^2$, the weighted sum of the squares of the differences between the observed and calculated intensities. The agreement between the observed (F_o) and calculated (F_c) structure factors was expressed by the residual index (R_1) [equation 2.1], which should be low for a satisfactory model. The agreement between the observed and calculated intensities was expressed by the parameter wR_2 [equation 2.2].

$$\mathbf{R_1 = [\ \Sigma\ |\ |F_o| - |\ F_c|\ |\ ]\ /\ \Sigma\ |F_o|} \qquad \mathbf{(2.1)}$$

$$\mathbf{wR_2 = \{[\ \Sigma\ w(F_o^2 - F_c^2)^2\ ]\ /\ [\ \Sigma\ w(F_o^2)^2\ ]\ \}^{1/2}} \qquad \mathbf{(2.2)}$$

The parameter w in equation 2.2 refers to the weighting scheme that was used in the final cycles of the refinement, and is defined in equation 2.3.

$$\mathbf{w = 1\ /\ [\ \sigma^2\ (F_o^2) + (aP)^2 + bP\ ]} \qquad \mathbf{(2.3)}$$

where the terms a and b are chosen to yield constant distributions of $\mathbf{w(F_o^2 - F_c^2)^2}$ with $\sin\theta$ and $\mathbf{(F_o\ /\ F_{max})^{1/2}}$ and P is defined in equation 2.4.

$$\mathbf{P = \ [\ max(F_o^2, 0) + 2F_c^2\ ]\ /\ 3} \qquad \mathbf{(2.4)}$$

The goodness of fit, **S**, is defined in equation 2.5

$$\mathbf{S = [\ \Sigma\ [w(F_o^2 - F_c^2)^2\ ]\ /\ (n - p)\ ]^{1/2}} \qquad \mathbf{(2.5)}$$

where **n** and **p** represent the number of reflections and total number of refined parameters respectively. For well behaved refinement **S** should be close to unity and the overdetermination ratio, n / p, should be at least ~ 10.

Powder X-ray Diffraction [PXRD]

PXRD is a technique in which diffraction patterns are obtained by irradiating a powdered crystalline material with X-rays. These patterns were recorded using a Huber Imaging Plate Guinier Camera 670. All samples were manually ground and packed into Lindemann capillaries with internal diameter of 1 mm and a glass thickness of 0.01 mm. The capillaries were obtained from Hilgenberg, Germany. Nickel-filtered CuKα radiation [λ = 1.5418 Å], produced at 40 kV and 20 mA by a Phillips PW1120/00 generator fitted with a Huber long fine-focus tube PW2273/20 and a Huber Guinier Monochromator Series 611/15, was employed.

For each successfully determined single crystal structure LAZY PULVERIX[108] was used to generate a computed PXRD trace. These were compared with experimental traces to establish whether any phase transformation had occurred upon grinding the material in the course of preparation for the analysis.

Computer Packages

The following computer packages were used in the crystal structure analyses of the various compounds:

- Pov-Ray[109] and Weblab ViewerPro[129] were used to generate molecular and structural diagrams.

- LAYER[112] was used to examine simulated graphic representations of the reciprocal lattice layers to confirm Laue symmetries and reflection conditions in cases where X-ray photographic data were absent.

- Ortep-3[116] was used to generate molecular diagrams with thermal ellipsoids drawn at a specified probability level.

- LAZYPULVERIX[108] was used to generate computed powder X-ray diffraction traces from single crystal X-ray structures. The input for this program included space group information, fractional atomic coordinates and thermal parameters.

- X-SEED[105] was used as a graphical interface from which LAZYPULVERIX,[108] LAYER,[112] SHELXS-97[104] and SHELXL-97[113] could be run.

- PLATON was used to calculate the geometrical parameters and non-bonded interactions, together with their associated standard deviations, of each structure. The geometrical parameters included bond distances, bond angles and torsion angles, while the non-bonded interactions included hydrogen bonding, π•••π and C-H•••π-ring interactions, as well as short intermolecular contacts.

- The Cambridge Structural Database (CSD)[82] was used to obtain unit cell parameters, space group information and fractional coordinates of structures where appropriate.

Additional Resources

Crystallographic information on each of the solved structures in this thesis has been stored on a compact disk, attached to the inside cover of this thesis. The files are stored in the folder Appendix A. The files have been saved in the subfolders with the abbreviation of each structure that was used in the thesis except atenolol, oxprenolol and metoprolol tartrate which are abbreviated in this Appendix A as aten, oxp and mett respectively. Table 2.1 lists the file types and the information that they contain.

Table 2.1 File types in Appendix A and the information that they contain

File extension	Contents
.HKL	Reflection data
.RES	SHELX type coordinate file
.CIF	Crystallographic Information File
.XL	SHELX output file
.LIS	PLATON output file listing all geometric parameters of a structure
.FCF	Structure factor tables
.SUP	PLATON output file summarising selected information from .LIS file in tabulated form

Chapter 3 – Antihypertensive Agents

Characterisation of Antihypertensive Agents

The solid-state physicochemical properties of the following racemic beta-blocker drugs, namely, atenolol, metoprolol tartrate and its free base, and oxprenolol hydrochloride and its free base have been studied. The current commercially available substances are atenolol, atenolol hydrochloride, metoprolol tartrate and oxprenolol hydrochloride.

Free Base Preparation

The free bases of metoprolol and oxprenolol were prepared by adding an excess of 0.1 M NaOH to aqueous solutions of metoprolol tartrate and oxprenolol hydrochloride. Following this, each resulting base was extracted into dichloromethane, which was then allowed to evaporate slowly resulting in crystals of each free base. Each product was washed with water to eliminate impurities, and subsequently each product was recrystallised from n-hexane at 30°C and allowed to evaporate slowly at ambient temperature.

Crystallisation Of Antihypertensive Agents

The main aspect investigated was the possibility that each of these substances might crystallise in more than one crystal form, a phenomenon termed polymorphism. Various solvents, including a combination of solvents and various crystallization methods were employed. The most common method used was preparation of solutions at room temperature, and allowing them to evaporate slowly to yield crystals by slow evaporation. The high solubility of metoprolol tartrate and oxprenolol hydrochloride in water rendered this solvent unsuitable for single crystal preparation; thus organic solvents were used to prepare solutions of these salts. Vapour diffusion, crystallisation from binary solvents and sublimation methods were unsuccessful in giving new polymorphic forms and only resulted in the isolation of existing forms. Some of these solvents are listed in Table 3.1, and the concentration of each solution was maintained at 10 mg/ml.

Table 3.1 Solvents used to isolate crystal forms of antihypertensive agents

Method			
Crystallisation from single solvents	atenolol	metoprolol	oxprenolol
n-Hexane	Form I	Form I and Form II [#]	Form I
Dichloromethane	Form I	Form I	Form I
Acetone	Form I	Form I	Form I
Chloroform	Form I	Form I	Form I
Ethyl acetate	Form I	Form I	Form I
Ethanol	Form I	Form I	Form I
Methanol	Form I	Form I	Form I
Benzyl alcohol	Form I	Form I	Form I
Diethyl ether	Form I	Form I	Form I
Cyclohexane	Form I	Form I	Form I
1,4-Dioxane	Form I	Form I	Form I
1-Propanol	Form I	Form I	Form I
Toluene	Form I	Form I	Form I
Benzene	Form I	Form I	Form I
Ethyl benzene	Form I	Form I	Form I
n-Propyl acetate	Form I	Form I	Form I
Carbon tetrachloride	Form I	Form I	Form I
Water [*]	Form I	Form I	Form I
Tetrahydrofuran	Form I	Form I	Form I
Isopropanol	Form I	Form I	Form I
DMSO	Form I	Form I	Form I
DMF	Form I	Form I	Form I
Acetonitrile	Form I	Form I	Form I
Crystallisation from binary solvents			
Ethyl acetate : DMSO (2:1 v/v)	Form I	Form I	Form I
n-Hexane : Acetone (3:1 v/v)	Form I	Form I	Form I
n-Hexane : Toluene (1:1 v/v)	Form I	Form I	Form I
Chloroform : DMSO (2:1 v/v)	Form I	Form I	Form I
Acetone : DMSO (2:1 v/v)	Form I	Form I	Form I
Acetonitrile : DMF (2:1 v/v)	Form I	Form I	Form I
Chloroform : 1-Propanol (2:1 v/v)	Form I	Form I	Form I
DMF : Methanol (1:2 v/v)	Form I	Form I	Form I

[#] Crystals of Form I of metoprolol were grown at room temperature whereas those for Form II were grown at 5°C.

[*] The solutions of the free bases atenolol, metoprolol and oxprenolol were prepared at 40°C and left at room temperature to crystallise since these substances are insoluble in water at ambient temperature.

Microanalysis

The C, H, N microanalysis results of the unsolvated crystallised products are listed in Table 3.2. In addition, metoprolol tartrate and oxprenolol hydrochloride were purified by recrystallisation from binary solvent systems of ethyl acetate:DMSO (2:1 v/v) and acetone:DMSO (2:1 v/v) respectively.

The experimental values of %C, %H and %N for these products agree with their respective calculated values within experimental error thus showing a high degree of purity and also that no chemical reaction had occurred between these substances and the solvents in which they were dissolved.

Table 3.2 C, H, N microanalysis results [n = 2] for antihypertensive agents

Substance	**Experimental** [#]			**Calculated**		
	%C	**%H**	**%N**	**%C**	**%H**	**%N**
Atenolol $C_{14}H_{22}N_2O_3$	63.34	8.01	10.25	63.13	8.33	10.51
Metoprolol free base $C_{15}H_{25}NO_3$	67.52	9.49	5.15	67.38	9.63	5.24
Oxprenolol free base $C_{15}H_{23}NO_3$	67.85	8.66	5.19	67.90	8.74	5.28
Metoprolol tartrate $(C_{15}H_{25}NO_3)_2 \cdot C_4H_6O_6$	59.56	8.26	4.05	59.61	8.24	4.09

Oxprenolol hydrochloride	**%C**	**%H**	**%N**	**%Cl**	**%C**	**%H**	**%N**	**%Cl**
$C_{15}H_{23}NO_3 \cdot HCl$	59.57	7.88	4.57	11.83	59.69	8.02	4.64	11.75

[#] Experimental error = ± 0.3 %

Thermal Analyses

Hot Stage Microscopy

HSM was performed to characterise the thermal behaviour visually for crystals of antihypertensive agents. The temperature range used was 25-250°C. During heating, no colour changes or other thermal events were observed except the melting of these substances. The HSM micrographs are therefore not included in this section.

Differential Scanning Calorimetry and Thermogravimetric Analysis

The DSC results for the atenolol, metoprolol, oxprenolol free bases, metoprolol tartrate and oxprenolol hydrochloride are shown in Figure 3.1 (a), (b), (c), (d) and (e) respectively and the results [given as average of triplicate experiments] are summarised in Table 3.3. The DSC traces for all these substances show sharp fusion endotherms which are indicative of their high purity. Metoprolol and oxprenolol free bases have lower melting points relative to that of atenolol. No significant endotherms or exotherms associated with decomposition appear in the DSC traces.

TGA traces for antihypertensive agents clearly indicated no mass loss in all five cases, confirming the lack of included solvent. These results correlate well with the HSM findings [not shown]. The decomposition onset temperatures of 140, 128, 176 and 223°C for metoprolol free base, oxprenolol free base, metoprolol tartrate and oxprenolol hydrochloride respectively were observed from TGA traces and for atenolol there was no discernible decomposition.

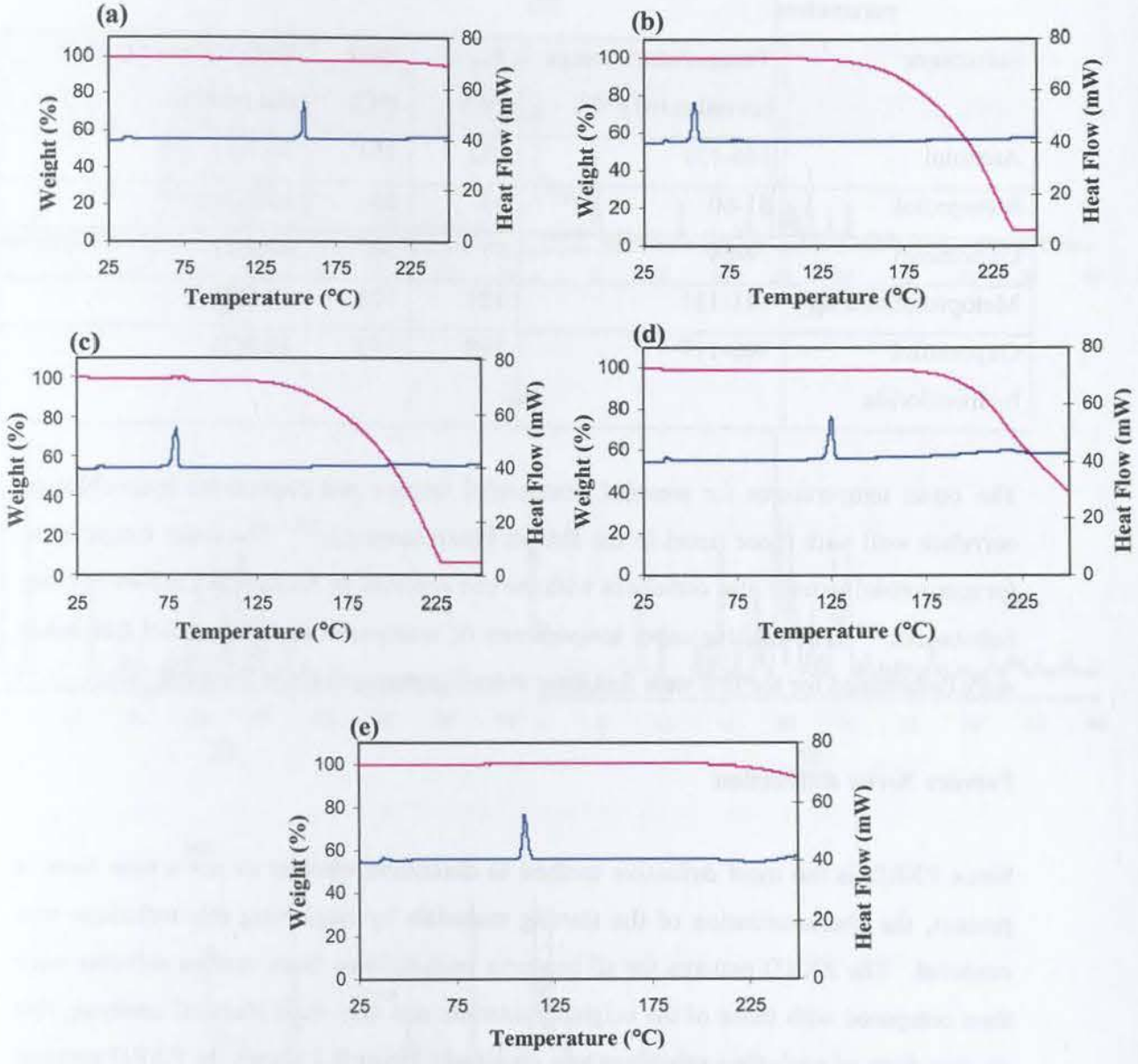

Figure 3.1 TGA [pink] and DSC [blue] traces for the (a) atenolol, (b) metoprolol and (c) oxprenolol free bases, (d) metoprolol tartrate and (e) oxprenolol hydrochloride.

Table 3.3 Summary of the DSC events [n = 3] for atenolol, metoprolol, oxprenolol free bases, metoprolol tartrate and oxprenolol hydrochloride showing endotherm parameters

Substance	**Temperature range investigated (°C)**	**T_{on} (°C)**	**Peak (°C)**	**Enthalpies of fusion (kJ mol^{-1})**
Atenolol	146-159	152	154	36.7(1)
Metoprolol	51-60	52	55	36.8(2)
Oxprenolol	74-84	77	80	47.4(2)
Metoprolol tartrate	111-131	121	124	68.6(2)
Oxprenolol hydrochloride	105-117	108	110	38.8(2)

The onset temperatures for atenolol, metoprolol tartrate and oxprenolol hydrochloride correlate well with those listed in the British Pharmacopoeia.[110] The onset temperature for metoprolol tartrate also correlates with the one reported in Analytical Profiles of Drug Substances.[111] The melting onset temperatures of metoprolol and oxprenolol free bases were determined for the first time and there is no literature reference for them.

Powder X-ray diffraction

Since PXRD is the most definitive method to determine whether or not a new form is present, the characterisation of the starting materials by employing this technique was essential. The PXRD patterns for all products recrystallised from various solvents were then compared with those of the original materials and they were identical implying that no new form of each drug substance was obtained. Figure 3.2 shows the PXRD patterns of the antihypertensive agents in the 2θ-range 4-40°.

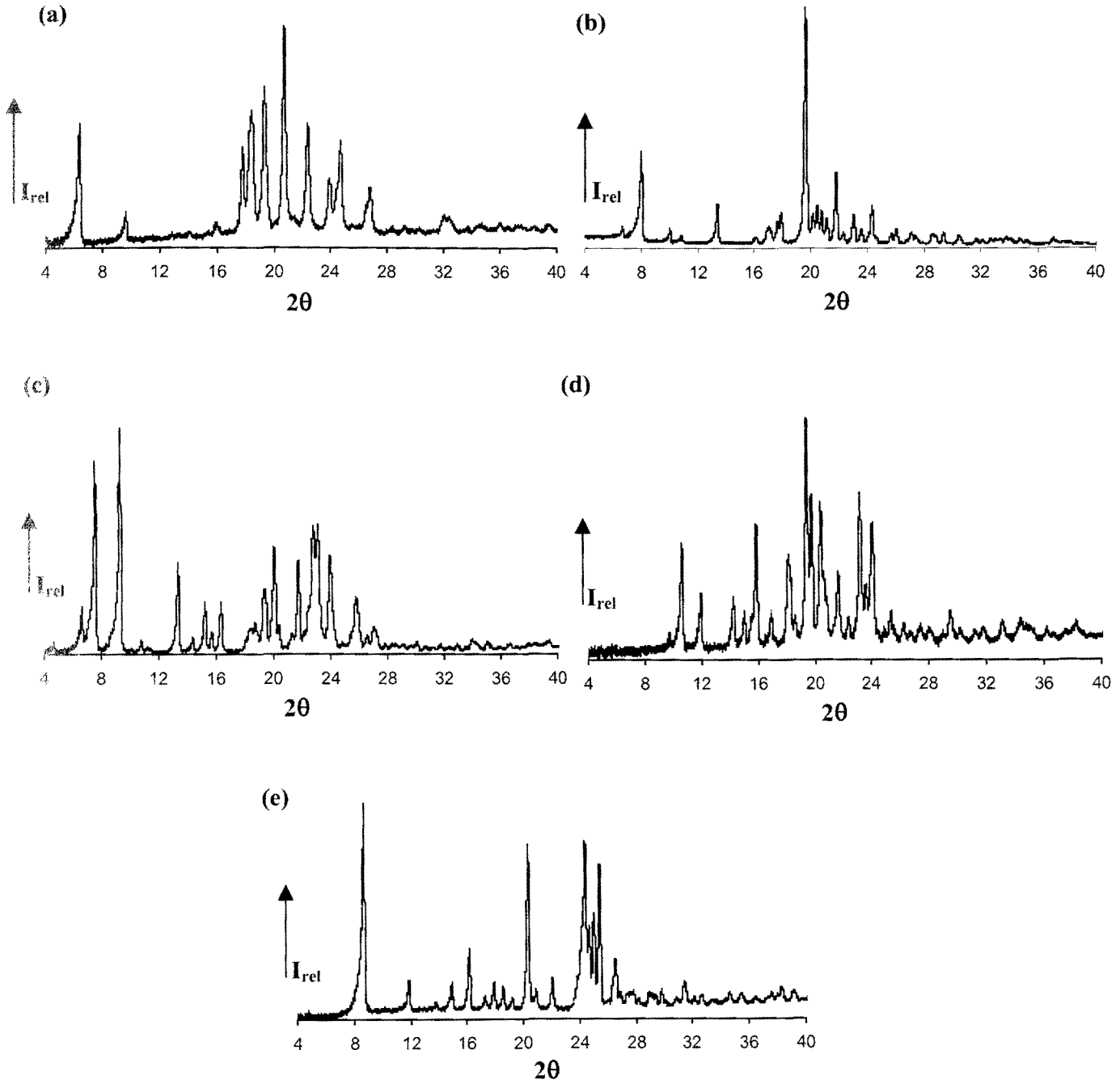

Figure 3.2 Experimental PXRD traces of (a) atenolol, (b) metoprolol, (c) oxprenolol, (d) metoprolol tartrate and (e) oxprenolol hydrochloride.

X-ray Crystallographic Analysis of Oxprenolol hydrochloride

Single Crystal X-ray Diffraction

X-ray photography

Preliminary unit cell parameters were determined by X-ray photographic techniques. An oscillation photograph showed m_x symmetry while the corresponding zero-level Weissenberg photograph showed two-fold symmetry. The combined information gave 2/m Laue symmetry and therefore the monoclinic crystal system was deduced.

Phase identification

A check of the Cambridge Crystallographic Database (CCD) during the initial literature survey showed that unit cell parameters reported for this compound by Leger *et al*[28] were a = 10.48, b = 22.11 and c = 7.48 Å, β = 103.9°, Z = 4 with the space group $P2_1/c$. Preliminary unit cell parameter determination on a Nonius Kappa CCD diffractometer indicated that oxprenolol hydrochloride isolated by the author crystallises in the monoclinic system with the following dimensions: a = 10.48, b = 22.11, c = 7.43 Å, β = 103.9°. The crystals were therefore not considered further.

X-ray Crystallographic Analysis of Atenolol

Single Crystal X-ray Diffraction

X-ray photography

X-ray photographic techniques were used to determine the preliminary unit cell parameters and Laue symmetry of atenolol. The Laue symmetry was then used to deduce the crystal system of this substance. An oscillation photograph showed two-fold

symmetry while the corresponding zero-level Weissenberg photograph showed *mm* symmetry. The combined information indicated Laue 2/m symmetry and thus the monoclinic crystal system was assigned.

Data-collection and space group determination

The crystals of atenolol obtained from various solvents were in the form of extremely thin laminae [shown in Figure 3.3] and data collected from them were generally not of high quality. The data-collection described and the resulting structural model are based on the best intensity data of several sets collected over many months using different crystal specimens. Diffraction intensities were collected on a Nonius Kappa CCD diffractometer at low temperature [173K]. Preliminary unit cell parameter determination at room temperature was performed to assess the quality of the crystal and also to ensure that no phase transition was effected on cooling the crystal. Inspection of the reciprocal lattice layers with LAYER[112] showed the reflection conditions hkl: h + k = 2n; h0l : l = 2n. The program XPREP[103] was used to determine the space group of atenolol. It indicated the monoclinic space groups C2/c (space group No. 15) or Cc (space group No. 9) based on the reflection conditions. Intensity statistics provided by XPREP[103] showed $|E^2 - 1| = 1.006$, indicating a centrosymmetric space group and therefore C2/c was chosen as the correct space group.

Figure 3.3 Thin plate-like crystals of atenolol.

Structure solution and refinement

SHELXS-97[104] was used for the structure solution of atenolol. An E-map based on correctly phased reflections revealed the positions of all non-hydrogen atoms and allowed their placement. SHELXL-97[113] was then used to refine these atoms isotropically on F^2. The atom C14 [Figure 3.4] was observed to be disordered over two positions and these were assigned site occupancy factors of x and 1-x, with x variable. The relative site occupancies estimated from peak heights were 0.62 and 0.38 for the atoms C14A and C14B respectively. The population parameters finally refined to 0.58 and 0.42. The carbon atoms of the isopropyl group C17 and C18 were also each disordered over two sites and they were each assigned s.o.f.'s of y, 1-y and z, 1-z, with y and z variables for carbon atoms C17 and C18 respectively. The s.o.f.'s of carbon atoms C17A, C17B, C18A and C18B refined to 0.55 and 0.45 with atoms C17A and C18A occupying major positions. Anisotropic refinement was performed on all non-hydrogen atoms with satisfactory isotropic thermal parameters. The difference Fourier map revealed the positions of few hydrogen atoms and this is attributed to the poor quality of the crystal. Hydrogen atoms were placed in fixed geometric positions using a riding model. These hydrogen atoms were refined isotropically with thermal parameters equal to 1.2 times those of their parent atoms. In the final cycle of refinement, least-squares weights of the form described in Chapter 2 were employed. The crystal and refinement data for atenolol are presented in Table 3.4.

Table 3.4 Crystal and refinement data for atenolol

Empirical formula	$C_{14}H_{20}N_2O_3$
Formula weight / g mol^{-1}	264.32
Crystal system	Monoclinic
Space group	C2/c
a / Å	54.94(1)
b / Å	5.520(1)
c / Å	9.707(2)
β / °	99.80(3)
Volume / $Å^3$	2901(1)
Z	8
Density $_{calc}$ / g cm^{-3}	1.210
μ(MoKα) / mm^{-1}	0.086
F(000)	1136
Temperature of data collection / K	173
Crystal size / mm^3	0.15 x 0.50 x 0.80
Range scanned θ / °	$2 \leq \theta \leq 25$
Index ranges	h: -62, 48 k: -6, 5 l: -9, 11
Dx / mm	55
Total no. of reflections collected	4869
Total no. of unique reflections	2227
No. of reflections with $I > 2\sigma(I)$	1330
No. of parameters	167
S	1.44
R_1 ($I > 2\sigma(I)$)	0.1160
No. of reflections omitted	8
wR_2 (all reflections)	0.3889
Weighting scheme	a = 0.2 b = 0.0
$(\Delta / \sigma)_{mean}$	< 0.001
Δρ excursions / e $Å^{-3}$	0.68 and –0.55

Description of the atenolol structure

Atenolol crystallises in the monoclinic space group C2/c with Z = 8 molecules per unit cell. This indicates one molecule per asymmetric unit since C2/c has eight equivalent positions. The ADDSYM function in PLATON[114] indicated no extra crystallographic symmetry for the atenolol, reaffirming the correct choice of space group for this structure. Since the compound is racemic, the crystal contains equal numbers of molecules of (R-)- and (S-)-configuration, the chiral centre being C9. Due to the disorder described, both (R-)- and (S-)- configurations appear in the asymmetric unit, and this is an unusual phenomenon. The atoms C14, C17 and C18 are each disordered over two positions. One terminal of the atenolol molecule consists of the hydrophobic isopropyl group while the other end consists of the amide group. The diagrams of the atenolol molecule [chemical structural diagram, stick and Ortep diagrams] and its numbering scheme are presented in Figures 3.4 and 3.5.

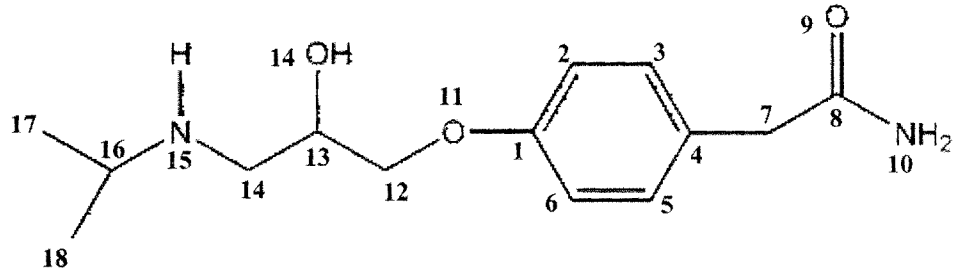

Figure 3.4 A chemical structural diagram of atenolol and its numbering scheme.

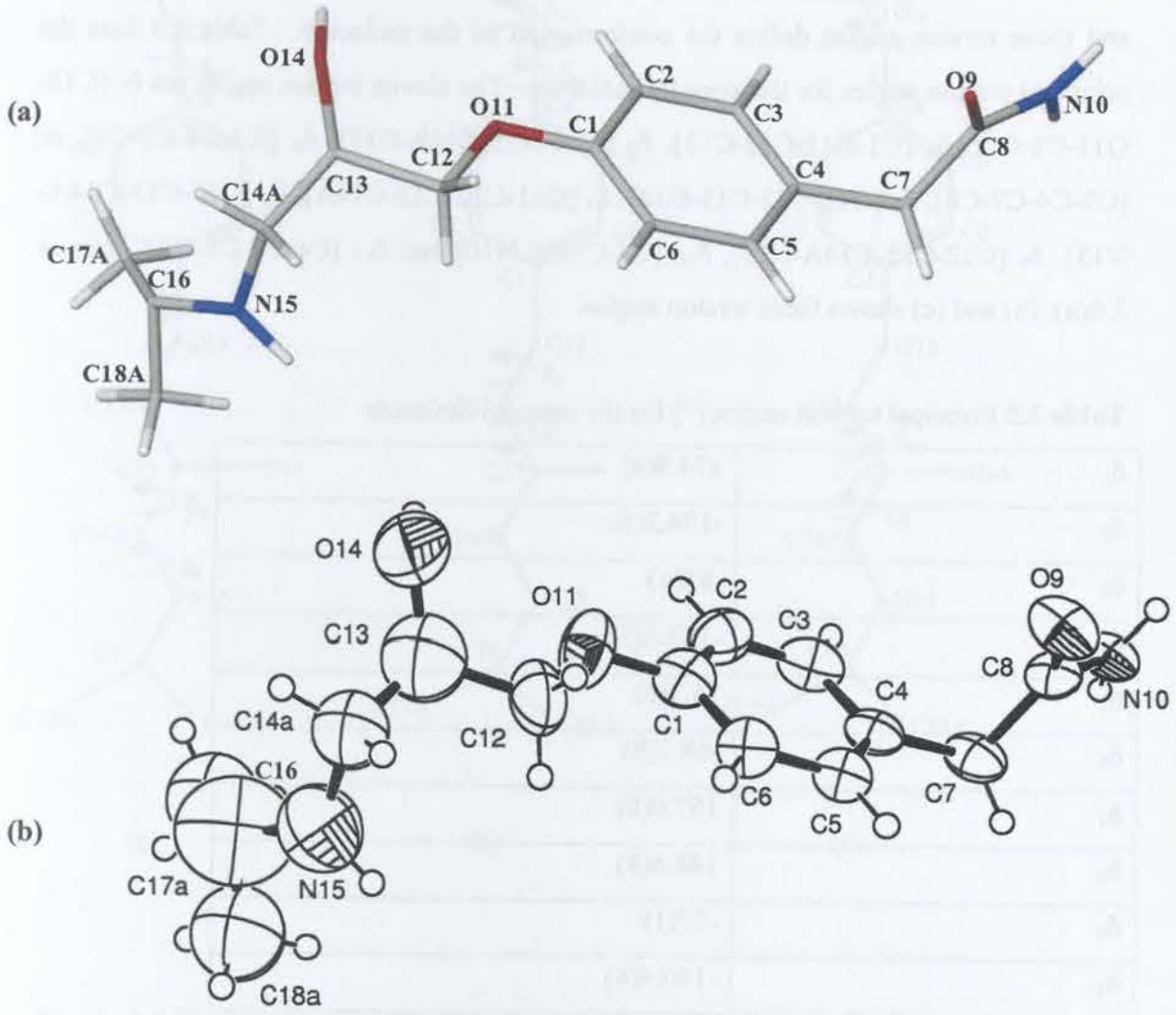

Figure 3.5 (a) The molecular structure of atenolol, (b) ORTEP diagram and the atomic numbering scheme. In both (a) and (b) the disordered components C14B, C17B, C18B and their accompanying hydrogen atoms are omitted for clarity.

Molecular conformation of atenolol

There are eleven principal torsion angles of the atenolol backbone that were identified, and these torsion angles define the conformation of the molecule. Table 3.5 lists the principal torsion angles for the atenolol molecule. The eleven torsion angles are δ_1 [C12-O11-C1-C2], δ_2 [C1-O11-C12-C13], δ_3 [C16-N15-C14A-C13], δ_4 [C5-C4-C7-C8], δ_5 [C3-C4-C7-C8], δ_6 [O11-C12-C13-O14], δ_7 [O11-C12-C13-C14A], δ_8 [O14-C13-C14A-N15], δ_9 [C12-C13-C14A-N15], δ_{10} [C4-C7-C8-N10] and δ_{11} [C4-C7-C8-O9]. Figure 3.6(a), (b) and (c) shows these torsion angles.

Table 3.5 Principal torsion angles [°] for the atenolol molecule

δ_1	174.9(4)
δ_2	-174.3(5)
δ_3	-85(1)
δ_4	-102.3(5)
δ_5	75.7(6)
δ_6	-68.7(8)
δ_7	157.0(8)
δ_8	148.6(8)
δ_9	-77(1)
δ_{10}	-140.4(4)
δ_{11}	41.0(6)

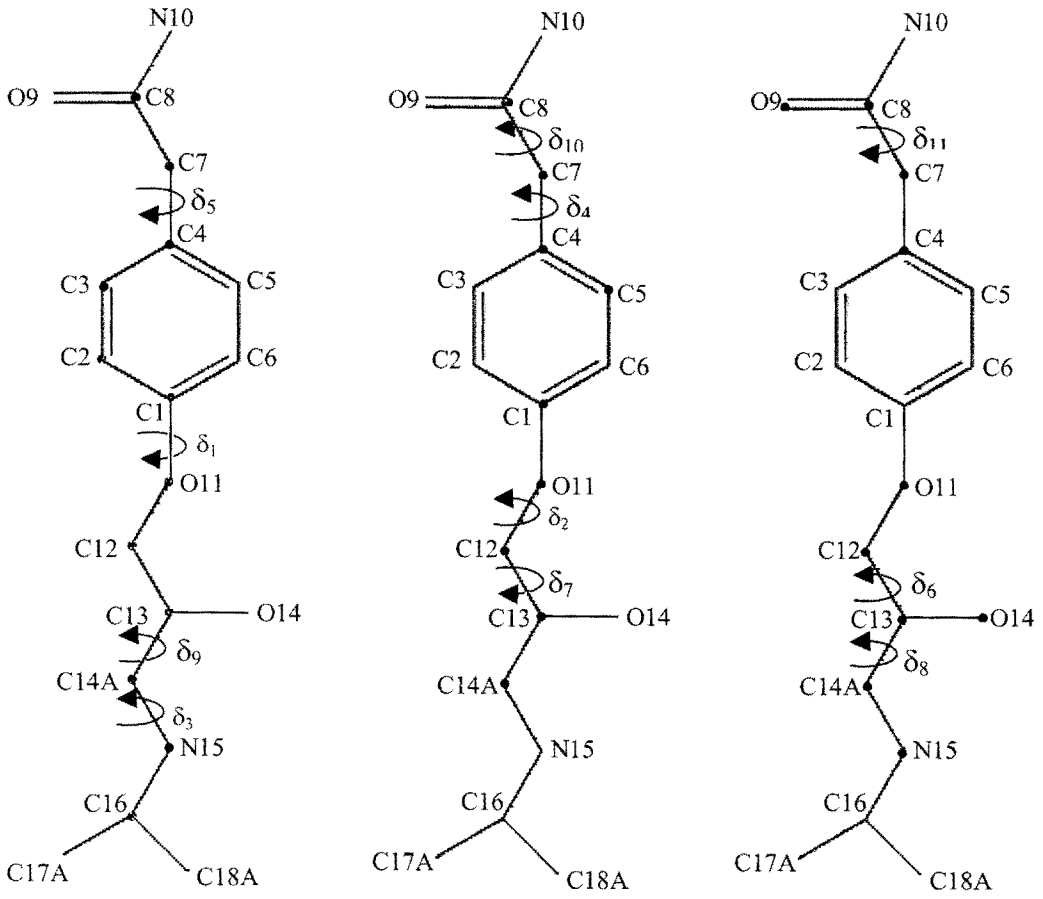

Figure 3.6 Diagram showing the principal torsion angles (a) δ_1, δ_3, δ_5, δ_9 (b) δ_2, δ_4, δ_7, δ_{10} (c) δ_6, δ_8 and δ_{11} for the atenolol molecule. The carbon atoms C14A, C17A and C18A [major positions] were chosen.

Hydrogen bonding and C-H•••π interactions in the atenolol structure

A PLATON[114] geometrical structure analysis revealed three intermolecular hydrogen bonds, namely O14-H14•••N15, N10-H10A•••O9 and N10-H10B•••O9 and one C12-H12A•••C_g interaction. These hydrogen bonds are presented in Table 3.6. C_g refers to the centre of gravity of the aromatic ring of the atenolol molecule. Distances for π•••π interactions were too long [~ 5 Å] to be regarded as significant interactions of this type, thus they are not included.

Table 3.6 Hydrogen bonding and C-H•••π interactions of the atenolol structure

Interaction	**H•••A / Å**	**D•••A / Å**	**D-H•••A / °**	**Symmetry code** [#]
O14-H14•••N15	2.12	2.96(1)	177	x, 1+y, z
N10-H10A••• O9	2.01	2.889(5)	174	1/2-x, 5/2-y, 1-z
N10-H10B•••O9	2.02	2.863(4)	160	x, 2-y, -1/2+z
C-H•••π	**H•••C_g** [*] **/ Å**	**C•••C_g / Å**	**C-H•••C_g** [*] **/ °**	**Symmetry code** [#]
C12-H12A•••C_g	2.871	3.742(7)	147	x, 1-y, 1/2+z

[#] Symmetry code applied to second unit of the interaction

[*] Cg = centre of gravity of the aromatic ring

Other close contact distances are presented in Table 3.7 and Figure 3.7(a) illustrates the intermolecular hydrogen bonding interactions between the amide oxygen atom O9 and the amine hydrogen atoms H10A and H10B of nitrogen atom N10. The atom H10A connects the atenolol molecules along the a-axis while the atom H10B connects the molecules along the c-axis. Figure 3.7(b) is a diagram projected down the c-axis illustrating the hydrogen bonding interaction between the hydroxyl hydrogen atom H14 and the atom N15 of a translated molecule. This hydrogen bond connects the atenolol molecules along the b-axis.

Table 3.7 Close contact distances for the atenolol structure

Interaction	Distance / Å	Symmetry code [#]
O11•••H14	2.85	x, y, z
O11•••H14C	2.84	x, y, z
O11•••H14B	2.84	x, 1-y, 1/2+z
O14•••O11	2.882(6)	x, y, z
O14•••H14B	2.77	x, 1+y, z
O14•••H2	2.59	x, 2-y, ½+z
N15•••H12B	2.83	x, y, z
O14•••H15	2.79	x, 1+y, z
C1•••H3	2.94	x, -y, ½+z
C1•••H12A	3.00	x, 1-y, -½+z
C2•••H14B	2.90	x, 1-y, -½+z
C4•••H6	2.99	x, 1-y, -½+z
C14A•••H14	2.57	x, -1+y, z
C8•••H10A	2.88	½-x, 5/2-y, 1-z

[#] Symmetry code applied to second unit of interaction

For distances involving a H atom all e.s.d's < 0.01.

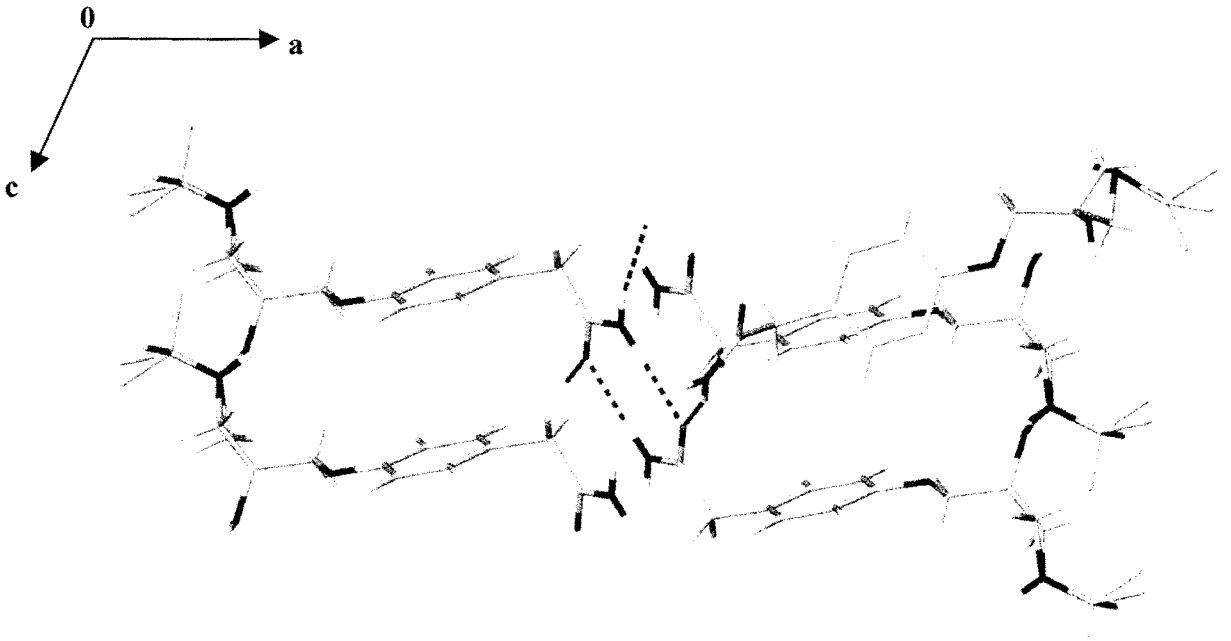

Figure 3.7(a) Diagram illustrating intermolecular N10-H10A•••O9 and N10-H10B•••O9 hydrogen bonding interactions between the atenolol molecules viewed down the b-axis.

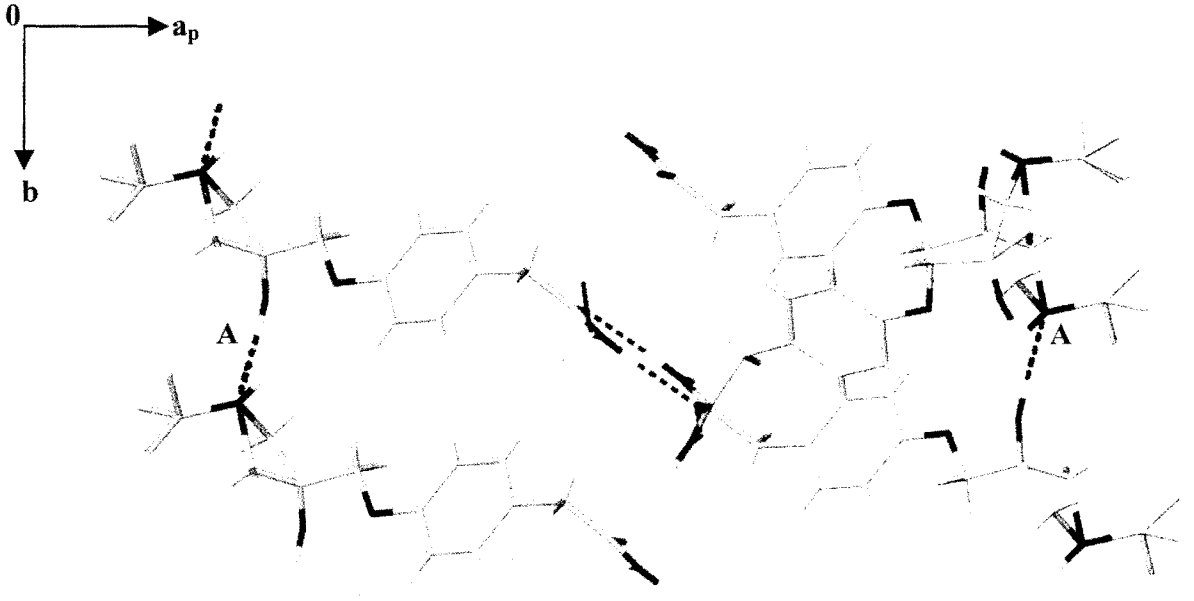

Figure 3.7(b) Diagram illustrating the intermolecular O14-H14•••N15 hydrogen bond [labelled **A**] connecting the atenolol molecules along the b-axis.

Crystal packing

Figure 3.8 presents the crystal packing of the atenolol structure viewed down the b-axis. The intermolecular hydrogen bonds N10-H10A•••O9 and N10-H10B•••O9 link the molecules as double ribbons running in the [001] direction. The hydrophobic ends of the isopropyl groups of the adjacent molecules form bridges connecting the neighbouring molecules along the a-axis. In addition the O14-H14•••N15 hydrogen bond links the atenolol molecules along the b-axis. There is faster crystal growth in the yz-plane owing to these hydrogen bonds relative to the growth along the x-direction. This therefore results in thin plate-like crystals of atenolol. Further attempts to grow better crystals of atenolol will be described in the **Conclusion** to this Chapter.

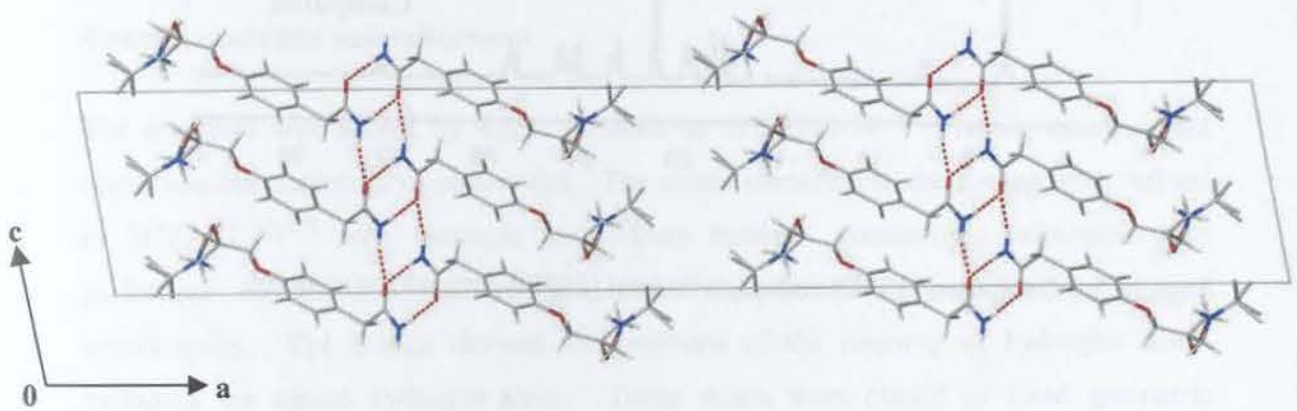

Figure 3.8 Crystal packing diagram for the atenolol down the b-axis. The intermolecular hydrogen bonding is shown in red.

Powder X-ray diffraction

The computed and experimental PXRD patterns for atenolol are presented in Figure 3.9. The close match of the patterns indicates that no phase transformation took place on grinding the atenolol for PXRD sample preparation. A slight shift of the experimental trace to lower 2θ values when compared to the computed trace is attributed to the difference in temperature at which the information for the respective traces was obtained.

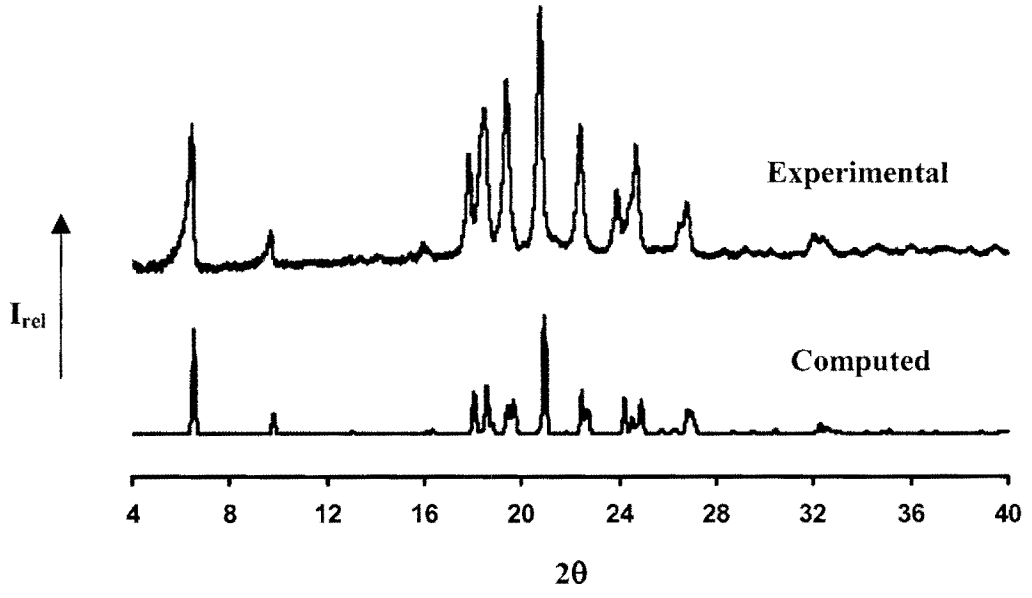

Figure 3.9 Computed [173K] and experimental [295K] patterns for atenolol.

X-ray Crystallographic Analysis of metoprolol free base

Data-collection and space group determination

Diffraction intensity data for metoprolol free base were collected on a Nonius Kappa CCD diffractometer at 173(2) K using graphite-monochromated MoKα radiation. A suitable crystal was mounted on a glass fibre, covered in Paratone N oil[115] to glue the crystal to the fibre on freezing. Inspection of the intensity-weighted reciprocal lattice revealed Laue 2/m symmetry, indicating the monoclinic crystal system. XPREP[103] indicated the possible space groups $P2_1/n$, Pn and P2/n. The reflections were then investigated with LAYER[112] and found to satisfy the conditions h0l: h + l = 2n; 0k0: k = 2n which uniquely identify the space group as $P2_1/n$ [alternative setting of space group $P2_1/c$, No. 14]. Intensity statistics provided by XPREP[103] showed $|E^2-1|=1.019$, confirming a centrosymmetric space group. Metoprolol free base will be referred to hereinafter as Form I since a second form of this substance will be discussed later.

Structure solution and refinement

The structure was solved by direct methods in SHELXS-97.[104] The asymmetric unit comprises one molecule of metoprolol. The atoms identified in the E-map were refined in SHELXL-97[113] with isotropic temperature factors. Anisotropic refinement was performed on all the non-hydrogen atoms whose temperature factors behaved satisfactorily. The E-map showed the positions of the majority of hydrogen atoms including the amino hydrogen atom. These atoms were placed in fixed geometric positions and were refined using a riding model with isotropic thermal parameters 1.2 times those of their parent atoms. The hydroxyl and amino hydrogen atoms were revealed by the Fourier-map and refined freely. The final refined O-H and N-H distances were 0.92 and 0.85 Å respectively. The methyl hydrogen atoms were placed using the rotating refinement strategy [AFIX 137] with the methyl hydrogen atoms refined with isotropic temperature factors 1.5 times those of their parent atoms. The crystal data and refinement parameters are presented in Table 3.8.

Table 3.8 Crystal and refinement parameters for metoprolol [Form I]

Formula unit	$C_{15}H_{25}NO_3$
Formula weight / g mol^{-1}	267.4
Crystal system	Monoclinic
Space group	$P2_1/n$
a / Å	16.1940(5)
b / Å	5.4409(2)
c / Å	17.8670(7)
β / °	100.63(2)
Volume / $Å^3$	1547.3(1)
Z	4
$Density_{calc}$ / g cm^{-3}	1.148
μ(MoKα) / mm^{-1}	0.079
F(000)	584
Crystal size / mm^3	0.25 x 0.27 x 0.50
Temperature / K	173(2)
Range scanned θ / °	$1 \leq \theta \leq 28$
Dx / mm	45
Index ranges	h: -20, 21 k: -6, 7 l: -23, 19
No. of measured reflections	7072
No. of unique reflections	3449
No. of reflections with $I > 2\sigma(I)$	2245
No. of least-squares parameters	183
No. of reflections omitted	4
R_{int}	0.032
R_σ	0.055
S	1.02
R_1 [$I > 2\sigma(I)$]	0.0469
wR_2	0.1191
Weighting scheme parameters	a = 0.0529 b = 0.1184
$(\Delta / \sigma)_{mean}$	< 0.001
Δρ excursions / e $Å^{-3}$	0.16, -0.24

Description of the metoprolol structure

Metoprolol [Form I] crystallises in the monoclinic space group $P2_1/n$ with Z = 4 formula units per unit cell. Thus the asymmetric unit, given in stick representation and as an ORTEP[116] diagram, is shown in Figure 3.10(a) and (**b**) respectively and it consists of one metoprolol molecule. This compound consists of a racemic mixture of optical isomers of the base. The chiral centre for this compound is C9 and the molecule with (R-)-configuration is shown.

(a)

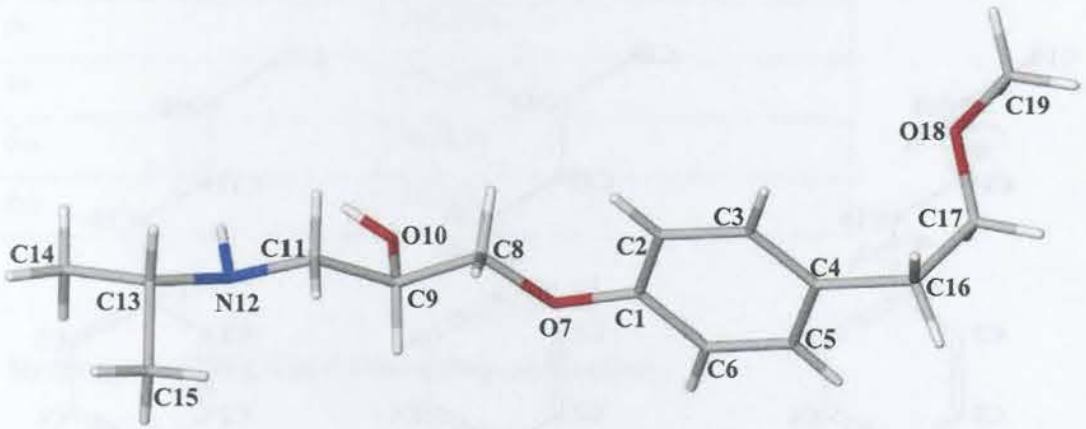

(b)

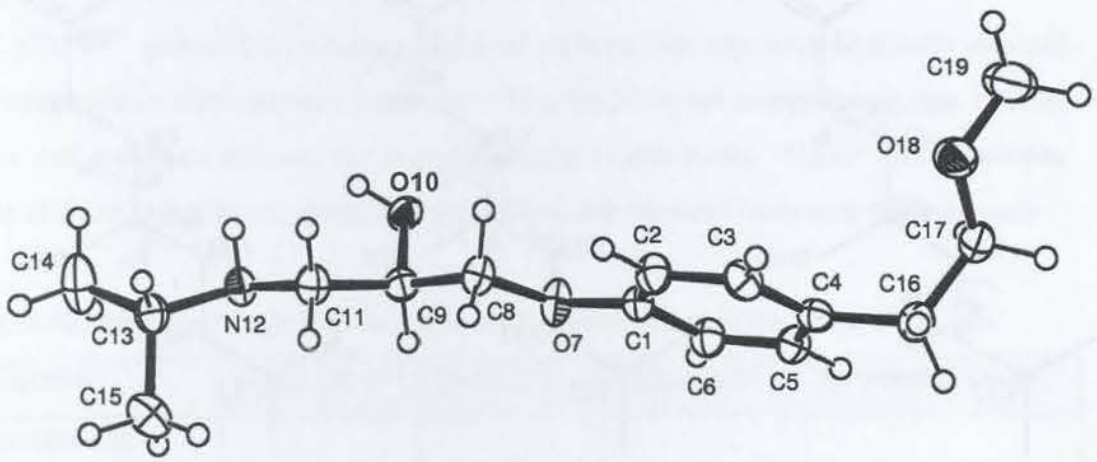

Figure 3.10 (a) The molecular structure of the metoprolol free base, (b) ORTEP diagram and its numbering scheme.

Molecular conformation of metoprolol [Form I]

Eleven principal torsion angles of the metoprolol molecule were identified that define the conformation and these are shown in Figure 3.11(a), (b) and (c). The eleven torsion angles are δ_1 [C1-O7-C8-C9], δ_2 [C8-O7-C1-C2], δ_3 [C19-O18-C17-C16], δ_4 [C13-N12-C11-C9], δ_5 [C3-C4-C16-C17], δ_6 [C5-C4-C16-C17], δ_7 [O7-C8-C9-C11], δ_8 [O7-C8-C9-O10], δ_9 [C8-C9-C11-N12], δ_{10} [O10-C9-C11-N12] and δ_{11} [C4-C16-C17-O18]. These torsion angles are presented in Table 3.9.

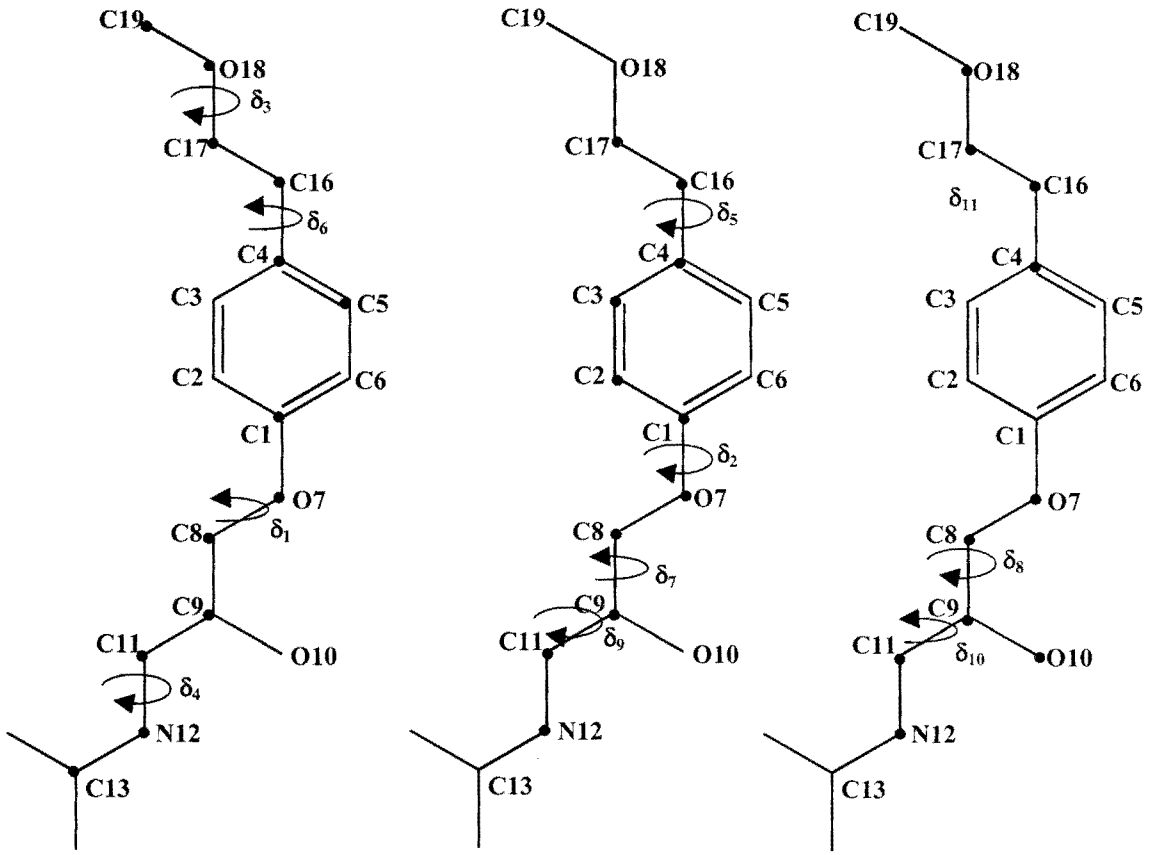

(a) (b) (c)

Figure 3.11 Schematic diagram of the principal torsion angles (a) δ_1, δ_3, δ_4 and δ_6 (b) δ_2, δ_5, δ_7 and δ_9 (c) δ_8, δ_{10} and δ_{11} for the metoprolol molecule.

Table 3.9 Principal torsion [°] for metoprolol

δ_1	-177.6(1)
δ_2	174.2(1)
δ_3	-177.5(1)
δ_4	163.5(1)
δ_5	-97.9(2)
δ_6	81.9(2)
δ_7	162.8(1)
δ_8	-75.6(1)
δ_9	176.1(1)
δ_{10}	54.7(2)
δ_{11}	73.1(2)

Hydrogen bonding and C-H•••π-ring interactions

A PLATON[114] geometrical structure analysis showed two crystallographically distinct pairs of intermolecular hydrogen bonds involving the hydroxyl and amine groups, both as donors and acceptors and one C-H•••π interaction [Table 3.10]. Figure 3.12 illustrates details of these interactions; those labelled 1 and 1' are identical inversion-related bonds

Table 3.10 Hydrogen bonds and the C-H•••π-ring interactions in the Form I structure

Interaction	**H•••A / Å**	**D•••A / Å**	**D-H•••A / °**	**Symmetry code** [#]
Intermolecular				
O10-H•••N12	1.90(2)	2.809(2)	174(2)	1-x, -y, 1-z
N12-H12•••O10	2.48 (2)	3.193(2)	142(1)	1-x, 1-y, 1-z
C-H•••π	**H•••Cg** [*] **/ Å**	**C•••Cg / Å**	**C-H•••Cg / °**	**Symmetry code** [#]
C2-H2•••Cg	3.022	3.687(2)	128.2	1/2-x, 1/2+y, 3/2-z

[#] Symmetry code is applied to the second unit of the interaction

[*] Cg = Centre of gravity of the aromatic ring of the metoprolol molecule

of the type O-H•••N [unique bond O10-H•••N12] while another distinct pair of inversion-related bonds of the type N-H•••O [unique N12-H12•••O10] is labelled 2 and 2'. These metoprolol molecules are thus linked in infinite arrays by ribbons of hydrogen bonds propagating parallel to the crystal b-axis. The pyramidal geometry associated with N12 in Figures 3.10 and 3.12 is pronounced and consistent with the approach of the O10-H group of an inversion-related molecule onto the plane defined by C11, N12 and C13, as hydrogen bond formation occurs.

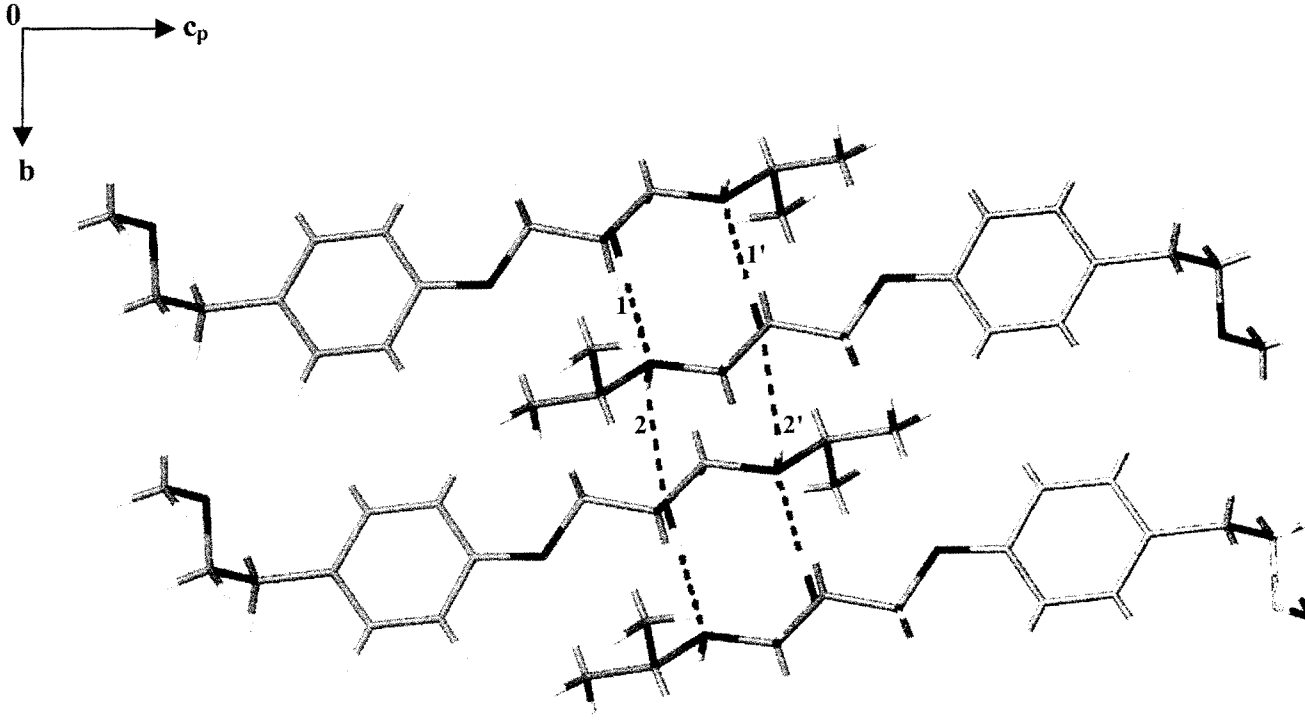

Figure 3.12 Diagram illustrating the O-H•••N and N-H•••O hydrogen bonding motif in metoprolol projected down the a-axis.

Crystal packing

Figure 3.12 presents a portion of the crystal packing of the metoprolol [Form I] structure viewed down the a-axis while Figure 3.13 is the crystal packing projected down the b-axis. The intermolecular N12-H12•••O10 hydrogen bonds [labelled **2**, **2'**] indicate that this interaction links inversion-related metoprolol molecules into dimers in the xz-plane. Cohesion along the b-axis is effected by the O10-H•••N12 hydrogen bonds.

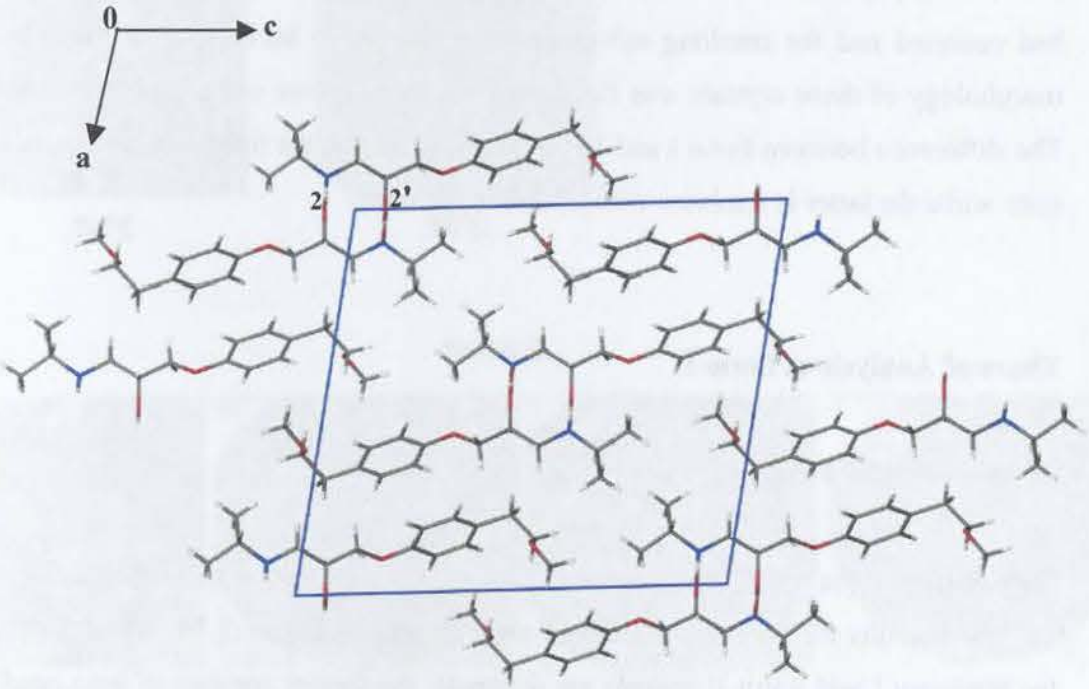

Figure 3.13 Crystal packing diagram for metoprolol with the intermolecular N12-H12•••O10 hydrogen bonds viewed down the b-axis.

Isolation of a Second Crystalline Modification of Metoprolol Free Base

In addition to the Form I crystal structure that has been discussed, crystals of a second form were grown at 5°C. The crystals were prepared by heating and stirring a solution of the drug in n-hexane in a sealed flask at 40°C for five minutes. This was followed by a hot filtration to remove any impurities. The solution was then allowed to cool to room temperature before being placed in the refrigerator at 5°C. Spherically-shaped, transparent crystals of the drug were obtained after three days.

Preliminary physicochemical studies indicated that an inclusion of the n-hexane solvent had occurred and the resulting solvate will be referred to hereinafter as Form II. The morphology of these crystals was different from those grown under ambient conditions. The difference between Form I and Form II crystals is that the former is in the unsolvated state while the latter is a solvate with n-hexane included.

Thermal Analysis of Form II

HSM results for Form II

HSM proved to be a useful technique to observe the desolvation of n-hexane from Form II. HSM results for Form I and Form II are presented in Figure 3.14. The crystal habits for the Form I and Form II crystals are different; the former consists of long needle-like rectangular crystals whilst the latter has globular crystals. The events displayed by these crystals are different; the Form I crystals remain transparent until they melt in the temperature range 56-58°C whereas Form II crystals begin to turn opaque at 35°C. They begin to melt at 54°C while still losing solvent, and are completely molten at 56°C. Negligible bubbling was observed since the host-guest ratio of Form II is 8:1.

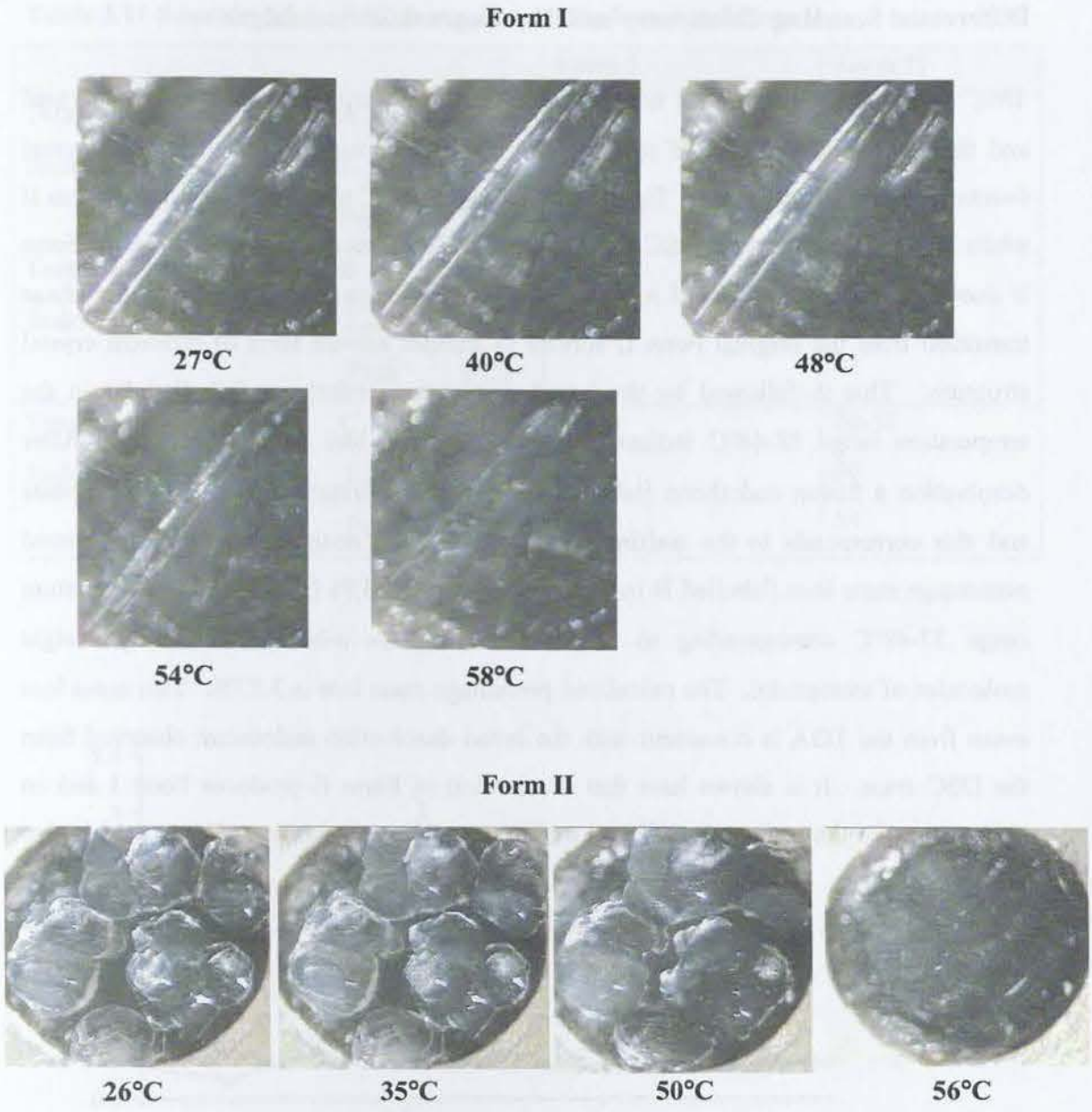

Figure 3.14 HSM photographs taken at various temperatures for crystals of Form I and Form II.

Differential Scanning Calorimetry and Thermogravimetric Analysis

DSC analyses were performed in the 25-100°C temperature range for both the solvated and the non-solvated forms of metoprolol. Table 3.11 summarises the DSC thermal events for Form I and Form II. Figure 3.15 shows the DSC traces for Form I and Form II while Figure 3.16 shows the DSC and TGA results for Form II. The DSC trace for Form II shows an exotherm [labelled A] in the temperature range 32-37°C indicating a phase transition from the original Form II solvate to another solvate form of different crystal structure. This is followed by the broad desolvation endotherm [labelled B] in the temperature range 38-48°C indicative of the n-hexane loss from the crystal. After desolvation a fusion endotherm [labelled C] in the temperature range 49-58°C appears and this corresponds to the melting of Form II. TGA analysis for Form II showed percentage mass loss [labelled B in Figure 3.16] of 3.81(3)% [n = 3] in the temperature range 37-49°C corresponding to one molecule of the n-hexane solvent per eight molecules of metoprolol. The calculated percentage mass loss is 3.87%. This mass loss event from the TGA is consistent with the broad desolvation endotherm observed from the DSC trace. It is shown later that desolvation of Form II produces Form I and an explanation for the apparently different melting temperatures shown in Figure 3.15 is also presented.

Table 3.11 Summary of the DSC thermal events for Form I and Form II

			Form I	Form II
Temperature range	A	(°C)		32-37
Exotherm A	T_{on}	(°C)		33
	Peak	(°C)		35
Temperature range	B	(°C)		38-48
Endotherm B	T_{on}	(°C)		39
	Peak	(°C)		42
Temperature range	C	(°C)	51-60	49-58
Endotherm C	T_{on}	(°C)	52	50
	Peak	(°C)	55	54

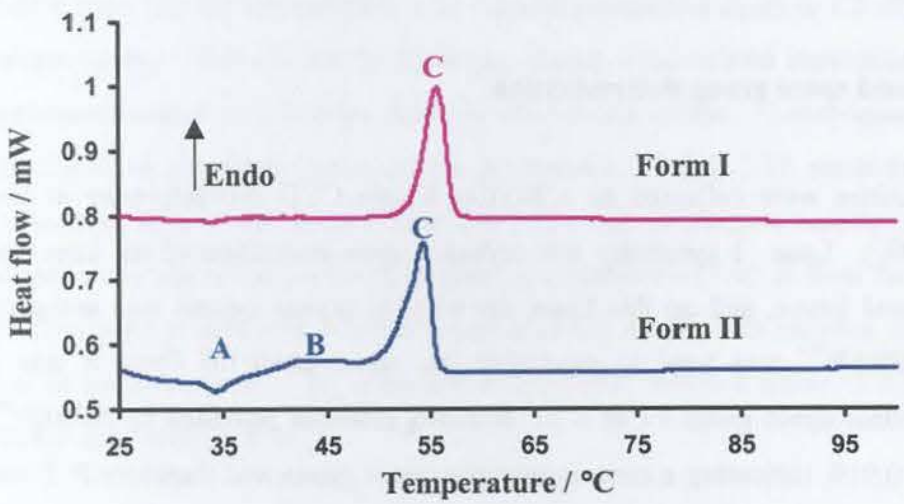

Figure 3.15 DSC traces for Form I and Form II of metoprolol free base.

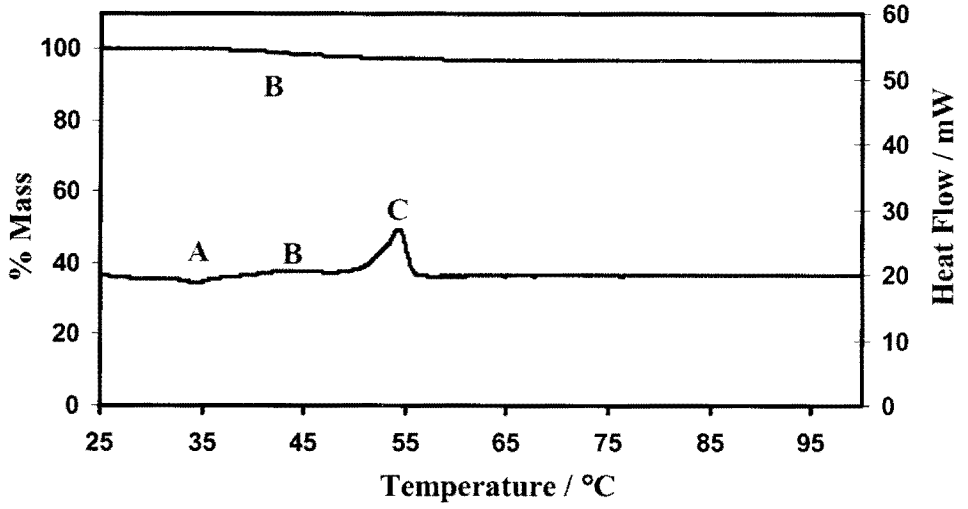

Figure 3.16 TGA and DSC traces for Form II.

X-ray Crystallographic Analysis of Form II

Data-collection and space group determination

Diffraction intensities were collected on a Nonius Kappa CCD diffractometer at low temperature [113K]. Laue $\bar{1}$ symmetry was revealed upon inspection of the intensity-weighted reciprocal lattice, and on this basis, the triclinic crystal system was assigned. The program XPREP[103] was used to determine the space group of Form II and it indicated the triclinic space group P1 or P $\bar{1}$. Intensity statistics provided by XPREP[103] showed $|E^2-1| = 0.919$, indicating a centrosymmetric space group and therefore P $\bar{1}$ was chosen. The successful refinement of the structure in this space group confirmed its choice. Since the free base was known to be racemic, the centrosymmetric space group was expected.

Structure solution and refinement

The asymmetric unit consists of eight molecules of metoprolol and one of n-hexane. SHELXD[117] was used to solve the structure by direct methods and it showed the positions of all the non-hydrogen atoms of Form II except atom C19A and the n-hexane molecule. For the first refinement in SHELXL-97[113] the atoms were refined isotropically. After the first refinement the Fourier map revealed positions for the atom C19A and the carbon atoms of the n-hexane molecule.

Due to the poorly defined geometry found for the n-hexane molecule, distance constraints of 1.46(5) Å were placed on all five C-C bonds. The difference Fourier map revealed most of the hydrogen atoms on the host molecules including the amino and hydroxyl hydrogen atoms. All of the amino hydrogen atoms were allowed to refine with restrained N-H distances of 1.000(5) Å while all the hydroxyl hydrogen atoms were refined freely. Most of the aromatic ring hydrogen atoms located in subsequent difference Fourier maps were placed in fixed geometric positions using a riding model. The methyl hydrogen atoms were refined isotropically with thermal parameters equal to 1.5 times those of their parent atoms. The rest of the hydrogen atoms were refined isotropically with thermal parameters equal to 1.2 times those of their parent atoms. Least-squares weights were employed in the final cycles of the refinement. Table 3.11 presents the crystal and refinement data for the Form II structure. The highest electron density peak of 0.94 e $Å^{-3}$ at the end of the refinement was situated at a distance of 1.61 Å from the atom O18H and was regarded as possible residual disorder of this atom. This electron density peak could not be modelled due to the abnormal bond angles which it made with the atoms C17H, O18H and O18H, C19H.

Table 3.11 Crystal and refinement parameters for Form II of metoprolol

Formula unit	$8(C_{15}H_{25}NO_3)\bullet(C_6H_{14})$
Formula weight / g mol^{-1}	2225.05
Crystal system	Triclinic
Space group	$P\bar{1}$
a / Å	15.715(1)
b / Å	15.700(1)
c / Å	30.942(2)
α / °	85.925(2)
β / °	78.662(2)
γ / °	60.833(2)
Volume / Å^3	6533.3(6)
Z	2
Density$_{calc}$ / g cm^{-3}	1.131
μ(MoKα) / mm^{-1}	0.077
F(000)	2436
Crystal size / mm^3	0.05 x 0.25 x 0.40
Temperature / K	113
Range scanned θ / °	$1 \leq \theta \leq 24$
Dx / mm	44
Index ranges	h: -16, 17 k: -16, 17 l: -34, 34
No. of measured reflections	22923
No. of unique reflections	14980
No. of reflections with $I > 2\sigma(I)$	7645
No. of least-squares parameters	1442
No. of reflections omitted	11
R_{int}	0.061
R_σ	0.1462
S	1.04
R_1 [$I > 2\sigma(I)$]	0.0997
wR_2 (All reflections)	0.2945
Weighting scheme parameters	a = 0.1165 b = 19.009
$(\Delta / \sigma)_{mean}$	0.019
Δρ excursions / e Å^{-3}	0.94, -0.61

Description of the Form II structure

Form II crystallises in the triclinic space group P $\bar{1}$ with sixteen molecules of metoprolol and two molecules of n-hexane per unit cell, which indicates eight molecules of metoprolol and one molecule of n-hexane per asymmetric unit since this space group has two general equivalent positions. An ORTEP[116] diagram for the metoprolol molecules and a stick model for the n-hexane molecule of the Form II structure are presented in Figure 3.17. The Form II molecules are labelled **A-H** and the numbering shown in molecule A is the same for all eight Form I molecules. The smaller thermal ellipsoids of the Form II structure show their reduced thermal motion except for C17H, O18H and C19H with U_{iso} = 0.112, 0.221 and 0.223 Å^2 respectively. The carbon atoms C1, C2, C3, C4, C5 and C6 for the n-hexane molecule have higher thermal motion; their U_{iso} parameters refined to the final values of 0.286, 0.202, 0.209, 0.229, 0.274 and 0.365 Å^2 respectively. For clarity only one metoprolol molecule and the n-hexane solvent molecule are labelled. The n-hexane molecule acts as a pseudo-centrosymmetric centre relative to the eight metoprolol molecules in the asymmetric unit; however in the ORTEP[116] diagram in Figure 3.17 molecules have been arranged separately to clearly show the molecular conformations and thermal motion of the atoms for each molecule. Thermal ellipsoids were drawn at the 50% probability level. The configuration at the C9 atom for the molecules chosen as the asymmetric unit is (S-) for the molecules **A-H**. However, for each molecule there is a counterpart in the crystal with the chirality (R-) for the molecules corresponding to **A-H**, a requirement of the centrosymmetric space group.

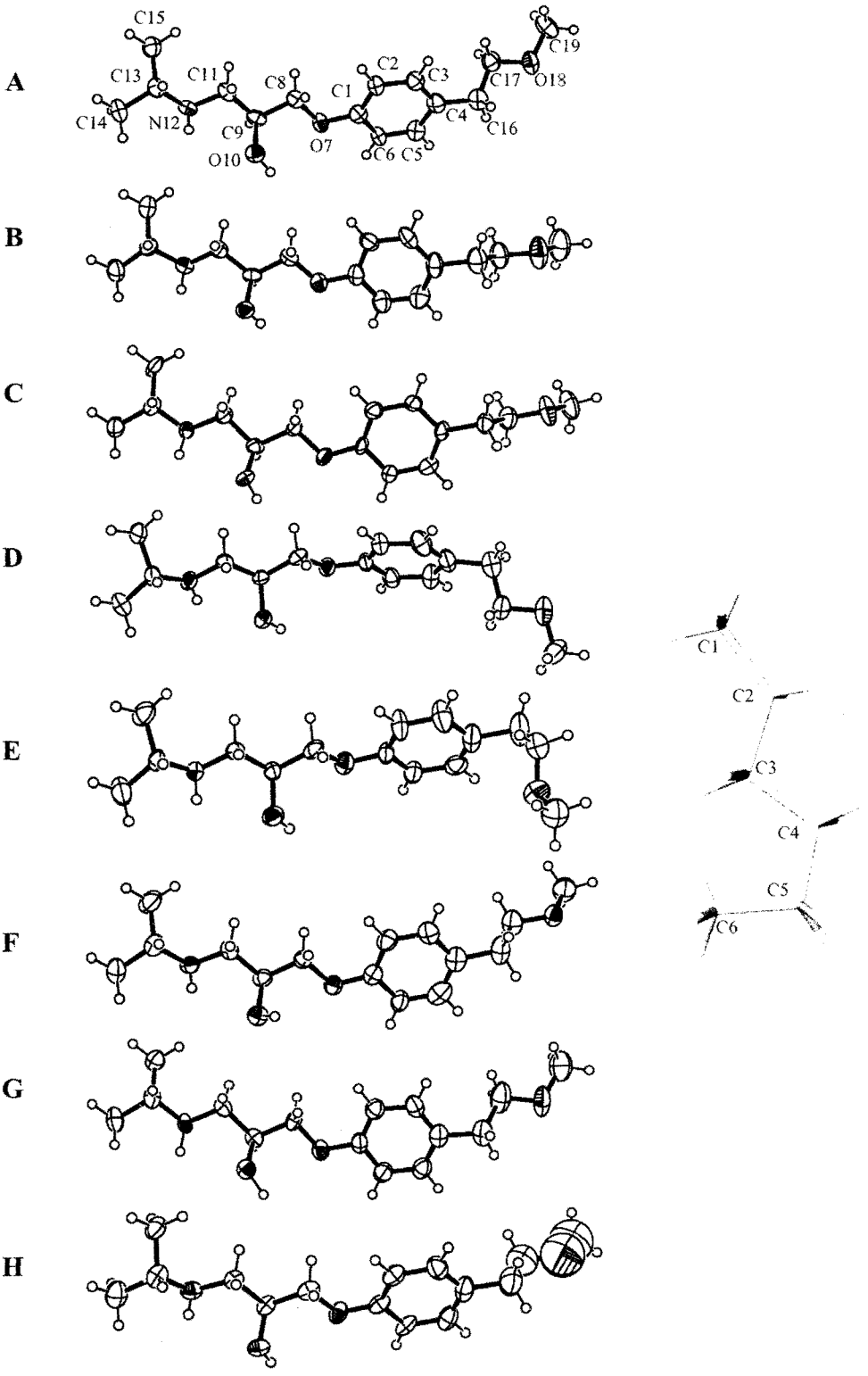

Figure 3.17 ORTEP diagram for the metoprolol molecules and stick model diagram for the n-hexane molecule of Form II.

Molecular conformation of metoprolol [Form II]

Since there are eight crystallographically independent molecules of metoprolol in the asymmetric unit, each metoprolol molecule can have unique values for its torsion angles. This is also confirmed by visual inspection of the molecules in Figure 3.17. The reader is referred to Figure 3.11 on page 60 for the key to the conformational parameters of the metoprolol molecule.

Table 3.12 lists the principal torsion angles for the molecules labelled **A-H** as calculated by PLATON.[114] The signs of the torsion angles are those for the chosen asymmetric unit with eight metoprolol molecules. Table 3.12 highlights the close agreement of the torsion angle magnitudes [δ_1, δ_2, δ_3, δ_4, δ_7, δ_8, δ_9 and δ_{10}] of the molecules labelled **A-H**. The molecules labelled **A-D** and **F-H** show close agreement of the torsion angle δ_{11} magnitude.

Table 3.12 Principal torsion angles [°] for Form II

Torsion angle / °	**A**	**B**	**C**	**D**
δ_1	-173.8(6)	-172.6(6)	-177.8(6)	-160.3(8)
δ_2	-175.8(7)	176.9(6)	-178.8(7)	171.8(8)
δ_3	-171.8(6)	-175(1)	-178.7(7)	179.1(7)
δ_4	170.1(6)	166.3(6)	164.5(6)	164.9(8)
δ_5	-58(1)	67(1)	70(1)	-72(1)
δ_6	125.5(9)	-114(1)	-113.0(8)	104(1)
δ_7	-171.9(6)	-175.5(6)	-175.4(6)	-166.3(7)
δ_8	69.6(7)	66(1)	68(1)	74(1)
δ_9	173.6(6)	170.1(6)	175.1(6)	174.7(7)
δ_{10}	-65(1)	-68(1)	-65(1)	-64(1)
δ_{11}	-177.3(6)	-177.4(9)	179.1(6)	174.4(7)
Torsion angle / °	**E**	**F**	**G**	**H**
δ_1	-168.9((7)	-174.9(7)	-173.6(7)	-178.4(7)
δ_2	169.9(8)	178.9(8)	-179.9(7)	179.9(7)
δ_3	179.0(9)	-177.1(8)	-168.4(9)	173(1)
δ_4	167.8(7)	163.4(7)	169.8(7)	162.5(6)
δ_5	68(1)	-85(1)	-52(1)	70(1)
δ_6	-114(1)	94(1)	133(1)	-114(1)
δ_7	-167.3(7)	-174.3(7)	-173.2(6)	-176.0(6)
δ_8	73(1)	67(1)	68(1)	65(1)
δ_9	177.0(7)	172.0(7)	174.0(6)	175.2(6)
δ_{10}	-61(1)	-66(1)	-64(1)	-62(1)
δ_{11}	69(1)	179.4(8)	-176.4(8)	-180(1)

Hydrogen bonding and C-H•••π ring interactions

Table 3.13 lists all the hydrogen bonds for Form II molecules as calculated by PLATON.[114] The total of seven N12-H•••O10 intramolecular hydrogen bonds help to stabilise the conformations of these Form II molecules. The formation of N-H•••O intramolecular hydrogen bonds explains the *gauche* relationship between atoms O10 and N12. Rotation around the C9-C11 bond, described by the δ_9 and δ_{10} torsion angles, affects the donor•••acceptor distances for these intramolecular interactions. Due to the presence of these intramolecular hydrogen bonds the δ_{10} torsion angles for molecules **A-H** are therefore very close to a minimum. There are two intermolecular hydrogen bonds

illustrated in stereo in Figure 3.18, namely, O10C-H10C•••N12A and O10A-H18•••N12D that provide additional stability to the Form II structure. Each metoprolol molecule plays a dual function in which it acts as a proton donor [O10A-H•••N12D] and a proton acceptor [O10C-H•••N12A] as shown for metoprolol molecule labelled **A**. There are six O10-H•••N12 hydrogen bonds and three C8-H•••O10 hydrogen bonds between symmetry related molecules in the Form II crystal structure.

PLATON revealed ten C-H•••π ring interactions, listed in Table 3.14, for the Form II structure, nine of which have symmetry operations other than x, y, z indicating that all these nine interactions are between molecules of different asymmetric units. There were no indications of π•••π interactions.

Table 3.13 Hydrogen bonding interactions for Form II

Interaction	**H•••A / Å**	**D•••A / Å**	**D- H•••A / °**
Intramolecular			
N12C-H2•••O10C	2.40(2)	2.82(1)	102
N12H-H30•••O10H	2.40(2)	2.82(1)	107
N12G-H9•••O10G	2.40(2)	2.84(1)	106
N12B-H26•••O10B	2.50(2)	2.87(1)	102
N12F-H31•••O10F	2.40(2)	2.85(1)	111
N12D-H32•••O10D	2.20(2)	2.80(1)	118
N12A-H33•••O10A	2.50(2)	2.84(1)	100
Intermolecular			
O10C-H10C•••N12A	1.98	2.79(1)	163
O10D-H10D•••N12B [i]	1.94	2.77(1)	166
O10E -H10E•••N12F [ii]	1.96	2.79(1)	170
O10H-H10H•••N12G [iii]	1.95	2.77(1)	164
O10G-H16•••N12E [ii]	1.70(2)	2.79(1)	171
O10A-H18•••N12D	1.60(2)	2.70(3)	168
C8B-H8B2•••O10B [i]	2.57	3.56(1)	172
C8C-H8C2•••O10C [iv]	2.52	3.49(1)	166
C8H-H8H2•••O10H [v]	2.47	3.44(1)	167
Related by symmetry operation:			
i) -x, -y, -z ii) -x, -y, 1-z iii) -x, 1-y, 1-z iv) -x, -y, -z			
v) 1-x, 1-y, 1-z vi) 1+x, y, z			

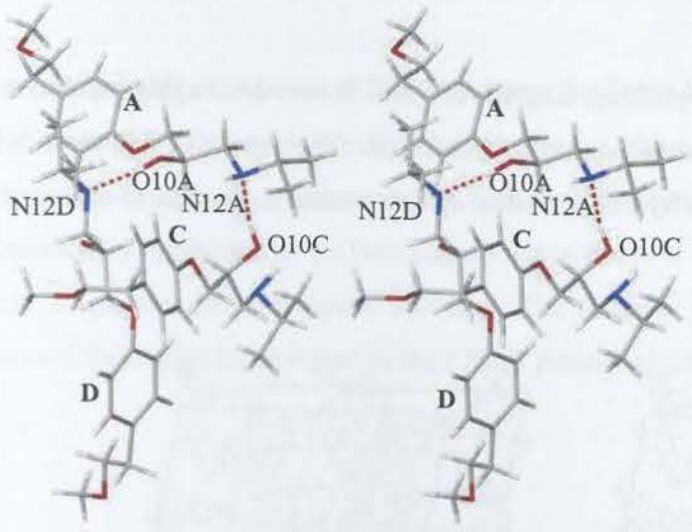

Figure 3.18 Stereo view of the N-H•••O intermolecular hydrogen bonding involving metoprolol molecules **A**, **C** and **D** in Form II. The remaining molecules of the asymmetric unit are omitted for clarity.

Table 3.14 C-H•••π ring interactions for Form II

Interaction	H•••Cg / Å	C•••Cg / Å	C-H•••Cg * / °	Symmetry code #
C13A-H13A•••Cg1	3.03	3.98(1)	159	-x, 1-y, -z
C13B-H13B•••Cg2	2.86	3.82(1)	159	-x, -y, -z
C13C-H13C•••Cg3	2.67	3.61(1)	156	1-x, -y, -z
C13F-H13F•••Cg6	2.96	3.90(1)	155	-x, -y, 1-z
C13G-H13G•••Cg7	2.93	3.87(1)	155	-x, 1-y, 1-z
C13H-H13H•••Cg8	2.69	3.61(1)	153	1-x, 1-y, 1-z
C14G-H14T•••Cg5	3.17	3.99(1)	143	-1+x, 1+y, z
C15B-H15F•••Cg4	3.30	4.16(1)	147	-x, -y, -z
C15E-H15N•••Cg6	3.27	4.20(1)	158	x, -1+y, z

Symmetry code applies to the second unit of the interaction

* CgX = centre of gravity of the aromatic ring of molecule X

Crystal packing

Figure 3.19 presents the stereo packing diagram of Form II viewed roughly parallel to the b-axis. There are two n-hexane molecules in a unit cell. The repetitive pattern in which one metoprolol molecule forms hydrogen bonds with two other molecules is observed.

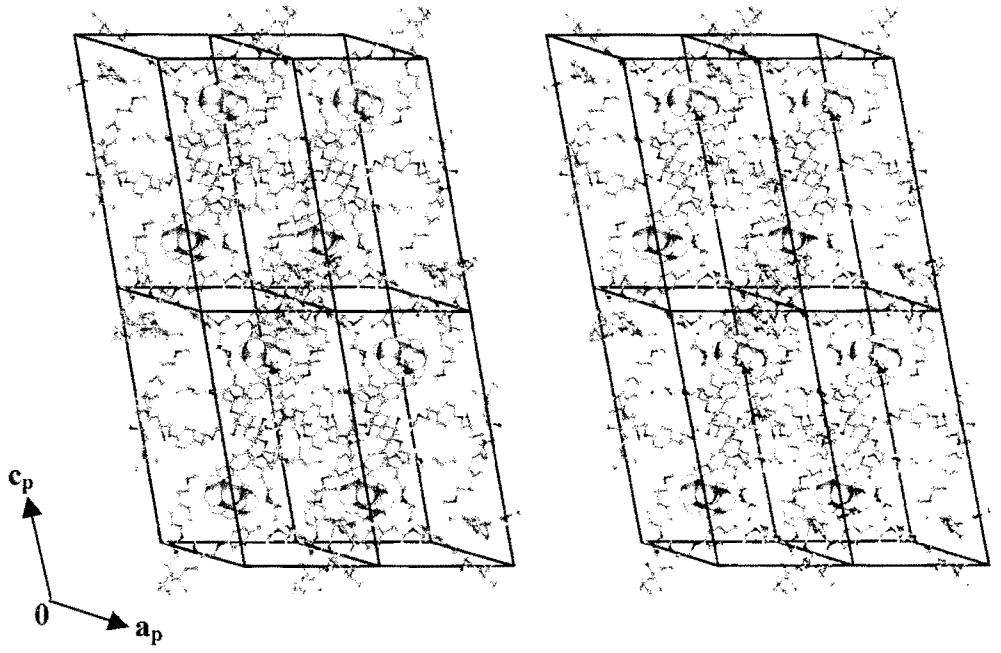

Figure 3.19 Stereo packing diagram for the Form II structure. Four unit cells are illustrated and hydrogen bonds are shown in dotted black lines.

Powder X-ray diffraction

The computed and experimental PXRD patterns for Form II are presented in Figure 3.20. The close match of these patterns indicates that no phase transformation took place on grinding this compound. The remarkable shift of the experimental PXRD pattern from the baseline is attributed to the wet sample since Form II had to be soaked in n-hexane solvent to prevent loss of crystal solvent. The removal of crystals from their mother liquor and their grinding resulted in the PXRD pattern of the unsolvated Form I.

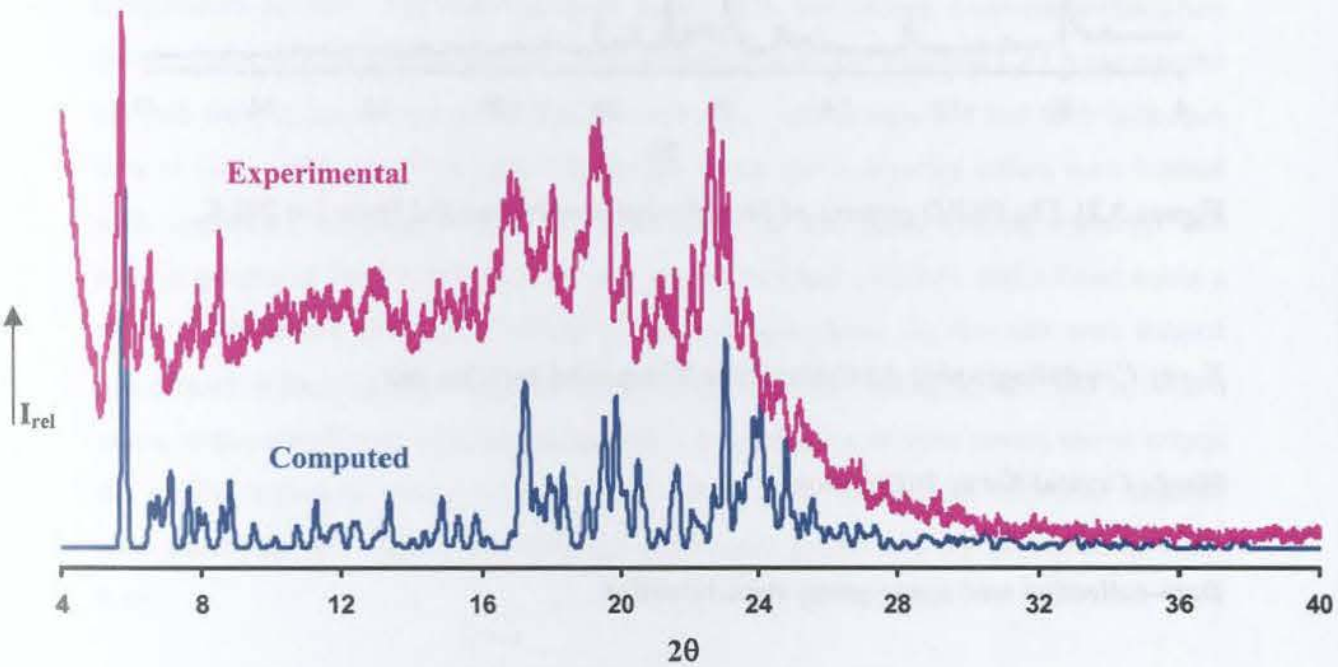

Figure 3.20 Experimental [113 K] and computed patterns [293 K] of Form II.

Since the melting temperature of Form II is slightly lower than that of Form I from the DSC traces in Figure 3.15, the possibility existed that desolvated Form II might be different from Form I. To investigate this, the solvated Form II was heated for 2 hours at 35°C and after its desolvation, its PXRD pattern was recorded and found to be identical to that of Form I. However the desolvated material had a very fine texture compared to

that of the unsolvated Form I, and this was considered to be the reason for the difference in thermal behaviours. The PXRD patterns for the dried Form II and Form I [unsolvated form] are presented in Figure 3.21.

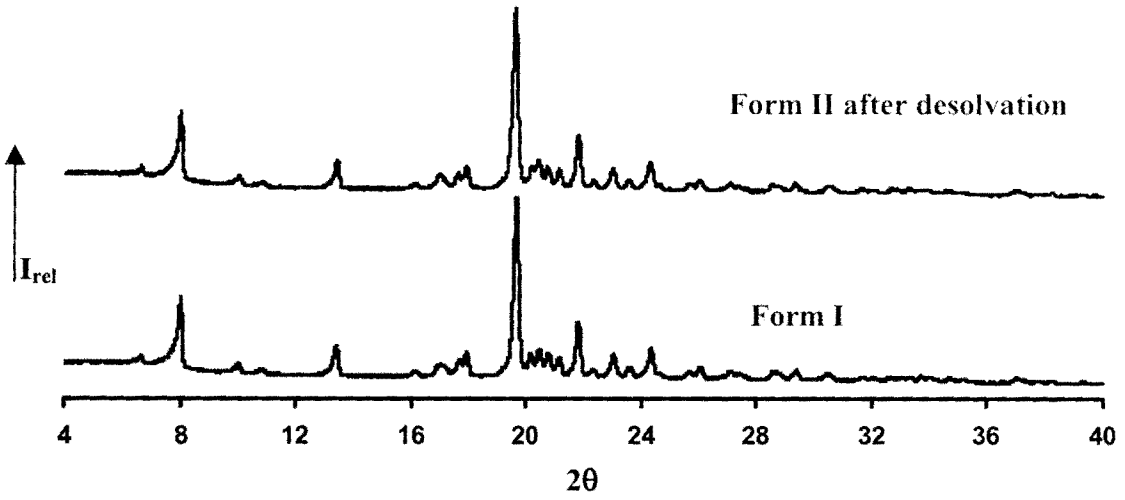

Figure 3.21 The PXRD patterns of Form II after desolvation and Form I at 293 K.

X-ray Crystallographic Analysis of the Metoprolol tartrate salt

Single Crystal X-ray Diffraction

Data-collection and space group determination

Diffraction intensity data for the salt Metoprolol tartrate were collected on a Nonius Kappa CCD diffractometer at 173(1)K. A suitable crystal was mounted under paratone oil to glue the crystal to the fibre on freezing. The overall symmetry of the reciprocal lattice [Laue symmetry] was determined as 2/m indicating that the crystal belongs to the monoclinic system. XPREP[103] indicated the space group $P2_1$ or $P2_1/m$ based on the reflection conditions 0k0: k = 2n. The intensity statistic $|E^2-1| = 0.839$ provided by XPREP[103] is intermediate between non-centrosymmetric structures [0.736] and

centrosymmetric structures [0.968] and the correct space group was therefore not distinguished by this parameter. However, on the basis of the known chiral nature [2R, 3R-configuration] of the tartrate ion, the non-centrosymmetric space group $P2_1$ was chosen. The reason for the value of 0.839 for $|E^2-1|$ was subsequently rationalised.

Structure solution and refinement

SHELXS-97[104] was used to solve the structure of the metoprolol tartrate salt by direct methods. The unit cell volume showed that the asymmetric unit comprises four metoprolol cations and two tartrate anions. The E-map showed the positions of all the non-hydrogen atoms and these were placed and refined in SHELXL-97[113] with isotropic temperature factors. The non-hydrogen atoms with satisfactory isotropic temperature factors were refined anisotropically. The equalisation of the terminal C-O bond lengths on both tartrate anions was proof that the carboxylic acid groups had lost their hydrogen ions to form a salt; thus two amino hydrogen atoms per metoprolol cation were located with tetrahedral geometry. The hydrogen atoms of the freely rotating hydroxyl and methyl groups of the Form I cations were placed in fixed positions and refined using a rotating refinement strategy. The rest of the hydrogen atoms for this salt were located and placed in fixed geometric positions and refined using a riding model. All hydrogen atoms were refined with thermal parameters 1.2 times those of their parent atoms except the methyl hydrogen atoms, which refined with thermal parameters 1.5 times those of their parent atoms. The crystal data and refinement parameters are presented in Table 3.15.

Table 3.15 Crystal and refinement parameters for metoprolol tartrate

Formula unit	$2(C_{15}H_{25}NO_3)^+ \cdot C_4H_4O_6^{2-}$
Formula weight / g mol^{-1}	682.77
Crystal system	Monoclinic
Space group	$P2_1$
a / Å	8.4395(2)
b / Å	45.653(1)
c / Å	9.6019(3)
β / °	90.733(2)
Volume / Å^3	3699(2)
Z	4
Density$_{calc}$ / g cm^{-3}	1.230
μ(MoKα) / mm^{-1}	0.09
F(000)	1480
Crystal size / mm^3	0.15 x 0.25 x 0.40
Temperature / K	173(1)
Range scanned θ / °	$2 \leq \theta \leq 24$
Index ranges	h: -9, 8 k: -46, 49 l: -9, 9
Dx / mm	45
No. of measured reflections	5168
No. of unique reflections	5168
No. of reflections with $I > 2\sigma(I)$	4554
No. of least-squares parameters	545
S	1.03
R_1 [$I > 2\sigma(I)$]	0.0691
No. of reflections omitted	2
wR_2 (all reflections)	0.1827
R_{int}	0.000
R_σ	0.0376
Weighting scheme parameters	a = 0.0739 b = 10.076
$(\Delta / \sigma)_{mean}$	< 0.001
Δρ excursions / e Å^{-3}	0.36, -0.30

Description of the structure

Metoprolol tartrate[118] is a 2:1 salt consisting of a racemic mixture of optical isomers of the protonated base and naturally occurring *dextro*-tartaric acid anion. The composite is optically active, which is consistent with crystallisation of the compound in the polar space group $P2_1$. The crystallographic asymmetric unit, as illustrated in the diagram in Figure 3.22, comprises a pair of 2:1 units in which the four cations are related by a pseudo-inversion centre. The two crystallographically independent tartrate ions, both of which have the 2R, 3R-configuration, are located near the pseudo-inversion centre. It is the presence of this pseudo-inversion centre that gave rise to the observed value of $|E^2-1| = 0.839$ for the intensity data. The numbering scheme for the molecules of the asymmetric unit is presented in Figure 3.23.

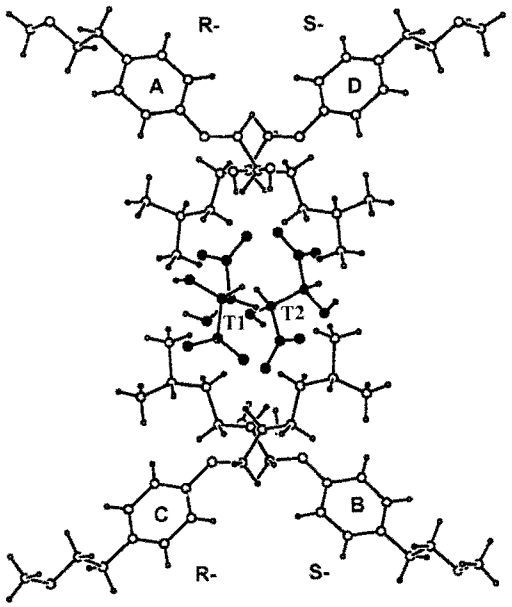

Figure 3.22 Diagram of the asymmetric unit of Metoprolol tartrate. Metoprolol cations are labelled **A**, **B**, **C** and **D**, and for clarity the individual atoms are not numbered. The tartrate ions are labelled **T1** and **T2**.

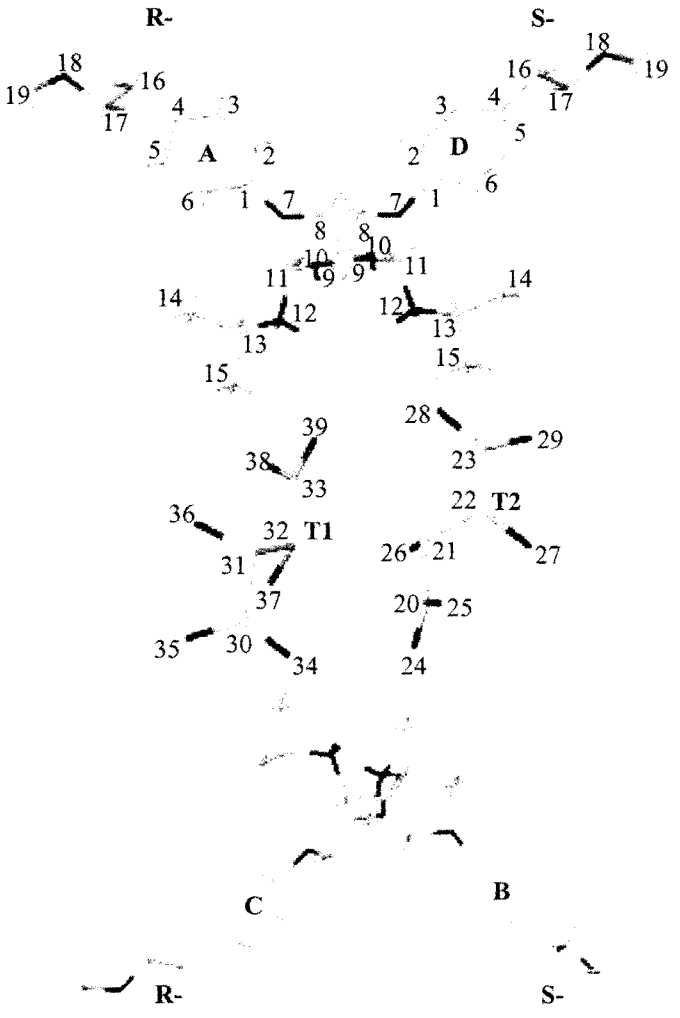

Figure 3.23 The numbering scheme of the metoprolol molecules and the tartrate ions in the asymmetric unit. Only the numbering scheme of metoprolol **A** and **D** molecules is shown. Molecules **B** and **C** have the same numbering scheme as **A** and **D** molecules.

Molecular conformation of Metoprolol tartrate

Table 3.16 lists eleven principal torsion angles defining the conformations of the four independent cations, two of S- and two of R- configuration present in the crystal of the salt [See Figure 3.11 for δ_n definitions]. These cations have essentially the same conformation. The torsion angles δ_5 and δ_{11} with the rotation around the C4-C16 and C16-C17 bonds respectively, show that the side chain with respect to the methoxyethyl side-chain, lies below the phenyl ring and is fully extended.

Table 3.16 Principal torsion angles [°] for the independent cations **A-D** in Form I tartrate

Torsion angle / °	**A (R-)**	**B (S-)**	**C (R-)**	**D (S-)**
δ_1	-170.8(8)	165.9(8)	-168.8(9)	169.3(8)
δ_2	-14(1)	11(1)	-15(1)	9(1)
δ_3	175.5(9)	-176.9(9)	178.3(9)	-175.2(9)
δ_4	-175.7(7)	176.6(7)	-169.8(8)	175.5(8)
δ_5	95(1)	-91(1)	91(1)	-89(1)
δ_6	-84(1)	89(1)	-90(1)	86(1)
δ_7	172.7(7)	-170.5(7)	168.6(8)	-168.8(8)
δ_8	-69(1)	66(1)	-69(1)	68(1)
δ_9	-155.7(8)	161.2(8)	-155.5(9)	158.1(8)
δ_{10}	86(1)	-76(1)	83(1)	-81(1)
δ_{11}	175.6(9)	176.5(8)	179.1(8)	-175.0(8)

The torsion angles in this Table are arranged as in Tables 3.9 and 3.12

Hydrogen bonding and C-H•••π ring interactions

A PLATON[114] geometrical structure analysis revealed extensive hydrogen bonds that involve all of the tartrate carboxylate O atoms, the –OH and $-NH_2^+$ functions of the metoprolol cations. These interactions are shown in Figure 3.24. Two cations of S-configuration are bridged by one of the two crystallographically independent tartrate ions via N^+-H•••O^- [carboxylato] hydrogen bonds. The second tartrate ion bridges two cations of R-configuration in an analogous fashion. Cations of R-and S-configuration are linked via additional N^+-H•••O^- and O-H•••O^- [carboxylato] bonds giving rise to an infinite series of hydrogen bonded rings and chains in the crystal. Hydrogen bonding involves eight crystallographically distinct N^+-H•••O^- bonds [N•••O distance range 2.72(1)-2.82(1)Å] and they are presented in Table 3.17.

PLATON[114] also revealed six C-H•••π ring interactions for the metoprolol salt. All these interactions have symmetry operations other than x, y, z indicating that all the interactions are between molecules of different asymmetric units and they are listed in Table 3.18. The π•••π-ring distances were not considered as representing significant interactions as they were all either greater than or equal to 5Å.

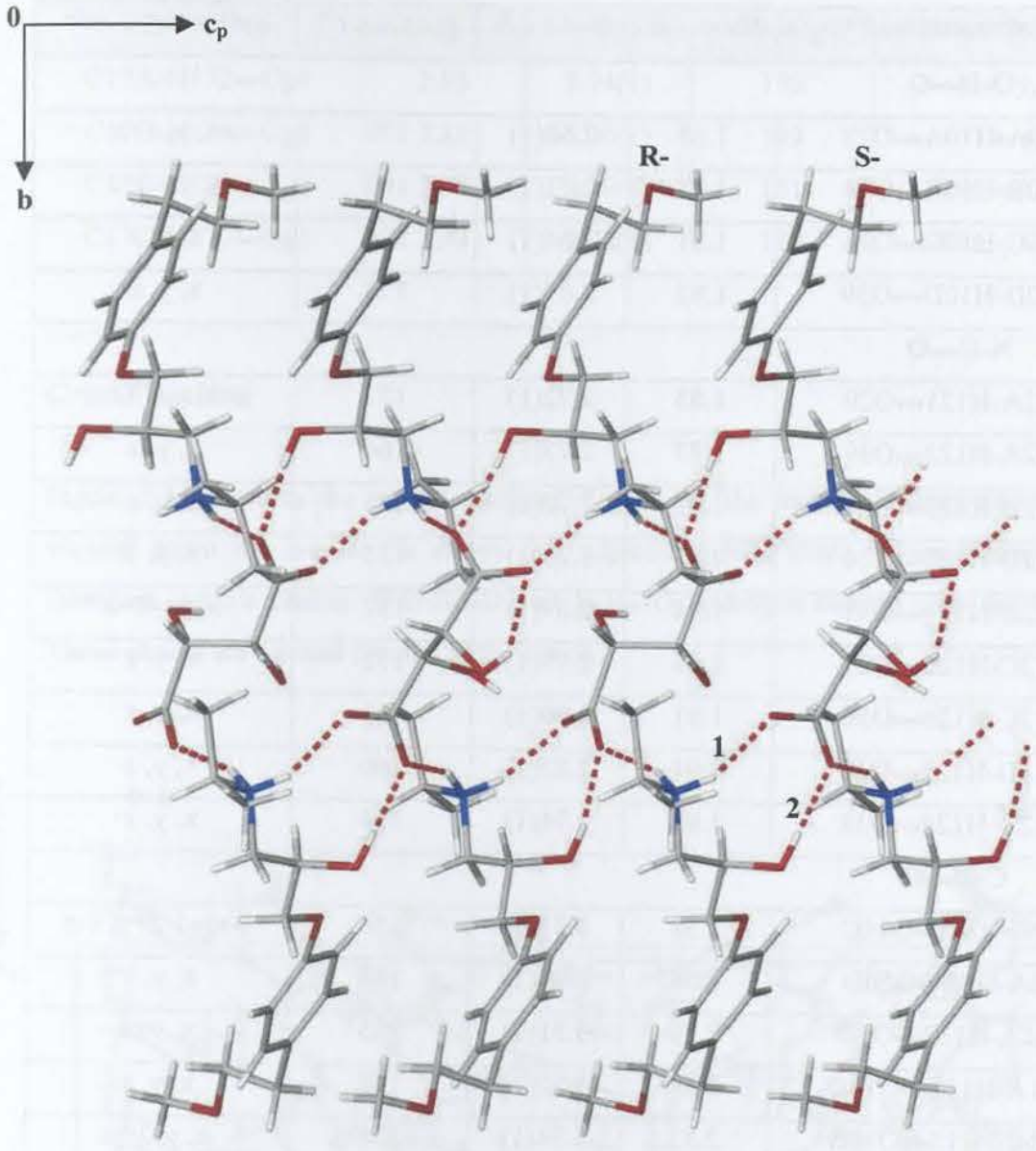

Figure 3.24 Hydrogen bonding interactions involving N^+-H•••O^- and O-H•••O^- [labelled **1** and **2** respectively] of the metoprolol salt.

Table 3.17 Hydrogen bonds for Metoprolol tartrate

Hydrogen bond	H•••A / Å	D•••A / Å	D-H•••A / °	Symmetry Code
O-H•••O				
O10A-H10A•••O28	1.85	2.68(1)	170	x, y, 1+z
O10B-H10B•••O34	1.88	2.71(1)	168	x, y, -1+z
O10C-H10C•••O24	1.81	2.64(1)	174	x, y, z
O10D-H10D•••O39	1.82	2.65(1)	175	x, y, z
N-H•••O				
N12A-H121•••O29	1.85	2.72(1)	157	x, y, 1+z
N12A-H122•••O39	1.87	2.77(1)	164	x, y, z
N12B-H123•••O24	1.92	2.77(1)	153	x, y, z
N12B-H123•••O26	2.52	3.23(1)	135	x, y, z
N12B-H124•••O35	1.94	2.81(1)	157	x, y, -1+z
N12C-H125•••O25	1.93	2.77(1)	152	x, y, z
N12C-H126•••O34	1.91	2.80(1)	161	x, y, z
N12D-H127•••O28	1.94	2.82(1)	160	x, y, z
N12D-H128•••O38	1.88	2.74(1)	154	x, y, z
C-H•••O				
C3D-H3D•••O18C	2.58	3.43(1)	150	1-x, -1/2+y, 1-z
C8A-H82•••O10D	2.58	3.43(1)	144	x, y, x
C11A-H112•••O7D	2.59	3.51(1)	155	x, y, z
C11A-H112•••O10D	2.59	3.37(1)	135	x, y, z
C11C-H115•••O10B	2.53	3.34(1)	139	x, y, 1+z
C11D-H117•••O10A	2.57	3.36(1)	138	x, y, -1+z
C15A-H151•••O38	2.51	3.42(1)	155	-1+x, y, z
C15C-H158•••O35	2.58	3.48(1)	152	-1+x, y, z

Table 3.18 C-H•••π ring interactions for Metoprolol tartrate

Interaction	H•••Cg / Å	C•••Cg / Å	C-H•••Cg / °	Symmetry Code
C17A-H172•••Cg4	2.85	3.74(1)	150	1+x, y, z
C17B-H174•••Cg3	2.88	3.76(1)	149	-1+x, y, z
C17C-H175•••Cg2	2.90	3.79(1)	151	1+x, y, 1+z
C17D-H177•••Cg1	2.94	3.82(1)	148	-1+x, y, -1+z

Crystal packing

Figure 3.25 presents the crystal packing diagram of the metoprolol tartrate structure viewed down the a-axis. It shows that adjacent motifs share common anions and therefore infinite chains of O-H•••O and N-H•••O hydrogen bonded ions are formed. These chains are stacked parallel to the c-axis.

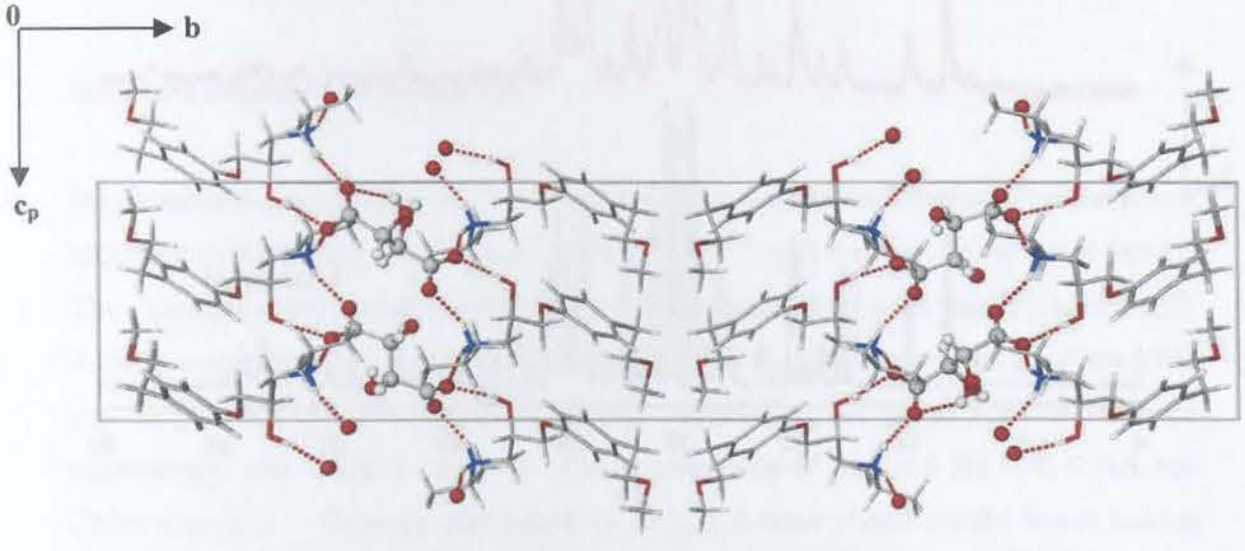

Figure 3.25 Diagram illustrating the crystal packing of metoprolol tartrate down the a-axis. The intermolecular hydrogen bonding is shown in red dotted lines and the tartrate ions are presented in ball and stick mode.

Powder X-ray diffraction

The experimental and computed traces for the metoprolol tartrate structure are presented in Figure 3.26. The PXRD pattern for this salt has been reported previously,[118] although its resolution is lower than that in Figure 3.26. These traces show a very close match with each other which indicates that metoprolol tartrate did not transform on grinding for sample preparation and that the computed trace can serve as reference for the identification of this salt. The slight shift to lower 2θ values for the experimental trace is due to the difference in temperatures at which the information for the traces was obtained.

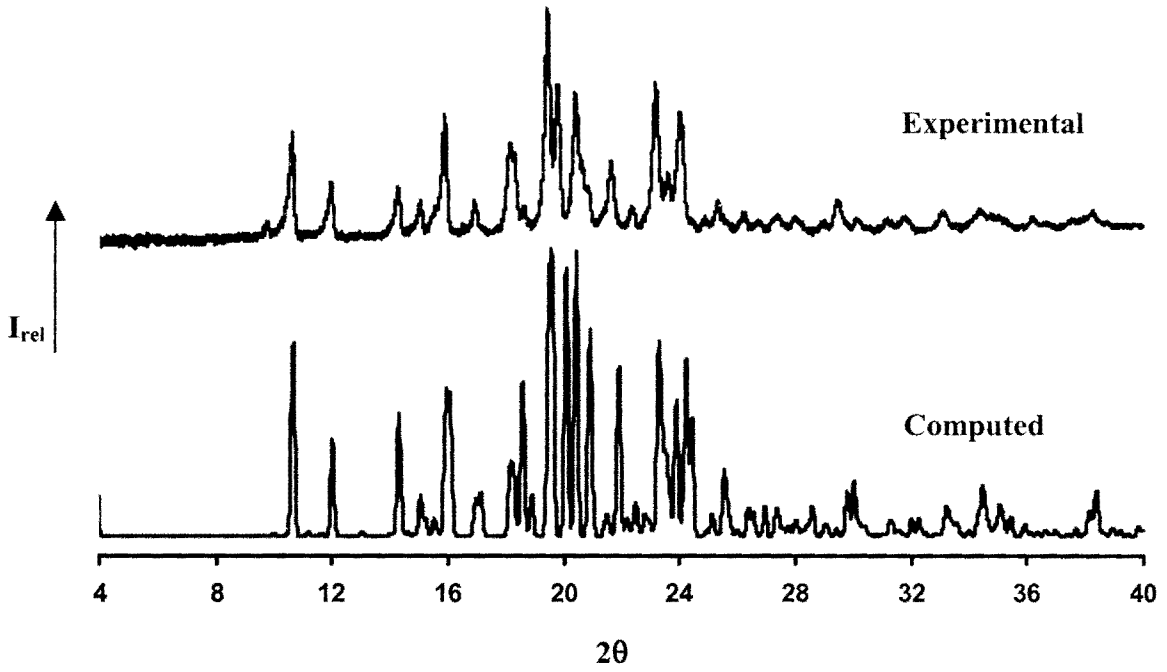

Figure 3.26 Computed [173K] and experimental [295K] PXRD traces for metoprolol tartrate.

X-ray Crystallographic Analysis of Oxprenolol Free Base

Single Crystal X-ray Diffraction

Data-collection and space group determination

X-ray intensity data-collection for oxprenolol free base was performed at 173(2)K on a Nonius Kappa CCD diffractometer. A suitable crystal was mounted under paratone N oil[115] to glue the crystal to the glass fibre on freezing. Laue $\bar{1}$ symmetry was revealed upon inspection of the intensity-weighted reciprocal lattice indicating the triclinic crystal system. Program XPREP[103] indicated the two possible space groups, namely, P1 and P $\bar{1}$, and furthermore the intensity statistics provided by this program showed $|E^2-1| = 0.908$, indicating a centrosymmetric space group and therefore P $\bar{1}$ was chosen. This choice was justified by the successful refinement of the structure in this space group. The centrosymmetric space group was expected since the free base had been prepared from the racemic hydrochloride salt.

Structure solution and refinement

Direct methods in SHELXS-97[104] were used to solve the oxprenolol structure. The atoms identified in the E-map were refined in SHELXL-97[113] with isotropic temperature factors. The asymmetric unit comprises two oxprenolol molecules labelled **A** and **B** [Figure 3.27]. A Fourier map revealed that C18 and C19 were each disordered over two positions. For a given pair of C18 and C19, site-occupancy factors of x, 1-x and y, 1-y were assigned respectively, with x and y variables. The refined value of the s.o.f. for both C18A and C19A was 0.53. Distance constraints of 1.25(5) Å were placed on the bonds linking these disordered atoms to the parent atoms. A Fourier map showed the majority of the hydrogen atoms and they were placed in fixed geometric positions using a riding model except for the hydroxyl and amino hydrogen atoms which were located in subsequent difference Fourier maps. These hydrogen atoms were allowed to refine with O-H and N-H distances restrained to 1.000(5) Å. All the non-hydrogen atoms with satisfactory

isotropic thermal parameters were refined anisotropically. Least-squares weights were employed in the final cycles of the refinement. The crystal and refinement parameters are presented in Table 3.19.

Table 3.19 Crystal and refinement parameters for oxprenolol

Formula unit	$C_{15}H_{25}NO_3$
Formula weight / $gmol^{-1}$	267.35
Crystal system	Triclinic
Space group	P $\bar{1}$
a / Å	4.9271(2)
b / Å	16.384(1)
c / Å	18.952(1)
α / °	81.437(1)
β / °	87.091(1)
γ / °	83.707(2)
Volume / $Å^3$	1502.8(1)
Z	4
$Density_{calc}$ / g cm^{-3}	1.173
μ(MoKα) / mm^{-1}	0.081
F(000)	576
Crystal size / mm^3	0.10 x 0.10 x 0.40
Temperature / K	173(2)
Range scanned θ / °	$1 \leq \theta \leq 28$
Index ranges	h: -5, 6 k: -18, 21 l: -20, 24
Dx / mm	35
No. of measured reflections	9426
No. of unique reflections	6411
No. of reflections with $I > 2\sigma(I)$	2356
No. of least-squares parameters	362
S	1.04
R_1 [$I > 2\sigma(I)$]	0.0937
No. of reflections omitted	1
wR_2	0.3291
R_{int}	0.044
R_σ	0.2023
Weighting scheme parameters	a = 0.1201 b = 1.9005
$(\Delta / \sigma)_{mean}$	0.01
$\Delta\rho$ excursions / $e.Å^{-3}$	0.67, -0.54

Description of the structure

Oxprenolol crystallises in the triclinic space group P $\bar{1}$ with Z = 4 molecules per unit cell. This indicates two molecules per asymmetric unit since P $\bar{1}$ has two equivalent positions. An ORTEP[116] stereo diagram of the asymmetric unit is presented in Figure 3.27. The relatively small thermal ellipsoids of the oxprenolol structure indicate its reduced thermal motion, which led to a higher precision of its structural determination. The crystal is racemic and the unit cell contains two molecules with R- and two with S-configuration. Molecules **A** and **B** in the asymmetric unit both have R-configuration at the C9 stereogenic centre. In general, the S-enantiomers of beta-blockers are more potent than the R-enantiomers.[119]

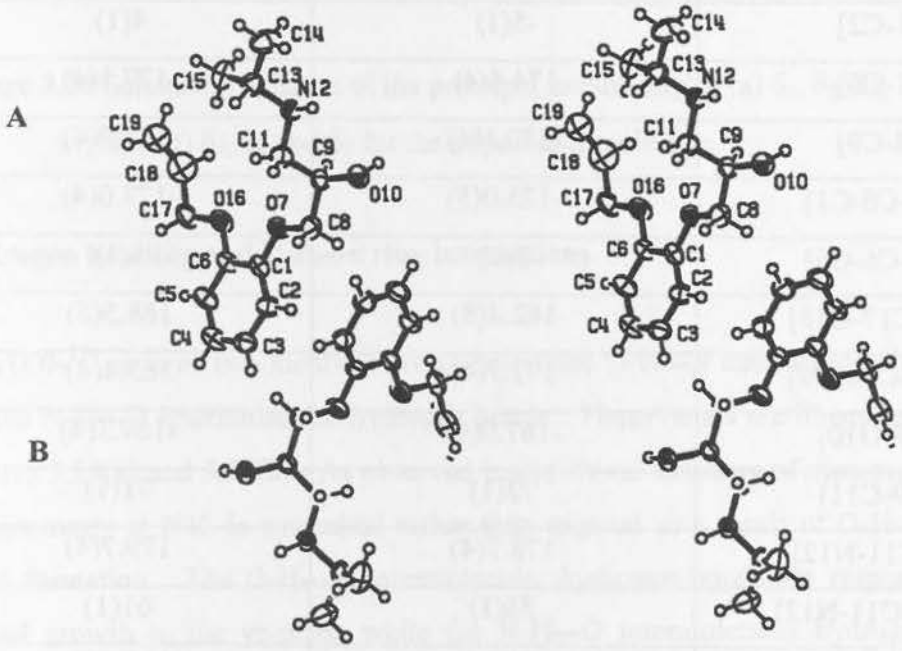

Figure 3.27 Stereo view of the ORTEP diagram for the two crystallographically independent oxprenolol molecules **A** and **B**. Thermal ellipsoids are drawn at the 50% probability level. Atomic numbering for molecule **B** follows that used for molecule **A**. For clarity only the major disordered components of atoms C18A and C19A are drawn.

Molecular conformation of oxprenolol

The principal torsion angles for the two crystallographically independent oxprenolol molecules **A** and **B**, both of which have the R-configuration at atom C9 are listed in Table 3.20 and are illustrated in Figure 3.28. Comparison of the data shows that these molecules have essentially the same conformation. The values for torsion angles δ_{10} and δ_{11} correspond to the atoms C11, N12, C13, C14 and C15 of the side chain lying above the phenyl ring plane for both **A** and **B** molecules.

Table 3.20 Principal torsion angles [°] for the two crystallographically independent **A** and **B** oxprenolol molecules

Torsion angle	A	B
δ_1 [C8-O7-C1-C2]	-5(1)	4(1)
δ_2 [C8-O7-C1-C6]	174.4(4)	-177.1(4)
δ_3 [C1-O7-C8-C9]	-170.1(4)	-177.9(4)
δ_4 [C17-O16-C6-C1]	-173.0(5)	-177.0(4)
δ_5 [C17-O16-C6-C5]	8(1)	5(1)
δ_6 [C6-O16-C17-C18]	162.4(8)	168.5(5)
δ_7 [C13-N12-C11-C9]	171.7(4)	163.4(4)
δ_8 [O7-C8-C9-O10]	-167.0(4)	-169.3(4)
δ_9 [O7-C8-C9-C11]	72(1)	71(1)
δ_{10} [C8-C9-C11-N12]	178.7(4)	179.7(4)
δ_{11} [O10-C9-C11-N12]	58(1)	61(1)
δ_{12} [O16-C17-C18-C19]	-159.7(3)	115.6(7)

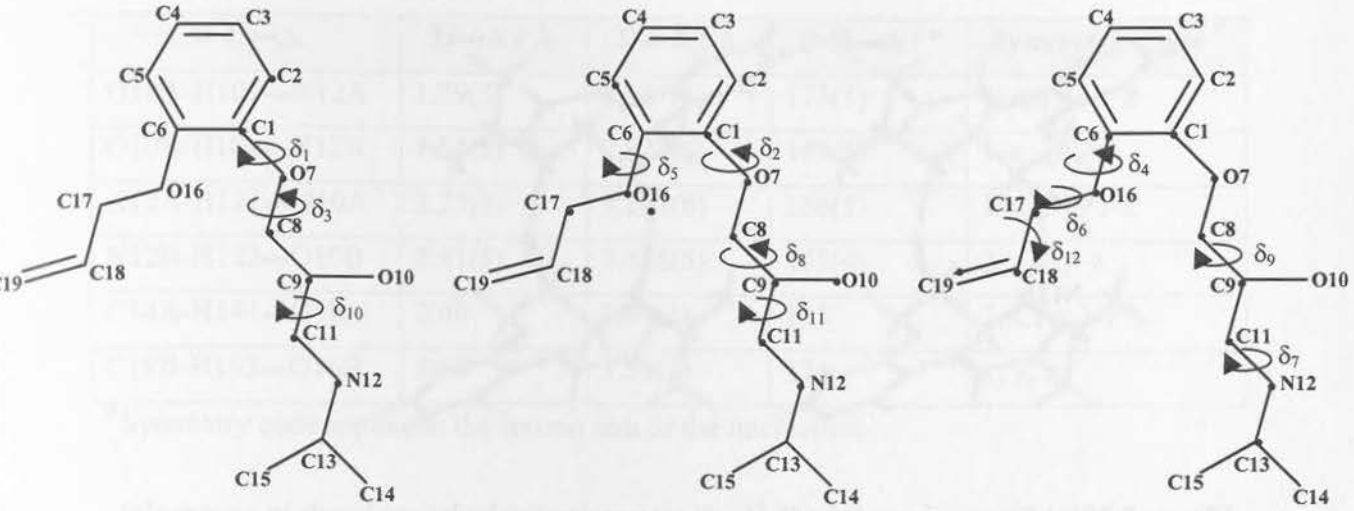

Figure 3.28 Schematic diagram of the principal torsion angles (a) δ_1, δ_3, δ_{10} (b) δ_2, δ_5, δ_8, δ_{11} (c) δ_4, δ_6 and δ_7 for the oxprenolol molecule.

Hydrogen bonding and C-H•••π ring interactions

PLATON[114] showed two identical inversion-related O-H•••N and two identical inversion-related N-H•••O intermolecular hydrogen bonds. These bonds are illustrated in stereo in Figures 3.29(a) and 3.29(b). As observed in the crystal structure of metoprolol free base, the geometry at N12 is pyramidal rather than trigonal as a result of O-H•••N hydrogen bond formation. The O-H•••N intermolecular hydrogen bonds are responsible for the crystal growth in the yz-plane while the N-H•••O intermolecular hydrogen bonds are responsible for the crystal growth along the shortest axis, a. These hydrogen bonds contribute to the stability of this crystal. The O-H•••N hydrogen bond connects the oxprenolol molecules within the same unit cell. PLATON[114] also revealed two additional C-H•••O intermolecular hydrogen bonds that stabilise the oxprenolol structure, namely, C14A-H141•••O10A and C19B-H193•••O16B. Table 3.21 presents these hydrogen bonds.

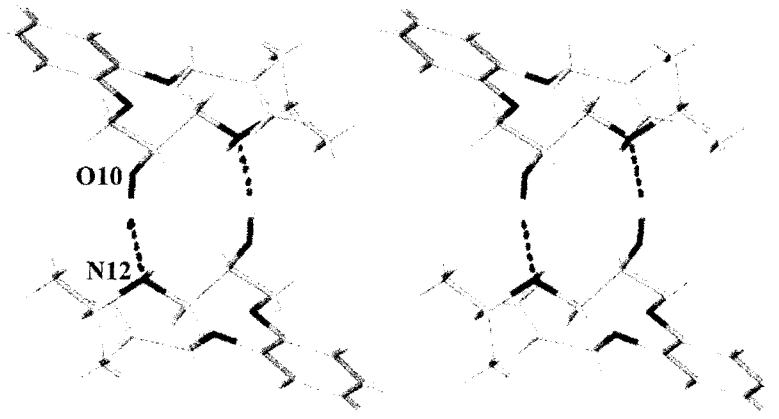

Figure 3.29(a) Stereo view of the O-H•••N intermolecular hydrogen bonds in oxprenolol.

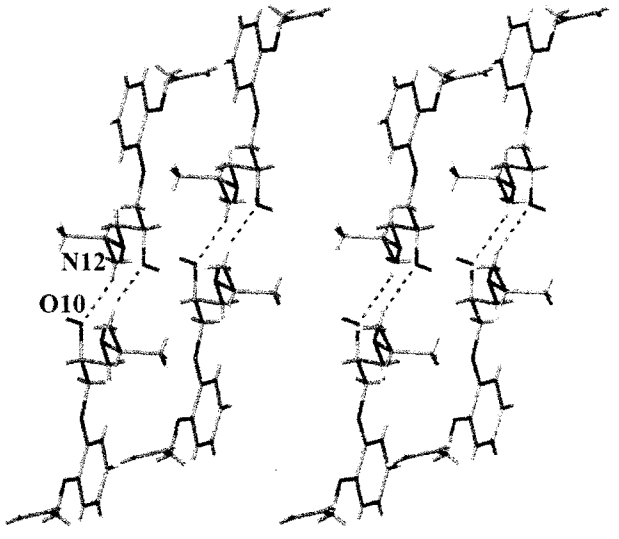

Figure 3.29(b) Stereo view of the N-H•••O intermolecular hydrogen bonds in oxprenolol.

Table 3.21 Hydrogen-bonding interactions for oxprenolol

D-H•••A	H•••A / Å	D•••A / Å	D-H•••A / °	Symmetry Code #
O10A-H101•••N12A	1.79(5)	2.787(6)	173(1)	1-x, 1-y, 1-z
O10B-H102•••N12B	1.84(5)	2.821(6)	163(5)	1-x, -y, -z
N12A-H121•••O10A	2.27(3)	3.207(6)	156(3)	1-x, 1-y, 1-z
N12B-H122•••O10B	2.41(5)	3.338(5)	153(4)	2-x, -y, -z
C14A-H141•••O10A	2.60	3.44(1)	143	2-x,1-y,1-z
C19B-H193•••O16B	2.58	3.53(1)	174	x, y, z

Symmetry code applies to the second unit of the interaction

Three C-H•••π ring interactions were indicated by PLATON[114] and these are presented in Table 3.22.

Table 3.22 C-H•••π ring interactions for oxprenolol

Interaction	H•••Cg / Å	C•••Cg / Å	C-H•••Cg / °	Symmetry Code #
C2B-H2B•••Cg	3.093	3.874(6)	141	x, y, z
C17A-H17B•••Cg	2.732	3.631(6)	151	-1+x, y, z
C17B-H174•••Cg	3.121	4.063(6)	160	-1+x, y, z

Symmetry code applies to the second unit of the interaction

Crystal packing

The crystal packing of the oxprenolol structure projected down the a-axis is presented in Figure 3.30. It shows identical inversion-related hydrogen bonds of the type O-H•••N labelled **1** and **1'** for the oxprenolol molecule **A**, with O•••N 2.787(6) Å and the angle O-H•••N 173(1)°. The identical inversion-related hydrogen bonds of the type O-H•••N for the oxprenolol molecule **B** are labelled **2** and **2'**, with O•••N 2.821(6) Å and the angle O-H•••N 163(5)°. For clarity the N-H•••O intermolecular hydrogen bonds are not shown in this diagram. Both centrosymmetrically related molecules act as proton donors and acceptors.

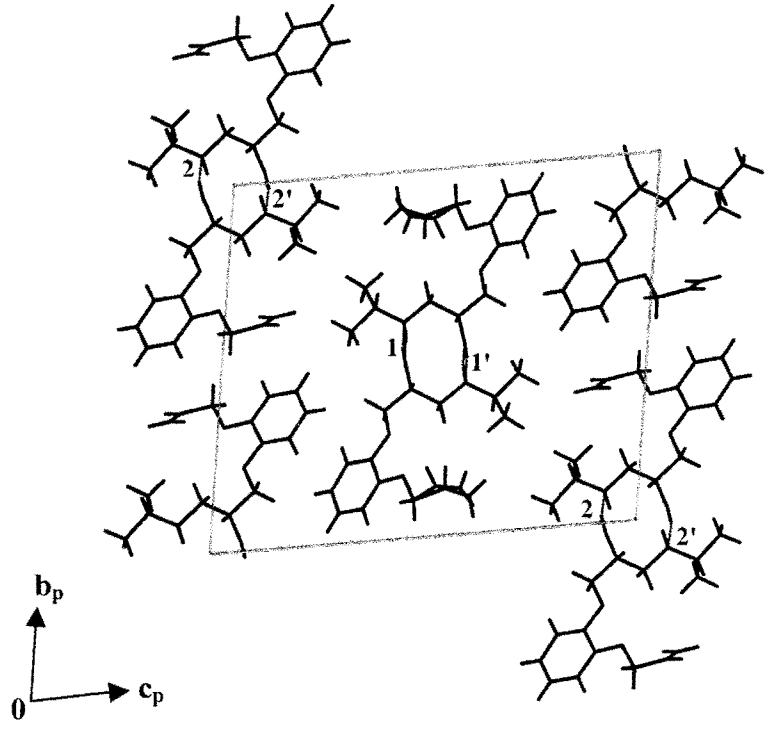

Figure 3.30 Crystal packing diagram of oxprenolol viewed down the a-axis. Hydrogen bonds shown in red are of the O-H•••N type.

Powder X-ray diffraction

Experimental and computed PXRD patterns of oxprenolol are presented in Figure 3.31. The correctness of the single crystal structural model is shown by the close agreement between the computed and experimental patterns. The relative intensity distribution of the peaks of the experimental pattern is similar to that of the computed pattern indicating the lack of preferred orientation in the analysed sample. The slight shifts of the experimental pattern with respect to the computed pattern to lower 2θ are due to temperature differences at which the respective traces were obtained.

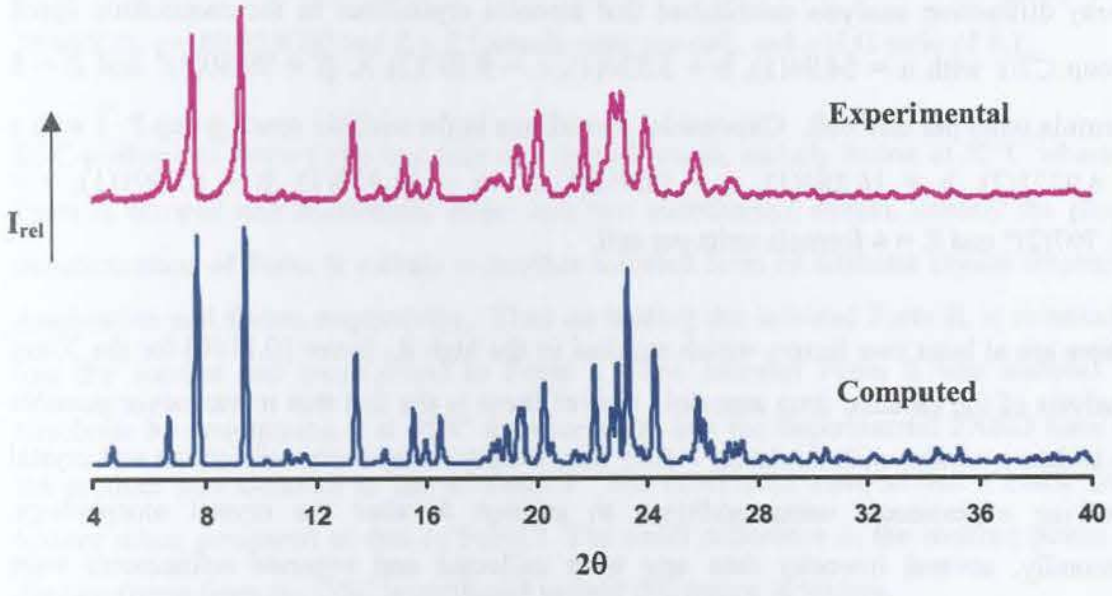

Figure 3.31 Computed [173(2)K] and experimental PXRD patterns [295K] of oxprenolol.

Conclusion

The main objective of the study described in this chapter was to isolate and characterise by thermal, spectroscopic, microanalytical and diffraction methods, racemic antihypertensive agents. The two novel free bases, namely oxprenolol and metoprolol were prepared from the salts of oxprenolol hydrochloride and metoprolol tartrate respectively.

TGA analysis showed that two salts, namely metoprolol tartrate and oxprenolol hydrochloride, and three free bases, were unsolvated. DSC analysis revealed only one thermal event for each, namely fusion with melting points of 152, 52, 77, 121 and 108°C for atenolol, metoprolol, oxprenolol, metoprolol tartrate and oxprenolol hydrochloride respectively.

X-ray diffraction analysis established that atenolol crystallises in the monoclinic space group C2/c with a = 54.94(1), b = 5.520(1), c = 9.707(2) Å, β = 99.80(3)° and Z = 8 formula units per unit cell. Oxprenolol crystallises in the triclinic space group $P\bar{1}$ with a = 4.9271(2), b = 16.384(1), c = 18.952(1) Å, α = 81.437(1), β = 87.091(1), γ = 83.707(2)° and Z = 4 formula units per cell.

There are at least two factors which resulted in the high R_1 factor [0.1160] for the X-ray analysis of the racemic drug atenolol. One of these is the fact that it was never possible to isolate a crystal with thickness > 0.15 mm, despite many recrystallisations and crystal growing experiments using additives to attempt to alter the crystal morphology. Secondly, several intensity data sets were collected and separate refinements were performed. In all cases, the two-fold disorder of atoms C14, C17 and C18 was observed, indicating that this is an inherent feature of the crystallisation of atenolol.

As regards the first factor, it has long been recognised that the presence of small amounts of impurities or additives have substantial effects on the kinetics of crystal nucleation, growth morphology and dissolution.[120,121] The presence of impurities may also

profoundly influence the growth of a crystal. Attempts were made to grow atenolol crystals in the presence of various additives used in small amounts with the aim of controlling or inhibiting the crystal growth along the longest dimension. However these attempts were unsuccessful. Some of the additives used were benzoic acid, D-and L-tartaric acid, acetylsalicylic acid, 4-acetamidophenol and acetanilide. These additives have similar molecular structure to that of atenolol except D- and L-tartaric acid.

Two forms of metoprolol [Form I and Form II] were isolated and characterised by thermal and diffraction methods. Form I is the unsolvated form and it was crystallised from either n-hexane or water. Form II is the solvate in which n-hexane is included. Form II crystals were obtained at 5°C from n-hexane. Form I crystallises in the monoclinic space group $P2_1/n$ with a = 16.1940(5), b = 5.4409(2), c = 17.8670(7) Å, β = 100.63(2)° and Z = 4 formula units per unit cell. Form II crystallises in the triclinic space group $P\bar{1}$ with a = 15.7147(6), b = 15.7002(9), c = 30.942(2) Å, α = 85.925(2), β = 78.662(2), γ = 60.833(2)° and Z = 2 formula units per cell, and a H:G ratio of 8:1.

DSC analysis of Form I showed only one thermal event, namely fusion at 52°C whereas Form II showed one exothermic event and two endothermic events, namely the phase transformation of Form II solvate to another solvated form of different crystal structure, desolvation and fusion respectively. Thus on heating the solvated Form II, it eventually lost the solvent and transformed to Form I. The solvated Form II was allowed to desolvate by maintaining it at 35°C for four hours and the experimental PXRD trace of the product was identical to that of Form I. The desolvated material had a much finer texture when compared to that of Form I. The small difference in the melting points of the two forms from the DSC is attributed to their difference in texture.

Previous studies have shown that solvation/desolvation processes of some solvates improve their technological properties such as flowability, texture, particle size distribution and compressibility.[122,123] Furthermore when Form II crystals were exposed to air they became opaque spontaneously and the PXRD pattern of the product was

identical to that of Form I. It was concluded that Form II is metastable and it readily transforms to Form I, the more stable form.

Metoprolol tartrate crystallises in the monoclinic space group $P2_1$ with a = 8.4395(2), b = 45.653(1), c = 9.6019(3) Å, β = 90.733(2)° and Z = 4 formula units per cell. The metoprolol and oxprenolol free bases prepared from metoprolol tartrate and oxprenolol hydrochloride respectively were considered to be of novel interest, given that very little information regarding their structures, thermal behaviour and possible exploitation for medicinal purposes has been published. The inclusion of these free bases in cyclodextrins as a route for modifying their delivery properties has been explored and it is described in the chapters that follow.

Chapter 4 – γ-CD Inclusion Complexes

Complex preparation

Crystalline complexes of metoprolol and oxprenolol free bases with γ-CD were obtained from evaporation of hot aqueous solutions [~ 60°C] of cyclodextrin and drug in 1:1 molar ratios at an elevated temperature of 40°C. Colourless rods were obtained on standing for a period of one to two weeks at an elevated temperature. Due to the high solubility of the host and its complexes in both aqueous solution and organic solvents the density of the crystal was not measured. The complexes of γ-CD with each drug, grown at a higher temperature, will be referred to as METGCD and OXPRGCD respectively and will be described herein.

Microanalysis

The host-guest ratios of the γ-CD complexes were determined by carbon, hydrogen and nitrogen microanalysis of the partially hydrated complexes. Prior to microanalysis, the crystals of the complexes were kept in open vials for a week to allow water vapour equilibrium to be reached. Each of the METGCD and OXPRGCD complexes crystallises in a 3:2 host:guest ratio. The microanalysis results are presented in Table 4.1.

Table 4.1 C, H, N microanalysis results [n = 3] for METGCD and OXPRGCD

Complex	**Experimental** *			**Calculated**		
	%C	%H	%N	%C	%H	%N
METGCD $3(C_{48}H_{80}O_{40})\cdot2(C_{15}H_{25}NO_3)\cdot35.4H_2O$	41.20	7.18	0.55	40.90	7.19	0.72
OXPRGCD $3(C_{48}H_{80}O_{40})\cdot2(C_{15}H_{23}NO_3)\cdot39.9H_2O$	40.86	7.12	0.55	40.63	7.11	0.54

* Standard deviation in experimental percentage ~ 0.3

Thermal analysis

HSM was used to analyse the thermal behaviour of the complexes upon heating at a constant rate of 10°C / min. The analyses were done under silicone oil to assess the presence of included water as would be indicated by bubble formation. The visual interpretations of the changes observed in the crystals of METGCD and OXPRGCD upon heating are illustrated in Figures 4.1 and 4.2 respectively. Photographs of the METGCD and OXPRGCD crystals were recorded at the start of the analysis at room temperature [22 and 25°C respectively].

The beginning of opacity and the cracking of the METGCD crystal were observed at 112°C and vigorous bubbling was observed from 120°C and stopped at 140°C. The first signs of decomposition took place at 230°C and it was noticed by the change in the colour of the crystals. Accompanying decomposition was the further bubbling of the METGCD crystals at 250°C and it continued until 300°C.

For OXPRGCD initial bubbling of the crystals was observed at 100°C and vigorous bubbling took place at 108°C and continued until 130°C. At 198°C the first signs of decomposition were observed and its associated bubbling took place from 220°C.

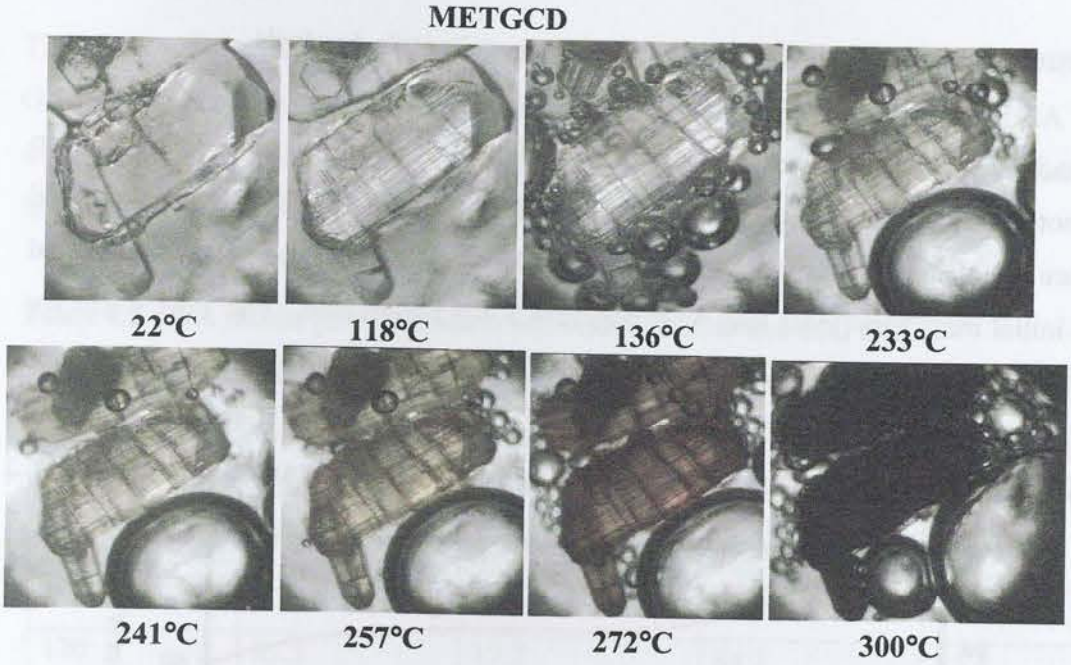

Figure 4.1 HSM photographs taken at various temperatures for crystals of the METGCD complex.

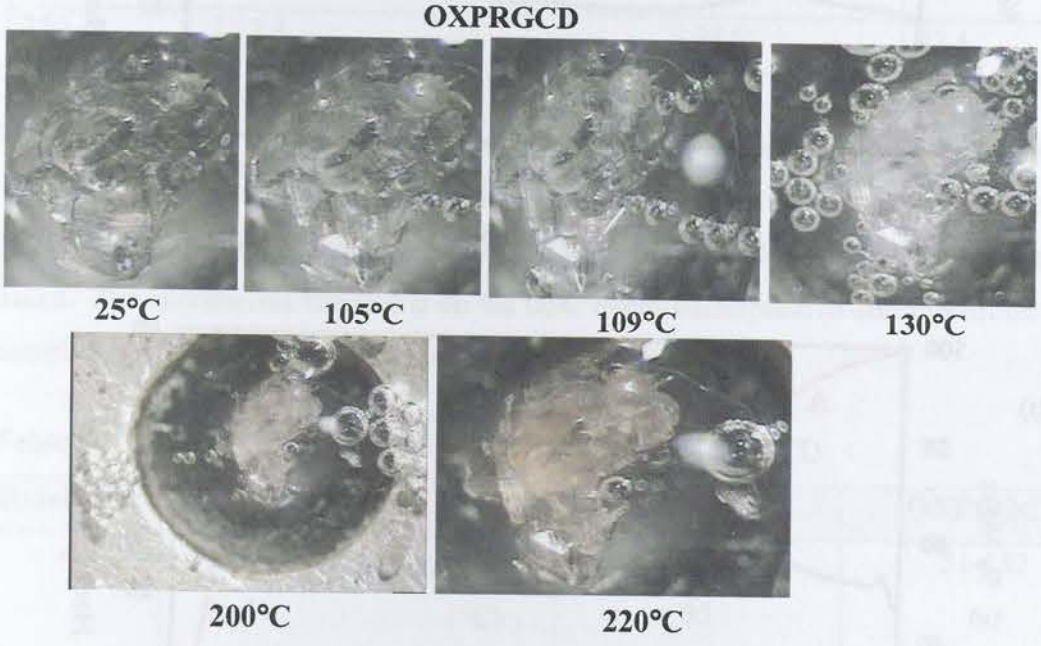

Figure 4.2 HSM photographs taken at various temperatures for crystals of the OXPRGCD complex.

Differential Scanning Calorimetry and Thermogravimetric Analysis

DSC and TGA analyses were performed on fresh crystals directly after removal from their mother liquor. DSC and TGA traces for METGCD and OXPRGCD are presented in Figure 4.3. The water content of the METGCD and OXPRGCD complexes, indicated by the initial mass loss [mass loss A] in Figure 4.3 was determined. The TGA traces for the METGCD and OXPRGCD complexes show mass loss of 12.6% and 14.0% respectively in the temperature range 30-150°C. This establishes the γ-CD:drug:H_2O ratio of 3:2:35.4 and 3:2:39.9 for the METGCD and OXPRGCD complexes respectively.

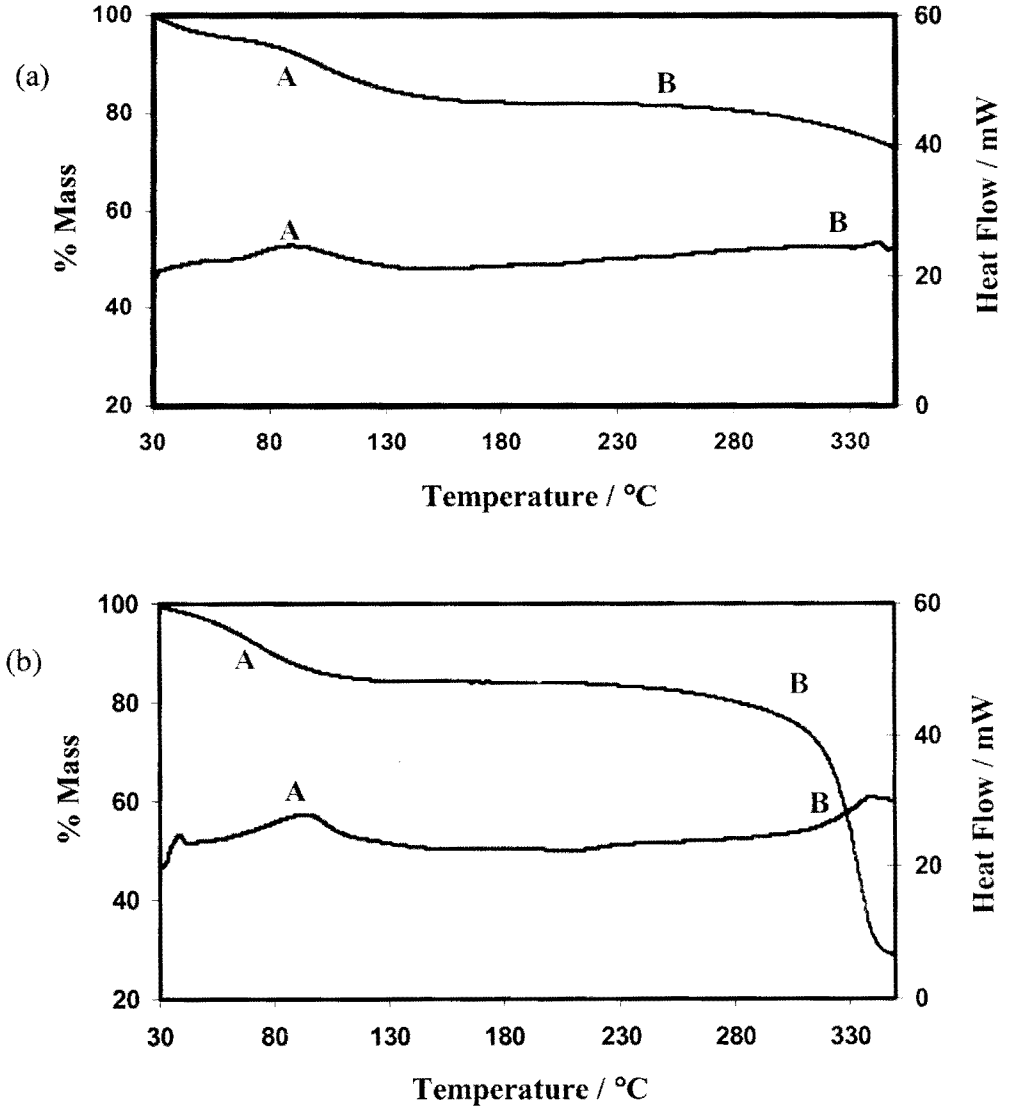

Figure 4.3 TGA [pink] and DSC [blue] traces of (a) METGCD and (b) OXPRGCD.

The onset of decomposition [labelled B] at 240 and 292°C for the METGCD and OXPRGCD complexes respectively is indicated by further mass loss on the TGA traces of the complexes. The TGA results over the whole range of the analyses are summarised in Table 4.2.

Table 4.2 TGA results [n = 4] summarised for METGCD and OXPRGCD

Temp (°C)	METGCD		OXPRGCD	
	% Mass	% Mass Loss	% Mass	% Mass Loss
30	100	0	100	0
60	95.5	4.5	95.2	4.8
100	90.3	9.7	86.0	14
170	82.3	17.7	84.2	15.8
250	81.5	18.5	82.6	17.4
300	79.4	20.6	77.5	22.5
350	72.8	27.2	28.9	71.1

The DSC traces for both METGCD and OXPRGCD show an initial endotherm [labelled A in Figure 4.3], which is characteristic of hydrated complexes. These endotherms are indicative of dehydration that corresponds to the initial mass loss [labelled A] in the TGA traces. The endotherms labelled B on the DSC traces correspond to decomposition of the complexes. The DSC results are summarised in Table 4.3.

Table 4.3 DSC results summarised for METGCD and OXPRGCD

Endotherm	Parameter	METGCD	OXPRGCD
A	Temperature range (°C)	47-156	51-157
	T_{on} (°C)	55	60
	Peak (°C)	85	94
B	Temperature range (°C)	332-348	315-346
	T_{on} (°C)	336	317
	Peak (°C)	344	340

X-ray Crystallographic Analysis of METGCD

Single Crystal X-ray Diffraction

Data-collection and space group determination

On cooling the METGCD crystal in a stream of N_2 gas, the mosaicity of the crystal increased from 1.2 to 3.1°. Thus X-ray intensity data were collected on a Nonius Kappa CCD diffractometer at room temperature [299K] using graphite-monochromated MoKα radiation. XPREP[103] indicated two space group options, $P42_1m$ and $P42_12$. Since the host molecule is chiral, the non-centrosymmetric space group $P42_12$ was selected.

Structure solution and refinement

All γ-CD complexes crystallise in the tetragonal crystal system, space group $P42_12$ and contain three crystallographically independent host molecules that are stacked on top of one another.[124] However, since the γ-CD molecules lie on a four-fold rotation axis, only the coordinates of two glucose units need to be determined for each CD. The structure was solved using the published coordinates for the non-hydrogen CD atoms [excluding the primary hydroxyl oxygen atoms] of the isomorphous 12-crown-4-γ-CD complex.[125] The reason for exclusion of the O6 atoms was to model their possible disorder using the electron density peak heights of their disordered components. The glucopyranose units of the asymmetric unit host molecules were labelled **A1-A2**, **B1-B2** and **C1-C2** respectively. SHELXL-97[113] was used to refine this initial model and to locate the remaining asymmetric unit atoms. In the initial and subsequent difference Fourier maps, the O6 atoms were located. The O6 atoms for the **A1** and **C1** glucopyranose units were each disordered over two sites [the minor disordered component was labelled O7] and they were allowed to refine with s.o.f.'s of x and 1-x for the major and minor disordered components respectively. The temperature factors for the disordered components of **A1** and **C1** glucopyranose units were fixed at 0.09 and 0.07 $Å^2$ respectively [the average values of the isotropic temperature factors of the ordered O6 atoms]. The x values finally

refined to 0.84 and 0.68 for A1 and C1 respectively. The isotropic thermal parameters for all host atoms refined satisfactorily and these atoms were thus subsequently refined anisotropically, except for the disordered O6 atoms. The hydrogen atoms were placed using a riding model and they were all refined isotropically with isotropic temperature factors 1.2 times those of their parent atoms.

The four-fold rotation axis runs directly through the γ-CD cavity and the guest included in this cavity should be disordered at least four-fold. This will always be true unless the guest has four-fold symmetry (C_4) of its own, as is the case for γ-CD inclusion complexes with 12-crown-4 and its metal ion coordination complexes as guests.[125,126,127] This requirement made the interpretation of the difference Fourier map very difficult. The abnormal geometries and distances between the electron density peaks in the host cavities, as well as their low electron densities made it impossible to place any guest atoms. After the placement of all host atoms and oxygen atoms for water molecules, seven of the highest peaks in the map did consistently appear on the four-fold rotation axis. However, the distances between them were abnormally long when compared to the distances between bonded atoms of the metoprolol molecule.

Seventeen sites were identified as water molecules. These were placed with fixed isotropic temperature factors [0.09 $Å^2$ which was the value for O1W] and their site-occupancy factors were allowed to vary, except for O1W which was assigned a full s.o.f. All the water molecules except O1W were disordered as shown by their closeness to the other neighbouring water molecules. The total site-occupancy for all the water molecules at the end of the refinement was 5.2 which translated to 20.8 water molecules for the three independent host molecules. This is considerably less than 35.4 water molecules as calculated from the TGA analysis. Therefore reliable information for the number of water molecules present in the METGCD complex was best obtained from thermal analysis rather than X-ray diffraction. The crystal and refinement parameters are presented in Table 4.4 while the s.o.f.'s of the water molecules are presented in Table 4.5.

Table 4.4 Data collection and refinement parameters for METGCD at 299K

Formula unit	$3(C_{48}H_{80}O_{40})$ •2 $(C_{15}H_{25}O_3N_1)$•35.4H_2O
Formula weight / g mol^{-1}	5062.2
Crystal system	Tetragonal
Space group	$P42_12$
a / Å	23.7279(2)
c / Å	23.0900(3)
Volume / $Å^3$	13000.0(2)
Z	2
Density $_{calc}$ / gcm^{-3}	1.292
μ(MoKα) / mm^{-1}	0.098
F(000)	4470
Temperature of data collection / K	299
Crystal size / mm^3	0.20 x 0.40 x 0.40
Range scanned θ / °	$2 \leq \theta \leq 27$
Index ranges	h: -24, 29 k: -29, 29 l: -27, 28
Dx / mm	46
Total no. of reflections collected	51896
Total no. of unique reflections	13150
No. of reflections with $I > 2\sigma$ (I)	9237
No. of parameters	675
R_{int}, R_σ	0.0463, 0.0477
S	1.07
R_1 (for 8420 reflections)	0.0913
No. of reflections omitted	41
wR_2	0.2785
Weighting scheme	a = 0.1839 b = 4.2155
Δρ excursions / e. $Å^{-3}$	0.85 and –0.94

Table 4.5 Site-occupancy factors for the water molecules of the METGCD structure

Molecule	**s.o.f.**	**Molecule**	**s.o.f.**	**Molecule**	**s.o.f.**
O1W	1	O4BW	0.27	O6DW	0.11
O2AW	0.29	O5AW	0.26	O7W	0.39
O2BW	0.37	O5BW	0.20	O8W	0.22
O3AW	0.52	O6AW	0.21	O9W	0.33
O3BW	0.37	O6BW	0.12	O10W	0.09
O4AW	0.36	O6CW	0.22		

Description of the METGCD structure

The METGCD structure consists of three crystallographically independent host molecules, located on a four-fold rotation axis. Therefore the asymmetric unit consists of only six glucopyranose units, two from each host molecule. Figure 4.4(a) shows a side view of the three crystallographically independent molecules while Figure 4.4(b) shows the asymmetric unit with the labelling scheme of its atoms.

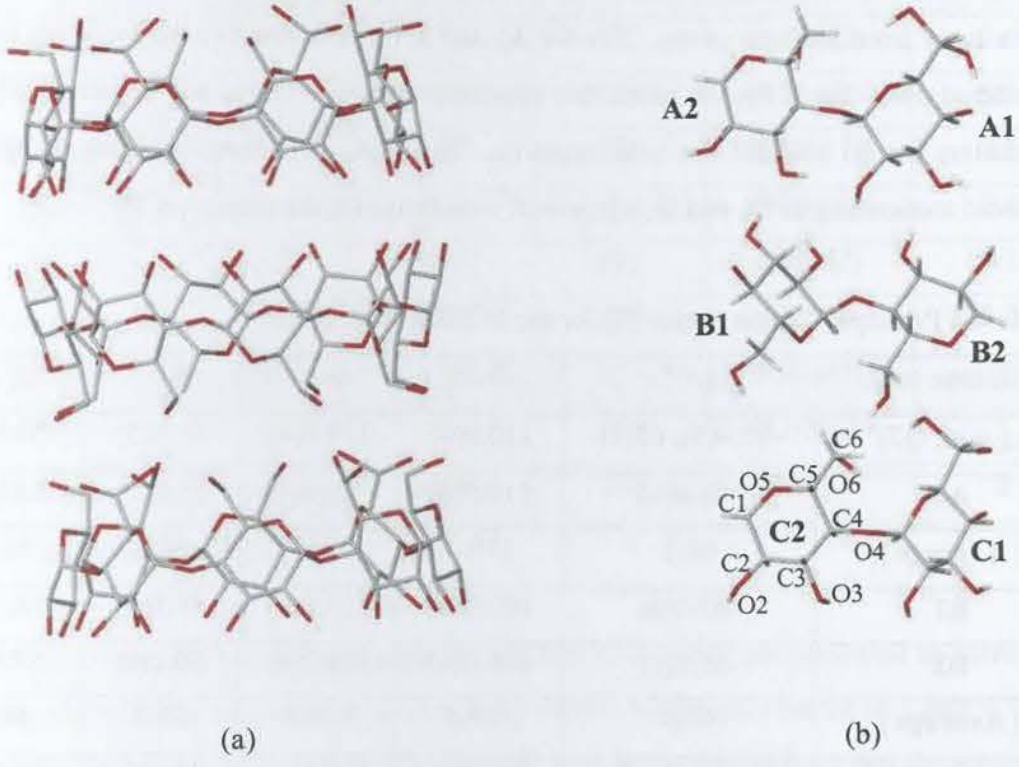

(a) (b)

Figure 4.4 (a) Three crystallographically independent γ-CD host molecules viewed from the side in the METGCD structure (b) The asymmetric unit with glucose unit **C2** showing representative labelling.

Geometrical analysis of the METGCD complex structure

The glucose residues of all three CDs are in the $^4C_1$ chair conformation. The geometrical parameters that describe the conformations of the METGCD host molecules are presented in Tables 4.6-4.8. The principal torsion angles are presented in Table 4.6. The rotation around the C5-C6 bond is described by the **ω** parameter and this gives the direction of the freely rotating C6-O6 bond. The positive sign of **ω** shows that the C6-O6 bond points towards the host cavity while the negative sign indicates that the C6-O6 bond points away from the host cavity. For the **A1** and **C1** glucose units corresponding to the disordered positions of the O6 atom, this parameter is both positive and negative. The **ω** parameters for **B1** and **B2** are both negative. The glycosidic torsion angles **Φ**, **ψ** and pyranoid torsion angles Θ_1 and Θ_2 agree well with those for the parent γ-CD.[137]

Table 4.6 Principal torsion angles [°] for the METGCD structure

Glucose unit	ω / °	Φ / °	ψ / °	Θ_1 / °	Θ_2 / °
A1 (O6, O7)#	-72.9(5), 63(1)	110.9(4)	127.6(4)	56.6(5)	-58.6(4)
A2	-68.6(6)	110.5(4)	125.9(4)	55.6(5)	-56.8(5)
| Average |	68.2	110.7	126.7	56.1	57.7
B1	-62.0(6)	109.0(4)	129.6(4)	56.3(5)	-58.1(5)
B2	-59.6(6)	108.0(4)	128.2(4)	60.2(5)	-59.6(5)
| Average |	60.8	108.5	128.9	58.2	58.8
C1 (O6, O7)#	-63.0(6), 83.7(6)	106.9(4)	128.9(4)	55.6(5)	-58.0(6)
C2	-59.7(5)	107.3(4)	128.6(4)	57.8(4)	-58.8(4)
| Average |*	68.8	107.1	128.7	56.7	58.4

The disordered O6 atoms result in two ω values
* Unweighted average of all recorded values

The parameters for the O4-octagons of the METGCD structure are presented in Table 4.7. The parameters listed are the radii (**r**) from the O4-octagon centroid to O4 atom distance, the O4•••O4' side lengths (**l**), the O4•••O4'•••O4" angle (**a**), the deviation of each O4 atom from the mean O4 plane (**d**) and the O4•••O4'•••O4"•••O4"' torsion angle (**t**).

The values for the **r**, **l**, and **a** parameters show that, in addition to the four-fold symmetry of each host molecule required by the space group $P42_12$, the unique residues also have very close values both within and between host molecules. This is also confirmed by the near-zero values of the O4 torsion angles and the small deviations of the O4 atoms from the mean O4 plane of each host molecule.

Table 4.7 The geometrical parameters of the O4-octagons of the METGCD structure

Glucose unit	r / Å	l / Å	a / °	d / Å	t / °
A1	5.88	4.50	135	-0.004(2)	0.5
A2	5.88	4.49	135	0.004(2)	0.5
Average	**5.88**	**4.49**	**135**	**0.004** *	**0.5**
B1	5.88	4.50	134	-0.001(2)	0.1
B2	5.85	4.50	136	0.001(2)	0.1
Average	**5.86**	**4.50**	**135**	**0.001** *	**0.1**
C1	5.92	4.50	133	0.015(2)	2
C2	5.84	4.50	137	-0.015(2)	2
Average	**5.88**	**4.50**	**135**	**0.015** *	**2**

* Root-mean-square deviation

The tilt and intersaccharidic angles for the METGCD structure are presented in Table 4.8. In keeping with the high degree of symmetry shown by the parameters in Table 4.7, the tilt angles are all positive. The relatively small positive angles indicate that the secondary sides of the CD host molecules are only slightly more open than their primary sides, rendering them the shape of a truncated cone.

Table 4.8 φ and τ parameters for the METGCD structure

Glucose unit	φ / °	τ_1 / °	τ_2 / °
A1	116.5(3)	12.2(1)	13.0(1)
A2	116.7(3)	12.0(1)	11.7(1)
Average	**116.6**	**12.1**	**12.3**
B1	116.4(3)	14.6(1)	15.4(1)
B2	116.9(3)	14.1(1)	15.4(1)
Average	**116.6**	**14.3**	**15.4**
C1	115.2(3)	15.6(1)	15.0(1)
C2	117.7(3)	15.1(1)	15.0(1)
Average	**116.4**	**15.3**	**15.0**

Guest inclusion

The location of the host molecule on a four-fold rotation axis and the guest molecule being not symmetrical and disordered over four positions resulted in the unsuccessful modelling of the latter. The stereo diagram of the highest electron density peaks [0.82-0.40 e $Å^{-3}$] in the host cavities is presented in Figure 4.5.

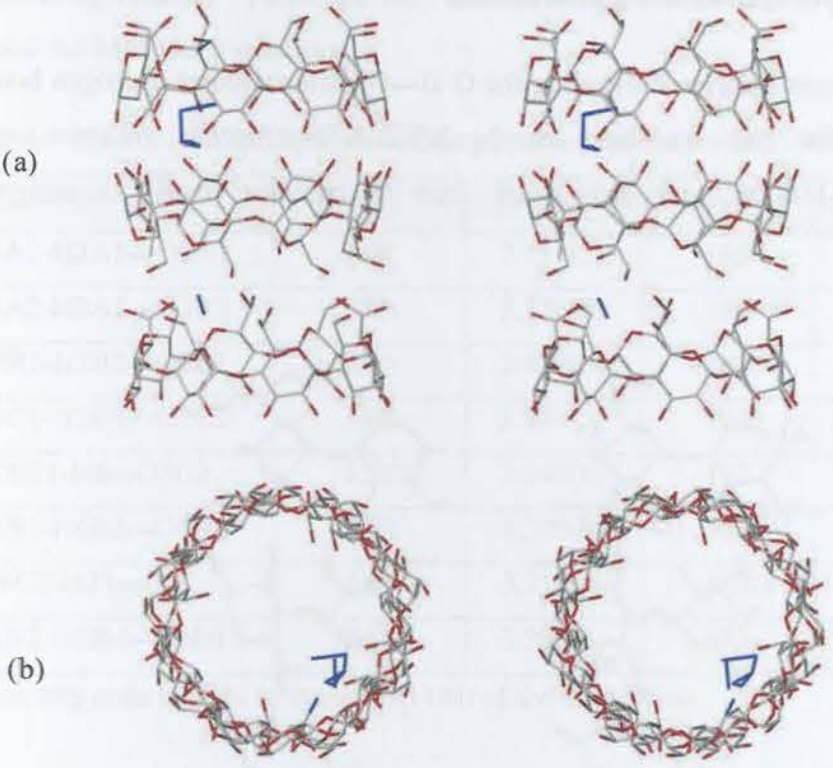

Figure 4.5 (a) Side and (b) top stereo views of the electron density in the METGCD host cavities. Only the unique peaks attributable to the guest are shown (in blue).

Hydrogen bonding interactions of the METGCD structure

The trimer exhibits head-to-head, head-to-tail and tail-to-tail orientations of the γ-CD host molecules. These orientations are stabilised by intra- and intermolecular hydrogen bonded interactions of the CDs. The host hydrogen bonds of the METGCD structure were calculated using PLATON.[114]

Intramolecular hydrogen bonding interactions

Figure 4.6 is a stereo diagram illustrating the O-H•••O intramolecular hydrogen bonding interactions for the host molecules of the METGCD structure. These are the characteristic O3-H•••O2' hydrogen bonds that are present in β-CD and γ-CD complexes.[124,128]

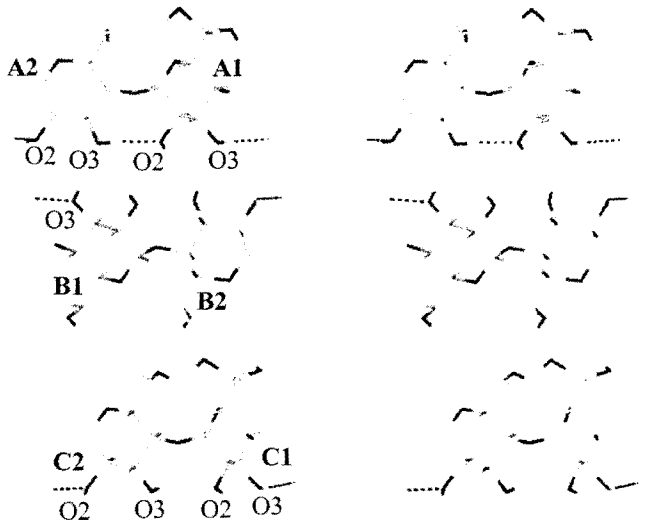

Figure 4.6 Stereo diagram of the METGCD asymmetric unit showing intramolecular hydrogen bonding interactions.

Table 4.9 lists four unique O-H•••O and four unique C-H•••O intramolecular hydrogen bonds that stabilise the METGCD structure. Host molecule **A** has one unique O3-H•••O2' hydrogen bond present and the four-fold symmetry of this molecule requires three other identical hydrogen bonds. Host molecule **B** has a unique O3•••H-O2' hydrogen bond present that connects the **B1** glucose residue to its neighbouring residue making a total of four of these interactions. In the host molecule **C** there is a unique 'O2•••H-O3 and O3-H•••O2' hydrogen bond present that connect **C2** and **C1** glucose units respectively to each

neighbouring residue. There are four intramolecular C6-H•••O5' hydrogen bonds that stabilise the METGCD structure.

Table 4.9 Intramolecular hydrogen bonding interactions for the METGCD structure

Hydrogen bond	H•••A / °	D•••A / °	D-H•••A / °	Symmetry Code[#]
O3A1-H2A1•••O2A2	1.98	2.787(5)	165	1/2+y, 1/2-x, z
O3A2-H2A2•••O2A1	1.96	2.776(5)	174	x, y, z
O2B2-H2B2•••O3B1	2.16	2.877(5)	147	1/2+y, 1/2-x, z
O3C1-H2C1•••O2C2	2.08	2.874(5)	163	1/2+y, 1/2-x, z
C6C1-H6•••O5C2	2.58	3.348(6)	133	1/2+y, 1/2-x, z
C6B1-H6B2•••O5B2	2.57	3.309(6)	133	1/2-y, -1/2+x, z
C6C2-H21•••O5C1	2.58	3.313(6)	132	x, y, z
C6B2-H6B4•••O5B1	2.55	3.295(8)	133	x, y, z

[#] Symmetry code applies to the second unit of the interaction

Intermolecular hydrogen bonding interactions

Table 4.10 lists the intermolecular hydrogen bonds for the METGCD structure. There are seven unique O-H•••O hydrogen bonds and these are illustrated in a stereo diagram in Figure 4.7. The head-to-head arrangement of the host molecules **A** and **B** results in them being hydrogen bonded to each other via their O3 atoms. The tail-to-tail arrangement of the host molecules **B** and **C** permits them to be hydrogen bonded to each other via their O6 atoms. There are four C-H•••O hydrogen bonds that contribute to the stability of the METGCD structure.

Table 4.10 Intermolecular hydrogen bonding interactions

Hydrogen bond	H•••A / °	D•••A / °	D-H•••A / °	Symmetry Code[#]
O2A1-H2A1•••O3C2	1.98	2.787(5)	167	1-y, 1-x, 1-z
O2B1-H2B1•••O3A2	2.50	3.234(5)	150	x, y, z
O3B1-H3B2•••O3A2	2.00	2.817(4)	171	x, y, z
O3B2-H3B1•••O3A1	2.01	2.793(4)	160	x, y, z
O6B2-H6B3•••O6C2	2.01	2.814(6)	169	x, y, z
O2C1-H3C1•••O3A1	2.02	2.837(5)	173	1-y, 1-x, 1-z
O3C2-H2C2•••O2A1	2.13	2.787(5)	137	1-y, 1-x, 1-z
C1B1-H1B1•••O6C2	2.48	3.452(6)	173	1-y, 1-x, 1-z
C2C1-H18•••O2B2	2.60	3.505(6)	154	1-y, 1-x, 1-z
C2C2-H20•••O2B1	2.51	3.412(5)	153	1-y, 1-x, 1-z
C1C1-H4C1•••O3B2	2.39	3.279(6)	150	1-y, 1-x, 1-z

[#] Symmetry code applies to the second unit of the interaction

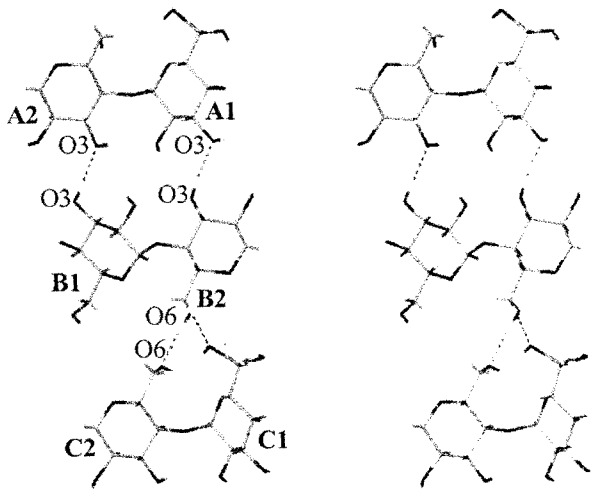

Figure 4.7 Stereo diagram showing the intermolecular O-H•••O hydrogen bonding.

Water interactions

Table 4.11 presents water interactions for the METGCD structure. Water molecules play an essential role in the stabilisation of trimeric γ-CD structures. The water molecules lie mainly in the interstitial channels forming a network of hydrogen bonds between the columns of γ-CD molecules.

Table 4.11 Water interactions for the METGCD structure

Hydrogen bond	D•••A / °	Symmetry Code[#]
O6B1•••O1W	2.80(1)	x, y, z
O2C2•••O2WA	2.76(2)	x, y, z
O3A2•••O2WA	2.96(2)	1-x, 1-y, 1-z
O2C2•••O2WB	2.67(2)	x, y, z
O3A2•••O2WB	2.84(2)	1-x, 1-y, 1-z
O2A2•••O3WA	2.73(1)	x, y, z
O2A2•••O3WB	2.79(1)	x, y, z
O3C1•••O3WB	2.69(2)	-½+x, ½-y, 1-z
O5A2•••O4WA	3.04(2)	y, x, 2-z
O3B1•••O6WA	2.96(2)	1-y, 1-x, 1-z
O2B2•••O6WC	3.02(3)	3/2-x, -½+y, 1-z
O3B1•••O6WD	2.87(5)	1-y, 1-x, 1-z
O5B2•••O7W	3.08(1)	x, y, z
O6B2•••O7W	2.77(1)	x, y, z
O6C1•••O8W	2.72(2)	x, y, z
O6A2•••O9W	2.79(2)	x, y, z
O4WA•••O3WA	2.75(2)	x, y, z
O5WA•••O1W	2.86(3)	x, y, z
O6WB•••O3WA	2.56(5)	1-y, 1-x, 1-z
O6WC•••O3WA	2.74(3)	1-y, 1-x, 1-z

[#] Symmetry code applies to the second unit of the interaction

The water molecules are bonded directly to the hydroxyl oxygen atoms of the γ-CD or bonded to other water molecules. The host•••water interactions are more predominant than the water•••water interactions [sixteen host•••water interactions vs. four water•••water interactions].

Crystal packing

A WebLab Viewer[129] diagram of the crystal packing of the METGCD, projected down the c-axis, is shown in Figure 4.8. This illustrates interstitial location of the water molecules and the endless channels down this axis. The diameter of the interstice is fairly large [almost comparable to that of the host cavities] and is a result of the channels arranging in a square pattern, as opposed to a more closely packed hexagonal arrangement. In a study of the dehydration kinetics of γ-CD•clofibric acid•15.5H_2O[130] it was suggested that the wide interstices enhance diffusion of the water molecules along the z-direction upon heating the crystals.

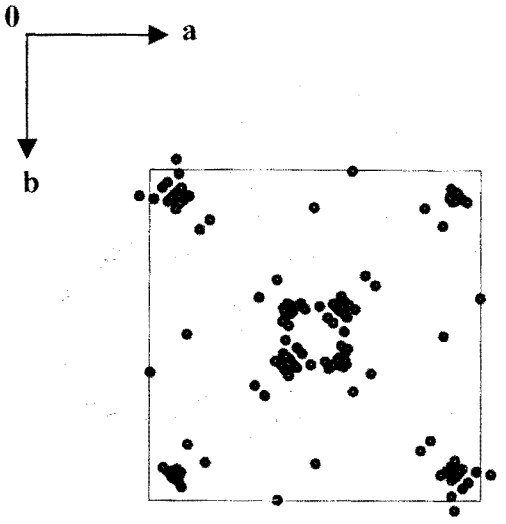

Figure 4.8 A WebLab Viewer diagram of the γ-CD trimer and interstitial water molecules projected along the c-axis.

Powder X-ray diffraction

The experimental and computed PXRD patterns for METGCD are shown in Figure 4.9. There is a close match between the two PXRD patterns. Differences in relative intensities of the peaks in the experimental trace when compared to the computed pattern are due to preferred orientation effects in the former and incomplete modelling of the guest and water in the latter. The traces were obtained at similar temperatures and thus there was no angular shift for corresponding peaks, which is mainly observed for experiments carried out at different temperatures.

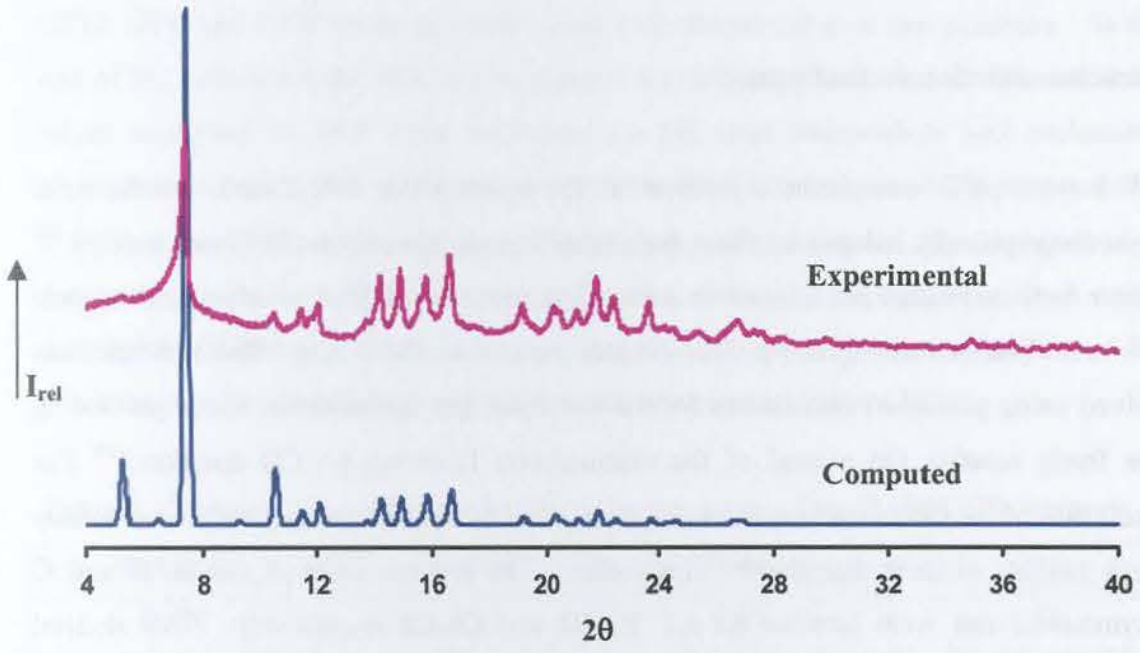

Figure 4.9 Computed [299K] and experimental [295K] patterns for METGCD.

X-ray Crystallographic Analysis of OXPRGCD

Single Crystal X-ray Diffraction

Data-collection and space group determination

The mosaicity of the OXPRGCD crystal increased on cooling it in a stream of N_2 vapour and thus X-ray intensity data were collected on a Nonius Kappa CCD diffractometer at room temperature using graphite-monochromated MoKα radiation. Inspection of the reciprocal lattice layers with LAYER[112] indicated the reflection condition h00: h =2n. Since the host is chiral, XPREP indicated the space group of $P42_12$

Structure solution and refinement

All known γ-CD complexes crystallise in the space group $P42_12$ and contain three crystallographically independent host molecules that are stacked on top of one another.[124] These host molecules are located on a four-fold rotation axis that is orthogonal to their O4 mean planes running down their cavities parallel to the c-axis. The structure was solved using published coordinates for the non-hydrogen cyclodextrin atoms [excluding the freely rotating O6 atoms] of the isomorphous 12-crown-4-γ-CD complex.[125] The exclusion of the O6 atoms was to model their possible disorder using the electron density peak heights of their disordered components. The glucose units of the **A**, **B** and **C** asymmetric unit were labelled **A1-A2**, **B1-B2** and **C1-C2** respectively. This skeletal structure was refined with SHELXL-97[113] and the difference Fourier map revealed the positions of most of the remaining non-hydrogen atoms. The O6 atoms for the **A2** and **C2** glucose units were disordered over two positions [the minor disordered component was labelled O7]. The placement of the disordered O6 atoms was based on their initial peak heights. For each given pair of O6 atoms in the **A2** and **C2** glucose units fixed U_{iso} values of 0.1 and 0.07 $Å^2$ [the average value for the ordered oxygen atoms for A and C glucose units] were assigned respectively and the site occupancy factors of x and 1-x were assigned, with x variable. The final site-occupancy factors from the major positions

for **A2** and **C2** glucose units refined to 0.65 and 0.88 respectively. All the non-hydrogen atoms of the host except for the disordered O6 atoms were refined anisotropically which was then followed by the placement of the hydrogen atoms using a riding model.

The modelling of the guest was unsuccessful since the four-fold rotation axis requires that any included asymmetrical guest in the γ-CD host cavity should at least be four-fold disordered. In addition, the unacceptable geometries and distances between the electron density peaks contributed to the difficulty of interpreting the difference Fourier map. Twelve sites were identified as water molecules. These were placed with a fixed isotropic temperature factor of 0.09 $Å^2$ except for O1W [isotropic temperature factor for the O1W atom with full s.o.f.] and their site-occupancy factors were allowed to vary. O2W, O3W and O7W water molecules were each disordered over two positions. At the end of the refinement the total site-occupancy for the unique water molecules was 4.94, which translated to 19.8 water molecules for the three independent host molecules. Comparison of this value with that obtained from the TGA analysis clearly shows that it is far less than 39.9 water molecules. Therefore the information for the water content of these crystals for the OXPRGCD complex is best obtained from thermal analysis rather than X-ray diffraction. The s.o.f.'s of the water molecules are presented in Table 4.12, while the crystal and refinement parameters are presented in Table 4.13.

Table 4.12 Site-occupancy factors for the water molecules of the OXPRGCD structure

Molecule	s.o.f.	Molecule	s.o.f.
O1W	1	O6W	0.48
O2WA	0.27	O7WA	0.27
O2WB	0.48	O7WB	0.33
O3WA	0.46	O8W	0.22
O3WB	0.31	O9W	0.16
O4W	0.39	O10W	0.25
O5W	0.36		

Table 4.13 Data collection and refinement parameters for OXPRGCD at 293K

Formula unit	$3(C_{48}H_{80}O_{40}) \cdot 2(C_{15}H_{23}NO_3) \cdot 39.9H_2O$
Formula weight / g mol^{-1}	5141.0
Crystal system	Tetragonal
Space group	$P42_12$
a / Å	23.7413(2)
c / Å	23.0924(2)
Volume / $Å^3$	13016.0 (2)
Z	2
Density $_{calc}$ / gcm^{-3}	1.395
μ(MoKα) / mm^{-1}	0.098
F(000)	4444
Temperature of data collection / K	293
Crystal size / mm^3	0.18 x 0.25 x 0.28
Range scanned θ / °	$2 \leq \theta \leq 25$
Index ranges	h: -27, 27 k: -19, 19 l: -26, 23
Dx / mm	44
Total no. of reflections collected	19797
Total no. of unique reflections	10363
No. of reflections with $I > 2\sigma$ (I)	7834
No. of parameters	659
R_{int}, R_σ	0.0290, 0.0467
S	1.17
R_1 (for 8420 reflections)	0.0934
No. of reflections omitted	16
wR_2	0.2882
Weighting scheme	a = 0.2 b = 0
Δρ excursions / e. $Å^{-3}$	0.84 and –0.79

Description of the structure

OXPRGCD crystallises in the tetragonal space group $P42_12$ in a 3:2 γ-CD:oxprenolol molar ratio with Z = 2 formula units per unit cell and 39.9 water molecules in the formula unit. The asymmetric unit comprises three crystallographically independent host molecules that are located on a four-fold rotation axis with two glucose units from each host molecule. Two γ-CD molecules form a head-to-head dimer while the third is attached to the O6 side of the dimer in a tail-to-tail mode. Figure 4.10 presents a side

view of the three crystallographically independent host molecules as well as the asymmetric unit with its atom labelling scheme.

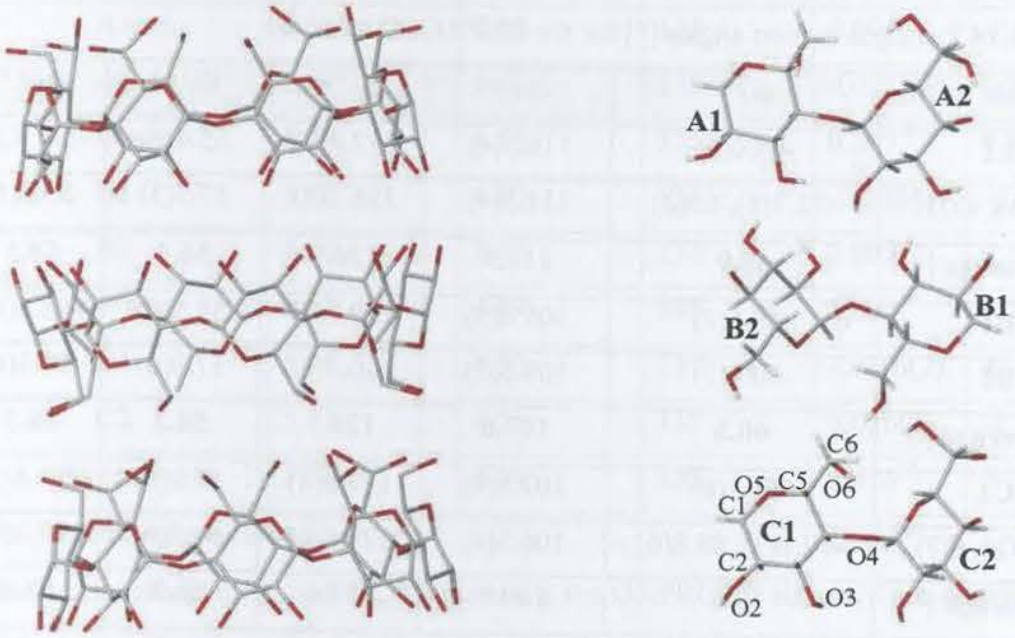

(a) (b)

Figure 4.10 (a) Three crystallographically independent γ-CD host molecules viewed from the side in the OXPRGCD structure (b) The asymmetric unit with glucose unit **C1** showing representative labelling.

Geometrical analysis of the OXPRGCD complex structure

The glucose residues are all in the $^4C_1$ chair conformation and their geometrical parameters are presented in Tables 4.14-4.16. The principal torsion angles are shown in Table 4.14. The primary hydroxyl or O5-C5-C6-O6 torsion angle (ω) adopts two orientations namely (+)-*gauche* and (-)-*gauche* conformations for the **A2** and **C2** glucose units corresponding to the disordered positions of the O6 atom for these residues. The minor components of the disordered O6 atom adopt a (+)-*gauche* conformation, that is their O7-H bonds point toward the centre of the CD cavity whilst the major components point away from the centre of the CD cavity. The ω parameter for the **A1**, **B1**, **B2** and **C1** glucose residues is negative indicating that O6-H for each of these glucose residues is

directed away from the CD host cavity. The **Φ**, **ψ**, **Θ_1** and **Θ_2** torsion angles are in good agreement with those for the parent γ-CD.[137]

Table 4.14 Principal torsion angles [°] for the OXPRGCD structure

Glucose unit	**ω / °**	**Φ / °**	**ψ / °**	**Θ_1 / °**	**Θ_2 / °**
A1	-68.0(6)	110.5(4)	127.4(4)	55.4(6)	-58.1(5)
A2 (O6, O7)[#]	-73.7(6), 65(2)	111.3(4)	126.1(4)	57.5(5)	-59.0(5)
| Average |	**68.9**	**110.9**	**126.7**	**56.4**	**58.5**
B1	-60.6(7)	105.6(5)	129.1(4)	59.5(6)	-58.4(6)
B2	-60.4(7)	109.6(5)	130.3(4)	57.0(6)	-58.3(6)
| Average |	**60.5**	**107.6**	**129.7**	**58.2**	**58.3**
C1	-60.1(6)	107.3(4)	127.8(4)	57.9(5)	-59.4(5)
C2 (O6, O7)	-62.0(7), 89.8(6)	106.5(4)	129.5(4)	54.7(6)	-57.3(6)
| Average |[*]	**70.6**	**106.9**	**128.6**	**56.3**	**58.3**

[#] The disordered O6 atoms result in two ω values

[*] Unweighted average of all recorded values

Data defining the O4-octagons in OXPRGCD appear in Table 4.15. These parameters were defined earlier for METGCD [Table 4.7 and preceding text]. The values of these parameters are similar to those found in the METGCD structure.

Table 4.15 The geometrical parameters of the O4-octagons of the OXPRGCD structure

Glucose unit	r / Å	l / Å	a / °	d / Å	t / °
A1	5.88	4.49	135	0.007(3)	-0.9
A2	5.89	4.51	135	-0.007(3)	0.9
Average	**5.88**	**4.50**	**135**	**0.007** [#]	**0.9**
B1	5.85	4.50	136	-0.003(2)	-0.3
B2	5.90	4.49	134	0.003(2)	0.3
Average	**5.87**	**4.49**	**135**	**0.003** [#]	**0.3**
C1	5.84	4.50	137	-0.016(2)	2
C2	5.93	4.51	133	0.016(2)	-2
Average	**5.88**	**4.50**	**135**	**0.016** [#]	**2**

[#] Root-mean-square deviation

The intersaccharidic, φ, and tilt, τ, angles for the OXPRGCD structure are presented in Table 4.16. The tilt angles for the glucose residues are all positive and they range from 3.8 to 14.3°. These relatively small positive tilt angles indicate that the O2, O3 side of the CD is slightly more open than the O6 side of the CD molecules; thus the CD molecules appear with the shape of a truncated cone.

Table 4.16 φ and τ parameters for the OXPRGCD structure

Glucose unit	φ / °	τ_1 / °	τ_2 / °
A1	116.1(4)	12.0(1)	4.3(4)
A2	117.7(4)	12.2(1)	3.3(2)
Average	**116.9**	**12.1**	**3.8**
B1	118.0(4)	13.6(1)	5.5(1)
B2	115.8(4)	15.0(1)	4.2(2)
Average	**116.9**	**14.3**	**4.8**
C1	117.8(4)	14.8(2)	6.6(1)
C2	114.7(4)	12.8(2)	4.8(2)
Average	**116.2**	**13.8**	**5.7**

Guest inclusion

As mentioned earlier, any guest molecule included in the CD cavity should be disordered at least four-fold, unless it possesses four-fold symmetry itself.[65] Figure 4.11 is a stereo diagram of the highest electron density peaks [0.78-0.3 eÅ^{-3}] in the CD host cavity.

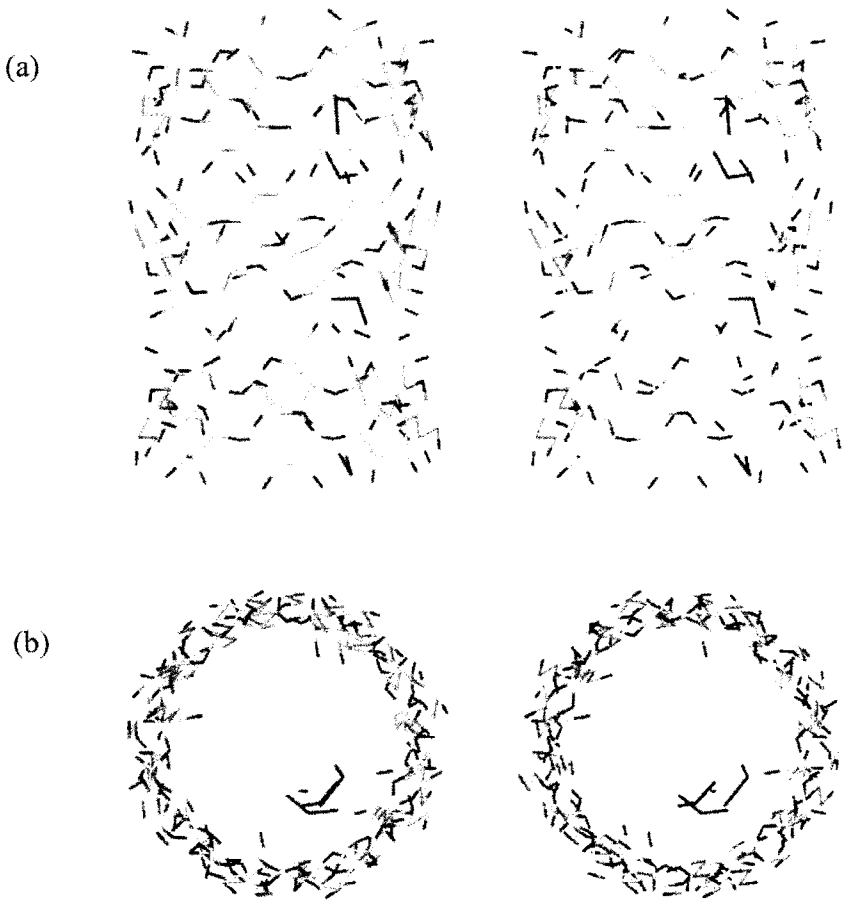

Figure 4.11 (a) Side and (b) top stereo views of the electron density in the OXPRGCD host cavities. Only the unique peaks attributable to the guest are shown [in blue].

Hydrogen bonding interactions of the OXPRGCD structure

The three crystallographically independent γ-CD molecules **A**, **B** and **C** form a trimer arranged in head-to-head [**A-B**], tail-to-tail [**B-C**] and head-to-tail [**A-C^{i}**, **i** = x, y, 1+z] fashion. These arrangements are stabilised by direct hydrogen bonded interactions between the CD host molecules. PLATON[114] was used to calculate several of these interactions exclusively involving host atoms of the OXPRGCD structure. These interactions are classified as intra- and intermolecular hydrogen bonding interactions.

Intramolecular hydrogen bonding interactions

Table 4.17 lists three unique O-H•••O and four unique C-H•••O intramolecular hydrogen bonds. All three O-H•••O intramolecular hydrogen bonds are characteristic of O3-H•••O2' bonds. All C-H•••O intramolecular hydrogen bonds are characteristic of C6-H•••O5' hydrogen bonds which also contribute to the stabilisation of the γ-CD host molecules. A diagram illustrating these unique bonds is presented in Figure 4.12(a). The **A** and **C** host molecules each have one unique O3-H•••O2' hydrogen bond present with the four-fold symmetry of these molecules requiring three other identical hydrogen bonds.

Table 4.17 Intramolecular hydrogen bonding interactions for the OXPRGCD structure

Hydrogen bond	H•••A / °	D•••A / °	D-H•••A / °	Symmetry Code [#]
O3C2-H3C2•••O2C1	2.07	2.881(6)	170	1/2+y, 1/2-x, z
O3A1-H3A1•••O2A2	1.94	2.758(5)	173	x, y, z
O3A2-H3A2•••O2A1	1.98	2.795(5)	170	1/2+y, 1/2-x, z
C6C2-H2•••O5C1	2.57	3.369(6)	130	1/2+y, 1/2-x, z
C6C1-H6C2•••O5C2	2.56	3.293(7)	132	x, y, z
C6B1-H23•••O5B2	2.57	3.302(9)	133	x, y, z
C6B2-H6B4•••O5B1	2.57	3.316(8)	134	1/2-y, -1/2+x, z

[#] Symmetry code applies to the second unit of the interaction

Intermolecular hydrogen bonding interactions

The diagram illustrating the intermolecular hydrogen bonding interactions is presented in Figure 4.12(b) and these bonds are listed in Table 4.18. There are seven unique O-H•••O hydrogen bonds. The O3-H•••O3' hydrogen bonds connect the two host molecules **A** and **B** in a head-to-head fashion. The O6-H•••O2' hydrogen bond links the **C** and **A** molecules of adjacent sets of three crystallographically independent γ-CD host molecules in a head-to-tail mode. There are three intermolecular C-H•••O hydrogen bonds that stabilise the OXPRGCD structure.

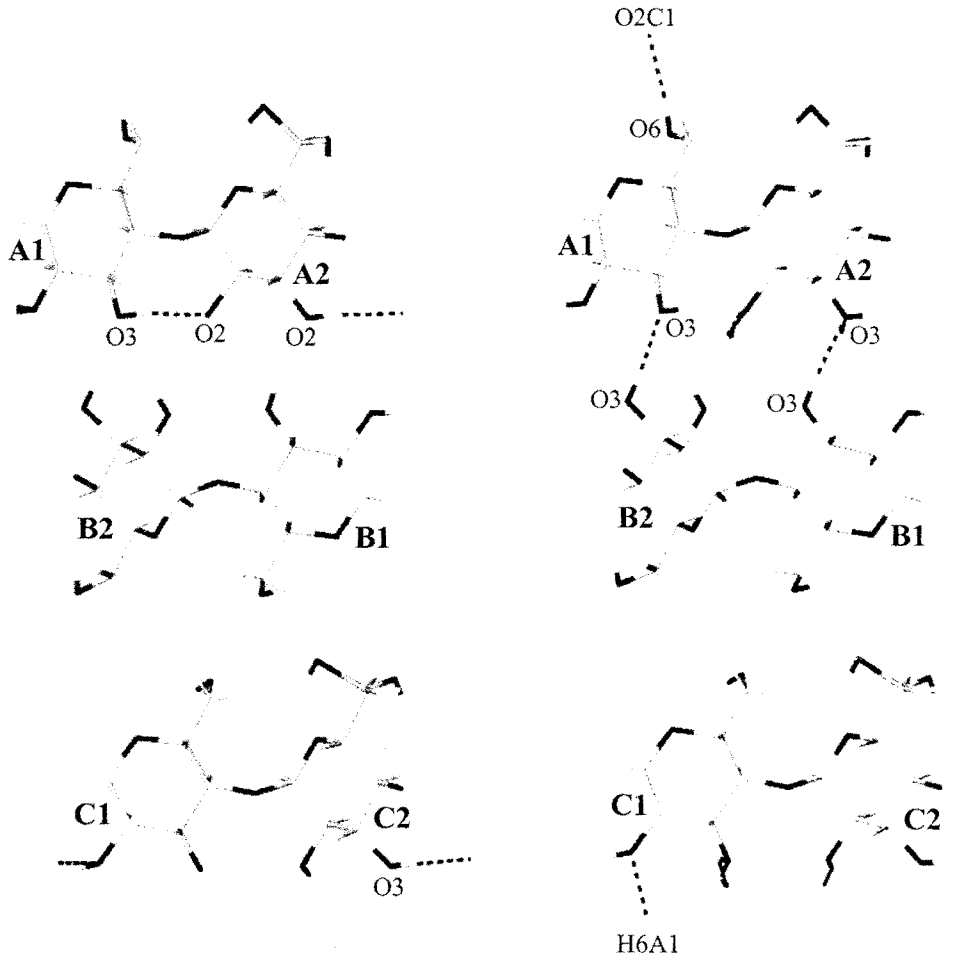

Figure 4.12 OXPRGCD asymmetric unit diagram illustrating the (a) intramolecular and (b) intermolecular O-H•••O hydrogen bonding.

Table 4.18 Intermolecular hydrogen bonding interactions

Hydrogen bond	H•••A / °	D•••A / °	D-H•••A / °	Symmetry Code [#]
O3C1-H3C1•••O2A2	2.09	2.792(5)	144	1-y, 1-x, 1-z
O2C2-H2C2•••O3A2	2.03	2.837(6)	166	1-y, 1-x, 1-z
O6A1-H6A1•••O2C1	2.08	2.855(6)	159	x, y, 1+z
O2A2-H2A2•••O3C1	2.00	2.792(5)	163	1-y, 1-x, 1-z
O3B1-H3B1•••O3A2	2.03	2.795(5)	154	x, y, z
O2B2-H2B2•••O3A1	2.44	3.247(5)	169	x, y, z
O3B2-H3B2•••O3A1	2.02	2.828(5)	170	x, y, z
C1C2-H1C2•••O3B1	2.41	3.292(6)	150	1-y, 1-x, 1-z
C2C1-H11•••O2B2	2.51	3.408(6)	153	1-y, 1-x, 1-z
C1B2-H1B2•••O6C1	2.48	3.458(7)	174	1-y, 1-x, 1-z

[#] Symmetry code applies to the second unit of the interaction

Water interactions

The water molecules, which lie mainly in the interstitial channels, play a significant role in the stabilisation of trimeric γ-CD structures. These form a network of hydrogen bonds between the columns of γ-CD molecules. The host•••water interactions exceed the water•••water interactions [twenty one host•••water versus one water•••water interaction]. The water molecules not hydrogen bonded to other water molecules form hydrogen bonds with the hydroxyl oxygen atoms of the γ-CD molecules thus enhancing the rigidity of the structure.

Table 4.19 Water interactions for the OXPRGCD structure

Hydrogen bond	**D•••A / °**	**Symmetry Code** [#]
O6B2•••O1W	2.784(7)	x, y, z
O6C1•••O1W	2.869(7)	x, y, z
O2C1•••O2WA	2.80(3)	x, y, z
O3A1•••O2WA	3.03(3)	1-y, 1-x, 1-z
O3A1•••O2WB	2.85(2)	1-y, 1-x, 1-z
O2C1•••O2WB	2.67(2)	x, y, z
O2A1•••O3WA	2.73(1)	x, y, z
O3C2•••O3WA	2.95(2)	-1/2+x, ½-y, 1-z
O2A1•••O3WB	2.73(2)	x, y, z
O3C2•••O3WB	2.72(2)	½+x, ½-y, 1-z
O6A1•••O5W	2.80(2)	x, y, z
O6B1•••O6W	2.73(1)	x, y, z
O5B1•••O6W	3.01(1)	x, y, z
O5A1•••O7B	3.01(2)	y, x, 2-z
O2B1•••O8W	3.07(3)	½+y, ½-x, z
O6C2•••O9W	2.58(3)	½+x, ½-y, 1-z
O3B2•••O10W	3.11(2)	x, y, z
O1W•••O4W	2.84(2)	x, y, z
C2C1•••O2WA	3.32(3)	x, y, z
C2C1•••O2WB	3.37(2)	x, y, z
C2A1•••O3WB	3.33(2)	x, y, z
C1A1•••O7WB	3.33(2)	y, x, 2-z

[#] Symmetry code applies to the second unit of the interaction

Crystal packing

The γ-CD molecules are stacked to form a channel-type structure. The repeating unit in the column consists of three γ-CD molecules. Two γ-CD molecules form a head-to-head dimer whilst the third γ-CD molecule is attached to the dimer in a head-to-tail mode. Figure 4.13 is a projection down the c-axis of the structure and the water molecules are clearly seen to be located in the interstitial channels.

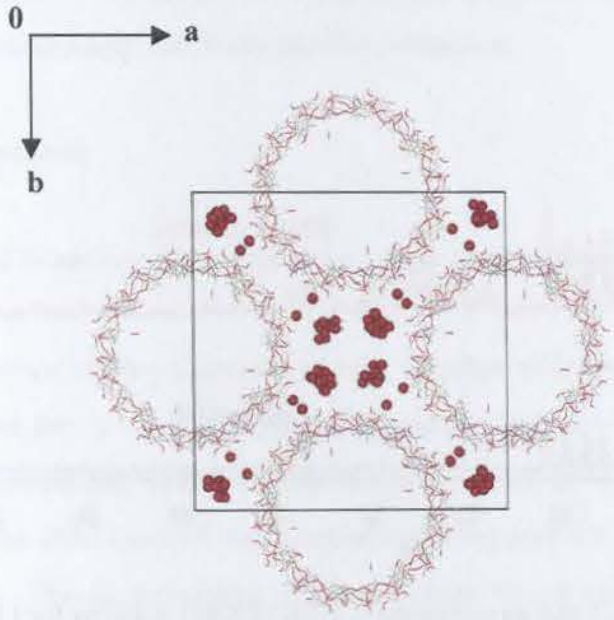

Figure 4.13 A WebLab Viewer diagram of OXPRGCD trimer and interstitial water molecules projected along the c-axis.

Powder X-ray diffraction

The computed and experimental PXRD patterns for the OXPRGCD structure are presented in Figure 4.14. Differences in relative intensities of the peaks in the experimental trace when compared to the computed pattern are pronounced. They are attributed to preferred orientation in the experimental sample and to unsuccessful modelling of the guest in the computed pattern. The traces were obtained at similar temperatures and thus angular shifts for corresponding peaks were not observed.

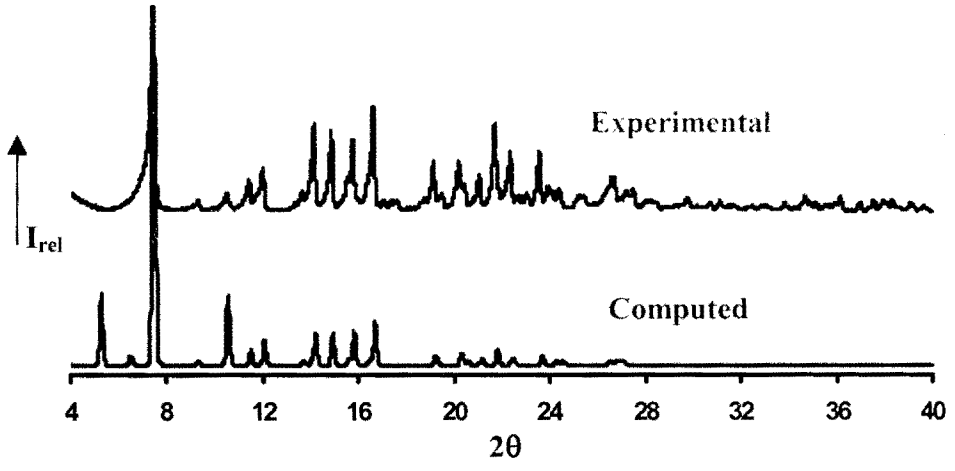

Figure 4.14 Computed [299K] and experimental [295K] PXRD patterns for OXPRGCD.

Characterisation of the Kneaded Atenolol -γ-CD Product (ATGCD)

An attempt to obtain single crystals of an inclusion complex between atenolol and γ-CD by employing the co-precipitation method in which atenolol was dissolved in a small volume of methanol and the solution slowly added to the saturated solution of γ-CD was unsuccessful. The γ-CD paste was prepared as follows: a small amount of water was added to 50 mg of γ-CD and this mixture was kneaded to form a paste. The equivalent amount of the drug atenolol was slowly added to this paste while kneading the two components for 1h. The characterisation and comparison of the kneaded product to the physical mixture were carried out using various analytical techniques such as DSC, TGA, infra-red spectroscopy and X-ray powder diffraction.

Thermal analysis

Differential Scanning Calorimetry and Thermogravimetric Analysis

The DSC trace of the kneaded product together with the trace of the uncomplexed atenolol and the 1:1 γ-CD to drug physical mixture are shown in Figure 4.15. The characteristic melting endotherm for atenolol occurs at 152°C. This fusion is clearly visible in the DSC trace of the uncomplexed drug and the physical mixture of this drug with γ-CD. The disappearance of the pure drug fusion endotherm was observed in the DSC trace of the kneaded product, indicating that an inclusion complex had been formed in the solid state. This complex will hereinafter be referred to as ATGCD. The location of drug molecules inside the γ-CD host cavities alters the characteristics of the original crystalline phase of atenolol.

The asymmetric shape of the dehydration endotherm [labelled A] in Figure 4.16 suggests that water loss from the ATGCD complex is a multi-stage process. The DSC onset of decomposition occurs at 290°C and the results are summarised in Table 4.20.

The TGA trace for the ATGCD complex presented in Figure 4.16 shows weight loss due to water [labelled A] from 30°C to 160°C. From 200°C onwards weight losses due to chemical decomposition are observed. A summary of the observed percentage weight loss is presented in Table 4.21.

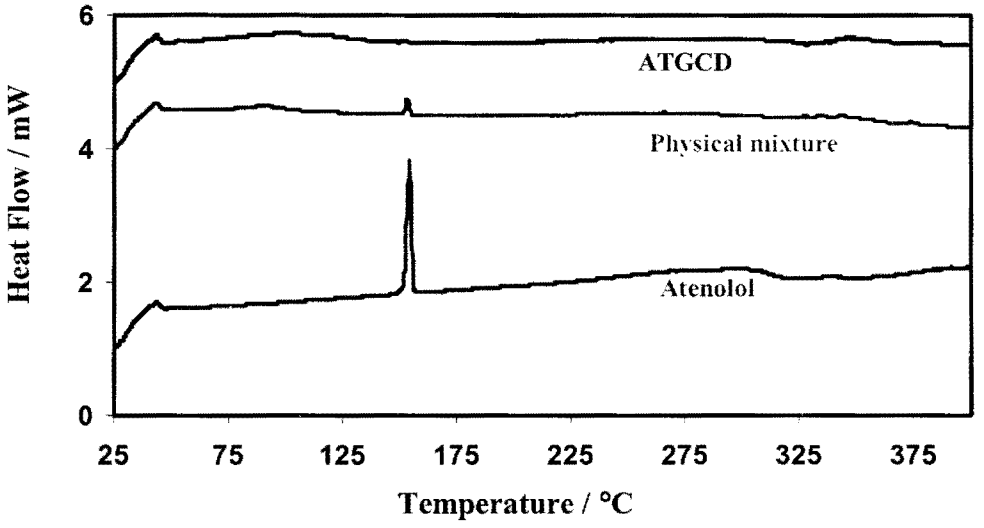

Figure 4.15 DSC traces of the γ-CD atenolol complex, 1:1 physical mixture and uncomplexed atenolol.

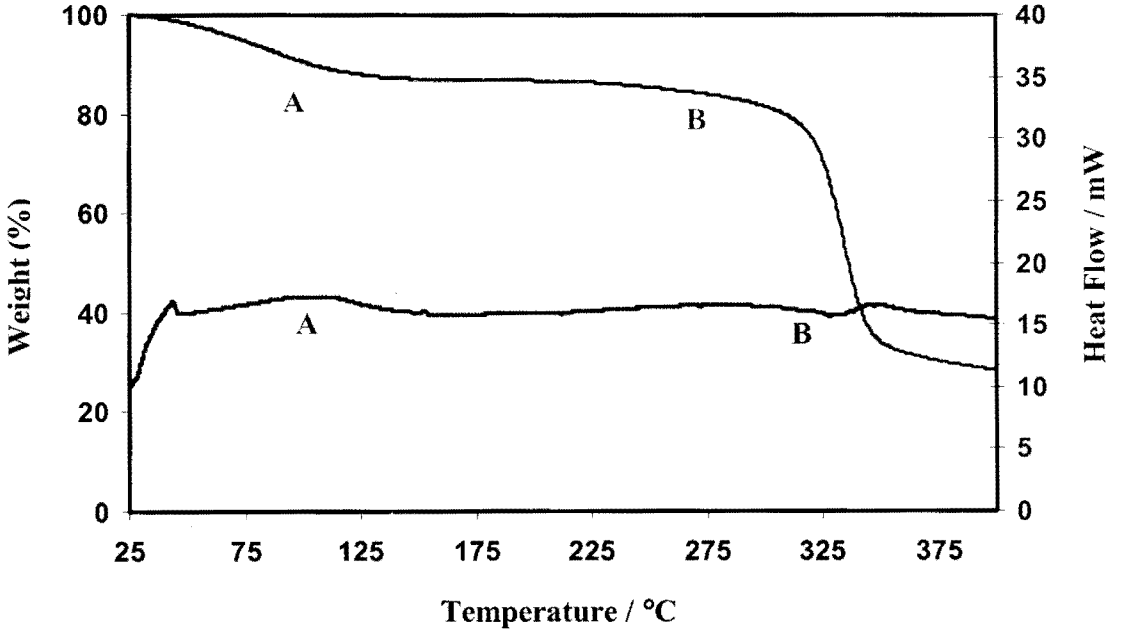

Figure 4.16 TGA and DSC trace for the ATGCD complex.

Table 4.20 Summary of the DSC thermal events for ATGCD

Endotherm	Parameter	ATGCD
A	Temperature range (°C)	48-148
	T_{on} (°C)	49
	Peak (°C)	100
B	Temperature range (°C)	280-348
	T_{on} (°C)	271
	Peak (°C)	328

Table 4.21 TGA results [n=2] summarised for ATGCD

Temperature / °C	ATGCD	
	% Mass	% Mass Loss
25	100	0
70	95.6	4.4
100	90.4	9.6
140	87.3	12.7
200	86.8	13.2
250	85.5	14.4
300	81.4	18.6
350	34.0	66.0
400	28.3	71.7

Fourier Tranform Infrared Spectroscopy (FTIR)

The assignment of the infrared bands of atenolol was based on what has been previously reported.[131] Since the molecule of atenolol has a carbonyl functional group, the FTIR spectroscopic technique was used to observe whether or not the carbonyl [C=O] stretching frequency of this molecule was affected by complexation [Figure 4.17]. The

C=O, -N-C=O and the arylether stretching frequencies of atenolol in the ATGCD complex [Figure 4.17 (b)] are displaced to 1662, 1513 and 1159 cm^{-1} respectively from the measured values of 1636, 1516 and 1179 cm^{-1} for the uncomplexed atenolol drug molecule [Figure 4.17 (a)]. This significant shift in frequency indicates that the guest inclusion into the γ-CD host cavity has occurred. Furthermore this shift in frequency is attributed to the known presence of strong hydrogen bonding interaction between carbonyl and amine groups [N-H•••O and O-H•••N] in the crystals of the guest[132] (dealt with in Chapter 3) and the probable absence of hydrogen bonding of this type in the CD complex. The stretching mode of the $-NH_2$ group of atenolol shows two sharp infrared bands at 3352 and 3168 cm^{-1}. However the large number of hydroxyl groups and water molecules in the host molecule γ-CD, mask the $-NH_2$ bands in this region.

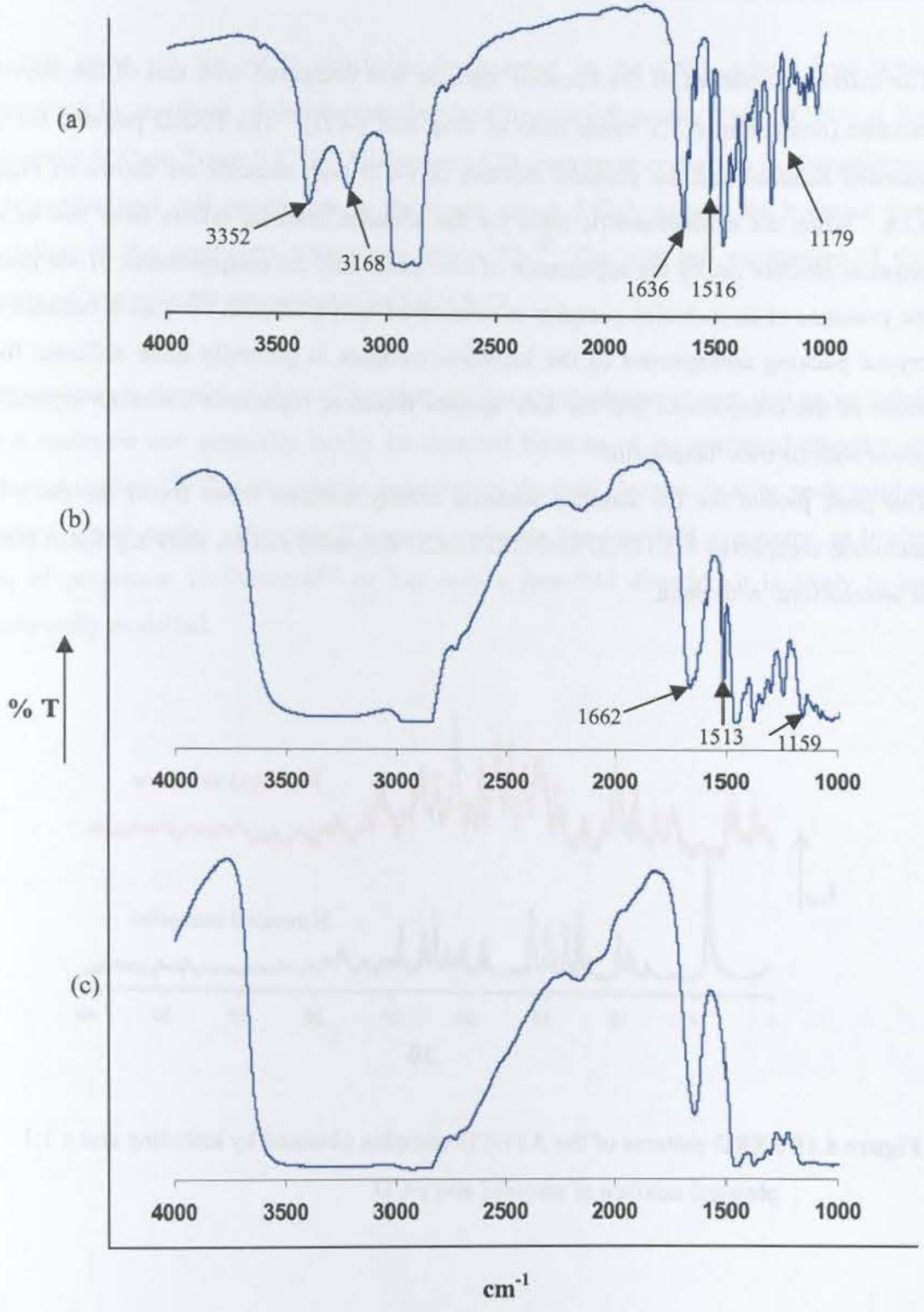

Figure 4.17 FTIR spectra for the (a) atenolol, (b) ATGCD complex and (c) γ-CD.

Powder X-ray diffraction

The diffraction pattern of the kneaded material was compared with that of the physical mixture [containing a 1:1 molar ratio of drug and γ-CD]. The PXRD patterns for the kneaded material and the physical mixture of γ-CD with atenolol are shown in Figure 4.18. When the diffractometric trace for the kneaded material differs from that of the physical mixture i.e. by the appearance of new peaks and the disappearance of old peaks, the presence of an inclusion complex is considered 'very probable'.[133] This is because the crystal packing arrangement of the inclusion complex is generally quite different from those of the components and the new species therefore represents a distinct crystalline phase with its own 'fingerprint'.

The peak profile for the kneaded material clearly matches those found for the γ-CD inclusion complexes METGCD and OXPRGCD discussed earlier, showing that ATGCD is isostructural with them.

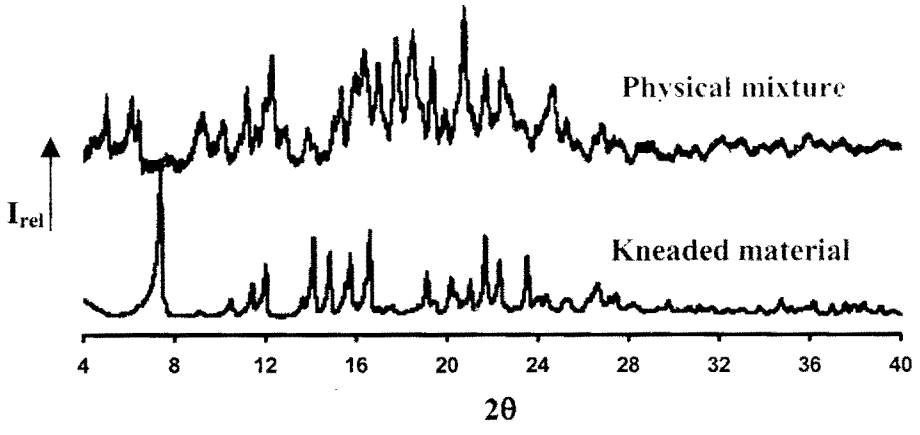

Figure 4.18 PXRD patterns of the ATGCD complex obtained by kneading and a 1:1 physical mixture of atenolol and γ-CD.

Discussion

To date there are ten γ-CD structures documented in the CSD, while three were determined by members of the Supramolecular Chemistry Research Unit (SCRU) at the University of Cape Town (UCT). All known γ-CD complexes crystallise in channel-type with similar unit cell parameters in the space group $P42_12$, except the hydrates that crystallise in the cage-form with space group $P2_1$.[65] The unit cell parameters of the known γ-CD structures are presented in Table 4.22.

The continuous channel of the γ-CD molecules has a wide diameter such that an included guest molecule can generally hardly be detected because of its statistical disorder or diffusive motion.[134] This disorder is indicated by the low electron density peak heights inside the host cavity. However if a guest molecule has four-fold symmetry, as in the case of potassium 12-Crown-4[135] or has only a four-fold disorder, it is likely to be successfully modelled.

Table 4.22 Unit cell parameters of the known γ-CD structures

Guest	**a / Å**	**b / Å**	**c / Å**	**α / °**	**β / °**	**γ / °**	**CSD Refcode**
Space group $P2_1$							
$11H_2O$	20.287	22.079	16.858	90	105.07	90	CIMSAS
$14H_2O$	16.847	11.098	20.271	90	104.97	90	CIWMIE10
Space group $P42_12$							
12-Crown-4	23.808	23.808	23.175	90	90	90	DOCYID
12-Crown-4•LiSCN	23.750	23.750	22.920	90	90	90	FEJFIJ
12-Crown-4•KCl	23.842	23.842	23.132	90	90	90	FEJPOP
Polyrotaxane	23.370	23.370	23.910	90	90	90	MOPBUO
Methanol	23.808	23.808	23.140	90	90	90	NUNRIX
12-Crown-4-NaCl	23.816	23.816	23.072	90	90	90	SAJNAS
1-Propanol (Form I)	23.840	23.840	23.227	90	90	90	SEBJAO
1-Propanol (Form II)	23.809	23.809	23.207	90	90	90	SIBJES
UCT SCRU							
Clofibric acid	23.650	23.650	23.640	90	90	90	UCT SCRU[136]
Cyclizine	23.824	23.824	23.083	90	90	90	UCT SCRU[137]
Tulobuterol	23.731	23.731	23.069	90	90	90	UCT SCRU[138]
Metoprolol	23.728	23.728	23.090	90	90	90	This work
Oxprenolol	23.741	23.741	23.092	90	90	90	This work

Conformation of the host

The asymmetric unit of all known γ-CD complexes consists of six glucose units of three crystallographically independent γ-CD molecules arranged to form a trimer. These complexes crystallise in the space group $P42_12$ and they are located on a four-fold rotation axis; thus each γ-CD molecule has eight glucose residues. The maintainance of the round shape of the γ-CD structures is via the intramolecular [O2•••O3' and O3•••O2'] as well as the intermolecular [O3•••O3'] hydrogen bonding interactions which remarkably minimise the degree of tilt angles of the glucose units to the lowest values.

Hydrogen bonding interactions of the host

The hydroxyl groups of the secondary hydroxyl end of the γ-CD complexes are held together by hydrogen bonded interactions similar to those found in β-CD complexes [discussed in Chapter 5]. This rim of hydrogen bonds is a general feature observed for all β- and γ-CD complexes and serves to stabilise the macrocyclic conformation of the CD. The hydroxyl groups of the primary hydroxyl end are hydrogen bonded to the hydroxyl groups on the secondary rim of their neighbouring γ-CD molecules.

Water interactions

Water interactions play an essential role in the stabilisation of trimeric γ-CD structures. These water molecules lie mainly in the interstitial channels that have fairly large diameters due to the arrangement of the γ-CD trimers. They form a network of hydrogen bonds between the columns of γ-CD molecules. The hydrogen bonding interactions are between the hydroxyl oxygen atoms of the γ-CD and water and between water molecules.

Crystal packing

The WebLab diagrams showing the crystal packing of the METGCD and OXPRGCD structures are presented in Figure 4.19. Both structures are projected down the c-axis. The γ-CD trimers stack to form the 'endless' channels down this axis and the interstitial location of the water molecules is shown. The square pattern arrangement of the channels as opposed to a more closely-packed hexagonal arrangement results in the diameter of the interstices being fairly large. In a study of the dehydration kinetics of γ-CD•clofibric acid•15.5(H_2O) complex[130] it was suggested that these wide interstices facilitate diffusion of the water molecules along the z-direction upon heating the crystals.

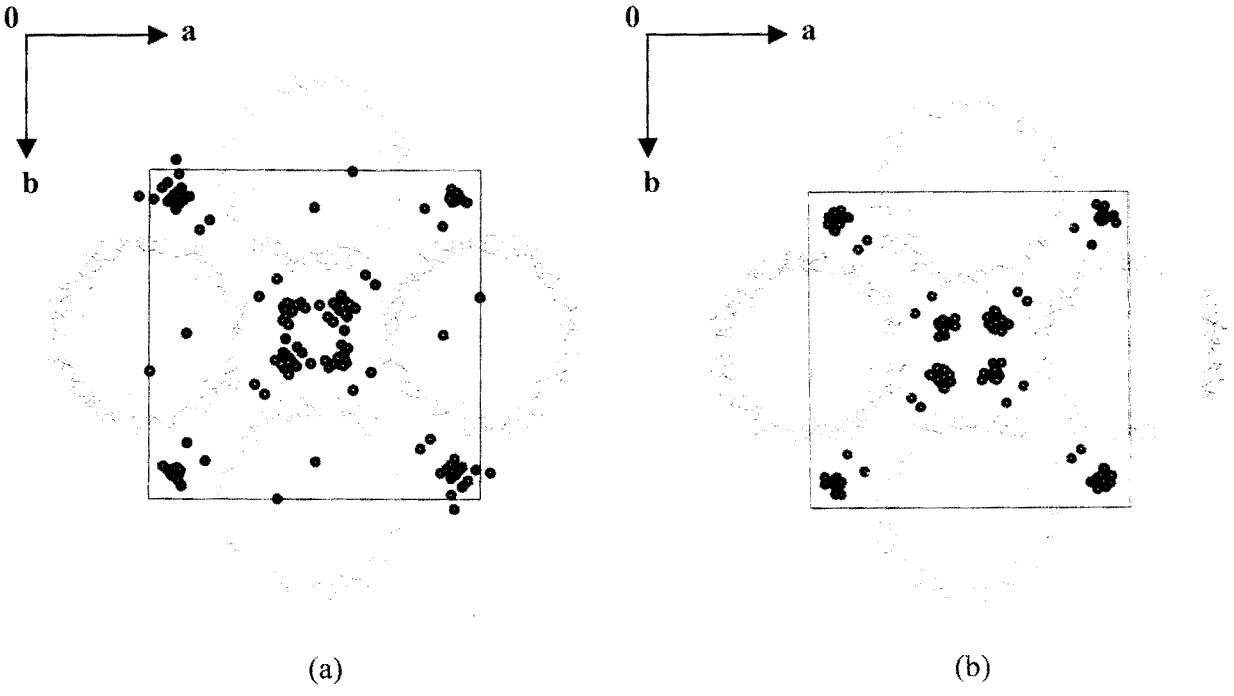

Figure 4.19 Crystal packing of the (a) METGCD and (b) OXPRGCD structures down the c-axis with the interstitial water molecules included.

Powder X-ray diffraction

The experimental PXRD trace of ATGCD and the computed traces of OXPRGCD and METGCD are presented in Figure 4.20 (a), (b) and (c) respectively. The three PXRD patterns of these γ-CD complexes, with different guest molecules being included, are in close agreement with one another indicating that three inclusion complexes are isostructural. The term isostructurality refers to two or more crystalline phases having identical or quasi-identical packing motifs.[74] This implies that the unit cell parameters and internal arrangements of molecules for such closely related structures are similar.

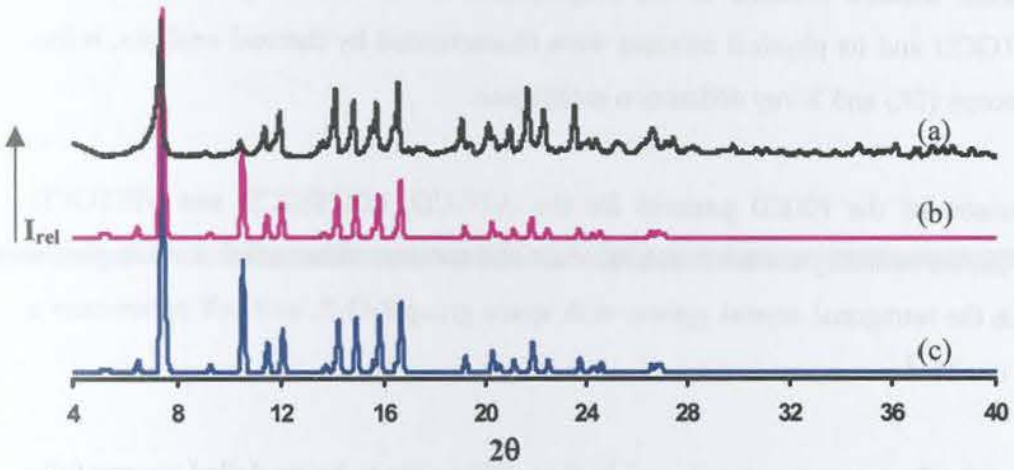

Figure 4.20 (a)The experimental trace of the ATGCD complex and the computed traces of (b) OXPRGCD and (c) METGCD complexes at room temperature [293K].

Conclusion

Complexes of γ-CD with metoprolol, oxprenolol and atenolol have successfully been prepared. Single crystals for γ-CD complexes with metoprolol [METGCD] and oxprenolol [OXPRGCD] as guest molecules were obtained at an elevated temperature. These complexes were characterised by elemental analysis, thermal and X-ray diffraction techniques. The host:guest:H_2O ratios for METGCD and OXPRGCD were established from a combination of information from elemental analysis and TGA to be 3:2:35.4 and 3:2:39.9 respectively.

The unsuccessful attempt to obtain single crystals of a γ-CD-atenolol complex from the co-precipitation method resulted in the employment of the kneading method. The kneaded ATGCD and its physical mixture were characterised by thermal analysis, infra-red spectroscopy (IR) and X-ray diffraction techniques.

The comparison of the PXRD patterns for the ATGCD, OXPRGCD and METGCD complexes shows that they are isostructural with one another. Thus all three complexes crystallise in the tetragonal crystal system with space group $P42_12$, unit cell parameters a = b ~ 23.7, c ~ 23 Å.

The prerequisite for a guest molecule inside the γ-CD cavity to be modelled successfully is that it should have a four-fold symmetry. The guest molecules metoprolol and oxprenolol could therefore not be modelled. However the host and water molecules for these complexes were successfully modelled and their geometrical parameters and interactions explained.

Chapter 5 – β-CD Inclusion Complexes

Complex Preparation

Crystalline complexes of atenolol, metoprolol and oxprenolol free bases with β-CD were obtained from both slow cooling and evaporation of hot aqueous solutions [~ 50°C] of cyclodextrin and drug in 1:1 molar ratios at room temperature (RT). Crystalline material was obtained on standing for a period of two to four weeks at RT. The complexes of β-CD with each drug, grown under ambient conditions, will be referred to as ATBCD, METBCD and OXPRBCD respectively and will be described herein.

Microanalysis

The host-guest ratios of the β-CD complexes were determined by carbon, hydrogen and nitrogen microanalysis of the partially hydrated complexes and the results are presented in Table 5.1. Microanalysis indicated a 2:1 host:guest molar ratio for each of the ATBCD, METBCD and OXPRBCD complexes. Prior to microanalysis, the crystals of these complexes were kept in open vials for a week to allow water vapour equilibrium to be reached and the water content thereafter was determined using thermogravimetric analysis.

Table 5.1 C, H, N microanalysis results [n = 3] for the β-CD complexes

Complex	**Calculated**			**Experimental** [#]		
	%C	**%H**	**%N**	**%C**	**%H**	**%N**
ATBCD $2(C_{42}H_{70}O_{35}) \cdot C_{14}H_{22}N_2O_3 \cdot 12H_2O$	42.83	6.80	1.02	42.65	6.73	1.18
METBCD $2(C_{42}H_{70}O_{35}) \cdot C_{15}H_{25}NO_3 \cdot 13.6H_2O$	42.73	6.96	0.50	42.09	6.69	0.54
OXPRBCD $2(C_{42}H_{70}O_{35}) \cdot C_{15}H_{23}NO_3 \cdot 12H_2O$	43.21	6.85	0.51	43.30	6.95	0.81

[#] Precision ± 0.3%

Thermal Analysis

HSM results for the β-CD complexes

HSM was used to analyse the thermal behaviour of the complexes upon heating at a constant rate of 10°C / min. Figures 5.1 and 5.2 illustrate the visually observed changes in the crystals upon heating. The crystals were removed from the mother liquor and submerged in silicone oil in order to prevent preliminary dehydration and to facilitate observation of dehydration upon heating. The ATBCD, METBCD and OXPRBCD crystallised as transparent prisms.

In general, dehydration of all the β-CD complexes was observed at room temperature once the crystals were taken out of the mother liquor; however, for the HSM analysis the crystals were quickly covered in silicone oil. Thus initial water loss from the ATBCD complex was noticed at 74°C and at 150°C the crystals had become totally opaque and the fragmentation of the crystals was noticed. Decomposition of the complex was observed from 230°C onwards and by 350°C extensive decomposition of the complex had taken place.

In the METBCD complex, initial cracking was observed from 36°C and very small bubbles were released at 90°C. By 98°C more pronounced bubbles were liberated and at 140°C the crystals were completely dehydrated. By 150°C the crystals had a glue- like appearance, with poorly defined edges. The onset of decomposition was observed at 190°C.

In the OXPRBCD crystals, bubbling was initially seen at 90°C and continued to 100°C at which the crystals were slightly opaque. The release of bubbles became more vigorous from 110°C and continued to 130°C, finally stopping at 140°C. By 150°C the crystals were totally opaque and had lost the sharpness of their edges. Decomposition commenced at 280°C. Between 300°C and 350°C the crystals showed melting and became darker.

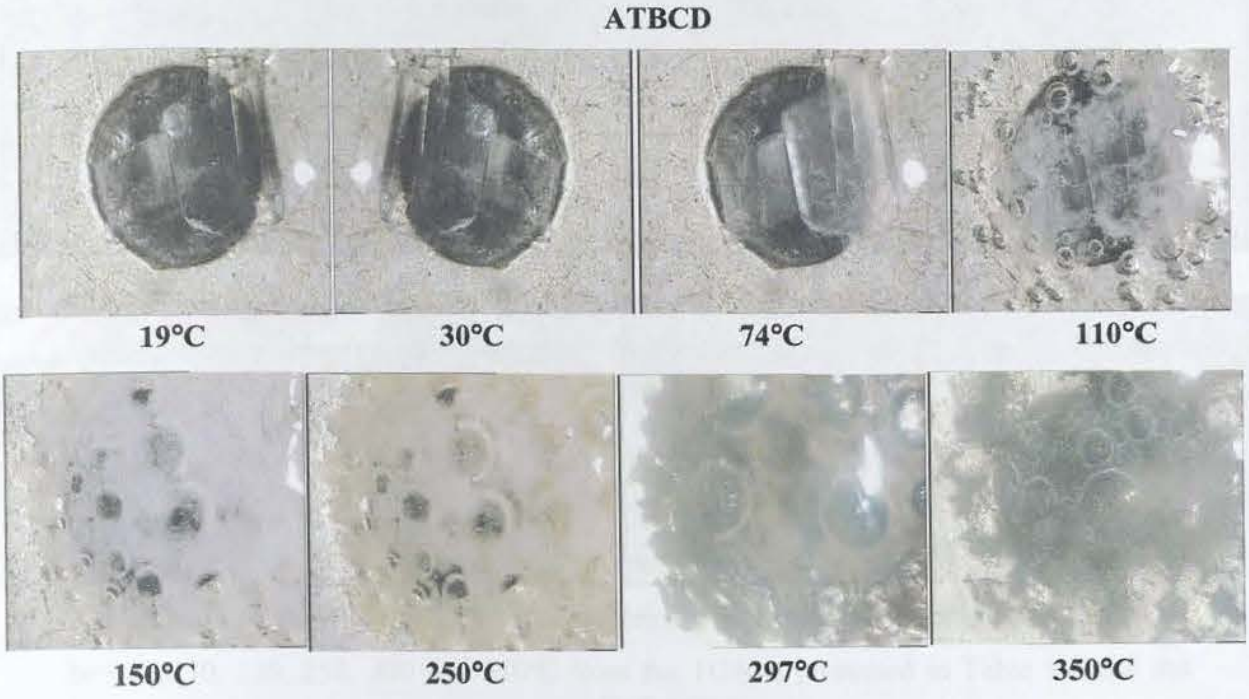

Figure 5.1 HSM photographs taken at various temperatures for crystals of the ATBCD complex.

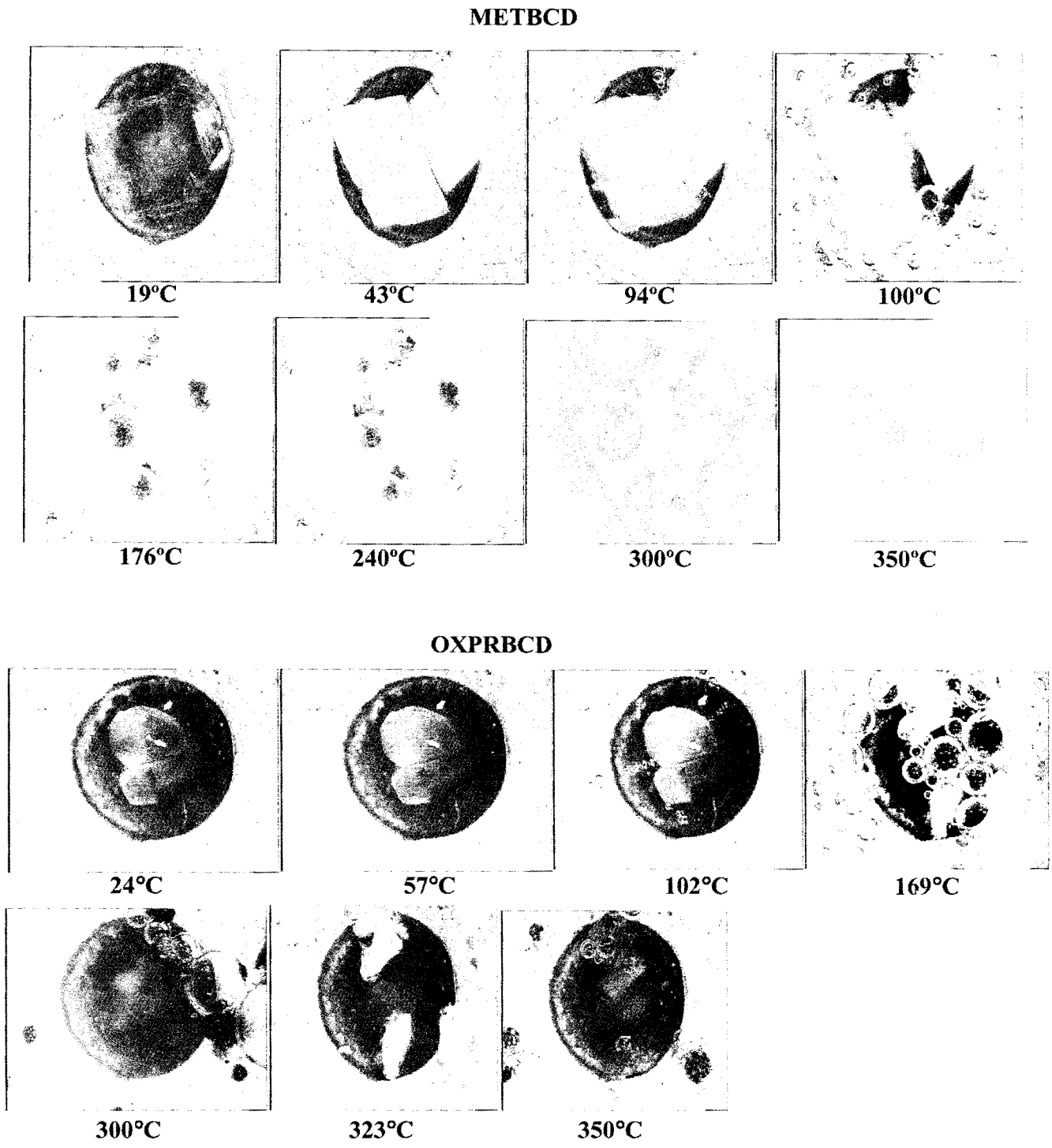

Figure 5.2 HSM photographs taken at various temperatures for crystals of the METBCD and OXPRBCD complexes.

Differential Scanning Calorimetry and Thermogravimetric Analysis

Figure 5.3 shows the DSC traces of the ATBCD, METBCD and OXPRBCD complexes together with the traces of the corresponding uncomplexed drug and the 1:1 β-CD-drug physical mixture. The characteristic fusion endotherms for atenolol, metoprolol and oxprenolol [labelled A in Figure 5.3] occur at 154, 52 and 80°C respectively and are clearly visible in the DSC traces of the uncomplexed drug and physical mixtures of these drugs with β-CD. In each case the disappearance of the fusion endotherm of the drug was observed in the magenta DSC traces of Figure 5.3, which indicated that an inclusion complex had been formed in the solid state. Individual drug molecules encapsulated within the cavities of the cyclodextrin molecules no longer exhibit the characteristic fusion endotherm of their original crystalline phase.

A summary of the observed percentage weight losses over the temperature intervals between 30, 150, 250, 300 and 350°C from the TGA is presented in Table 5.2 and the TGA results for the ATBCD, METBCD and OXPRBCD complexes are shown in Figures 5.4 (a), (b) and (c) respectively.

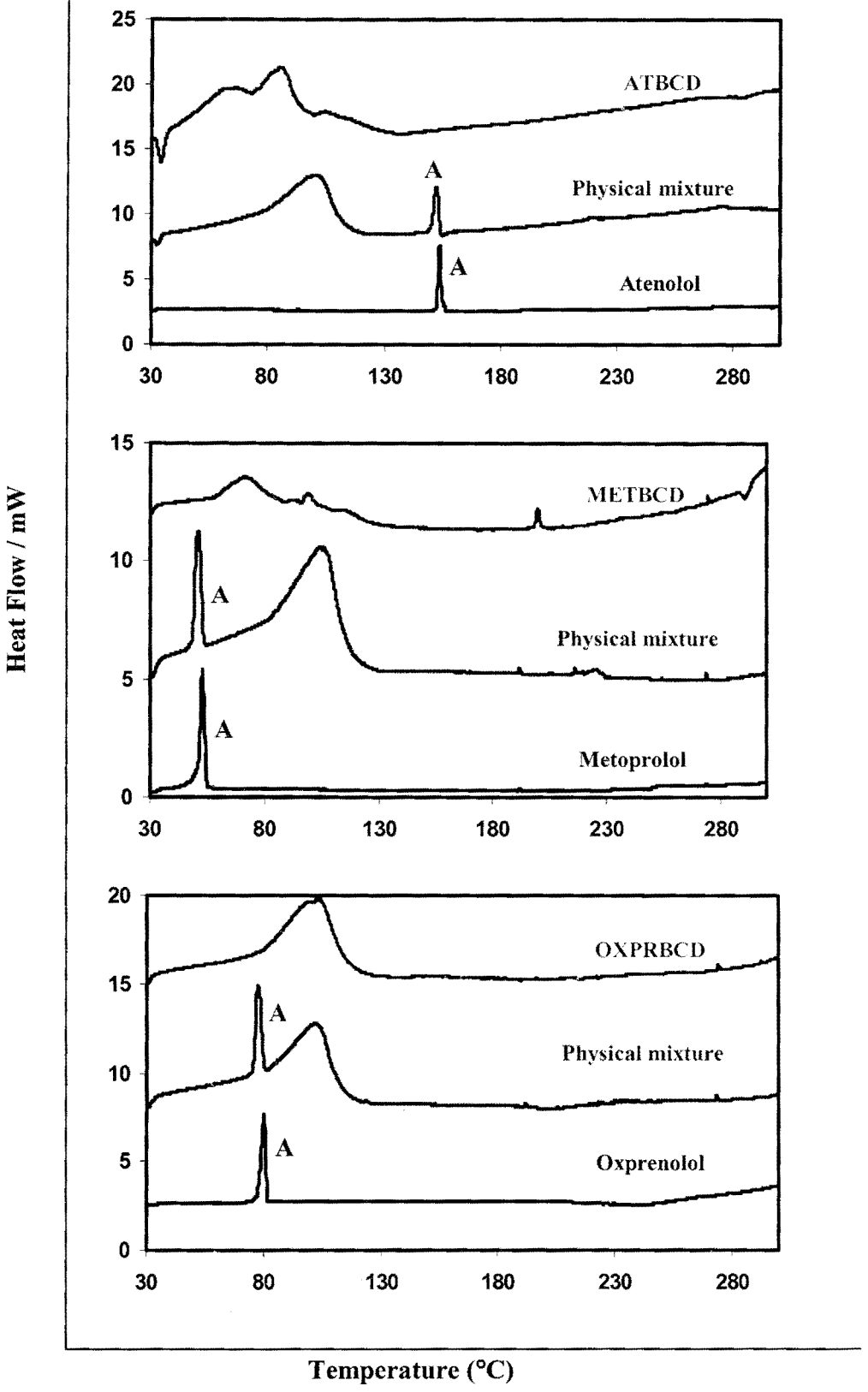

Figure 5.3 DSC traces of the β-CD-β-blocker complexes, physical mixtures and uncomplexed β-blocker drugs.

Table 5.2 The percentage weight losses for the ATBCD, METBCD and OXPRBCD complexes at various temperatures

Temp (°C)	ATBCD		METBCD		OXPRBCD	
	% Mass	% Mass Loss	% Mass	% Mass Loss	% Mass	% Mass Loss
30	100	-	100	-	100	-
150	83.9	16.1	83.2	16.8	88.8	11.2
250	83.7	16.3	81.9	18.1	85.6	14.4
300	83.2	16.8	75.9	24.1	82.3	17.7
350	76.2	23.8	19.6	80.4	27.8	72.2

The DSC results for the ATBCD, METBCD and OXPRBCD complexes are shown in Figure 5.4 (a), (b) and (c) respectively and the results are summarised in Table 5.3. All the complexes tend to have similar profiles. The complexes show a broad asymmetric endotherm [labelled A] with a leading edge, which is associated with water loss. These endotherms cover the same temperature range for water loss as observed from TGA (weight loss due to water loss is labelled A for the TGA traces). For ATBCD the peak of the water loss endotherm [labelled A] occurs at 86°C. However, this peak contains two shoulders occurring at 65°C and 106°C indicating that water loss from this complex is obviously a multi-stage process. The water loss from the METBCD complex shows a sequence of endothermic events on DSC, which is also characteristic of a multi-stage dehydration process. The main endothermic peak [labelled A] occurs at 72°C, with smaller but relatively distinct peaks at 99°C and 116°C. The asymmetric shape of the dehydration endotherm is an indication that the water loss from these complexes is a multi-step process. The OXPRBCD complex displays a characteristic single dehydration endotherm [labelled A] with the main peak at 103°C. The presence of a single endotherm from the OXPRBCD complex indicates that water loss occurs in a single step. For the METBCD complex, the decomposition onset is indicated by a smaller endotherm at approximately 200°C [labelled B] followed by an exotherm at 291°C [labelled C].

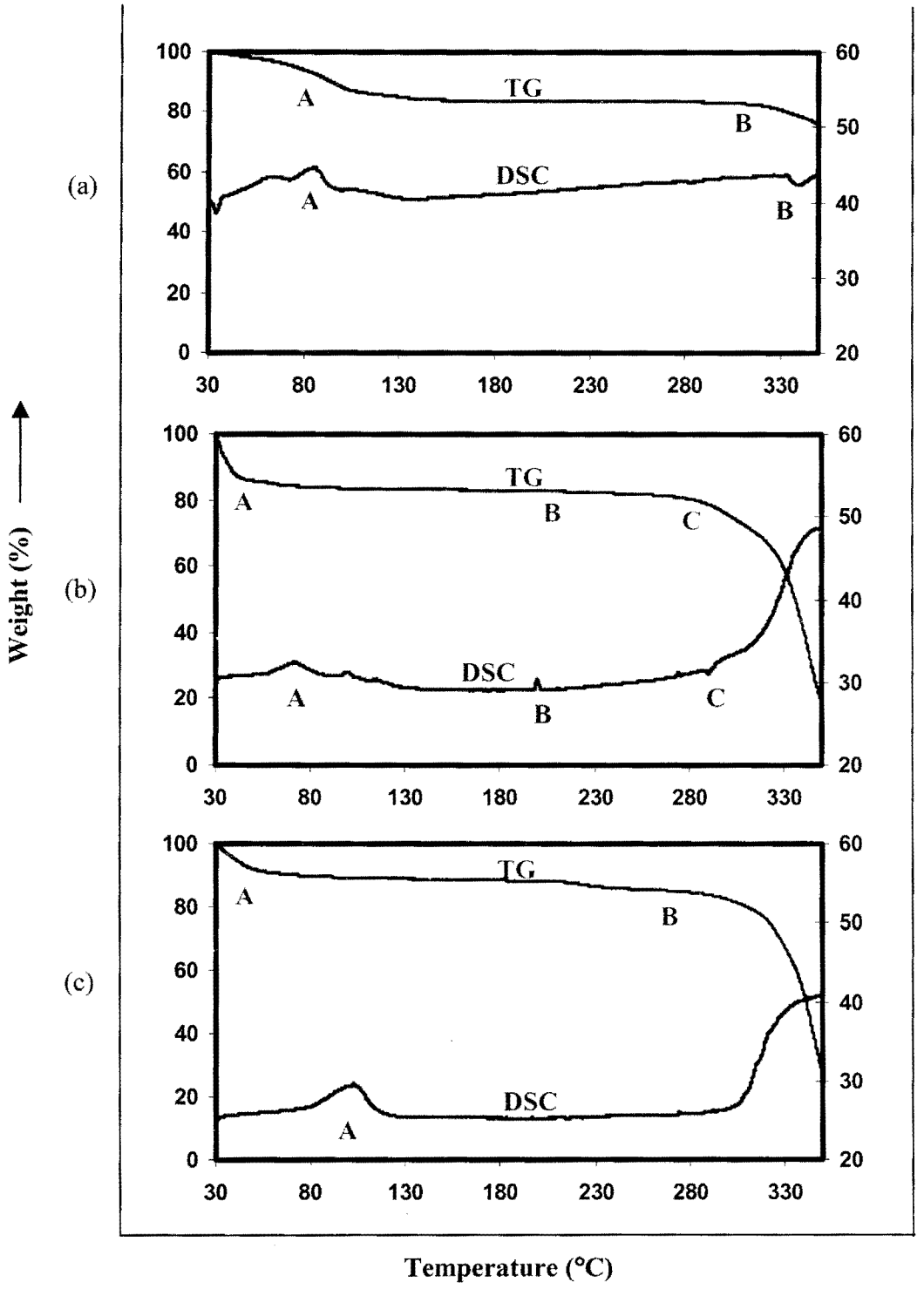

Figure 5.4 TGA and DSC traces for the (a) ATBCD (b) METBCD and (c) OXPRBCD complexes.

The ATBCD complex shows an exotherm with a peak at approximately 338°C [labelled B]. This exotherm most likely indicates a phase change occurring in the already partially decomposing complex. The decomposition of the crystalline β-CD host molecule occurs above 290°C as compared to that of the two complexes, namely METBCD and OXPRBCD which begins well below the decomposition temperature of β-CD, and this is associated with either the beginning of further mass loss or the decomposition of the guest molecules included in the complexes. The TGA traces also show very large weight losses from 270°C onwards for the OXPRBCD and METBCD complexes and from 300°C onwards for the ATBCD complex. The thermal stability of the inclusion complexes is solely based on the analysis of the onset of decomposition for the complexes. The stability follows the order ATBCD > METBCD ~ OXPRBCD, which does not follow a similar thermal stability order to that of the pure drug substances since the melting temperature of oxprenolol is higher than that of metoprolol as shown in Table 5.3.

Table 5.3 Summarised DSC results for the β-CD complexes

			ATBCD	**METBCD**	**OXPRBCD**
Temperature range	A	(°C)	30-138	30-140	30-139
Endotherm A	T_{on}	(°C)	30	30	30
	Peak	(°C)	86	72	103
Endotherm B	T_{on}	(°C)		198	
Exotherm B	T_{on}	(°C)	329		
Exotherm C	T_{on}	(°C)		286	
			atenolol	oxprenolol	metoprolol
Endotherm for fusion of pure drugs (°C)			152	78	49

Experimental PXRD Analysis

Figures 5.5 and 5.6 show the PXRD patterns of the ATBCD and METBCD complexes, obtained from the kneading and co-precipitation methods together with the XRD patterns of the physical mixture of β-CD with the appropriate drug. The diffractometric traces of the kneaded and co-precipitated materials were compared with those of the physical mixture consisting of a 1:1 molar ratio of drug and β-CD. The diffraction patterns of the kneaded and co-precipitated materials were different from that of the physical mixture indicating inclusion complex formation had occurred.[139] The diffractometric traces for the kneaded and co-precipitated materials in Figure 5.6 are in good correspondence, showing that the same crystalline complex METBCD was produced by the different procedures used.

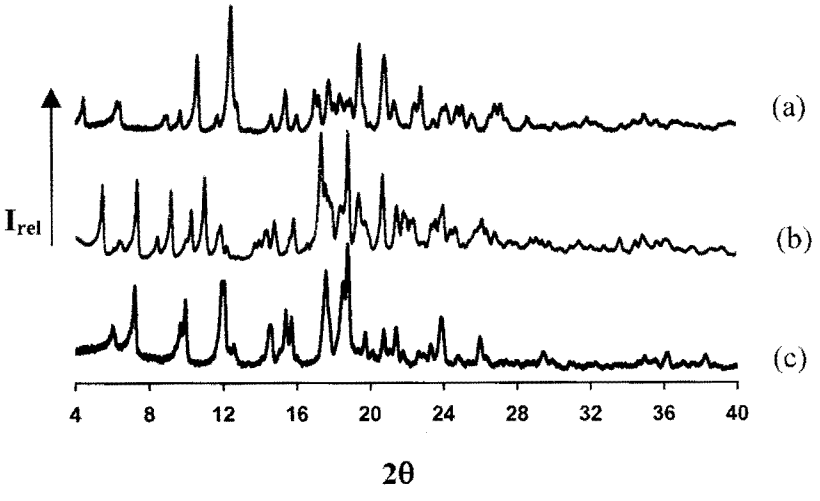

Figure 5.5 XRD patterns of the ATBCD (a) 1:1 physical mixture (b) kneaded and (c) co-precipitated materials.

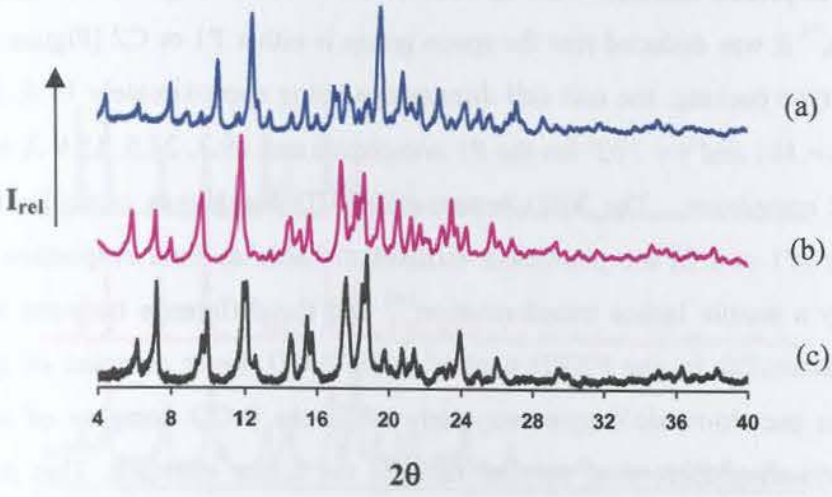

Figure 5.6 XRD patterns of the METBCD (a) 1:1 physical mixture (b) kneaded and (c) co-precipitated materials.

From the observation that the PXRD traces for ATBCD prepared by the kneading and co-precipitation methods are different [Fig. 5.5], it was concluded that the original (untreated) phases are not isostructural.[74] The former complex was subsequently recrystallised from water and unit cell parameters were determined from single crystals. These parameters matched those of single crystals of ATBCD obtained by co-precipitation, both sets corresponding to the triclinic intermediate (IM) packing phase described by Mentzafos *et al.*,[140] space group P1, with a ~ 18, b ~15, c ~ 15 Å. It was also confirmed that the complex prepared by kneading yielded an experimental PXRD pattern corresponding to the published reference pattern for this phase [73] [Fig. 5.7]. The conclusion drawn from the above observations was that when single crystals prepared by co-precipitation were ground for the purpose of PXRD analysis, they transformed into another phase.

Two crystalline forms of a β-CD complex, in which a common single guest is included, had been previously reported.[154] However, the two crystal forms were obtained at different temperatures. The phase transformation of β-CD complexes from one form to another upon grinding is reported by the author in this work for the first time. The experimental PXRD patterns of crystals obtained after the crystallisation of the kneaded

material and co-precipitated material were identical, and in comparing them with those published by Caira,[73] it was deduced that the space group is either P1 or C2 [Figure 5.8], both with channel type packing, the unit cell dimensions being approximately 15.6, 15.6, 15.9 Å, α = 101, β = 101 and γ = 103° for the P1 complexes and 19.3, 24.5, 15.9 Å and β = 109° for the C2 complexes. The XRD patterns of β-CD complexes crystallising in these space groups [P1 or C2] are practically indistinguishable as their respective unit cells are related by a simple lattice transformation[140] and the difference between these structures is not discernible by the PXRD method. The β-CD dimer complex of space group P1 possesses pseudo-twofold symmetry only while the β-CD complex of space group C2 has a crystallographic diad passing through the dimer interface. This subtle relationship consequently has led in more than one instance to the wrong space group being used for complex structure refinement.[141]

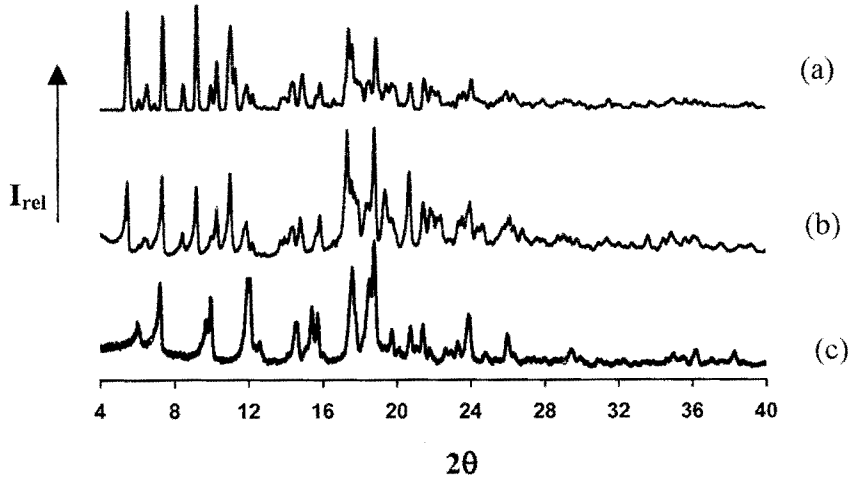

Figure 5.7 XRD traces of the (a) reference pattern for intermediate β-CD dimeric complexes (Space group P1) (b) kneaded ATBCD and (c) recrystallised ATBCD after kneading.

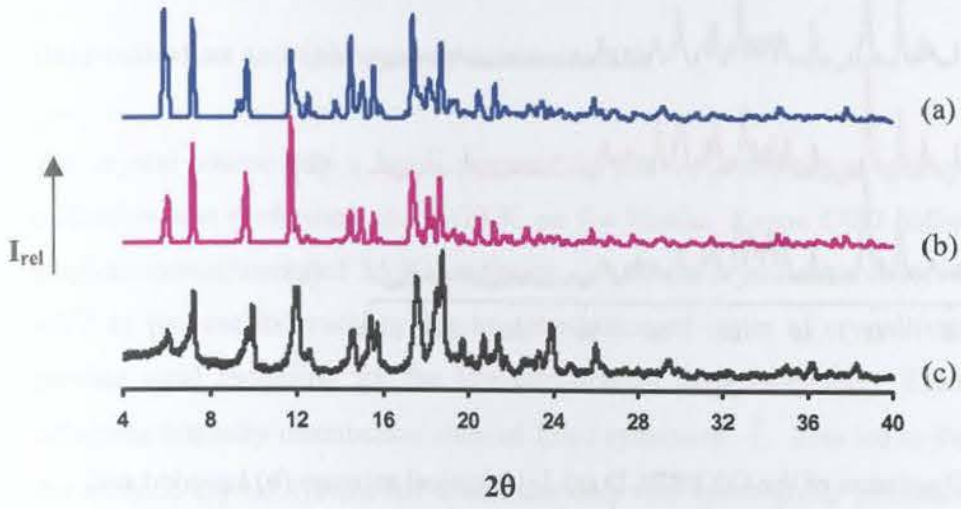

Figure 5.8 XRD traces of the reference patterns (a) C2 (b) P1 and (c) co-precipitated ATBCD.

The diffraction patterns of the physical mixture [consisting of a 1:1 molar ratio of drug and β-CD], kneaded and co-precipitated materials for OXPRBCD are shown in Figure 5.9. The XRD pattern of the kneaded material was similar to that of the physical mixture and different from that of the co-precipitated material indicating that complex formation did not occur from kneading but occurred by co-precipitation.[139]

In Figure 5.10 the PXRD traces of the co-precipitated ATBCD and METBCD complexes resemble each other closely, and they are considered as isostructural.[74] The experimental PXRD pattern for the co-precipitated OXPRBCD complex does not match the pattern for either ATBCD or METBCD.

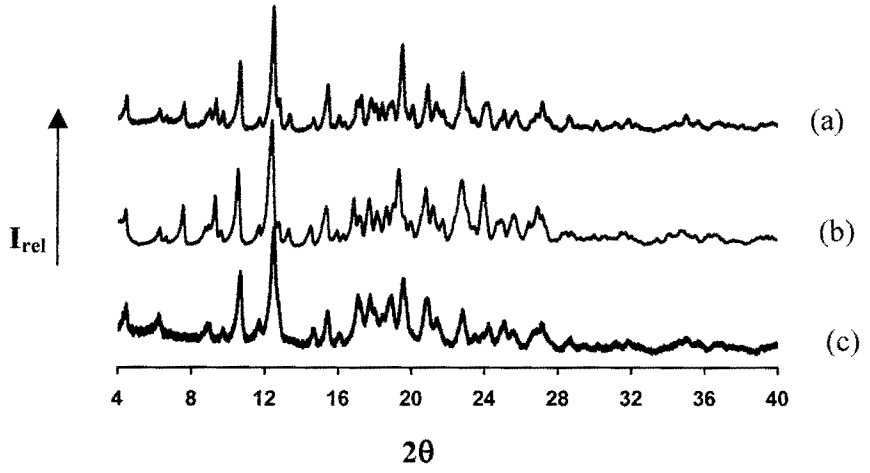

Figure 5.9 XRD patterns of the OXPRBCD (a) 1:1 physical mixture (b) kneaded and (c) co-precipitated materials.

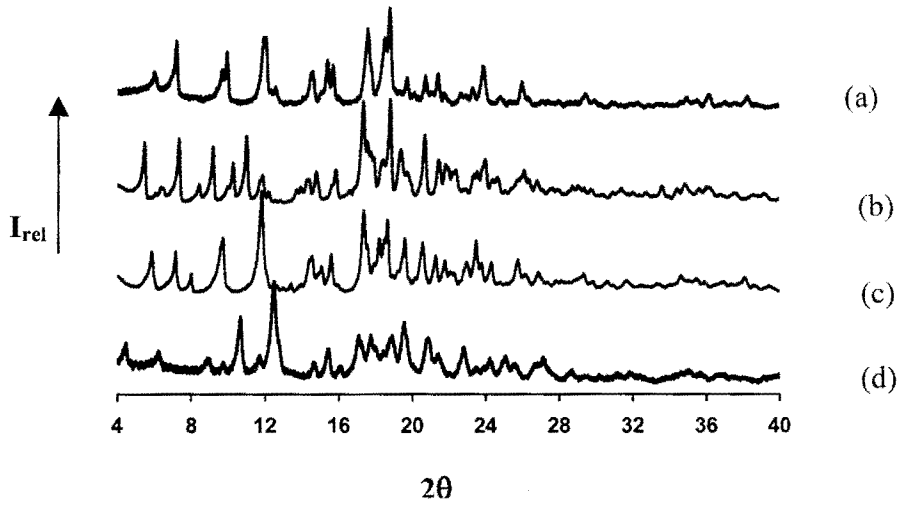

Figure 5.10 PXRD patterns of the (a) co-precipitated ATBCD, (b) kneaded ATBCD, (c) METBCD and (d) co-precipitated OXPRBCD complexes.

X-ray Crystallographic Analysis of the ATBCD Structure

Data-collection and space group determination

The crystal source was a batch prepared by the co-precipitation method. X-ray data-collection was performed at 193(2) K on the Nonius Kappa CCD diffractometer using graphite-monochromated MoKα radiation. A single crystal was covered in Paratone N oil[115] to prevent its cracking due to dehydration of water of crystallisation and also to provide rigid mounting for the low-temperature data collection. Examination of the reflection intensity distribution showed Laue symmetry $\bar{1}$. This led to the assignment of the triclinic crystal system for which the only two space group possibilities are P1 and P $\bar{1}$. Since the host β-CD molecule is chiral, the former space group was chosen.

Structure solution and refinement

The ATBCD complex crystallises in the triclinic crystal system, space group P1 with two crystallographically independent β-CD molecules, one guest molecule and 16.8 water molecules comprising the asymmetric unit of the structure. The structure was solved using published coordinates of the non-hydrogen atoms (excluding the freely rotating primary hydroxyl O atoms) of the two independent β-CD molecules of the isomorphous β-CD-nonanoic acid complex.[142] The difference Fourier map after refinement in SHELX-97[113] revealed the positions of most of the primary hydroxyl oxygen atoms. After refinement of five water molecules, their average fixed U_{iso} of 0.06 $Å^2$ was applied to the remaining water molecules and their site-occupancy factors (s.o.f. 's) were allowed to vary. After further refinement it was found that one of the primary hydroxyl O atoms was disordered over two positions [O63 and O66]. For the disordered O atom, a fixed U_{iso} of 0.06 $Å^2$ [the average of U_{eq} for the chemically equivalent ordered atoms] was assigned and s.o.f.'s of x and 1-x were also assigned, with x variable. The major positions refined to s.o.f.'s of 0.54 and 0.46 for O63 and O66 respectively. The BLOC instruction

was applied for the independent refinement of the host atoms and all non-hydrogen host atoms with $U_{iso} \leq 0.06$ Å^2 were refined anisotropically.

The sequential addition of hydrogen atoms was performed ranging from tertiary C-H, secondary -CH_2 and hydroxyl hydrogen atoms in a riding-model with U_{iso} set at 1.2 times those of the parent atoms. Oxygen atoms of water molecules were located over 33 sites. Water molecules O1W to O6W were assigned full site-occupancy and were refined anisotropically with the final temperature factors U_{eq} in the range 0.04-0.10 Å^2. The remaining water molecules were refined isotropically with a fixed U_{iso} of 0.06 Å^2, the average U of the preceding six water molecules. From O7W to O25W the refinement proceeded with varying site-occupancies. A total number of 17.2 water molecules was accounted for per asymmetric unit as compared to the 16.8 water molecules obtained from TGA results. The site-occupancies of the water molecules are listed in Table 5.4. Crystal data and parameters for its data-collection are listed in Table 5.5.

Table 5.4 Site-occupancy values of the water molecules in the asymmetric unit

Water molecule	**s.o.f.**	**Water molecule**	**s.o.f.**	**Water molecule**	**s.o.f.**
O1W	1. 00	O2W	1.00	O3W	1.00
O4W	1.00	O5W	1.00	O6W	1.00
O7W	0.83	O8A	0.64	O8B	0.40
O9W	0.63	O10W	0.62	O11W	0.56
O12A	0.53	O12B	0.42	O13W	0.57
O14A	0.86	O14B	0.37	O15A	0.38
O15B	0.40	O15C	0.30	O16W	0.31
O17W	0.25	O18A	0.32	O18B	0.26
O19A	0.36	O19B	0.23	O20W	0.30
O21A	0.28	O21B	0.29	O22W	0.29
O23W	0.24	O24W	0.28	O25W	0.27

No attempt was made to locate the hydrogen atoms of water molecules since most of them were disordered over two positions. Eighty four low-angle reflections were omitted as they were truncated by the beam-stop.

Table 5.5 Crystal data and refinement parameters for the ATBCD structure

Complex formula	$2(C_{42}H_{70}O_{35})\cdot C_{14}H_{22}N_2O_3\cdot 16.8H_2O$
Formula weight	2839.0
Crystal system	Triclinic
Space group	P1
a / Å	17.952(1)
b / Å	15.404(1)
c / Å	15.371(1)
α / °	102.87(4)
β / °	113.33(3)
γ / °	99.3(3)
Volume / $Å^3$	3653.89(4)
Z	1
$Density_{calc}$ / g cm^{-3}	1.292
μ(MoKα) / mm^{-1}	0.106
F(000)	1338
Crystal size / mm^3	0.20 x 0.25 x 0.25
Temperature / K	193(2)
Range scanned θ / °	$2 \leq \theta \leq 26$
Index ranges	h : -21, 21 k : -18, 18 l : -18, 18
Dx / mm	42
No. of measured reflections	26557
No. of unique reflections	26557
No. of reflections with $I > 2\sigma(I)$	22613
No. of least-squares parameters	1511
R_{int}, R_σ	0.000, 0.0382
R_1 ($I > 2\sigma(I)$)	0.0889
S	1.04
No. of reflections omitted	84
wR_2	0.2685
Weighting scheme parameters	a = 0.1948, b = 3.2999
Δρ excursions / e $Å^{-3}$	-1.03, 0.90

Overall description of the ATBCD structure

The two CDs were labelled **CD(A)** and **CD(B)**. The glucopyranose units of each of the CDs are numbered from one to seven, so that the glucose residues of **CD(A)** are **A1**, **A2**, **A3**, **A4**, **A5**, **A6** and **A7**. The host-numbering scheme is illustrated in Figure 5.11.

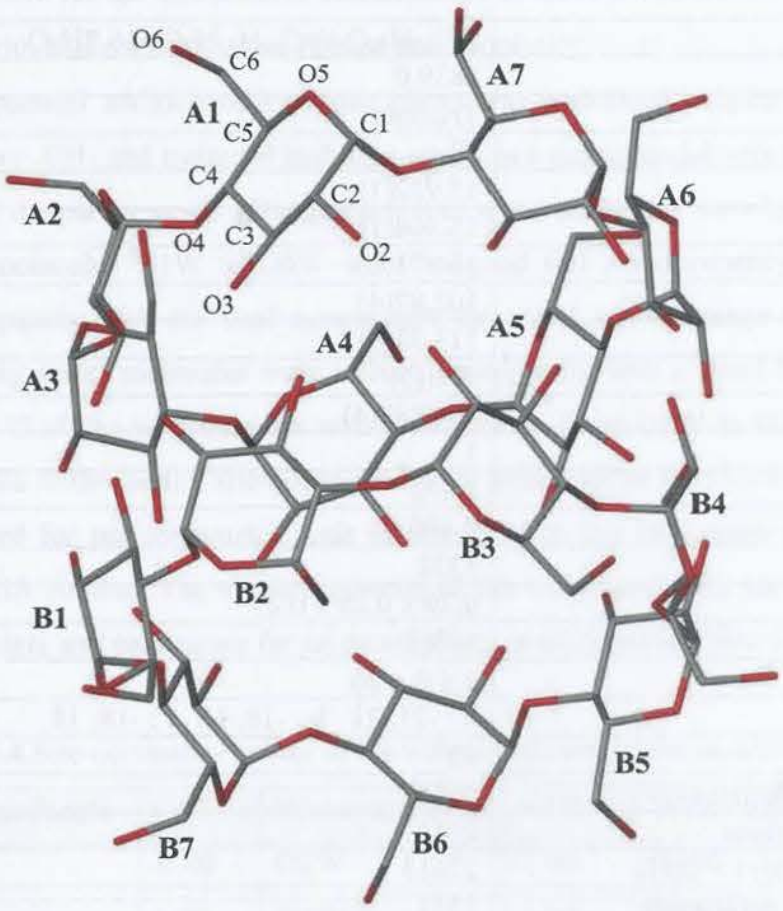

Figure 5.11 Macrocyclic structure and numbering scheme of glucose residues in the asymmetric unit of ATBCD.

The geometrical parameters that describe the conformation of cyclodextrin molecules as discussed in Chapter 1 [Introduction], are listed for the ATBCD structure in Tables 5.6-5.8. Table 5.6 lists the principal torsion angles for the ATBCD host molecule. These include the O5-C5-C6-O6 torsion angle [ω], the glycosidic torsion angles Φ = O5(n)-C1(n)-O4(n-1)-C4(n-1) and ψ = C1(n)-O4(n-1)-C4(n-1)-C3(n-1) and the two pyranoid torsion angles Θ_1 (C2-C3-C4-C5) and Θ_2 (C3-C4-C5-O5) used to describe the conformational relationships around the C4 atom of each glucose unit. All the glucose subunits are in the $^4C_1$ chair conformation. In host molecule A, one of the primary hydroxyl groups is disordered over two positions, O6A7 and O6C7. The (-)- *gauche*

conformation is adopted by the majority of the primary hydroxyl groups, i.e. the C6-O6 bonds point away from the centre of the cavity [indicated by the negative ω parameter]. The C6-O6 bonds for O6A7 [major position] and O6A3 point inside the cavity, thus making these primary hydroxyls adopt the (+)-*gauche* conformation [indicated by the positive ω parameter]. The Φ, ψ, Θ_1 and Θ_2 torsion angles agree closely with those observed for the parent β-CD.[60]

Table 5.6 Principal torsion angles [°] for ATBCD

Glucose unit	ω / °	Φ / °	ψ / °	Θ_1 / °	Θ_2 / °
CD(A)					
A1	-66.8(5)	113.7(4)	123.3(4)	54.8(5)	-52.7(5)
A2	-57.0(6)	116.4(4)	125.9(4)	56.7(5)	-51.7(6)
A3	61.0(6)	116.8(4)	128.7(4)	52.6(6)	-51.3(5)
A4	-67.9(5)	113.4(5)	126.6(4)	55.4(5)	-51.6(5)
A5	-67.4(6)	116.9(4)	131.3(4)	57.8(5)	-58.1(6)
A6	-64.9(5)	109.3(4)	124.4(4)	52.3(5)	-50.2(5)
A7 (O6A7, O6C7)*	63.0(8), -76.0(6)	112.5(5)	129.8(5)	57.1(5)	-57.0(5)
| Average |	**64**	**114.1**	**127.1**	**55.2**	**53.2**
CD(B)					
B1	-66.1(5)	113.6(4)	123.4(4)	54.4(5)	-54.0(5)
B2	-59.1(5)	116.3(4)	126.8(4)	56.0(5)	-53.6(5)
B3	-61.5(7)	114.2(4)	129.0(4)	54.5(6)	-53.3(6)
B4	-68.1(5)	114.1(5)	-114.1(5)	55.5(5)	-51.5(5)
B5	-67.7(9)	115.8(4)	131.5(4)	57.8(6)	-57.6(6)
B6	-67.4(6)	111.1(5)	124.1(4)	52.8(5)	-50.7(5)
B7	-66.0(8)	114.1(5)	129.7(5)	55.2(6)	-54.0(6)
| Average |	**65.1**	**114.2**	**125.5**	**55.2**	**53.5**

* Two values for the ω parameter as a result of the disorder of the O6 atom

Table 5.7 lists the geometric parameters of the O4 heptagon of the ATBCD structure for the two crystallographically independent β-CD molecules **A** and **B** making the dimer. These geometric parameters are the radii [**r**], the O4•••O4' distances [**l**], the O4•••O4'•••O4" angles [**a**], the O4•••O4'•••O4"•••O4'" torsion angles [**t**] and the deviations of each of the O4 atoms from the mean O4 plane [**d**]. The average value of parameter **d** is larger for **CD(A)** than for **CD(B)**. This is accompanied by larger torsion angles for the **CD(A)** host molecule as compared to those of **CD(B)**. The **r**, **l** and **a** parameters do not vary substantially within each β-CD molecule, thus reflecting the near ideal seven-fold symmetry of the O4-heptagons. The low values of the **d** and **t** parameters also indicate this symmetry. The O4 mean planes of the **A** and **B** host molecules are also nearly parallel, as indicated by the angle of 1.02(4)° that these make with each other.

Table 5.7 O4-heptagon for the ATBCD structure

Glucose unit	r / Å	l / Å	a / °	d / Å	t / °
CD(A)					
A1	4.89	4.47	132	-0.009(2)	0.2
A2	5.06	4.33	128	-0.004(3)	-1.5
A3	5.22	4.32	124	0.028(3)	2.7
A4	4.90	4.49	132	-0.034(3)	-2.5
A5	4.97	4.28	130	0.016(3)	1.3
A6	5.17	4.40	126	-0.001(3)	-0.6
A7	5.06	4.31	128	0.004(3)	0.5
| Average |	**5.04**	**4.37**	**129**	**0.014**	**1.3**
CD(B)					
B1	4.99	4.39	129	-0.005(2)	0.3
B2	5.00	4.38	129	-0.003(3)	-0.2
B3	5.11	4.30	127	-0.001(3)	0.7
B4	5.01	4.43	129	0.012(3)	-1.1
B5	4.95	4.31	130	-0.015(3)	0.7
B6	5.07	4.36	127	0.002(3)	0.1
B7	5.05	4.35	128	0.008(3)	-0.4
| Average |	**5.03**	**4.36**	**128**	**0.007**	**0.5**

The other important features of the macrocyclic structure such as the intersaccharidic bond angle (φ), and the tilt angles [τ_1 and τ_2] are listed in Table 5.8. The definition of these parameters is given in Chapter 1.

Table 5.8 φ, and τ for the ATBCD structure

Glucose unit	φ / °	τ_1 / °	τ_2 / °
CD(A)			
A1	117.4(4)	4.5(1)	5.5(2)
A2	117.7(4)	4.3(1)	6.4(1)
A3	118.1(3)	6.3(1)	7.3(1)
A4	118.7(4)	4.9(1)	6.7(2)
A5	117.4(4)	11.9(1)	12.3(2)
A6	117.6(4)	6.9(1)	8.9(1)
A7	118.6(4)	9.8(1)	4.9(2)
Average	**117.9**	**6.9**	**7.4**
CD(B)			
B1	117.4(4)	4.5(1)	5.6(1)
B2	117.4(3)	4.3(1)	7.4(2)
B3	118.5(3)	6.3(1)	9.0(2)
B4	117.6(4)	4.9(1)	7.1(1)
B5	117.7(4)	11.9(1)	11.1(2)
B6	116.8(4)	6.9(1)	6.6(3)
B7	118.4(4)	9.8(1)	10.3(3)
Average	**117.7**	**6.9**	**8.2**

The conformations of the two crystallographically independent β-CD molecules, **A** and **B**, are not significantly different. A high degree of planarity of the whole O(4) heptagon is observed and based on the O(4)•••O(4') distances [**A** and **B** averages being 4.37Å and 4.36Å (Table 5.5) compared to 4.38Å, the distance of the regular heptagon] and O(4)•••O(4')•••O(4") angles, a seven-fold symmetry is evident. The O(4) angles shown in Table 5.7 [**A** and **B** average values being 129° and 128° respectively], do not differ significantly from 128.3°, the angle of the regular heptagon, meaning that there is a very slight distortion of the cavity due to the inclusion of the guest. The small deviation of the O(4) atoms from the mean O(4) plane also confirms the high degree of planarity.

The tilt angles of the glucopyranose units are very small and positive resulting in the truncation of the O(6) end of the β-CD molecule giving it a cone shape with the secondary rim being wider than the primary rim. The O(2)•••O(3') distance values [**A**(average) = 2.79Å, **B**(average) = 2.77Å] are characteristic of strong intramolecular hydrogen bonds corresponding to the flip-flop system described by Saenger[143,144] to maintain the structural rigidity of the β-CD molecule.

Guest inclusion

Due to abnormal distances and angles between the electron density peaks, the guest could not be located beyond a diffuse electron density cloud located within the cyclodextrin cavity and thus could not be modelled. The maximum and minimum residual electron densities were 0.90 and 0.43 e $Å^{-3}$ respectively. Since elemental analysis and UV spectroscopy confirmed the host-guest mole ratio of 2:1, the low R_1 of 0.09 for observed data indicated that the guest is extensively disordered [Figures 5.12(a) and (b)] since it effectively does not contribute to the X-ray scattering. This disorder of the guest is a very rare case for the intermediate packing system if compared with other β-CD complexes of the same packing system reported so far in the CSD.[82] It is not possible to ascertain whether the disorder is statistical or whether the guest molecule is undergoing a high degree of thermal motion or is actaully migrating through the channels despite intensity data-collection having been recorded at a temperature well below ambient.

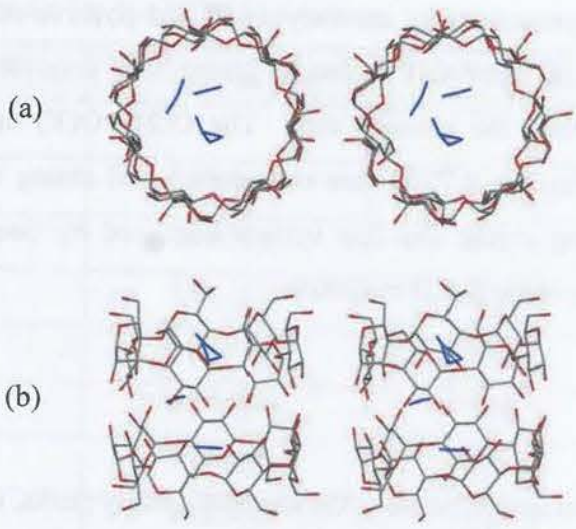

Figure 5.12 Stereo-view of the (a) top and (b) side faces of the β-CD dimer in the ATBCD structure illustrating the peaks of highest electron density in the dimer cavity.

Host hydrogen bonding interactions of the ATBCD structure

PLATON[114] was used to calculate several hydrogen bonding interactions for the ATBCD structure exclusively involving host atoms. These host hydrogen bonding interactions are categorised based on whether they occur within or between dimers, respectively referred to as intra- and inter-dimer host hydrogen bonding interactions.

Intra-dimer hydrogen bonds

The intra-dimer host hydrogen bonding interactions are presented in Table 5.9. There are nine intramolecular O-H•••O hydrogen bonds [four for **CD(A)** and five for **CD(B)**] that stabilise the macrocyclic conformation of the β-CD molecule and the orientation of one glucose unit relative to its neighbours. There are eleven intermolecular, intra-dimer O-H•••O hydrogen bonds that connect the two host molecules into a head-to-head dimer, and these involve the O2 and O3 atoms on the secondary sides of the β-CD molecules. A stereo diagram of all the intra- and intermolecular intra-dimer O-H•••O hydrogen bonds is presented in Figure 5.13. The O2 and O3 atoms that are not engaged in O2•••O3'

intramolecular hydrogen bonds are involved in hydrogen bonds to the other host molecule of the dimer. It has recently been shown for the first time with the aid of synchrotron data that the O3•••O3' hydrogen bonds bind the dimer in the 2(β-CD)•(1,12)-dodecanedioic acid structure.[145]

Table 5.9 Intra-dimer hydrogen bonds

Interaction	H•••A / Å	D•••A / Å	D-H•••A / °
Intramolecular			
O3A1-H3A1•••O2A2	1.98	2.71(1)	144
O3A2-H3A2•••O2A3	2.11	2.78(1)	137
O3A7-H3A7•••O2A1	2.05	2.79(1)	147
O3A4-H173•••O2A5	1.91	2.80(1)	155
O3B2-H3B2•••O2B3	2.11	2.80(1)	139
O3B3-H3B3•••O2B4	2.02	2.77(1)	148
O3B4-H3B4•••O2B5	2.11	2.81(1)	141
O2B6-H2B6•••O3B5	2.01	2.76(1)	149
O3B6-H3B6•••O2B7	2.08	2.80(1)	143
Host•••host			
O2A3-H2A3•••O3B7	2.44	3.18(1)	147
O3A3-H3A3•••O3B7	2.04	2.87(1)	168
O2A5-H2A5•••O3B5	2.47	3.23(1)	150
O3A5-H3A5•••O3B5	2.01	2.83(1)	169
O2A6-H2A6•••O3B4	2.30	3.01(1)	142
O3A6-H3A6•••O3B4	1.92	2.76(1)	174
O3B1-H3B1•••O3A2	1.97	2.79(1)	165
O2B3-H2B3•••O3A7	2.48	3.17(1)	139
O2B5-H2B5•••O3A5	2.53	3.21(1)	139
O3B5-H3B5•••O3A5	2.01	2.83(1)	167
O3B7-H3B7•••O3A3	2.05	2.87(1)	165

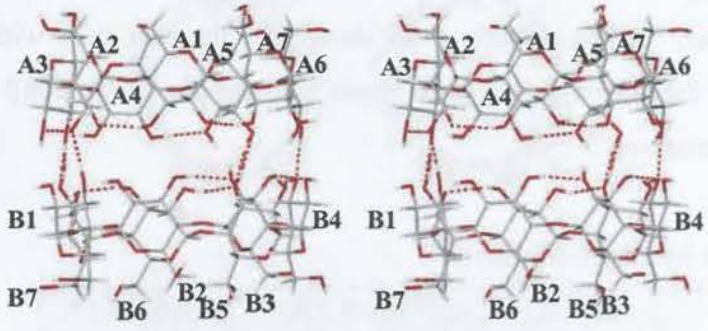

Figure 5.13 Stereo diagram of the intra-dimer O-H•••O hydrogen bonding for the ATBCD structure.

Inter-dimer hydrogen bonds

Table 5.10 lists the inter-dimer hydrogen bonding interactions. These interactions are categorised as intra-layer [within the same layer] and inter-layer [between adjacent layers]. There are seven unique C-H•••O intra-layer hydrogen bonding interactions, namely C1-H•••O2' and C2-H•••O3' hydrogen bonds. The hydrogen atoms on C1 and C2 allow the cyclodextrin molecules to interact with the atoms of neighbouring β-CD molecules.

On the other hand there are six inter-layer O-H•••O hydrogen bonding interactions, of which only one is of type O6-H•••O5' and the remaining five being O6-H•••O6' hydrogen bonds.

Table 5.10 Inter-dimer hydrogen bonding interactions for the ATBCD structure

Interaction	H•••A / Å	D•••A / Å	D-H•••A / °	Symmetry code *
Intra-layer				
C2A1-H1•••O3A4	2.42	3.38(1)	161	x, y, 1+z
C1A1-H1A1•••O2A5	2.58	3.38(1)	137	x, y, 1+z
C2A6-H11•••O3A2	2.35	3.30(1)	157	x, 1+y, z
C2B1-H15•••O3B4	2.37	3.36(1)	168	x, -1+y, z
C2B6-H25•••O3B2	2.34	3.30(1)	161	x, y, -1+z
C1A6-H1A6•••O2A3	2.55	3.40(1)	142	x, 1+y, z
C1B1-H1B1•••O2B5	2.52	3.31(1)	136	x, -1+y, z
Inter-layer				
O6A6-H29•••O6A2	2.31	2.87(1)	125	x, 1+y, z
O6A1-H30•••O6A4	2.14	2.77(1)	131	x, y, 1+z
O6B1-H6BC•••O6B4	2.13	2.74(1)	130	x, -1+y, z
O6A3-H6AC•••O6B3	1.99	2.75(1)	151	-1+x, -1+y, -1+z
O6A4-H6AD•••O6A1	2.10	2.77(1)	136	x, y, -1+z
O6B3-H6BG•••O5A3	2.27	3.10(1)	171	1+x, 1+y, 1+z

* Symmetry code applied to the second unit of the interaction

Water interactions

The summary of the close contacts involving water molecules, together with their averages and ranges, for the ATBCD structure, is presented in Table 5.11. The total number of water molecules accounted for by single crystal X-ray analysis was 17.2 as compared to 16.8 obtained from the TGA. These water molecules were located around the periphery of the host molecules. The unsuccessful modelling of the guest made it difficult to ascertain the possible presence of water within the host cavities. Intermolecular and intramolecular O-H•••O' hydrogen bonds and interactions due to water molecules form cooperative networks which enhance the rigidity of the host. The intermolecular hydrogen bonding across the secondary hydroxyl ends of two symmetry-independent β-CD molecules causes these molecules to exist as a head-to-head dimer.

The water sub-layer forming the interface between two adjacent dimeric layers contributes to the cohesiveness of the crystal structure.[140]

Table 5.11 Water interactions for the ATBCD structure

Type	Number of interactions	Range (Å)	Average (Å)
O2A•••Water	9	2.68-3.20	2.92
O3A•••Water	6	2.77-3.23	2.93
O5A•••Water	1	3.09	3.09
O6A•••Water	10	2.68-2.89	2.76
C2A•••Water	5	3.24-3.41	3.31
C6A•••Water	5	3.31-3.41	3.35
Total Host(A) •••Water	**36**		
O2B•••Water	9	2.55-3.08	2.78
O3B•••Water	6	2.76-3.10	2.92
O5B•••Water	4	3.04-3.19	3.12
O6B•••Water	11	2.69-2.98	2.80
C2B•••Water	6	3.04-3.34	3.22
C5B•••Water	1	2.77	2.77
C6B•••Water	3	2.05-3.38	2.91
Total Host(B) •••Water	**40**		
Water•••Water	**22**	2.53-3.09	2.87

Crystal packing of the ATBCD structure

Figure 5.14 presents a stereo view of the crystal packing down the a-axis for the ATBCD structure and it shows channels produced by the cavities of the dimers being parallel to the a-axis and perpendicular to the O(4) plane. This implies that layers are stacked parallel to the yz-plane of the structure. The crystalline ATBCD inclusion complex consists of head-to-head dimeric β-CD molecules.

This diagram [Figure 5.14] also illustrates the location of the water molecules where they act as the 'glue' that maintains the crystal structure.

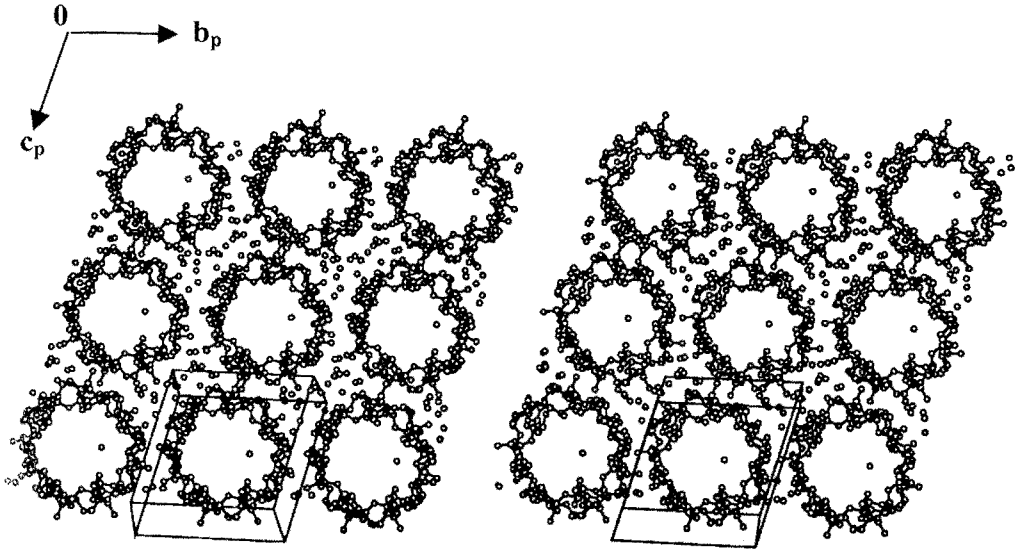

Figure 5.14 Stereo view of the crystal packing down the a-axis for the ATBCD structure. Water oxygen atoms are shown as isolated spheres.

An intermediate (IM) type packing mode is observed for the ATBCD structure which is characteristic for β-CD dimeric complexes that crystallize in the space group P1 with cell dimensions similar to those reported here.[140] In the intermediate type structures, the β-CD dimers are arranged as close packed layers stacking on top of each other with a significant shift. A number of structures with this IM packing mode, crystallizing in P1 have been reported[142,146,147,148,149,150,151,152,153,154,155] The relative average shift of consecutive dimers, when the dimers are viewed perpendicular to their mean O(4) planes is 6.0(2) Å for IM type structures crystallizing in the space group P1.[140] This value is almost equal to the inner diameter of the β-CD molecule at the primary rim and is slightly larger than the average radius of the O(4) heptagon. In Figure 5.14 the packing diagram shows that the dimers are arranged in dimeric layers parallel to the yz-plane of the structure. The isolation and structure elucidation of a cyclodextrin inclusion complex of the IM type-packing mode in which the guest is completely disordered is a rare case. The author is unaware of any β-CD inclusion complex of this nature.

Powder X-ray diffraction

The experimental and computed PXRD patterns for ATBCD as well as the reference pattern for IM [space group P1] type complexes are presented in Figure 5.15. The computed pattern was calculated from the above refinement based on crystals obtained by co-precipitation. The experimental and computed patterns do not match and this is attributed to a phase transformation that occurs upon grinding these crystals. The computed PXRD pattern for the ATBCD complex and the IM [P1] type reference pattern are in good agreement with each other and this furthermore is the evidence that a phase transformation had occurred upon grinding the co-precipitated ATBCD crystals.

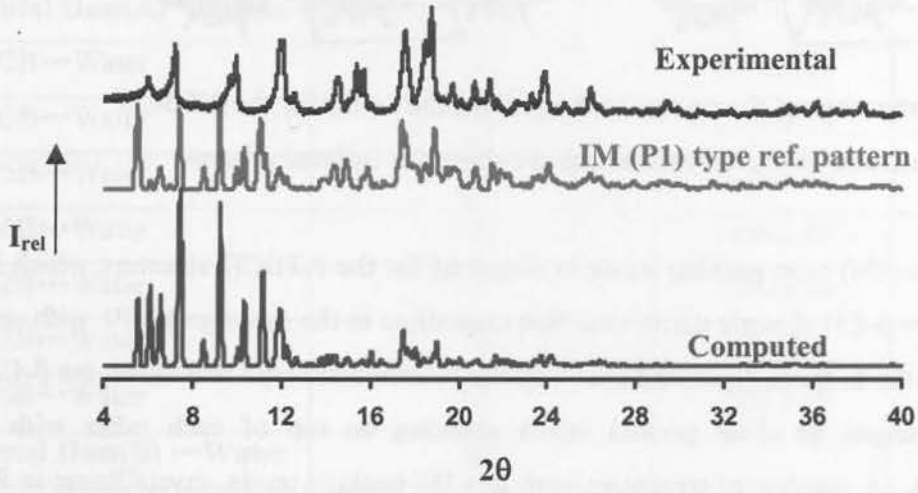

Figure 5.15 Computed [193K] and experimental [295K] PXRD traces for ATBCD; shown also is a reference pattern.

Inclusion of (S)-Atenolol in β-CD

A study of the inclusion of the racemic anti-inflammatory drug, ibuprofen, in β-CD by Brown[156] resulted in the complex with space group C2, and the cell parameters a = 19.41, b = 24.41, c = 15.92 Å, β = 108.89° and Z = 4, in which the guest was completely disordered. A later study of the inclusion complex between β-CD and the enantiopure (S)-ibuprofen, the more active form, by Susana *et al*,[157] resulted in a complex with space

group C2, cell parameters a = 19.41, b = 24.41, c = 15.90 Å, β = 109.03°, Z = 4 and the guest was successfully modelled.

An attempt to include racemic atenolol [guest] in β-CD [host] as described in the previous section, resulted in the guest being completely disordered in the cavity of the host. The disorder of the guest was attributed to both (R)- and (S)- enantiomers that are present in equal amounts in the original guest sample, competing to be included in the cyclodextrin cavity. Various methods were utilised to isolate the biologically active (S)-atenolol[158] and among those the direct enantiomeric resolution of racemic atenolol by Bhushan[159] was carried out using normal-phase TLC on silica gel plates impregnated with L-aspartic acid as the chiral selector. However, this was unsuccessful. A further attempt to synthesize (S)-atenolol according to the method of Kitaori *et al*[160] was performed using p-hydroxyphenylacetamide and (R)-epichlorohydrin. This procedure was also unsuccessful in producing resolved enantiomers. Eventually (S)-atenolol, purchased from Sigma Aldrich, was used for β-CD inclusion with the objective of successfully modelling the guest in the inclusion complex.

Complex Preparation

The crystalline complex of (S)-atenolol with β-CD was prepared by the co-precipitation method in which the drug was slowly added to a hot saturated β-CD solution [1:1 host-guest molar ratio]. The solution was stirred for four hours. The crystals were obtained from both slow cooling and evaporation of the aqueous solution. The inclusion complex between (S)-atenolol and β-CD will be referred to hereinafter as SATBCD.

Microanalysis

The host-guest ratio was determined by C, H and N microanalysis of the partially hydrated complex. Prior to microanalysis, the crystals were kept in an open vial for a week to allow water vapour equilibrium to be reached. Microanalysis showed that the

SATBCD complex crystallises in a 2:1 host:guest ratio. The microanalysis results are presented in Table 5.12.

Table 5.12 C, H, N microanalysis results [n = 3] for SATBCD

Complex	Experimental *			Calculated		
	%C	%H	%N	%C	%H	%N
SATBCD $2(C_{42}H_{70}O_{35})\bullet C_{14}H_{22}N_2O_3\bullet 10H_2O$	43.11	6.92	1.00	43.33	6.75	1.03

* E.s.d. in experimental percentage ~ 0.25

Thermal analysis

HSM was used to analyse and to compare the thermal behaviours of ATBCD [prepared using racemic atenolol] and SATBCD [prepared using enantiopure (S)- atenolol]. HSM results for the ATBCD and SATBCD complexes are presented in Figure 5.16. The flat plate-like appearance for both complexes shows that they have similar crystal habits. In addition both complexes display similar thermal events, i.e. initial cracking and bubbling indicating loss of water, followed by decomposition.

The ATBCD crystals started cracking at 74°C as they began to lose their water of crystallisation. Thereafter significant cracking was observed from 100°C and by 148°C the crystals had become totally opaque. These dehydrated crystals remained unchanged till shortly before 230°C. The discoloration of the complex from 250°C onwards was evidence of its decomposition and by 350°C extensive decomposition of the complex had taken place. The SATBCD crystals began cracking at 61°C and became more opaque as the temperature increased to 80°C. Bubbles were observed at 89°C and became more vigorous by 102°C. The severe cracking and breaking apart of crystals was caused by dehydration. Decomposition was observed as the crystals began to discolour at a temperature of 242°C. Thus the thermal properties for the ATBCD and SATBCD crystals are similar.

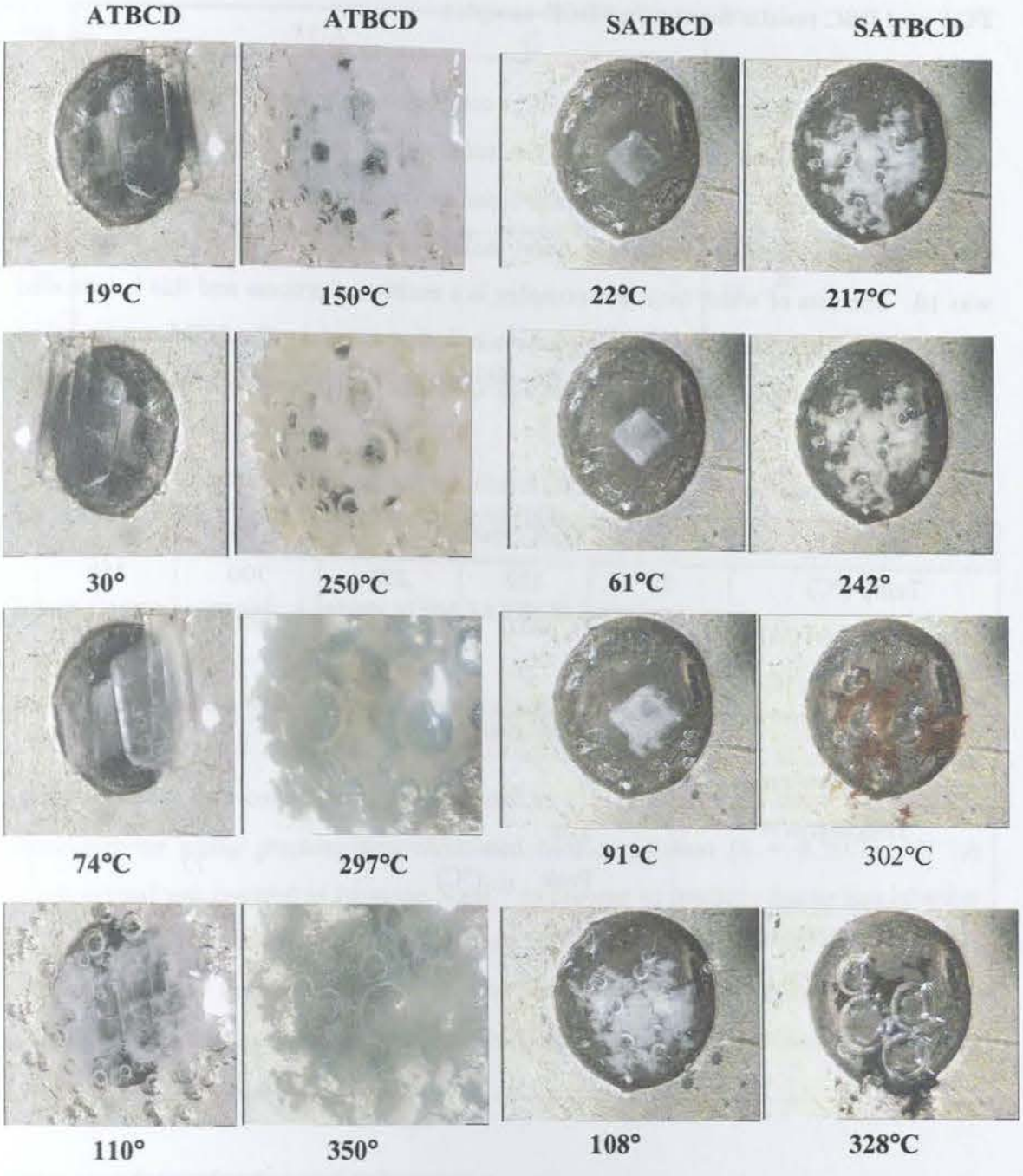

Figure 5.16 HSM photographs at various temperatures for crystals of the ATBCD and the SATBCD complexes.

TGA and DSC results for the SATBCD complex

The DSC and TGA traces for the SATBCD complex are shown in Figure 5.17 and the results are summarised in Table 5.13. TGA results show that water loss is complete by 130°C and this event is consistent with the broad asymmetric endotherm labelled A in the DSC trace. The calculated number of water molecules per CD from the TGA weight loss was 16. The loss of water from this complex is a multi-step process and this is indicated by the asymmetric shape of the dehydration endotherm and by the HSM results. The further mass loss on the TGA traces from 318°C labelled C is the onset of decomposition.

Table 5.13 Summaries of TGA and DSC results for the SATBCD complex

TGA results					
Temp (°C)	30	130	250	300	350
Sample weight (%)	100	90.0	89.5	88.2	34.1
Δ Weight loss (%)	-	10	0.50	1.30	54.1
DSC results					
Temperature range	A	(°C)	30 – 93		
Endotherm A	Ton	(°C)	63		
	Peak	(°C)	77		
Temperature range	B	(°C)	92 – 130		
Endotherm B	Ton	(°C)	93		
	Peak	(°C)	99		

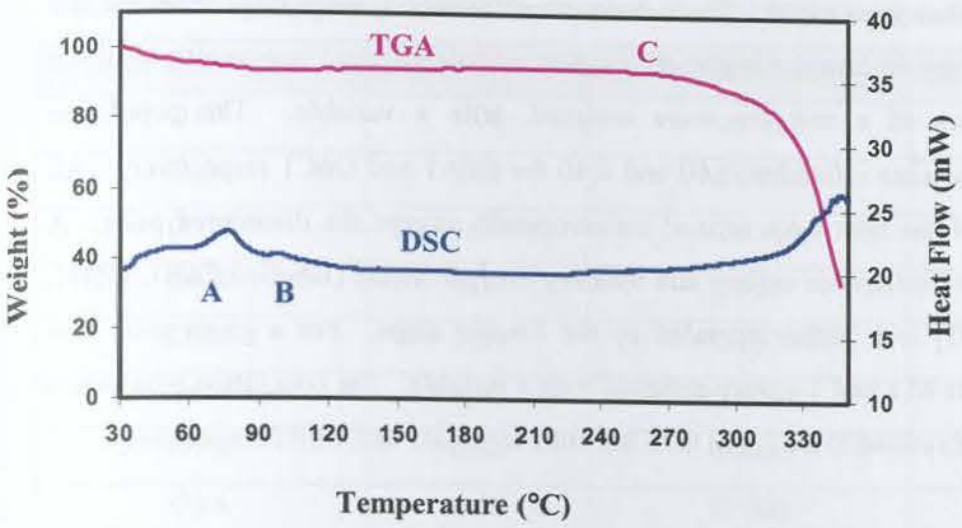

Figure 5.17 TGA and DSC traces for the SATBCD complex.

X-ray Crystallographic Analysis of the SATBCD Structure

Data-collection and space group determination

X-ray intensity data-collection was performed at 113(2) K on the Nonius Kappa CCD diffractometer using graphite-monochromated MoKα radiation [λ = 0.71073 Å]. A single crystal was covered in Paratone N oil[115] to prevent its cracking due to loss of water of crystallisation and also to provide rigid mounting for the low-temperature data collection. Laue symmetry $\bar{1}$ from a preliminary survey of the reflection intensities indicated the triclinic crystal system. The chiral nature of the β-CD molecule determined the space group as P1.

Structure determination and refinement

The co-ordinates for the non-hydrogen β-CD atoms of the isomorphous β-CD-atenolol complex described earlier in this chapter [deprived of the primary hydroxyl atoms] were used to solve the structure. The refinement of this fragment was performed with SHELX-97.[113] The difference Fourier map that followed showed the positions of the

primary hydroxyl oxygen atoms. The subsequent difference Fourier maps revealed that one of the primary hydroxyl oxygen atoms was disordered over two positions. Site occupancy factors of x and 1-x were assigned, with x variable. The population parameters of the sites refined to 0.60 and 0.40 for O6A1 and O6C1 respectively. All oxygen atoms of the host were refined anisotropically except the disordered pairs. A disordered pair of methylene carbon and hydroxyl oxygen atoms [labelled C6B1, C6D1, O6B1 and O6D1] was further revealed by the Fourier maps. For a given pair, site-occupancy factors of z and 1-z were assigned with z variable. The population parameters of the major sites refined to s.o.f.'s of 0.75 and 0.81 for C6B1 and O6B1 respectively.

After the complete location of all non-hydrogen atoms of the host, the placement of the cyclodextrin hydrogen atoms was carried out. Hydrogen atom positions were calculated for idealised geometries based on stereochemical requirements. These atoms were included in a riding model, with U_{iso} set to 1.2 times the U_{iso} of the parent atom. A common variable temperature factor was assigned to all the primary hydroxyl hydrogen atoms and they were located using the AFIX 83 instruction.

Oxygen atoms of water molecules were located over thirty seven sites. Water molecules O1W to O6W were assigned a full site occupancy factor and were refined anisotropically with final equivalent isotropic temperature factors U_{eq} ranging between 0.05 and 0.10 $Å^2$. The remaining water molecules were refined isotropically with a constant U_{iso} of 0.05 $Å^2$ [the average U value of the first six water molecules]. The site-occupancies of these water molecules were allowed to vary. Most of the water molecules were disordered over two positions with the exception of O16W which is disordered over three positions labelled O16A, O16B and O16C. Table 5.14 lists the site-occupancies of the water molecules. A total of 17.0 water molecules in the asymmetric unit were found which closely agreed with the 16 water molecules calculated from thermogravimetric analysis. Crystal data and data-collection parameters are listed in Table 5.15.

Table 5.14 Site-occupancy values of the water molecules in the asymmetric unit

Water molecule	s.o.f.	Water molecule	s.o.f.
O1W	1.00	O15A	0.37
O2W	1.00	O15B	0.32
O3W	1.00	O16A	0.36
O4W	1.00	O16B	0.22
O5W	1.00	O16C	0.16
O6W	1.00	O17W	0.29
O7W	0.84	O18A	0.28
O8A	0.65	O18B	0.24
O8B	0.42	O19A	0.25
O9W	0.59	O19B	0.18
O10A	0.45	O20W	0.23
O10B	0.32	O21A	0.27
O11A	0.58	O21B	0.19
O11B	0.36	O22W	0.30
O12A	0.33	O23A	0.23
O12B	0.34	O23B	0.18
O13A	0.40	O24W	0.19
O13B	0.34	O25W	0.20
O14W	0.54	O26W	0.20

No attempt was made to place hydrogen atoms of water molecules because of the disorder observed for most of them. The highest and lowest residual electron density peaks of 0.93 and 0.37 e $Å^{-3}$ respectively were found within the cavity. An attempt was made to refine the highest electron density peak as oxygen and it was assigned a constant U_{iso} of 0.1 $Å^2$ and the site-occupancy factor refined to only 0.3. Thereafter attempted sequential refinement of the inner cavity electron density peaks as carbon atoms followed. Due to the abnormal distances and angles between the peaks the refinement was terminated and it was noted that the guest was disordered.

Table 5.15 Crystal and refinement parameters for the SATBCD structure

Complex formula	$2(C_{42}H_{70}O_{35})\bullet C_{14}H_{22}N_2O_3\bullet 16H_2O$
Formula weight	2824.6
Crystal system	Triclinic
Space group	P1
a / Å	17.8931(2)
b / Å	15.3823(1)
c / Å	15.3211(1)
α / °	102.828(4)
β / °	113.365(4)
γ / °	99.309(4)
Volume / $Å^3$	3624.63(5)
Z	1
$Density_{calc}$ / g cm^{-3}	1.294
μ(MoKα) / mm^{-1}	0.107
F(000)	1336
Crystal size / mm^3	0.23 x 0.25 x 0.25
Temperature / K	113 (2)
Range scanned θ / °	$4 \leq \theta \leq 28$
Index ranges	h : -22, 22 k : -19, 19 l : -19, 19
Dx / mm	33
No. of measured reflections	30242
No. of unique reflections	30242
No. of reflections with $I > 2\sigma(I)$	26432
No. of least-squares parameters	1118
R_{int}, R_σ	0.000, 0.0311
R_1 ($I > 2\sigma(I)$)	0.0954
S	1.38
No. of reflections omitted	172
wR_2	0.3049
Weighting scheme parameters	a = 0.2, b = 0
Δρ excursions / e $Å^{-3}$	-0.62, 0.93

Geometrical analysis of the SATBCD structure

The asymmetric unit of the SATBCD complex comprises two crystallographically independent β-CD molecules, one disordered guest molecule and 16 water molecules. The two CDs will be referred to as **CD(A)** and **CD(B)**. The glucose residues of each of the CDs are numbered from one to seven, so that the glucose residues of **CD(A)** are **A1** to **A7**. Figure 5.18 shows the host numbering scheme.

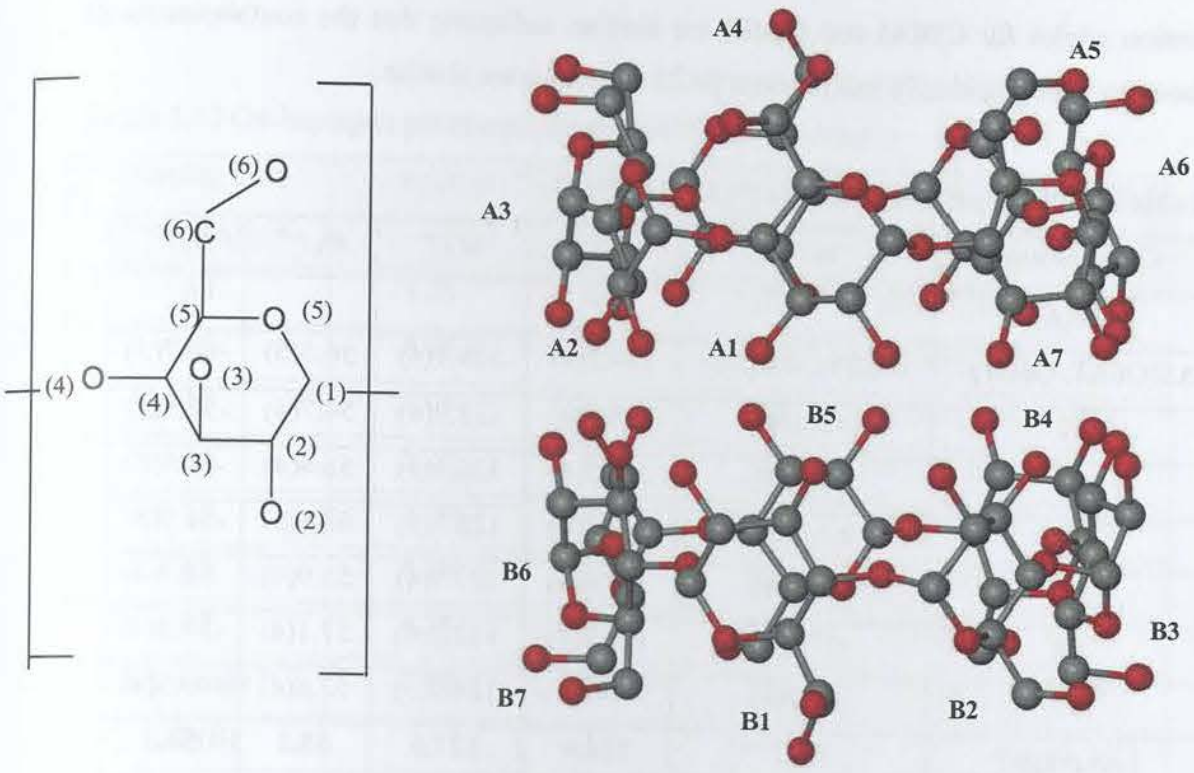

Figure 5.18 Macrocyclic structure and numbering scheme of glucose residues.

The shape of the macrocycle resembles that of a hollow cylinder. All fourteen glucopyronose units adopt the usual $^4C_1$ chair conformation. In the host molecules **A** and **B**, one carbon atom of the methylene group and two hydroxyl groups are disordered over two positions respectively [host **A**: O6A1 and O6C1; host B: C6B1, C6D1, OB1 and O6D1].

The geometrical data that describe the conformations of cyclodextrin molecules, as discussed in Chapter 1- Introduction, are listed for the SATBCD structure in Tables 5.16-5.18. The principal torsion angles for the SATBCD host molecule are listed in Table 5.16. In the SATBCD structure, all the C6-O6 bonds are in the (-)-*gauche* conformation. The C6-O6 bonds for glucose units **A1** and **B1** are in both the (-)- and (+)-*gauche* conformations, because of the disorder of their O6 atoms. The respective conformations of the major and minor components of the disorder for the **A1** and **B1** glucose units are

described by the (+)-*gauche* conformations. The average values for **Φ**, **ψ**, **Θ_1** and **Θ_2** torsion angles for **CD(A)** and **CD(B)** are similar, indicating that the conformations of these crystallographically independent β-CD molecules are similar.

Table 5.16 Principal torsion angles [°] for SATBCD

Glucose unit	ω / °	Φ / °	ψ / °	Θ_1 / °	Θ_2 / °
CD(A)					
A1(O6A1, O6C1) *	63.2(7), -74.1(8)	114.2(4)	129.1(4)	56.5(5)	-56.7(5)
A2	-65.1(4)	113.5(4)	123.9(4)	54.7(4)	-52.9(4)
A3	-54.5(5)	116.3(4)	126.1(3)	56.4(4)	-51.8(5)
A4	61.0(5)	117.5(4)	128.7(3)	53.1(5)	-51.9(5)
A5	-66.8(4)	113.4(4)	127.7(4)	55.9(4)	-52.7(4)
A6	-67.7(5)	116.9(4)	132.2(4)	57.1(4)	-57.2(4)
A7	-65.2(4)	110.1(3)	124.7(3)	52.6(4)	-49.7(4)
| Average |	**64.7**	**114.6**	**127.5**	**55.2**	**53.3**
CD(B)					
B1(O6B1, O6D1) #	-60(1), 67(4)	115.1(4)	128.7(3)	55.3(5)	-53.7(5)
B2	-66.4(4)	113.9(4)	125.3(4)	55.7(5)	-51.7(4)
B3	-68.9(8)	115.1(4)	131.4(4)	57.1(5)	-57.6(5)
B4	-67.6(4)	110.6(4)	122.7(4)	53.6(4)	-51.6(4)
B5	-64.7(7)	114.7(4)	129.5(4)	55.3(5)	-53.0(5)
B6	-67.1(4)	112.9(4)	122.7(4)	54.4(4)	-53.8(4)
B7	-59.6(4)	117.3(3)	126.1(3)	56.4(4)	-52.9(4)
| Average | *	**65.2**	**114.2**	**126.6**	**55.4**	**53.5**

Two values for the ω parameter as a result of the disorder of the O6 atom
* Unweighted average of all recorded values

Table 5.17 lists the parameters of the O4-heptagon. The **r**, **a** and **l** parameters, which respectively describe the distance of the O4-heptagon centroid to each O4 atom, the distance between adjacent O4 atoms and the angle between three adjacent O4 atoms, do not vary substantially within each β-CD molecule, thus showing the near ideal seven-fold

symmetry of the O4-heptagons. The low values of the **d** and **t** parameters also indicate this symmetry.

Table 5.17 O4-heptagon parameters for the SATBCD structure

Glucose unit	r / Å	l / Å	a / °	d / Å	t / °
CD(A)					
A1	5.05	4.32	128	0.009(2)	0.8
A2	4.88	4.47	132	-0.009(2)	0.1
A3	5.06	4.32	128	-0.005(2)	-1.5
A4	5.22	4.32	124	0.026(2)	2.7
A5	4.89	4.49	132	-0.034(2)	-2.9
A6	4.96	4.28	130	0.022(2)	1.9
A7	5.18	4.38	125	-0.010(2)	-1.2
| Average |	**5.03**	**4.37**	**128**	**0.016**	**1.6**
CD(B)					
B1	5.11	4.30	127	0.003(2)	0.6
B2	5.02	4.43	129	0.014(2)	-1.4
B3	4.94	4.31	130	-0.020(2)	1.2
B4	5.07	4.37	127	0.007(2)	-0.3
B5	5.05	4.34	128	0.006(2)	-0.1
B6	4.99	4.38	129	-0.002(2)	-0.2
B7	4.98	4.40	130	-0.008(2)	0.1
| Average |	**5.02**	**4.36**	**129**	**0.009**	**0.6**

Table 5.18 lists the other important features of the macrocyclic structure such as the intersaccharidic bond angle (φ) and the tilt angles [τ_1 and τ_2] for the SATBCD structure. The φ angles for both host molecules are close to the average values for other β-CD molecules.[61] All the tilt angles for host molecules **A** and **B** are positive and their values

are fairly small and are within a fairly narrow range [4.3-12.5 and 4.0-11.5° for host molecules **A** and **B** respectively].

Table 5.18 φ and τ parameters for the SATBCD structure

Glucose unit	φ / °	τ_1 / °	τ_2 / °
CD(A)			
A1	118.1(3)	8.9(1)	10.0(2)
A2	117.2(3)	4.3(1)	5.8(2)
A3	118.3(3)	4.6(1)	6.6(1)
A4	117.6(3)	6.1(1)	7.2(1)
A5	118.4(3)	4.7(1)	7.0(2)
A6	117.4(3)	11.8(1)	12.5(1)
A7	117.1(3)	7.0(1)	8.8(1)
Average	**117.7**	**6.8**	**8.3**
CD(B)			
B1	117.9(3)	7.8(1)	8.4(2)
B2	118.5(4)	5.3(1)	7.2(1)
B3	117.9(3)	10.8(1)	11.5(2)
B4	117.5(3)	5.3(1)	6.3(2)
B5	118.2(3)	9.1(1)	10.1(2)
B6	117.7(3)	4.0(1)	4.8(1)
B7	117.6(3)	5.4(1)	6.8(2)
Average	**117.9**	**6.8**	**7.9**

Guest interaction

Microanalysis indicated that one guest molecule was included in two β-CD molecules. The guest molecule, however, could not be visualised beyond a diffuse electron density cloud as it was extensively disordered. The highest and lowest electron density peaks within the cavity range between 0.93 and 0.37 e $Å^{-3}$, and are illustrated in stereo in Figure

5.19. The abnormal distances and angles associated with these peaks made it impossible to model a guest molecule and the mode of complexation therefore could not be established. The Fourier map did not reveal any recognisable fragment upon the refinement of the first two highest electron density peaks within the cavity as oxygen atoms, followed by a subsequent refinement of the remaining electron density peaks as carbon atoms, refining one atom at a time at a constant U_{iso} of 0.1 $Å^2$. This condition persisted even when the investigation of the difference Fourier maps extended to examination of the residual two hundred peaks.

(a)

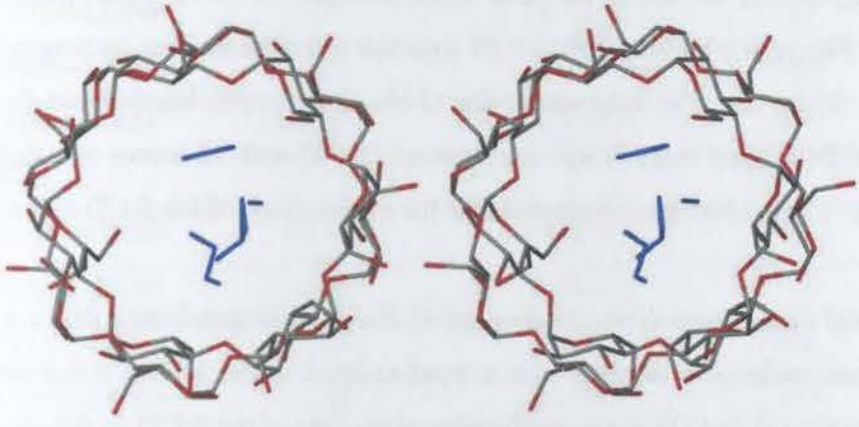

(b)

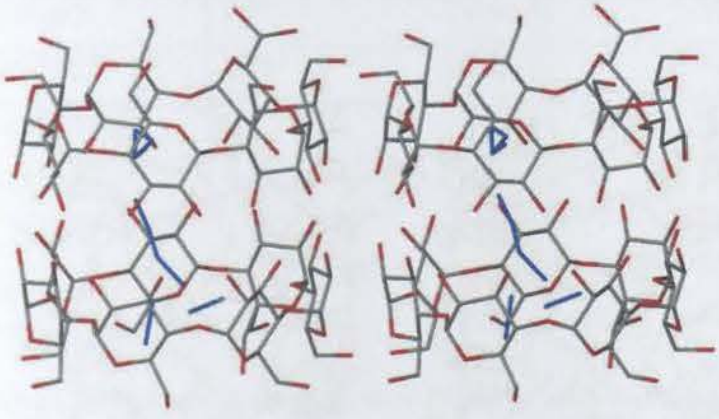

Figure 5.19 Stereo views of the (a) top and (b) side faces of the β-CD dimer in SATBCD showing the electron density in the dimer cavity.

Hydrogen bonding interactions of the host

The calculation of several hydrogen bonding interactions for the SATBCD structure involving host atoms was by means of PLATON.[114] The hydrogen bonding interactions that occur within dimers are referred to as intra- while those that occur between dimers are known as intermolecular hydrogen bonding interactions.

Intra-dimer hydrogen bonds

A stereo diagram of all the intra- and intermolecular O-H•••O hydrogen bonds is presented in Figure 5.20 whilst Table 5.19 lists the intra-dimer host hydrogen bonding interactions. There are nine intra-molecular O-H•••O hydrogen bonds [four for **CD(A)** and five for **CD(B)**] and these bonds are between the O2 and O3 atoms of neighbouring glucose units. These hydrogen bonds stabilise the round shape of the β-CD molecules.[140]

There is a total of ten intra-dimer, host•••host O-H•••O hydrogen bonds that connect the two β-CD host molecules together into a head-to-head dimer in the asymmetric unit. These involve the O2 and O3 atoms on the secondary rims of the β-CD molecules.

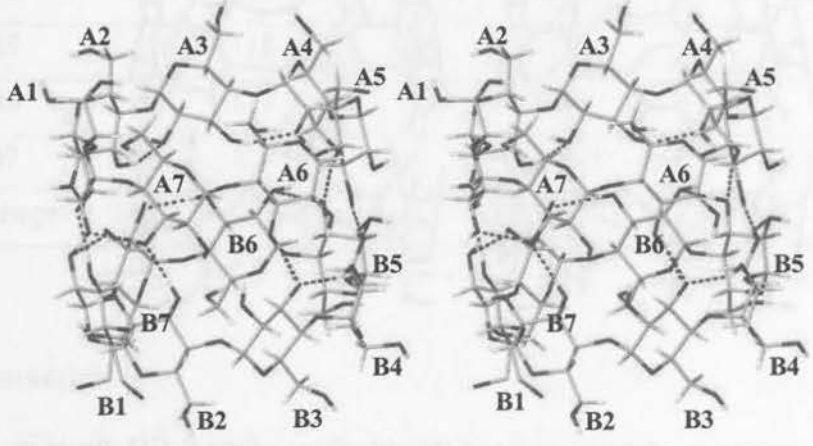

Figure 5.20 Stereo diagram showing intra- and inter-molecular hydrogen bonding for the SATBCD structure. Only O-H•••O hydrogen bonding atoms are shown.

Table 5.19 Intra-dimer O-H•••O hydrogen bonds

Interaction	H•••A / Å	D•••A / Å	D-H•••A / °
Intramolecular			
O3A1-H3A1•••O2A2	2.04	2.78(4)	147
O3A2-H3A2•••O2A3	1.98	2.71(4)	145
O3A3-H3A3•••O2A4	2.10	2.78(4)	137
O3A7-H3A7•••O2A1	2.05	2.81(4)	151
O2B4-H2B4•••O3B3	2.00	2.76(4)	149
O3B4-H3B4•••O2B5	2.06	2.78(4)	143
O3B5-H3B5•••O2B6	1.95	2.72(4)	151
O3B6-H3B6•••O2B7	2.02	2.74(4)	144
O3B7-H3B7•••O2B1	2.09	2.78(5)	138
Host•••Host			
O2A4-H2A4•••O3B5	2.43	3.17(5)	147
O3A4-H3A4•••O3B5	2.02	2.85(5)	168
O3A5-H3A5•••O3B4	1.89	2.70(5)	162
O2A6-H2A6•••O3B3	2.46	3.21(5)	149
O3A6-H3A6•••O3B3	1.97	2.80(5)	169
O2A7-H2A7•••O3B2	2.29	3.00(4)	141
O2B1-H2B1•••O3A1	2.47	3.15(5)	139
O3B1-H3B1•••O3A1	1.98	2.80(5)	164
O3B2-H3B2•••O3A7	1.94	2.75(5)	160
O2B3-H2B3•••O3A6	2.51	3.19(5)	139

The O2 and O3 atoms that are not involved in O2•••O3' intra-molecular hydrogen bonds participate in hydrogen bonding to the other host molecule of the dimer. Previous neutron diffraction studies of carbohydrate crystal structures by Steiner,[161] indicates that oxygen atoms adjacent to C-H donors enhance their donor strength.

The mobility of the O2 and O3 hydrogen atoms has been highlighted in previous neutron diffraction studies[143,144] due to the dynamic switching between O2•••O3' and O3•••O2'. In

Table 5.19 the O3•••O3' hydrogen bond candidates for the SATBCD structure are found to have shorter and more favourable O-H•••O geometries than O2•••O3' hydrogen bonds.

Inter-dimer hydrogen bonds

The inter-dimer hydrogen bonds are classified into two categories, namely, (i) intra-layer [within the same layer] and (ii) inter-layer [between adjacent layers] and these bonds are listed in Table 5.20. The arrangement of dimers is of the intermediate type, consisting of the disrupted channel motif of the SATBCD that will be dealt with in the section titled 'Crystal packing'.

There are twelve unique intra-layer hydrogen bonds of which only four are O-H•••O hydrogen bonds, the rest being C-H•••O hydrogen bonds, the former being an O6-H •••O6' and the latter being C2-H•••O3' hydrogen bonds. The external location of the C1 and C2 hydrogen atoms of the cyclodextrin molecules enables them to interact with the atoms of neighbouring β-CD host molecules.

There is only one inter-layer hydrogen bond, namely the O6-H•••O6' hydrogen bond. This small number of strong O-H•••O hydrogen bonds for the inter-layer dimeric interactions shows that dimers are more weakly associated between the dimeric layers than within them.

Table 5.20 Inter-dimer hydrogen bonds for the SATBCD structure

Interaction	H•••A / Å	D•••A / Å	D-H•••A / °	Symmetry code *
Intra-layer				
O6B6-H6BA•••O6B2	2.14	2.74(1)	128	x, -1+y, z
O6A2-H6AC•••O6A5	2.09	2.72(1)	132	x, y, 1+z
O6A7-H6AD•••O6A3	2.32	2.86(1)	123	x, 1+y, z
O6A5-H6AE•••O6A2	2.07	2.72(1)	134	x, y, -1+z
C2A2-H3•••O3A5	2.40	3.36(1)	160	x, y, 1+z
C1A2-H1A2•••O2A6	2.57	3.36(1)	137	x, y, 1+z
C2A7-H13•••O3A3	2.33	3.27(1)	156	x, -1+y, z
C2B6-H25•••O3B2	2.34	3.33(1)	168	x, -1+y, z
C1A7-H1A7•••O2A4	2.54	3.38(1)	142	x, 1+y, z
C1B4-H1B4•••O2B1	2.59	3.40(1)	138	x, y, -1+z
C1B6-H1B6•••O2B3	2.51	3.30(1)	136	x, -1+y, z
C2B4-H21•••O3B7	2.33	3.29(1)	162	-1+x, -1+y, z
Inter-layer				
O6A4-H6AF•••O6B1	1.92	2.69(1)	152	-1+x, -1+y, z

* Symmetry code applied to the second unit of the interaction

Water interactions

TGA analysis of the SATBCD structure showed a total of sixteen water molecules as compared to seventeen which were modelled over thirty seven sites because of the majority of these water molecules having partial site-occupancies. The location of water molecules was around the peripheries of the host molecules. These water molecules maintain the host structure or connect the host and guest molecules. They also act as the packing space fillers among the β-CD dimer units. The unsuccessful modelling of the guest molecule because of its disorder made it difficult to observe the possible presence of water molecules within the host cavities and therefore no attempts were made to do so. Close contacts between water and the SATBCD structure are listed in Table 5.21.

There are two separate water networks formed between the dimers, one linking the primary [O6] and the other linking the secondary [O2 and O3] hydroxyl groups. Since the secondary hydroxyl oxygen atoms donate their H atoms in the hydrogen bonding scheme within the dimer or between dimers in the lattice, the water molecules act as H atom donors. There are six water molecules that are hydrogen bonded to **CD(A)** and five water molecules to **CD(B)**. The remaining six water molecules are linked to the CD by other water molecules and they do not interact with the host at all.

Table 5.21 Summary of close contacts between water and the SATBCD structure

Contact atom	No. of interactions	Range / Å	Mean Distance / Å
O2A	14	2.53-3.19	2.84
O3A	8	2.74-3.20	2.86
O5A	2	3.05-3.22	3.13
O6A	14	2.66-3.04	2.78
C1A	1	2.92	2.92
C2A	9	2.72-3.40	3.17
C4A	1	2.78	2.78
C6A	7	2.84-3.36	3.25
Total Host(A)•••Water	**56**		
O2B	15	2.50-3.16	2.74
O3B	8	2.77-2.99	2.88
O5B	4	3.01-3.16	3.09
O6B	10	2.70-2.98	2.80
C2B	9	2.73-3.38	3.13
C4B	2	2.78-3.35	3.06
C5B	1	2.77	2.77
C6B	5	2.84-3.42	3.18
Total Host(B)•••Water	**54**		
Water•••Water	**20**	2.68-3.09	2.87

Crystal packing of the SATBCD structure

The crystalline SATBCD inclusion complex consists of head-to-head β-CD dimers with one disordered guest molecule and included water molecules. A stereo view of the crystal packing down the a-axis for the SATBCD structure is presented in Figure 5.21 which illustrates the "endless" channels produced by the cavities of the dimers. The dimeric layers are thus stacked parallel to the yz-plane of the structure.

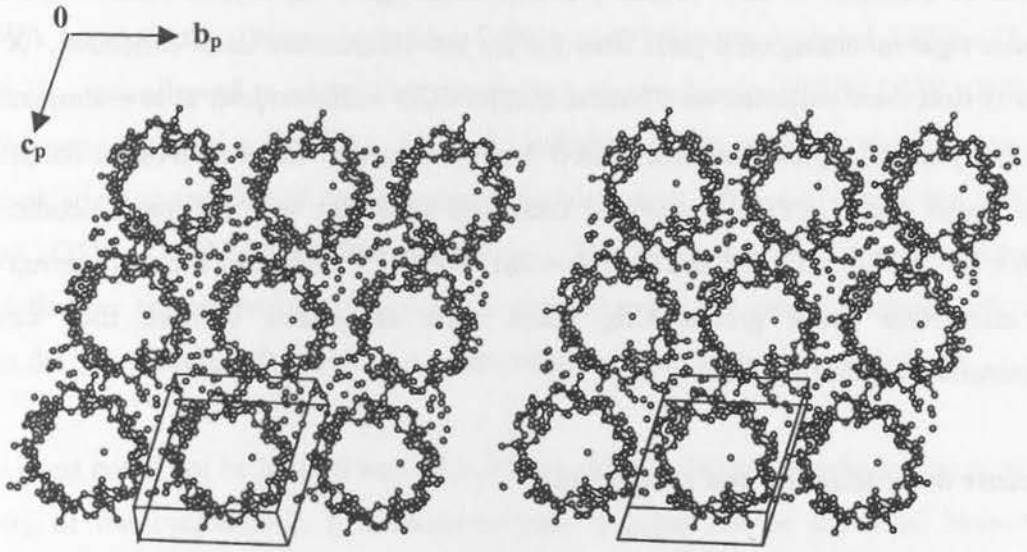

Figure 5.21 Stereo view of the crystal packing down the a-axis for the SATBCD structure. The water oxygen atoms are shown as isolated spheres.

Due to the high cost of the enantiopure (S)-atenolol there was insufficient material to record the experimental PXRD pattern of the SATBCD complex. However, later in this chapter the comparison of the computed PXRD patterns for the ATBCD and the SATBCD complexes is shown.

X-ray Crystallographic Analysis of the METBCD Structure

Data-collection and space group determination

A crystalline complex of metoprolol free base with β-CD was obtained from slow cooling and slow evaporation of a hot aqueous solution [~ 50°C] of β-CD and metoprolol in a 1:1 molar ratio at ambient temperature. A single crystal of desirable size was selected from a batch. The instability of the crystal when exposed to air required it to be covered in Paratone N oil[115] which prevents cracking of the crystal surface and also provides rigid mounting on a glass fibre for the low temperature data- collection. X-ray intensity data were collected on a Nonius Kappa CCD diffractometer at low temperature [193(2) K] using graphite-monochromated MoKα radiation. Inspection of the reciprocal lattice layers with LAYER[112] revealed Laue 2/m symmetry with reflection conditions: hkl: h + k = 2n, h0l: (h = 2n) and 0k0: (k = 2n). XPREP[103] indicated the space group C2. The alternative space groups Cm, C2/m were eliminated because they cannot accommodate a chiral CD host.

Structure determination and refinement

The published co-ordinates for the non-hydrogen cyclodextrin atoms [excluding the primary hydroxyl oxygen atoms] of the isomorphous (2)-(Poly(tris(ethylene glycol)))-(β-cyclodextrin)-polyrotaxane octahydrate[162] were used to solve the structure. The difference Fourier map, after refinement in SHELX-97,[113] revealed the positions of most of the primary hydroxyl oxygen atoms. Further refinement showed that two of these atoms were disordered over two positions [O6G2 and O6I2, O6G6 and O6J6]. For a given pair, a constant U_{iso} of 0.08 Å^2 [the average of U_{eq} for the chemically equivalent ordered atoms] was assigned and site-occupancy factors [s.o.f.'s] of x and 1-x were assigned with x variable. The major positions refined to s.o.f. values of 0.55 and 0.66 for O6G2 and O6G6 respectively. All non-hydrogen host atoms with U_{iso} 0.08 Å^2, except the disordered pair, were refined anisotropically.

Hydrogen atoms were placed in idealised positions in a riding model with U_{iso} set at 1.2 times those of the parent atoms. All the primary hydroxyl hydrogen atoms were given a common variable isotropic temperature factor and were placed using the AFIX 147 instruction.

Oxygen atoms of water molecules were placed over 10 sites. Two of these water molecules [O4W and O7W] were disordered over two positions. For a given pair, a constant U_{iso} of 0.1 $Å^2$ was assigned and s.o.f.'s of x and 1-x were assigned with x variable. The s.o.f.'s of the major positions refined to 0.67 and 0.55 for O4WA and O7WA respectively. Water molecules O1W and O2W were assigned full s.o.f.'s and their U_{iso} was allowed to vary. The remaining water molecules [O3W, O5W, O6W and O8W] were assigned a fixed U_{iso} of 0.1 $Å^2$ and their s.o.f.'s were allowed to vary. The refined site-occupancies of these water molecules were 0.85, 0.67, 0.64 and 0.47 for O3W, O5W, O6W and O8W respectively. The total number of water molecules modelled per asymmetric unit was 6.5 as compared to the 8.0 water molecules calculated from the TGA results. The hydrogen atoms of water molecules were not located.

The guest could not be located beyond a diffuse electron density cloud situated inside the cavity of the cyclodextrin host molecule and it could not be modelled because of abnormal distances and angles between electron density peaks. The unsuccessful modelling of the guest molecule resulted in the convergence of the refinement to the R_1 factor of 0.11 for observed data [$I > 2\sigma(I)$]. The maximum and the minimum residual electron density peaks inside the cavity were 0.65 and 0.30 e $Å^{-3}$ respectively. Table 5.22 lists crystal data and refinement parameters for the METBCD structure.

Table 5.22 Crystal data and refinement parameters for the METBCD structure

Complex formula	$2(C_{42}H_{70}O_{35})\bullet C_{15}H_{25}NO_3\bullet 16H_2O$
Formula weight	2825.6
Crystal system	Monoclinic
Space group	C2
a / Å	18.825(1)
b / Å	24.469(2)
c / Å	15.502(1)
β / °	110.295(3)
Volume / $Å^3$	6697.3(8)
Z	2
$Density_{calc}$ / g cm^{-3}	1.402
μ(MoKα) / mm^{-1}	0.112
F(000)	2615
Crystal size / mm^3	0.18 x 0.25 x 0.35
Temperature / K	193(2)
Range scanned θ / °	$2 \leq \theta \leq 25$
Index ranges	h: -22, 22 k: -26, 28 l: -18, 18
Dx / mm	30
No. of measured reflections	9525
No. of unique reflections	9525
No. of reflections with $I > 2\sigma(I)$	7250
No. of least-squares parameters	738
R_{int}, R_σ	0.000, 0.0876
R_1 ($I > 2\sigma(I)$)	0.1051
S	1.22
No. of reflections omitted	25
wR_2	0.3155
Weighting scheme parameters	a = 0.2, b = 0.000
$(\Delta / \sigma)_{mean}$	<0.001
Δρ excursions / e $Å^{-3}$	0.45, 0.88

Geometrical analysis of the METBCD structure

METBCD crystallises in the space group C2 in a 2:1:16 β-CD:metoprolol:H_2O molar ratio with Z = 2 formula units [formula unit defined in Table 5.22] per unit cell. The β-CD molecule is rotated through a diad parallel to the b-axis to produce the other half of the dimer. A diagram of the asymmetric unit of the METBCD complex is presented in Figure 5.22. The seven glucosidic residues have been assigned the Gn notation. The

disordered positions were denoted **I** and **J** respectively. The glucose units are denoted as **G1**, **G2**, **G3**, **G4**, **G5**, **G6** and **G7**.

The geometrical parameters that describe the conformations of cyclodextrin molecules as discussed in **Chapter 1 – Introduction**, are listed for the METBCD structure in Tables 5.23-5.25. The glucose residues are all in the $^4C_1$ chair conformation. Table 5.23 presents the principal torsion angles. The C6-O6 bonds of the **G1**, **G4**, **G5** and **G7** residues are pointing away from the cavity and are thus adopting the (-)-*gauche* conformation.

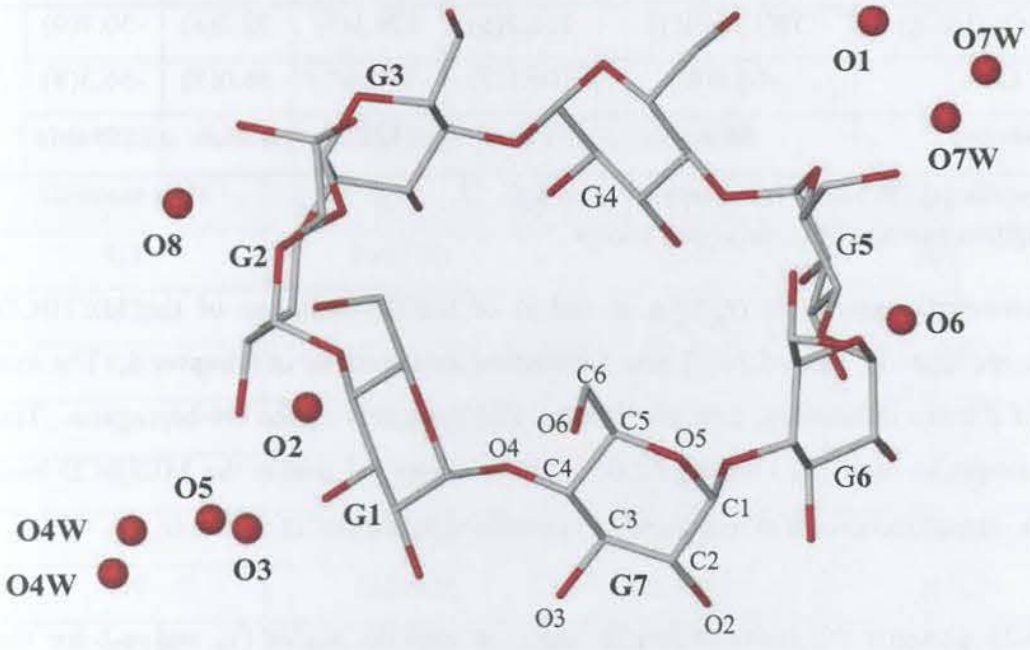

Figure 5.22 Macrocyclic structure of the METBCD complex and the numbering scheme of glucose residues and water oxygen atoms with the hydrogen atoms excluded. The host is viewed from the primary face.

The C6-O6 bond of the **G3** residue points toward the cavity and is in the (+)-*gauche* conformation. The O6 atoms of the **G2** and **G6** residues are disordered over two

positions. The major and minor positions of the O6 atoms for the G2 and G6 residues respectively, adopt the (-)-*gauche* conformation.

Table 5.23 Principal torsion angles [°] for the METBCD structure

Glucose unit	ω / °	Φ / °	ψ / °	Θ_1 / °	Θ_2 / °
G1	-68.4(8)	112.2(6)	128.6(6)	56.7(8)	-56.1(8)
G2 (O6G2, O6I2) *	-55(1), 72(1)	113.9(7)	126.4(7)	53.2(8)	-52.4(8)
G3	62(1)	110.8(7)	127.6(7)	53.3(8)	-53.1(8)
G4	-65.9(8)	109.9(7)	-115.3(7)	54.4(8)	-51.8(8)
G5	-61(1)	118.0(6)	-110.0(7)	59.4(8)	-58.2(8)
G6 (O6G6, O6J6) *	58(1), -45(1)	116.2(6)	129.1(6)	52.2(8)	-50.7(9)
G7	-64.4(8)	106.1(7)	-110.8(7)	56.0(8)	-56.3(8)
| Average |*	**55.4**	**112.4**	**121.1**	**55.0**	**54.1**

The disordered O6 atoms result in two ω values
* Unweighted average of all recorded values

The geometrical parameters (**r**, **l**, **a**, **d** and **t**) of the O4-heptagon of the METBCD structure are listed in Table 5.24. These parameters are described in **Chapter 1**. The low values of **d** and **t** indicate the near ideal seven-fold symmetry of the O4-heptagons. The narrow ranges in radii [**r**], O4 lengths [**l**], and O4 angles [**a**] within the METBCD host molecule, are an indication of high rigidity maintained by the β-CD molecule.

Table 5.25 presents the intersaccharidic angle, φ and tilt angles [τ_1 and τ_2] for the METBCD structure. The intersaccharradic angle φ is close to the average value for other β-CD molecules.[61] All the tilt angles for the host molecule are positive.

Table 5.24 O4-heptagon parameters for the METBCD structure

Glucose unit	r / Å	l / Å	a / °	d / Å	t / °
A1	4.92	4.36	130	0.083(4)	-1.6
A2	5.09	4.35	128	0.023(4)	-3.2
A3	5.17	4.31	125	-0.096(4)	3.1
A4	4.89	4.51	132	0.019(4)	2.3
A5	5.00	4.31	130	0.093(4)	-4.6
A6	5.23	4.38	124	-0.067(4)	0.4
A7	4.98	4.41	131	-0.055(4)	3.9
| Average |	**5.04**	**4.38**	**129**	**0.062**	**2.7**

Table 5.25 φ and τ parameters for the METBCD structure

Glucose unit	φ / °	τ_1 / °	τ_2 / °
G1	116.7(6)	9.7(2)	9.6(1)
G2	117.9(6)	9.0(2)	11.1(3)
G3	119.5(6)	7.9(2)	9.6(3)
G4	119.8(5)	2.4(2)	3.3(1)
G5	117.5(6)	10.2(2)	10.2(1)
G6	117.4(5)	10.5(2)	12.8(1)
G7	120.4(5)	6.6(2)	8.3(1)
Average	**118.5**	**8.0**	**9.3**

Guest inclusion

As mentioned earlier in this chapter, the guest could not be successfully modelled due to the high degree of disorder in the difference Fourier map shown by the abnormal distances and angles between electron density peaks. However microanalysis [on page 2 of Chapter 5] clearly indicated that the two β-CD host molecules crystallise with one

guest molecule. The highest and the lowest electron density peaks [0.65-0.33 e $Å^{-3}$] inside the host cavity are illustrated in stereo in Figure 5.23. There is no recognisable fragment of the metoprolol molecule shown by the difference Fourier map that could be used as a starting model for further refinements. A further attempt to refine the first two electron peak densities inside the cavity as oxygen atoms and refining other peak densities one by one as carbon atoms while their U_{iso} was kept constant, was also not successful.

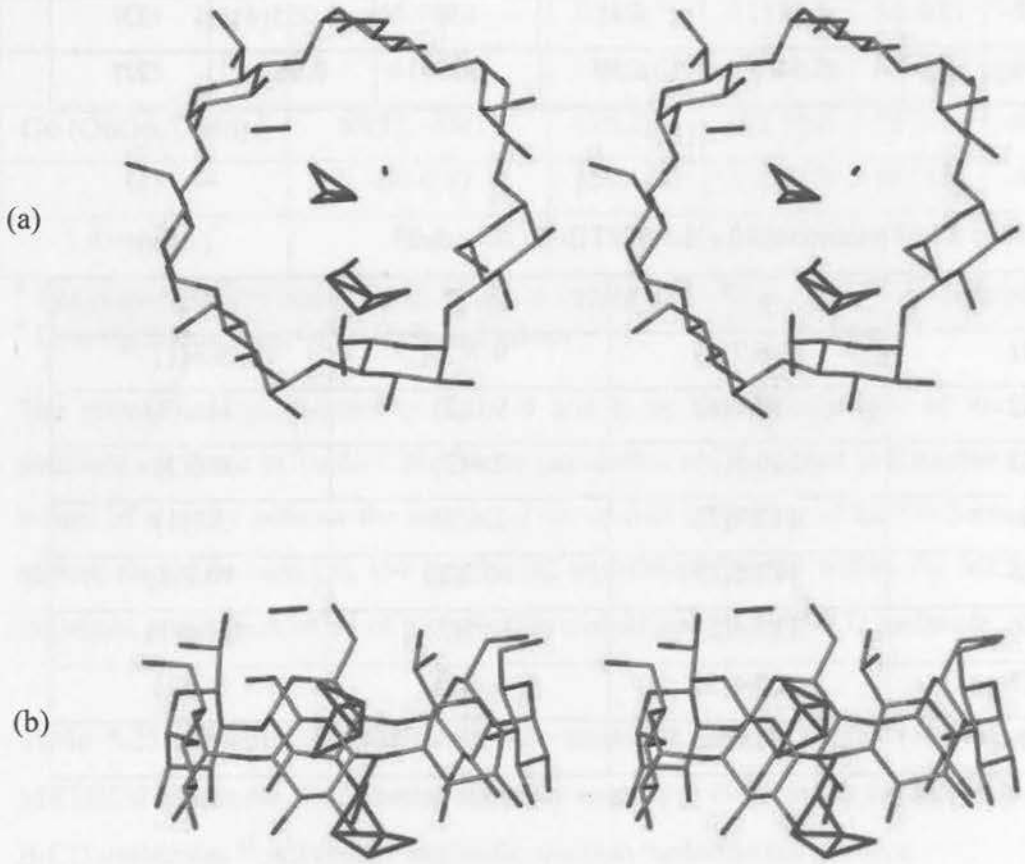

Figure 5.23 Stereo views of the (a) primary and (b) side faces of the crystallographically unique β-CD molecule in METBCD showing the electron density in the cavity.

Hydrogen bonding interactions of the host

PLATON[114] was used to calculate host hydrogen bonding interactions for the METBCD structure. These host hydrogen bonding interactions are categorised with respect to whether they occur within or between host molecules, and they are referred to as intra- and intermolecular host hydrogen bonding interactions respectively.

Intramolecular host hydrogen bonds

The intramolecular host hydrogen bonds are presented in Table 5.26. The conformation of the β-CD macrocycle is stabilised through a total of six intramolecular O2•••O3' and O3•••O2' hydrogen bonds corresponding to the flip-flop system described by Saenger.[143,144] Furthermore the conformation of the β-CD molecule is stabilised by four intramolecular C-H•••O hydrogen bonds.

Table 5.26 Summary of the intramolecular host hydrogen bonds for METBCD

Interaction	H ••• A / Å	D ••• A / Å	D – H•••A /
Intramolecular			
O2G1-H2G1•••O3G7	2.03	2.81(1)	152
O3G3-H3G3•••O2G4	1.98	2.79(1)	163
O2G4-H2G4•••O3G3	2.01	2.79(1)	153
O3G4-H3G4•••O2G5	1.93	2.75(1)	169
O3G6-H3G6•••O2G7	2.19	2.91(1)	144
O2G7-H2G7•••O3G6	2.12	2.91(1)	155
C6G3-H8•••O5G4	2.59	3.45(1)	146
C6G2-H6G3•••O5G3	2.57	3.44(1)	147
C6G7-H23•••O5G1	2.58	3.36(1)	136
C6G6-H6G9•••O5G7	2.47	3.45(1)	147

Intermolecular host hydrogen bonds

There are two O3•••O3', three O6•••O6', one O2•••O2', one O6•••O5' intra-layer hydrogen bonds. In addition to these there are four intra-layer hydrogen bonds of the type C-H•••O, and they are all presented in Table 5.27.

Table 5.27 Intermolecular host hydrogen bonds

Interaction	H ••• A / Å	D ••• A / Å	D – H•••A /	Symmetry code [#]
Intra-layer				
O2G2-H2G2•••O2G4	1.94	2.76(1)	165	1/2-x, -1/2+y, -z
O3G2-H3G2•••O3G7	2.22	2.75(1)	121	1-x, y, -z
O6G3-H20•••O6G6	2.07	2.85(2)	156	1-x, y, 1-z
O6G7-H22•••O5G5	2.56	3.10(1)	123	3/2-x, -1/2+y, 1-z
O6G7-H22•••O6G5	2.00	2.81(1)	162	3/2-x, -1/2+y, 1-z
O6G4-H6G5•••O6G7	2.04	2.85(1)	160	-1/2+x, 1/2+y, z
O3G5-H3G5•••O3G4	1.99	2.82(1)	170	1-x, y, -z
C2G2-H4•••O3G5	2.44	3.33(1)	149	-1/2+x, -1/2+y, z
C1G2-H1G2•••O2G6	2.60	3.50(1)	150	-1/2+x, -1/2+y, z
C2G4-H9•••O3G7	2.40	3.38(1)	168	-1/2+x, 1/2+y, z
C1G4-H1G4•••O2G1	2.51	3.30(1)	136	-1/2+x, 1/2+y, z

[#] Symmetry code applied to the second unit of the interaction

Water interactions

TGA analysis for the METBCD structure showed it to have 8 water molecules per asymmetric unit of which 6.5 were modelled over ten sites. The water molecules were located on the periphery of the host molecule. The unsuccessful modelling of the guest made it impossible to observe whether or not there was water present inside the cavity of the host and no attempts were thus made to do so. Two networks of water molecules form hydrogen bonds to primary and secondary hydroxyl groups. These water molecules play an essential role in stabilising the crystal packing. Five primary hydroxyls, namely

O6G1, O6G4, O6G5, O6G6 and O6G7 are attached to at least one water molecule each. The water molecules O1W, O2W and O7WB that interact with the O6 rim of the cyclodextrin form links between adjacent dimers in the same layer. The water molecules O4WB, O5W, O6W and O8W that interact with the secondary rim form part of an infinite sub-layer of water molecules that run between the cyclodextrin channels. Only two water molecules, O3W and O4WA, do not interact directly with a cyclodextrin host molecule but are linked to other water molecules. Hydrogen bonding distances between the cyclodextrin host and these water molecules are shown in Table 5.28.

Table 5.28 Hydrogen bonding distances involving water molecules

Interaction	Distance / Å	Symmetry code *
O1W•••O6G4	2.72(1)	-1/2+x, 1/2+y, z
O1W•••O5G7	3.18(1)	1-x, y, 1-z
O1W•••O6G7	2.92(1)	1-x, y, 1-z
O2W•••O5G1	3.04(1)	x, y, z
O2W•••O6G1	2.67(1)	x, y, z
O2W•••O6G5	2.89(1)	1/2-x, 1/2+y, 1-z
O2W•••O5G6	2.93(1)	1/2-x, 1/2+y, 1-z
O2W•••O6G6	3.07(1)	1/2-x, 1/2+y, 1-z
O4WB•••O2G3	2.86(1)	x, y, z
O5W•••O3G1	2.73(1)	1-x, y, 1-z
O5W•••O3G3	3.11(1)	-1/2+x, 1/2+y, -1+z
O5W•••O2G6	2.83(1)	1/2-x, 1/2+y, 1-z
O6W•••O3G2	2.79(1)	-1+x, y, z
O6W•••O3G4	3.13(1)	1/2-x, 1/2+y, -z
O6W•••O2G5	2.61(1)	-1/2+x, 1/2+y, z
O4WB•••O3G6	2.85(1)	x, y, z
O7WB•••O5G3	3.21(1)	1+x, y, z
O7WB•••O6G6	2.95(1)	1-x, y, 1-z
O8W•••O2G3	2.63(1)	-x, y, -z
O1W•••O7WA	2.66(1)	x, y, z
O1W•••O7WB	2.75(1)	x, y, z
O2W•••O3W	2.83(1)	-1/2+x, -1/2+y, z
O4WB•••O7WA	3.13(1)	x, y, z
O6W•••O6W	3.16(1)	1-x, y, -z

* Symmetry code applied to the second unit of the interaction

Crystal packing of the METBCD structure

A stereo diagram of the METBCD complex viewed down the c-axis in Figure 5.24 illustrates the "endless" channels formed by the dimer columns.

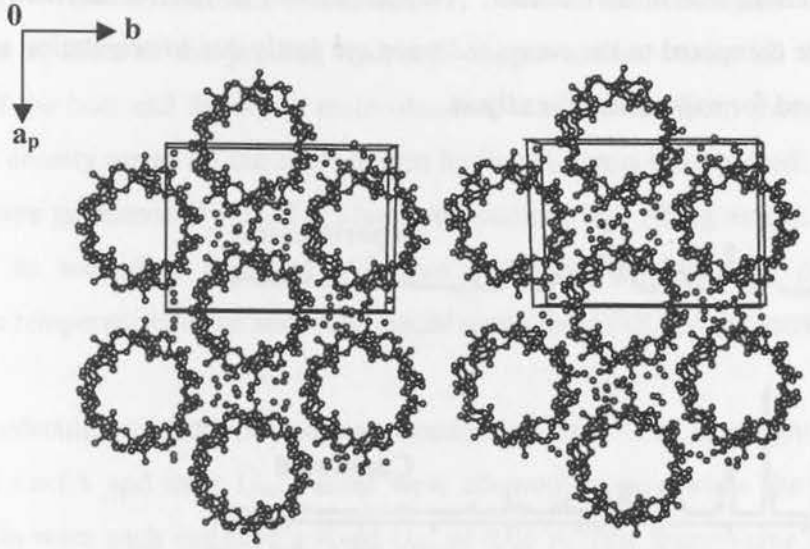

Figure 5.24 Stereo diagram of the METBCD complex viewed down the c-axis illustrating water molecules that connect adjacent host molecules and the "endless" channels formed by the β-CD host molecules.

The METBCD structure is characteristic of the channel type packing motif for β-CD dimers.[163,164,165,166,167,168,169,170,171,172,173] The arrangement of dimers is in C-centered layers and they are stacked upon each other parallel to the c-axis to form almost linear channels. Mentzafos *et al*[140] reported the relative average shift of consecutive dimers as 2.7(2) Å, when the dimers are viewed perpendicular to their mean O(4) planes for channel type structures crystallising in the space group C2. The channels of the β-CD structures crystallising in the space group C2 are the most linear channels observed for all known types of β-CD packing arrangements.

Disorder of the included guest is often observed in structures of the channel (CH) type packing mode crystallising in the space group C2.[37-47] The same phenomenon was observed for the METBCD structure.

Powder X-ray diffraction

Figure 5.25 presents the computed and experimental PXRD traces for METBCD. The two patterns show a high degree of correlation despite the guest not being modelled in the single crystal structure due to its disorder. The differences in relative intensities of the experimental trace compared to the computed trace are partly due to orientation effects in the sample prepared for experimental analysis.

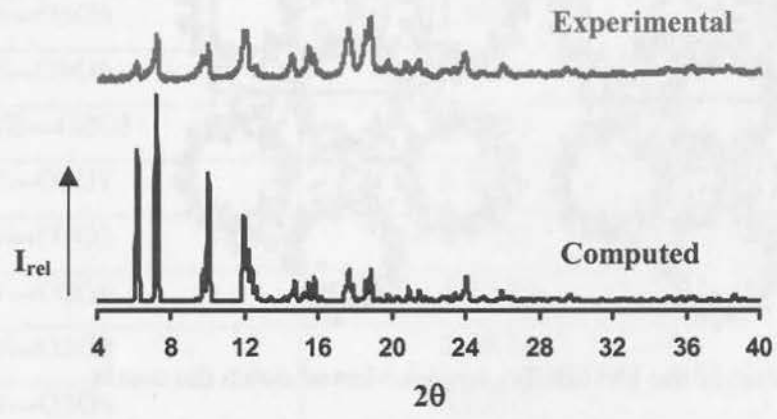

Figure 5.25 Computed [193K] and experimental [295K] PXRD traces for METBCD.

X-ray Crystallographic Analysis of OXPRBCD

Data-collection and space group determination

X-ray intensity data-collection was performed at 172(2) K on the Nonius Kappa CCD diffractometer using graphite-monochromated MoKα radiation. A single crystal was mounted on a glass fibre and covered in Paratone N oil[115] to provide a rigid mounting for the low temperature data-collection and to prevent cracking due to loss of water of crystallisation. Laue symmetry $\bar{1}$, upon inspection of the intensity-weighted reciprocal lattice, indicated the triclinic crystal system. Since the β-CD host molecule is chiral, the space group P1 was correctly indicated by the program XPREP.[103]

Structure determination and refinement

The structure was solved using the published coordinates for the non-hydrogen CD atoms (excluding primary hydroxyl oxygen atoms) of the isomorphous 4-*t*-butylbenzoic acid complex.[148] After refinement in SHELX-97,[113] the difference Fourier map revealed the positions of most of the primary hydroxyl oxygen atoms. Once all the non-hydrogen atoms of the host and the water molecules had been located from subsequent difference electron density maps, all the cyclodextrin hydrogen atoms were placed. These hydrogen atoms were geometrically fixed at idealised positions in a riding model. All the primary as well as secondary hydroxyl hydrogen atoms were assigned a common variable isotropic temperature factor and were placed using the AFIX 137 instruction.

Water molecules were distributed over twenty nine sites. The first eight water molecules had full s.o.f.'s and their U_{iso} values were allowed to vary while the remaining water molecules were each assigned a fixed U_{iso} of 0.06 $Å^2$ [the mean value for the first eight water molecules] while their site-occupancy factors were allowed to refine. The site-occupancies of the water molecules varied in the range 0.85-0.27 and are listed in Table 5.26. The total number of water molecules accounted for per asymmetric unit was 19.7, as compared to 21 water molecules expected from the TGA results. The hydrogen atoms of water molecules were not located.

Table 5.26 Site occupancy values of the water molecules

Water molecule	s.o.f.	Water molecule	s.o.f.
O1W	1.0	O15W	0.69
O2W	1.0	O16W	0.74
O3W	1.0	O17W	0.61
O4W	1.0	O18W	0.62
O5W	1.0	O19W	0.55
O6W	1.0	O20A	0.64
O7W	1.0	O20B	0.29
O8W	1.0	O21W	0.56
O9A	0.85	O22W	0.47
O9B	0.31	O23A	0.45
O10W	0.82	O23B	0.30
O11W	0.76	O24W	0.34
O12W	0.78	O25W	0.30
O13W	0.63	O26W	0.27
O14W	0.70		

Modelling of the oxprenolol guest

The subsequent difference Fourier map revealed the position of the phenyl ring of the oxprenolol guest molecule at the interface of the two β-CD molecules that form a dimer. Elemental analysis indicated that a single oxprenolol molecule was present for every two β-CD molecules. Upon the placement of the tertiary hydrogen atoms of the β-CD host molecules, a difference map calculated near the end of the refinement revealed electron density peaks forming the shape of a second phenyl ring within the cavity along the primary hydroxyl side of **CD(A)**, with significantly lower occupancy. Initially it was thought that the guest was possibly disordered over two positions within the β-CD host cavity. However attempts to model the guest accordingly were unsuccessful. After careful inspection of the map, peaks were chosen that corresponded to the position of the

phenyl ring situated at the interface between **CD(A)** and **CD(B)**. The map showed co-planar density peaks for the ortho-oxygen atoms on the phenyl ring. The atoms of the phenyl ring were constrained as a rigid hexagon using the AFIX 66 instruction. This was followed by the placement of the side chain atoms. A single isotropic temperature factor was used for all the non-hydrogen atoms of the guest [initial U_{iso} = 0.15 Å^2] and this refined to a final value of 0.23 Å^2. The guest hydrogen atoms were included in geometrically calculated positions and were assigned a common isotropic temperature factor. The diffuse, relatively high electron density peaks [0.65-1.2 e Å^{-3}] and [0.66-0.92 e Å^{-3}] remained in the cavity of the host molecules **A** and **B** respectively after the final refinement. The final structural model is deficient on several counts [poor modelling of the guest, a relatively high refined global U_{iso} value for the guest molecule that was placed, low residual electron density in one host cavity that could not be modelled but which probably indicates guest present at very low occupancy]. In modelling the guest by placing and refining only a single molecule within the host dimer, its site-occupancy was assigned as 1.0 only to account for the 2:1 host-guest stoichiometry indicated by chemical analysis. The shortcomings of the model, suggesting that one β-CD molecule of the dimer is effectively unoccupied by guest, is recognised however. Crystal data and data-collection parameters are listed in Table 5.27.

Table 5.27 Crystal and refinement parameters for the OXPRBCD structure

Empirical formula	$2(C_{42}H_{70}O_{35})\cdot C_{15}H_{23}NO_3\cdot 21H_2O$
Formula weight / g mol^{-1}	2913.63
Crystal system	Triclinic
Space group	P1
a / Å	18.1503(4)
b / Å	15.4082(2)
c / Å	15.3226(2)
α / °	102.434(1)
β / °	113.484(1)
γ / °	99.646(1)
Volume / $Å^3$	3681.3(1)
Z	1
$Density_{calc}$ / g cm^{-3}	1.314
μ (MoKα) / mm^{-1}	0.116
F(000)	1504
Temperature of data collection / K	172(2)
Crystal size / mm^3	0.35 x 0.35 x 0.49
Range scanned θ / °	$2 \leq \theta \leq 26$
Dx / mm	40
No. of measured reflections	18413
No. of unique reflections	18413
No. of reflections with $I > 2\sigma(I)$	15323
No. of parameters	1581
S	1.28
R_1 (15323 reflections with $I > 2\sigma(I)$)	0.1004
No. of reflections omitted	28
wR_2	0.2965
Weighting scheme	a = 0.2 b = 0
$(\Delta / \sigma)_{mean}$	0.028
Δρ excursions / e $Å^{-3}$	-0.71 and 1.21

Geometrical analysis of the OXPRBCD structure

The asymmetric unit comprises two crystallographically independent host molecules, one guest molecule and 21 water molecules. The two CDs will be referred to as **CD(A)** and **CD(B)**. The glucose residues of each of the CDs are numbered one to seven, so that the glucose residues of **CD(A)** are **A1**, **A2**, **A3**, **A4**, **A5**, **A6** and **A7**. The interface insertion of the oxprenolol guest phenyl ring and the short side chain between the two **CD(A)** and

CD(B) host molecules are illustrated in Figure 5.26. The longer side chain of the guest extends along the cavity of **CD(B)**. The host numbering scheme is also shown in Figure 5.26.

The geometrical parameters for the two independent β-CD molecules are listed in Tables 5.28-5.30. The principal torsion angles are presented in Table 5.28. These include the radii (**r**), side lengths (**l**), O4•••O4'•••O4" angles (**a**), the deviation of each O4 from the mean O4 plane (**d**) and the O4•••O4'•••O4"•••O4"' torsion angle (**t**). Other important parameters are the intersaccharidic bond angle (φ) and the tilt angles (τ_1 and τ_2). These parameters are defined in Chapter 1. The glucose residues are all in the $^4C_1$ chair conformation and the values of the torsion angles are consistent with the average values obtained for β-CD structures.

The ω parameter indicates whether the direction of the C6-O6 bond is towards [positive] or away from [negative] the host cavity. In the OXPRBCD structure, all the C6-O6 bonds are in the (-)-*gauche* conformation, except that for glucopyranose unit **A7** which is in the (+)-*gauche* orientation. The **Φ, ψ, Θ1** and **Θ2** torsion angles in Table 5.28 agree closely with those observed for the β-CD host molecule.[60]

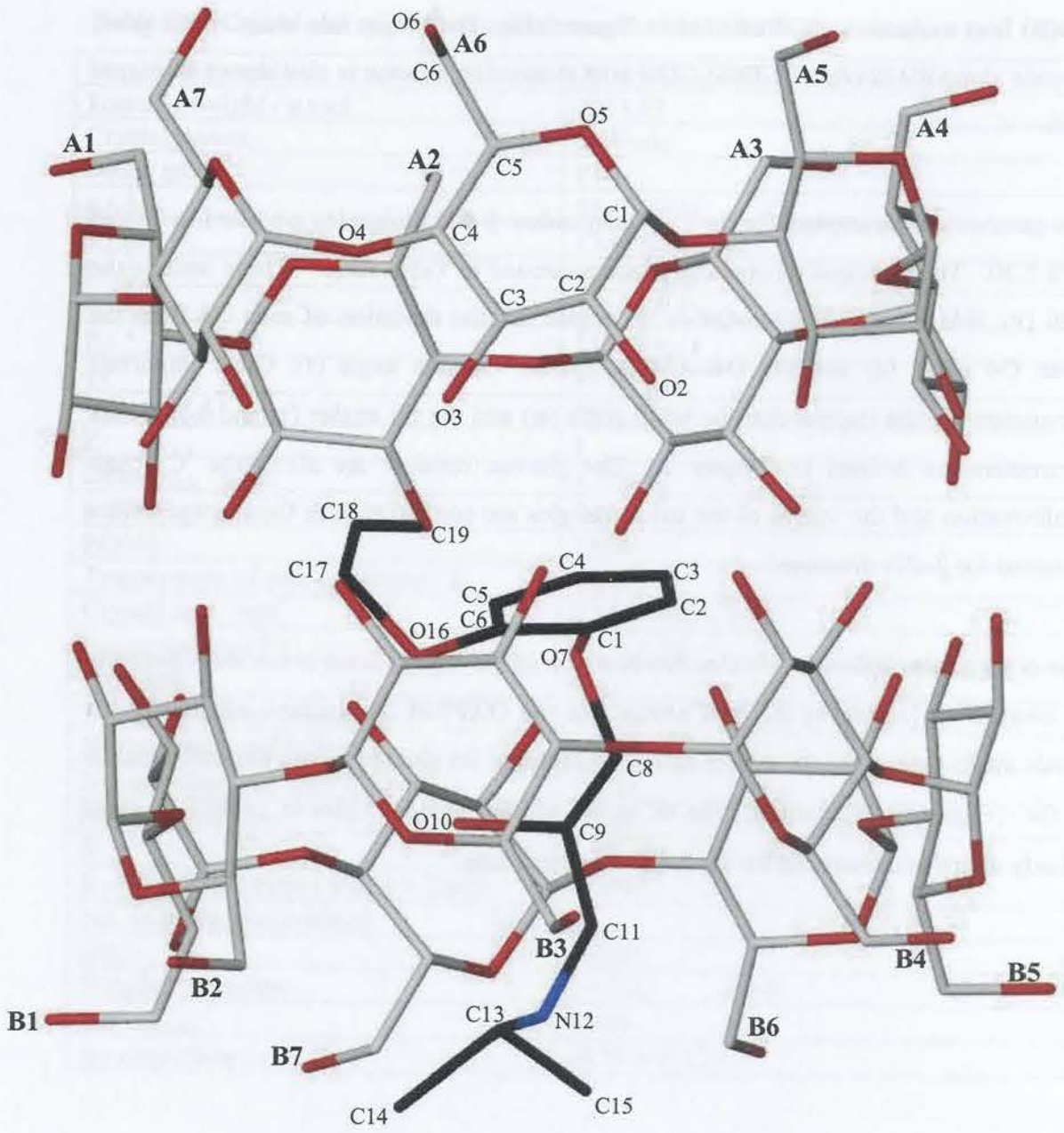

Figure 5.26 The interface insertion of the guest phenyl ring and its short side chain between the **CD(A)** and **CD(B)** host molecules and the numbering scheme of the CD molecules and the oxprenolol guest molecule. The hydrogen atoms for the β-CD host molecule and the oxprenolol guest molecule are omitted for clarity.

Table 5.28 Principal torsion angles [°] for the OXPRBCD

Glucose unit	ω / °	Φ / °	ψ / °	Θ_1 / °	Θ_2 / °
CD(A)					
A1	-65.5(7)	115.5(6)	126.3(6)	56.0(7)	-51.3(7)
A2	-66.5(8)	116.3(6)	131.1(6)	56.8(7)	-58.9(7)
A3	-64.6(8)	111.8(6)	125.3(6)	51.7(7)	-50.0(7)
A4	-75(1)	113.3(7)	-127.4(7)	57.3(8)	-55.7(8)
A5	-65.7(7)	113.0(6)	128.0(6)	54.8(7)	-51.5(7)
A6	-57.9(7)	116.1(6)	-126.6(6)	55.4(7)	-51.1(8)
A7	62.5(9)	115.7(6)	-112.7(7)	54.7(8)	-54.7(8)
| Average |	**65.4**	**114.5**	**125.3**	**55.2**	**53.3**
CD(B)					
B1	-71.0(7)	114.2(6)	125.1(6)	51.3(7)	-49.8(7)
B2	-65.0(8)	115.7(7)	127.8(7)	54.4(8)	-51.4(8)
B3	-65.0(7)	115.0(6)	-116.2(6)	54.6(7)	-53.6(7)
B4	-58.9(8)	116.9(6)	126.0(6)	55.8(7)	-53.6(7)
B5	-58.2(9)	115.5(6)	128.6(6)	55.1(8)	-52.1(9)
B6	-65.9(7)	115.5(7)	124.2(6)	54.6(7)	-50.1(7)
B7	-69.3(9)	117.4(6)	127.6(6)	55.3(8)	-54.0(8)
| Average |	**64.8**	**115.7**	**125.1**	**54.4**	**52.2**

[#] The disordered O6 atoms result in two ω values

The **r**, **l** and **a** parameters in Table 5.29, respectively describe the distance of the O4-heptagon centroid to each O4 atom, the distance between adjacent O4 atoms and the angle between three adjacent O4 atoms. These parameters do not vary substantially within each β-CD molecule, thus reflecting the near ideal seven-fold symmetry of the O4-heptagons. This symmetry is also indicated by the low values of the **d** and **t** parameters, which respectively describe the deviation of each O4 atom from the mean O4 plane and the torsion angle defined by four adjacent O4 atoms.

Table 5.29 O4-heptagon parameters for the OXPRBCD structure

CD(A)	r / Å	l / Å	a / °	d / Å	t / °
A1	4.92	4.49	132	-0.024(4)	-2.0
A2	4.96	4.32	130	0.014(4)	+1.5
A3	5.19	4.35	125	-0.008(4)	-1.3
A4	5.06	4.37	128	0.015(4)	+1.4
A5	4.88	4.44	132	-0.016(4)	-0.6
A6	5.10	4.36	127	0.001(4)	-0.8
A7	5.20	4.31	125	0.019(4)	+1.8
| Average |	**5.04**	**4.38**	**128**	**0.014**	**1.3**
CD(B)					
B1	5.07	4.35	128	-0.009(4)	-0.5
B2	5.09	4.36	128	0.012(4)	-0.1
B3	4.99	4.42	130	0.001(4)	-0.9
B4	5.00	4.35	129	-0.022(4)	+0.9
B5	5.10	4.35	128	0.011(4)	0.7
B6	5.06	4.40	128	0.024(4)	-2.2
B7	4.94	4.36	131	-0.035(4)	+1.9
| Average |	**5.04**	**4.37**	**129**	**0.016**	**1.0**

The φ angles [presented in Table 5.30] for both host molecules are close to the average values for other β-CD molecules.[61] All the tilt angles [τ_1 and τ_2] for both host molecules **A** and **B** are positive indicating that each glucose residue leans towards the centre of the cavity. This gives the cyclodextrin the characteristic truncated cone shape with the secondary rim being wider than the primary rim. The O4 mean planes of the **A** and **B** host molecules are nearly parallel, as indicated by the angle of 0.54(5)° that these make with each other. The phenyl ring of the oxprenolol guest molecule situated at the interface of host molecules **A** and **B**, makes angles of 25.9(1) and 25.3(1)° respectively with the O4 mean planes of these host molecules.

Table 5.30 φ and τ parameters for OXPRBCD

Glucose unit	φ / °	τ_1 / °	τ_2 / °
CD(A)			
A1	118.7(5)	3.7(1)	6.2(3)
A2	118.0(5)	10.8(2)	10.9(2)
A3	118.1(5)	6.9(2)	8.9(2)
A4	119.1(5)	7.3(2)	8.3(4)
A5	118.3(5)	5.0(1)	7.5(4)
A6	116.8(5)	5.0(2)	7.6(2)
A7	119.9(5)	5.3(2)	6.1(2)
Average	**118.4**	**6.3**	**7.9**
CD(B)			
B1	116.9(5)	4.7(1)	6.4(4)
B2	119.4(5)	7.4(2)	8.9(4)
B3	116.3(5)	4.5(1)	5.4(2)
B4	118.0(5)	5.4(1)	6.7(3)
B5	118.0(5)	7.2(2)	7.3(3)
B6	117.9(5)	3.5(2)	5.0(1)
B7	120.0(5)	7.0(2)	7.8(3)
Average	**118.1**	**5.7**	**6.8**

Conformation and configuration of the guest molecule

The conformation of the oxprenolol molecule in OXPRBCD is discussed next relative to its conformation as the uncomplexed drug discussed in Chapter 3. The principal torsion angles for the uncomplexed oxprenolol molecules A and B and the complexed oxprenolol guest molecule are presented in Table 5.31, while Figure 5.27 is a repeat of Figure 3.28 in Chapter 3, illustrating the definitions of the torsion angles. The reader is referred to Chapter 3 for more background information. The configuration at the chiral center C9 of the included oxprenolol molecule is (R-), which will be dealt with in the Discussion

section of this chapter. The torsion angles δ_2, δ_3, δ_4, δ_6 and δ_8 of the complexed oxprenolol have a smaller out-of-plane twist than those of the uncomplexed drug oxprenolol. This indicates that inclusion allows for less rotational freedom around the C1-O7, O7-C8, C6-O16, O16-C17 and C8-C9 bonds for the torsion angles δ_2, δ_3, δ_4, δ_6 and δ_8 respectively.

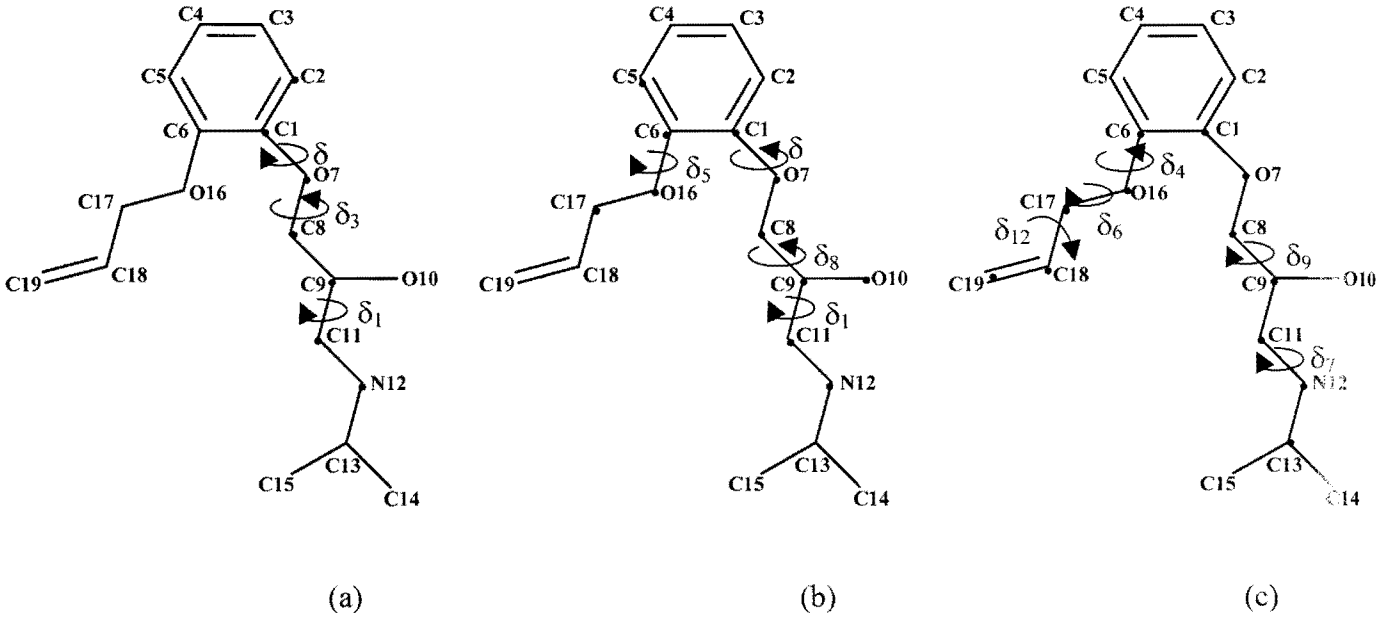

Figure 5.27 Schematic diagram of the principal torsion angles (a) δ_1, δ_3, δ_{10} (b) δ_2, δ_5, δ_8, δ_{11} (c) δ_4, δ_6 and δ_7 for the oxprenolol molecule.

Table 5.31 Principal torsion angles [°] of oxprenolol in OXPRBCD and the oxprenolol molecules **A** and **B** in the uncomplexed drug molecule

Torsion angle / °	OXPRBCD [(R-)]	Molecule A [(R-)]	Molecule B [(R-)]
δ_1	-76(1)	-5(1)	4(1)
δ_2	104(1)	174(4)	-177(4)
δ_3	-76(3)	-170(4)	-178(4)
δ_4	116(2)	-173(5)	-177(4)
δ_5	-65(3)	8(1)	5(1)
δ_6	-83(2)	162.4(8)	168(5)
δ_7	151(2)	172(4)	163(4)
δ_8	-58(3)	-167(4)	-169(4)
δ_9	-173(2)	72(1)	71(1)
δ_{10}	-177(4)	179(4)	180(4)
δ_{11}	59(4)	58(1)	61(1)
δ_{12}	-5.7(3)	-159.7(3)	115.6(7)

Hydrogen bonding interactions

PLATON[114] was used to calculate several hydrogen bonding interactions for the OXPRBCD structure. The host hydrogen bonding interactions are categorised with respect to whether they occur within or between dimers, referred to as intra- and inter-dimer host hydrogen bonding interactions respectively.

Intra-dimer host hydrogen bonds

The intra-dimer host hydrogen bonding interactions, guest and host-guest hydrogen bonding interactions are presented in Table 5.32. There are thirteen intramolecular intra-dimer hydrogen bonds, six of which are the O2•••O3' and the remaining ones are O3•••O2' hydrogen bonds. These hydrogen bonds are responsible for the small tilt angles and they also maintain the relatively 'round' shapes of the β-CD molecules.[140] There are eight

unique intermolecular intra-dimer O-H•••O hydrogen bonds that connect the two host molecules into a head-to-head dimer, and these involve the O2 and O3 atoms on the secondary sides of the β-CD molecules. A stereo diagram showing all the intra- and intermolecular intra-dimer O-H•••O hydrogen bonds is presented in Figure 5.28. The O2 and O3 atoms that are not involved in O2•••O3' intramolecular hydrogen bonds, form hydrogen bonds with the other host molecule of the dimer. There are two intramolecular hydrogen bonds of the guest molecule, namely O10-H10A•••O7 and C19-H19A•••O7.

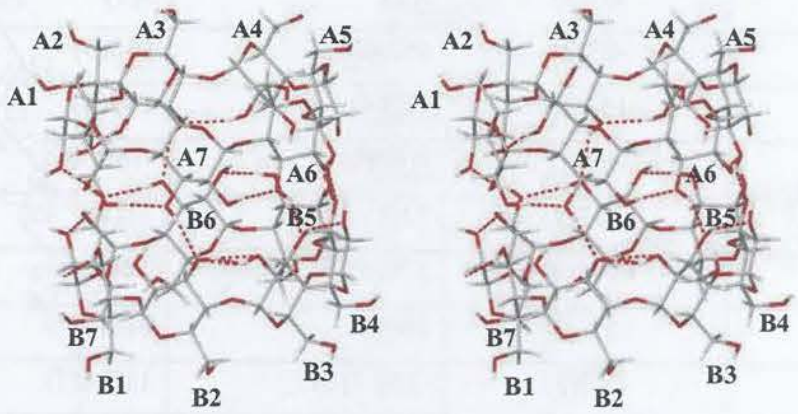

Figure 5.28 Stereo diagram of the intra-dimer hydrogen bonding for the OXPRBCD structure.

Table 5.32 Intra-dimer host hydrogen bonds

Interaction	H•••A / Å	D•••A / Å	D-H•••A / °
Intramolecular			
O2A1-H2A1•••O3A7	2.11	2.789(8)	138
O2A4-H2A4•••O3A3	2.07	2.829(8)	149
O2A3-H2A3•••O3A2	1.97	2.792(8)	168
O3A1-H3A1•••O2A2	2.19	2.793(7)	128
O2A6-H2A6•••O3A5	1.90	2.715(9)	162
O2A7-H2A7•••O3A6	1.96	2.792(8)	168
O3B2-H3B2•••O2B3	1.89	2.717(8)	167
O2B3-H2B3•••O3B2	1.99	2.717(8)	145
O3B3-H3B3•••O2B4	1.99	2.730(8)	147
O3B4-H3B4•••O2B5	1.98	2.799(8)	167
O3B5-H3B5•••O2B6	2.03	2.735(9)	142
O3B6-H3B6•••O2B7	1.95	2.784(8)	174
O3B7-H3B7•••O2B1	2.17	2.744(8)	126
Guest			
O10-H10A•••O7	2.60	2.91(3)	103
C19-H19A•••O7	2.04	2.89	149
Host•••guest			
C17-H17B•••O3B1	2.59	3.48	150
Host•••Host			
O2A5-H2A5•••O3B4	2.42	3.041(8)	131
O3A3-H3A3•••O3B6	2.14	2.77(1)	132
O3A5-H3A5•••O3B4	2.03	2.795(9)	150
O3A6-H3A6•••O3B3	2.10	2.804(9)	141
O3A7-H3A7•••O3B2	2.14	2.840(9)	140
O2B2-H2B2•••O3A7	2.27	3.10(1)	167
O2B4-H2B4•••O3A5	2.30	3.11(1)	161
O2B5-H2B5•••O3A4	2.33	3.121(9)	157

Inter-dimer host hydrogen bonds

Table 5.34 lists the inter-dimer hydrogen bonds. The discussion of the hydrogen bonds between dimers is in terms of whether they are within the same layer [intra-layer] or between adjacent layers [inter-layer]. The OXPRBCD structure has only twelve unique intra-layer hydrogen bonds of which only four are O-H•••O hydrogen bonds the latter being C1-H•••O2 and C2-H•••O3 hydrogen bonds. The hydrogen atoms of C1 and C2 are located on the outside of the cyclodextrin molecules, thus allowing them to interact with the atoms of neighbouring β-CD molecules.

Table 5.34 Inter-dimer hydrogen bonds for the OXPRBCD

Interaction	H•••A / Å	D•••A / Å	D-H•••A / °	Symmetry code *
Intra-layer				
O6A3-H6A5•••O6A6	2.27	2.870(9)	139	x, 1+y, z
O2B1-H2B1•••O2A5	1.92	2.750(8)	168	x, y, -1+z
O6B3-H6B5•••O6B6	1.98	2.78(1)	160	x, -1+y, z
O6B4-H6B7•••O6B1	2.29	3.08(1)	159	x, y, 1+z
C2A3-H7•••O3A6	2.34	3.30(1)	160	x, 1+y, z
C2A5-H12•••O3A1	2.43	3.394(9)	161	x, y, 1+z
C1A3-H1A3•••O2A7	2.55	3.39(1)	141	x, 1+y, z
C2B1-H21•••O3B4	2.39	3.345(9)	160	x, y, -1+z
C2B3-H26•••O3B6	2.37	3.34(1)	162	x, -1+y, z
C1A5-H1A5•••O2A2	2.58	3.396(9)	139	x, y, 1+z
C1B1-H1B1•••O2B5	2.55	3.400(9)	143	x, y, -1+z
C1B3-H1B3•••O2B7	2.48	3.32(1)	141	x, -1+y, z

Water interactions

TGA analysis showed that the asymmetric unit of the OXPRBCD structure contains 21 water molecules, of which 19.7 were modelled over twenty nine sites since some of them

had only partial s.o.f.'s. The water molecules were located around the periphery of the host molecules. These water molecules play an essential role as mediators which construct the host matrix structure or connect the host and the guest molecules, as well as acting as the packing space fillers among the β-CD dimer units. Table 5.35 presents the close contacts involving water molecules together with their averages and ranges for the OXPRBCD structure.

Table 5.35 Water close contacts for the OXPRBCD structure

Contact atom	Number of interactions	Range / Å	Average Distance / Å
O2A	6	2.68-3.18	2.90
O3A	4	2.85-3.10	2.91
O5A	2	3.15-3.18	3.16
O6A	10	2.68-2.96	2.76
Total Host(A)•••Water	**22**		
Guest•••Water	1	2.99	2.99
O2B	8	2.68-3.11	2.52
O3B	5	2.87-3.21	2.98
O5B	3	2.94-3.10	3.04
O6B	13	2.40-2.98	2.76
Total Host(B)•••Water	**29**		
Water•••Water	**24**	2.56-3.18	2.81

The two separate water networks are formed between the dimers, one connecting the primary and the other connecting the secondary hydroxyl groups. The water molecules that interact with the O6 rim of the cyclodextrin form bridges between adjacent dimers in the same layer, while those that interact with the secondary rim form part of an infinite sub-layer of water molecules that run between the cyclodextrin channels. Since the hydrogen atoms at the secondary hydroxyl side participate in the hydrogen bonding scheme within the dimer /between dimers in the lattice, it is deduced that water molecules would act as H atom donors.

Crystal packing of the OXPRBCD structure

A stereo diagram of the crystal packing viewed down the b-axis for the OXPRBCD structure is presented in Figure 5.29. This stacking mode has been classified as type IM (for 'intermediate'), which is characteristic for β-CD complexes crystallising in the space group P1 with cell dimensions similar to those reported here with a ~ 18 Å and b, c ~ 15 Å each.[140] A number of structures with this IM packing motif have been described in the space group P1.[142,146,147,148,174,175,176,177,178,179,180,181,182,183,184,185]

The channels are more deformed at the interdimeric interface than for the CH type structures. The relative average shift of consecutive dimers, when the dimers are viewed perpendicular to their mean O4 planes is 6.0(2) Å for IM type structures crystallising in the space group P1.[140] The guest molecule occupies only one CD cavity and the other host cavity is apparently empty. This phenomenon has been previously observed for the inclusion of cyclizine in β-CD.[137] On the other hand, as explained earlier, evidence for a second guest molecule with very low site-occupancy was found in the 'empty' CD, but its modelling was unsuccessful. The endless channels projected down the a-axis produced by the cavities of the dimers are presented in Figure 5.30. Hence the dimeric layers are stacked parallel to the yz-plane of the structure.

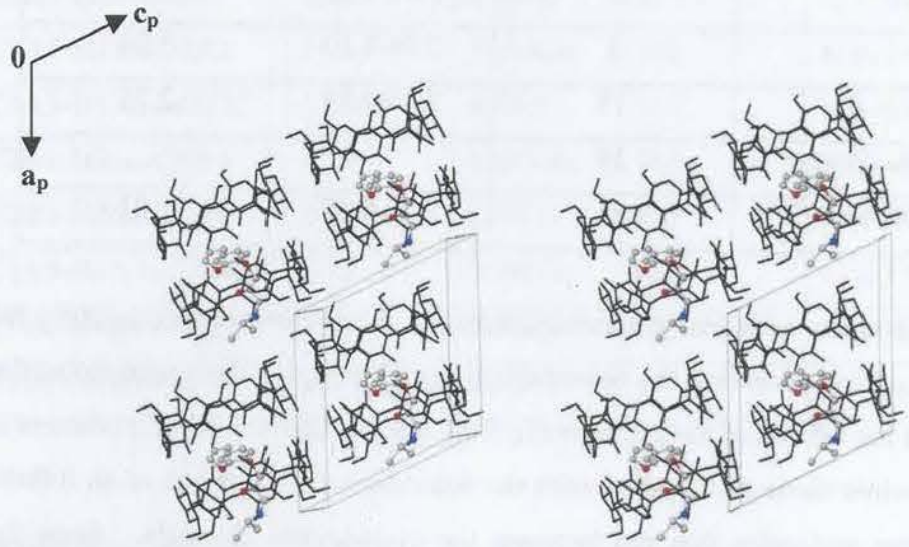

Figure 5.29 Stereo packing diagram of the OXPRBCD structure viewed down the b-axis with the guest molecule represented in red, grey and blue.

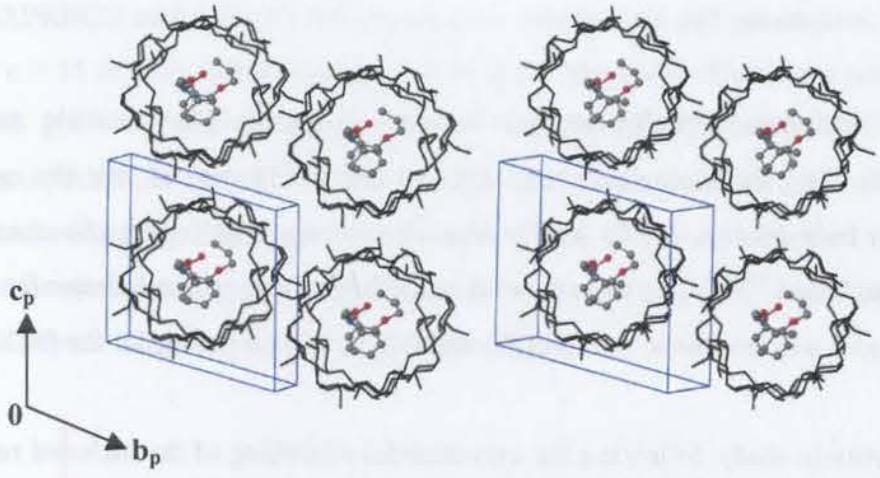

Figure 5.30 Stereo packing diagram of the OXPRBCD structure viewed down the a-axis.

Powder X-ray diffraction

The computed and experimental PXRD traces for OXPRBCD as well as the reference pattern for β-CD dimeric complexes crystallising in space group $P2_1$ [unit cell parameters a ~ 21, b ~ 10 and c ~ 15 Å] are presented in Figure 5.31. The computed and experimental PXRD traces do not match. This is attributed to a phase transformation of these crystals into another form on grinding. The experimental PXRD trace does, however match that of the reference pattern shown.

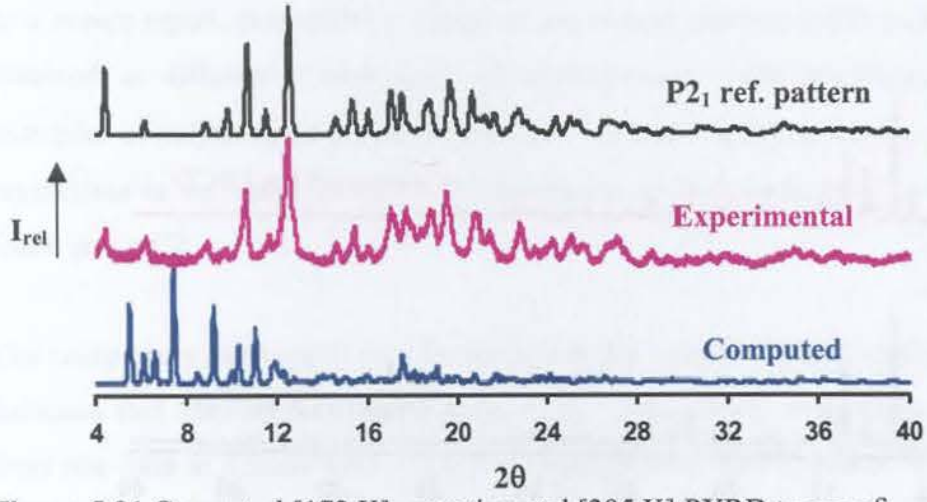

Figure 5.31 Computed [172 K], experimental [295 K] PXRD traces of OXPRBCD and $P2_1$ reference pattern.

Conclusion

The previous inclusion complex studies between ibuprofen [the racemic and its enantiopure (S)-form, the biologically active form] and β-CD showed that the racemic drug could not be modelled due to its disorder whereas the enantiopure (S)- form was successfully modelled.[156,157] The unsuccessful modelling of the racemic ibuprofen guest due to its disorder was attributed to both (R)- and (S)-forms competing for the β-CD host cavity.

Based on the present study, following the unsuccessful modelling of the included racemic atenolol due to its disorder in the β-CD host compound, the biologically active (S)-form of atenolol was included in β-CD. However, even for this complex, the drug molecule could not be modelled. The unit cell parameters and the conformations of the host molecules of ATBCD and SATBCD are similar; thus they are isostructural,[74] and they crystallise in space group P1 with the intermediate packing arrangement.

The experimental PXRD pattern of SATBCD was not recorded due to the small amount of enantiopure drug sample used to obtain these complex crystals. However, the computed patterns of the ATBCD and the SATBCD complexes are shown in Figure 5.32 and these two patterns are identical, confirming isostructurality of the host structures.

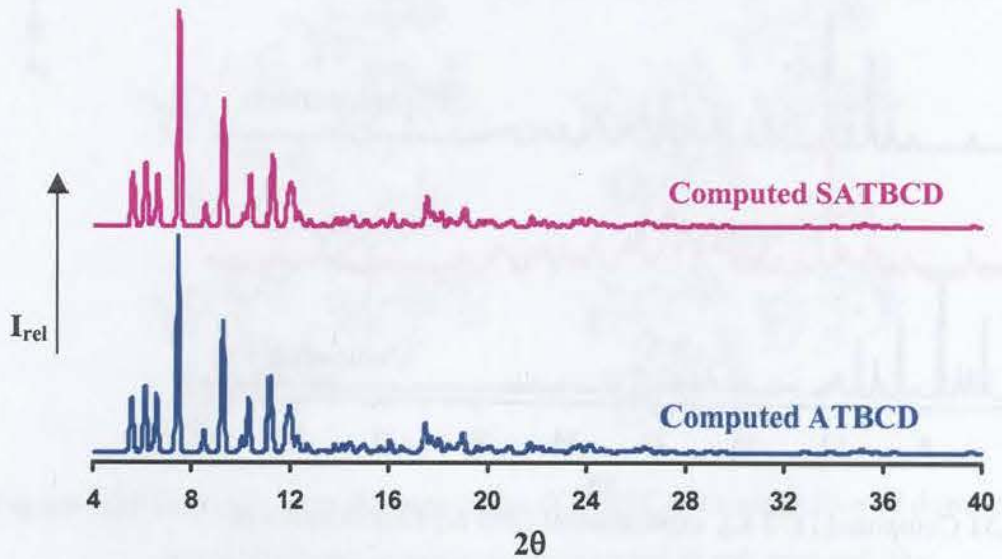

Figure 5.32 Computed XRD traces for ATBCD [193 K] and SATBCD [113 K].

The OXPRBCD and ATBCD complexes have similar unit cell parameters, i.e. a ~ 18 Å and b, c ~ 15 Å each and they crystallise in space group P1. These two complexes have different guest molecules included, namely oxprenolol and atenolol. The computed patterns of ATBCD and OXPRBCD [Figure 5.33] are very similar and thus they appear to be isostructural.[74] These computed patterns from single crystals clearly indicate that the forementioned complexes have similar unit cell parameters and packing arrangements irrespective of the different included guest molecules.

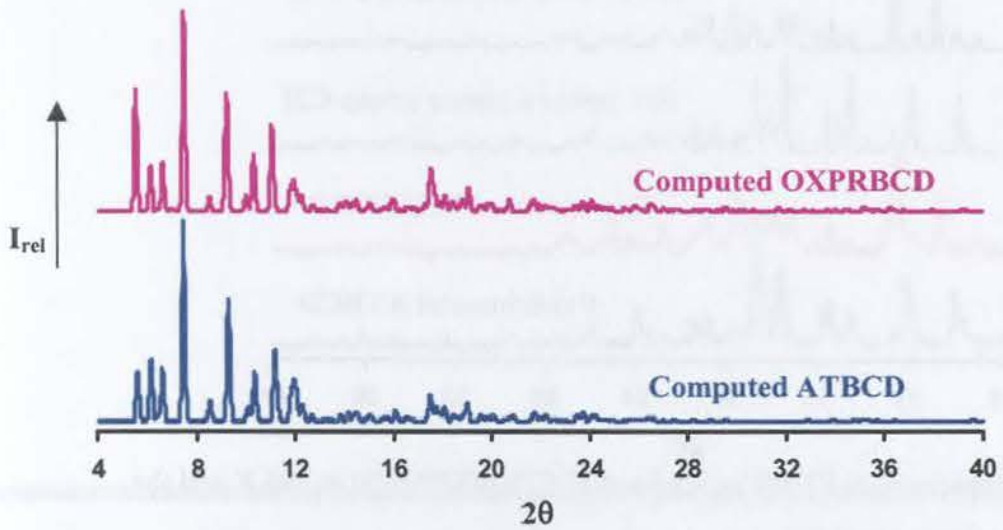

Figure 5.33 Computed patterns for ATBCD [193 K] and OXPRBCD [172 K].

In a recent report, two different forms of the methyl paraben-β-CD inclusion complex, obtained at different temperatures of crystallisation, were highlighted as the first examples of polymorphic β-CD complexes.[154] At room temperature, the species isolated crystallises in the space group P1; crystallisation at 5°C produces a monoclinic crystal, space group C2.

The comparison between the experimental and the computed PXRD patterns of ATBCD indicates that they do not match [Figure 5.16]. This clearly shows that a phase change from one form to a more stable form occurs on grinding these crystals. The experimental trace of the ATBCD complex, however, matches the reference pattern for dimeric β-CD complexes crystallising in space group C2 [Figure 5.34].

The experimental PXRD pattern of OXPRBCD is different from its computed pattern [Figure 5.31] indicating that a phase transformation occurred upon grinding these crystals. The experimental PXRD pattern of this complex matches the reference pattern for dimeric β-CD complexes crystallising in space group $P2_1$ [unit cell parameters a ~ 21, b ~ 10 and c ~ 15 Å] [Figure 5.36].

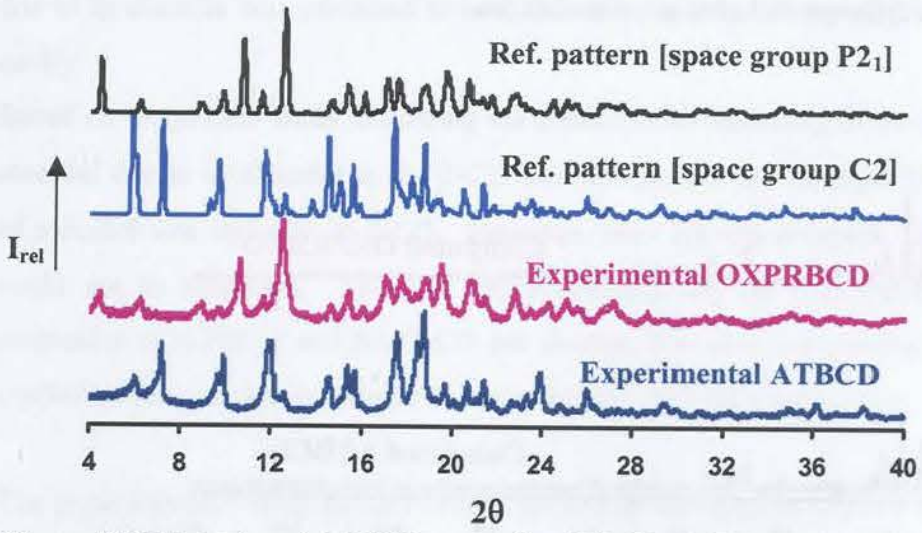

Figure 5.34 Experimental PXRD traces for ATBCD, OXPRBCD at 295 K and the reference patterns.

The results presented here highlight the fact that both PXRD and single crystal XRD must be used in conjunction to establish whether crystal transformations occur upon grinding. In this study the ATBCD and OXPRBCD complexes produced new forms when ground into powder. Evidence for this was the mismatch between computed PXRD patterns and the experimental ones. Although the two complexes [ATBCD and OXPRBCD] crystallise in the space group P1 with the intermediate packing arrangement, their experimental PXRD patterns when compared with the reference patterns indicate that the ATBCD complex transforms into a phase of space group C2 upon grinding, while the OXPRBCD complex transforms into a phase of space group $P2_1$. Such phase transformations induced by grinding have not, to our knowledge been reported previously for cyclodextrin inclusion complexes.

Chapter 6 – TRIMEB Inclusion Complexes

Complex Preparation

Various methods and techniques were applied in preparing the TRIMEB complexes. A crystalline complex of TRIMEB with metoprolol was prepared by dissolving an equimolar amount of each substance in distilled water at ambient temperature. The solution of metoprolol with TRIMEB was filtered and incubated in an oven set at approximately 60°C. Crystals were obtained after three days. The TRIMEB complex with metoprolol will be referred to hereinafter as METTMB.

Two different forms of TRIMEB complexes with oxprenolol were obtained. The first form [OXPTMB(I)] was obtained by employing the co-solvent method in which oxprenolol was dissolved in a small volume of methanol and the resulting solution was slowly added to the TRIMEB solution while the second form [OXPTMB(II)] was obtained by preparing a slurry using equimolar amounts of TRIMEB and oxprenolol at ambient temperature. The resulting solutions were filtered and stored in an oven set at approximately 60°C. Crystals of these two forms were obtained on standing for a period of 48 hours and they were all colourless crystals. The high solubility of the host in both aqueous solution and organic solvents made it impossible to measure the density of the crystals.

Microanalysis

The host to guest ratios of the TRIMEB complexes were determined by carbon, hydrogen and nitrogen microanalysis and the results are given as the average of duplicate determinations. The host-guest stoichiometry for the METTMB and OXPTMB(I) complexes was established as 1:1 whilst that for OXPTMB(II) was 2:1 and the results are reported in Table 6.1. The water content present in each complex was calculated from the initial mass loss obtained from the TGA traces.

Table 6.1 Carbon, hydrogen and nitrogen microanalytical results for the TRIMEB complexes

Complex	Calculated (%)			Experimental (%) #		
	C	H	N	C	H	N
METTMB $C_{63}H_{112}O_{35}\cdot C_{15}H_{25}NO_3\cdot 1.3H_2O$	54.44	8.18	0.81	54.42	8.21	0.92
OXPTMB(I) $C_{63}H_{112}O_{35}\cdot C_{15}H_{23}\ NO_3\cdot 0.6H_2O$	55.27	8.03	0.83	55.09	8.15	0.94
OXPTMB(II) $2(C_{63}H_{112}O_{35})\cdot C_{15}H_{23}\ NO_3\cdot 7.2H_2O$	53.89	7.98	0.45	53.85	7.52	0.46

Precision ± 0.3%

Thermal Analysis

HSM results for the TRIMEB complexes

The HSM results for METTMB are presented in Figure 6.1 while those for OXPTMB(I) and OXPTMB(II) are presented in Figure 6.2. The analyses were performed under silicone oil to observe bubbling due to the presence of included solvent. The slow release of bubbles indicates the loss of water from the complexes. Water loss for the METTMB, observed with very few small bubbles, took place over a temperature range of 79 to 117°C. The melting of this complex commenced at 146°C and ended at 152°C.

The rectangular shaped crystals of OXPTMB(I) showed water loss in the temperature range 83-119°C. The crystals also showed signs of melting from 119°C and were completely melted at 124°C.

The needle shaped crystals of OXPTMB(II) showed water loss from 78°C, represented by very tiny bubbles and this water loss continued until 113°C. The crystals started melting from 115°C and were completely melted by 124°C.

None of these TRIMEB complexes showed signs of opacity even when water loss was observed by the formation of bubbles, which was subsequently followed by their melting.

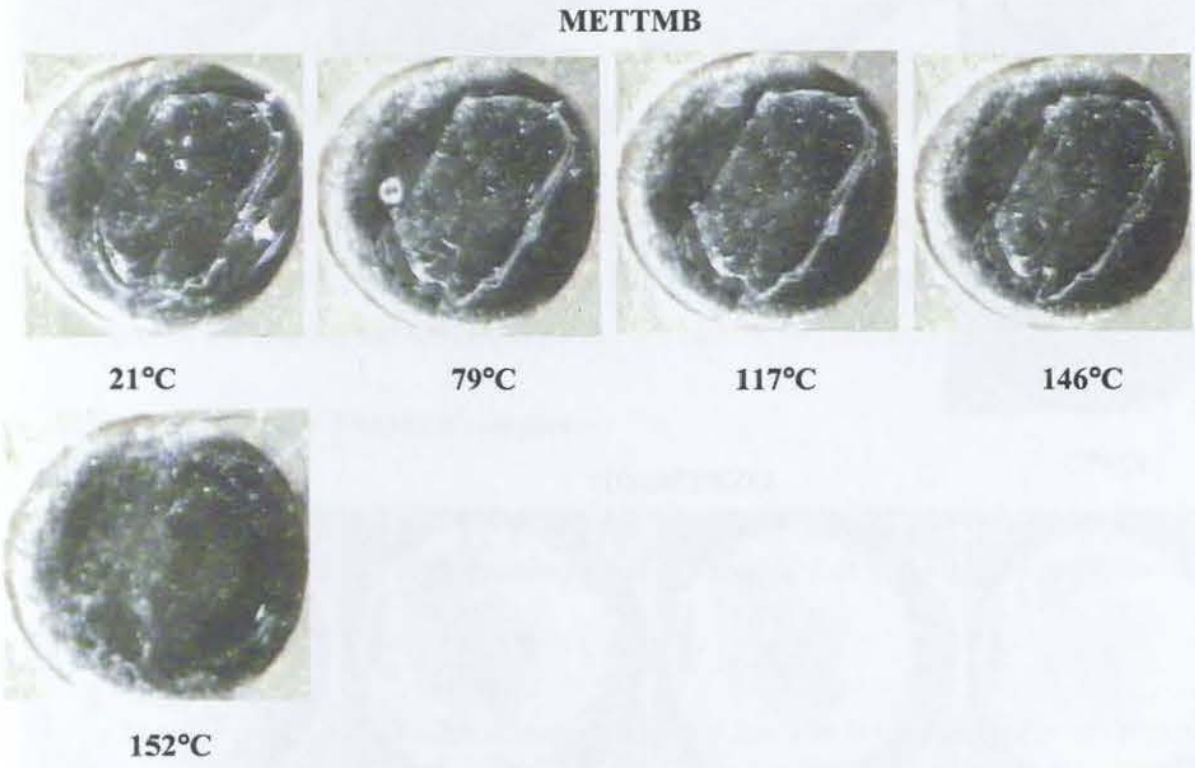

Figure 6.1 HSM photographs taken at various temperatures for crystals of the METTMB complex.

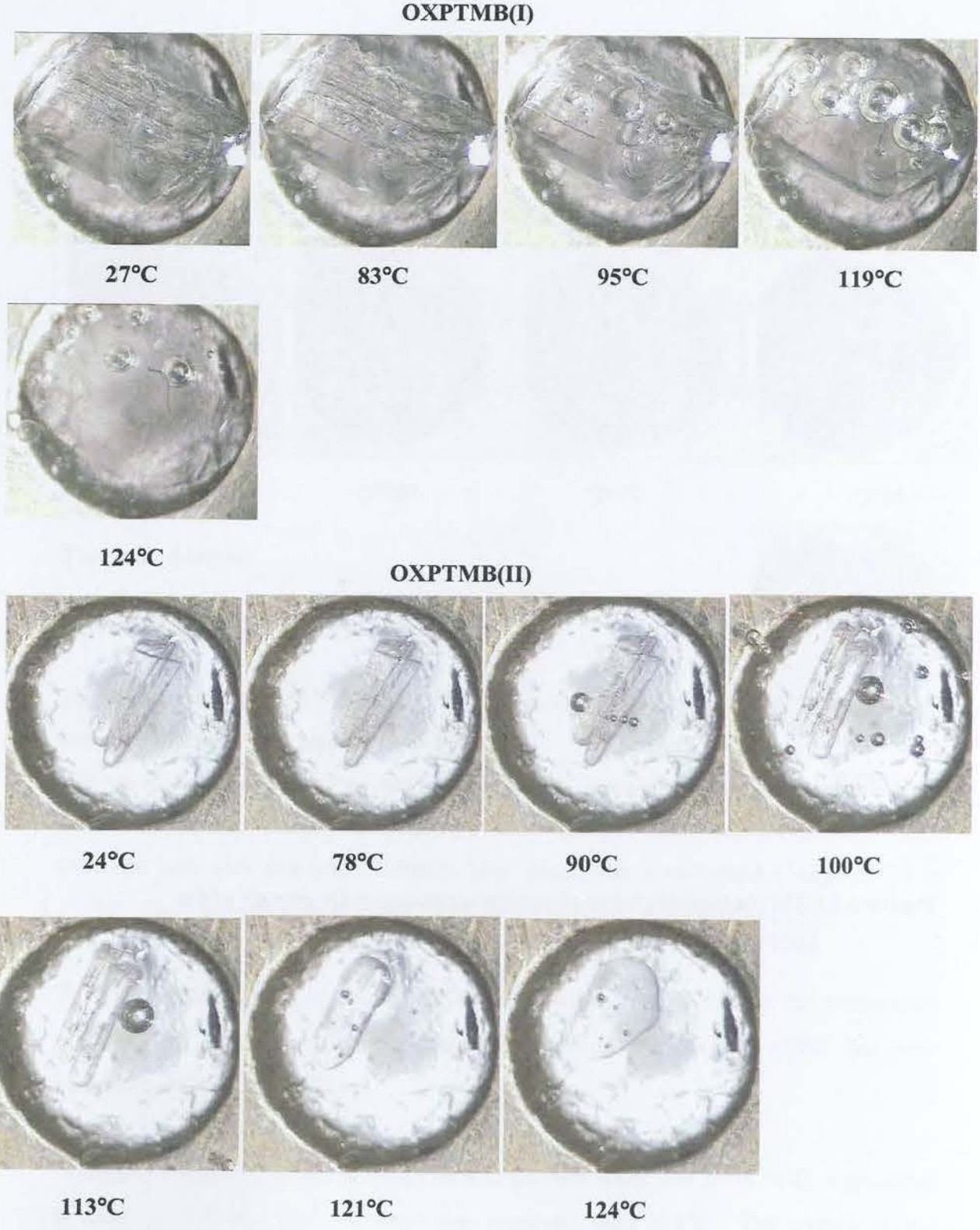

Figure 6.2 HSM photographs taken at various temperatures for crystals of OXPTMB(I) and OXPTMB(II).

TGA results for the TRIMEB complexes

The TGA results for the METTMB, OXPTMB(I) and OXPTMB(II) complexes are shown in Figures 6.3 (a), (b) and (c) respectively. Table 6.2 presents a summary of the observed percentage weight losses over the temperature intervals between 30, 100, 120, 140, 160, 180 and 200°C. Weight losses from 30 to 100°C represent water loss from the complexes. A very small percentage weight loss is noted from 100 to 160°C and from 160°C onwards percentage weight losses observed are due to decomposition of the complexes. The percentage mass losses that indicate the stoichiometry with respect to water as shown in Table 6.1 for the METTMB, OXPTMB(I) and OXPTMB(II) complexes are 1.3, 0.6 and 4.0 [± (0.1)% in each case, n = 4] respectively.

DSC results for the TRIMEB complexes

The DSC results for the METTMB, OXPTMB(I) and OXPTMB(II) complexes are shown in Figure 6.3 (a), (b) and (c) respectively and the summary of the results is presented in Table 6.3.

The broader endothermic events corresponding to water loss for all TRIMEB complexes was noted in the temperature range 30-100°C, which agreed well with an observed mass loss in the TGA traces labelled A.

The onset temperature of fusion occurs at 135, 111 and 109°C for the METTMB, OXPTMB(I) and OXPTMB(II) complexes respectively. The thermal stability of the inclusion complexes was centred on the analysis of the onset temperature of fusion for the complexes. The stability follows the order of METTMB > OXPTMB(I) ~ OXPTMB(II). The much lower melting point in comparison with the melting points of complexes of unsubstituted cyclodextrins is indicative of the weaker intermolecular interactions and is expected since methylation of all the hydroxyl groups precludes host-host intermolecular hydrogen bonding. The DSC traces do not show any indication of the endotherms corresponding to the pure drugs.

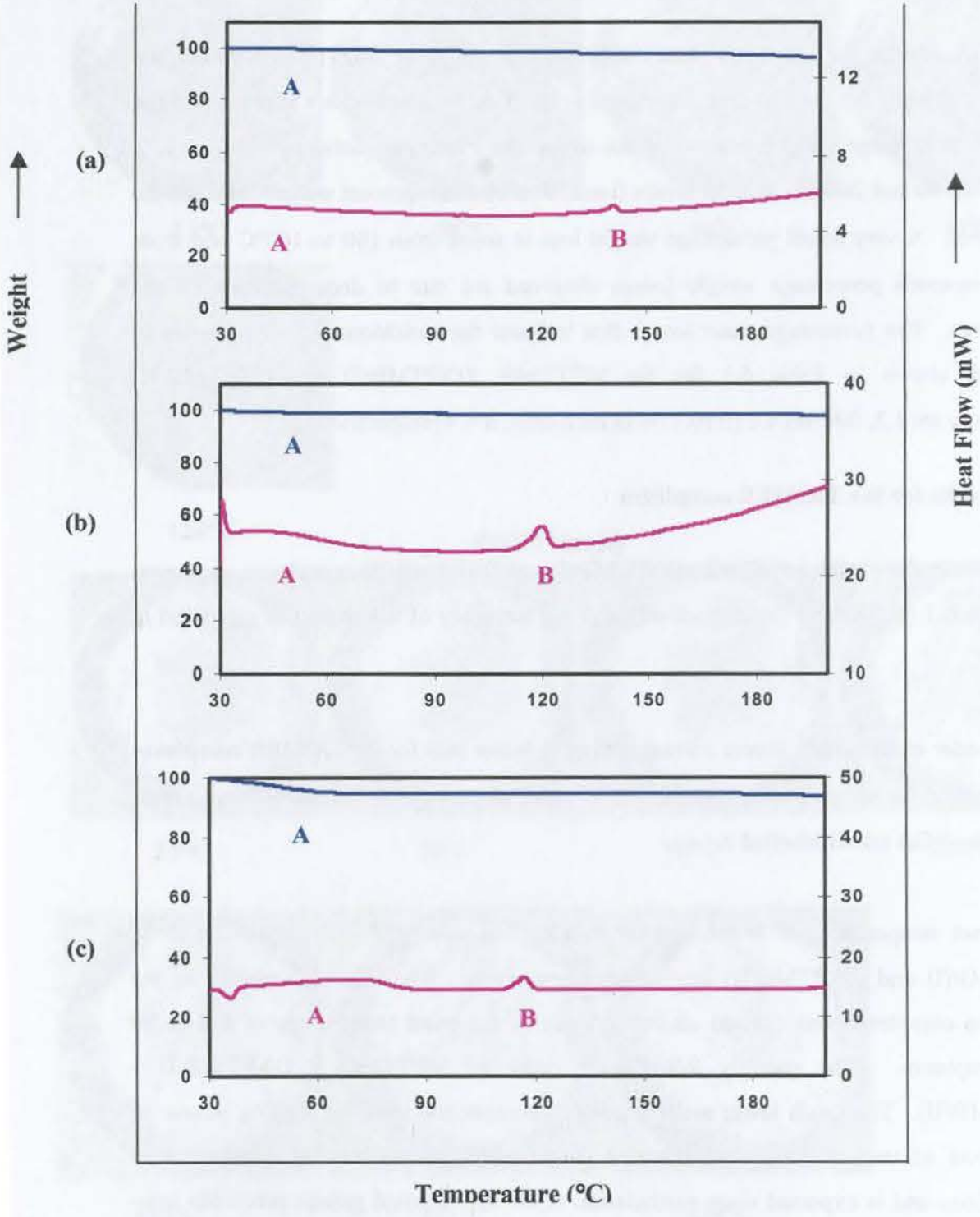

Figure 6.3 TGA [blue] and DSC [pink] traces for the (a) METTMB (b) OXPTMB(I) (c) OXPTMB(II) complexes.

Table 6.2 The percentage weight losses for the TRIMEB complexes

Temp (°C)	METTMB		OXPTMB(I)		OXPTMB(II)	
	Sample weight (%)	Δ Weight loss (%)	Sample weight (%)	Δ Weight loss (%)	Sample weight (%)	Δ Weight loss (%)
30	100	-	100	-	100	-
100	98.7	1.3	99.4	0.6	96.0	4.0
120	98.1	1.9	98.6	1.4	94.9	5.1
140	98.0	2.0	98.5	1.5	94.9	5.1
160	97.8	2.2	98.4	1.6	94.9	5.1
180	97.4	2.6	98.4	1.6	94.6	5.4
200	97.0	3.0	98.0	2.0	94.0	6.0

Table 6.3 Summarised DSC results for the TRIMEB complexes

		METTMB	OXPTMB(I)	OXPTMB(II)
Temperature range	A (°C)	30-90	30-90	30-90
Temperature range	B (°C)	135-144	111-125	109-123
Endotherm B	Ton (°C)	137	111	109
	Peak (°C)	141	120	117
Guest		Metoprolol	Oxprenolol	
melting points of uncomplexed drug substances (°C)		49	78	

Experimental PXRD Analysis

Figures 6.4, 6.5 and 6.6 illustrate the PXRD patterns for the METTMB, OXPTMB(I) and OXPTMB(II) complexes respectively together with the PXRD patterns of the physical

mixture of TRIMEB with the appropriate drug. The PXRD patterns for the METTMB, OXPTMB(I) and OXPTMB(II) complexes are distinctive and they differ significantly from those of the 1:1 physical mixtures. This confirms that complexation of the TRIMEB with each drug occurred to produce a new phase.

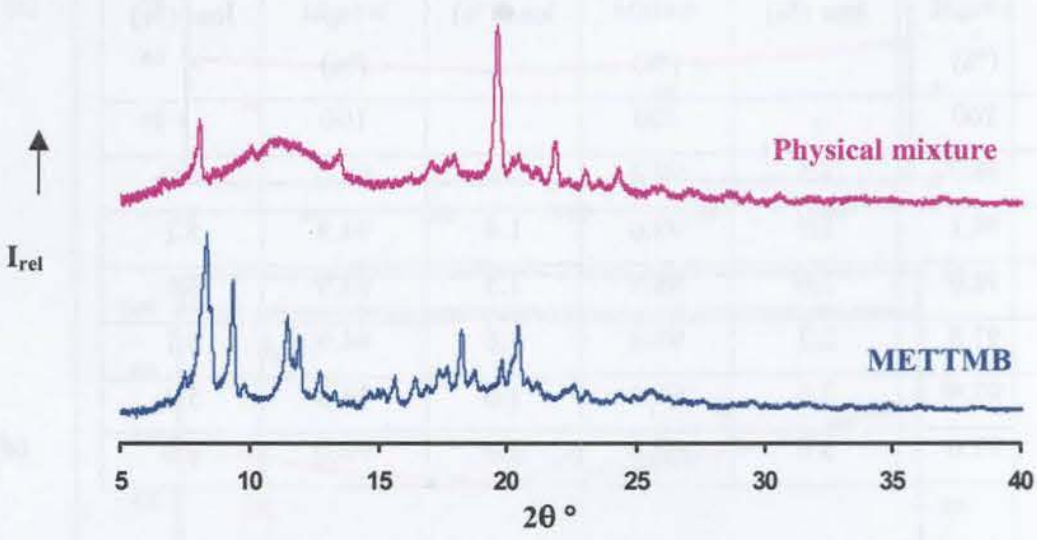

Figure 6.4 PXRD patterns of the METTMB complex and a 1:1 physical mixture of metoprolol and TRIMEB.

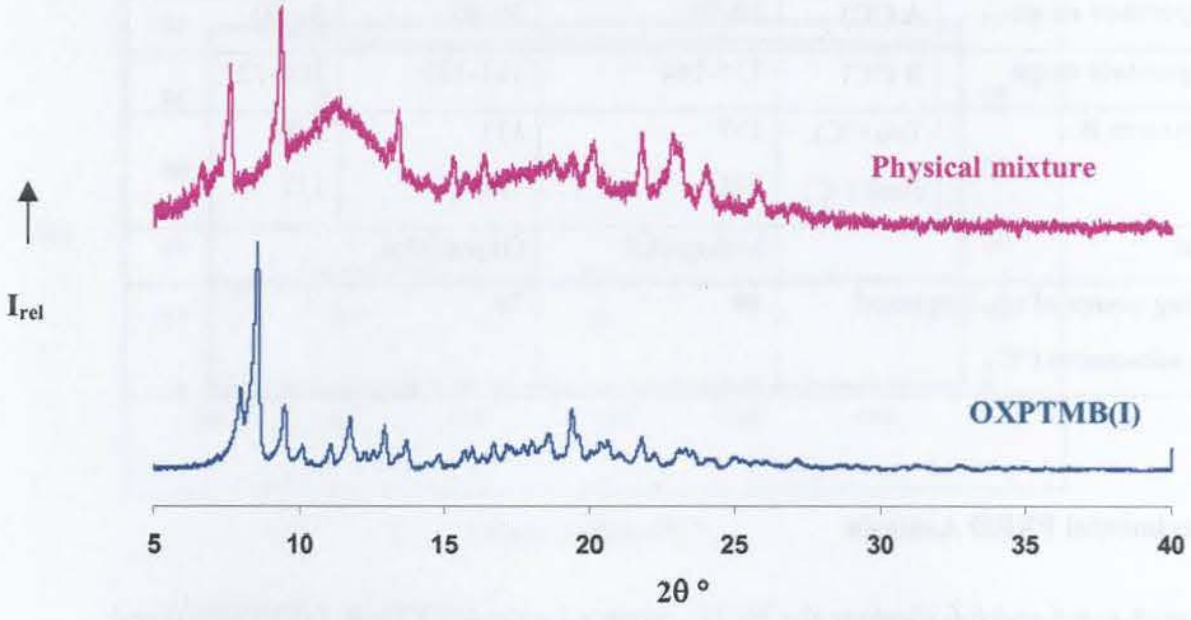

Figure 6.5 PXRD patterns of a 1:1 physical mixture of oxprenolol and TRIMEB and OXPTMB(I).

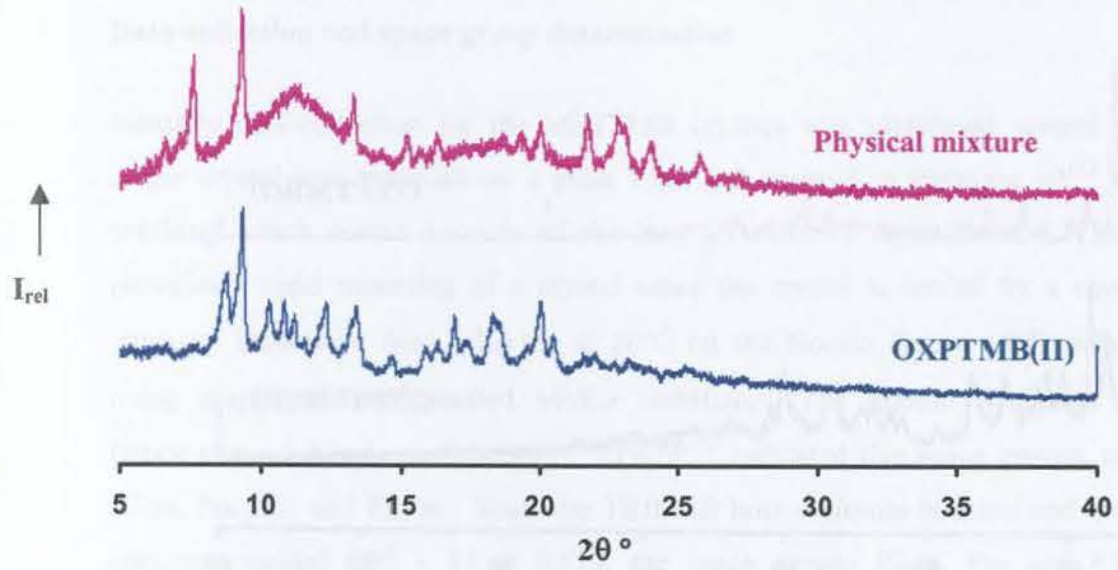

Figure 6.6 PXRD patterns of a 1:1 physical mixture of oxprenolol and TRIMEB and OXPTMB(II).

The experimental PXRD traces of the OXPTMB(I) and OXPTMB(II) crystals illustrated in Figure 6.7 clearly show that two different forms of inclusion complex between oxprenolol and TRIMEB exist. The most common crystalline modification for TRIMEB complexes is that crystallising in the orthorhombic space group $P2_12_12_1$ [OXPTMB(I)] with a ~ 14, b ~ 22, c ~ 28.[186,187,188,189,190,191,192] A comparison of the PXRD trace for OXPTMB(I) with the reference trace of Caira[186] [Figure 6.8] indicated that there is a fair resemblance between these PXRD traces, suggesting that OXPTMB(I) crystallises in the space group $P2_12_12_1$. However there are a few recently reported TRIMEB complexes belonging to the monoclinic crystal system with space group $P2_1$.[85,86] However, the unique axes in these crystal forms have different lengths and they are therefore not isostructural. Thus, so far, there are no reference traces for these complexes belonging to the monoclinic crystal system.

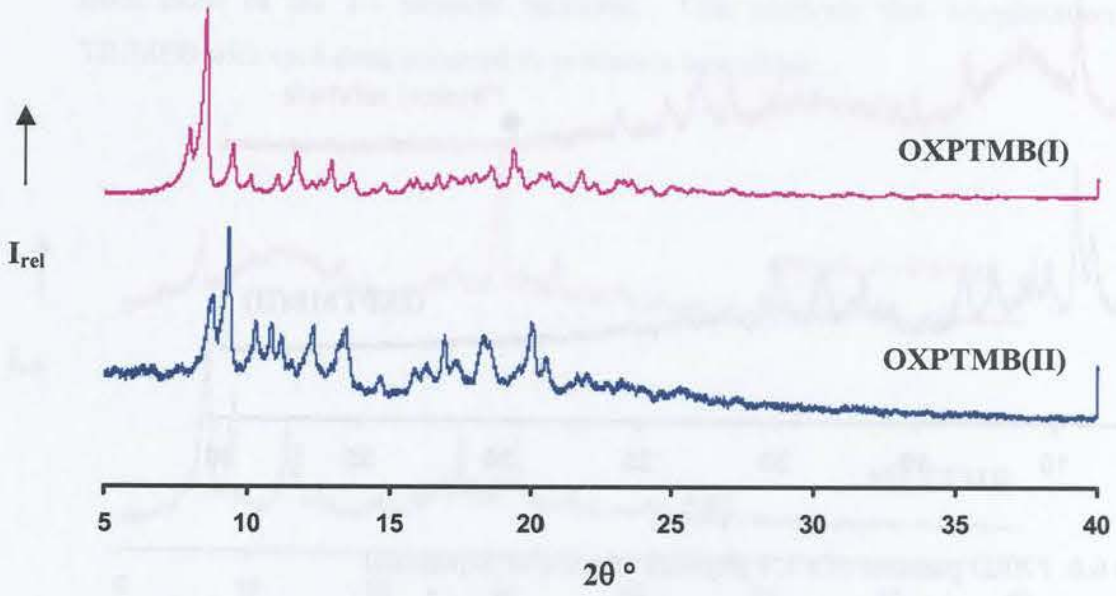

Figure 6.7 Experimental PXRD patterns of the OXPTMB(I) and OXPTMB(II) complexes.

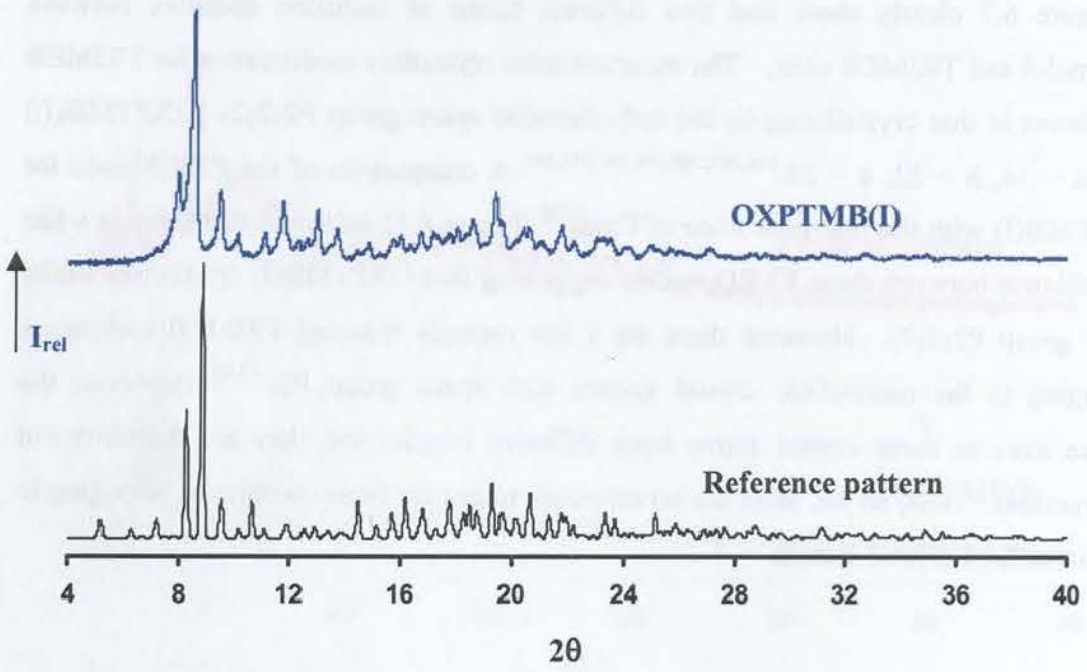

Figure 6.8 Experimental PXRD pattern of the OXPTMB(I) and the reference pattern.

X-ray Crystallographic Analysis of METTMB

Data-collection and space group determination

Intensity data-collection for the METTMB crystals was performed several times. A single crystal was mounted on a glass fibre and covered in Paratone oil[115] to prevent cracking which occurs because of the loss of water of crystallization. This oil also provides a rigid mounting of a crystal when the crystal is cooled by a stream of N_2 vapour. Data were first collected at 20°C on the Nonius Kappa CCD diffractometer using graphite-monochromated MoKα radiation. The intensity-weighted reciprocal lattice showed 2/m Laue symmetry. XPREP[103] indicated five space groups, namely P2, P2/m, Pm, $P2_1$ and $P2_1/m$. Since the TRIMEB host molecule is chiral and the intensity statistics yielded $|E^2 - 1| = 0.819$, the space groups P2/m, Pm and $P2_1/m$ were eliminated. This value is close to 0.736 expected for non-centrosymmetric structures. Inspection of the zero levels of the reciprocal lattice with LAYER[112] showed the reflection condition to be 0k0: k = 2n which uniquely identifies the space group as $P2_1$. The other two crystals for which data-collections were performed at -100°C and -160°C will be briefly mentioned later under the discussion in this chapter and a comparison of the three resulting structural models will also be presented.

Structure solution and refinement

The structure was solved using the SHELXD[117] program. The input had the following parameters, namely FIND and PLOP (peaklist optimization) and the program was allowed to run for one hour and the final correlation coefficient (CC) was 72 percent. In general the CC value of 65% or greater indicates that the structure is almost certainly solved. The E-map revealed most of the non-hydrogen atoms of the asymmetric unit that included two independent CD molecules. Preliminary inspection of the intensity-weighted reciprocal lattice layers showed that the intensities of reflections hkl alternate between strong and weak. Strong reflections are presented as follows: 0kl, 2kl, 4kl, etc and the weak reflections are 1kl, 3kl, 5kl, etc. This indicated that the unit cell contents in the interval x = 0 to x = 0.5 are approximately repeated in the interval x = 0.5 to x = 1.0.

Information with respect to any structural differences between the contents of these two intervals is contained in the weak-intensity layers hkl with h = 2n + 1. The O6, C7, C8 and C9 atoms of each methylglucose residue were initially deleted from the model as these are frequently found to display disorder in TRIMEB complexes. After refinement in SHELX-97,[113] the difference Fourier map revealed the positions of most of the remaining non-hydrogen atoms. All host atoms were initially refined isotropically. After further refinement it was found that the atom C9 on O6B1 was disordered. The atom O6 on C6A2, C6A4 and C6B2 was also disordered leading to disorder in the C9 atom on C6A2, C6A4 and C6B2. Two alternative positions were found for each disordered atoms. For a given pair, a fixed U_{iso} of 0.10 Å^2 was assigned and site-occupancy factors [s.o.f.'s] of x and 1-x were assigned, with x variable. Distance constraints were placed on some of the bonds on these disordered atoms since the observed lengths were either abnormally long or too short.

A distance constraint was also placed on bond lengths involving several other atoms since they were either abnormally long or too short. All non-hydrogen atoms with $U_{iso} \leq$ 0.10 Å^2 were refined anisotropically. The total amount of water loss observed from TG is 1.3 H_2O molecules and it is believed that these water molecules are severely disordered; it was difficult to locate them since the Fourier map revealed peaks of density below 1 e Å^{-3}. Once all the non-hydrogen atoms of the host had been placed from the subsequent difference electron density map, the positions of the methine and methylene hydrogen atoms on the CD were calculated. These hydrogen atoms were geometrically fixed at idealised positions in a riding model and were included in the refinement with an isotropic temperature factor of 1.2 times those of their parent atoms. Location of the guest molecule was problematic. There were five significant electron density peaks remaining unaccounted for at the end of the refinement with heights in the range 0.74-0.93 e Å^{-3}, the highest electron density peak being situated outside the cavity of **CD(B)** while the remaining four electron density peaks were found inside the cavity of **CD(A)**, situated higher up along the primary side of this host molecule. No reasonable structural modelling of the guest molecule was therefore possible. Crystal data and data-collection parameters are listed in Table 6.4

Table 6.4 Data-collection and refinement parameters for METTMB at 293K

Complex formula	$C_{63}H_{112}O_{35}•C_{15}H_{25}NO_3•1.3H_2O$
Formula weight / g mol^{-1}	1720.3
Crystal system	Monoclinic
Space group	$P2_1$
a / Å	21.4632(2)
b / Å	14.8321(2)
c / Å	27.5114(4)
β / °	97.97(4)
Volume / Å^3	8673.5(2)
Z	4
Density $_{calc}$ / g cm^{-3}	1.314
μ(MoKα) / mm^{-1}	0.089
F(000)	3688
Temperature of data-collection / K	293(2)
Crystal size / mm^3	0.50 x 0.50 x 0.60
Range scanned θ / °	$2 \leq \theta \leq 28$
Index ranges	h : -27, 27 k : -18, 18 l : -34, 34
Dx / mm	59
Total no. of reflections collected	33090
Total no. of unique reflections	16123
No. of reflections with $I > 2\sigma(I)$	14143
No. of parameters	1499
S	1.37
R_1 (for 14143 reflections)	0.1525
wR_2	0.4477
R_{int} R_σ	0.0809 0.0809
Weighting scheme	a = 0.2 b = 0
$(\Delta/\sigma)_{mean}$	< 0.034
Δρ excursions / e Å^{-3}	0.93 and -0.90

Geometrical analysis of the METTMB structure

METTMB crystallises in a 1:1 TRIMEB:metoprolol molar ratio in the monoclinic space group $P2_1$ with two crystallographically independent TRIMEB molecules, 1.3 H_2O molecules and Z = 4 complex formula units per unit cell. A diagram of the METTMB structure is presented in Figure 6.9. The methylglucose units of the two independent host molecules are denoted **A1** to **A7** and **B1** to **B7** and the numbering of one methylglucose

unit is shown. The geometrical parameters used to describe the structural features of the CD host, as described in Chapter 1 are listed in Tables 6.5-6.7.

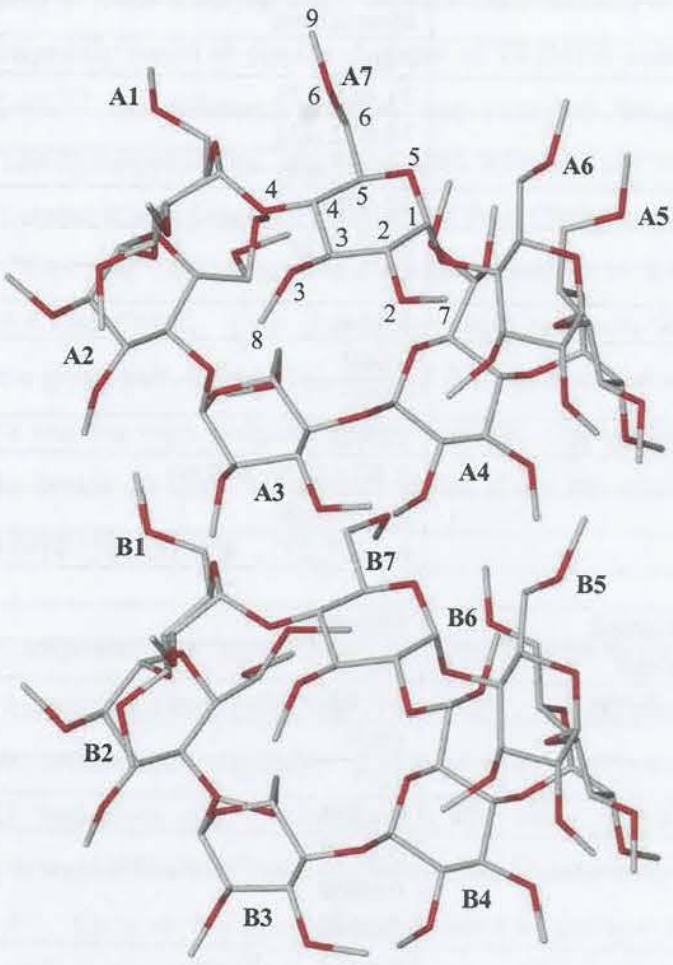

Figure 6.9 Oblique view of the host molecules of the asymmetric unit of the METTMB complex. The labelling for the **A7** residue is shown. Hydrogen atoms and electron density peaks for the disordered guest are omitted for clarity.

Table 6.5 Torsion angles (°) for METTMB

CD(A)	ω	Φ	Ψ	Θ_1	Θ_2
A1	-70 (1)	108.9(9)	136.1(8)	51(1)	-48(1)
A2 *	-43(2), 12(2)	104.8(9)	139.2(8)	53(1)	-58(1)
A3	-74(1)	80.0(9)	97.1(8)	55(1)	-61(1)
A4 *	-36(1), 77(1)	123.1(7)	163.2(7)	48(1)	-51(1)
A5	-64(1)	97.7(8)	126.4(7)	43(1)	-45(1)
A6	-68(1)	91.7(8)	105.3(8)	52(1)	-55(1)
A7	-67(1)	106.0(10)	136.9(9)	54(1)	-58(1)
CD(B)					
B1	-75(1)	105.9(9)	128.6(9)	53(1)	-51(1)
B2 *	-85(1), 59(1)	112.8(9)	152.6(8)	57(1)	-59(1)
B3	-80(1)	79.3(9)	93.6(8)	43(1)	-47(1)
B4	-62(1)	108.5(8)	165.6(7)	43(1)	-47(1)
B5	77(1)	99.7(7)	127.9(7)	47(1)	-49(1)
B6	-70(1)	90.8(9)	102.0(8)	54(1)	57(1)
B7	71(1)	111.9(8)	139.0(9)	50(1)	-55(1)
| Average | *	**64.1**	**101.5**	**129.5**	**50**	**53**

* Oxygen atoms are disordered over two positions

* Unweighted average of all recorded values

The principal torsion angles of the independent TRIMEB molecules are listed in Table 6.5. The ω parameter [describing the direction of the C6-O6 bonds with respect to the cavity] is positive for **B5**, **B7**, and for **A2** and **B2** [minor position O6] and for **A4** [major position O6], thus indicating that the C6-O6 bonds are pointing toward the cavity. The ω parameter is negative for **A1**, **A3**, **A5**, **A6**, **A7**, **B1**, **B3**, **B4** and **B6** and for the **A2**, **B2** [major position O6] and for the **A4** [minor position O6], indicating that the C6-O6 bonds are pointing pointing away from the cavity. The C9 methyl carbon atoms of the methylglucopyranose unit for which ω is positive extend along the primary rim attempting to close this side of the host molecule and this is clearly illustrated in Figure 6.8. The O6-C9 bond is *trans* to C5-C6 for all residues except for O(6C4)-C(9C4) [major

position on **A4**], O(6C2)-C(9C2) and O(6D2)-C(9D2) [minor positions on **A2** and **B2** respectively] where the bonds are *gauche*. On the secondary rim the C7 and C8 methyl carbons point away from each other to avoid steric hindrance. The methylglucopyranose units are all in the $^4C_1$ chair conformation and the conformation around the C4 atoms, described by the parameters Θ_1 and Θ_2, depicts minimal deviation from the ideal values for such residues. The O4 heptagon parameters are listed in Table 6.6. These include the radii [**r**], i.e. the distances O4G*n*•••Cg, where Cg is the centre of gravity of the seven O4G*n* atoms [*n* = 1-7], the O4•••O4' distances [**l**], the O4•••O4'•••O4" angles [**a**], the deviations of each of the O4 atoms from the mean O4 plane [**d**] and the O4•••O4'•••O4"•••O4'" torsion angles [**t**].

Table 6.6 O4 heptagon parameters for METTMB

CD(A)	r / Å	l / Å	a / °	d / Å	t / °
A1	5.27	4.28	118	-0.456(4)	8
A2	4.40	4.46	139	0.560(4)	-36
A3	4.92	4.24	128	0.158(4)	20
A4	5.42	4.25	116	-0.574(4)	17
A5	4.79	4.55	134	0.118(4)	-19
A6	4.71	4.45	131	0.438(5)	-6
A7	5.25	4.28	128	-0.244(5)	16
CD(B)					
B1	4.97	4.43	125	-0.481(4)	11
B2	4.40	4.42	141	0.501(4)	-36
B3	5.35	4.29	118	0.234(4)	14
B4	5.28	4.36	120	-0.608(4)	20
B5	4.55	4.56	138	0.102(4)	-23
B6	4.97	4.33	127	0.445(5)	-5
B7	5.40	4.25	121	-0.194(5)	12
| Average |	**4.98**	**4.37**	**127**	**| 0.365 |**	**17**

The O4 heptagons of the METTMB differ significantly from a regular heptagon of a parent β-cyclodextrin. The evidence of that is observed in Figure 6.10. The increasing and decreasing patterns of the numerical variation in **r**, **l**, and **a** parameters in Table 6.6 confirm this significant difference between METTMB and the parent β-cyclodextrin. The **d** and **t** parameters also indicate the significant deviation of the individual O4 atoms from the O4 mean plane. This is due to the tilt angles described below.

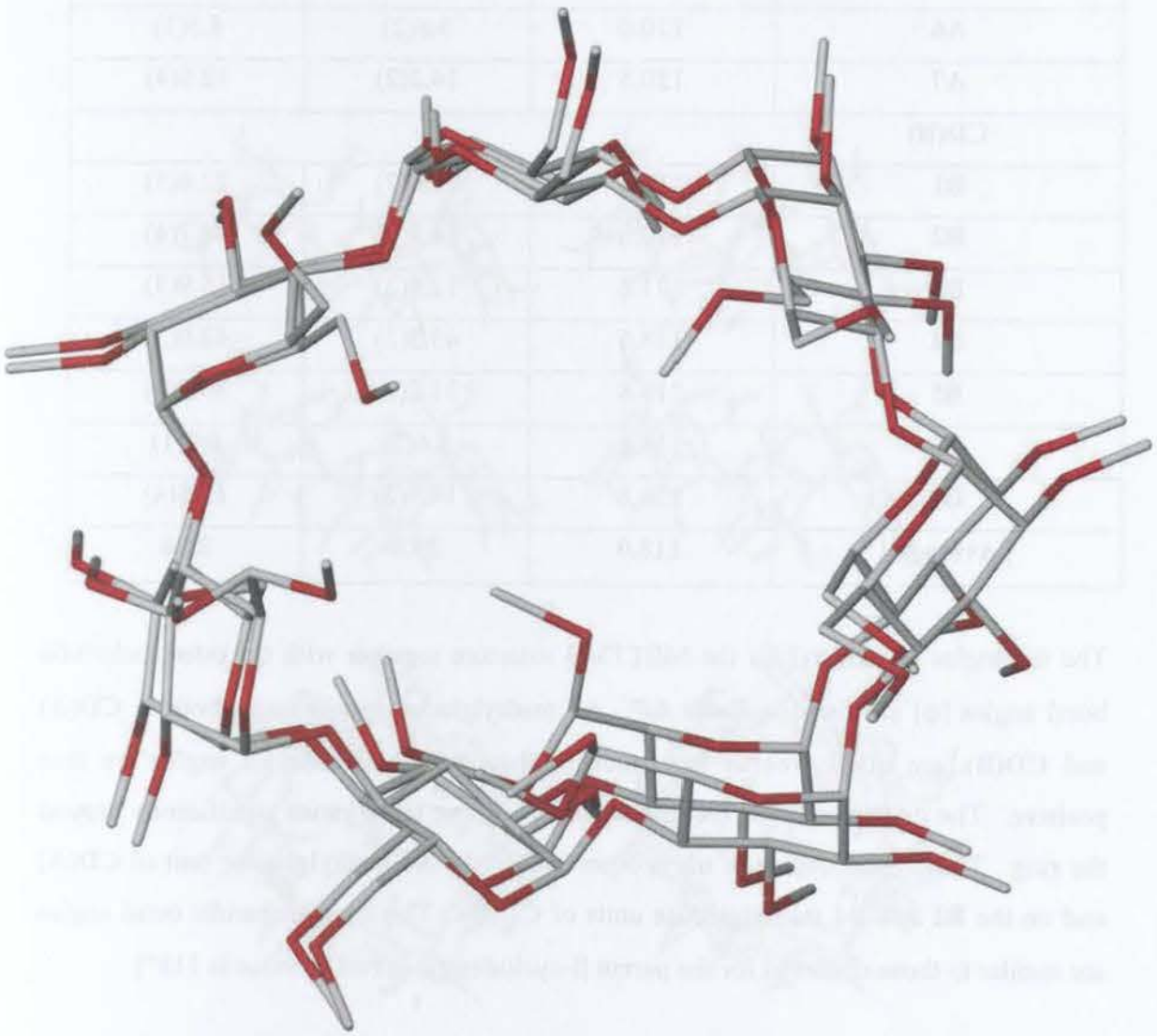

Figure 6.10 View of the independent CD molecules of the METTMB complex from the host primary face of **CD(A)**, showing the ellipticity of the macrocycles.

Table 6.7 φ and τ parameters for METTMB

D(A)	φ / °	τ_1 / °	τ_2 / °
A1	118.4	29.8(2)	29.7(4)
A2	111.9	28.4(2)	33.9(3)
A3	117.2	17.4(3)	22.5(3)
A4	119.4	41.5(2)	37.8(2)
A5	118.7	26.6(2)	31.7(2)
A6	120.0	5.8(2)	8.5(1)
A7	120.5	14.2(2)	12.6(4)
CD(B)			
B1	116.7	21.6(2)	22.8(5)
B2	113.6	34.9(2)	44.7(4)
B3	121.6	12.5(2)	15.9(3)
B4	118.6	43.3(2)	42.0(2)
B5	116.8	31.2(2)	36.8(2)
B6	117.6	8.6(2)	8.9(1)
B7	120.8	14.5(2)	13.5(4)
| Average |	**118.0**	**23.6**	**25.8**

The tilt angles [τ_1 and τ_2] for the METTMB structure together with the intersaccharidic bond angles [φ] are listed in Table 6.7. All methylglucopyranose units, both in **CD(A)** and **CD(B)**, are tilted towards the inside of the cavity and their tilt angles are thus positive. The degree of tilt of the methylglucopyranose units varies significantly around the ring. The highest degree of tilt is observed for the **A4** methylglucose unit of **CD(A)** and on the **B2** and **B4** methylglucose units of **CD(B)**. The intersaccharidic bond angles are similar to those observed for the parent β-cyclodextrin [average value is 118°].

Guest inclusion

As stated earlier in the chapter, the guest could not be modelled due to the high degree of disorder that was prevalent in the difference Fourier map as indicated by the abnormal distances and angles between electron density peaks. However information from microanalysis showed that METTMB crystallised with one guest molecule per TRIMEB host molecule. The highest electron density peaks in the host cavities [0.42-0.75 e.Å^{-3}] are illustrated in stereo in Figure 6.11.

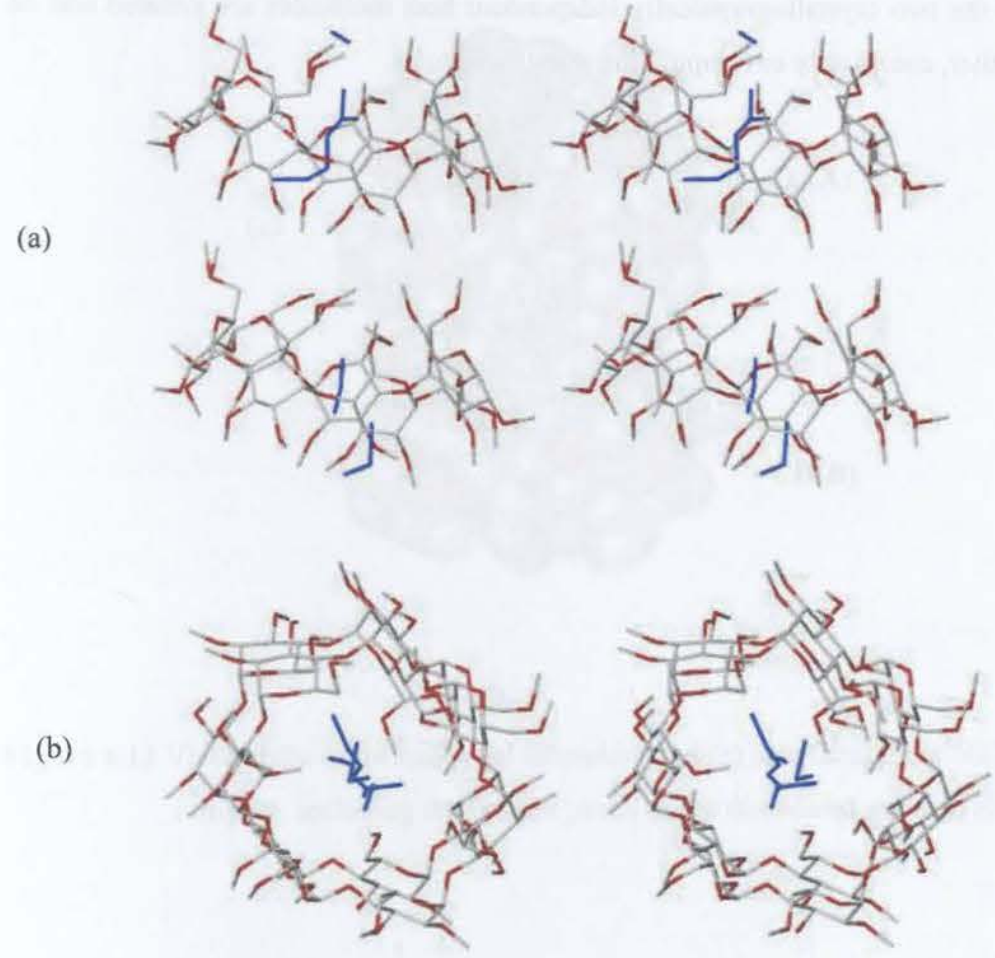

Figure 6.11 Stereoviews from (a) the sides and (b) onto the primary sides of the independent host molecules. Disordered guest peaks are in blue.

This clearly shows that the difference Fourier map did not reveal any recognisable fragment of the metoprolol molecule that could be used as a starting model for further refinements. Figures 6.12 (a)-(c) are space-filling diagrams presenting different views of the METTMB complex, including the electron density peaks [blue] for the disordered guest. Figure 6.12(a) is a view from the primary face of **CD(A)** illustrating the effect of the C9 methyl groups of the methylglucose units for which ω is positive. These O6 methyl groups thus point toward the cavity, effectively closing the primary rim of the CD. The view from the secondary face, illustrated in Figure 6.12(b), shows the open side of the TRIMEB molecule. The side view of the METTMB complex in Figure 6.12(c) shows how the two crystallographically independent host molecules are situated one on top of the other, completely enveloping the guest molecules.

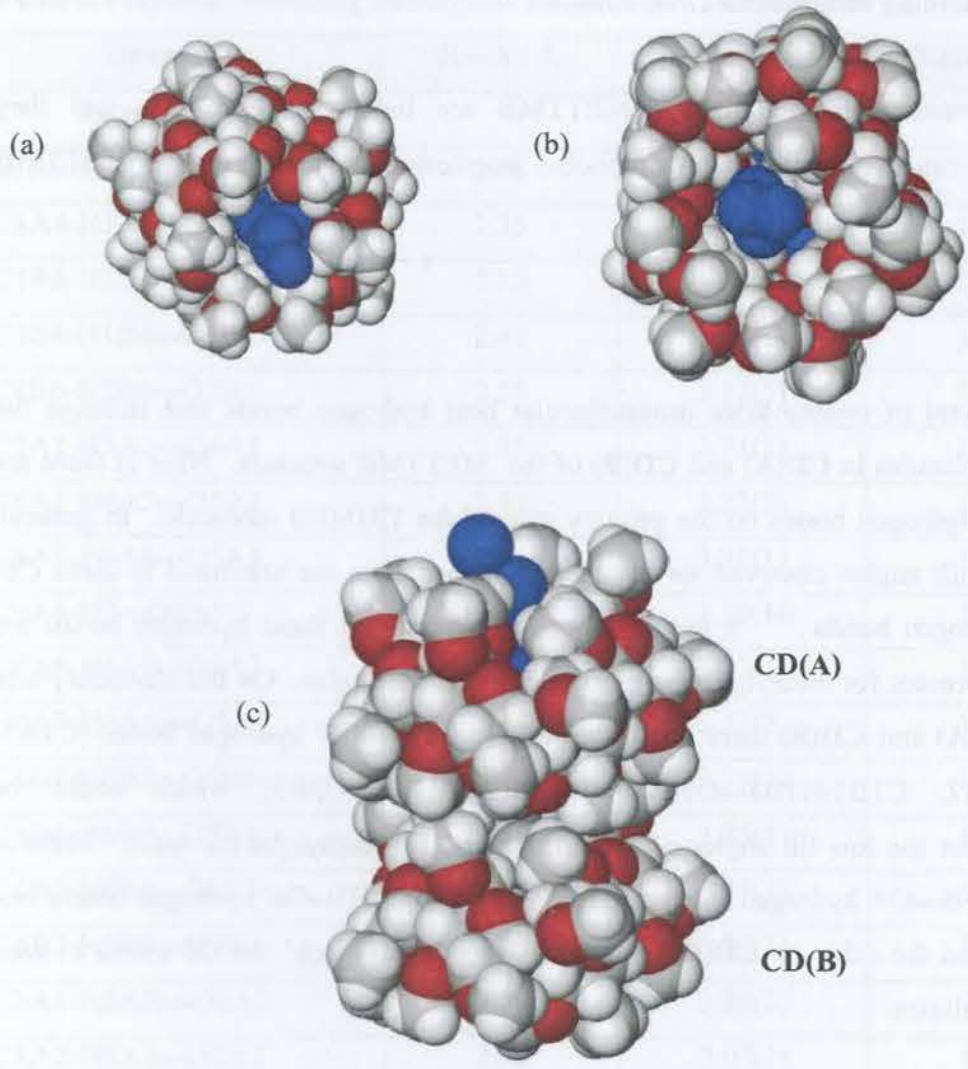

Figure 6.12 View of the (a) primary, (b) secondary and (c) side face of the METTMB complex, including the Fourier peaks of the disordered guest in blue.

Hydrogen bonding in the METTMB complex

Hydrogen bonding interactions for METTMB are listed in Table 6.8, and they complement van der Waals and hydrophobic interactions that stabilise the METTMB structure.

Intramolecular host interactions

There is a total of twenty three intramolecular host hydrogen bonds that stabilise the TRIMEB molecules in **CD(A)** and **CD(B)** of the METTMB structure. Nine of them are C6-H•••O5' hydrogen bonds on the primary side of the TRIMEB molecule. In general, the positive tilt angles observed for the methylglucose units are attributed to these C6-H•••O5' hydrogen bonds .[193] It has also been suggested that these hydrogen bonds are usually not present for methylglucose units with lower tilt angles. On the secondary side of both **CD(A)** and **CD(B)** there is a total of three C1-H•••O3' hydrogen bonds [C1A3-H1A3•••O3A2, C1B3-H1B3•••O3B2 and C1B6-H1B6•••O3B5] which could be responsible for the low tilt angles of the **A3**, **B3** and **B6** methylglucose units. There is only one C5-H•••O4' hydrogen bond on **CD(A)** and two C1-H•••O6' hydrogen bonds, one on **CD(A)** and the other on **CD(B)**, and these latter bonds 'lock' the O6 atoms in their observed positions.

Intermolecular host interactions

There are only two intermolecular host-host C-H•••O hydrogen bonds present in the METTMB structure. These are responsible for the stabilisation of the crystal structure in the absence of water molecules that fulfil this function in hydrated complexes.

Table 6.8 Hydrogen-bonding interactions for the METTMB structure

Interaction	H•••A / Å	D•••A / Å	D-H•••A / °
Intramolecular			
C1A3-H1A3•••O3A2	2.46	3.13(1)	125
C1A4-H1A4•••O6A3	2.35	3.20(1)	145
C1B3-H1B3•••O3B2	2.33	3.00(1)	125
C1B4-H1B4•••O6B3	2.42	3.22(1)	138
C1B6-H1B6•••O3B5	2.55	3.12(1)	117
C5A2-H5A2•••O4A1	2.15	2.71(1)	114
C6A1-H6A2•••O5A2	2.43	3.22(2)	138
C6A3-H6A4•••O5A4	2.51	3.31(1)	140
C6A4-H7•••O5A5	2.24	3.10(1)	149
C6A6-H6A8•••O5A7	2.53	3.27(1)	133
C6A7-H6AX•••O5A1	2.48	3.21(2)	132
C6B3-H6B2•••O5B4	2.44	3.21(1)	136
C6B4-H6B4•••O5B5	2.45	3.25(1)	139
C6B4-H6B4•••O6B5	2.60	3.45(1)	146
C6B7-H6B9•••O5B1	2.43	3.32(1)	154
C8A1-H8AH•••O2A2	2.59	3.20(2)	122
C8A2-H8A3•••O2A2	2.46	3.07(1)	121
C8A3-H8AX•••O4A3	2.48	3.07(2)	119
C8A7-H8A7•••O2A1	2.60	3.15(2)	117
C8B2-H8B3•••O2B2	2.45	2.98(1)	115
C8B6-H8BA•••O2B7	2.38	3.07(2)	128
C8B7-H8B8•••O2B1	2.32	3.12(2)	140
C9A3-H9A4•••O5A3	2.26	3.00(2)	133

Intermolecular	H•••A / Å	D•••A / Å	D-H•••A / °	Symmetry code [#]
C9A7-H9AY•••O3B1	2.49	3.34(2)	149	1-x, ½ +y, 2-z
C2B2-H2B2•••O6B6	2.52	3.50(1)	171	x, -1+y, z

[#] Symmetry code applied to second unit of interaction

Crystal packing

Figure 6.13 presents a stereo packing diagram of the METTMB complex. The channel-like packing arrangement along the a-axis, is similar to that found in the butamben-TRIMEB complex[85] (space group $P2_1$). The presence of 2_1-axes parallel to only one direction (the unique axis) yields a structure in which successive layers of complex units parallel to the b-axis have alternating polarities. This phenomenon is unusual for TRIMEB complexes, which normally crystallise in the space group $P2_12_12_1$, consistent with modulated channel-packing motifs.[194]

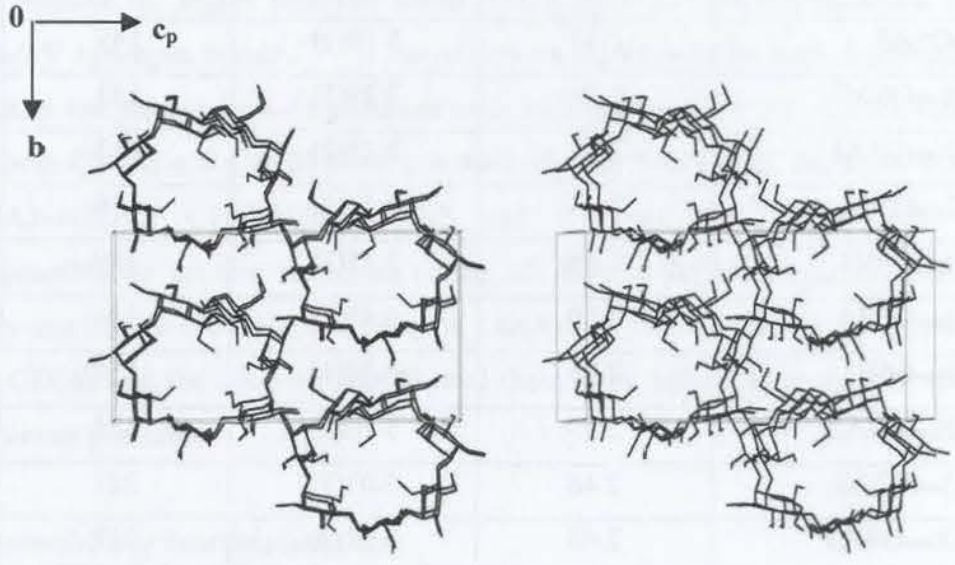

Figure 6.13 Stereo packing diagram of the METTMB complex viewed down the a-axis.

Powder X-ray diffraction

Figure 6.14 presents the computed and experimental PXRD patterns for METTMB. The patterns match in their number of peaks as well as their profiles. The close agreement between the two PXRD patterns indicates the lack of a phase change on grinding the complex and that the computed trace can serve as reference for METTMB identification. The information for both traces was obtained at room temperature.

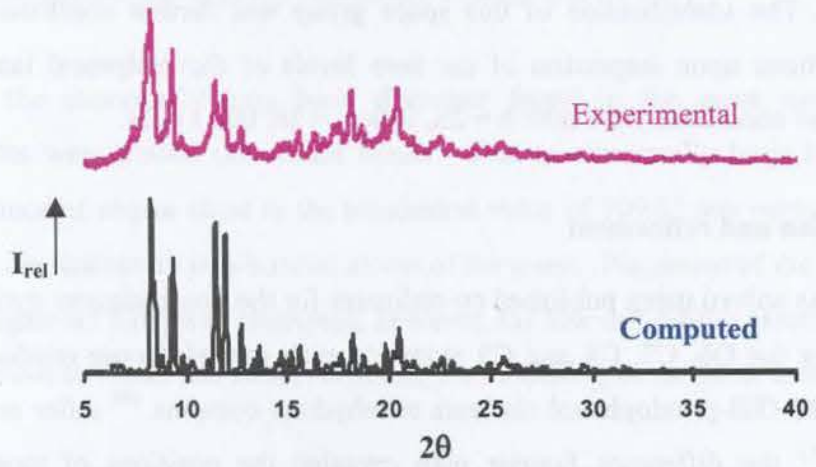

Figure 6.14 Computed and experimental [293K] PXRD traces of METTMB.

X-ray Crystallographic Analysis of OXPTMB(I)

Data-collection and space group determination

Data-collections were performed several times on this complex. A crystal of the complex was mounted on a glass fibre and covered in Paratone N oil[115] to prevent cracking due to loss of water of crystallisation. Data were collected at 113(2) K on the Nonius Kappa CCD diffractometer using graphite-monochromated MoKα radiation. The Laue *mmm* symmetry indicated that the OXPTMB(I) crystal belongs to the orthorhombic crystal system. XPREP[103] indicated the space group $P2_12_12_1$ that was suggested earlier by PXRD analysis. The identification of this space group was further confirmed by the reflection conditions upon inspection of the zero levels of the reciprocal lattice with LAYER.[112] These conditions were h00: h = 2n, 0k0: k = 2n, 00l: l = 2n.

Structure solution and refinement

The structure was solved using published co-ordinates for the non-hydrogen cyclodextrin atoms [excluding the O6, C7, C8 and C9 atoms of each methylglucose residue] of the isomorphous TRIMEB-p-iodophenol clathrate tetrahydrate complex.[186] After refinement in SHELX-97,[113] the difference Fourier map revealed the positions of most of the remaining non-hydrogen atoms. All the non-hydrogen atoms on the host with $U_{iso} \leq 0.1$ $Å^2$ were refined anisotropically.

Once all the non-hydrogen atoms of the host had been located from the subsequent difference electron density map, the positions of the methine and methylene hydrogen atoms were calculated and geometrically fixed at idealised positions in a riding model and were included in the refinement with an isotropic temperature factor of 1.2 times that of the attached carbon atom. The highest remaining electron density peak of 1.20 e $Å^{-3}$ was located at distances of 0.96 Å from C6G5 and 1.65 Å from O6G5. The possibility that this electron density peak represented a disordered oxygen atom was rejected on the basis of the unfavourable geometric position relative to those atoms already placed and it was also at an extremely short contact distance [0.96 Å] from the C6G5 atom. This

electron density peak [1.20 e $Å^{-3}$] was therefore refined as water with s.o.f. of less than one, since it was at a favourable hydrogen bonding distance from N12 [3.27 Å] and O10 [2.76 Å] atoms of the guest molecule. TGA showed that the OXPTMB(I) complex has a total of 0.6 H_2O molecules per asymmetric unit and it was successfully located. Distance constraints were placed on certain bonds of the TRIMEB host molecule.

The guest phenyl ring was modelled as a regular hexagon. The hydrogen atoms attached to the carbon atoms of the guest were also inserted at idealised positions and assigned a common isotropic temperature factor. The hydrogen atom of the hydroxyl group was located using the rotating group refinement strategy [AFIX 147].

Due to the abnormally long bond distances found in the guest molecule, distance constraints were placed on certain bonds. Due to abnormally large bond angles, the maintenance of angles close to the tetrahedral value of 109.5° was performed by placing distance constraints on non-bonded atoms of the guest. Placement of the C19 atom of the guest [Figure 6.15(b)] was attempted; however, the low and diffuse electron density made it impossible to locate this atom, rendering the modelling of the guest incomplete.

The very poor S and R_1 agreement indices for the OXPTMB(I) structure are attributed to several factors. Firstly the instability of this model led to the placement of distance constraints on certain bonds of both the TRIMEB host and oxprenolol guest molecules. Secondly the low and diffuse electron density peaks inside the host cavity in the range 1.04-0.30 e $Å^{-3}$ were used for guest modelling. Thirdly the high mosaicity [1.5%] and low data-completeness [89%] and finally the incomplete modelling of the guest also contributed to these poor factors. The study of this structure has, however, been pursued since a second crystalline form [OXPTMB(II)] of this complex was isolated and structural comparison was desirable. Crystal data and data-collection parameters are listed in Table 6.9.

Table 6.9 Data-collection and refinement parameters for OXPTMB(I) at 113K

Complex formula	$C_{63}H_{112}O_{35} \cdot C_{15}H_{23}NO_3 \cdot 0.6H_2O$
Formula weight / g mol^{-1}	1711.9
Crystal system	Orthorhombic
Space group	$P2_12_12_1$
a / Å	14.5974(5)
b / Å	21.7829(6)
c / Å	28.164(1)
Volume / $Å^3$	8955.4(5)
Z	4
Density $_{calc}$ / g cm^{-3}	1.269
μ(MoKα) / mm^{-1}	0.100
F(000)	3616
Temperature of data-collection / K	113(2)
Crystal size / mm^3	0.35 x 0.45 x 0.52
Range scanned θ / °	$2 \leq \theta \leq 25$
Index ranges	h: -16, 16 k: -25, 25 l: -32, 32
Dx / mm	50
Total no. of reflections collected	13684
Total no. of unique reflections	6842
No. of reflections with $I > 2\sigma(I)$	8420
No. of parameters	844
No. of reflections omitted	15
R_{int}, R_σ	0.0764, 0.0764
S	1.79
R_1 (for 8420 reflections)	0.1937
wR_2 (all reflections)	0.4827
Weighting scheme parameters	a = 0.2 b = 0.0
$(\Delta/\sigma)_{mean}$	< 0.022
$\Delta\rho$ excursions / e $Å^{-3}$	-1.54 and 1.20

Geometrical analysis of the OXPTMB(I) structure

The asymmetric unit of the OXPTMB(I) structure comprises a single TRIMEB molecule, its associated oxprenolol guest molecule and one water molecule. The glucose units are labelled **G1** to **G7**. The numbering scheme of the OXPTMB(I) complex is shown in Figure 6.15(a) while Figure 6.15(b) illustrates the chemical structural diagram of oxprenolol and its numbering scheme.

All seven methylglucose moieties of the TRIMEB molecule are in the $^4C_1$ chair conformation and the macrocycle is in the shape of an elliptically distorted and truncated cone. The O2-C7 bonds point away from the cavity whilst the O3-C8 bonds are directed toward the cavity. The geometrical data for the TRIMEB molecule are listed in Tables 6.10 to 6.12. The **ω** parameter in Table 6.10 shows that four C6-O6 bonds, on the glucose units **G1**, **G2**, **G4** and **G7**, are directed away from the cavity and thus adopt the (-)-*gauche* conformation and the remaining C6-O6 bonds on the glucose units **G3**, **G5** and **G6** point toward the centre of the cavity and are in the (+)- *gauche* conformation.

The geometric parameters of the O4 heptagon of OXPTMB(I) are listed in Table 6.11. The O4 heptagon of the host molecule in OXPTMB(I) significantly differs from a regular heptagon of a parent β-cyclodextrin. Generally, the bond angles and bond lengths conform to those of other known cyclodextrin complexes. There is also significant deviation of the individual O4 atoms from the O4 mean plane, and this is indicated by the **d** and **t** parameters. This significant deviation is attributed to tilt angles to be discussed next.

(a)

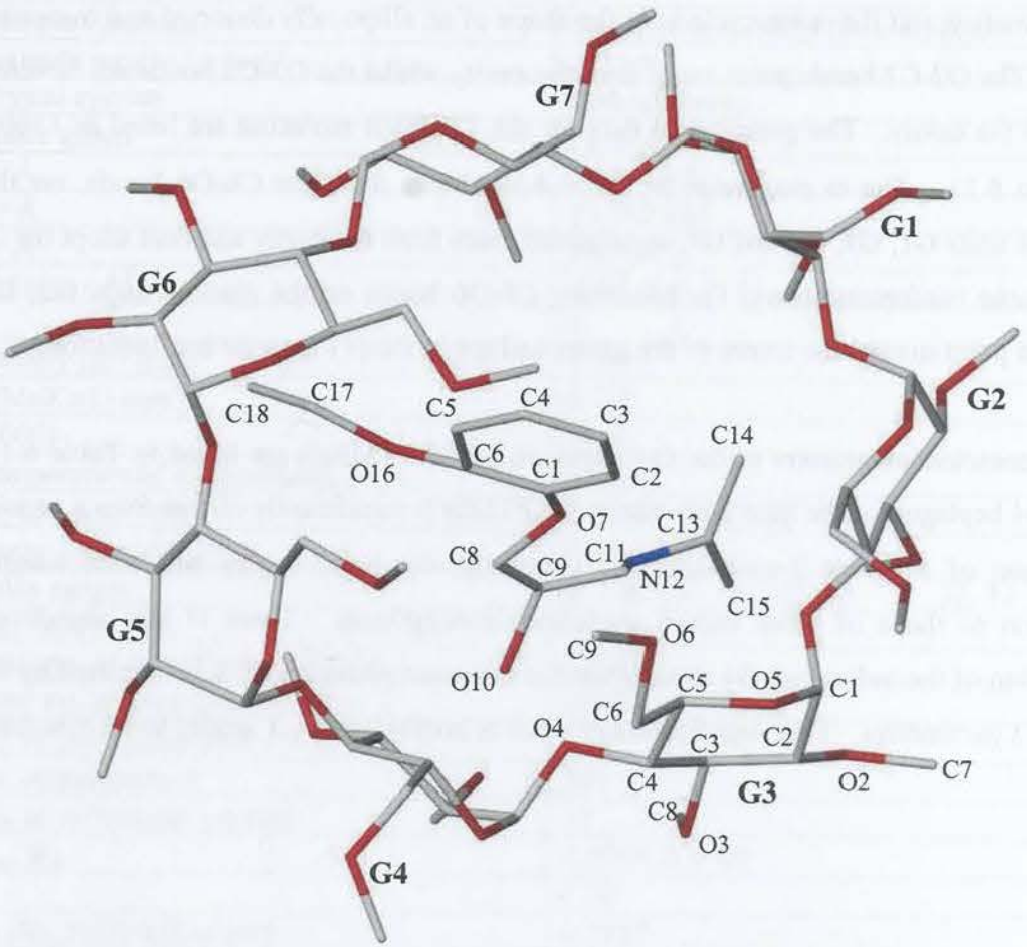

(b)

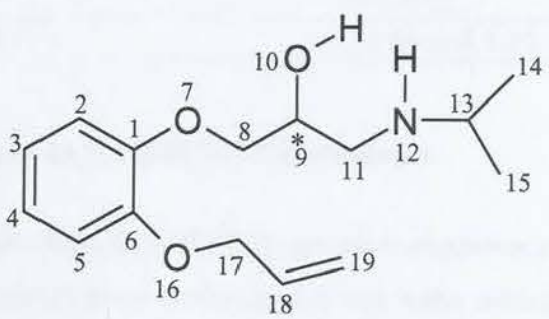

Figure 6.15(a) Macrocyclic structure and numbering scheme of glucose residues and guest molecule, with the hydrogen atoms excluded. The host is viewed from the primary face, (b) chemical structural diagram of oxprenolol with its numbering scheme.

Table 6.10 Torsion angles (°) for OXPTMB(I)

Glucose unit	ω	Φ	Ψ	Θ_1	Θ_2
G1	-66(1)	111(1)	145(1)	50(1)	-50(1)
G2	-77(1)	112(1)	139(1)	44(2)	-50(2)
G3	75(1)	106(1)	138(1)	46(1)	-50(2)
G4	-72(2)	83(1)	104(1)	45(2)	-47(2)
G5	62(2)	114(1)	151(1)	39(2)	-49(1)
G6	81(2)	104(1)	132(2)	33(2)	-38(2)
G7	-68(1)	93(1)	96(2)	60(1)	-63(1)
| Average |	**72**	**103**	**129**	**45**	**50**

Table 6.11 O4 heptagon parameters for OXPTMB(I)

Glucose unit	r / Å	l / Å	a / °	d / Å	t / °
G1	5.35	4.38	120	0.207(6)	18.8
G2	5.13	4.37	124	0.463(6)	7.0
G3	4.60	4.55	136	-0.413(7)	-26.6
G4	5.06	4.36	126	-0.291(8)	5.1
G5	5.40	4.10	116	0.588(8)	22.7
G6	4.66	4.61	137	-0.043(8)	-18.6
G7	4.72	4.23	132	-0.512(7)	-12.0
| Average |	**4.99**	**4.37**	**127**	**0.360**	**15.8**

Listed in Table 6.12 are the tilt angles [τ_1 and τ_2] for the OXPTMB(I) structure together with the intersaccharidic bond angles [φ]. All methylglucose units are tilted towards the inside of the cavity and their tilt angles are thus positive. The degree of tilt of the methylglucopyranose units varies significantly around the ring. The intersaccharidic bond angles are similar to those observed for β-CD molecules [average = 118°].

Table 6.12 φ and τ parameters for OXPTMB(I)

Glucose unit	φ / °	τ_1 / °	τ_2 / °
G1	112.7(9)	9.1(3)	11.6(2)
G2	120.6(9)	30.0(3)	29.2(5)
G3	117.7(9)	29.1(3)	38.2(4)
G4	114(1)	5.4(5)	9.9(4)
G5	120(1)	33.6(3)	32.5(4)
G6	118(1)	36.6(4)	39.1(8)
G7	114(1)	12.5(4)	12.3(3)
Average	**116.7**	**22.3**	**24.7**

Guest inclusion

The oxprenolol molecule is inserted into the cyclodextrin cavity from the secondary rim with the phenyl ring buried in the cavity and side chains extending to the outside of the cavity along the secondary side of the TRIMEB host molecule as illustrated in Figure 6.16. This phenomenon is also observed for the inclusion of the naproxen and (S)-ibuprofen molecules in the TRIMEB host cavity.[156,195] The phenyl ring is located very close to the centre of the TRIMEB cavity [the distance of the phenyl ring centroid to the O4-heptagon centroid is only 0.85 Å]. The phenyl ring makes an angle of 65.5(3)° with the O4 mean plane.

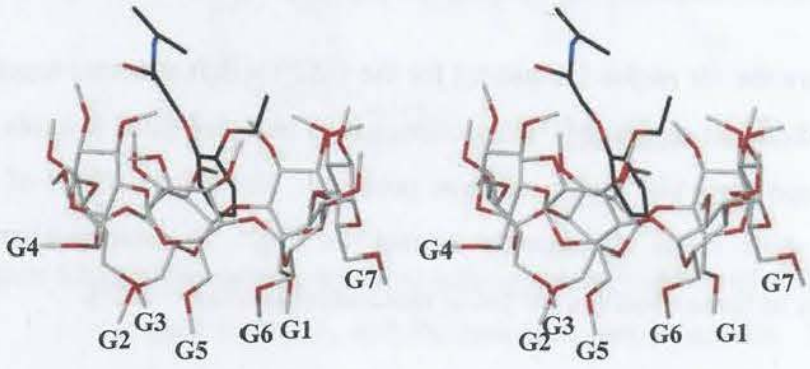

Figure 6.16 Stereo view illustrating the mode of guest inclusion in OXPTMB(I).

Figures 6.17(a)-(d) are space filling diagrams presenting different views of the OXPTMB(I) complex. Figure 6.17(a) is a view from the primary face showing the effect of the C9 methyl groups of the methylglucose units for which ω parameter is positive. These methyl groups thus point toward the TRIMEB cavity, 'sealing off' this side of the CD. The secondary face view, illustrated in Figure 6.17(b), shows the 'open' rim of the TRIMEB molecule and the location of the guest inside the host cavity is also clearly shown in this diagram. The extent to which the guest protrudes from the host cavity in a side view of the OXPTMB(I) complex is presented in Figure 6.17(c), and it shows that the ortho- side chains are protruding above the secondary rim of the TRIMEB molecule. Figure 6.17(d) is the same as Figure 6.17(c) with part of the host removed. The guest is not as fully included in the TRIMEB molecule on account of the host's cup-like shape as opposed to the toroidal shape of β-cyclodextrin.

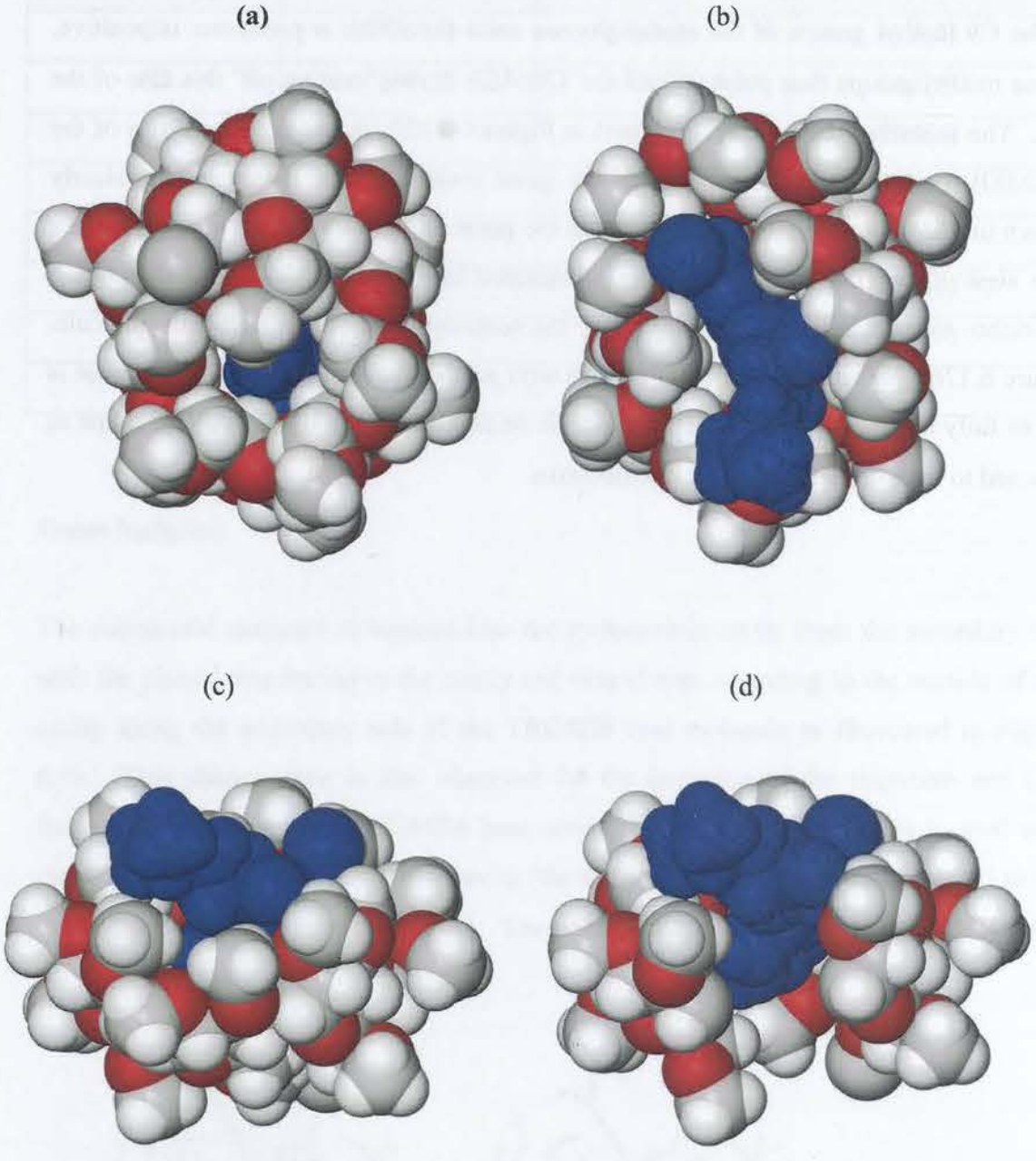

Figure 6.17 View of the (a) primary, (b) secondary and (c) side face of the OXPTMB(I) complex, while (d) is a view of the side with part of the host molecule removed.

Guest conformation and its configuration

The discussion of the conformation of the oxprenolol molecule in the OXPTMB(I) complex is relative to its conformation in the uncomplexed form [discussed in Chapter 3]. The principal torsion angles for the oxprenolol molecule in OXPTMB(I) and the uncomplexed oxprenolol are presented in Table 6.13, while Figure 6.18 is a repeat of Figure 3.25 [Chapter 3] illustrating the definitions of the torsion angles. The two oxprenolol molecules in the asymmetric unit of the uncomplexed drug were labelled as A and B, and in the Table below are referred to as OXPRFB(A) and OXPRFB(B) respectively. The principal torsion angle δ_1 of the drug molecule in OXPTMB(I) is much smaller than those of OXPRFB(A) and OXPRFB(B) and the reduction in this principal torsion angle is believed to contribute to the fitting of the oxprenolol drug into the TRIMEB host cavity . The majority of the principal torsion angles of the drug molecule in OXPTMB(I) are similar to those of the uncomplexed oxprenolol.

For more background the reader is referred to Chapter 3 on the conformation of the uncomplexed oxprenolol. The configuration at the chiral centre C9 of the included oxprenolol molecule is (R-); this will be dealt with in the Discussion section of this chapter.

Table 6.13 Principal torsion angles [°] of oxprenolol in OXPTMB(I) and uncomplexed oxprenolol

Principal torsion angles	Form I	OXPRFB(A)	OXPRFB(B)
δ_1 (C6-C1-O7-C8)	-38(1)	174.4(5)	-177.1(5)
δ_2 (C1-O7-C8-C9)	-170(1)	-170.1(4)	-177.9(4)
δ_3 (O7-C8-C9-O10)	146(1)	-167.0(4)	-169.3(4)
δ_4 (O10-C9-C11-N12)	77(2)	57.4(6)	60.0(6)
δ_5 (C8-C9-C11-N12)	-149(1)	178.6(4)	179.7(4)
δ_6 (C9-C11-N12-C13)	172(1)	171.7(4)	163.4(4)
δ_7 (C1-C6-O16-C17)	-165(1)	173.0(5)	-177.1(5)
δ_8 (C6-O16-C17-C18)	170(1)	163.2(9)	168.5(5)

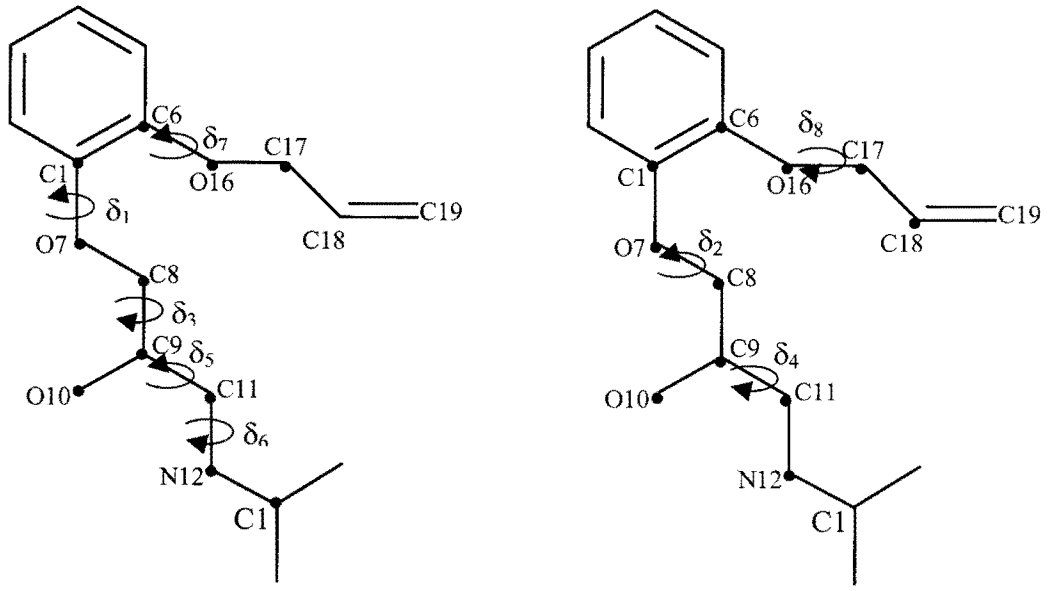

Figure 6.18 Schematic diagram of the principal torsion angles for the oxprenolol molecule.

Hydrogen bonding and C-H•••π ring interactions

Table 6.14 lists hydrogen bonding and C-H•••π ring interactions for OXPTMB(I). These bonds, in addition to van der Waals and hydrophobic interactions, contribute to the stabilisation of the OXPTMB(I) structure.

Intramolecular host interactions

The distorted conformation of the TRIMEB molecule relative to the conformation observed for the parent β-cyclodextrin molecule is stabilised by intramolecular C-H•••O hydrogen bonds, a common interaction found in carbohydrate crystal structures.[196] There is a total of eleven host hydrogen bonds that stabilise the TRIMEB molecule in OXPTMB(I). The C6-H•••O5' hydrogen bonds have been suggested as factors for the high positive tilt angles noted for the methylglucopyranose units in general,[193] and it has also been suggested that these hydrogen bonds are usually not present for methylglucopyranose units with lower tilt angles. There are four C6-H•••O5' hydrogen

bonds in the OXPTMB(I) structure, as observed in the TRIMEB monohydrate structure.[188] In addition there is one C1-H•••O3' hydrogen bond and a C1-H•••O6' hydrogen bond. Furthermore there are stabilising intramolecular hydrogen bonds within some of the glucose units, namely a C7-H•••O3' hydrogen bond and three C8-H•••O2' hydrogen bonds. All the C•••O distances are in the range 2.9-3.5 Å.

Host-guest interactions

There are four host-guest hydrogen bonds and one C-H•••π interaction. These interactions are all listed in Table 6.14 and they strengthen the association of the host and guest molecules. A C-H•••N hydrogen bond is formed between N12 and C6G6 on a symmetry related cyclodextrin. The O10-H10•••O2G4 hydrogen bond anchors the guest hydroxyl group to the secondary side of the host.

Host-host interactions

There is a total of six host-host C-H•••O hydrogen bonds present in the Form I structure. All these hydrogen bonds contribute to the stabilisation of the crystal structure in the absence of water molecules that fulfil this role in hydrated complexes. The symmetry codes for the C2G3-H2G3•••O6G7 [-1+x, y, z], C9G4-H9GA•••O3G6 [-1+x, y, z] and C4G7-H4G7•••O3G3 [1+x, y, z] hydrogen bonds show that they join the TRIMEB host molecules along the a-axis.

The symmetry codes for the C2G2-H2G2•••O5G5 [3/2-x, 1-y, ½+z], C2G5-H2G5•••O6G2 [3/2-x, 1-y, -½+z] and C9G2-H9G1•••O3G5 [3/2-x, 1-y, ½+z] hydrogen bonds indicate that they link the screw-related host molecules along the c-axis.

Table 6.14 Hydrogen-bonding and C-H•••π ring interactions for OXPTMB(I)

Interaction	H•••A / Å	D•••A / Å	D-H•••A / Å	Symmetry code [#]
Host				
C6G2-H6G4•••O5G3	2.44	3.07(1)	121	x, y, z
C6G2-H6G4•••O6G3	2.60	3.52(1)	156	x, y, z
C1G5-H1G5•••O6G4	2.44	3.12	125	x, y, z
C1G7-H1G7•••O3G6	2.42	3.05	121	x, y, z
C6G7-H6G8•••O5G1	2.57	3.26(2)	127	x, y, z
C8G3-H8G6•••O2G3	2.53	3.12(2)	118	x, y, z
C6G5-H6G9•••O5G6	2.06	2.98(2)	153	x, y, z
C8G7-H8GY•••O2G1	2.50	3.12(2)	120	x, y, z
C7G7-H7GX•••O3G7	2.35	2.94(3)	118	x, y, z
C6G4-H6GZ•••O5G5	2.28	3.09(2)	138	x, y, z
C8G1-H8GH•••O2G2	2.43	3.09(2)	124	x, y, z
Host-Guest				
O2G4•••H10-O10	2.34	2.91(2)	125	x, y, z
C6G6-H6GA•••N12	2.43	3.39(2)	163	2-x, ½+y, ½-z
O2G7•••H17B-C17	2.58	3.44(2)	145	x, y, z
C8G7-H8GX•••Cg*	3.24	4.16(2)	157	x, y, z
Host-host				
C2G2-H2G2•••O5G5	2.49	3.40(2)	151	3/2-x, 1-y, ½+z
C2G3-H2G3•••O6G7	2.54	3.48(1)	155	-1+x, y, z
C2G5-H2G5•••O6G2	2.41	3.35(2)	156	3/2-x, 1-y, -1/2+z
C4G7-H4G7•••O3G3	2.56	3.48(2)	152	1+x, y, z
C9G2-H9G1•••O3G5	2.48	3.23(1)	133	3/2-x, 1-y, ½+z
C9G4-H9GA•••O3G6	2.48	3.33(2)	145	-1+x, y, z

[#] Symmetry code applied to second unit of interaction

* Cg = Centre of gravity of the aromatic ring of the guest

Water interaction

Thermogravimetric analysis gave a weight loss corresponding to 0.6 of a water molecule per 1:1 complex unit, of which 0.4 was accounted for in the crystallographic analysis and referred to as OW1. This water is situated on the secondary side of the TRIMEB host molecule and makes hydrogen bonding contacts with the O10 and the N12 atoms of the oxprenolol guest. The OW1 also makes hydrogen bonding contact with the O5G7 and C6G3 atoms of the TRIMEB host molecule. Hydrogen bonding distances between the host, the guest and OW1 are listed in Table 6.15.

Table 6.15 Hydrogen bonding distances involving the OW1 water molecule

Interaction	Distance / Å	Symmetry code [#]
OW1•••O10	2.76(3)	x, y, z
OW1•••N12	3.27(3)	x, y, z
OW1•••O5G7	3.16(3)	2-x, -1/2+y, 1/2-z
OW1•••C6G3	3.26(3)	1-x, -1/2+y, 1/2-z

[#] Symmetry code applies to the second unit of the interaction

Crystal packing of the OXPTMB(I) structure

Extended stereo packing diagrams of the OXPTMB(I) structure showing projections as viewed down the a-, b- and c-axes are presented in Figure 6.19. Complex units pack in a screw-channel mode in a tail-to-head fashion, similar to the packing modes of naproxen and (S)-ibuprofen-TRIMEB complexes[156,195] [confirmed later in the Discussion Section of this Chapter by comparison of PXRD traces]. The crystal packing diagrams also show that there are no inter-guest interactions and also show that the two guest ortho-side chains do not protrude into the cavities of neighbouring host molecules.

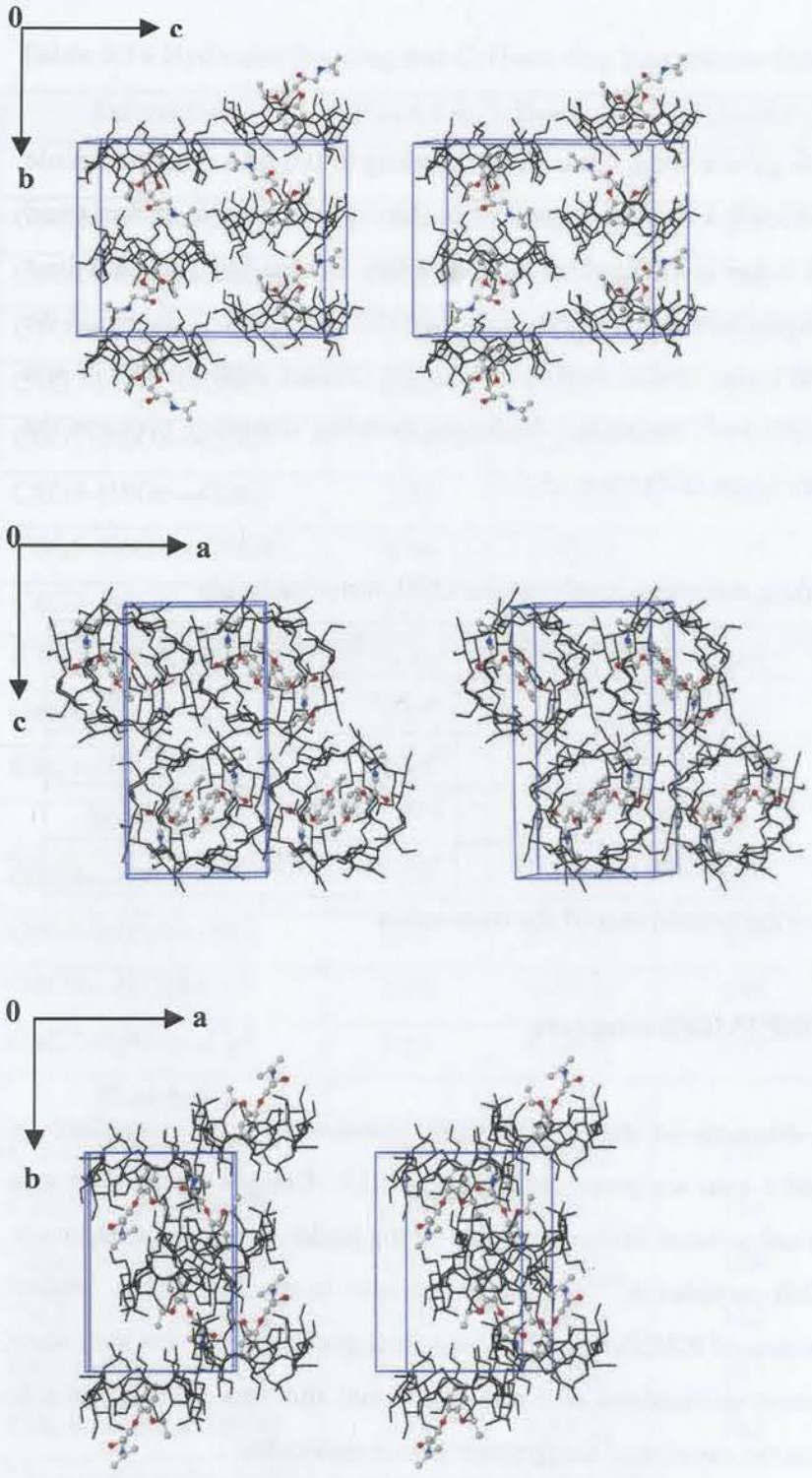

Figure 6.19 Stereo packing diagrams of the OXPTMB(I) structure down the a-, b- and c-axes respectively.

Powder X-ray diffraction

The calculated and experimental PXRD patterns for the OXPTMB(I) complex were successfully matched and are shown in Figure 6.20. The close match in peak positions [neglecting the shifts due to temperature difference] is evidence for the high purity of the sample, and it also indicates that there was no phase change on grinding the complex. A slight mismatch in relative peak intensities of the experimental trace with respect to the computed trace is due to preferred orientation effects in the sample.

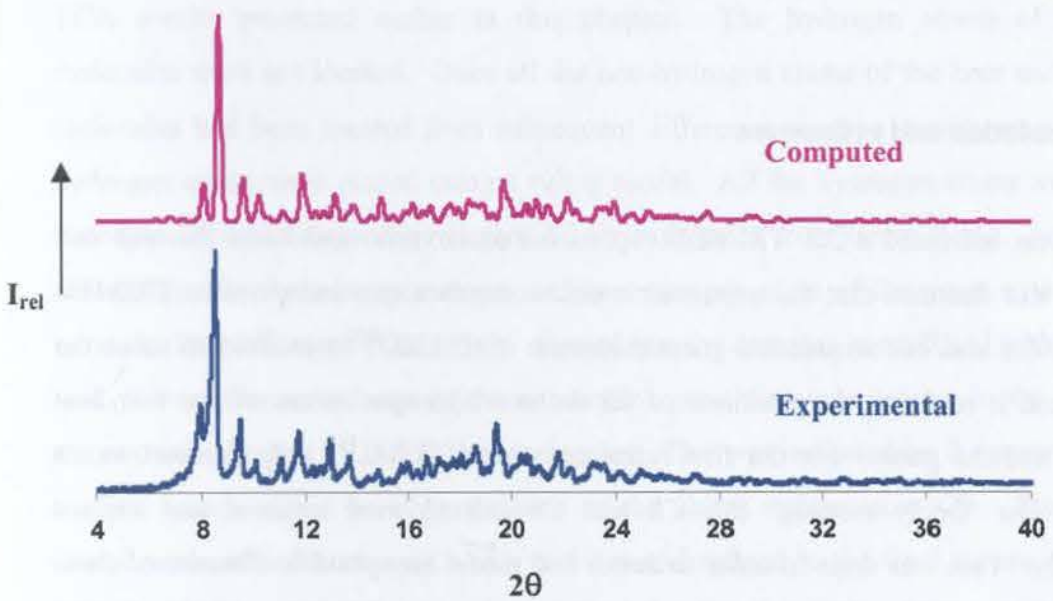

Figure 6.20 Computed [113K] and experimental [298K] PXRD traces for the OXPTMB(I) structure.

X-ray Crystallographic Analysis of the OXPTMB(II) Complex

Data-collection and space group determination

Intensity data were collected at 113 K on a Nonius Kappa CCD diffractometer using graphite-monochromated MoKα radiation [λ = 0.71073 Å]. A single crystal was mounted on a glass fibre and covered in Paratone oil[115] to provide rigid mounting for the low temperature data-collection and to prevent cracking due to loss of water of crystallisation. The Laue symmetry 2/m indicated that the crystal belongs to the monoclinic crystal system. XPREP[103] indicated the monoclinic space group $P2_1$ based on the reflection conditions 0k0: k = 2n. Inspection of the reciprocal lattice layers with LAYER[112] confirmed these reflection conditions. The intensity statistics yielded $|E^2-1|$ = 0.727 which is close to the numerical value of 0.736 expected for non-centrosymetric structures.

Structure solution and refinement

Microanalysis indicated a 2:1 TRIMEB:oxprenolol molar ratio and from the unit cell volume it was deduced that the asymmetric unit comprises two independent TRIMEB host molecules and one oxprenolol guest molecule. SHELXD[210] was used to solve the structure and it revealed the positions of all the non-hydrogen atoms of the two host molecules and the guest. For the first refinement in SHELXL,[113] only the host atoms [excluding the 'freely rotating' C7, C8 and C9 atoms] were retained and refined isotropically. This was done in order to detect and model any possible disorder of these freely rotating atoms based on peak heights of their associated electron densities in the difference Fourier map. The glucopyranose units of the two host molecules of the asymmetric unit were labelled **A1-A7** and **B1-B7** respectively. The subsequent difference Fourier maps revealed that one O6 atom and one C9 atom per host molecule [those of **A6** and **B1** respectively] were disordered over two positions. These disordered atoms were refined with s.o.f.'s of x and 1-x, the initial fraction x weighted according to the initial relative electron density peak heights of the disordered components. The

s.o.f.'s of O6A6 and O6B1 refined to the final x values of 0.62 and 0.52 respectively whilst the s.o.f.'s of C9A6 and C9B1 refined to the final x values of 0.57 and 0.61 respectively. All the freely rotating methyl carbon atoms, O2, O3, O4 and O6 atoms, except the disordered O6A6 and C9B1, were refined anisotropically. Refinement continued with the placement of water oxygen atoms, for which seven positions were located. O1W, O2W, O3W, O4W and O5W were assigned a full site-occupancy factor and refined anisotropically with a final temperature factor of U_{eq} in the range 0.01-0.08 $Å^2$. The remaining water molecules, with a site-occupancy factor of less than one, were assigned a fixed isotropic temperature factor of 0.06 $Å^2$ [the mean of the preceding U values] while the site-occupancies were allowed to vary. The site-occupancies of O6W and O7W are 0.72 and 0.64 respectively, amounting to an additional 1.4 water molecules per asymmetric unit. This gives a total of 6.4 water molecules per asymmetric unit which were accounted for in the model, as compared to the 7.4 water molecules expected from TGA results presented earlier in this chapter. The hydrogen atoms of the water molecules were not located. Once all the non-hydrogen atoms of the host and the water molecules had been located from subsequent difference electron density maps, the host hydrogen atoms were placed using a riding model. All the hydrogen atoms were refined isotropically with temperature factors 1.2 times those of their parent atoms. After further refinement, the three oxygen atoms and one nitrogen atom of the guest molecule were located. The difference Fourier map showed that the complex crystallised with both (R-) and (S-) enantiomeric forms of the oxprenolol guest molecule present in the cavities of the two independent TRIMEB host molecules. This was indicated by the presence of two oxygen atoms within bonding distance of the chiral carbon atom C9. These oxygen atoms were refined with s.o.f.'s of x and 1-x and refined to the final values of 0.60 and 0.40 for O10A and O10B respectively, which implies that 60 % of the enantiomeric (S-) and 40 % of the (R-) oxprenolol molecules are present inside the cavities of the two independent TRIMEB host molecules. The highest electron density peaks at the end of the refinement [0.40-0.70 e $Å^{-3}$] were situated around the interface of the TRIMEB molecules and inside the cavities of CD(A) and CD(B). Crystal data and data-collection parameters are listed in Table 6.16.

Table 6.16 Data-collection and refinement parameters for OXPTMB(II)

Complex formula	$2(C_{63}H_{112}O_{35})\bullet(C_{15}H_{23}NO_3)\bullet 7.4H_2O$
Formula weight / g mol^{-1}	3257.7
Crystal system	Monoclinic
Space group	$P2_1$
a / Å	15.1356(1)
b / Å	28.8092(2)
c / Å	19.7017(2)
α / °	90
β / °	101.70(3)
γ / °	90
Volume / $Å^3$	8412.3(1)
Z	2
Density $_{calc}$ / g cm^{-3}	1.272
μ(MoKα) / mm^{-1}	0.104
F(000)	3462
Temperature of data-collection / K	113
Crystal size / mm^3	0.45 x 0.52 x 0.55
Range scanned θ / °	$2 \leq \theta \leq 26$
Index ranges	h: -15, 15 k: -28, 27 l: -20, 20
Dx / mm	54
Total no. of reflections collected	82113
Total no. of unique reflections	16386
No. of reflections with $I > 2\sigma(I)$	27186
No. of parameters	1480
R_{int}, R_σ	0.0360, 0.0360
S	1.014
R_1 (for 8420 reflections)	0.0639
wR_2	0.1708
No. of reflections omitted	72
Weighting scheme	a = 0.0893, b = 9.5408
$(\Delta/\sigma)_{mean}$	< 0.025
Δρ excursions / e $Å^{-3}$	0.70 and –0.62

Description of the structure

OXPTMB(II) crystallises in a 2:1 TRIMEB:oxprenolol molar ratio in the monoclinic space group $P2_1$ with Z = 2 complex formula units per unit cell. A diagram of the asymmetric unit of the OXPTMB(II) complex is presented in Figure 6.21. The

glucopyranose units of the host molecules labelled **A** and **B** are denoted **A1-A7** and **B1-B7** respectively, with the glucopyranose atom numbering scheme shown.

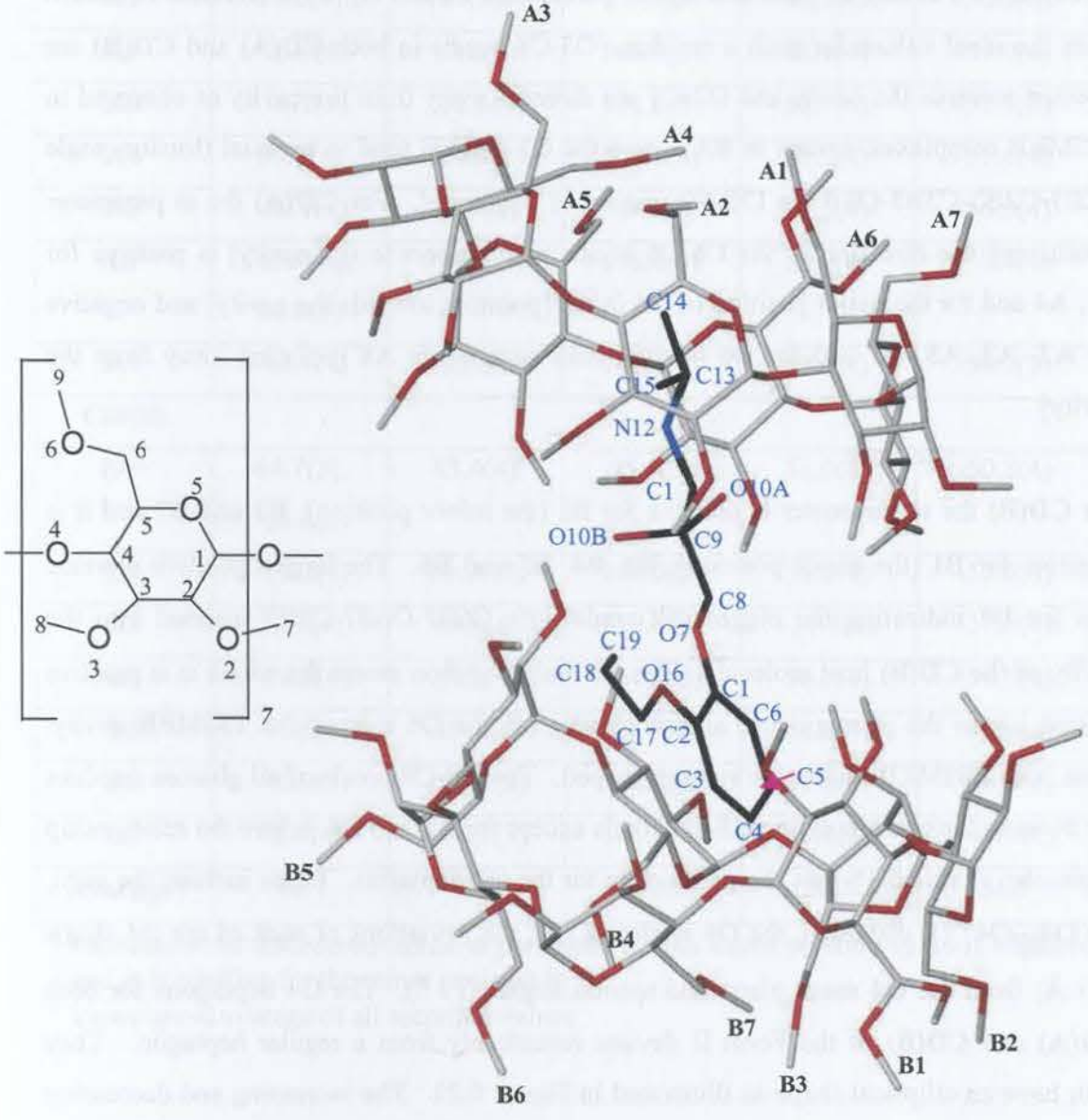

Figure 6.21 A side view of the asymmetric unit of the OXPTMB(II) complex. The carbon atoms of the guest are in black. Hydrogen atoms are omitted for clarity.

Table 6.17 lists some of the principal torsion angles for the two TRIMEB host molecules [**CD(A)** and **CD(B)**]. All methylglucose residues adopt the $^4C_1$ chair conformation

except the **B3** methylglucose unit that adopts the unusual $^{0}S_{2}$ skew boat conformation. The inverted conformation $^{1}C_{4}$ that is less stable was not observed. The conformations around the C4 atoms, as described by the parameters Θ_1 and Θ_2, show minimal deviation from the ideal values for such a residue. O3-C8 bonds in both **CD(A)** and **CD(B)** are directed towards the cavity and O2-C7 are directed away from the cavity as observed in TRIMEB complexes, except in **B3**, where the O2 and O3 tend to be axial (torsion angle O2B3-C2B3-C3B3-O3B3 = 178.4°) instead of equatorial. For **CD(A)** the ω parameter [describing the direction of the C6-O6 bonds with respect to the cavity] is positive for **A1**, **A4** and for the major position of O6 in A6 [pointing towards the cavity] and negative for **A2**, **A3**, **A5**, **A7** and for O6 of the minor position in **A6** [pointing away from the cavity].

For **CD(B)** the ω parameter is positive for **B1** [the minor position], **B3** and **B7** and it is negative for **B1** [the major position], **B2**, **B4**, **B5** and **B6**. The largest positive ω value was for **B7** indicating the biggest tilt angle with C6B7-O6B7-C9B7 inserted into the cavity of the **CD(B)** host molecule. The C9 methyl carbon atoms for which ω is positive extend across the primary rim, almost closing off the O6 side of the TRIMEB cavity. Thus both TRIMEB molecules are cup-shaped. The O6-C9 bonds of all glucose residues are *trans* to the corresponding C5-C6 bonds except for **A2** and **B4**, where the relationship is *gauche*. Table 6.18 lists the parameters for the O4 heptagon. These include the radii, the O4•••O4′ (**l**) distances, the O4 angles (**a** / °), the deviations of each of the O4 atoms (**d** / Å) from the O4 mean plane and torsion angles (**t** / °). The O4 heptagons for both **CD(A)** and **CD(B)** of the Form II deviate remarkably from a regular heptagon. They both have an elliptical shape as illustrated in Figure 6.22. The increasing and decreasing patterns of the numerical values for **r**, **l** and **a** parameters also confirm this. The **d** and **t** paramaters also indicate the significant deviation of the individual O4 atoms from the O4 mean plane and this is attributed to the tilt angles to be shortly described in this section. The O4•••O4'•••O4" angle of **B3** is the smallest angle and this is due to the large tilt angles [τ_1 and τ_2] of **B4**.

Table 6.17 Principal torsion angles [°] for OXPTMB(II)

CD(A)	ω	Φ	ψ	Θ_1	Θ_2
A1	76.0(4)	109.1(3)	137.9(3)	48.7(4)	-50.5(4)
A2	-75.9(4)	89.8(3)	106.9(3)	48.1(4)	-51.0(4)
A3	-74.1(3)	108.5(3)	141.6(3)	56.7(4)	-57.5(3)
A4	69.6(4)	104.1(3)	162.6(3)	49.1(4)	-51.6(4)
A5	-68.1(4)	83.7(4)	90.0(3)	54.3(4)	-56.5(4)
A6$^{\chi}$	-63.4(6), 66.0(5)	115.2(3)	138.6(3)	50.0(4)	-50.4(4)
A7	-69.1(4)	108.6(3)	141.1(3)	57.4(4)	-59.7(3)
CD(B)					
B1$^{\chi}$	64.7(5), -66.4(6)	83.4(4)	95.6(3)	51.0(4)	-50.8(4)
B2	-71.2(4)	104.9(3)	150.0(3)	51.1(4)	-52.6(4)
B3	72.4(4)	95.8(4)	129.8(3)	-31.7(4)	-30.0(4)
B4	-59.5(4)	84.2(4)	167.4(3)	56.2(4)	-59.5(4)
B5	-71.6(4)	56.2(4)	83.7(4)	50.2(4)	-50.8(4)
B6	-70.9(3)	107.6(3)	162.9(3)	52.8(4)	-56.9(3)
B7	92.4(4)	106.7(3)	141.9(3)	47.1(4)	-49.4(4)
| Average |*	**70.7**	**97.0**	**132.1**	**50.3**	**51.9**

$^{\chi}$ Represents the disordered atoms. ω parameter for the minor position in A6 is negative and it is positive for the minor position in B1.

* Unweighted average of all recorded values

Table 6.18 Geometrical parameters of the O4 heptagon for OXPTMB(II)

CD(A)	r / Å	l / Å	a / °	d / Å	t / °
A1	4.91	4.38	129	0.241(2)	-18
A2	5.03	4.49	128	0.371(2)	-5
A3	5.23	4.19	118	-0.498(2)	25
A4	4.63	4.42	140	-0.011(2)	-16
A5	5.03	4.23	125	0.392(2)	-7
A6	5.17	4.49	125	-0.069(2)	10
A7	4.93	4.31	129	-0.425(2)	11
CD(B)					
B1	5.06	4.31	118	-0.669(2)	-9
B2	4.63	4.68	143	0.039(2)	10
B3	5.63	4.59	99	0.962(2)	25
B4	4.48	4.34	138	-0.847(2)	-55
B5	4.95	4.36	122	-0.474(2)	25
B6	5.06	4.20	120	0.921(2)	32
B7	4.78	4.40	135	0.067(2)	-28
| Average |	**4.97**	**4.38**	**126**	**0.428**	**20**

The tilt angles for the OXPTMB(II) structure together with the intersaccharidic bond angles are presented in Table 6.19. Five of the methylglucose units for both **CD(A)** and **CD(B)** have positive tilt angles and the remaining two glucose moieties **A2** and **A5** in **CD(A)** and **B1** and **B5** in **CD(B)** have negative tilt angles. This shows that the majority of the methylglucose units are tilted towards the inside of the cavity on the O6 side. The **A4**, **B4** and **B7** methylglucose moieties have the largest positive tilt angles. The intersaccharidic bond angles except the one for **B4**, are close to what is observed for the parent β-CD molecule.

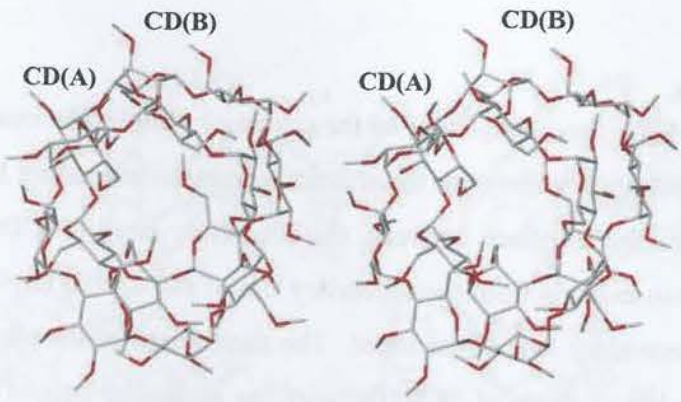

Figure 6.22 Stereo view of the crystallographically independent **CD(A)** and **CD(B)** TRIMEB host molecules of OXPTMB(II) showing the elliptical shape. The skew boat conformation of the B3 unit [top of the figure] is also evident.

Table 6.19 φ, and τ parameters for OXPTMB(II)

CD(A)	φ	τ_1	τ_2
A1	116.0(2)	32.4(1)	36.9(1)
A2	116.3(3)	-6.4(1)	-6.4(4)
A3	117.3(3)	17.4(1)	19.6(1)
A4	119.0(3)	47.7(1)	53.2(1)
A5	115.1(3)	-9.7(1)	-9.8(1)
A6	117.3(3)	9.0(1)	10.2(4)
A7	118.6(2)	27.7(1)	27.4(1)
CD(B)			
B1	114.9(3)	-9.9(1)	-11.6(1)
B2	118.8(3)	15.1(1)	16.0(1)
B3	118.2(3)	30.0(1)	35.8(1)
B4	116.6(3)	43.3(1)	68.0(2)
B5	116.0(3)	-15.4(1)	-17.3(1)
B6	117.9(3)	39.0(1)	39.8(2)
B7	118.1(2)	45.7(1)	54.1(1)
| Average |	**117.1**	**24.9**	**29.0**

Guest inclusion

As shown earlier in Figure 6.21, the phenyl ring of the oxprenolol molecule inserts into the **CD(B)** cavity from the secondary rim with the shorter side chain extending from the secondary face of **CD(B)** to the interface between the secondary rims of **CD(A)** and **CD(B)**. The longer side chain extends from the secondary rim of the **CD(B)** cavity to the **CD(A)** cavity through the secondary face of the latter. The mean plane of the phenyl ring defined by atoms C1-C6 makes an angle of 28.3(10)° with the molecular axis of the host **CD(B)** molecule defined as being orthogonal to its O4 mean plane. Figure 6.23 illustrates the numbering scheme of the oxprenolol guest molecule and Figure 6.24 is a stereo view illustrating the mode of guest inclusion in the OXPTMB(II) complex.

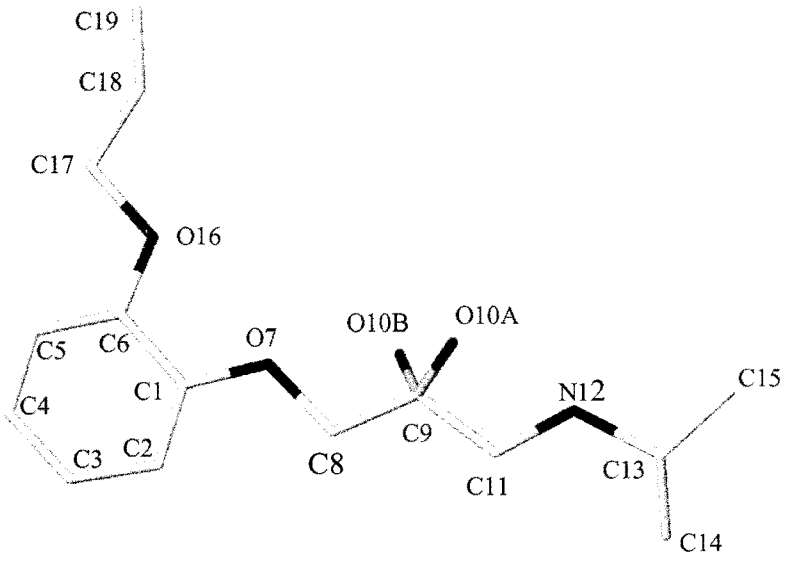

Figure 6.23 Numbering scheme of the oxprenolol guest molecule.

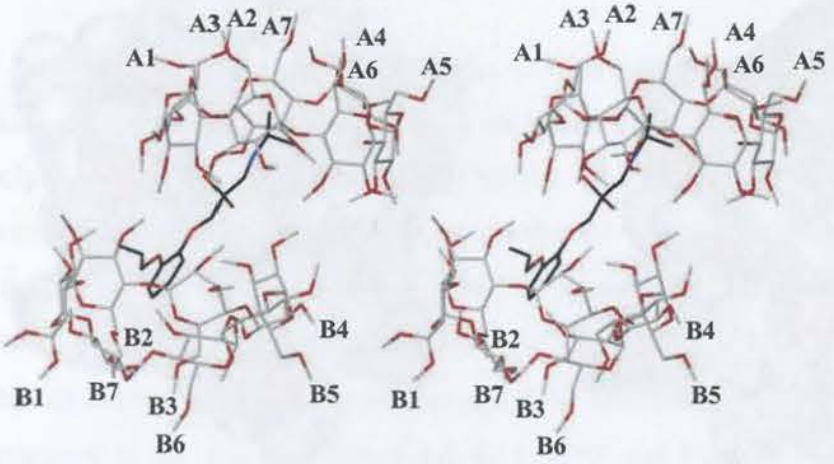

Figure 6.24 Stereo view showing the mode of guest inclusion in the OXPTMB(II) complex.

Space-filling diagrams showing different views of the OXPTMB(II) complex are shown in Figure 6.25 (a)-(d). Figures 6.25(a) and (b) present a view from the primary faces of **CD(A)** and **CD(B)** respectively, showing the effect of the C9 methyl groups of the methylglucose units for which the ω parameter is positive. In addition to the positive ω parameter for **A4** and **B7** glucopyranose units, their largest tilt angles also contribute to the effective 'sealing off' of the O6 sides of the cavities by the C9 methyl groups. The view of the side faces in Figure 6.25(c) clearly shows the protrusion of the short side chain at the interface of the secondary rims between the cavities of **CD(A)** and **CD(B)** host molecules. Since the asymmetric unit has two crystallographically independent host TRIMEB molecules which are head-to-head to each other, the guest is fully buried inside the cavities of these two host molecules as the primary faces are closed off by the C9 methyl groups. Figure 6.25(d), with part of the host atoms removed, shows the extent of insertion of the oxprenolol guest molecule into the host cavities.

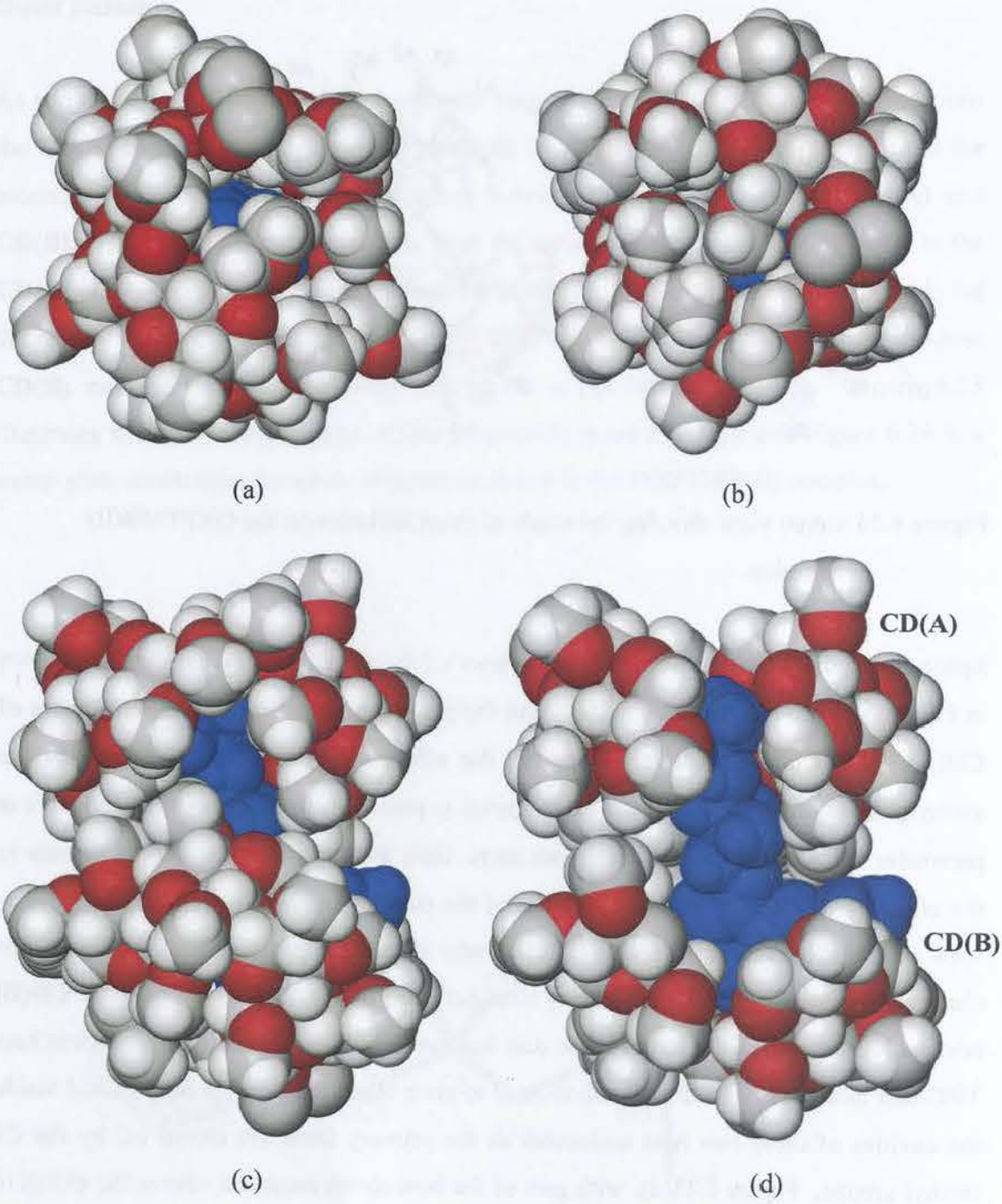

Figure 6.25 View of the (a), (b) primary faces for **CD(A)** and **CD(B)** respectively, (c) side faces for **CD(A)** and **CD(B)** of the OXPTMB(II) complex and (d) is a side view with part of the host molecule removed.

Guest conformation and its configuration

The conformation of the oxprenolol guest is defined by eleven torsion angles. These torsion angles are discussed relative to those of the uncomplexed oxprenolol. The principal torsion angles for the OXPTMB(II) and the uncomplexed oxprenolol are presented in Table 6.20. Figure 6.26 is a repeat of Figure 3.25 [Chapter 3], illustrating the definitions of the torsion angles. The configuration at the chiral centre C9 of the included oxprenolol molecule is (R-, S-) due to the disorder described earlier. The δ_1 and δ_{10} entries for the torsion angles of the oxprenolol in OXPTMB(II) correspond to the two orientations of the phenyl ring around the C1-O7 and C6-O16 bonds. These torsion angles [δ_1 and δ_{10}] agree closely with those of the uncomplexed oxprenolol molecule and δ_{10} for the oxprenolol in OXPTMB(II) is close to 180° and is in agreement with that for OXPRFB(B). The δ_3 and δ_4 angles of 74.5(5) and -53.6(6)° in the OXPTMB(II) complex are significantly different from the angles observed in the uncomplexed oxprenolol molecules.

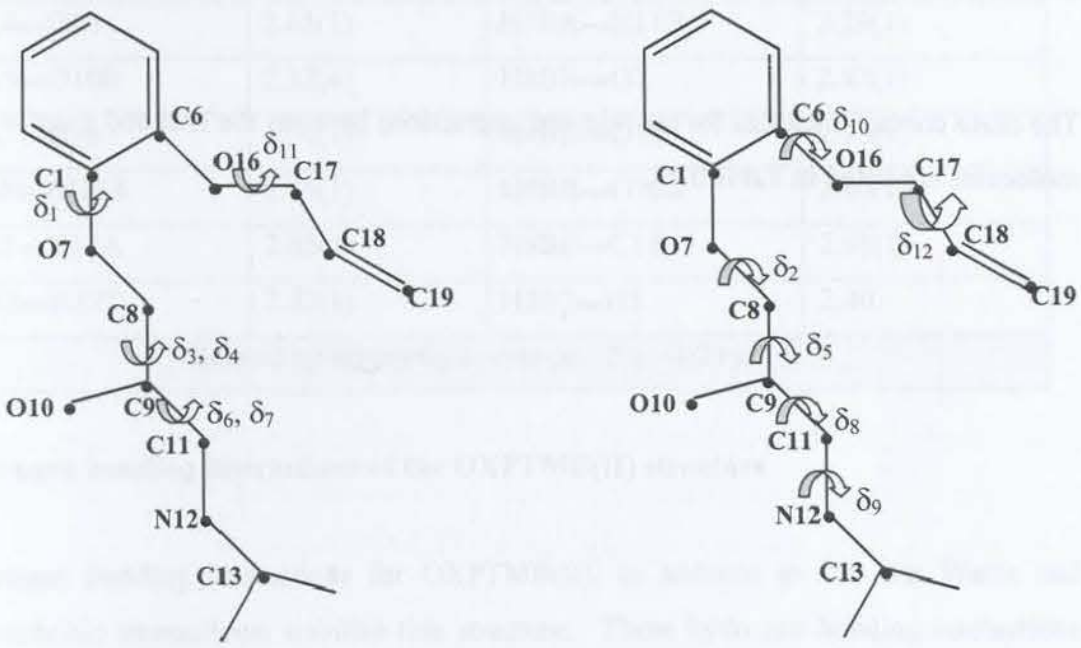

Figure 6.26 Schematic diagram of the principal torsion angles (δ) for the oxprenolol in OXPTMB(II).

Table 6.20 Principal torsion angles [°] of oxprenolol in OXPTMB(II) and uncomplexed oxprenolol

Principal torsion angles	OXPTMB(II)	OXPRFB(A)	OXPRFB(B)
δ_1 C6-C1-O7-C8	-175.1(4)	174.4(5)	-177.1(5)
δ_2 C1-O7-C8-C9	178.5(4)	-170.1(4)	-177.9(4)
δ_3 O7-C8-C9-O10A	74.5(5)	-167.0(4)	-169.3(4)
δ_4 O7-C8-C9-O10B	-53.6(6)	-167.0(4)	-169.3(4)
δ_5 O7-C8-C9-C11	177.2(5)	70.9(5)	70.6(5)
δ_6 O10A-C9-C11-N12	-67.5(6)	57.4(6)	60.0(6)
δ_7 O10B-C9-C11-N12	54.7(8)	57.4(6)	60.0(6)
δ_8 C8-C9-C11-N12	-179.3(5)	178.6(4)	179.7(4)
δ_9 C9-C11-N12-C13	166.3(5)	171.7(4)	163.4(4)
δ_{10} C1-C6-O16-C17	179.1(4)	173.0(5)	-177.1(5)
δ_{11} C6-O16-C17-C18	-179.0(4)	163.2(9)	168.5(5)
δ_{12} O16-C17-C18-C19	-130.7(6)	-159.7(3)	115.6(7)

The close contact distances for the relevant interactions between the host and guest molecules are listed in Table 6.21.

Table 6.21 Close contact distances for the OXPTMB(II) structure

Interaction	Distance / Å	Interaction	Distance / Å
O4A1•••O10A	3.03(1)	O4B2•••H3	2.51(2)
O2A2•••H10A	2.07(6)	O6B2•••H19B [i]	2.44(3)
O2A2•••H9L	2.80(1)	O2B3•••H3	2.76
C3A1•••O10A	3.26(4)	O2B5•••H8A	2.82(1)
C8A1•••H10A	2.89(1)	O2B5•••H10B	2.16(6)
C7A2•••O16	3.34(1)	O4B7•••H5	2.66(1)
C7A2•••C18	3.42(2)	O6B7•••H4	2.82(1)
C7A2•••H10A	2.75(1)	C7B3•••H2	3.02(1)
C8A2•••O10B	3.23(1)	C7B5•••H10B	2.78(1)
C9A4•••H15A	3.02(1)	C9B7•••H4	3.08(2)
C8A7•••H8B	3.04(1)	H3B1•••H5	2.57(2)
H3A1•••O10A	2.42(3)	H7B3•••H19A	2.42(2)
H5A1•••H13	2.58(2)	H9B1•••H19B [i]	2.51(1)
H8A1•••H10A	1.97(4)	H7B8•••H2	2.30(1)
H7A4•••O16	2.65(1)	H7BA•••H11B	2.29(1)
H8A5•••O10B	2.32(4)	H8BB•••O7	2.82(1)
H5A7•••H13	2.54(1)	H8BB•••O16	2.73(1)
H8AH•••H11A	2.45(1)	H8BB•••O10B	2.80(1)
O2B1•••H17A	2.63(1)	H8BE•••C18	2.98(1)
H8BE•••H17B	2.52(1)	H5B7•••H5	2.40
[i] Related by symmetry operation : 2-x, -1/2+y, 1-z			

Hydrogen bonding interactions of the OXPTMB(II) structure

Hydrogen bonding interactions for OXPTMB(II), in addition to van der Waals and hydrophobic interactions, stabilise this structure. These hydrogen bonding interactions are presented in Table 6.22 and Table 6.23 respectively.

Intramolecular host interactions

The conformation of the TRIMEB host molecules is stabilised by eighteen intramolecular C-H•••O hydrogen bonds [seven are for **CD(A)** and eleven are for **CD(B)**]. There is a total of seven hydrogen bonds of the type C6-H•••O5'. These and other C-H•••O hydrogen bonds are listed in Table 6.22.

Host-guest interactions

There are four host-guest hydrogen bonding interactions. The L-shaped molecular conformation for the oxprenolol [Figure 6.23] allows the terminal olefinic hydrogen atom to engage in intermolecular hydrogen bonding with the host [C19-H19B•••O6B2] related by 2-x, ½+y, 1-z symmetry. The C3-H3•••O4B2, C3A1-H3A1•••O10A and C8A1-H8A1•••O10A hydrogen bonds enhance the association of the host with the guest.

Host-host interactions

There are eight host-host C-H•••O hydrogen bonds in the OXPTMB(II) structure. Each of **CD(A)** and **CD(B)** has four of these bonds, that contribute to the stability of the crystal structure. The negative tilt angles of the **A5**, **B1** and **B5** residues are maintained by hydrogen bonds C2A5-H2A5•••O3A1, C4B1-H4B1•••O3B4 and C9B5-H9BX•••O3B7.

Inter-dimer host hydrogen bonds of OXPTMB(II)

There is one unique intra-layer C7B2-H7B4•••O2A6 hydrogen bond to a neighbouring unit. The location of the C7 hydrogen atoms on the outside of the **CD(B)** cavity allows them to interact with the atoms of neighbouring TRIMEB molecules.

Table 6.22 Hydrogen bonding interactions for the OXPTMB(II) complex

Interaction	H•••A / Å	D•••A / Å	D-H•••A / Å	Symmetry code*
CD(A)				
C8A1-H8A3•••O2A1	2.47	3.09	121	x, y, z
C6A2-H6A4•••O5A3	2.46	3.19	130	x, y, z
C6A3-H6A6•••O5A4	2.32	3.11	136	x, y, z
C1A4-H1A4•••O6A3	2.53	3.22	126	x, y, z
C1A5-H1A5•••O3A4	2.35	3.06	127	x, y, z
C6A5-H6AX•••O5A6	2.52	3.31	136	x, y, z
C6A7-H6AZ•••O5A1	2.50	3.18	126	x, y, z
CD(B)				
C1B1-H1B1•••O3B7	2.47	3.13	123	x, y, z
C6B2-H6B2•••O5B3	2.52	3.21	126	x, y, z
C6B2-H6B2•••O6B3	2.46	3.42	162	x, y, z
C6B3-H6B3•••O5B4	2.50	3.16	125	x, y, z
C7B3-H7B9•••O4B3	2.58	3.20	121	x, y, z
C9B4-H9B7•••O5B4	2.45	3.07	121	x, y, z
C1B5-H1B5•••O3B4	2.31	2.97	123	x, y, z
C5B5-H5B5•••O6B4	2.36	3.29	154	x, y, z
C6B5-H6B8•••O5B6	2.33	3.16	141	x, y, z
C8B5-H8BC•••O4B5	2.50	3.10	119	x, y, z
C1B6-H1B6•••O6B5	2.58	3.37	136	x, y, z
Host-guest				
C19-H19B•••O6B2	2.44	3.36	165	2-x, ½+y, 1-z
C3-H3•••O4B2	2.51	3.34	147	x, y, z
C3A1-H3A1•••O10A	2.42	3.26	141	x, y, z
C8A1-H8A1•••O10A	2.51	3.33	141	x, y, z
Host-host [CD(A)]				
C2A3-H2A3•••O6A7	2.31	3.23	153	1-x, ½+y, -z
C2A5-H2A5•••O3A1	2.45	3.36	151	-1+x, y, z
C2A7-H2A7•••O5A3	2.51	3.36	144	1-x, -½+y, -z
C2A7-H2A7•••O6A3	2.55	3.43	147	1-x, -½+y, -z

* Symmetry code applies to the second unit of the interaction

Table 6.23 Hydrogen bonding interactions for the OXPTMB(II) complex

Interaction	H•••A / Å	D•••A / Å	D-H•••A / Å	Symmetry code*
Host-host [CD(B)]				
C4B1-H4B1•••O3B4	2.38	3.36	167	1+x, y, z
C2B4-H2B4•••O6B1	2.51	3.49	164	-1+x, y, z
C9B5-H9BX•••O3B7	2.54	3.34	139	-1+x, y, z
C7B6-H7BD•••O2B4	2.52	3.37	144	1-x, ½+y, 1-z
Intra-layer				
C7B2-H7B4•••O2A6	2.44	3.26	140	1+x, y, z

* Symmetry code applies to the second unit of the interaction

Water interactions

Two of the water molecules [O5W and O7W] are situated inside the **CD(A)** cavity and O2W and O3W are located at the periphery of the **CD(A)** with the O2W filling a small intermolecular space between complex units. The O1W, O4W and O6W are located at the interface between the secondary rims of **CD(A)** and **CD(B)** TRIMEB molecules and O6W also fills a small intermolecular space between complex units. The O5W water molecule does not bond to the host but is hydrogen bonded to the other water molecules [O1W and O7W] and to the N12 and O10B atoms of the guest molecule. Figure 6.27 presents a schematic diagram illustrating the location of water molecules between the host molecules and Table 6.24 presents hydrogen bonding distances between the host, the guest and these water molecules.

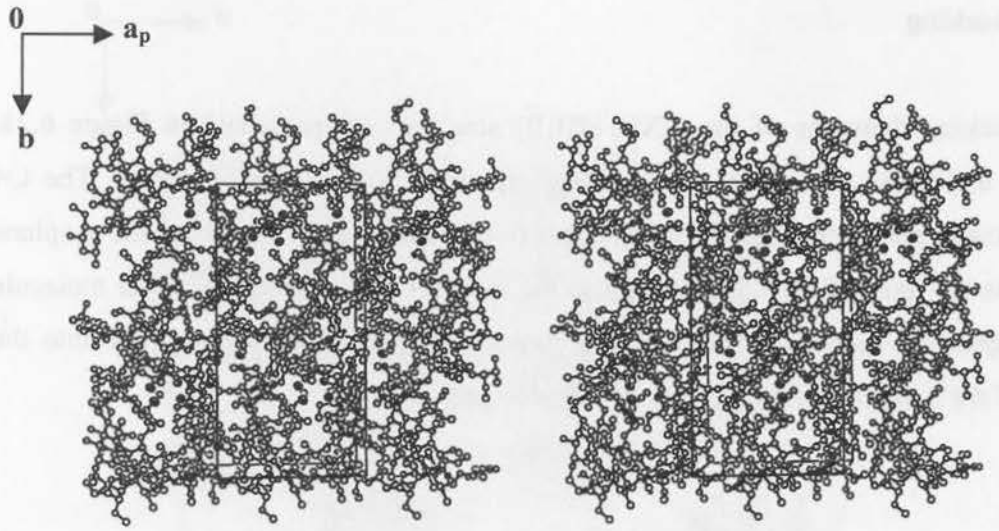

Figure 6.27 A stereo diagram viewed down the c-axis, shows the location of water oxygen atoms [filled ellipsoids] between the host CD molecules.

Table 6.24 Hydrogen bonding distances involving the water molecules

Water-host interaction	**Distance / Å**
O1W•••O3B5	2.83(5)
O2W•••O3A6	2.82(5)
O2W•••O3B6 ^{i}	2.84(4)
O3W•••O3A3	2.81(5)
O3W•••O2A4	2.81(4)
O4W•••O2A3	2.96(5)
O6W•••O3B3 ^{j}	3.02(6)
O7W•••O2A5	2.68(7)
Water-guest interaction	
O5W•••N12	2.90(7)
O5W•••O10B	3.2(1)
Water-water interaction	
O1W•••O4W	2.90(5)
O1W•••O6W	2.83(8)
O1W•••O5W	2.72(5)
O5W•••O7W	2.73(8)
Related by symmetry operations: ^{i} = 1-x, -1/2+y, 1-z , ^{j} = 1-x, 1/2+y, 1-z	

Crystal packing

Crystal packing diagrams of the OXPTMB(II) structure are presented in Figure 6.28. TRIMEB molecules pack in a screw-channel mode in a tail-to-tail fashion. The O4 heptagon mean planes for the two independent host molecules are parallel to the xy-plane with the cavity axes of the CDs parallel to the c-axis. The oxprenolol guest molecule fully occupies the cavities of the CD host molecules and it does not protrude into the cavities of the neighbouring TRIMEB host molecules.

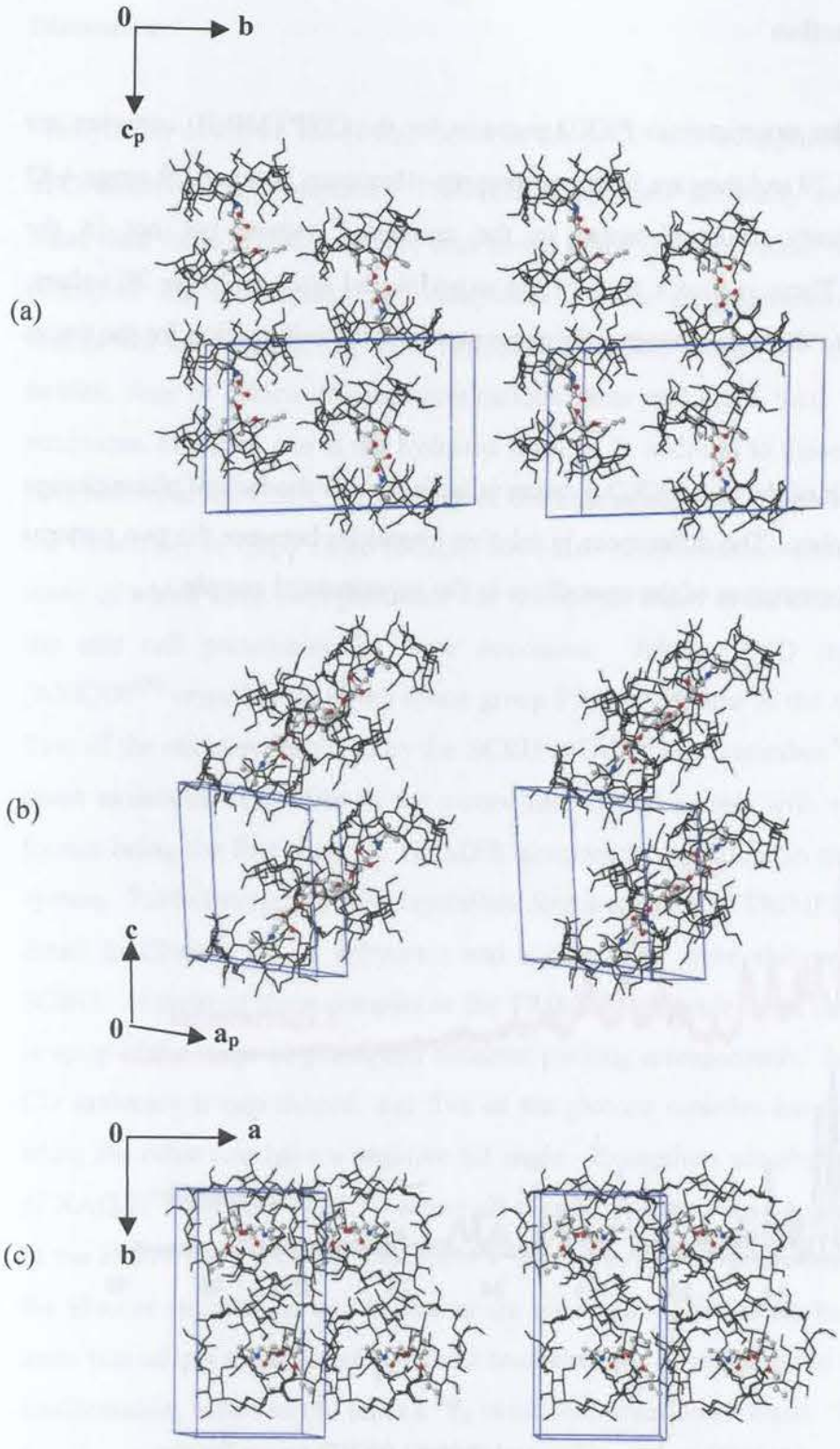

Figure 6.28 Stereo packing diagrams of the OXPTMB(II) structure down the (a) a- (b) b- and (c) c-axes respectively.

Powder X-ray diffraction

The computed and the experimental PXRD patterns for the OXPTMB(II) complex are presented in Figure 6.29 and they are in fair agreement. However, between 2θ range 4-8° there are low intensity peaks observed in the computed pattern but not in the experimental one. There is also a shift of the experimental trace to lower 2θ values. These are attributed to the temperature differences at which the information for the traces was obtained.

The reasonable match of the two PXRD patterns is indicative of the lack of phase change on grinding the complex. The differences in relative intensities between the two patterns are due to preferred orientation of the crystallites in the experimental sample.

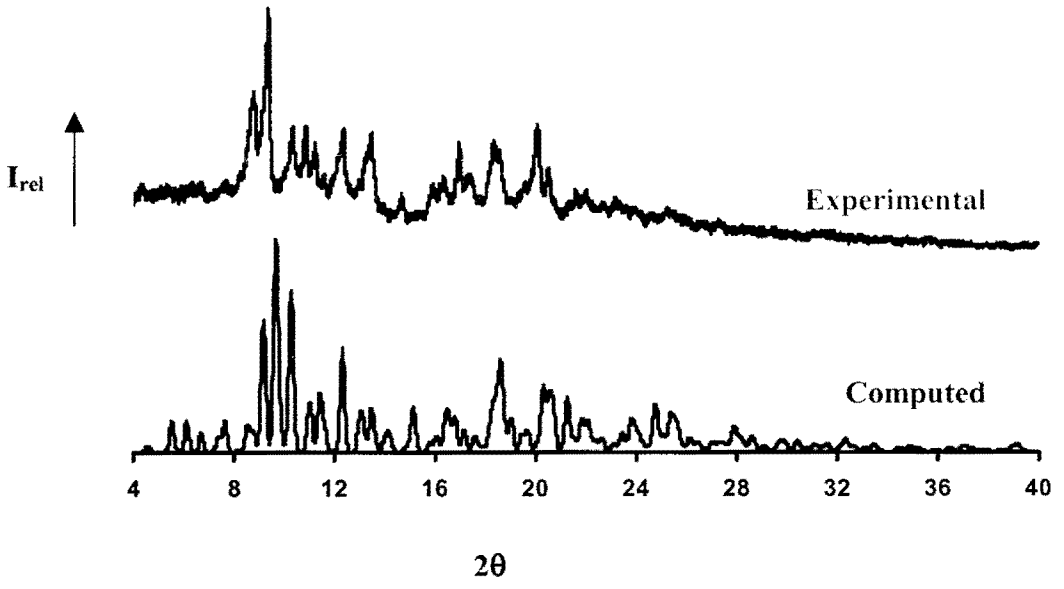

Figure 6.29 Computed [160K] and experimental [298K] PXRD traces for the OXPTMB(II) structure.

Discussion

Methylation of O2-H, O3-H and O6-H of the β-CD molecule produces heptakis(2, 3, 6-tri-O-methyl)- β-cyclodextrin. TRIMEB compounds are many times more soluble in water than those of β-CD and are thus useful in the pharmaceutical industry.[197] This then prompted the investigation of complexes of the antihypertensive agents [atenolol, metoprolol and oxprenolol] with TRIMEB. To date the CSD[198] contains only sixteen entries, four of which are redeterminations, thus making a total of twelve TRIMEB structures, of which one is the hydrated form. In addition to these TRIMEB structures obtained from the CSD,[198] members of the Supramolecular Chemistry Research Unit at the University of Cape Town [SCRU] have also determined several TRIMEB structures, some of which have been published but are not yet listed in the CSD.[198] Table 6.25 lists the unit cell parameters for these structures. All the CSD structures except one [ASIQOI[199] crystallising in the space group $P2_1$], crystallise in the space group $P2_12_12_1$. Two of the structures isolated by the SCRU at UCT, with butamben[85] and (E)-ajoene[86] as guest molecules crystallise in the monoclinic crystal system with space group $P2_1$, the former being the first reported TRIMEB structure to crystallise in the monoclinic crystal system. Furthermore, two new crystalline forms of the host TRIMEB [to be described in detail in Chapter 8], an anhydrate and a trihydrate, were also prepared by the UCT SCRU. In most of these complexes the TRIMEB molecule has a common conformation in spite of the range of guests and different packing arrangements. In these structures the CD molecule is cup-shaped, and five of the glucose moieties have a positive tilt angle, while the other two have a negative tilt angle. Exceptions are observed in the structures of XAQJII[200] and QOYLIZ,[190] where all the glucose moieties adopt a positive tilt angle. In the HEZWAK[188] and the GELKEN[189] structures two distinct conformations for one of the glucose residues in two instances are observed. The former has one of its glucose units that adopts the inverted $^1C_4$ chair conformation as compared to the normal $^4C_1$ chair conformation, while in the latter a $^0S_2$ twist conformation is found. The trial model used for the structure solution of OXPTMB(I) as mentioned earlier, was obtained from CAMPIP,[186] whose unit cell parameters [Table 6.25] agree closely with those of OXPTMB(I), one of the two necessary conditions for successful solution using the

Table 6.25 Known TRIMEB structures and their unit cell parameters

REFCODE	Space group	a / Å	b / Å	c / Å	α	β	γ
CSD structures							
ASIQOI[199]	$P2_1$	11.680	28.230	15.020	90	112.63	90
CAMPIP[186]	$P2_12_12_1$	14.997	21.368	28.205	90	90	90
COYXAP10[201](2)[#]	$P2_12_12_1$	15.092	21.714	28.269	90	90	90
COYXET20[201](2)	$P2_12_12_1$	15.271	21.451	27.895	90	90	90
EKOGOA[202]	$P2_12_12_1$	15.113	15.223	35.876	90	90	90
GELKEN10[189](2)	$P2_12_12_1$	15.669	20.798	25.486	90	90	90
HEZWAK[188](2)	$P2_12_12_1$	14.818	19.362	26.510	90	90	90
PAFSOE[189]	$P2_12_12_1$	14.890	21.407	28.540	90	90	90
QOYLIZ[190]	$P2_12_12_1$	10.936	25.530	29.640	90	90	90
RONWOG[191]	$P2_12_12_1$	15.232	21.327	27.597	90	90	90
XAQJII[203]	$P2_12_12_1$	11.149	25.664	29.427	90	90	90
ZIFQOU[204]	$P2_12_12_1$	15.179	21.407	27.670	90	90	90
UCT SCRU							
TRIMEB with:							
Butamben[85]	$P2_1$	10.891	14.858	27.583	90	99.62	90
(E)-ajoene[86]	$P2_1$	11.553	27.715	14.605	90	109.39	90
(Z)-ajoene[86]	$P2_12_12_1$	15.102	21.520	27.313	90	90	90
$3H_2O$[205]	$P2_12_12_1$	16.205	16.287	30.099	90	90	90
none[205]	$P2_12_12_1$	15.951	16.577	28.941	90	90	90
clofibric acid[136]	$P2_12_12_1$	11.601	26.284	28.882	90	90	90
psoralen[206]	$P2_12_12_1$	10.945	25.652	29.939	90	90	90
clofibrate[136]	$P2_12_12_1$	15.010	21.490	27.700	90	90	90
tulobuterol[138]	$P2_12_12_1$	15.063	21.290	27.671	90	90	90
This work							
metoprolol	$P2_1$	21.463	14.832	27.511	90	97.97	90
oxprenolol(i)	$P2_12_12_1$	14.597	21.783	28.164	90	90	90
oxprenolol(ii)	$P2_1$	15.136	28.809	19.702	90	101.70	90

[#] Number of re-determinations in parentheses

isomorphous replacement method. All the structures reported to date have larger tilt angles than those observed in complexes of native β-CD molecules. This can be attributed to two factors, namely steric hindrance involving the methyl groups attached to O3 which are directed towards the cavity and the host's inability to form O2•••O3' intramolecular hydrogen bonds since O2, O3 and O6 are methylated.[181] The flexibility of the TRIMEB macrocycle is therefore enhanced by the absence of these hydrogen bonds. The guest insertion into the TRIMEB host cavity alters the conformation of the macrocycle to accommodate the guest, i.e. inclusion involving induced fit,[207] thus further contributing to the flexibility of the macrocyle. The conformation of TRIMEB is however stabilised by several C-H•••O' intramolecular hydrogen bonds.[138,195,208]

In this study, complexes of TRIMEB with metoprolol and oxprenolol have been crystallised and the crystal structures have been elucidated. Several data-collections were performed on each of these complexes since the difficulties which were encountered were of the doubling of one or two of the axes upon cooling and poor crystal qualities leading to high mosaicity on attempting to collect data at low temperature.

TRIMEB-metoprolol (METTMB) complex

Data-collection of METTMB was performed at room temperature [293K], at 173K and at 113K. The crystal structures for data collected at 173K and 113K were not elaborated earlier in this chapter because of their significantly high R_I factors. However the comparison of the host conformation in all these TRIMEB complexes at three different temperatures will be made later in this section.

A preliminary inspection of the intensity-weighted reciprocal lattice layers of METTMB at 173 and 293K showed that the intensities of reflections hkl alternate between strong and weak, with strong reflections presented as follows: 0kl, 2kl, 4kl. This indicated that the unit cell contents in the interval x = 0 to x = 0.5 are approximately repeated in the interval x = 0.5 to x =1.0. The intensity-weighted reciprocal lattice layer for the METTMB data collected at 113K however, did not show this. The unit cell parameters

of this METTMB [113K] were similar to those of the TRIMEB-butamben complex,[85] thus these two structures are isostructural. Figure 6.30 shows the stereo view from the primary face [top] and the side view [bottom] of the overlay of the hosts of METTMB [113K] and the TRIMEB-butamben complex [113K],[85] illustrating their close conformations. The metoprolol guest molecule was still disordered at this temperature and could not be modelled.

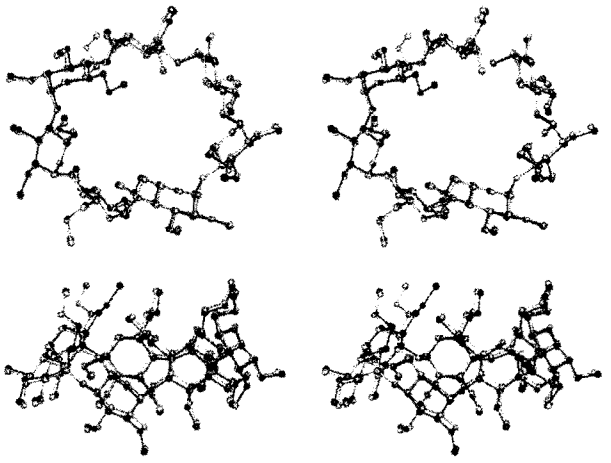

Figure 6.30 Stereo view of the overlay of the hosts of METTMB [red] and TRIMEB-butamben[85] [blue] showing their close conformations.

Table 6.26 lists the cell parameters and mosaicity of the METTMB crystal at three different temperatures, namely 113, 173 and 293K. A comparison of data-collections at these three temperatures shows that there is no significant difference in the unit cell parameters at 293 and 173K. However a slight increase in mosaicity and a significant difference between the R_I factors is observed. For data-collection at 113K the a-axis is halved, while b- and c-axes are similar to the corresponding axes at 173 and 293K. Comparison of the computed PXRDs for METTMB at these three different temperatures was carried out [Figure 6.31]. There are very small peaks at $2\theta = 7.3°$ and 8.8° for the METTMB structure at 293K which are not evident for this structure at 173K and 113K. Furthermore two peaks observed at $2\theta = 7.8°$ and 12.4° for METTMB at 293 and 173K are not evident at 113K. The origin of these [relatively trivial] differences is described below.

Table 6.26 Unit cell parameters of METTMB at different temperatures [K]

	293	173	113
Crystal system	Monoclinic	Monoclinic	Monoclinic
Space group	$P2_1$	$P2_1$	$P2_1$
a / Å	21.4632(2)	20.9641(4)	10.3288(4)
b / Å	14.8321(2)	14.8573(4)	14.7624(8)
c / Å	27.5114(4)	27.5055(8)	27.3653(13)
β / °	97.9686(4)	98.6421(8)	98.7769(17)
Crystal mosaicity / °	0.582(1)	0.754(2)	1.909(2)
R_1	0.1525	0.2357	0.2211
Data completeness / %	95.1	84.8	93.6

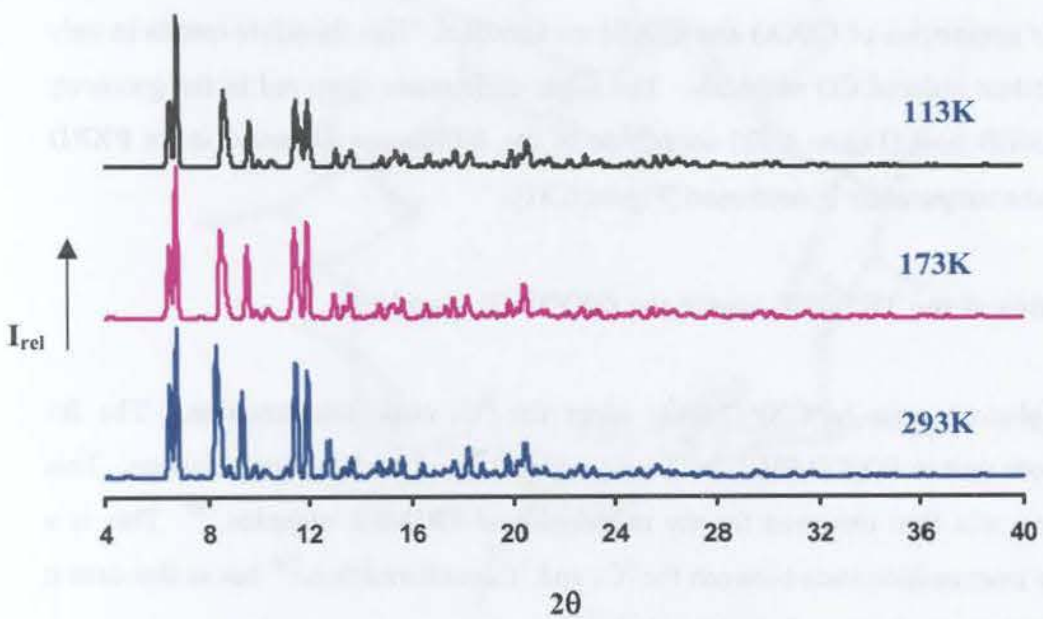

Figure 6.31 Computed PXRDs for the METTMB structure at 293, 173 and 113K.

Conformation of the TRIMEB host for METTMB at various temperatures

The conformation of the TRIMEB host molecule in the METTMB complex at various temperatures is illustrated in Figure 6.32. Comparison of the two crystallographically independent macrocycles **CD(A)** [red] and **CD(B)** [grey] for the TRIMEB host molecule at 293K indicates that their geometries are significantly different. The atoms O6A2 and O6A4 in **CD(A)** are disordered over two positions while in **CD(B)** the atoms C9B1 and O6B2 are disordered over two sites. The bonds O6B7-C9B7, O6B5-C9B5 and O6D2-C9D2 [minor position] of the **CD(B)** molecule point towards the cavity while in **CD(A)** only the bonds O6A2-C9A2 and O6A4-C9A4 [major positions] point towards the cavity.

At 173K the atoms O6A4 and O6A5 are disordered over two sites and the bonds O6A4-C9A4 and O6A5-C9A5 point towards the centre of the cavity. In **CD(B)** all atoms are ordered and all O6-C9 bonds are pointing away from the cavity.

At 113K the geometries of **CD(A)** and **CD(B)** are identical. This therefore results in only one independent ordered CD molecule. The slight differences observed in the geometry of the TRIMEB host [Figure 6.32] contribute to the differences observed in its PXRD patterns as the temperature is decreased [Figure 6.31].

Conformation of the TRIMEB host in the OXPTMB complexes

All methylglucose units in OXPTMB(I) adopt the $^4C_1$ chair conformation. The **B3** methylglucose unit in OXPTMB(II) adopts an unusual $^0S_2$ skew boat conformation. This conformation was first observed for the m-iodophenol-TRIMEB complex.[189] This is a high energy intermediate state between the $^4C_1$ and $^1C_4$ conformation,[209] but in this case it is stabilised by the inclusion of oxprenolol.

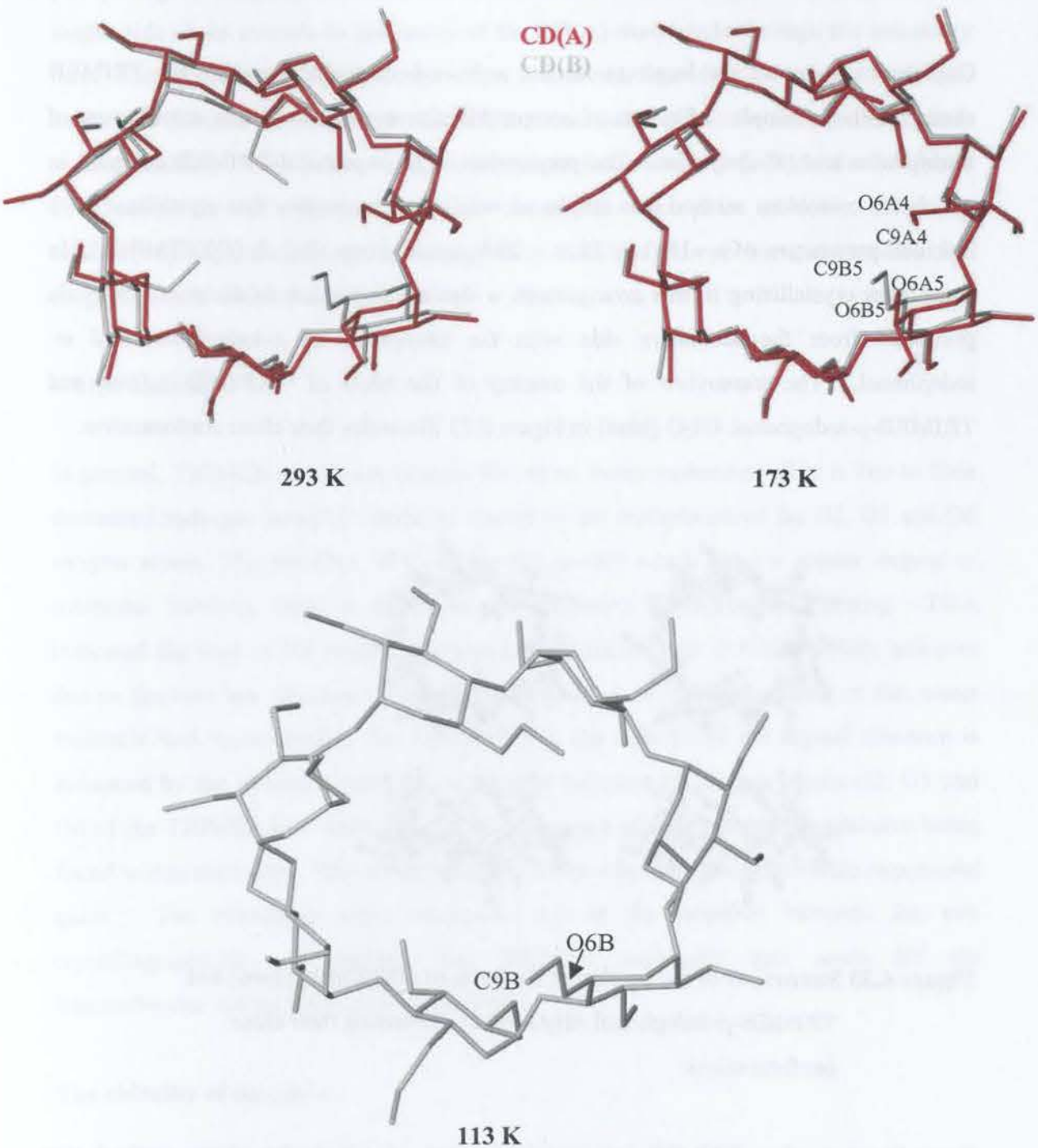

Figure 6.32 Conformation of the TRIMEB macrocycle for the METTMB complex at 293K, 173K and 113K.

Oxprenolol guest inclusion

Oxprenolol is one of the larger molecules to have been included within the TRIMEB cavity. Other examples of guests of comparable size are naproxen, the enantiomers of flurbiprofen and (S)-ibuprofen. The preparation of an oxprenolol-TRIMEB complex in which the co-solvent method was employed resulted in a complex that crystallised with unit cell parameters of a ~15, b ~ 21, c ~ 28Å, space group $P2_12_12_1$ [OXPTMB(I)]. In complexes crystallising in this arrangement, a significant portion of the guest molecule protrudes from the secondary side with the exceptions of *p*-iodophenol and *m*-iodophenol. The stereoview of the overlay of the hosts of OXPTMB(I) [red] and TRIMEB-p-iodophenol.$4H_2O$ [blue] in Figure 6.33 illustrates their close conformation.

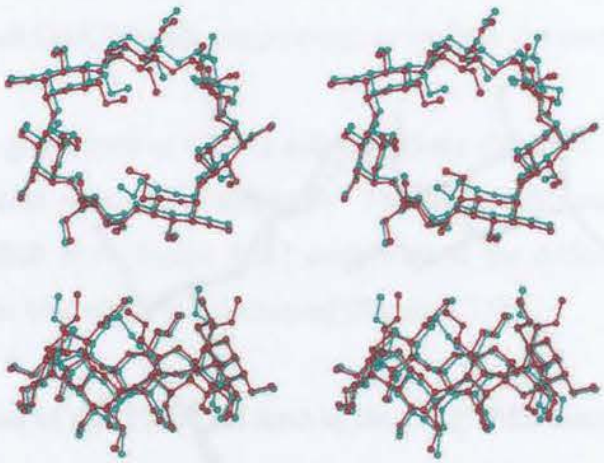

Figure 6.33 Stereoview of the overlay of the hosts of OXPTMB(I) [red] and TRIMEB-*p*-iodophenol.$4H_2O$ [blue] illustrating their close conformations.

Crystallisation of a TRIMEB-oxprenolol complex in which the slurry method was employed resulted in the monoclinic complex with unit cell parameters a = 15.136, b = 28.809, c = 19.702 Å, β = 101.70°, space group $P2_1$, with two crystallographically independent TRIMEB host molecules and one oxprenolol guest molecule in the asymmetric unit. The oxprenolol guest molecule occupies both cavities of the host. The

phenyl ring of the guest is located on the secondary rim of **CD(B)** macrocycle and the longer side chain extends to the cavity of the **CD(A)** macrocycle through the secondary face. The shorter side chain, because of the L-conformation of the oxprenolol molecule, extends to the interface of the two TRIMEB macrocycles which are arranged in a head-to-head fashion. This head-to-head arrangement is believed to provide the non-polar environment for the oxprenolol molecule since it is a non-polar molecule. Thus the relatively hydrophilic primary rim is kept away from the hydrophobic guest molecule as suggested by Lichtenhaler *et al.*[60, 72]

Water molecules

In general, TRIMEB complexes contain few or no water molecules. This is due to their decreased hydrogen bonding capability caused by the methylation of the O2, O3 and O6 oxygen atoms. The presence of these methyl groups which have a greater degree of rotational freedom, helps to maximise the efficiency of the crystal packing. TGA indicated the total of 0.6 water molecules in the formula unit of OXPTMB(I); however due to the very low electron density peaks [below 1 e $Å^{-3}$] the modelling of this water molecule was unsuccessful. For OXPTMB(II), the stability of the crystal structure is enhanced by the hydrogen bonding interactions between the oxygen atoms O2, O3 and O6 of the TRIMEB host molecule and water oxygen atoms, two water molecules being found within the cavity. One water molecule forms a hydrogen bond with the oxprenolol guest. The remaining water molecules are at the interface between the two crystallographically independent host TRIMEB molecules and some fill the intermolecular spaces between complex units.

The chirality of the guest

The ability of CDs to resolve racemic compounds has been studied.[194] The increased flexibility of methylated CD hosts renders them more suitable for chiral recognition as they are able to change their conformation to accommodate a specific enantiomer. Since the included metoprolol molecule in METTMB is disordered and could not be modelled,

its chirality could not be determined. For the OXPTMB(I) complex the TRIMEB host molecule exclusively accommodates the (R-)-enantiomer, while in the OXPTMB(II) complex the (R-) and (S-)-enantiomers are encapsulated to similar extents.

Crystal packing

In the METTMB structure, the TRIMEB molecules are related by the two-fold screw axis parallel to the b-axis. This structure is characterised as a screw-channel type packing mode and the complex units pack in a head-to tail fashion. This packing arrangement is similar to that occurring in the TRIMEB-butamben complex.[85]

In the OXPTMB(I) structure, complex units stack in columns in a head-to-tail mode, forming continuous channels along the b-axis. The O6-C9 methoxy groups almost completely seal off the O6 side of the molecule thus preventing the longer side chain from extending into the cavity of the neighbouring host molecule; instead, it protrudes from the secondary side of the host molecule.

In the OXPTMB(II) structure, the two crystallographically independent TRIMEB host molecules pack in a screw-channel mode in a tail-to-tail fashion. The guest molecule is completely buried in the cavity of each complex unit. The O6-C9 methoxy groups completely block the O6 side of the host molecules in each complex unit. Thus there is no interaction or contact between guest molecules in neighbouring complex units.

Chapter 7 – TRIMEA and DIMEB Inclusion Complexes

Complex Preparation

Single crystals of the TRIMEA complex of metoprolol were prepared by adding to a saturated, aqueous solution of TRIMEA in ice an equivalent amount of metoprolol. The resulting solution was filtered and incubated at approximately 60°C. Crystals were obtained on standing for a week and were colourless needles. The density of the crystals was not measured due to the high solubility of the host in both aqueous solution and organic solvents. Various attempts to prepare TRIMEA complexes with atenolol and oxprenolol including co-precipitation, co-solvent [with methanol and ethanol] and kneading methods were unsuccessful. Thus, this section focuses on only one complex of TRIMEA as a host with metoprolol as a guest molecule. The complex of TRIMEA with metoprolol will be referred to hereinafter as METTMEA.

Microanalysis

The host:guest ratio of the METTMEA complex was determined by C, H and N microanalysis. These data are presented in Table 7.1 and indicated a 2:1 host:guest ratio for the METTMEA complex, with one water molecule per formula unit.

Table 7.1 C, H, N microanalysis results [n = 2] for the METTMEA complex

Complex	**Experimental** [#]			**Calculated**		
	% C	% H	% N	% C	% H	% N
METTMEA $2(C_{54}H_{96}O_{30})\cdot(C_{15}H_{25}NO_3)\cdot H_2O$	54.25	7.78	0.74	54.00	8.07	0.51

[#] The experimental error is ± 0.30 %

Thermal Analysis

Hot Stage Microscopy

Hot stage microscopic [HSM] analysis of the METTMEA crystals was performed under silicone oil to detect the presence of possible included water, as this would be shown by bubble formation upon heating. Since TGA indicated the presence of only one water molecule per formula unit for this complex, which comprises two TRIMEA host molecules and one guest molecule, bubbling that emanated from the crystal was not pronounced. The METTMEA crystal remained clear throughout the heating process. In the temperature range 81-115°C a very tiny bubble was observed emanating from the crystal. The HSM analysis in the temperature range180-200°C displayed melting.

Figure 7.1 HSM photographs of METTMEA at various temperatures.

Differential Scanning Calorimetry and Thermogravimetric Analysis

Figure 7.2 presents the TGA and DSC analyses of the single crystals of the METTMEA complex. The TGA trace from 30°C to 100°C showed percentage water loss of 0.72 ± 0.02 % [n = 3] corresponding to one water molecule per formula unit [Table 7.1]. The lack of an endothermic peak for dehydration in the DSC trace is consistent with the low water content of the crystal. The DSC trace of the METTMEA complex showed three events labelled A, B and C respectively. The endotherm labelled A, with the onset temperature of 170.2°C, is due to a phase transition of the anhydrous complex prior to melting. The fusion endotherm [labelled B] has the onset temperature of 179.6°C and the subsequent exotherm [labelled C], with the onset temperature of 184.6°C is attributed to the beginning of decomposition of the METTMEA complex. This exotherm corresponds to the onset of decomposition from the TGA [labelled C].

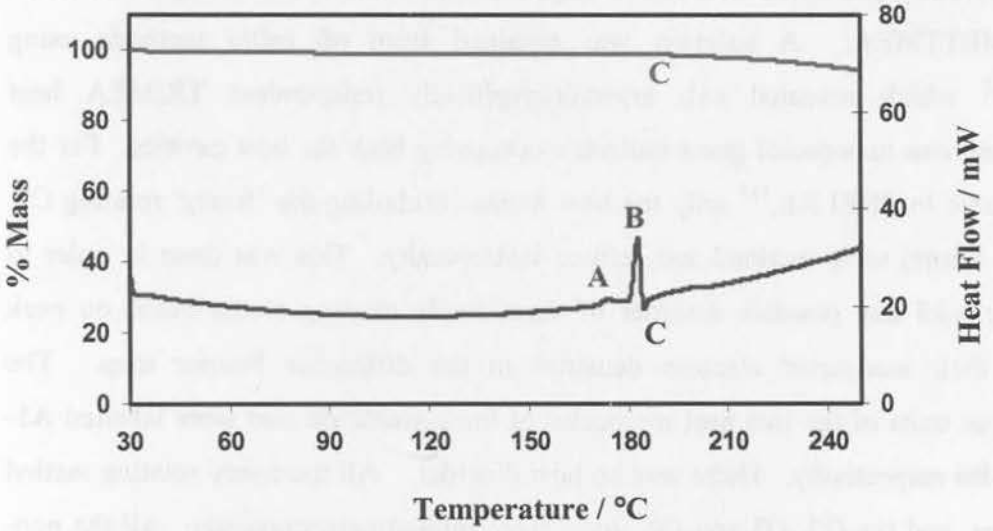

Figure 7.2 DSC and TGA traces of the METTMEA complex.

Table 7.1 Summary of TGA results for METTMEA

Temp (°C)	30	100	150	200	240
Sample weight (%)	100	99.3	99.0	98.3	94.5
Δ Weight loss (%)	-	0.72	1.0	1.7	5.5

X-ray Crystallographic Analysis of METTMEA

Data-collection and space group determination

Intensity data were collected on a Nonius Kappa CCD diffractometer at 113K using graphite-monochromated MoKα radiation. Laue symmetry 2/m was deduced for the intensity data which thus indicated the monoclinic system. Inspection of the zero levels of the reciprocal lattice with LAYER[112] showed the reflection condition to be 0k0: k = 2n. XPREP[103] indicated the possible space groups $P2_1$ and $P2_1/m$. Since the host is chiral the former space group was chosen.

Structure solution and refinement

The structure of METTMEA could not be solved by isomorphous replacement since there were no previously published TRIMEA complexes with similar unit cell parameters to those of METTMEA. A solution was obtained from *ab initio* methods using SHELXD,[210] which revealed two crystallographically independent TRIMEA host molecules and one metoprolol guest molecule occupying both the host cavities. For the first refinement in SHELXL,[113] only the host atoms [excluding the 'freely' rotating C7, C8 and C9 atoms] were retained and refined isotropically. This was done in order to detect and model any possible disorder of these freely rotating atoms based on peak heights of their associated electron densities in the difference Fourier map. The glucopyranose units of the two host molecules of the asymmetric unit were labelled **A1-A6** and **B1-B6** respectively. There was no host disorder. All the freely rotating methyl carbon atoms, and the O2, O3 and O6 atoms were refined anisotropically. All the non-hydrogen atoms of the guest were also refined anisotropically. The host and the guest hydrogen atoms were placed using a riding model and were refined isotropically with the temperature factors U_{iso} equal to 1.2 times those of their parent atoms and the methyl hydrogen atoms refined with temperature factors of 1.5 times of the methyl carbon atoms.

The TGA analysis indicated the presence of one water molecule included in the complex. This water molecule was located outside the cavity of **CD(B)**. An electron density peak of 1.46 e $Å^{-3}$ very close to the atom O10 was initially thought to form a disordered pair with O10 and it was referred to as O10B. The two oxygen atoms were assigned an s.o.f. of x and 1-x and refined with their U_{iso} fixed at 0.05 $Å^2$. Due to the abnormal angles and the distance of the atom O10B from C9 it was realised that it does not form a disordered pair with the atom O10 and it was deleted. There were a few, relatively high electron-density peaks [1.46-0.69 e $Å^{-3}$] remaining inside the cavities of **CD(A)** and **CD(B)** after the final refinement but no chemical significance could be assigned to them. Crystal and refinement parameters for METTMEA are presented in Table 7.2.

Table 7.2 Crystal and refinement parameters for the METTMEA structure

Empirical formula	$2(C_{54}H_{96}O_{30}) \cdot (C_{15}H_{25}NO_3) \cdot H_2O$
Formula weight / g mol^{-1}	2736.0
Crystal system	Monoclinic
Space group	$P2_1$
a / Å	13.5228(2)
b / Å	23.4723(3)
c / Å	22.5602(4)
β / °	98.063 (1)
Volume / $Å^3$	7090.1(2)
Z	2
Density $_{calc}$ / g cm^{-3}	1.281
μ(MoKα) / mm^{-1}	0.103
F(000)	2952
Temperature of data collection / K	113
Crystal size / mm^3	0.10 x 0.30 x 0.40
Range scanned θ / °	$2 \leq \theta \leq 26$
Index ranges	h: -16, 16 k: -28, 28 l: -27, 27
Dx / mm	39
Total no. of reflections collected	44646
Total no. of unique reflections	25708
No. of reflections with $I > 2\sigma(I)$	19635
No. of parameters	1369
R_{int}, R_σ	0.0483, 0.0721
$(\Delta / \sigma)_{mean}$	< 0.001
S	1.04
R_1 (for 19635 reflections)	0.1144
No. of reflections omitted	150
wR_2	0.3301
Weighting scheme	a = 0.127 b = 50.902
Δρ excursions / e $Å^{-3}$	1.46 and –0.56

Description of the structure

METTMEA crystallises in the space group $P2_1$ in a 2:1:1 TRIMEA:metoprolol:water molar ratio with Z = 2 formula units per unit cell. A diagram of the asymmetric unit of the METTMEA complex is presented in Figure 7.3. The methylglucose units of the **CD(A)** and **CD(B)** host molecules are denoted **A1-A6** and **B1-B6** respectively. The **CD(A)** and **CD(B)** host molecules of the asymmetric unit are arranged in a head-to-tail mode with the secondary side of **CD(A)** facing the primary side of **CD(B)**.

The mean O4 plane of the **CD(A)** host molecule is orientated at an angle of 2.01(3)° to the mean O4 plane of the **CD(B)** host molecule. The geometrical parameters used to describe the structural features of the CD host molecules, as explained in Chapter 1, are listed in Tables 7.3-7.5. Table 7.3 lists some of the principal torsion angles of the two TRIMEA molecules, **CD(A)** and **CD(B)**. The ω parameter [describing the direction of the C6-O6 bonds with respect to the cavity] is positive for **A1**, **A4**, **A5** and **A6** [pointing towards the cavity] and negative for **A2** and **A3** [pointing away from the cavity] for molecule **CD(A)**. For molecule **CD(B)** the ω parameter is positive for **B1**, **B4**, **B5** and **B6** and negative for **B2** and **B3**. The C9 methyl carbon atoms of the methylglucose units for which ω is positive extend across the primary rim to effectively close this side of the **CD(A)** as illustrated in Figure 7.3. On the secondary rim of the **CD(B)**, O2-C7 bonds point away from the cavity while the O3-C8 bonds point toward the cavity.

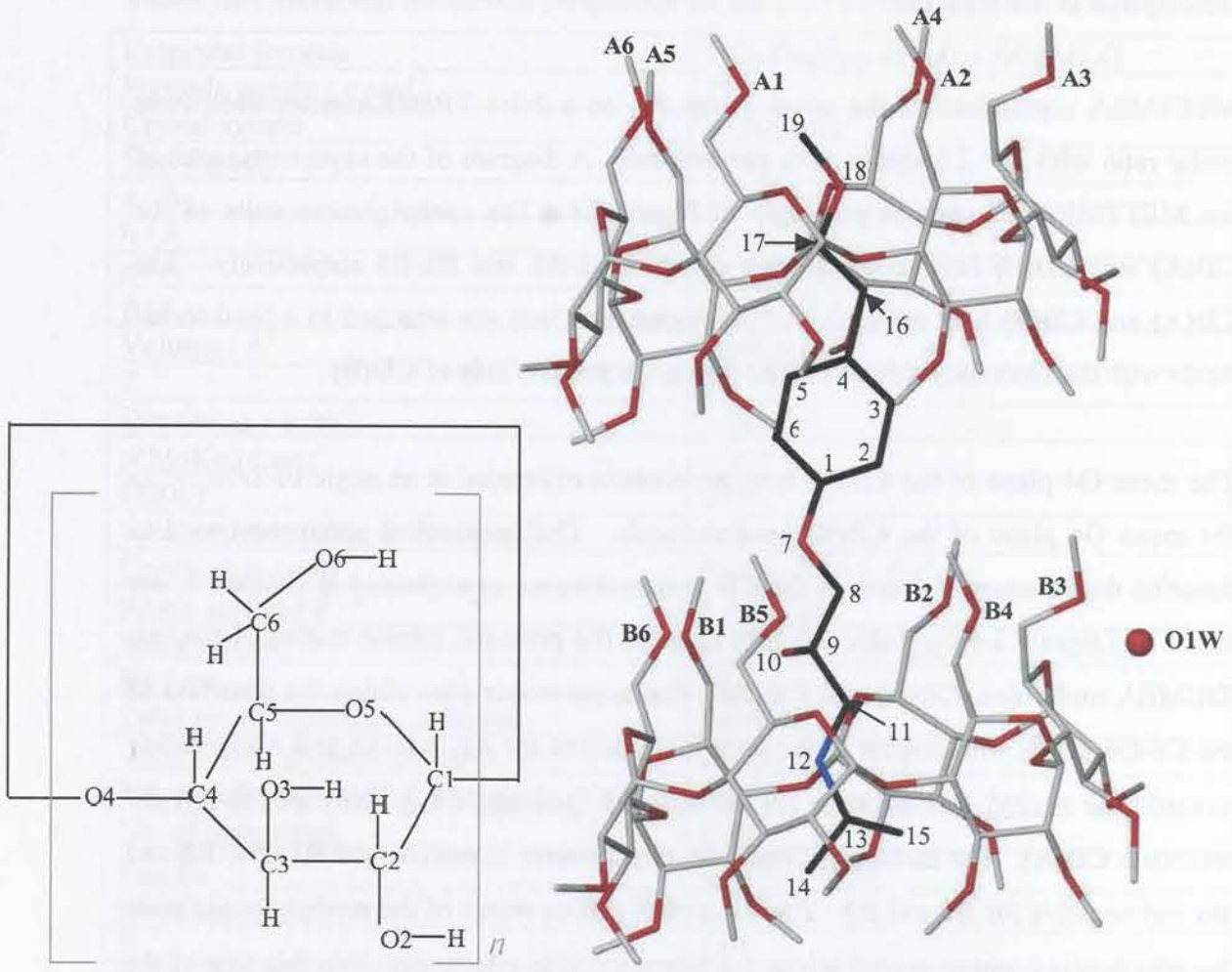

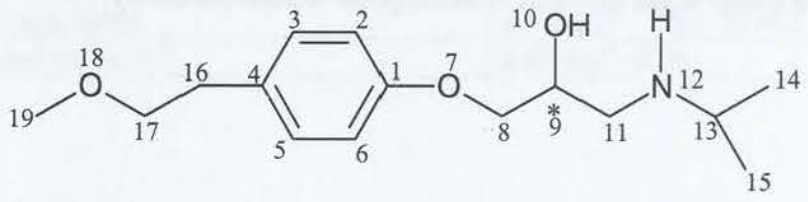

Figure 7.3 Side view of the METTMEA complex with the numbering schemes of the host and the guest. For clarity the guest carbon atoms are shown in black and there is one water molecule present in the complex. A chemical formula diagram of the guest molecule with its numbering scheme is also shown.

Table 7.3 Torsion angles [°] for METTMEA

CD(A)	ω	Φ	ψ	Θ_1	Θ_2
A1	63.5(9)	97.7(7)	114.1(7)	49.9(9)	-50.4(9)
A2	-70.8(9)	110.7(8)	143.0(7)	51.9(9)	-54.3(9)
A3	-67.1(8)	104.0(8)	131.4(7)	43.3(10)	-42.9(9)
A4	64.2(9)	99.7(8)	115.0(7)	51.5(9)	-54.8(8)
A5	64.8(8)	109.2(8)	141.6(7)	50.6(9)	-49.5(8)
A6	69.4(8)	105.5(7)	136.1(7)	45.5(9)	-43.8(9)
| Average |	**66.6**	**104.5**	**130.2**	**48.8**	**49.3**
CD(B)					
B1	67.2(9)	98.6(7)	119.3(7)	48.0(9)	-49.8(9)
B2	-69.1(8)	111.8(7)	140.5(6)	52.1(9)	-55.0(8)
B3	-63.1(9)	104.6(7)	132.4(7)	43.5(9)	-43.6(9)
B4	57.2(9)	99.4(8)	-125.1(7)	48.3(9)	-54.6(9)
B5	62.9(9)	112.3(7)	-93.8(8)	50.0(9)	-47.3(9)
B6	72.1(9)	103.5(8)	133.3(7)	51.1(9)	-47.3(9)
| Average |	**65.3**	**105.0**	**124.1**	**48.8**	**49.6**

There is steric hindrance between the methyl group attached to the O3 atom and the O2 atom of the adjacent glucose unit. Consequently, methylglucose units incline their O6 atoms [on the primary rim] toward the cavity to a much greater degree than do the glucose units of α-CD.[181] This large inclination increases the distance between the O2 and O3 atoms of adjacent methylglucose units, thus relieving their associated steric strain. The methylglucose units are all in the $^4C_1$ chair conformation and the conformations around the C4 atoms, as described by the parameters Θ_1 and Θ_2, show minimal deviation from the ideal values for α-CD. Table 7.4 lists the parameters for the O4-hexagons in the two independent host molecules. The two crystallographically independent **CD(A)** and **CD(B)** host molecules of the METTMEA complex have nearly identical conformations, and this is illustrated in Figure 7.4. The diagonal distances of the O4-hexagons for the **CD(A)** and **CD(B)** host molecules, are in the range 8.31-8.77 Å.

The slight ellipticity of the host is indicated numerically by the slight variations in the **r**, **l** and **a** parameters. The planarities of the O4-hexagons for both **CD(A)** and **CD(B)** as indicated by the **d** and **t** parameters are fairly high; the maximum deviations of O4 atoms from the planes are 0.24(4)Å and 0.25(5)Å for **CD(A)** and **CD(B)** respectively. These small deviations are due to the low tilt angles to be described.

Table 7.4 O4-hexagon parameters for METTMEA

Methylglucose unit	r / Å	l / Å	a / °	d / Å	t / °
A1	4.16	4.32	121	0.099(4)	10.3
A2	4.38	4.07	116	-0.238(4)	-11.5
A3	4.18	4.41	122	0.138(4)	1.4
A4	4.17	4.22	121	0.103(4)	10.2
A5	4.39	4.22	116	-0.237(4)	-11.3
A6	4.19	4.28	122	0.134(4)	1.3
| Average |	**4.24**	**4.25**	**120**	**0.158**	**7.7**
B1	4.15	4.33	122	0.084(4)	9.6
B2	4.39	4.11	116	-0.238(4)	-11.2
B3	4.23	4.41	121	0.145(4)	1.1
B4	4.16	4.22	122	0.105(4)	11.1
B5	4.39	4.24	116	-0.254(4)	-12.7
B6	4.22	4.27	121	0.158(4)	2.7
| Average |	**4.26**	**4.26**	**120**	**0.164**	**8.1**

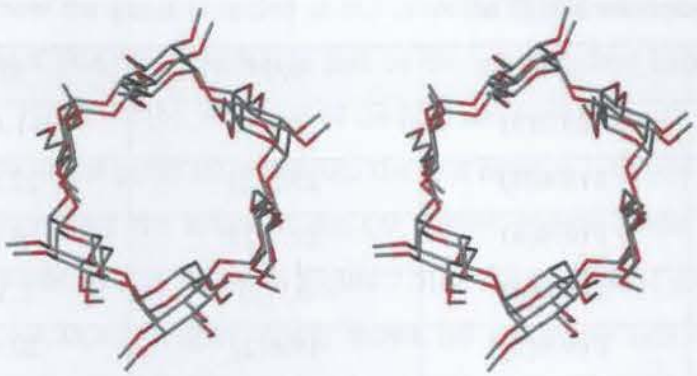

Figure 7.4 Stereo diagram of the TRIMEA molecules [**CD(A)** and **CD(B)**] in the asymmetric unit viewed from the secondary face of **CD(A)**, illustrating their nearly identical conformations.

The tilt angles for the METTMEA structure together with the intersaccharidic bond angles are listed in Table 7.5. Five methylglucose units of each CD have positive tilt angles, those for **A1** and **B4** being negative, indicating that the majority of the methylglucose units are tilted towards the inside of the cavity on the O6 side. The tilt angles τ_1 and τ_2, defined as the angles made by the O4 plane and the planes through C1, C2, C3, C4, C5, O5 and C1, C4, O4, O4 of each methylglucose residue respectively, are in the range 0.1-24.6° and 1.2-24.4° for **CD(A)** and **CD(B)**. The intersaccharidic bond angles are close to those observed for β-CD molecules.

Table 7.5 φ and τ parameters for METTMEA

Methylglucose unit	φ / °	τ_1 / °	τ_2 / °
A1	120.2(6)	-1.4(2)	-1.6(1)
A2	118.8(6)	23.5(2)	22.5(3)
A3	117.4(6)	21.7(2)	24.0(2)
A4	119.0(6)	0.7(2)	2.1(1)
A5	119.8(6)	19.6(2)	20.4(1)
A6	118.4(6)	21.5(2)	20.6(2)
| Average |	**118.9**	**14.7**	**15.2**
B1	117.4(6)	0.1(2)	1.2(1)
B2	120.6(6)	22.8(2)	21.1(3)
B3	119.2(6)	20.9(2)	23.4(2)
B4	117.5(6)	-4.0(2)	-4.4(2)
B5	119.6(6)	24.6(2)	24.4(2)
B6	118.5(6)	19.1(2)	23.1(2)
| Average |	**118.8**	**15.2**	**16.3**

Guest inclusion

The extended conformation of the included metoprolol guest molecule results in its having a length of approximately 15 Å. The metoprolol molecule is encapsulated in the cavity of the TRIMEA dimer as shown in Figure 7.3. The two TRIMEA molecules are arranged so as to fully include the bulky guest molecule. The phenyl ring moiety is located at the secondary side of the **CD(A)** molecule and it extends to the interface between the secondary side of **CD(A)** and the primary side of **CD(B)**. The longer side chain extends from the interface to the cavity of the **CD(B)** molecule, with the O10 atom of the guest in hydrogen bonding contact with the atoms O6B1 [2.51(1) Å] and O6B6 [2.37(1) Å] of the **CD(B)** host molecule. The shorter side chain is located inside the cavity of the **CD(A)** host molecule. Figures 7.5(a)-(d) are space-filling diagrams presenting different views of the METTMEA complex. Figure 7.5(a) is a side view

showing how the guest is sealed at the interface by the methyl groups on the secondary face of the **CD(A)** host molecule and on the primary face by those of the **CD(B)** host molecule. Figure 7.5(b), with part of the host removed, presents a side view of the degree of insertion of the guest molecule into the host cavities. A view from the primary face of **CD(A)** illustrating the effect of the C9 methyl groups of the methylglucose units for which ω is positive, is shown in Figure 7.5(c). These methyl groups tend to seal off this side of the **CD(A)**. Figure 7.5(d) shows the secondary side or the 'open side' of the TRIMEA molecule **CD(B)** and how the guest is encapsulated in the cavity.

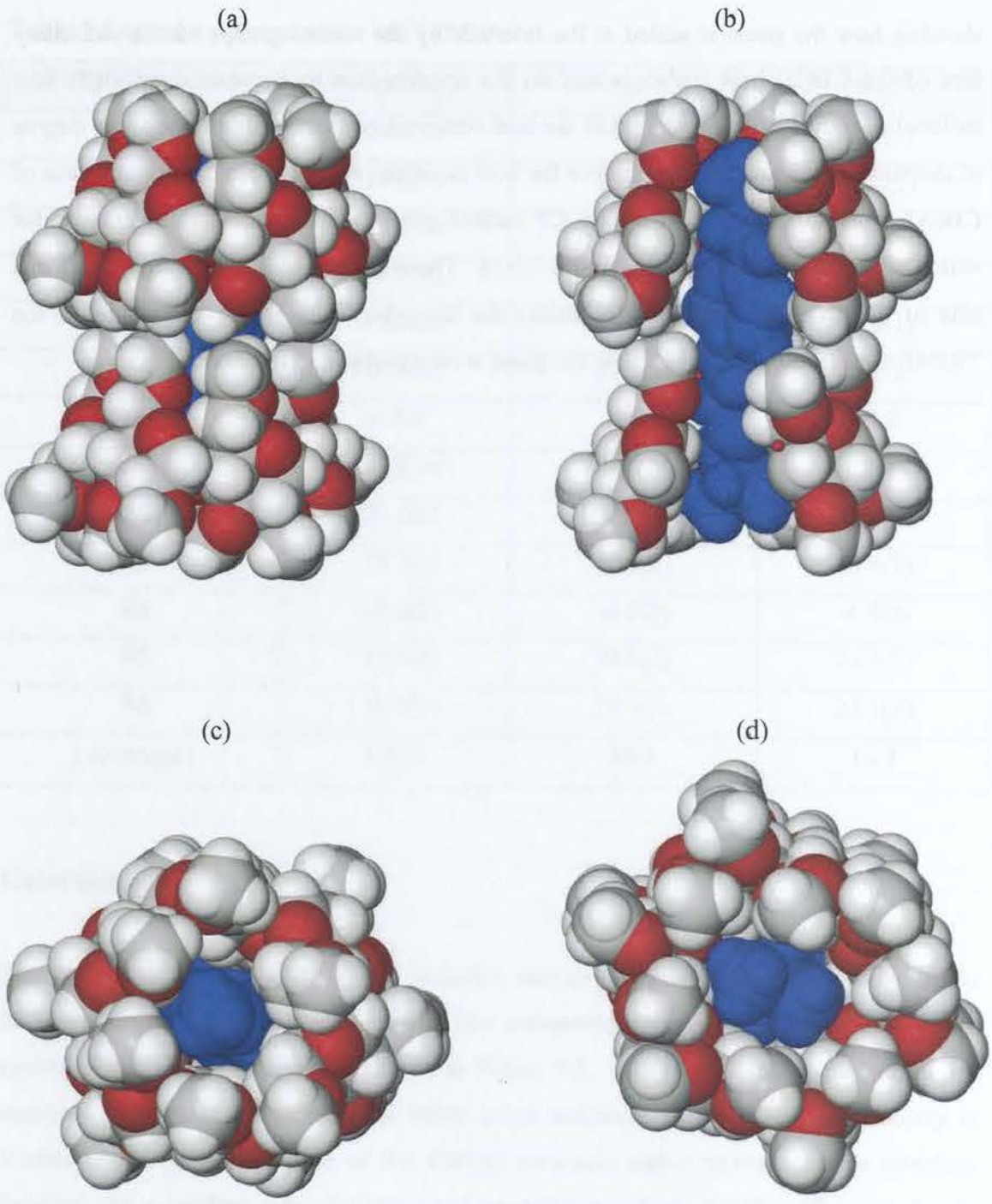

Figure 7.5 Views of the 2:1 complex unit (a) from the side face, (b) from the side with part of the host molecule removed, (c) from the primary and (d) secondary faces.

Conformation and configuration of the guest molecule

The conformation of the metoprolol molecule in METTMEA is discussed next relative to its conformation in the uncomplexed Forms I and II of metoprolol discussed in Chapter 3. The principal torsion angles for the metoprolol molecule in METTMEA, Form I and Form II are presented in Tables 7.6 and 7.7, while Figure 7.6 is a repeat of Figure 3.15, illustrating the definitions of the torsion angles. The configuration at the chiral centre C9 of the included metoprolol molecule is (S-), and this will be elaborated in the Discussion section of this chapter. Because of this configuration of the included metoprolol guest molecule, the comparison of the torsion angles is between the (S-) form of the complexed drug and the (S-) enantiomers of Form I and Form II. The δ_1, δ_2, δ_3, δ_4, δ_7 and δ_9 torsion angles agree closely with those for Form I and Form II. The δ_6 torsion angle for the complexed metoprolol is significantly smaller than those of Form I and Form II. This indicates that the plane of the aromatic ring is nearly parallel to the metoprolol backbone

Table 7.6 Principal torsion angles [°] of metoprolol in METTMEA and Form I

Torsion angle / °	Form I *	METTMEA
δ_1	177.7 (2)	-174(1)
δ_2	-174.2(2)	-174(2)
δ_3	177.5(2)	179(1)
δ_4	-163.5(2)	-176(1)
δ_5	98.0(2)	-165(1)
δ_6	-81.8(2)	15(2)
δ_7	-162.8(2)	-172(1)
δ_8	74.7(2)	80(1)
δ_9	-176.1(2)	178(1)
δ_{10}	-54.2(2)	-74(1)
δ_{11}	-73.2(2)	179(1)

* For the (S)-enantiomer for comparison with the guest

and this smaller torsion angle also facilitates the inclusion of the guest into the TRIMEA cavity.

Table 7.7 Principal torsion angles [°] for Form II

Torsion angle / °	**B**	**C**	**D**	**E**
δ_1	-172.6(6)	-177.8(6)	-160.3(8)	-168.9((7)
δ_2	176.9(6)	-178.8(7)	171.8(8)	169.9(8)
δ_3	-175(1)	-178.7(7)	179.1(7)	179.0(9)
δ_4	166.3(6)	164.5(6)	164.9(8)	167.8(7)
δ_5	67(1)	70(1)	-72(1)	-114(1)
δ_6	-114(1)	-113.0(8)	104(1)	68(1)
δ_7	-175.5(6)	-175.4(6)	-166.3(7)	-167.3(7)
δ_8	66(1)	68(1)	74(1)	73(1)
δ_9	170.1(6)	175.1(6)	174.7(7)	177.0(7)
δ_{10}	-68(1)	-65(1)	-64(1)	-61(1)
δ_{11}	-177.4(9)	179.1(6)	174.4(7)	69(1)
Torsion angle / °	**F**	**G**	**H**	
δ_1	-174.9(7)	-173.6(7)	-178.4(7)	
δ_2	178.9(8)	-179.9(7)	179.9(7)	
δ_3	-177.1(8)	-168.4(9)	173(1)	
δ_4	163.4(7)	169.8(7)	162.5(6)	
δ_5	94(1)	133(1)	-114(1)	
δ_6	-85(1)	-52(1)	70(1)	
δ_7	-174.3(7)	-173.2(6)	-176.0(6)	
δ_8	67(1)	68(1)	65(1)	
δ_9	172.0(7)	174.0(6)	175.2(6)	
δ_{10}	-66(1)	-64(1)	-62(1)	
δ_{11}	179.4(8)	-176.4(8)	-180(1)	

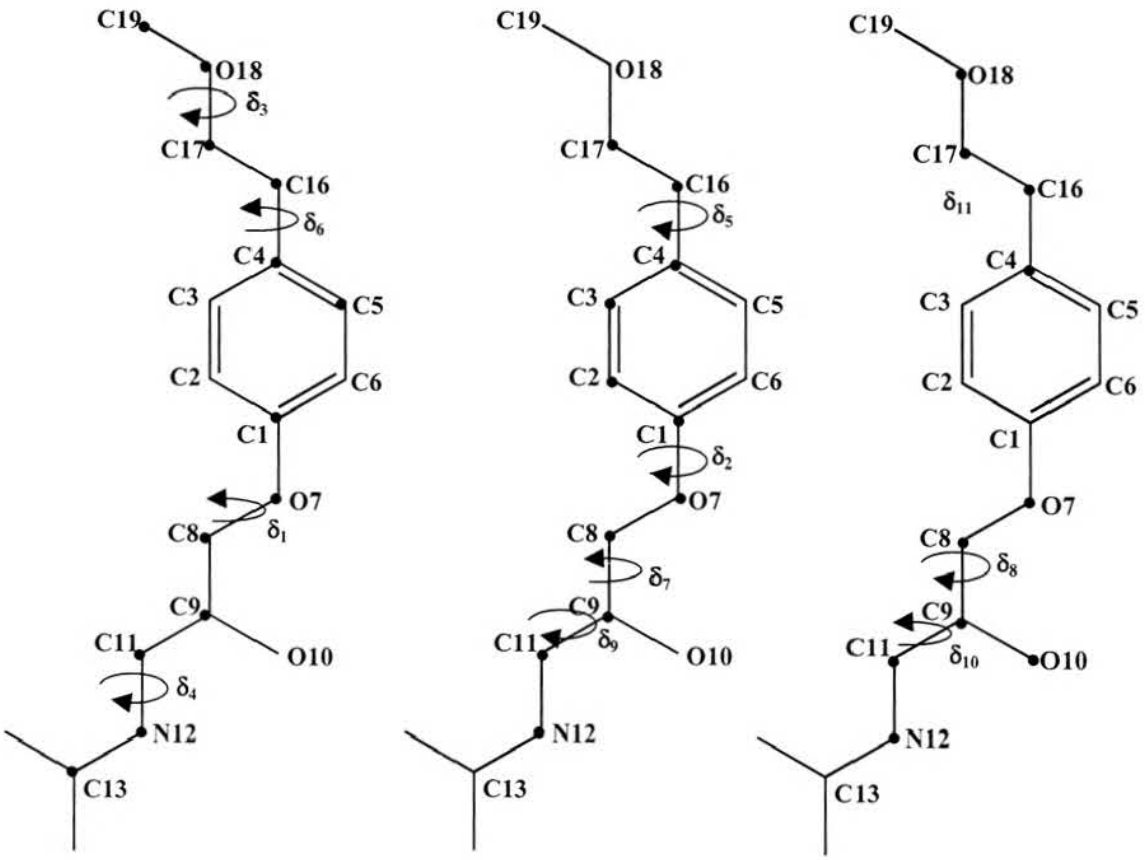

Figure 7.6 Schematic diagram of the principal torsion angles (a) δ_1, δ_3, δ_4, δ_6 (b) δ_2, δ_5, δ_7, δ_9 (c) δ_8, δ_{10} and δ_{11} for the metoprolol molecule.

Hydrogen bonding and C-H•••π ring interactions

Apart from van der Waals and hydrophobic interactions that stabilise the METTMEA structure, hydrogen bonding and C-H•••π ring interactions were identified and are listed in Table 7.8.

Intramolecular host interactions

There is a total of twelve intramolecular host hydrogen bonds [six for each of **CD(A)** and **CD(B)**] that stabilise the structure of the TRIMEA molecules in METTMEA. In order to further minimise the steric hindrance between the methyl group attached to the O3 and O2 atoms of the adjacent methylglucose unit, the C6-H•••O5' hydrogen bonds cause the C6-O6 bonds of the **A2** and **B2** methyglucose units to point away from the host cavity [their ω parameter is negative]. The C6-H•••O6' hydrogen bonds 'lock' the O6 atoms in their observed positions in their rotation around the C5-C6 bond [defined by the ω parameter in Table 7.3]. The other hydrogen bond on the secondary side of the TRIMEA molecules is the C8-H•••O2' hydrogen bond, which 'locks' the C8 methyl groups in their observed positions on their respective methylglucose units. There are no intramolecular guest interactions.

Host-guest interactions

There are seven host-guest hydrogen bonds and two C-H•••π ring interactions that are listed in Table 7.8. These hydrogen bonds enhance the association of the host and guest molecules. The strongest interactions are O10-H10•••O6B1 and O10-H10•••O6B6 in which bifurcated binding between the O10 atom of the metoprolol guest molecule and atoms O6B1 and O6B6 of the TRIMEA host molecule occurs and this is illustrated in Figure 7.7.

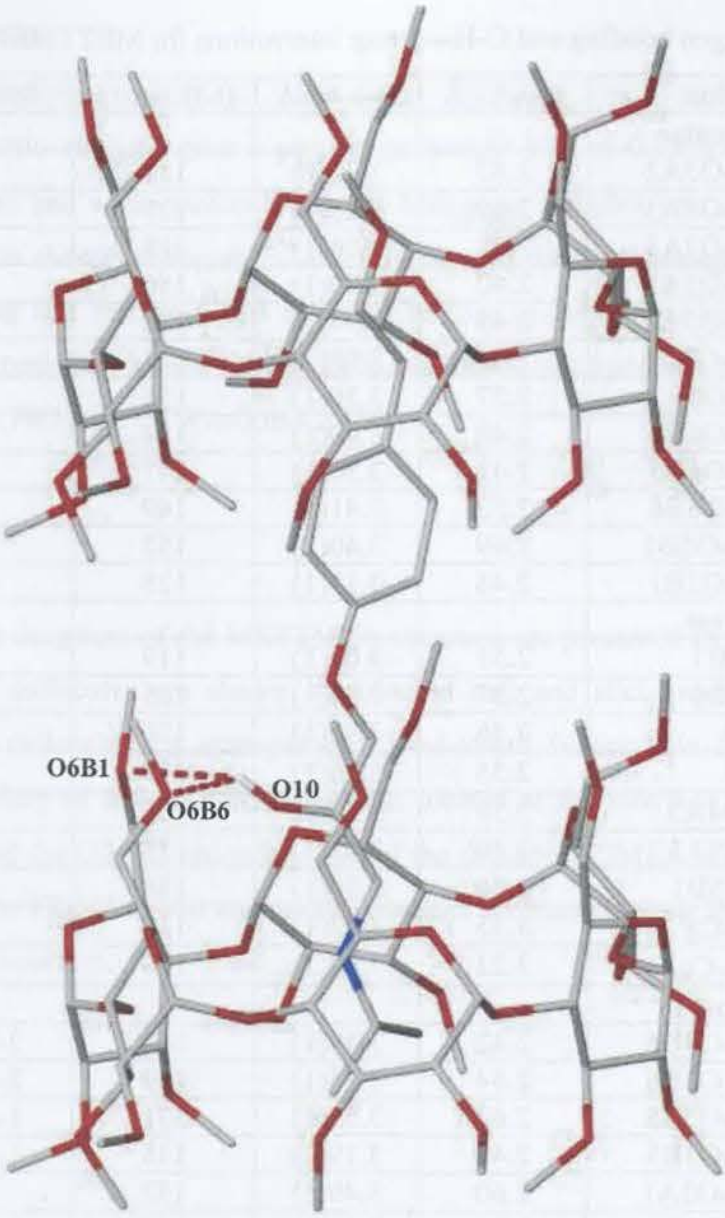

Figure 7.7 Bifurcated binding of the O10 atom of the metoprolol guest molecule to the O6B1 and O6B6 atoms of the TRIMEA **CD(B)** host molecule.

Host-host intermolecular interactions

There are nine host-host intermolecular C-H•••O hydrogen bonds that are present in the METTMEA structure and these contribute to the stabilisation of the crystal structure.

Table 7.8 Hydrogen bonding and C-H•••π ring interactions for METTMEA

Interaction	H•••A / Å	D•••A / Å	D-H•••A / °	Symmetry code[a]
Intramolecular				
C6A1-H6A1•••O5A2	2.42	3.32(1)	151	x, y, z
C6A2-H6A4•••O5A3	2.59	3.28(1)	127	x, y, z
C8A3-H8A8•••O2A3	2.48	3.06(1)	118	x, y, z
C6A4-H6A7•••O5A5	2.40	3.30(1)	150	x, y, z
C6A5-H6A9•••O5A6	2.43	3.34(1)	152	x, y, z
C8A6-H8AE•••O2A6	2.44	3.08(1)	123	x, y, z
C6B1-H6B1•••O5B2	2.37	3.30(1)	156	x, y, z
C6B3-H6B6•••O6B4	2.48	3.40(1)	154	x, y, z
C6B4-H6B7•••O5B5	2.43	3.30(1)	147	x, y, z
C6B5-H6B9•••O5B6	2.52	3.41(1)	149	x, y, z
C6B6-H6BY•••O5B1	2.49	3.40(1)	152	x, y, z
C8B6-H8BF•••O2B1	2.48	3.17(1)	128	x, y, z
Host-guest				
O10-H10•••O6B1	2.51	3.01(1)	119	x, y, z
O10-H10•••O6B6	2.37	2.94(1)	125	x, y, z
C9-H9•••O6B5	2.56	3.30(1)	130	x, y, z
C9-H9•••O6B6	2.55	3.16(1)	119	x, y, z
C16-H16A•••O4A3	2.59	3.57(1)	169	x, y, z
O18•••H5A3-C5A3	2.49	3.42(1)	155	x, y, z
O10•••H5B1-C5B1	2.56	3.36(1)	138	x, y, z
C8A1-H8A1•••Cg[#]	3.35	3.92(1)	119	x, y, z
C8A4-H8AY•••Cg[#]	3.23	3.92(1)	130	x, y, z
Host-host				
C2A2-H2A2•••O5B6	2.42	3.39(1)	165	2-x, 1/2+y, 1-z
C9A2-H9A6•••O3B6	2.54	3.34(1)	139	2-x, 1/2+y, 1-z
C2A3-H2A3•••O5B5	2.60	3.59(1)	171	1-x, 1/2+y, 1-z
C9A3-H9A9•••O3B5	2.42	3.19(1)	135	1-x, 1/2+y, 1-z
C7A4-H7AZ•••O3A1	2.60	3.49(1)	152	-1+x, y, z
C2B2-H2B2•••O5A6	2.34	3.33(1)	169	2-x, 1/2+y, 1-z
C9B2-H9B6•••O3A6	2.53	3.25(1)	130	2-x, 1/2+y, 1-z
C2B3-H2B3•••O5A5	2.41	3.40(1)	173	1-x, 1/2+y, 1-z
C2B6-H2B6•••O6A2	2.39	3.31(1)	153	2-x, -1/2+y, 1-z

[a] Symmetry code applied to second unit of interaction

Cg[#] Centre of gravity of the aromatic ring of the guest

Water interactions

Thermogravimetric analysis gave a percentage weight loss of 0.72 ± 0.02 % [n = 3] corresponding to one water molecule per 2:1 host:guest complex unit. This water was accounted for in the crystallographic analysis by placement of a single water oxygen atom and giving it a full s.o.f. and allowing its U_{iso} to vary. The water molecule is situated at the periphery of the **CD(B)** molecule and forms hydrogen bonding contacts O1W•••O6B3 2.79(1) and O1W•••O5B4 2.80(1) Å.

Crystal packing

Crystal packing diagrams of the METTMEA structure are presented in Figure 7.8. The included guest molecules are shown in coloured ball and stick mode. The dimeric TRIMEA host molecules are arranged in a head-to-tail fashion. In Figure 7.7(a) the phenyl ring moiety of the metoprolol guest is located at the interface between the O6 primary side and the O2, O3 secondary side of the dimeric TRIMEA host molecules. In Figure 7.7(b) the TRIMEA host and guest molecules are stacked along the c-axis forming a channel-type structure.

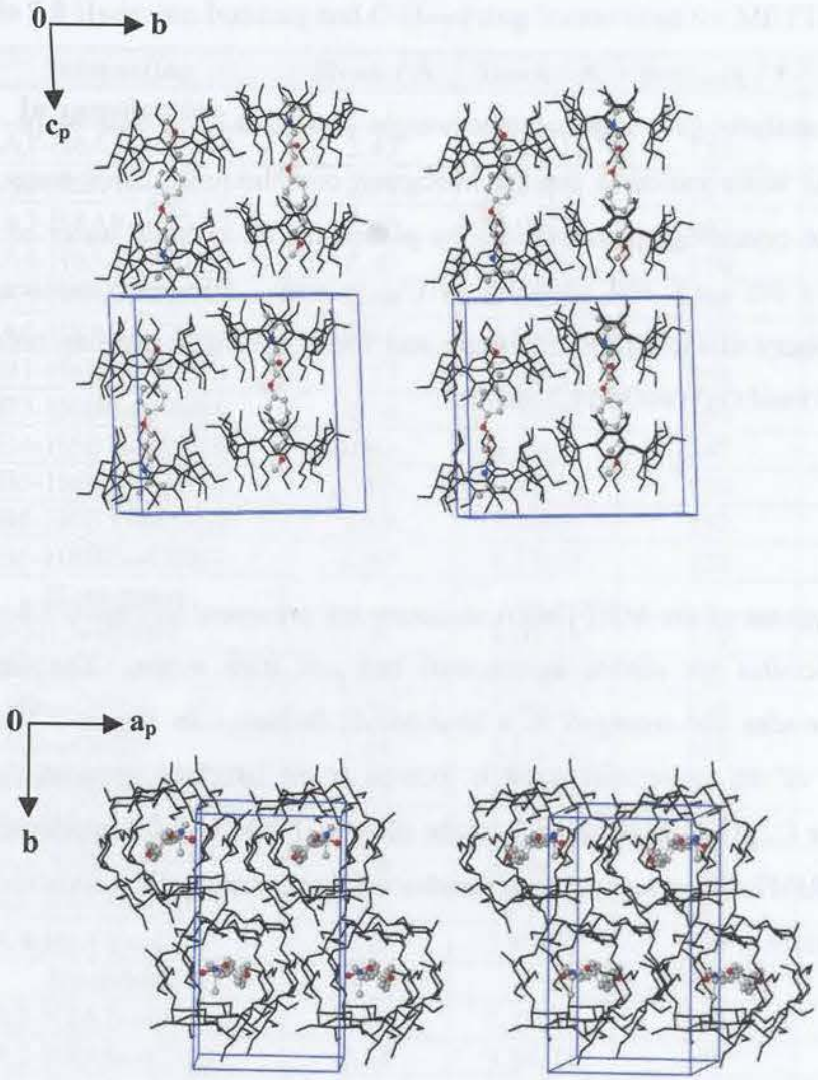

Figure 7.8 Crystal packing diagrams of METTMEA down the (a) a- and (b) c-axes respectively. The antiparallel arrangement of complex units created by the screw-axis parallel to b is evident.

Powder X-ray diffraction

The computed and experimental PXRD traces for METTMEA are presented in Figure 7.9. Since the information for the two traces was obtained at different temperatures, the experimental trace is slightly shifted to lower 2θ values. However the patterns match in their number of peaks as well as their profiles. The close agreement shows that there was no phase change on grinding the complex.

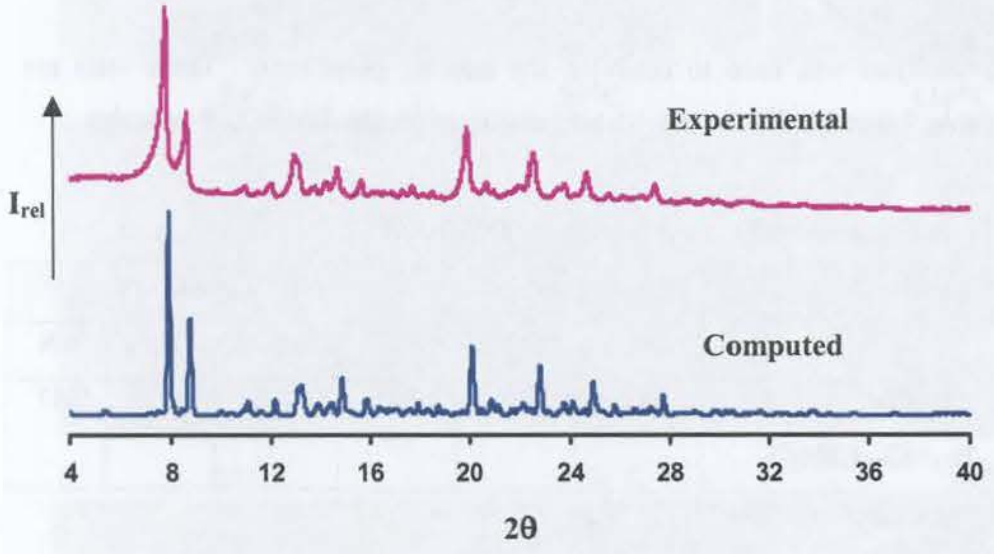

Figure 7.9 Computed [113K] and experimental [295K] PXRD traces for METTMEA.

DIMEB Inclusion Complex with Oxprenolol Free Base

Complex Preparation

The DIMEB complex of oxprenolol [hereinafter referred to as DMBOXP] was prepared by the co-precipitation method in which an equimolar amount of the drug was slowly added to a saturated solution of the DIMEB. The solution was stirred overnight in ice, filtered and allowed to crystallise at 60°C over a period of a few days.

Microanalysis

C, H, N microanalysis was used to establish the host to guest ratio. These data are presented in Table 7.9 and indicated a 1:1 host:guest ratio for the DMBOXP complex.

Table 7.9 C, H, N microanalysis results [n = 2] for DMBOXP

Complex	Experimental [#]			Calculated		
	%C	%H	%N	%C	%H	%N
DMBOXP $C_{56}H_{98}O_{35}\bullet C_{15}H_{23}NO_3\bullet 4.8H_2O$	52.90	7.48	0.88	52.70	7.69	0.87

[#] The experimental error is ± 0.30 %

Thermal Analyses

Hot Stage Microscopy

The visual characterisation of the DMBOXP crystals on heating is shown in Figure 7.10. The crystals were covered in silicone oil to determine the presence of possible included water molecules. At 20°C, the starting temperature, the crystals were clear; however, from 99°C bubbling began and stopped at 140°C. From 148-233°C vigorous bubbling was observed and this was evidenced on TGA as a mass loss equivalent to the dissociation of one guest molecule per host molecule. At 268°C the crystals showed

signs of decomposition, indicated by the light orange colour. The crystals gradually became darker up to 350°C at which point bubbling occurred as a result of the increased rate of decomposition.

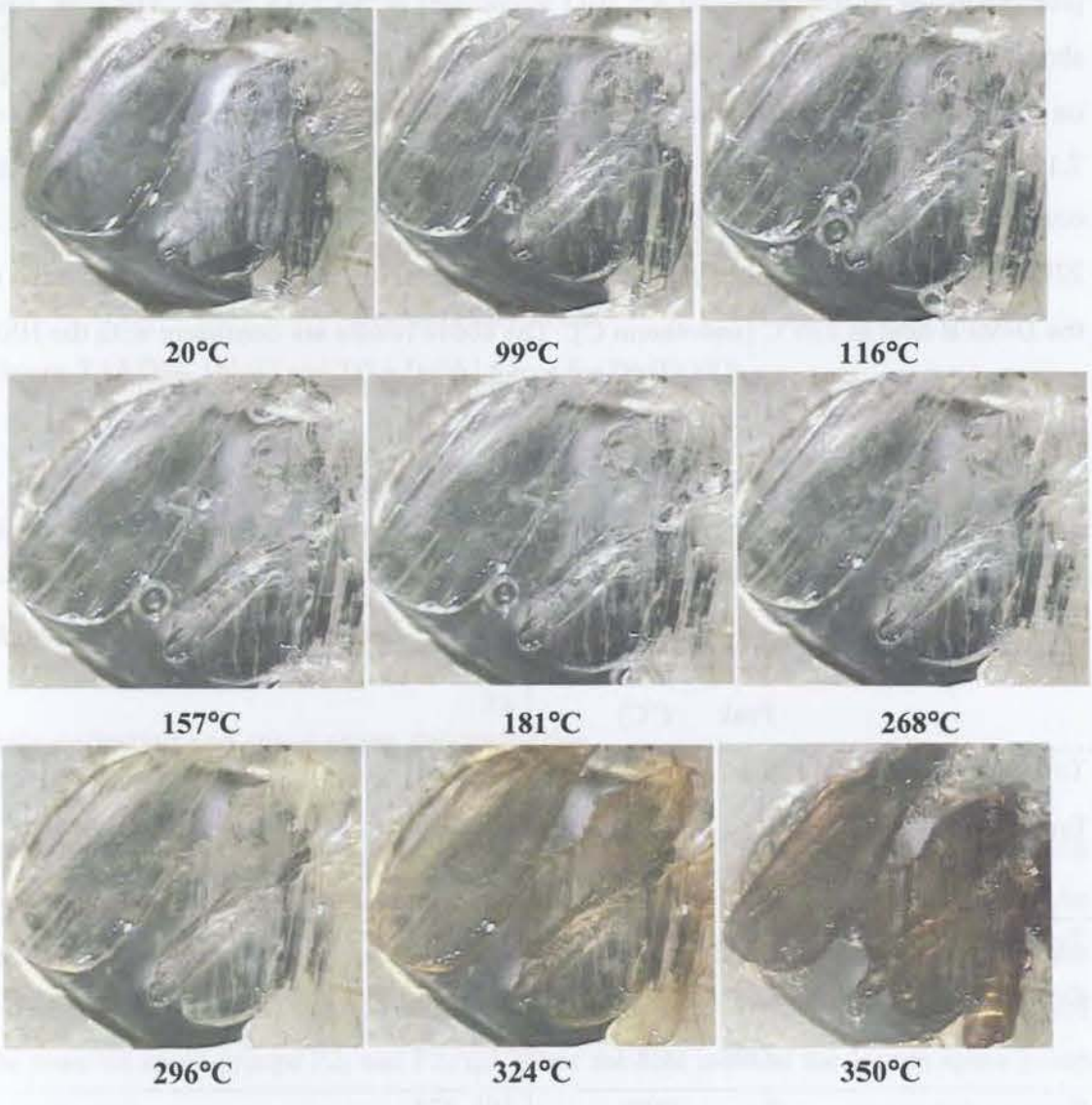

Figure 7.10 HSM photographs of DMBOXP.

Differential Scanning Calorimetry and Thermogravimetric Analysis

The TGA and DSC analyses of the single crystals of the DMBOXP complex are presented in Figure 7.10. An endothermic event [endotherm A] representing water loss in the range 30-110°C clearly corresponds to an observed percentage mass loss of 5.1% [corresponding to the calculated 4.8 H_2O molecules] in the TGA trace. The DSC trace shows an endothermic event in the temperature range 144-161°C [endotherm B], which on the TGA [mass loss in the range 138-202°C] corresponds to a percentage mass loss of 7.12% equal to half of a guest per host molecule. This indicates the dissociation of the complex, an event which is in general observed for DIMEB complexes. The peak at 229°C [exotherm D] possibly indicates the phase transition prior to the decomposition of the DIMEB host at 370°C [endotherm C]. The above results are consistent with the HSM analysis. The summary of the DSC thermal events is presented in Table 7.10.

Table 7.10 Summarised DSC results for the DMBOXP complex

			DMBOXP
Temperature range	A	(°C)	30-80
Endotherm A	T_{on}	(°C)	30
	Peak	(°C)	47
Temperature range	B	(°C)	144-161
Endotherm B	T_{on}	(°C)	147
	Peak	(°C)	153
Temperature range	D	(°C)	224-234
Exotherm D	T_{on}	(°C)	227
	Peak	(°C)	229
Temperature range	C	(°C)	366-374
Endotherm C	T_{on}	(°C)	369
	Peak	(°C)	370

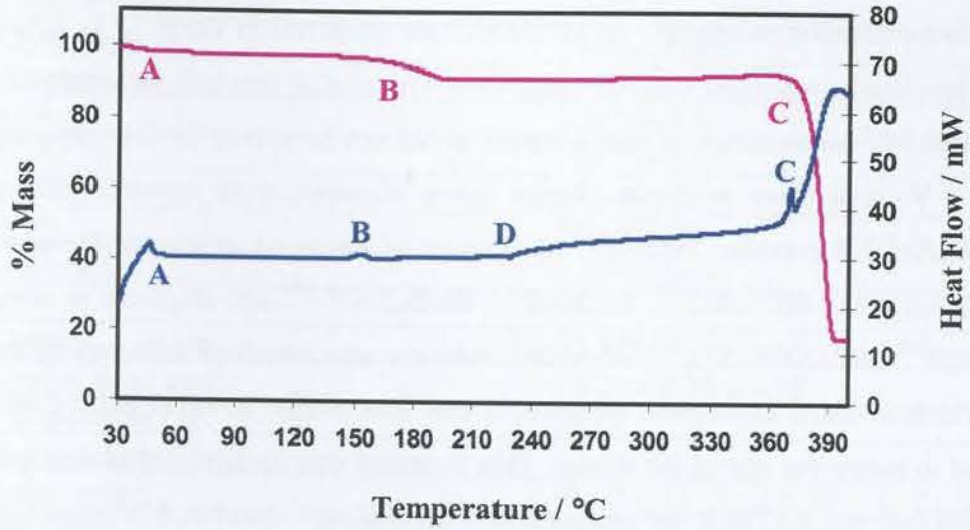

Figure 7.10 DSC [blue] and TGA [pink] traces for DMBOXP.

X-ray Crystallographic Analysis of DMBOXP

Single Crystal X-ray Diffraction

Data-collection and space group determination

Intensity data were collected on a Nonius Kappa CCD diffractometer at 173K using graphite-monochromated MoKα radiation. The intensities displayed Laue symmetry 2/m indicating the monoclinic system. Inspection of the zero levels of the reciprocal lattice with LAYER[112] showed the reflection condition to be 0k0 : k = 2n. XPREP[103] indicated the possible space groups $P2_1$ and $P2_1/m$. Since the host is chiral the former space group was chosen.

Attempted structure solution and refinement

Crystal and data-collection parameters for DMBOXP are presented in Table 7.11. Since there are no previously published DIMEB complexes with similar unit cell parameters to those of DMBOXP, the structure of this complex could not be solved by isomorphous replacement. Various other methods, despite many attempts, were unsuccessful in solving the DMBOXP complex structure. A number of strategies employed included structure solution using SHELXD[210], SIR2002[211], SHELXS-97[104] and fragment phasing using PATSEE[212] and SHELXD.[210] A partial solution was obtained using program SHELXD, which revealed incomplete asymmetric unit host atoms; however these could not be refined to locate the rest of the atoms. This fragment was further used as an input model in SHELXD and PATSEE for rotational and translational searches. Unfortunately this was also unsuccessful in providing a satisfactory solution. Since the asymmetric unit consists of four host molecules, this indicates that the unit cell contains eight host molecules; therefore, although the crystals were strongly diffracting, the unsuccessful attempts to solve the structure are attributed to the large size of the structure, which the available programs could not handle.

Table 7.11 Crystal and data-collection parameters for DMBOXP

Formula unit	$C_{56}H_{98}O_{35}•C_{15}H_{23}NO_3•4.8H_2O$
Formula weight / g mol^{-1}	1683.2
Crystal system	Monoclinic
Space group	$P2_1$
a / Å	20.5580(3)
b / Å	26.7588(3)
c / Å	30.6404(5)
β / °	90.073(7)
Volume / Å^3	16855.5(4)
Z	8
Density$_{calc}$ / g cm^{-3}	1.329
Crystal size / mm^3	0.25 x 0.25 x 0.35
Temperature / K	173
Range scanned θ / °	$2 \leq \theta \leq 25$
Index ranges	h: -11, 11 k: -18, 18, l: -21, 20
Dx / mm	52
No. of measured reflections	52369
No. of unique reflections	52369
No. of reflections with I > 2σ(I)	17507
R_{int}, R_σ	0.2275, 0.1381

Discussion

The syntheses and various chemical and physical properties of permethylated cyclodextrins [of which one of them is hexakis(2, 3, 6-tri-O-methyl)-α-cyclodextrin, referred to as TRIMEA], have been reported.[213,214,215] To date the CSD[82] documents thirteen TRIMEA structures, of which one is the hydrated form and three of these structures are redeterminations, thus making a total of ten unique TRIMEA structures. The unit cell parameters for these structures as well as those for METTMEA, are listed in Table 7.12. The CSD structures crystallise in the space groups $P2_1$, $P2_12_12_1$ and $C222_1$. The TRIMEA complex structure with metoprolol, is reported in this work by the author for the first time. Moreover, despite the fact that this complex crystallises in the monoclinic space group $P2_1$, it is the first TRIMEA complex structure to be reported with two crystallographically independent host molecules.

Table 7.12 Unit cell parameters of the known TRIMEA structures

Guest	a / Å	b / Å	c / Å	α / °	β / °	γ / °	CSD Refcode
CSD structures							
Space group$P2_1$							
benzaldehyde	11.604	23.832	13.593	90	106.11	90	BOHWUQ[216]
p-nitrophenol	11.307	14.578	22.118	90	93.62	90	BUDKEQ[222]
iodoacetic acid	11.590	23.285	13.901	90	106.98	90	BUPDIZ[217]
(S)-mandelic acid	13.123	23.187	13.113	90	107.19	90	CECMAY10[218]
(R)-mandelic acid	11.624	23.739	13.786	90	106.56	90	CECMEC[218]
(R)-1-phenylethanol	11.604	23.669	13.824	90	106.72	90	JEJWOK[219]
(S)-1-phenylethanol	11.586	23.641	13.762	90	106.45	90	JEJXAX[219]
metoprolol	13.523	23.472	22.560	90	98.06	90	This work
Space group $P2_12_12_1$							
(R)-1,7-dioxaspiro(5,5) undecane	14.636	21.637	23.450	90	90	90	QOYLEV[190]
none	15.424	18.167	23.128	90	90	90	TEVCEC[220]
Space group $C222_1$							
1,7-dioxaspiro(5,5) undecane	24.002	14.812	21.792	90	90	90	RACVIA[221]

Conformation of the host molecule

In general, the macrocyclic ring of permethylated cyclodextrins is remarkably distorted from the regular polygonal symmetry observed in the corresponding parent CDs, and the former have more conformational flexibility than the latter.[186,222] The reason for the distortion of the ring is the lack of O2•••O3' hydrogen bonds[186] that are responsible for the round structure of the parent molecules. Therefore it is expected that the stereo-selectivity of permethylated cyclodextrins in complex formation is higher than that of the parent cyclodextrins.[223] Hence a study of complex formation between TRIMEA and the racemic free bases, namely atenolol, oxprenolol and metoprolol was pursued. However, attempts to form complexes with atenolol and oxprenolol were unsuccessful and the only complex formed was that with the metoprolol free base reported.

Guest Inclusion

Metoprolol is one of the larger molecules to have been included within the TRIMEA cavity. Although the METTMEA complex crystallises in the monoclinic space group $P2_1$, common to some known TRIMEA complexes, its cell parameters are different from those of known complexes. Since the included guest molecule adopts an extended conformation, two independent TRIMEA host molecules are arranged in a head-to-tail fashion to accommodate the entire guest molecule. The phenyl ring is located at the interface between the secondary rim of the **CD(A)** molecule and the primary rim of the **CD(B)** molecule.

Chirality of the guest

The chirality of the metoprolol guest molecule at C9 atom was found to be (S-) and there was no sign of disorder, e.g. as two superimposed enantiomers. This indicated that there was resolution of the drug, at least for the chosen crystal. The study of the resolution of racemic compounds using cyclodextrins has been conducted.[194] Unlike the native CDs, the permethylated CDs have been found to be more suitable for chiral recognition due to the increased flexibility of the hosts, enabling them to change their conformation to accommodate a specific enantiomer. Due to time constraints, no further experiments were conducted in order to ascertain whether the selection of the (S)-enantiomer of the metoprolol guest molecule extended to the entire batch of crystals.

Crystal packing

The crystal packing of METTMEA is consistent with what is observed in TRIMEA complexes crystallising in the space group $P2_1$, i.e. head-to-tail packing of the host molecules down the c-axis. The two independent TRIMEA host molecules position themselves in such a way that the entire guest is encapsulated, which is a rare phenomenon for TRIMEA complexes.

DIMEB-Oxprenolol Complex

DMBOXP crystallises in a 1:1 host:guest ratio as shown by microanalysis. TGA also showed that this complex has $4.8H_2O$ water molecules per formula unit. The dissociation of the guest at 138-202°C before the decomposition of the host at ~ 370°C was also evidence of a 1:1 host:guest ratio. It crystallises in the monoclinic space group $P2_1$ with a = 20.56, b = 26.76, c = 30.64 Å, β = 90.07° and Z = 8 complex units per unit cell. Attempts to solve the structure were unsuccessful.

Chapter 8 – Novel Crystalline Form of TRIMEB

Permethylation of β-cyclodextrin [β-CD] in which the hydroxyl groups O2, O3 and O6 have been methylated results in a product called heptakis(2, 3, 6-tri-O-methyl)-β-cyclodextrin, referred to as TRIMEB. This substance is widely used as a solubilising agent and as host for the encapsulation of organic molecules,[194] including drugs.[224] The molecular structure of this substance is shown in Figure 8.1. To date there are several reported TRIMEB crystalline inclusion complexes.[191,201,225,226] In 1994 single crystals of the TRIMEB host were isolated as the monohydrate.[188] A second structure determination of this phase was subsequently reported.[227] TRIMEB monohydrate crystallises in the orthorhombic crystal system in space group $P2_12_12_1$. Methylated β-cyclodextrins show different physical properties in comparison to the corresponding native CDs. Methylated CDs are much more soluble and, as such, are potentially more useful in the pharmaceutical industry.[228] These substances show a negative temperature coefficient for their aqueous solubility.[229] As permethylated CDs are more distorted relative to the regular polygonal structures of the corresponding native CDs, they thus have unique properties of macromolecular recognition in comparison to their native counterparts.[223,230] In this study a new form of TRIMEB has been separately, and simultaneously, isolated by the author and by Miss Pam Dean[231] [Supramolecular Chemistry Research Unit (SCRU), UCT].

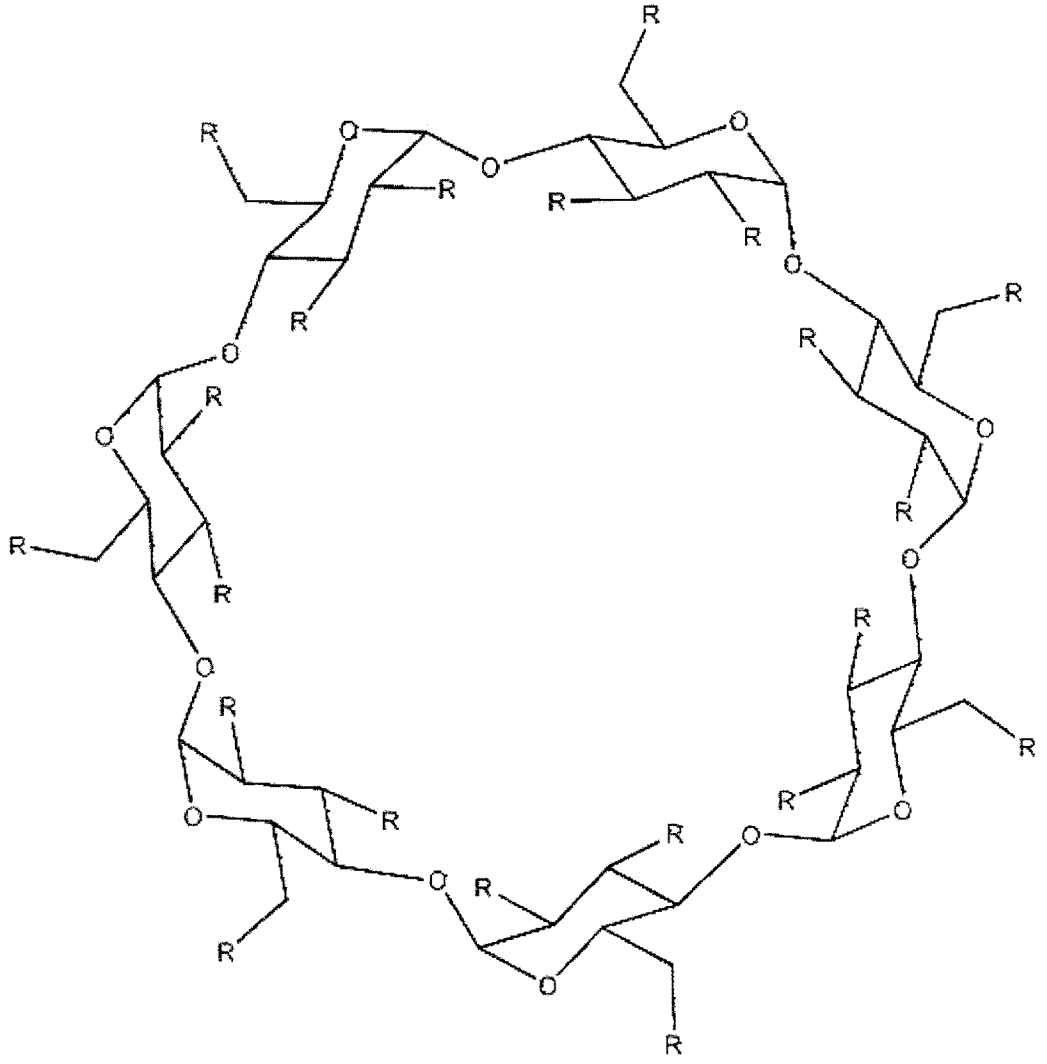

R = -OCH_3

Figure 8.1 The molecular structure of the host molecule TRIMEB.

Crystal Preparation

The attempt to prepare a new cyclodextrin complex between TRIMEB and the antihypertensive drug atenolol (4-[2-hydroxy-3-[(1-methylethyl)amino]propoxy] benzeneacetamide), either in the form of enantiopure (S)-atenolol or as the racemate resulted in a new crystalline form of TRIMEB. A slurry method was employed, in which 20 mg of atenolol and 100 mg of TRIMEB were stirred in 10 ml of water. The suspension was stirred in ice for 19 hours, filtered and placed in an oven set at 60°C. One large colourless crystal was obtained upon inspection after one month. This crystal

was then cut into smaller fragments. As described below, this species turned out to be a new crystalline form of TRIMEB, referred to hereinafter as NTMB.

Characterisation of the NTMB Form

Various analytical techniques such as microanalysis, thermal, infra-red, proton NMR, PXRD, and single crystal X-ray analysis, were utilised to characterise this new product in order to ascertain that there was no drug substance present in it.

Microanalysis

The water content is based on the result of thermogravimetric analysis. The molecular formula of the NTMB form is $C_{63}H_{112}O_{35}$•$2.9H_2O$. However, it should be noted that prior to microanalysis, TGA was performed on the NTMB crystals to dehydrate them. Therefore microanalysis was performed on the dehydrated material, referred to as DTMB. The experimental results and the calculated values for DTMB are presented in Table 8.1.

Table 8.1 C, H, N microanalysis results [n = 3] for DTMB

DTMB $C_{63}H_{112}O_{35}$	**Calculated**	**Experimental** [#]
% C	52.93	53.14
% H	7.90	7.86

[#] The error in experimental values is ± 0.25%

Thermal analysis

Hot Stage Microscopy (HSM)

HSM was used to analyse the thermal behaviour of the NTMB crystals upon heating at a constant rate of 10°C / min. The crystals were covered in silicone oil to detect the

presence of the included water more clearly. This would be indicated by bubble formation. The changes observed in the NTMB crystal upon heating are illustrated in Figure 8.2. The starting temperature of the analysis was 23°C. The first signs of bubbling, accompanied by the opacity of the crystals, were observed at 58°C. Bubbling continued up to 122°C. The NTMB crystal began to melt around 146-151°C.

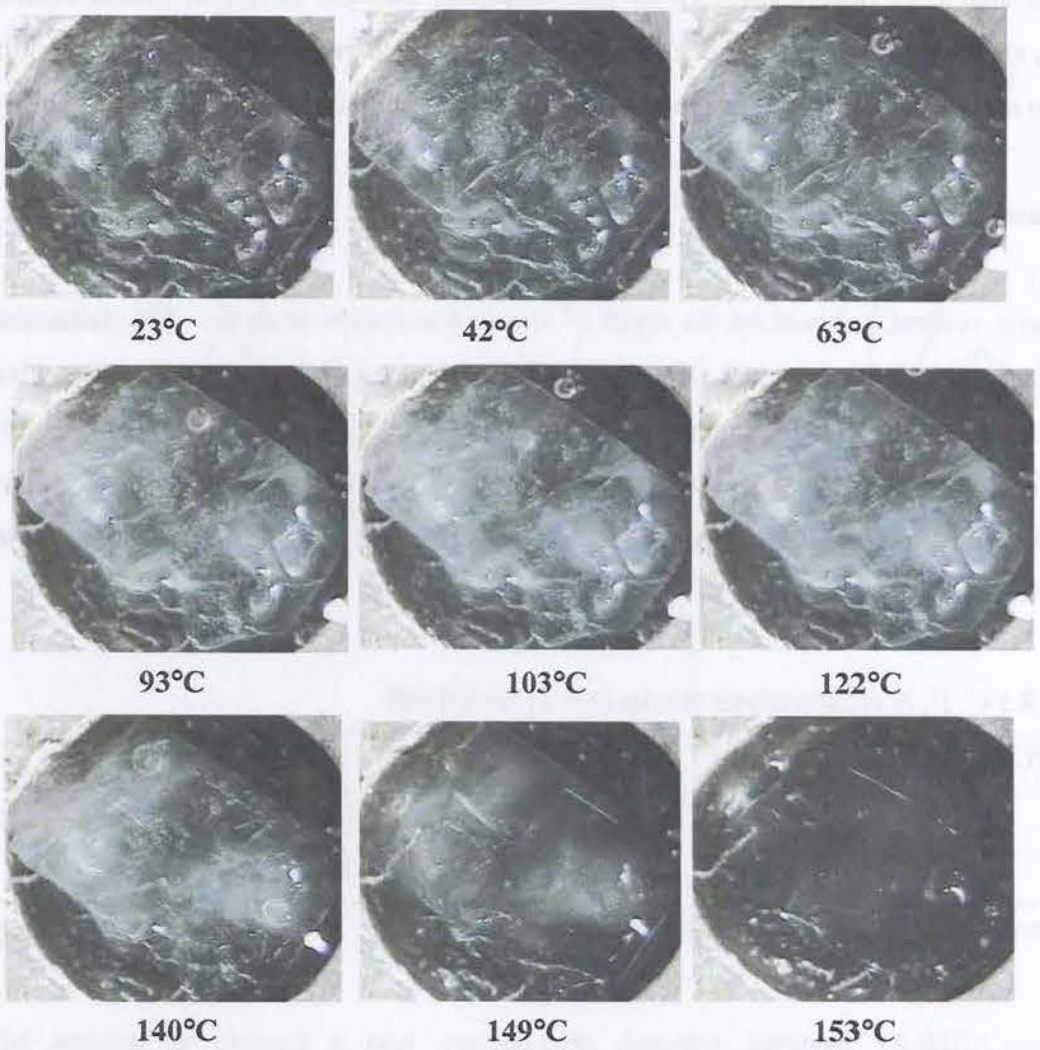

Figure 8.2 HSM photographs of the NTMB crystal upon heating under silicone oil.

Differential Scanning Calorimetry and Thermogravimetric Analysis

DSC and TGA analyses were performed on fresh crystals directly after removal from their mother liquor. TGA and DSC traces for NTMB are presented in Figure 8.3. The TGA trace [labelled A] shows a gradual weight loss of 3.3 ± 0.2% corresponding to 2.6-2.9 water molecules per TRIMEB molecule. A summary of the observed percentage weight loss as a function of temperature is presented in Table 8.2. Weight loss from 30 to 100°C represents water loss from the NTMB crystal. The DSC trace shows a very diffuse endotherm [labelled A] in the temperature range of the water loss, followed by fusion of the dehydrated NTMB [labelled B]. The DSC results are summarised in Table 8.3.

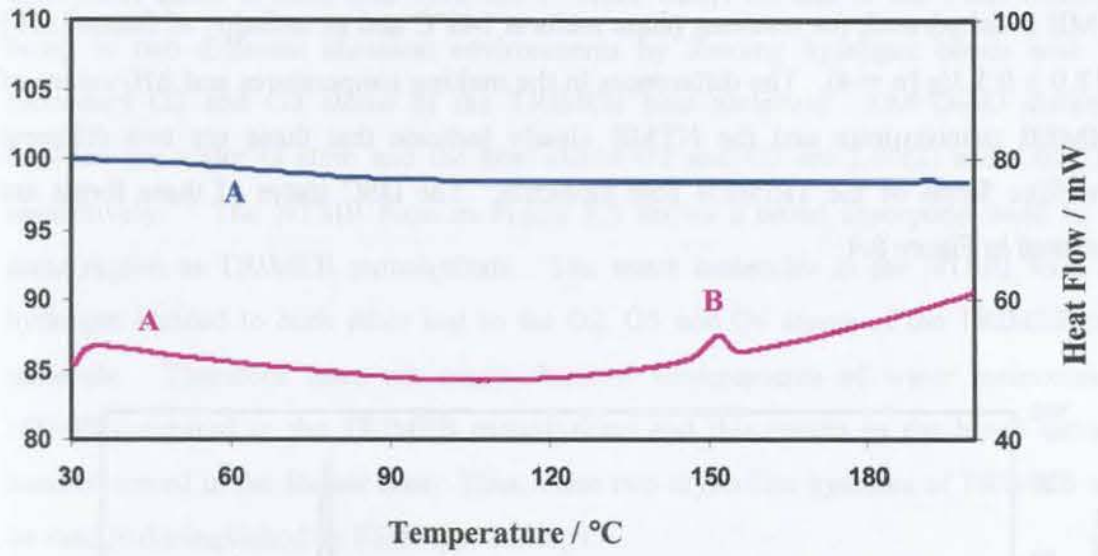

Figure 8.3 TGA [blue] and DSC [pink] traces for NTMB.

Table 8.2 TGA results [n = 3] summarised for NTMB

Temp (°C)	NTMB	
	% Mass	% Mass Loss
30	100	0
50	98.7	1.3
70	97.5	2.5
100	96.7	3.3
140	96.5	3.5

Table 8.3 DSC results summarised for NTMB

Endotherm	Parameter	NTMB
A	Temperature range (°C)	30-100
	T_{on} (°C)	35
	Peak (°C)	40
B	Temperature range (°C)	145-155
	T_{on} (°C)	148
	Peak (°C)	151

Following dehydration of TRIMEB monohydrate, the anhydrous phase melts at 157°C and its enthalpy of fusion [ΔH_f] is 39.1 ± 0.4 J/g [n = 4].[231] On the other hand, when NTMB is dehydrated, the resulting phase melts at 148°C and its enthalpy of fusion [ΔH_f] is 12.9 ± 0.5 J/g [n = 4]. The differences in the melting temperatures and ΔH_f values of TRIMEB monohydrate and the NTMB clearly indicate that these are two different crystalline forms of the TRIMEB host molecule. The DSC traces of these forms are presented in Figure 8.4.

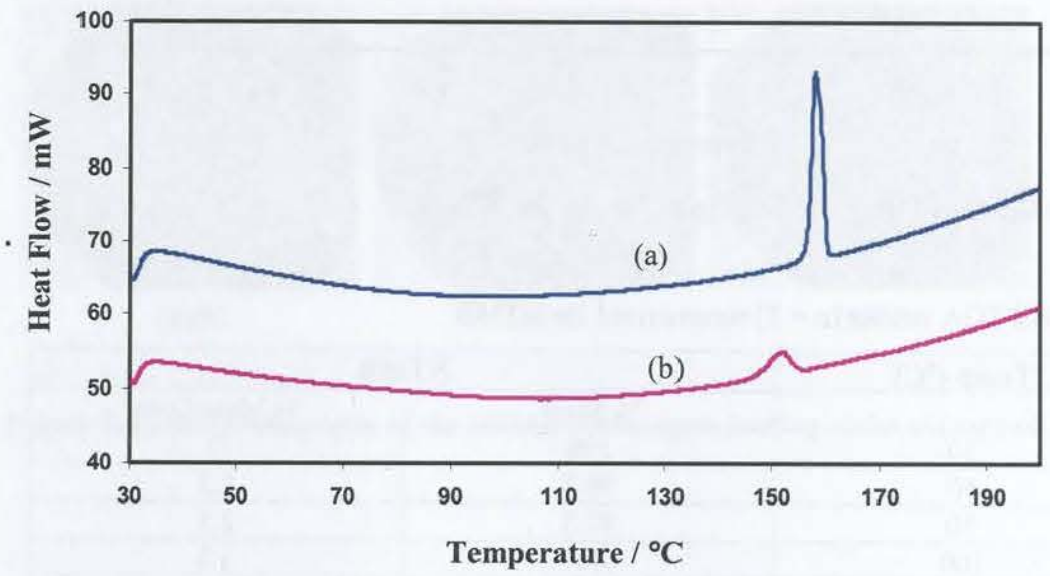

Figure 8.4 DSC traces for (a) TRIMEB monohydrate [blue] and (b) NTMB [pink].

Fourier Transform Infrared Spectroscopy (FTIR)

FTIR was used to determine whether there were any differences in the absorption bands between TRIMEB monohydrate and the NTMB form. Samples for FTIR spectroscopy were prepared as Nujol mulls. The IR-spectra for these two forms, including that of Nujol are shown in Figures 8.5 and 8.6.

In Figure 8.5 TRIMEB monohydrate has a sharp absorption band at 1638 cm^{-1} while the NTMB has a broad band in the same region. These bands correspond to the O-H bending vibration of water. In Figure 8.6 the O-H stretching vibrations of the included water for TRIMEB monohydrate and NTMB are shown. TRIMEB monohydrate has two absorption bands at 3508 and 3572 cm^{-1}. These bands are due to the water molecule being in two different chemical environments by forming hydrogen bonds with the secondary O2 and O3 atoms of the TRIMEB host molecule. The O•••O distances between the water O atom and the host atoms O2 and O3 are 2.80(2) and 3.03(2) Å respectively.[193] The NTMB form in Figure 8.6 shows a broad absorption band in the same region as TRIMEB monohydrate. The water molecules in the NTMB form are hydrogen bonded to each other and to the O2, O3 and O6 atoms of the TRIMEB host molecule. Therefore there are many chemical environments of water molecules in NTMB compared to the TRIMEB monohydrate and this results in the broad infrared band observed in the former case. Thus, these two crystalline hydrates of TRIMEB may be readily distinguished by FTIR spectroscopy.

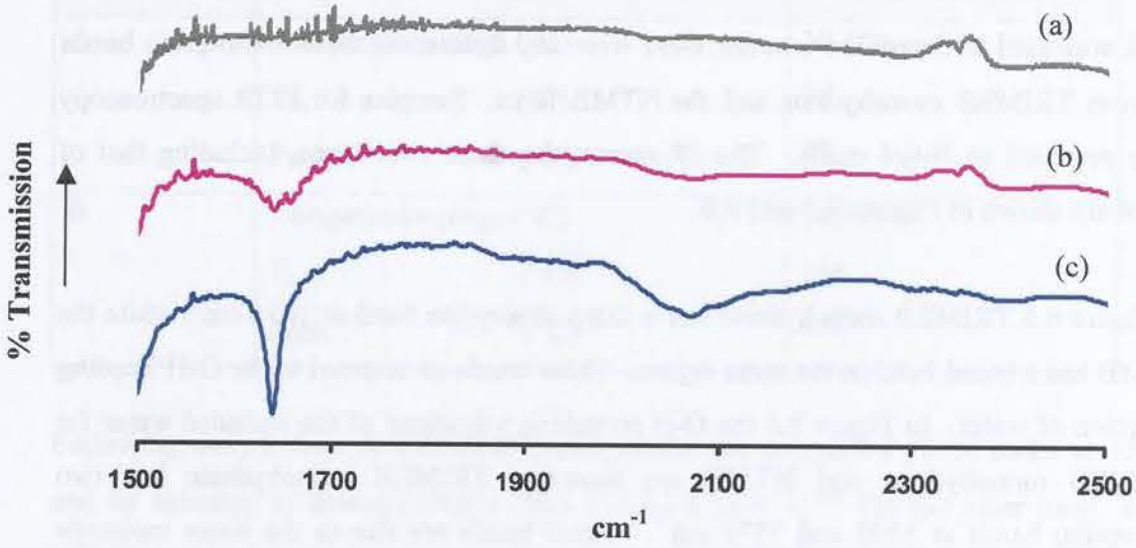

Figure 8.5 IR-spectra for (a) Nujol, (b) NTMB and (c) TRIMEB monohydrate in the frequency range 1500-2500 cm^{-1}.

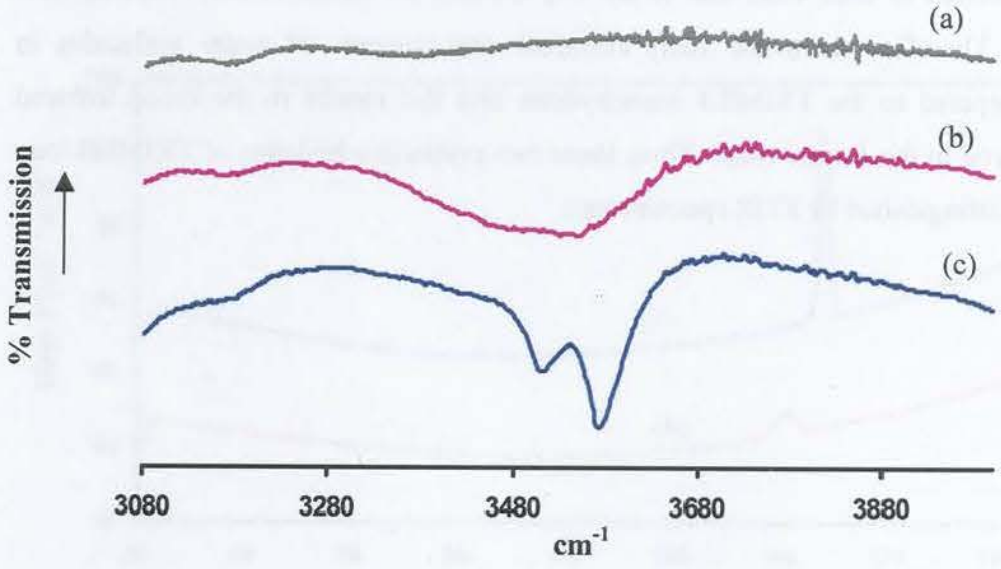

Figure 8.6 IR-spectra for (a) Nujol, (b) NTMB and (c) TRIMEB monohydrate in the frequency range 3080-3880 cm^{-1}.

Ultraviolet (UV) Spectroscopy

Since NTMB was isolated from a failed attempt to produce an inclusion complex between TRIMEB and atenolol, it was necessary to establish whether the crystals of NTMB contained any of the guest. Figure 8.7 presents the UV spectra for the NTMB form and atenolol. The UV absorption maxima of atenolol at 226 and 275 nm are in good agreement with those reported by Vesna Čaplar *et al.*[232] The NTMB form does not show any UV absorption spectra, indicating the absence of the drug atenolol in this product.

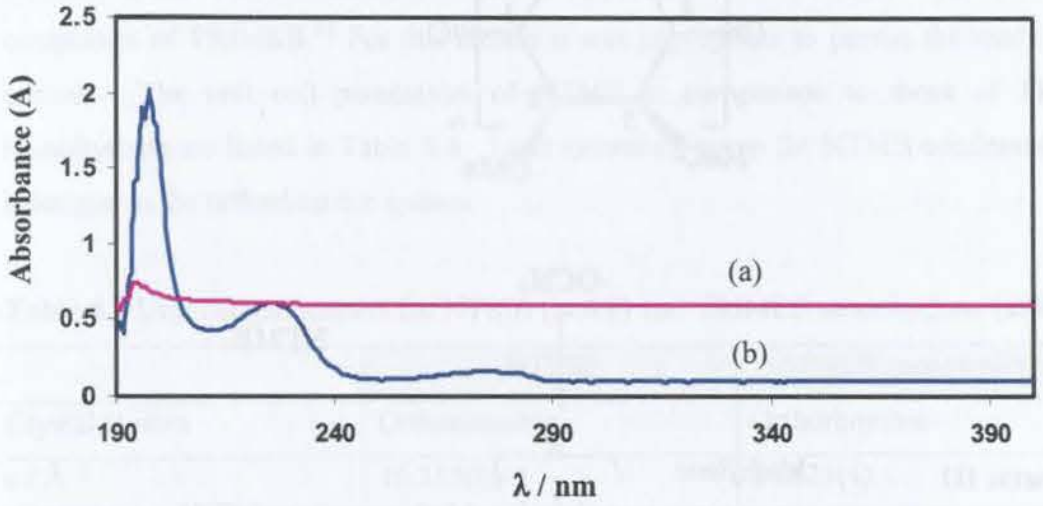

Figure 8.7 The UV spectra for (a) NTMB [pink] and atenolol [blue].

Proton Nuclear Magnetic Resonance (PNMR) Spectroscopy

The study of polymorphic substances in solution has no merit[233] since they show identical chemical properties. The aim of PNMR study of TRIMEB monohydrate and the NTMB form was to investigate whether or not they are chemically identical. The PNMR spectra for NTMB and TRIMEB monohydrate are presented in Figure 8.8. Proton NMR experiments were performed at 300 MHz with a Varian-Gemini 300 spectrometer. The ^{1}H NMR were recorded in D_2O solution at 295 ± 0.5 K. The doublet between 5.11 and 5.12 ppm is due to the tertiary anomeric H1 protons. The three methoxy protons

[-OCH_3], as a singlet, are located in the chemical shift range 3.18-3.40 ppm. The multiplets in the chemical shift range 3.65-3.82 ppm are due to the methylene protons [C6-H_2]. The doublet in the chemical shift range 3.16-3.18 ppm is due to the remaining tertiary [methine H2, H3, H4 and H5] protons. The two traces agree in all aspects and therefore chemical identity of the two crystals is established.

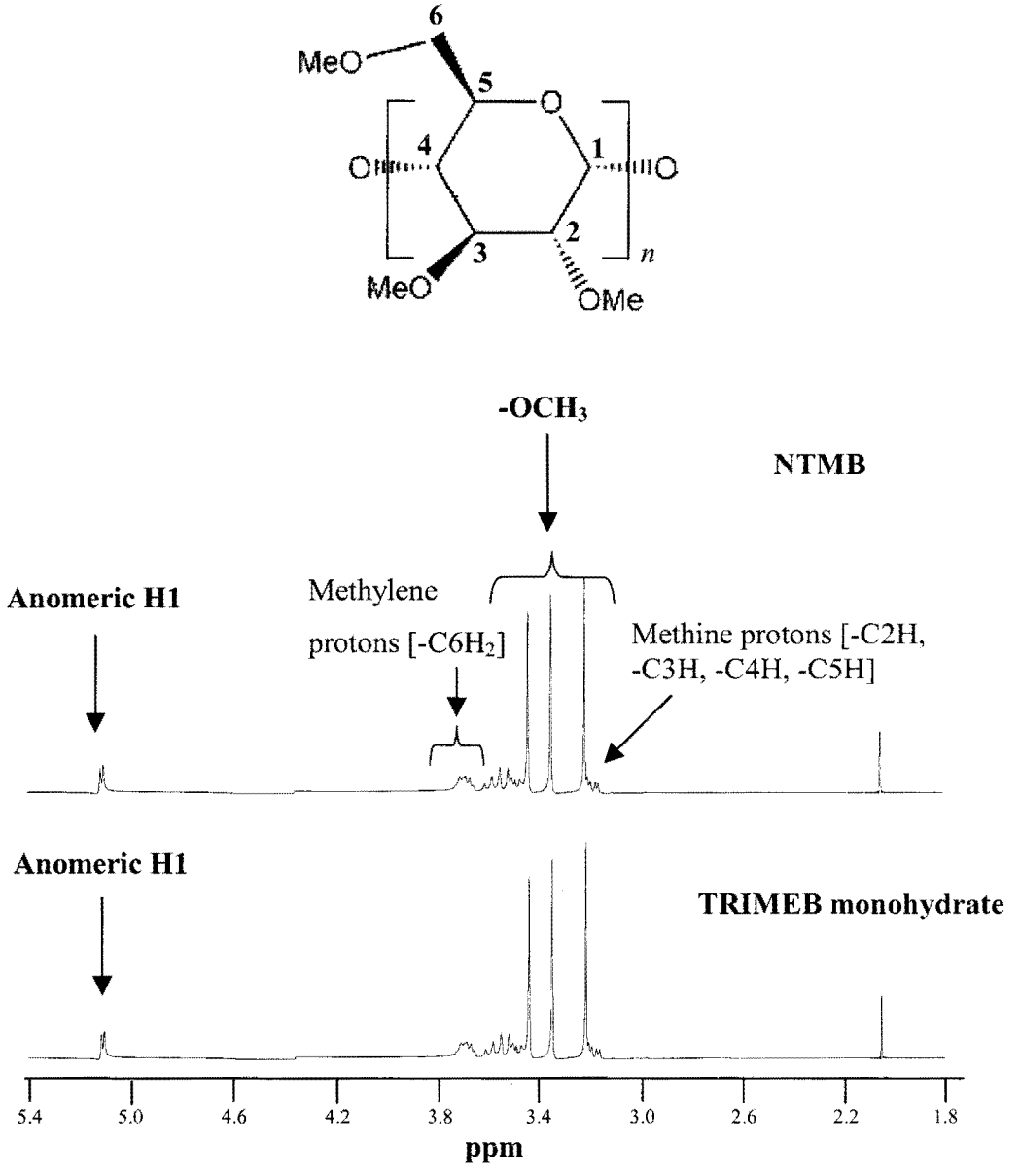

Figure 8.8 The PNMR spectra for NTMB and TRIMEB monohydrate.

X-ray Crystallographic Analysis of NTMB

Single Crystal X-ray Diffraction

Unit cell parameter determination

Unit cell parameter determination of the NTMB crystal was performed on a Nonius Kappa CCD diffractometer at room temperature. The measured unit cell parameters did not correspond with those of TRIMEB monohydrate nor with those of known inclusion complexes of TRIMEB.[82] For this reason it was appropriate to pursue the study of this species. The unit cell parameters of NTMB in comparison to those of TRIMEB monohydrate are listed in Table 8.4. Laue symmetry mmm for NTMB confirmed that it belonged to the orthorhombic system.

Table 8.4 Unit cell parameters for NTMB [at RT] and TRIMEB monohydrate [at RT]

	NTMB	TRIMEB monohydrate[188]
Crystal system	Orthorhombic	Orthorhombic
a / Å	16.215(1)	14.823(4)
b / Å	16.387(1)	19.382(9)
c / Å	30.099(1)	26.534(2)
Volume / Å^3	7997.8(1)	7623.2(2)
Z	4	4

Data-collection and space group determination

Diffraction intensity data for NTMB were collected on a Nonius Kappa CCD diffractometer at 193(2)K using graphite-monochromated MoKα radiation. A single crystal was mounted on a glass fibre and covered in Paratone N oil[115] to provide rigid mounting. The reflections were investigated with LAYER[112] and the systematic absences listed below indicated the space group $P2_12_12_1$.

hkl:	none
h00:	h = 2n + 1
0k0:	k = 2n + 1
00l:	l = 2n + 1

Structure solution and refinement

The structure was solved by SHELXD[117] *ab initio* methods and the positions of all the non-hydrogen atoms for NTMB were revealed in an E-map. Prior to the first refinement in SHELXL,[113] the O2, O3, O6 and C9 atoms for NTMB were deleted to account for any possibility of these atoms being disordered. The difference electron density map based on initial refinement in SHELXL[113] showed positions of most of these formerly deleted atoms. After further refinement it was found that the atom C7 on O2G6 was disordered over two positions. For a given pair on O2G6, a fixed U_{iso} of 0.08 Å^2 [the mean of U_{iso} for the chemically equivalent ordered atoms] was assigned and site-occupancy factors [s.o.f.'s] of x and 1-x were assigned, with x variable. After the refinement, the difference Fourier map showed positions of another disordered pair for C9 on O6G7. This pair was assigned a fixed U_{iso} of 0.12 Å^2 and the s.o.f.'s of y and 1-y, with y variable. The bond between atoms O6G7 and C97B was constrained as it was abnormally long. As the refinement proceeded, it was observed that the O6 atoms on C6G1 and C6G3 were disordered, leading to disorder in the corresponding C9 atoms. Two alternative positions were found for each disordered atom. The disordered pair on C6G1 was first refined and subsequently the disordered pair on C6G3 was refined. Prior to the refinement of these disordered atoms, a fixed U_{iso} of 0.07 Å^2 [the mean of U_{iso} for the chemically equivalent ordered atoms] was assigned and site-occupancy factors [s.o.f.'s] of z and 1-z were assigned, with z variable.

All the non-hydrogen atoms of NTMB except the disordered ones were refined anisotropically. This was followed by the placement of water oxygen atoms. Five positions were located for the water molecules. All the water oxygen atoms with s.o.f.'s less than one were assigned a fixed isotropic temperature factor of 0.12 Å^2 [the mean of

the preceding U_{iso} values] while the site-occupancies were allowed to vary. The total site occupancy summed to 2.9, in the expected range of 2.6-2.9, corresponding to the percentage weight loss of 3.3 ± 0.2% obtained from TGA analysis. The s.o.f.'s of the water molecules are presented in Table 8.5. The positions for most of the hydrogen atoms [except those of the water molecules] were revealed by the difference Fourier maps. All the hydrogen atoms were refined isotropically with temperature factors 1.2 times those of their parent atoms and the methyl hydrogen atoms with temperature factors 1.5 times those of their parent atoms. At the end of the refinement there were two electron density peaks with heights of 0.56 and 0.43 e $Å^{-3}$, the former being located at a distance of 1.1 Å from O3G4 and the latter at a distance of 3.0 Å from O61B. Crystal and refinement parameters for NTMB are presented in table 8.6.

Table 8.5 Site-occupancy factors for the water molecules of the NTMB structure

Molecule	s.o.f.
OW1	0.77
OW2	0.60
OW3	0.48
OW4A	0.66
OW4B	0.34

Table 8.6 Data collection and refinement parameters for NTMB at 193K

Formula unit	$C_{63}H_{112}O_{35}$•2.9H_2O
Formula weight / $gmol^{-1}$	1481.8
Crystal system	Orthorhombic
Space group	$P2_12_12_1$
a / Å	16.2051(1)
b / Å	16.2870(1)
c / Å	30.0989(3)
Volume / $Å^3$	7944.1(1)
Z	4
Density $_{calc}$ / gcm^{-3}	1.239
μ(MoKα) / mm^{-1}	0.102
F(000)	3196
Temperature of data collection / K	193(2)
Crystal size / mm^3	0.40 x 0.50 x 0.65
Range scanned θ / °	$3 \leq \theta \leq 28$
Index ranges	h: -21, 20 k: -20, 21 l: -38, 38
Dx / mm	56
Total no. of reflections collected	42815
Total no. of unique reflections	17741
No. of reflections with $I > 2\sigma$ (I)	13791
No. of parameters	896
R_{int}, R_σ	0.0330, 0.0426
S	1.02
R_1 (for 8420 reflections)	0.0631
No. of reflections omitted	33
wR_2	0.1756
$(\Delta / \sigma)_{mean}$	< 0.001
Weighting scheme	a = 0.0955 b = 2.5692
Δρ excursions / e $Å^{-3}$	0.61 and –0.43

Description of the structure

The asymmetric unit of the NTMB structure contains a single TRIMEB molecule and three water molecules located over five sites. The glucose units will be referred to as **G1**, **G2**, **G3**, **G4**, **G5**, **G6** and **G7** and the conformation and the numbering scheme of the NTMB structure are presented in Figure 8.9. The geomerical parameters used to describe the structural features of the CD host, as described in Chapter 1 are listed in Tables 8.7-8.9.

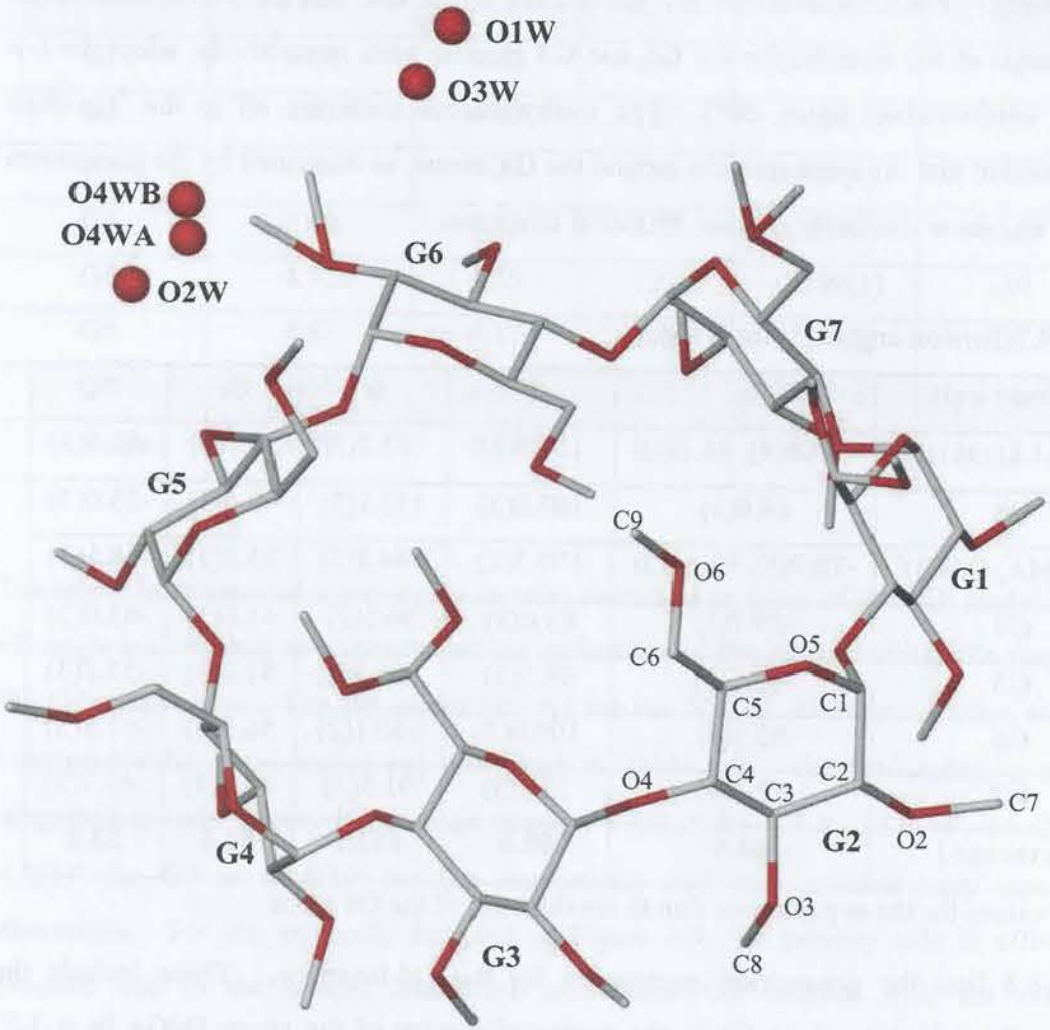

Figure 8.9 Macrocyclic structure and numbering scheme of NTMB with hydrogen atoms excluded, viewed from the primary rim.

Some of the principal torsion angles of the NTMB structure are listed in Table 8.7. The ω parameter indicates whether the direction of the C6-O6 bond is towards [positive] or away from [negative] the host cavity. In the NTMB structure, the C6-O6 bonds for glucose units **G2**, **G6** and **G7** adopt the (+)-*gauche* conformation [ω = +60°]. The C6-O6 bonds for the glucose units **G1** and **G3** are both in the (-)- and (+)-*gauche* conformations

as a result of the disorder of their O6 atoms. The (+)-*gauche* conformations describe the conformations of the minor components of the disorder for the **G1** and **G3** glucose units respectively. The C6-O6 bonds for the glucose units **G4**, **G5**, as well as the major components of the disorder for the **G1** and **G3** glucose units respectively, adopt the (-)-*gauche* conformation [ω = -60°]. The methylglucose units are all in the $^4C_1$ chair conformation and the conformation around the C4 atoms, as described by the parameters Θ_1 and Θ_2, show similarity to other TRIMEB structures.[138]

Table 8.7 Torsion angles [°] for NTMB

Glucose unit	ω	Φ	ψ	Θ_1	Θ_2
G1(O61A, O61B)*	-68.8(4), 48.1(8)	104.5(3)	143.2(3)	53.3(3)	-55.5(3)
G2	64.0(3)	107.0(3)	133.1(3)	49.6(3)	-53.0(3)
G3(O64A, O64B)*	-70.7(3), 43.4(12)	109.7(2)	144.2(2)	55.8(3)	-58.1(3)
G4	-79.7(3)	83.6(3)	96.2(2)	41.6(3)	-43.0(3)
G5	-71.7(3)	98.5(3)	166.3(2)	51.9(3)	-57.2(3)
G6	62.9(4)	109.0(3)	150.1(2)	56.3(3)	-61.8(3)
G7	72.1(4)	73.9(3)	91.3(3)	45.4(4)	-43.7(3)
| Average |	**64.6**	**98.0**	**132.1**	**50.6**	**53.2**

* Two values for the ω parameter due to the disorder of the O6 atom

Table 8.8 lists the geometrical parameters for the O4-heptagon. These include the O4G*n*•••Cg radii (**r**), where Cg is the centre of gravity of the seven O4G*n* [*n* = 1-7] atoms, the O4•••O4 distances (**l**), the O4•••O4'•••O4" angle (**a**), the deviations of each of the O4 atoms from the mean O4 plane (**d**) and the O4•••O4'•••O4"•••O4'" torsion angles (**t**). The extent of the ellipticity is measured by the seven 'radial' distances. For NTMB these radii span the narrower range 4.67-5.49 Å compared to the TRIMEB monohydrate range 3.41-5.94 Å.[193]

There are significant deviations of the individual O4 atoms from the O4 mean plane and these are indicated by the **d** and **t** parameters and are attributed to the tilt angles to be discussed shortly. The O4 angles (**a**) in the NTMB structure range from 112° to 136° and their average of 127° is close to the ideal value of 128.6° for a regular heptagon.

Table 8.8 O4-heptagon parameters for NTMB

Glucose unit	r / Å	l / Å	a / °	d / Å	t / °
G1	5.04	4.42	129	-0.178(1)	11
G2	4.82	4.47	127	-0.484(1)	-29
G3	4.81	4.24	136	0.467(1)	3
G4	5.49	4.41	112	0.369(1)	36
G5	4.72	4.55	129	-0.799(1)	-39
G6	4.67	4.17	135	0.178(2)	3
G7	5.36	4.43	118	0.448(2)	10
| Average |	**4.99**	**4.38**	**127**	**0.418**	**19**

Deviation from toroidal symmetry is usually described in terms of the 'tilt angle'.[62] The tilt angle is described as a measure of the inclination of the glucose units with respect to the O4 mean plane. The tilt angles [τ_1, τ_2] for the NTMB structure together with the intersaccharidic bond angles [φ] are listed in Table 8.9. The tilt angles, τ_1 and τ_2 magnitudes, span a very wide range, namely 1.1(1)° for **G7** to 53.0(4)° for **G6** and 4.3(1)° for **G7** to 66.5(1)° for **G6** respectively and this indicates very significant distortions. For the molecule depicted in Figure 8.9, the primary side is effectively blocked due to the unique orientation of residue **G6** coupled with the extended conformation of its side-chain C5 to C9. The large tilt angles observed for the NTMB structure are accounted for by the lack of O2•••O3' hydrogen bonds and steric strain.[189, 225,230] Six of the methyglucose units have positive tilt angles, those for **G4** being negative, indicating that the majority of the methylglucose units are tilted towards the inside of the cavity on the O6 primary side. The CPK space filling diagrams of the NTMB molecule are shown in Figure 8.10.

Table 8.9 φ and τ parameters for NTMB

Glucose unit	φ / °	τ_1 / °	τ_2 / °
G1	119.0(2)	16.9(1)	17.1(1)
G2	117.0(2)	27.7(1)	27.5(1)
G3	117.3(2)	34.9(1)	43.1(1)
G4	113.3(2)	-8.8(1)	-9.1(1)
G5	118.8(2)	43.2(1)	42.5(1)
G6	117.5(2)	53.0(4)	66.5(1)
G7	114.0(2)	1.1(1)	4.3(1)
| Average |	**116.7**	**26.5**	**30.0**

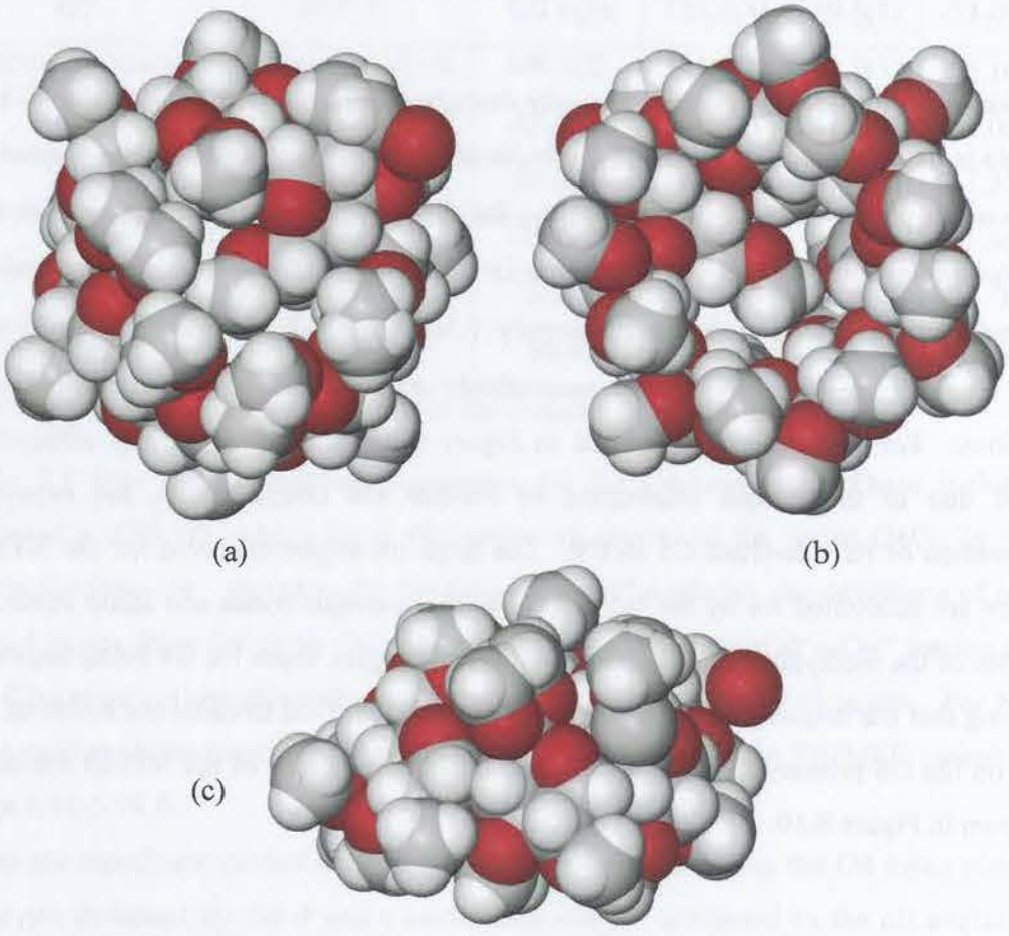

Figure 8.10 Space-filling diagram of the NTMB structure viewed from the (a) primary face, (b) secondary face and (c) side.

Hydrogen bonding interactions

Hydrogen bonding interactions for NTMB are listed in Table 8.10. These interactions, in addition to the known van der Waals and hydrophobic interactions, play a significant role in stabilising the NTMB structure.

Intramolecular host interactions

There are twelve intramolecular hydrogen bonds [Table 8.10], a common interaction found in carbohydrate crystal structures,[234] that stabilise the structure of NTMB. On the primary side of NTMB there are three C6-H•••O5' hydrogen bonds.

Host-host interactions

There are three host-host C-H•••O hydrogen bonds, namely C2G7-H07I•••O6G5, C9G2-H08G•••O2G7 and C4G7-H054•••O2G4, which are present in the NTMB structure. These bonds contribute to the stabilisation of the crystal structure and they connect the screw-related NTMB molecules.

Table 8.10 Hydrogen bonding interactions for NTMB

Interaction	H•••A / Å	D•••A / Å	D-H•••A / °	Symmetry code [#]
Intramolecular				
C6G2-H05A•••O5G3	2.34	3.25(4)	152	x, y, z
C7G2-H07G•••O3G1	2.59	3.19(5)	120	x, y, z
C8G3-H06G•••O2G3	2.58	3.15(4)	117	x, y, z
C1G4-H040•••O3G3	2.45	3.08(3)	120	x, y, z
C6G4-H06B•••O5G5	2.36	3.15(4)	136	x, y, z
C8G4-H07A•••O2G5	2.28	3.24(4)	166	x, y, z
C6G5-H06D•••O5G6	2.37	3.13(4)	133	x, y, z
C7G5-H08T•••O3G5	2.48	3.05(5)	117	x, y, z
C8G5-H08C•••O4G5	2.55	3.14(5)	119	x, y, z
C8G6-H09F•••O2G6	2.47	3.09(6)	121	x, y, z
C1G7-H066•••O3G6	2.34	3.04(4)	126	x, y, z
C8G7-H09A•••O2G1	2.53	3.21(6)	127	x, y, z
Host-host				
C2G7-H07I•••O6G5	2.59	3.43(5)	143	½-x, 1-y, ½+z
C9G2-H08G•••O2G7	2.60	3.43(4)	144	-½+x, 3/2-y, 1-z
C4G7-H054•••O2G4	2.59	3.58(4)	171	-½+x, 3/2-y, 1-z

[#] Symmetry code applied to second unit of interaction

Water interactions

Thermogravimetric analysis gave a percentage weight loss of 3.3% corresponding to the range of 2.6-2.9 water molecules per TRIMEB molecule. These water molecules are located outside the host cavity and are disordered over five sites. They are arranged in discontinuous channels parallel to the crystal b-axis where they are extensively hydrogen bonded to host oxygen atoms and to one another. Hydrogen bonding distances between the host and the water molecules, and between water molecules, are listed in Table 8.11.

Table 8.11 Hydrogen bonding distances involving the water molecules

Interaction	Distance / Å	Symmetry operator for the host oxygen atoms
Water-host		
OW1•••O3G1	2.87(1)	1/2-x, 2-y, -1/2+z
OW2•••O3G5	2.76(1)	x, y, z
OW2•••O2G6	3.22(1)	x, y, z
OW3•••O3G6	2.97(1)	x, y, z
OW3•••O2G2	3.15(1)	-½+x, 3/2-y, 1-z
OW3•••O3G2	3.23(1)	-½+x, 3/2-y, 1-z
OW4A•••O3G2	2.75(1)	½-x, 1-y, ½+z
OW4A•••O6G5	2.87(1)	x, y, z
OW4B•••O3G2	2.87(2)	½-x, 1-y, ½+z
Water-water		
OW2•••OW4B	2.85(2)	x, y, z

Crystal packing

The study of TRIMEB monohydrate showed that the collapsed structure of the uncomplexed TRIMEB molecule is due to the $^{1}C_4$ conformation adopted by the methylglucose unit **G2**.[195] This feature was interpreted as a response by the host molecule to minimise the hydrophobic cavity in the absence of a hydrophobic guest, thereby facilitating more efficient packing whilst avoiding accommodation of water molecules in a relatively hydrophobic environment.

In the NTMB form all the methylglucose units adopt the $^{4}C_1$ conformation; thus the structure of the uncomplexed TRIMEB molecule is not collapsed. Figure 8.11(a) and (b) and Figure 8.12 show three consecutive NTMB molecules viewed perpendicular to the a-axis. It is evident that the significant extent of self-inclusion (illustrated in Figures 8.11 and 8.12) is responsible for the host molecule retaining a relatively 'round' shape in the phase NTMB. This type of self-inclusion has also been observed in some DIMEB complexes[235] and in γ-CD hydrate.[65]

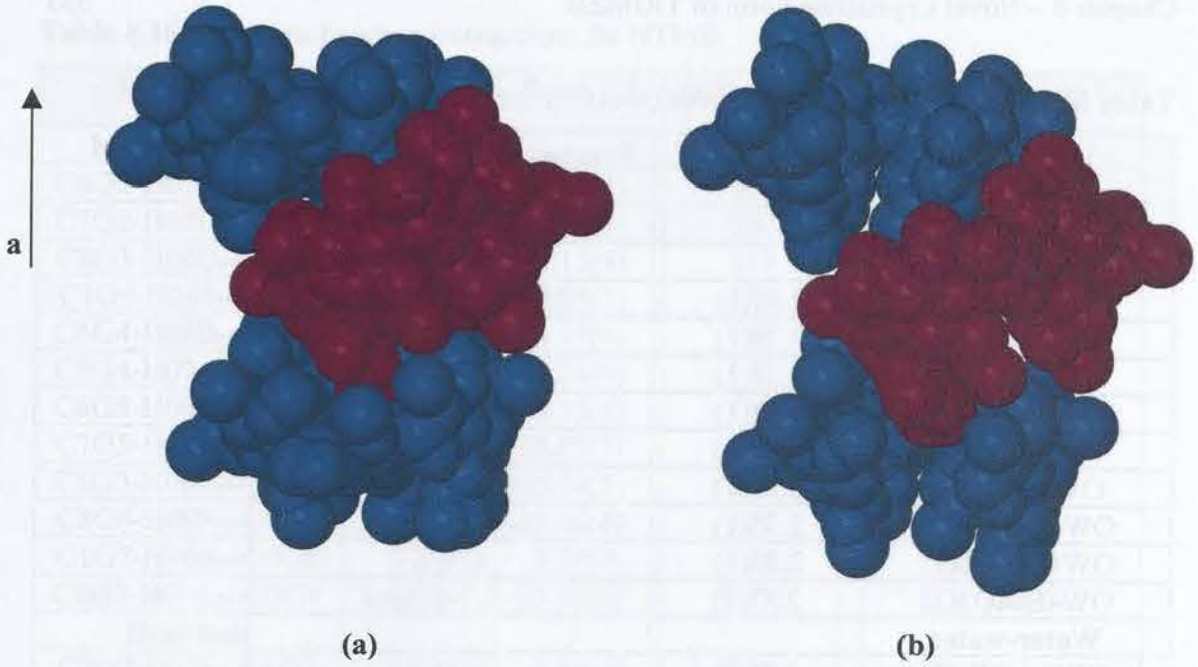

Figure 8.11 NTMB molecules viewed perpendicular to the a-axis with (a) CPK mode and (b) part of a host molecule removed to highlight the self-inclusion.

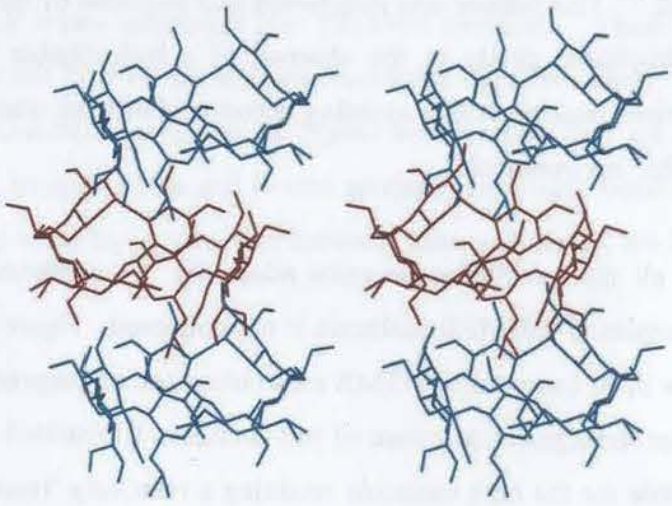

Figure 8.12 Stereo-view showing the self-inclusion referred to above.

The packing diagrams of the NTMB structure in Figure 8.13 show projections viewed down the a- and the b-axes. The NTMB molecules pack in a screw-channel mode in a head-to-tail fashion. The screw axis prohibits the existence of continuous channels.

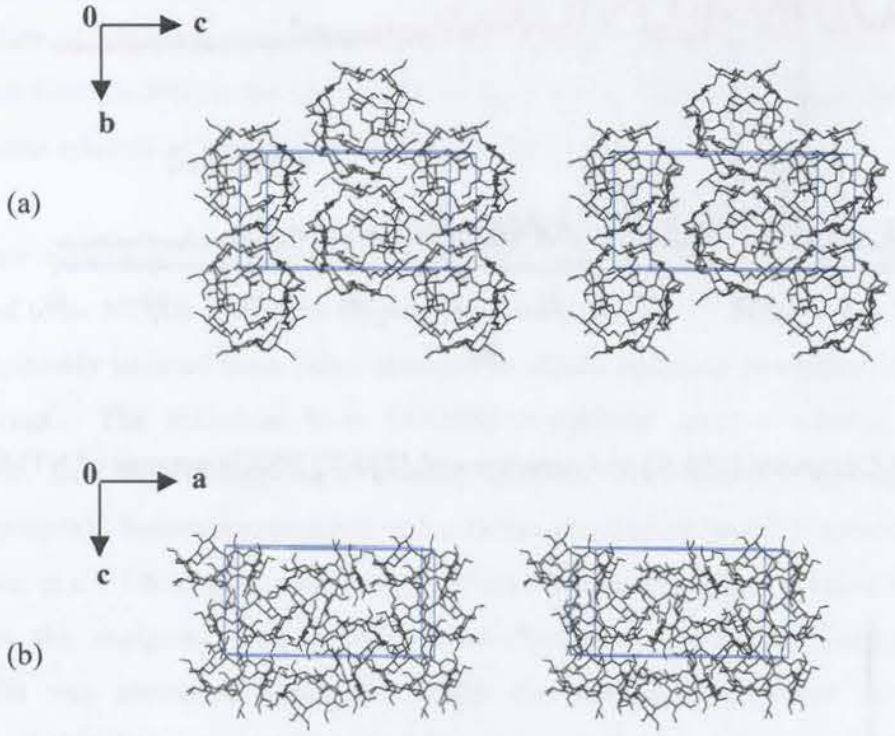

Figure 8.13 Stereo packing diagrams of NTMB down the (a) a- and (b) b-axes respectively.

Powder X-ray diffraction

The computed and experimental PXRD traces for NTMB are presented in Figure 8.14. The patterns match in their number of peaks as well as their profiles. The difference in temperatures at which the information for the traces was obtained resulted in the slight shift of the experimental trace to lower 2θ values. The lack of phase change on grinding is evidenced by the close agreement between these two traces. The computed PXRD trace of TRIMEB monohydrate in Figure 8.15 is readily distinguishable from that of NTMB.

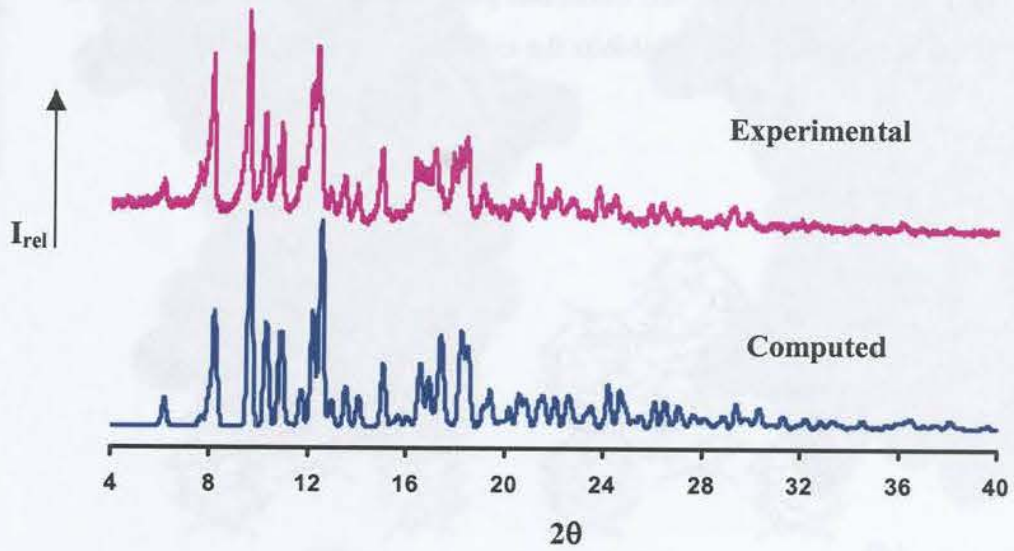

Figure 8.14 Computed [193 K] and experimental [295 K] PXRD patterns of NTMB.

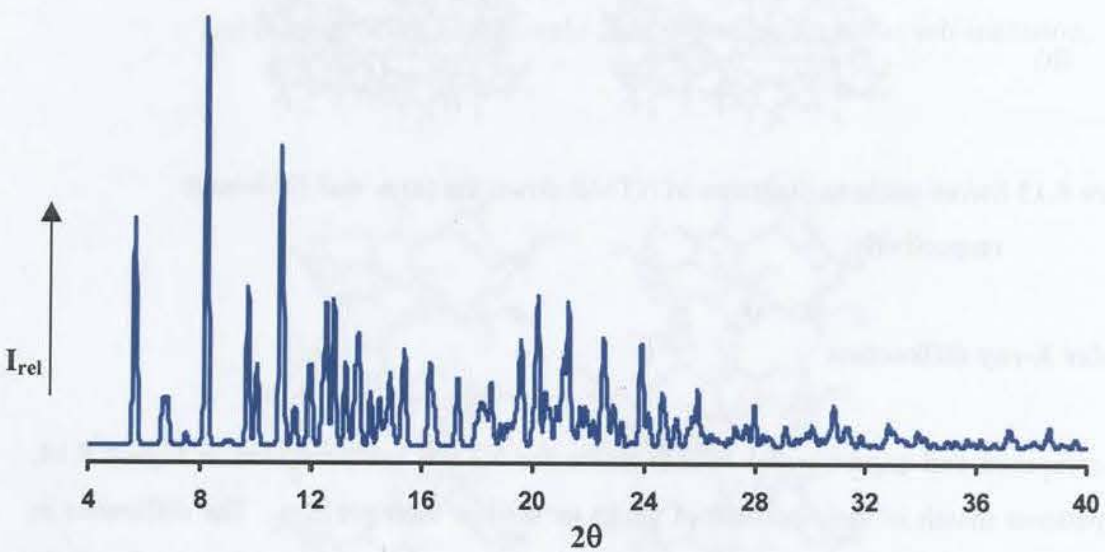

Figure 8.15 Computed [294 K] PXRD pattern of TRIMEB monohydrate.[188]

Discussion

Permethylated β-cyclodextrin [heptakis(2.3.6-tri-O-methyl)]-β- cyclodextrin, commonly known as TRIMEB, is widely used as a solubilising agent and as a host for the encapsulation of organic molecules,[194] including drugs.[224] The first crystal structural elucidation of TRIMEB monohydrate had been studied by the Supramolecular Chemistry Research Unit [SCRU] at the University of Cape Town. This form was crystallised from an aqueous solution of TRIMEB maintained at 50°C.[188]

Two new crystalline modifications of TRIMEB, namely, a trihydrate and an anhydrate [referred to as NTMB and TRIB respectively] were isolated.[205] Both crystal forms were serendipitously isolated from failed attempts to obtain inclusion complexes of TRIMEB with drugs. The trihydrate form [NTMB] crystallised from a solution containing TRIMEB and the antihypertensive drug atenolol (4-[2-hydroxy-3-[(1-methylethyl)-amino)propoxy] benzeneacetamide]), either in the enantiopure form (S)-atenolol or as the racemate, in a 1:1 host-guest molar ratio. When a similar experiment to obtain a complex between the analgesic drug bucetin (N-(4-ethoxyphenyl)-3-hydroxybutanamide) and TRIMEB was attempted, evidently NTMB also formed.[205] However, on prolonged heating, it dehydrated in a single crystal-to-single crystal transformation, producing the anhydrate TRIB. These new modifications of TRIMEB have unusually large crystals with round, rhombic prismatic habits, which contrast strongly with the flat elongated prisms of TRIMEB monohydrate. The shapes of TRIMEB monohydrate and NTMB are shown in Figure 8.16. In addition, the unit cell parameters for these crystal forms could not be reconciled with those of previous crystals containing the TRIMEB host molecule.

There is a trend for the formation of the NTMB form when drug substances of close structural likeness, e.g. atenolol and bucetin, are used as guests for complex formation with the TRIMEB host.

Figure 8.16 The comparison of the shapes of TRIMEB monohydrate [flat, elongated prism and NTMB [large pebble-shaped] crystals.

Conformation of the host

Dehydration of NTMB produced the anhydrate TRIB, whose host structure is practically isostructural with that of NTMB.[205] A comparison of the host conformations in these two phases follows.

All the methylglucose residues in NTMB and in TRIB adopt the $^4C_1$ chair conformation. Deviation from this occurs in TRIMEB monohydrate where one methylglucose residue is in the inverted $^1C_4$ conformation that results in the collapsed overall conformation.[188] The overall molecular conformation of NTMB closely resembles that of TRIB, but interestingly, there is molecular disorder in the former case [primary methoxy groups on **G1** and **G3**, each disordered over two positions]. An overlay of the host molecules in these crystals is presented in Figure 8.17. The host molecules are virtually superimposable with even the freely rotating methyl groups adopting similar conformations.

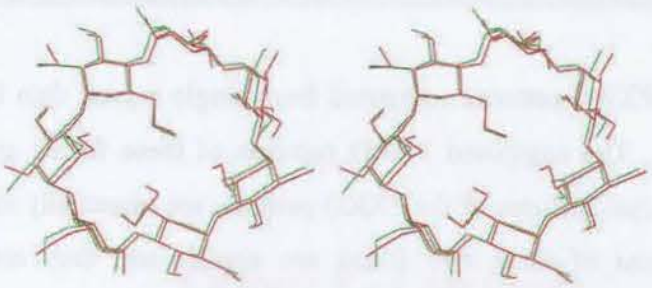

Figure 8.17 Stereo overlay of the TRIMEB hosts of NTMB [red] and TRIB [green].

Crystal packing

The crystal packing of NTMB is consistent with what is found in TRIB[205] and differs from the packing in TRIMEB monohydrate.[188] All these forms however, crystallise in the space group $P2_12_12_1$, i.e. head-to-tail packing of the host molecules parallel to the a-axis. The packing coefficients[236] for NTMB and TRIB are comparable at 67 and 64% respectively. Computation of the voids in NTMB yielded a total potential solvent volume[236] of only 51.5 $Å^3$ per unit cell [0.6%], whereas for TRIB, the void volume is 467.2 $Å^3$ (6.1%). The latter could accommodate ~ 3 water molecules per host molecule, which therefore implies that dehydration of NTMB leaves the crystal structure essentially intact but more porous than the NTMB phase. This was proven experimentally by performing cell parameter determination of the NTMB crystals freshly obtained from their mother liquor and after their dehydration. The comparison of the unit cell parameters between NTMB [crystals from the mother liquor] and TRIB [dehydrated crystals], is presented in Table 8.12.

Table 8.12 Unit cell parameters for the phases described in the text

Crystal	a / Å	b / Å	c / Å	Volume / $Å^3$
NTMB*	**16.205**	**16.287**	**30.099**	**7944.1**
TRIB#	**15.928**	**16.600**	**28.936**	**7652.7**

Dehydrated NTMB crystals

* Crystals from the mother liquor

Powder X-ray diffraction

Visual comparison of PXRD patterns computed from single crystal data for NTMB and TRIB was performed. The computed PXRD patterns of these forms are presented in Figure 8.18. The principal features of the PXRD patterns are essentially the same. Since the unit cell dimensions of these two forms are similar and they also show close similarity of the internal arrangement of their host molecules,[205] it is deduced that these two forms are isostructural. Thus, common atoms of the two structures have approximately the same co-ordinates.[75]

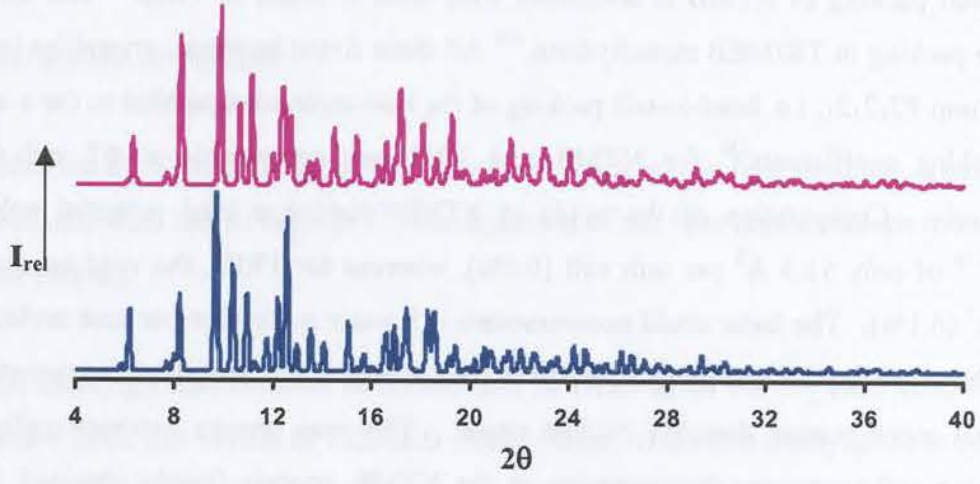

Figure 8.18 The computed patterns for NTMB [bottom] and TRIB [top].

Chapter 9 – Conclusion

In this study the racemic free bases of oxprenolol and metoprolol have been prepared from the commercially available salts oxprenolol hydrochloride and metoprolol tartrate respectively. The solid-state physicochemical properties of the forementioned substances, including atenolol were investigated in detail. Ten cyclodextrin inclusion complexes and a novel TRIMEB form have also been prepared. Various analytical techniques such as elemental analysis, thermal, X-ray diffraction and spectroscopic techniques were employed to identify and characterise these crystalline forms. This chapter will however highlight the novel discoveries made for metoprolol [the unsolvated and the solvated forms], phase transformations of the complexes formed between atenolol and oxprenolol with β-CD upon grinding, novel crystal form of the complex formed between metoprolol and TRIMEA, the TRIMEB- metoprolol complex, two different crystal forms of TRIMEB-oxprenolol complexes and finally the new TRIMEB host crystal structure.

Crystallisation of Racemic β-blocker Substances

The crystal forms of metoprolol tartrate salt, atenolol, metoprolol and oxprenolol free bases were prepared from different solvent systems. The main objective for employing these various solvents was to explore the possibility for each of these compounds to crystallise in more than one form. Two different crystal forms of metoprolol, namely Form I [unsolvated form] and Form II [solvated form] were prepared by recrystallisation from n-hexane at different temperatures.

Thermal analyses

Different thermal behaviours for the two forms of metoprolol were preliminarily assessed from hot stage microscopy [HSM]. Slight opacity of the crystals of Form II was observed at an elevated temperature indicating the loss of solvent.

TGA showed the mass loss of Form II confirming that it is a solvate and no mass loss for Form I indicating that it is a non-solvated form. DSC established that Form I and Form II

have different melting points. DSC analysis of Form II showed three thermal events, namely a phase transition from its original solvate form to another solvate form of different crystal structure, desolvation and fusion, while the DSC analysis of Form I showed a single thermal event [fusion].

TGA for metoprolol tartrate salt, atenolol and oxprenolol free bases indicated that they are all in the non-solvated form. DSC analysis of these substances showed only one thermal event [fusion].

X-ray diffraction

The crystal structures of two forms of metoprolol [Form I and Form II], atenolol, oxprenolol and metoprolol tartrate were successfully determined and they were reported in this work for the first time. The crystal structure of oxprenolol hydrochloride was not included in this work since it had been previously published.[28]

Single crystal X-ray diffraction revealed different asymmetric units for the two forms of metoprolol [Form I and Form II]. The asymmetric unit of Form I consists of one metoprolol molecule while the asymmetric unit of Form II consists of eight molecules of metoprolol and one included molecule of n-hexane. An O-H•••N intermolecular hydrogen bonding pattern is observed in Form II in which metoprolol molecules form a trimer.

Although Form I of metoprolol and oxprenolol crystallise in different space groups, there are similarities observed between the two species. The unit cell parameters of each are presented in Table 9.1 below. The shortest unit cell length of metoprolol is that of the b-axis while that of oxprenolol is the a-axis.

Table 9.1 Unit cell parameters of metoprolol [Form I] and oxprenolol

	Metoprolol	**Oxprenolol**
Formula unit	$C_{15}H_{25}NO_3$	$C_{15}H_{25}NO_3$
Crystal system	Monoclinic	Triclinic
Space group	$P2_1/n$	$P\bar{1}$
a / Å	16.1940(5)	4.9271(2)
b / Å	5.4409(2)	16.384(1)
c / Å	17.8670(7)	18.952(1)
α / °	90	81.437(1)
β / °	100.63(2)	87.091(1)
γ / °	90	83.707(2)
Volume / $Å^3$	1547.3(1)	1502.8(1)

Each crystal species [metoprolol and oxprenolol] contains two crystallographically distinct pairs of intermolecular hydrogen bonds, namely O-H•••N and N-H•••O with each distinct pair being related to another by a centre of inversion. The pyramidal geometry associated with N12 is pronounced. Thus the inversion-related metoprolol molecules are connected in the xz-plane by the N-H•••O hydrogen bonds and cohesion along the b-axis is effected by the O-H•••N hydrogen bonds, whereas for the oxprenolol molecule the O-H•••N hydrogen bonds are responsible for the crystal growth in the yz-plane while the N-H•••O hydrogen bonds are responsible for the crystal growth along the shortest axis, a.

Powder X-ray diffraction showed different patterns for Form I and Form II of metoprolol. The Form II crystals were unstable when taken out of their mother liquor; they became opaque within five minutes of exposure to air. Thus these crystals were ground while soaked in n-hexane and the experimental PXRD was performed.

Desolvation of Form II crystals was performed by maintaining them at 35°C for 1h. The resulting powder was of a very fine texture when compared to that of Form I. Texture of drug substances plays a very significant role in the pharmaceutical industry. The comparison of the PXRD patterns of Form I and the desolvated Form II showed that they

are identical, indicating that Form II upon desolvation transforms to the unsolvated Form I.

Phase Transformation of β-CD complexes

Two different forms of β-CD complexes with methyl paraben have been previously reported.[154] These forms were obtained at different temperatures. The first form, referred to as MPBCD was isolated at ambient temperature and crystallised in space group C2. The other form, referred to as MPBCD1 was isolated at 7°C and crystallised in space group P1 [intermediate packing arrangement (IM)] with unit cell parameters a ~ 18.0, b ~ 15.3, c ~ 15.4 Å, α ~ 104, β ~ 113 and γ ~ 99°. Based on thermal analysis it was discovered that MPBCD1 is more stable than the MPBCD form.

Inclusion complexes of atenolol and oxprenolol with β-CD, previously referred to as ATBCD and OXPRBCD respectively, crystallised in space group P1 [IM]. The experimental PXRD patterns for each of these complexes were different from their computed patterns. On comparison of the experimental patterns of ATBCD and OXPRBCD with those published by Caira[73] it was deduced that the former belongs to space group C2 while the latter belongs to space group $P2_1$. Phase transformation from one form to another occurred upon grinding single crystals of these complexes. Thus, in addition to employing temperature variation to effect crystallisation of different forms of a CD inclusion complex,[154] in the present work it has been discovered that mechanical grinding can also be used to generate new crystalline forms of such complexes.

Novel Crystal Form of the METTMEA Complex

Structure

The crystal structures of several TRIMEA complexes have been reported. These complexes crystallise in space groups $P2_1$, $P2_12_12_1$ and $C222_1$ with one guest molecule and one host molecule in the asymmetric unit. In this study SHELXD[117] was used to

solve the crystal structure of the complex formed between the host TRIMEA [permethylated α-CD] and the guest metoprolol, referred to as METTMEA. The METTMEA complex crystallises in space group $P2_1$ with two host molecules, one guest molecule and one water molecule in the asymmetric unit. The axis c (Å) and the angle β (°) are significantly different from those structures of TRIMEA complexes reported in the CSD.[82]

Elemental analysis indicated that the METTMEA complex uniquely crystallises with two host molecules and one guest molecule; this was also confirmed by the single crystal X-ray analysis of this complex. The two host molecules of the asymmetric unit are arranged in a head-to-tail fashion. The mean O4 planes of the host molecules are orientated at an angle of 2.01(3)° relative to each other. The geometries of the host molecules were mainly described in terms of their macrocyclic symmetries as defined by certain parameters of the O4-polygon as well as tilt angles of the individual glucopyranose units. The O4-polygon parameters included the radius of the polygon, the deviation of each O4 atom from the O4 atom mean plane as well as the distances, angles and torsion angles defined by adjacent O4 atoms. The macrocyclic symmetry of TRIMEA molecules deviates minimally from that of native α-CD molecules as a result of the lack of O2-H•••O3' and O3-H•••O2' hydrogen bonding. However the TRIMEA complex reported in this work was found not to be a member of any of the existing TRIMEA complex isostructural series.

Guest inclusion

The two TRIMEA host molecules are arranged in a head-to-tail mode such that the metoprolol molecule is fully buried within their cavities. The para-orientated side chains adopt a linear conformation; the phenyl ring of the guest is situated at the interface toward the secondary side of one host molecule. The longer side chain extends from the interface through the primary side of another TRIMEA host molecule into the host cavity. This host-guest interaction is stabilised not only by hydrophobic and van der Waals interactions but by a three-centre O10-H10•••O6B1 and O10-H10•••O6B6 hydrogen bonds in which bifurcated binding between the O10 atom of the metoprolol guest

molecule and atoms O6B1 and O6B6 of the TRIMEA host molecule occurs. Only the (S)-form of the metoprolol molecule is included. It has been reported that bifurcated hydrogen bonding can be utilised for the separation of racemic chiral compounds.[237]

Hydrogen bonding interactions

The lack of hydroxyl groups in TRIMEA means that strong hydrogen bonding interactions involving host atoms were precluded. Thus this complex contains only hydrogen bonds of the type C-H•••O. These bonds contribute to the stabilisation of the host conformation as well as the extended structure of the complex.

Crystal packing

The TRIMEA host molecules are stacked to form a head-to-tail channel-type structure. This channel type packing arrangement is consistent with other known TRIMEA complexes. The only major difference is that in this case there are two host molecules present and one guest molecule whereas in the known TRIMEA complexes there is one host molecule and one guest molecule involved.

TRIMEB-Metoprolol Complex [METTMB]

Crystal structure of METTMB – Data collected at various temperatures

A CSD[82] survey showed that TRIMEB complexes crystallise in the possible space groups $P2_1$ and $P2_12_12_1$ and in most cases guest molecules are successfully modelled. Data-collection of METTMB was performed at room temperature (because upon cooling the crystal deteriorated as previously discussed) and SHELXD was used to solve the structure. Elemental analysis indicated that this complex crystallises in 1:1 host-guest molar ratio. Although this complex crystallises in space group $P2_1$ with a = 21.46, b = 14.83, c = 27.51 Å, β = 97.97° and Z = 4, its unit cell parameters are different from those of other TRIMEB complexes that crystallise in the same space group. The asymmetric unit comprises two crystallographically independent host molecules and two guest

molecules. However due to the severe disorder, the metoprolol guest molecules could not be modelled.

The crystal structure for data collected at 173 K was similar to the one for data collected at room temperature; however the R_1 factor was higher for the former. A preliminary inspection of the intensity-weighted reciprocal lattice layers of METTMB at 173 and 293 K showed that the intensities of reflections hkl alternate between strong and weak, with strong reflections presented as follows: 0kl, 2kl, 4kl. This indicated that the unit cell contents in the interval x = 0 to x = 0.5 are approximately repeated in the interval x = 0.5 to x = 1.0.

The R_1 factor for data collected at 113 K for METTMB was significantly high. The intensity-weighted reciprocal lattice layer for the METTMB complex with these data did not show this alternation of intensities between weak and strong. The unit cell parameters of METTMB [113 K] are a = 10.34, b = 14.77, c = 27.35 Å, β = 98.43°, Z = 2, space group $P2_1$ and they are similar to those of the TRIMEB-butamben complex,[85] thus these two complexes are isostructural. For all data-collections of METTMB at various temperatures the metoprolol guest molecule could not be modelled due to its severe disorder. This is a very rare phenomenon for TRIMEB complexes.

Two Forms of the TRIMEB-Oxprenolol [OXPTMB] Complex

Crystal structures of the two forms of OXPTMB

Two different crystal forms of the TRIMEB-oxprenolol, previously referred to as OXPTMB(I) and OXPTMB(II), were isolated by employing different crystallisation methods. The former was obtained by employing the co-solvent method in which oxprenolol was dissolved in a small volume of methanol and the resulting solution was slowly added to the TRIMEB solution while the latter was obtained by preparing a slurry using equimolar amounts of TRIMEB and oxprenolol at room temperature. Elemental

analysis indicated a 1:1 host-guest molar ratio for OXPTMB(I) and a 2:1 host-guest molar ratio for OXPTMB(II).

The isomorphous replacement technique proved to be useful for the structure solution of the OXPTMB(I) complex while OXPTMB(II) was solved by SHELXD.[210] Crystal structure solution of these complexes provided unambiguous confirmation of complex formation and detailed information regarding the stoichiometry, mode of inclusion and host-guest interactions.

Description of the structure of OXPTMB(I)

OXPTMB(I) crystallises in space group $P2_12_12_1$ and its unit cell parameters [a = 14.60, b = 21.78, c = 28.16 Å and Z = 4] are similar to those of CAMPIP,[186] and upon refinement it was found that these two complexes are isostructural. The geometrical parameters of the TRIMEB host in this complex are similar to those of other TRIMEB complexes that crystallise in the same space group.[138,186]

The insertion of the oxprenolol guest molecule in OXPTMB(I) is similar to that observed for the inclusion of the naproxen and (S)-ibuprofen molecules in the TRIMEB host cavity.[156,238] The oxprenolol guest molecule is inserted into the cyclodextrin cavity through its hydrophobic phenyl ring moiety from the secondary rim of the host molecule. The side chains of the guest molecule extend along the secondary side of the TRIMEB host molecule to the outside of the cavity. The configuration at the chiral centre C9 of the included oxprenolol molecule is (R-).

The crystal packing of OXPTMB(I) is based on a screw-channel mode and the TRIMEB host molecules are arranged in a head-to-tail fashion similar to the packing modes of naproxen and (S)-ibuprofen-TRIMEB complexes.[156,195] It was observed from the crystal packing diagrams that there were no inter-guest interactions and that the two guest ortho-side chains do not protrude into the cavities of neighbouring host molecules.

Description of the structure of OXPTMB(II)

Several TRIMEB inclusion complexes e.g. those with indole-3-butyric acid, 2,4-dichlorophenoxyacetic acid,[239] 1-(p-bromophenyl) ethanol,[240] butamben,[85] (E)-ajoene[86] and 4-chlorophenoxyacetic acetic acid (4CPA),[241] have been previously reported to crystallise in space group $P2_1$. OXPTMB(II), which has been studied by the author, also crystallises in this space group. Apart from the different unit cell parameters of this complex when compared to the forementioned ones, the uniqueness of this complex is that its asymmetric unit comprises two crystallographically independent TRIMEB host molecules [arranged in a head-to-head fashion] and one guest molecule. This was initially indicated by elemental analysis and confirmed by X-ray analysis. The asymmetric unit of the TRIMEB complex reported by Tsorteki *et al*[241] comprises two complexes in 1:1 host-guest molar ratio.

All methylglucose residues adopt the $^4C_1$ chair conformation except one methylglucose unit with an unusual $^0S_2$ skew boat conformation and the host shows markedly distorted macrocyclic conformation. This type of conformation was first observed for the inclusion complex formed between the TRIMEB host molecule and the guest molecule m-iodophenol.[187]

The oxprenolol molecule is fully buried inside the TRIMEB host cavities. The conformation of the included oxprenolol guest molecule is such that the ortho-side chains form an L-shape relative to each other, with the shorter side chain extending along the secondary face of one host molecule to the outside of the host cavity. The longer side chain extends along the interface between the two TRIMEB host molecules through the secondary face of another TRIMEB host molecule to the host cavity. The crystal packing of OXPTMB(II) is unique. TRIMEB molecules in OXPTMB pack in a screw-channel mode in a tail-to-tail fashion. The O4 heptagon mean planes for the two independent host molecules are parallel to the xy-plane with the cavity axes of the CDs parallel to the c-axis. The oxprenolol guest molecule fully occupies the cavities of the CD host molecules and it does not protrude into the cavities of the neighbouring TRIMEB host molecules.

Therefore OXPTMB(II) is the first structure with two crystallographically independent TRIMEB host molecules and one included guest to be reported.

Novel Crystalline Forms of the Host TRIMEB

Heptakis(2,3,6-tri-O-methyl)-β-cyclodextrin, referred to as TRIMEB is a product formed upon methylation of the O2, O3 and O6 hydroxyl groups of the parent β-cyclodextrin host molecule. In 1994 single crystals of the TRIMEB host were isolated as the monohydrate from an aqueous solution of TRIMEB maintained at 50°C.[188] A second structure determination of this phase was subsequently reported.[242] This was the only form of TRIMEB encountered so far in cyclodextrin solid-state chemistry. TRIMEB monohydrate will be referred to hereinafter as Form I in view of recent isolation of two new crystalline modifications of TRIMEB.

A failed attempt to form an inclusion complex between TRIMEB and the antihypertensive drug atenolol (4-[2-hydroxy-3[(1-methylethyl)amino)propoxy] benzeneacetamide, either in the form of enantiopure (S)-atenolol or as the racemate, in a 1:1 host-guest molar ratio resulted in a new crystalline modification of TRIMEB, namely a trihydrate previously referred to as NTMB. Another failed attempt by Pam Dean [a former student in our laboratory] to form an inclusion complex from a solution containing TRIMEB and the analgesic drug bucetin (N-(4-ethoxyphenyl)-3-hydroxybutanamide) in a 1:1 molar ratio resulted in another crystalline modification of TRIMEB, an anhydrate, referred to as TRIB.[205] A prolonged heating of NTMB in which its dehydration occurred resulted in a single crystal-to-single crystal transformation producing TRIB. These new modifications of TRIMEB have unusually large crystals with round, rhombic prismatic habits, which contrast strongly with the flat elongated prisms of Form I. It was concluded that an attempt to form an inclusion complex between TRIMEB and drug substances of close structural likeness, e.g. atenolol and bucetin, used as guests, results in NTMB.

Description of Crystal Structures

All crystal forms of the TRIMEB molecule crystallise in the orthorhombic crystal system and space group $P2_12_12_1$. However the unit cell parameters of Form I are different from those of NTMB and TRIB. The volume of the asymmetric unit of Form I is significantly smaller than that of NTMB and similar to that of TRIB. The Table below lists the unit cell parameters of these forms.

Table 9.2 Unit cell parameters of Form I, Form II and Form III of TRIMEB

	a (Å)	b (Å)	c (Å)	V (Å^3)
Form I	14.818(4)	19.362(9)	26.51(2)	7606(6)
NTMB	16.2051(1)	16.2870(1)	30.0989(3)	7944.1(1)
TRIB	15.951(1)	16.577(1)	28.941(2)	7652.69(5)

The geometries of the host in NTMB and TRIB, which were mainly described in terms of their macrocyclic symmetries as defined by certain parameters of the O4-polygon as well as the tilt angles of the individual glucopyranose units are similar to each other but they are significantly different from the host geometry in Form I. In Form I six methylglucose residues are in the $^4C_1$ chair conformation and the remaining methylglucose unit adopts the most unusual inverted $^1C_4$ conformation. The collapsed structure of Form I because of the inversion of one methylglucose unit minimises the hydrophobic cavity in the absence of a hydrophobic guest. This also facilitates more efficient packing whilst avoiding accommodation of water molecules in a relatively hydrophobic environment.[188] All methylglucose residues in NTMB and TRIB adopt $^4C_1$ chair conformation, thus the TRIMEB structure in these two forms is not collapsed. The crystal packing of NTMB is consistent with what is found in TRIB and differs from the packing in Form I. The significant extent of self-inclusion in these two forms is responsible for the host molecule retaining their relatively 'round' shape. However the TRIMEB host molecules in all three forms are packed in a head-to-tail mode parallel to the a-axis. The principal features of the PXRD patterns for NTMB and TRIB are essentially the same. Since the unit cell dimensions of these two forms are similar and they also show close similarity of

the internal arrangement of their host molecules,[205] it is deduced that these two forms are isostructural. Thus, common atoms of the two structures have approximately the same co-ordinates.[75]

Final remarks

In the pharmaceutical industry, there is ever-increasing interest in the production of novel solid forms of drugs, be they established medicinal agents or new drug candidates. In this study, atenolol, metoprolol and oxprenolol were selected in an attempt to produce novel forms of these potent β-blockers that could have potential for further pharmaceutical development. These drugs displayed little tendency towards polymorphism and solvate formation under the conditions employed. The second method chosen for generating new entities was supramolecular modification *via* inclusion of these molecules in cyclodextrins, as CD-drug complexes are frequently reported to display significant advantages in delivery when compared to uncomplexed drugs. This study amply demonstrated the feasibility of producing such inclusion complexes by various methods. Furthermore, the complexes thus obtained were thoroughly characterized with respect to their chemical compositions, molecular and crystal structures, and thermal stabilities, providing information that is of great utility for their possible future formulation as alternatives to existing preparations.

In the process of investigating CD inclusion, several other significant findings emerged; these included previously unknown modes of guest inclusion, the serendipitous crystallization of novel forms of the CD host TRIMEB, and unexpected phase transformations of certain CD inclusion complexes resulting from mechanical grinding. These findings can therefore also be considered useful contributions to the field of cyclodextrin chemistry. Possible avenues for further investigation were identified and are summarised below.

Possible extension of the present study:

- The dissolution rate measurements for the inclusion complexes formed between atenolol, metoprolol and oxprenolol with cyclodextrins should be performed to compare their degree of enhanced solubility as compared to the uncomplexed drug substances.
- The phase transformation of the ATBCD and OXPRBCD crystals, upon grinding for recording the experimental PXRD patterns, from P1 [intermediate packing arrangement (IM)] to C2 and $P2_1$ respectively warrants further study. The ground materials should be recrystallised, and their unit cell parameters determined to observe whether or not they transform to their original crystal forms.
- The relationship between NTMB and TRIB, with respect to possible interconversion, should be investigated in detail.

References

References

---

1. J-M. Lehn, *Angew. Chem., Int. Ed. Engl.* (Nobel lecture), **27**, 89, **1988**.
2. H. Davy, *Philos. Trans. R. Soc.* London, **1**, 101, **1811**.
3. C. Rustichelli, G. Gamberini, V. Ferioli, M. C. Gamberini, R. Ficarra, S. Tommasini, *J. Pharm. Biomed. Anal.*, **23**, 41-54, **2000**.
4. L. Borka, J. K. Haleblian, *Acta pharm. Jugosl.*, **40**, 71-94, **1990**.
5. P. Corradini, *Chem. Ind. (Milan)*, **55**, 122-129, **1973**.
6. J. Bernstein, Polymorphism in Molecular Crystals – IUCr monographs on Crystallography, No. 14, Clarendon Press, Oxford, 4-5, **2002**.
7. H. P. Klug, L. E. Alexander, *X-ray diffraction procedures for polycrystalline and amorphous materials*. John Wiley and Sons, New York, 117, 253, 254, **1974**.
8. Y. Lian, S. M. Reutzel, G. A. Stephenson, *Pharm. Sci. Technol. To.*, **1**, 118-127, **1998**.
9. E. Mitscherlich, *Abhl. Akad. Berlin*, 43-48, **1822**.
10. G. B. Amici, *Ann. Chim. Phys., Ser. 3*, **12**, 114-120, **1844**.
11. E. Mallard, *Annales Mines*, **10**, 60-196, **1876**.
12. O. Lehmann, *Die Krystallanalyse oder die chemische Analyse durch Beobachtung der Krystallbildung mit Hülfe des Mikroskps*, Wilhelm Engelmann, Leipzig, 22, 23, 95, **1891**.
13. W. F. Ostwald, *Z. Phys. Chem.*, **22**, 289-330, **1897**.
14. G. Tammann, *Kristallisieren und Schemelzen*, Verlag von Johann Ambrosius Barth, Leipzig, **1903**.
15. K. K. Nass, Process implication of polymorphism in organic compounds. In *A. I. Che. E Symp. Ser.* No. 284, **1991**.
16. N. Garti, K. Sato, *Crystallisation and polymorphism of fats and fatty acids*, Marcel Dekker, Inc., New York, USA, **1988**.
17. Y. Matsuda, *J P Forum 2*, 38-53, **1993**.
18. T. Yoshikawa, T. Umeda, K. Kuroda, T. Kuroda, S. Asada, *Chem. Pharm. Bull.*, **29**, 194-199, **1981**.
19. M. Audran, Y. Lasserre, J. Rambaud, B. Pauvert, G. Berge, L. Maury, *Pharm. Acta*

Helv., **63**, 343-346, **1988**.

20. M. Otsuka, T. Matsumoto, N. Kaneniwa, *J. Pharm. Pharmacol.*, **41**, 665-669, **1989**.
21. R. J. Roberts, R. C. Rowe, *Int. J. Pharm.*, **129**, 79-94, **1996**.
22. K. Knapman, *Modern Drug Discovery*, **3**, 57, **2000**.
23. K. Stoschitzky, G. Zernig, W. Lindner, *J. Clin. Bas. Cardiol.*, **1**, 14-18, **1998**.
24. U. Thadani, C. Davidson, W. Singleton, S. H. Taylor, *Am. J. Med.*, **68**, 243, **1980**.
25. B. Magani, B. Mantovani, M. Brancaleoni, S. Gubelli, *Drugs*, **25**, 166. **1983**.
26. A. Mitrani, M. Oettinger, E. G. Alunader, M. Sharf, A. Klein, *Br. Obstet. Gynaecol.*, **82**, 651, **1975**.
27. C. M. E. Krogh (Editor), *Compendium of Pharmaceuticals and Specialties, 27th ed.*, Canadian Pharmaceutical Association, Ottawa, 1173-1174, **1992**.
28. J. M. Leger, M. Gadret, A. Carpy, *Acta Cryst.*, **B33**, 2156-2159, **1977**.
29. A. M. Barrett, R. Hull, D. J. LeCount, C. J. Squire, J. Carter (ICI Ltd.), *Ger. Offen.*, **73**, 120318, **1970**.
30. J. F. Giudicelli, J. R. Boissier, Y. Dumas, C. Advenier, *Compt. Rend. Soc. Biol.*, **167**, 232, **1973**.
31. L. Hansson, H. Aberg, S. Jameson, B, Karlberg, R. Malmcrona, *Acta Med. Scand.* **194**, 549, **1973**.
32. A. Amery, L. Billiet, R. Fagard, *N. Engl. J. Med.* **290**, 284, **1974**.
33. S. A. C. Wren, *Electrophoresis*, **16**, 2127, **1995**.
34. R. B. Miller, Y. Guertin, *J. Liq. Chrom.*, **15**, 1289, **1992**.
35. R. Bhushan, M. Arora, *Biomed. Chrom.*, **17**, 226-230, **2003**.
36. K. Kitaori, Y. Takehira, Y. Furukawa, H. Yoshimoto, J. Otera, *Chem. Pharm. Bull.*, **46**(3), 505-507, **1998**.
37. C. E. Baker, Pub., "Physicians' Desk Reference", 35th Ed., 906-908, **1981**.
38. A. Wade, Ed., "Martindale-The Extra Pharmacopoeia", 27th Ed., The Pharmaceutical Press, London, 1321-1322, **1977**.
39. M. Windholz, Ed., "The Merck Index", 9th Ed., Merck & Co., Inc., Rahway, N. J., 802-803, **1976**.
40. *Chemical Development* (Pharmaceutical Division, Switzerland), CIBA-GEIGY, Ltd.,

Personal Communication.

41. C. G. Regardh, K. O. Borg, R. Johansson, G. Johnsson, L. Palmer, *J. Pharmacokinet. Biopharm.*, **2**, 347-364, **1974**.
42. J. Szejtli, In: *Topics in Inclusion Science-Cyclodextrin Technology*, J. E. D. Davies (Eds.), **1998**, Kluwer Academic Publishers, Dordrecht, The Netherlands.
43. A. Villiers, *Compt. Rend.*, **112**, 536, **1891**.
44. F. Z. Schardinger, *Unters. Nahr. u. Genussm.*, **6**, 865, **1903**.
45. H. Pringsheim, *Chemistry of the Saccharides*; McGraw-Hill: New York, 280, **1932**.
46. H. Pringsheim, *A Comprehensive Survey of Starch Chemistry*; R. P. Walton, Ed.;Chemical Catalogue Co., Inc.: New York, NY, 35, **1928**.
47. P. Karrer, C. Nägeli, *Helv. Chim. Acta*, **4**, 169, **1921**.
48. A. Miekeley, *Ber. Dtsch. Chem. Ges.*, **65**, 69, **1932**.
49. K. Freudenberg, G. Blomquist, L. Ewald, K. Soff, *Ber. Dtsch. Chem. Ges.*, **69**, 1258, **1936**.
50. D. French, *Adv. Carbohydr. Chem.*, **12**, 189, **1957**.
51. F. Cramer, *Einschlussverbindungen (Inclusion Compounds)*; Springer-Verlag: Berlin, **1954**.
52. K. Freudenberg, F. Cramer, H. Plieninger, *Ger. Patent*, **895**, 769, **1953**.
53. J. A. Thoma, L. Stewart, *Starch, Chemistry and Technology I.*; R. L. Whistler, E. F. Paschall, Eds.; Academic Press: New York, 209, **1965**.
54. G. V. Caeser, *Starch and its Derivatives*; J. A. Radley, Ed.; Chapman and Hall: London, Chapter X, 290, **1986**.
55. W. Saenger, *Angew. Chem., Int. Ed. Engl.*, **19**, 344, **1980**.
56. W. Saenger, In: *Inclusion Compounds*, J. L. Atwood, J. E. D. Davies, D. D. MacNicol (Eds.), Oxford University Press, London, **2**, Ch 8, **1984**.
57. K. Harata, In: *Inclusion Compounds*, J. L. Atwood, J. E. D. Davies, D. D. MacNicol (Eds.), Oxford University Press, London, 5, Ch 9, **1984**.
58. W. Saenger, C. Betzel, B. E. Hingerty, G. M. Brown, *Nature*, 296, 581, **1982**.
59. K. B. Lipkowitz, K. Green, J. Yang, *Chirality*, **4**, 205, **1992**.
60. F. W. Lichtenthaler, S. Immel, *Starch.*, **48**, 225, **1996**.

61. F. W. Lichtenthaler, S. Immel, *Liebigs* Ann., 27, **1996**.

62. K. Harata, *Bull. Chem. Soc. Jpn.*, **52**, 2451, **1979**.

63. P. C. Manor, W. Saenger, *J. Am. Chem. Soc.*, **96**, 3630, **1976**.

64. K. Lindner, W. Saenger, *Carbohydr. Res.*, **99**, 103, **1982**.

65. K. Harata, *Bull. Chem. Soc. Jpn.*, **60**, 2763-2767, **1987**.

66. J. Szejtli, *Chem. Rev.*, **98**, 1743-1753, **1998**.

67. L. Lei, G. Qing-Xiang, *J. Incl. Phenom. Macro.*, **42**, 1-14, **2002**.

68. H. S. Frank, M. W. Evans, *J. Chem. Phys.*, **13**, 507, **1945**.

69. (a) J. L. Finney, A. K. Soper, *Chem. Soc. Rev.*, **23**, 1, **1994**. (b) A. A. Rashin, M. A. Bukatin, *J. Phys. Chem.*, **95**, 2942, **1991**.

70. M. Kitagawa, H. Hoshi, M. Sakurai, Y. Inoue, R. Chûjô, *Bull. Chem. Soc. Jpn.*, **61**, 4225, **1988**.

71. M. Sakurai, M. Kitagawa, H. Hoshi, Y. Inoue, R. Chûjô, *Chem. Lett.*, 895, **1988**.

72. F. W. Lichtenthaler, S. Immel, *Starch.*, **48**, 145, **1996**.

73. M. R. Caira, *Rev. Roum. Chim.*, **46**, 371-386, **2001**.

74. A. Kálmán, L. Párkányi, In: *Advances in Molecular Structure Research*, JAI Press Inc., 189-226, **1997**.

75. L. Fabián, A. Kálmán, *Acta Crystallogr., Sect.B, Struct. Sci.*, **55**, 1039-1049, **1999**.

76. W. Saenger, *Israel J. Chem.*, **25**, 43, **1985**.

77. M. J. Jozwiakowski, K. A. Connors, *Carbohydr. Res.*, **143**, 51, **1985**.

78. B. Casu, M. Reggiani, G. R. Sanderson, *Carbohydr. Res.*, **76**, 59, **1979**.

79. J. Szejtli, *J. Incl. Phenom.*, **1**, 135, **1983**.

80. B. W. Müller, U. Brauns, *Int. J. Pharm.*, **26**, 77, **1985**.

81. J. Phitha, *J. Pharm. Sci.*, **74**, 987, **1985**.

82. Cambridge Structural Database and Cambridge Structural Database System, Version 5.26, November **2004**, Cambridge Crystallographic Data Centre, University Chamical Laboratory, Cambridge, England.

83. K. Harata, *Chem. Commun.*, 191, **1999**.

84. K. Harata, *Bull. Chem. Soc. Jpn.*, **61**, 1939, **1988**.

85. M. R. Caira, S. A. Bourne, S. L. Vilakazi, L. Reddy, *Supramol. Chem.*, **16**, 279-285,

2004.

86. M. R. Caira, R. Hunter, S. A. Bourne, V. J. Smith, *Supramol. Chem.*, **16**(6), 395-403, **2004.**
87. R. L. Juliano (Ed.), *Drug Deliv. Syst.*, Oxford University Press, New York, **1980.**
88. P. Buri, A. Gumma (Eds.), *Drug Targeting*, Elsevier, Amsterdam, **1985.**
89. M. Szycher (Ed.), *High Performance Biomaterials*, A Comprehensive Guide to Medical and Pharmaceutical Applications, Technomic Publishing, PA, **1991.**
90. J. Szejtli (Ed.), *Cyclodextrins and their Inclusion Complexes*, Academia Kiado, Budapest, **1982.**
91. K. Uekama, *Pharmaceutical applications of cyclodextrin complexations*, Yakugaku Zasshi **101**, 857-873, **1981.**
92. K. Uekama, M. Otagiri, *CRC Crit. Rev. Ther. Drug Carrier Syst.* **3**, 1-40, **1987.**
93. V. J. Stella, R. A. Rajewski, Cyclodextrins: their future in drug formulation and delivery, *Pharm. Res.*, **14**, 556-567, **1997.**
94. T. Tokumura, M. Nambu, Y. Tsushima, K. Tatsuishi, M. Kayano, Y. Machida, T. Nagai, *J. Pharm. Sci.*, **75**, 391-394, **1986.**
95. K. Nakanishi, M. Masada, T. Nadai, K. Miyajima, *Chem. Pharm. Bull.*, 37, 211-214, **1989.**
96. F. Hirayama, K. Uekama, *Adv. Drug Deliv. Rev.*, **36**, 125-141, **1999.**
97. British Pharmacopoeia, *Medicinal and Pharmaceutical substan*ces, **1**, **1999.**
98. R. Ficarra, P. Ficarra, M. R. Di Bella, D. Raneri, S. Tommasini, M. L. Calabro, M. C. Gamberini, C. Rustichelli, *J. Pharm. Biomed. Anal.* **23**, 33-40, **2000.**
99. D. Giron, *Thermochim. Acta*, **1**, 248, **1965.**
100. Soft Imaging System GmbH, *Digital Solutions for Imaging and Microscopy*, Version 3.1 for Windows (Copyright **1987-2000**).
101. G. H. Stout L. H. Jensen, *X-ray Structure Determination: a Practical Guide*, ©**1989**, John Wiley & Sons, Inc., Ch5.
102. Z. Otwinowski, W. Minor, In: *Processing of X-ray Diffraction Data in Oscillation Mode in Methods in Enzymology*, Carter, C. W., Sweet, R. M. (Eds.), Academic Press, New York, 276, 307, **1996.**

103. *Data Preparation and Reciprocal Space Exploration*, Version 5.1, (Copyright Bruker Analytical X-ray Systems, **1997**).

104. G. M. Sheldrick, *SHELXS-97, Program for Crystal Structure Solution*, Institüt für Anorganische Chemie der Universität, Tammanstrasse 4, D-3400 Göttingen, Germany, **1997**.

105. L. J. Barbour, X-SEED, *A graphical interface to SHELX*, University of Missouri, Columbia, U.S.A, **1999**.

106. R. Miller, C. M. Weeks, In: *Direct Methods for Solving Macromolecular Structures*, Dordrecht (Ed.), Kluwer Academic Publishers, 389-400, **1998**.

107. I. Usón, G. M. Sheldrick, *Curr. Op. Struct. Biol.*, **9**, 643-648, **1999**.

108. K. Yvon, W. Jeitschko, E. Parthé, *J. Appl. Cryst.*, **10**, 73, **1977**.

109. Pov-Ray for Windows, Version 3.1e.watcom.win32, The persistence of vision development Team, © **1991-1999**.

110. British Pharmacopoeia, *Medicinal and Pharmaceutical substances*, **1**, **1999**.

111. *Anal. Profiles Drug. Subs.*, **12**, Academic Press Inc (London).

112. L. J. Barbour, LAYER, A computer program for the graphic display of intensity data as simulated precession photographs, *J. Appl. Cryst.*, **32**, 351, **1999**.

113. G. M. Sheldrick, SHELXL-97, *Program for the Refinement of Crystal Structures*, Institüt für Anorganische Chemie der Universität, Tammanstrasse 4, D-3400 Göttingen, Germany, **1997**.

114. A. L. Spek, *PLATON*, A multipurpose crystallographic tool, Version 10500 © **1980-2000.**

115. Paratone N oil (Exxon Chemical Co., TX, USA).

116. L. J. Farrugia, *Ortep-3 for Windows*, *J. Appl. Cryst.*, **30**, 565, **1997**.

117. G. M. Sheldrick, In: *Direct Methods for Solving Macromolecular Structures*, Dordrecht (Ed.), Kluwer Academic Publishers, 401-411, **1998**.

118. J. R. Luch, *Anal. Profiles Drug. Subs.*, **12**, 325, **1983**.

119. K. Stoschitzky, G. Zernig, W. Lindner, *J. Clin. Bas. Cardiol.*, **1**, 14, **1998**.

120. D. L. Klug, The influence of impurities and solvents on crystallisation. In: Myerson, A. (Ed.), Handbook of Industrial Crystallisation, Butterworths, New York, 65-87,

1993.

121. I. Weissbuch, L. Leiserowitz, M. Lahav, Tailor-made additives and impurities. In: Mersmann, A. (Ed.), Crystallisation Technology Handbook, Marcel Dekker, New York, 401-457, **1995**.
122. C. F. Lerk, A. C. Andreae, A. H. De Boer, G. K. Bolhuis, K. Zuurman, P. De Hoog, K. Kussendrager, J. Van Leverink, *J. Pharm. Pharmacol*, **35**, 747, **1983**.
123. J. M. Fachaux, A. M. Guyot-Hermann, J. C. Guyot, P. Conflant, M. Drache, J. P. Huvenne, R. Bouche, *Congr. Int. Technol. Pharm* 6^{th}, **5**, 213, **1992**.
124. T. Steiner, W. Saenger, *Acta Crystallogr.*, **B54**, 450-455, **1998**.
125. S. Kamitori, K. Hirotsu, T. Higuchi, *J. Chem. Soc., Chem. Commun.*, **109**, 2409, **1987**.
126. S. Kamitori, K. Hirotsu, T. Higuchi, *J. Chem. Soc., Chem. Commun.*, 690, **1986**.
127. S. Kamitori, K. Hirotsu, T. Higuchi, *Bull. Chem. Soc. Jpn.*, **61**, 3825, **1988**.
128. D. Mentzafos, I. M. Mavridis, G. le Bas, G. Tsoucaris, *Acta Crystallogr.*, **B47**, 746-757, **1991**.
129. WebLab ViewerPro Version 3.5 (Copyright **1999** by Molecular Simulations Inc., San Diego, CA).
130. M. R. Caira, S. A. Bourne, E. Mvula, *J. Therm. Anal. Calorim.*, **56**, 1329-1334, **1999**.
131. V. Čaplar, Z. Mikotić-Mihun, H. Hofman, J. Kuftinec, F. Kajfež, *Analytical Profiles of Drug Substances*, **13**, **1984**.
132. J. Villaverde, J. I. Pérez-Martinez, C. Maqueda, J. M. Ginés, E. Morillo, *Chemosphere*, 1-9, In Press, **2005**.
133. L. Szente, In Comprehensive Supramolecular Chemistry, Eds. J. L. Atwood, J. E. D. Davies, D. D. MacNicol and F. Vögtle, Pergamon, UK, Ch.8, **13**, 253-278, **1996**.
134. J. Ding, T. Steiner, W. Saenger, *Acta Crystallogr. Sect. B*, **47**, 731, **1991**.
135. J. A. Hamilton, L. J. Chen, *J. Am. Chem. Soc.*, **110**, 4379, **1988**.
136. E. N. Mvula, MSc Thesis, Preparation and Solid State Properties of Cyclodextrin Complexes of Selected Drug Molecules, University of Cape Town, South Africa, **1999**.

137. D. R. Dodds, PhD Thesis, Physicochemical Study of Inclusion of Drug Molecules in Cyclodextrins, University of Cape Town, South Africa, **1999**.

138. C. L. Oliver, PhD Thesis, Polymorphs, Cyclodextrin Inclusion Complexes and Salts of the Bronchodilator Tulobuterol, University of Cape Town, South Africa, **2004**.

139. L. Szente, In Comprehensive Supramolecular Chemistry, Eds. J. L. Atwood, J. E. D. Davies, D. D. MacNicol and F. Vögtle, Pergamon, UK, Ch.8, **3**, 253-278, **1996**.

140. D. Mentzafos, I. M. Mavridis, G. le Bas and G. Tsoucaris, *Acta Crystallogr., Sect. B*, **47**, 746-757, **1991**.

141. F. H. Herbstein and R. E. Marsh, *Acta Crystallogr., Sect. B, (Struct. Sci.)*, **54**, 677-686, **1998**.

142. A. Rontoyianni, I. M.Mavridis, *Acta Crystallogr.*, **C52**(9), 2277-2281, **1996**.

143. W. Saenger, C. Betzel, B. E. Hingerty, G. M. Brown, *Nature*, **296**, 581, **1982**.

144. W. Saenger, C. Betzel, B. E. Hingerty, G. M. Brown, *Angew.Chem., Int. Ed. Engl.*, **22**, 883, **1983**.

145. S. Makedonopoulou, I. M. Mavridis, *Acta Crystallogr.*, **B56**, 322-331, **2000**.

146. K. H. Jogun, J. J. Stezowski, *Nature*, **278**, 667, **1979**.

147. J. J. Stezowski, *Trans. Am. Crystallogr. Assoc.*, **20**, 73, **1985**.

148. A. Rontoyianni, I. M. Mavridis, E. Hadjoudis, A. J. M. Duisenberg, *Carbohydr. Res.*, **252**, 19, **1994**.

149. S. Makedonopoulou, A. Tulinsky, I. M. Mavridis, *Supramol. Chem.*, **11**, 73, **1999**.

150. T. J. Brett, J. M. Alexander, J. J. Stezowski, *J. Chem. Soc.*, 1105, **2000**

151. S. Makedonopoulou, I. M. Mavridis, *Carbohydr. Res.*, **335**, 213, **2001**.

152. J. L. Clark, J. J. Stezowski, *J. Am. Soc.*, **123**, 9880, **2001**.

153. J. M. Alexander, J. L. Clark, T. J. Brett, J. J. Stezowski, *Proc. Nat. Acad. Sci.*, **99**, 5115, **2002**.

154. M. R. Caira, E. J. C. de Vries, L. R. Nassimbeni, *Chem. Commun.*, **16**, 2058-2059, **2003**.

155. T. Bojinova, H. Gornitzka, N. Lauth-de Viguerie, I. Rico-Lattes, *Carbohydr. Res.*,

338, 381, **2003**.

156. G. R. Brown, MSc dissertation, The Physicochemical Characterisation of Cyclodextrin Inclusion Compounds with Non-Steroidal Anti-Inflammatory Drugs, University of Cape Town, South Africa, **1997**.
157. S. S. Braga, I. S. Gonçalves, E. Herdtweck, J. J. C. Teixeira-Dias, *New J. Chem.*, **27**, 597 – 601, **2003**.
158. K. Stoschitzky, G. Egginger, G. Zernig, W. Klein, W. Lindner, *Chirality*, **5**, 15-9, **1993**.
159. R. Bhushan, M. Arora, *Biomed. Chromatogr.*, **17**, 226 – 230, **2003**.
160. K. Kitaori, Y. Takehira, Y. Furukawa, H. Yoshimoto, *Chem. Pharm. Bull.*, **46**(3), 505 – 507, **1998.**
161. T. Steiner, W. Saenger, *J. Am. Chem. Soc.*, **114**, 10146 – 10154, **1992a.**
162. K. A. Udachin, L. D. Wilson, J. A. Ripmeester, *J. Am. Chem. Soc.*, **122**, 12375, **2000**.
163. J. A. Hamilton, M. N. Sabesan, L. K. Steinrauf, A. Geddes, *Biochem. Bioph. Res. Co.*, **73**, 659, **1976**.
164. M. Noltmeyer, W. Saenger, *J. Am. Chem. Soc.*, **102**, 2710, **1980**.
165. J. A. Hamilton, M. N. Sabesan, *Carbohydr. Res.*, **31**, 102, **1982**.
166. C. Betzel, B. E. Hingerty, M. Noltmeyer, G. Weber, W. Saenger, J. A. Hamilton, *J. Inclusion Phenom.*, **1**, 181, **1983**.
167. J. A. Hamilton, M. N. Sabesan, L. K. Steinrauf, *Carbohydr. Res.*, **33**, 89, **1981**.
168. G. le Bas, C. de Rango, N. Rysanek, G. Tsoucaris, *J. Inclusion Phenom.*, **2**, 861, **1984**.
169. I. M. Mavridis, E. Hadjoudis, G. Tsoucaris, *Mol. Cryst. Liq. Cryst.*, 186, 185, **1990**.
170. B. Klingert, G. Rihs, *J. Chem. Soc., Dalton Trans.*, 2749, **1991**.
171. I. M. Mavridis, E. Hadjoudis, G. Tsoucaris, *Carbohydr. Res.*, **11**, 220, **1991**.
172. D. Mentzafos, I. M. Mavridis, M. B. Hursthouse, *Acta Crystallogr.*, **C52**, 1220, **1996**.
173. N. Rysanek, G. le Bas, F. Villain, G. Tsoucaris, *Acta Crystallogr.*, **C52**, 2932, **1996**.
174. J. J. Stezowski, K. H. Jogun, E. Eckle, K. Bartels, *Nature (London)*, **274**, 617, **1978**.

175. H. Jogun, J. M. Maclennan, J. J. Stezowski, European Crystallographic Meeting, **1979**.

176. M. B. Hursthouse, C. Z. Smith, M. Thornton-Pett, J. H. P. Utley, *J. Chem. Soc., Chem. Commun.*, 881, **1982**.

177. J. A. Hamilton, M. N. Sabesan, *Acta Crystallogr., Sect. B*, **38**, 3063, **1982**.

178. M. Czugler, G. Geiger, J. J. Stezowski, *Z. Kristallogr.*, **54**, 162, **1983**.

179. K. Uekama, F. Hirayama, T. Imai, M. Otagiri, K. Harata, *Chem. Pharm. Bull.*, **31**, 3363, **1983**.

180. K. Uekama, F. Hirayama, T. Imai, M. Otagiri, K. Harata, *Chem. Pharm. Bull.*, **32**, 1662, **1984**.

181. K. Harata, K. Uekama, M. Otagiri, F. Hirayama, *J. Incl. Phenom.*, **1**, 279, **1984**.

182. I. Nakanishi, M. Arai, T. Fujiwara, K. Tomita, *J. Incl. Phenom.*, **2**, 689, **1984**.

183. F. Nishioka, I. Nakanishi, T. Fujiwara, K. Tomita, *J. Incl. Phenom.*, **2**, 701, **1984**.

184. T. Fijiwara, K. Tomita, I. Marseigne, J. Vicens, *Mol. Cryst. Liq. Cryst.*, **156**, 393, **1988**.

185. J. Vicens, T. Fujiwara, K. Tomita, *J. Incl. Phenom.*, **6**, 577, **1988**.

186. K. Harata, K. Uekama, M. Otagiri, F. Hirayama, *Bull. Chem. Soc*, **56**, 1732, **1983**.

187. K. Harata, *Chem. Commun.*, **14**, 928-929, **1988**.

188. M. R. Caira, V. J. Griffith, L. R. Nassimbeni, B. van Oudsthoorn, *J. Chem. Soc. Perkin Trans.2*, **10**, 2071-2073, **1994**.

189. K. Harata, F. Hirayama, H. Arima, K. Uekama, T. Miyaji, *J. Chem, Soc., Perkin Trans.2*, 1159-1166, **1992**.

190. S. Makedonopoulou, K Yannakopoulou, D. Mentzafos, V. Lamzin, A. Popou, I. M. Mavridis, *Acta Crystallogr. Sect. B : Struct. Sci.*, **57**, 399, **2001**.

191. G. R. Brown, M. R. Caira, L. R. Nassimbeni, B. van Oudshoorn, *J. Incl. Phenom.*, **26**, 281, **1996**.

192. A. Grandeury, S. Petit, G. Gouhier, V. Agasse, G. Couquerel, *Tetrahedron*, **14**, 2143, **2003**.

193. M. R. Caira, V. J. Griffith, L. R. Nassimbeni, B. van Oudtshoorn, *Supramol.*

Chem., **7**, 119-124, **1996**.

194. K. Harata, *Chem. Rev.* **98**, 1803-1827, **1998**.
195. Griffith, PhD Thesis, Physicochemical Characterisation of Cyclodextrin-Drug Complexes, University of Cape Town, South Africa, **1996**.
196. T. Steiner and W. Saenger, *J. Am. Chem. Soc.*, 114, 10146, **1992**.
197. J. Szejtli, *J. Incl. Phenom.*, **14**, 25, **1992**.
198. R. L. Gelb, L. M. Schwartz, B. Cardelino, H. S. Fuhrman, R. F. Johnson, D. A. Laufer, *J. Am. Chem. Soc.*, **103**, 1750, **1981**.
199. F. Tsorteki, K. Bethanis, D. Mentzafos, *Carbohydr. Res.*, 339, 233, **2004**.
200. A. Rontoyianni, I. M. Mavridis, *J. Incl. Phenom. Macro.*, **32**, 415-428, **2001**.
201. K. Harata, F. Hirayama, T. Imai, K. Uekama, M. Otagiri, *J. Incl. Phenom. Macro.*, **6**, 443, **1988**.
202. A. Grandeury, S. Petit, G. Gouhier, V. Agasse, G. Coquerel, Tetrahedron : *Asymm.*, **14**, 2143, **2003**.
203. A. Rontoyianni, I. M. Mavridis, *J. Incl. Phenom. Macro.*, **32**, 415-428, **2001**.
204. M. R. Caira, L. R. Nassimbeni, B. van Oudtshoorn, *J. Incl. Phenom. Mol.*, **20**, 277-290, **1995**.
205. M. R. Caira, S. A. Bourne, W. T. Mhlongo, P. M. Dean, *Chem. Commun.*, 2216-2217, **2004**.
206. M. R. Caira, S. A. Bourne, F. Giordano, S. L. Vilakazi, *Supramol. Chem.*, **2004.**
207. T. Steiner, W. Saenger, *Angew. Chem., Int. Ed. Engl.*, **37**, 3404, **1998**.
208. E. J. C. de Vries, PhD Thesis, Inclusion of Alkylparabens in Cyclodextrins, Uinversity of Cape Town, South Africa, **2003**.
209. M. K. Dowd, A. D. French, P. J. Reilly, *Carbohydr. Res.*, **1**, 264, **1994**.
210. G. M. Sheldrick, In: Direct Methods for Solving Macromolecular Structures, Dordrecht (Ed.), Kluwer Academic Publishers, **1998**, 401-411.
211. Giacovazzo, C., *SIR2002, Program for Crystal Structure Solution*, **2002**, Inst., di Ric. per lo Sviluppo di Metodologie Cristallografiche, CNR, Univ. of Bari, Italy.
212. Egert, E., Sheldrick, G., *Acta Crystallogr*, **1985**, A41, 262-268.
213. J. Boger, R. J. Corcoran, J. M. Lehn, *Helv. Chim. Acta*, 61, 2190-2218, **1978**.

214. B. Casu, M. Reggiani, *Carbohydr. Res.*, 76, 59-66, **1979**.

215. J. Szejtli, A. Lipták, I. Jodál, P. Fügedi, P. Nánási, A. Neszmélyi, *Starch / Stürke*, 32, 165-169, **1980**.

216. K. Harata, K. Uekama, M. Otagiri, F. Hirayama, Y. Sugiyama, *Bull. Chem. Soc. Jpn.*, 55, 3386, **1982**.

217. K. Harata, K. Uekama, M. Otagiri, F. Hirayama, *J. Chem. Soc. Jpn.*, 173, **1983**.

218. K. Harata, K. Uekama, M. Otagiri, F. Hirayama, *Bull. Chem. Soc. Jpn.*, 60, 497, **1987**.

219. K. Harata, *J. Chem. Soc., Perkin Trans.* 2, 799, **1990**.

220. T. Steiner, W. Saenger, *Carbohydr. Res.*, 282, 53, **1996**.

221. K. Yannakopoulou, D. Mentzafos, I.M. Mavridis, K. Dandika, *Angew. Chem.*, Int. Ed., 35, 2480, **1996**.

222. K. Harata, K. Uekama, M. Otagiri, F. Hirayama, *Bull. Chem. Soc. Jpn.*, **55**, 3904, **1982**.

223. K. Harata, K. Uekama, M. Otagiri, F. Hirayama, *Chem. Lett.*, 1807-1810, **1983**.

224. K. H. Frömming, J. Szejtli, *Cyclodextrins in Pharmacy*, Kluwer, Dordrecht, p.25, **1996**.

225. M. R. Caira, V. J. Griffith, L. R. Nassimbeni, *J. Incl. Phenom.*, **20**, 277-290, **1995**.

226. J. Frank, J. Holzwarth, W. Saenger, *Langmuir*, **18**, 5974-5976, **2002**.

227. T. Steiner, W. Saenger, *Angew. Chem., Int. Ed.*, **37**, 3404, **1998**.

228. J. Szejtli, *J. Incl. Phenom.*, **14**, 25, **1992**.

229. M. Okada, M. Kamachi, A. Harada, *Macromolecules*, **32**, 7202-7207, **1999**.

230. T. Loftsson, M. E. Brewster, *J. Pharm. Sci.*, **85**, 1017-1025, **1996**.

231. P. M. Dean, MSc. dissertation, Structural and Thermal Characterisation of NSAIDS and Cyclodextrin-NSAID Complexes, University of Cape Town, South Africa, **2005**.

232. V. Čaplar, Z. Mikotić-Mihun, H. Hofman, J. Kuftinec, F. Kajfež, *Analytical Profiles of Drug Substances*, **13**, 1-25, **1984**.

233. L. Borka, J. K. Haleblian, *Acta Pharm.*, **40**, 71-94, **1990**.

234. T. Steiner, W. Saenger, *J. Am. Chem. Soc.*, **114**, 10146, **1992**.

235. K. Harata, *J. Chem. Soc. Jpn.*, **61**, 1939, **1988**.

236. A. L. Spek, *J. Appl. Crystallogr.*, **36**, 7-13, **2003**.

237. S. G. Kim, K. H. Kim, Y. K. Kim, S. K. Shin, K. H. Ahn, *J. Am. Chem. Soc.*, **125**, 13819-13824, **2003**.

238. V. J. Griffith, PhD Thesis, Physicochemical Characterisation of Cyclodextrin-Drug Complexes, University of Cape Town, South Africa, **1996**.

239. F. Tsorteki, K. Bethanis, D. Mentzafos, *Carbohydr. Res.*, **339**(2), 233-240, **2004**.

240. A. Grandeury, S. Petit, G. Gouhier, V. Agasse, G. Coquerel, *Tetrahedron: Asym.*,**14**, 2143-2152, **2003**.

241. F. Tsorteki, K. Bethanis, N. Pinotsis, P. Giastas, D. Mentzafos, Acta Crystallogr., **B61**, 207-217, **2005**.

242. T. Steiner, W. Saenger, *Angew. Chem., Int. Ed. Engl.*, **37**, 3404, **1998**.

Appendix A

Appendix A

Supplementary crystallographic information for each of the solved structures in this thesis has been stored in the folder 'Appendix A' on the CD-ROM attached to the inside cover of this thesis. Each structure is stored in a subfolder that is named according to the structure abbreviation that was used in the thesis. Seven files are included for each of the structures elucidated and they contain the following information:

File extension	Contents
.HKL	Reflection data
.RES	SHELX type coordinate file
.CIF	Crystallographic Information File
.XL	SHELX output file
.LIS	PLATON output file listing all geometric parameters of a structure
.FCF	Structure factor tables
.SUP	PLATON output file summarising selected information from .LIS file in tabulated form